The Application of Body and Seismic Trace Shape Analysis to the Exploration of Turbidite Systems: Eocene Tay Sandstone Member, Gannet South, Central North Sea.

Thesis submitted as partial fulfillment of the requirements for the degree of Doctor of Philosophy (Ph.D.) in Geology & Geophysics

Yousuf Muhammed Rashid Al-Aufi
Department of Geology & Geophysics
University of Edinburgh
December 2003

**In the Name of God, the most Gracious
the most Merciful.**

A person remains to be knowledgeable as long as s/he seeks knowledge, once s/he feels that they have gained knowledge then they are ignorant.

"Indeed, in the creation of the heavens and the earth and the alternation of the night and day are signs for those of understanding".

The Quran, ch 3, verse 190.

Acknowledgements

All praises and thanks are due to God, the creator, the cherisher and the sustainer of the universe. God's blessings make possible all good deeds. May God's peace and blessings be upon all the messengers including Moses, Jesus and Muhammad.

This project was initiated by John Verbeek of Shell-Expro. I am grateful both to him and to Shell who provided me with a unique opportunity to work within their offices in Aberdeen. In addition to gaining my PhD, I had a marvellous opportunity to get work experience within Shell as I was based in the Geophysics Consultants team. Thanks to the whole team and others within Shell without mentioning the endless list.

No usual thanks are sufficient to express my gratitude towards PDO who not only sponsored my studies but also were very patient and kind throughout the years of the PhD.

Roger Scrutton was my supervisor. He is thanked for his guidance especially towards the end of my work.

Many thanks to all those who have kept me sane through the long years that I spent in the UK. I'm going to miss these guys both in Aberdeen and Edinburgh.

My gratitude extends to my beloved family, my parents and all the 20 brothers and sisters. Special thanks to my precious mum for being patient and giving me the help and care throughout my life and to my beloved wife for her continuous support, encouragement and patience and thank you for being part of my life. May God reward you all abundantly.

ABSTRACT OF THESIS

Due to their importance as source and host rocks of hydrocarbons, deepwater siliciclastic systems have been extensively investigated over the past 50 years through outcrop and laboratory studies, acoustic imaging of modern fans and deep-penetration seismic profiling of buried systems. Correct recognition and interpretation of turbidite systems is of great importance for evaluating reservoir geometry and distribution. In this regard it is necessary not only to consider the most appropriate sedimentological model, but also the range of controls that have been most influential in the deposition of any given sequence. Furthermore, due to the complex nature of these systems, understanding subtle stratigraphic features and identifying minor structures such as faults that are close to or below seismic resolution is especially valuable since such features and structures may have a dramatic effect on reservoir performance. The need to identify minor features has led to a marked increase in the focus on seismic attribute maps as the interpreter is challenged to provide more accurate and detailed results.

This project was devoted to the extraction of more quantitative information by integrating 3D seismic data with wireline logs and cores from 10 exploration wells drilled through the Tay system, Gannet South, Central North Sea and by introducing the innovative body and seismic trace shape analysis to the interpretation process.

The idea of analysing a seismic dataset based on variation of seismic trace shapes comes from the assumption that changes in lithology, rock properties and fluid content should affect seismic response in not only amplitude but the whole shape of the trace. This project utilizes the pattern recognition capability of the neural network technology to classify seismic traces based on their shapes. Both supervised and unsupervised classifications were applied on the Gannet South seismic dataset. Maps produced have revealed subtle geological features only expressed in the shape of the seismic trace and thus have substantially enhanced the understanding of the sand geometries of the turbidite system and the structural development and evolution of the basin. The results also provided clues to the timing, nature and extent of factors

controlling the sediment transport pathways in the area, and helped in the discovery of hydrocarbon pockets previously gone unnoticed.

A set of body shape parameters that would enable a distinctive description of different turbidite sand bodies were established. No single parameter is enough to uniquely describe all shapes but a combination of parameters could be used. The study also showed that the normalised polar representation of any shape can be significant for its recognition as well as for matching purposes. Unfortunately, the body shape analysis was hampered by the lack of accepted general turbidite models in the literature as well as inaccessibility to subsurface seismic datasets on which body shape analysis could have been applied in order to take the results further at this stage.

The Eocene Tay sediments of the Gannet South area preserve a three-dimensional setting of a relatively small turbidite system (30 km long and 10 km wide). The Tay Sandstone Member is relatively thin in this area as the maximum thickness is no more than 141 ms (approximately 700 ft). The thickest Tay package has been deposited on the basin floor where the system fans out. The system is moderately sandy and comprises layered and amalgamated sheets/lobes. Turbidity currents were point-sourced and flowed from west-southwest towards east-northeast.

The Tay Sandstone is a thin to thick-bedded, fine to medium-grained sandstone, interbedded with variably silty, fissile, green-grey to grey mudstones and siltstones. Coarse sands and gravels are completely absent in this area as shown by the cored wells. Generally speaking, the Tay Fan system displays a complex distribution, which is restricted to the southern parts of UK quadrants 21 and 22. Other workers in the area have attributed this distribution to salt movement during sedimentation. However, this study shows that salt movement during deposition is not the only factor controlling the Tay distribution as pre-sedimentation salt movement as well as highs resulted from previous periods of sedimentation have also played an important role in defining the channel pathways and locus of deposition.

The basin can be divided into three sub-basins. The onset of basin filling is interpreted to start first in the basin close to the shelf and progress successively seaward as each basin is filled to a spill point (fill and spill model). This is why the maximum amount of the youngest sand is observed at the deepest basin (Basin III) in well 22/26a-1. However, syn-sedimentary salt movement caused the highs that became buried to rise once again and stand in the way of the flow. In Basin I this caused younger sediments to be deposited while in Basin III the whole pathway was shifted and another lobe was deposited in a new position onlapping the previous one. Thus, the dispersal and accumulation of sediment and resulting morphology and architecture of the Gannet South Tay system have been strongly influenced by sea-floor topography at different levels. This model for the distribution and architecture of the Tay Sandstone Member and its relationship to evolution of basin geometry can provide a framework for the investigation for other deepwater fairways within the North Sea.

List of Figures

Chapter 1: Introduction

Chapter 2: Tectono-Stratigraphic Framework

Chapter 3: Seismic Data Interpretation

Chapter 4: Sedimentological and Petrophysical Framework

Chapter 5: Seismic Data to Well Log Tie

Chapter 6: Trace Shape Analysis

Chapter 7: Body Shape Analysis

Chapter 8: Synthesis and Conclusions

List of Tables

List of Appendices

Table of Content

Chapter One

Chapter One

Introduction

1.1 Rationale

The success of an exploration or production project hinges on the knowledge of the subsurface. This fact has been realised since 1920s when "surface geology" was no longer sufficient for new oil discoveries as the need for oil was increasing rapidly. The price of a barrel shot-up from $1.20 in 1916 to $3.36 in 1920 (Al-Aufi, 1996). By this time all the surface features (e.g. oil seepage), in the oil producing countries of that time, were drilled. The need to find a way to "see" underground was at its peak. The momentum of hydrocarbon exploration and production has relied on technological innovation. In the mid 1970s the 3D seismic technique was first presented to the world but it was not used significantly until late 1980s and early 1990s (Brown, 1993). According to Al-Aufi (1996), 3D seismic data accounts for approximately 30% of land acquisition and 75% of the marine acquisition. It is more than likely that these percentages are a lot higher today. This is because 3D seismic datasets are of significantly higher quality than the 2D datasets. Furthermore, the extremely dense grid lines make it possible to develop a more accurate structural and stratigraphic interpretation. Hence better understanding of the subsurface leads to optimised exploitation, such as minimising the number of wells required in an oil field.

Geoscientists are normally asked to estimate the petrophysical properties of lithologies and the uncertainties involved in these estimatins. However, the success of exploration or production ventures does not depend only on the geologists getting it right, but on what is technically achievable. The development of three-dimensional

seismic imaging combined with major advancement in wireline logs technology has provided a unique opportunity to predict reservoir geometries and properties with improved certainty and in a more efficient way. However, despite these advances in the subsurface imaging methods and tools, they are still not able to lead to a full description of the subsurface. All that they are capable of is to give a prediction of what could be found. Furthermore, now that most of the established world class petroleum provinces, e.g. North Sea basin, have reached a mature state of development, exploration focus has shifted away from targeting structural to more subtle stratigraphic plays making the challenge of providing more accurate maps even greater than at any other time.

In this project, the author attempts to contribute to advancing the understanding of the subsurface by devoting the project to the extraction of more quantitative information from 3D seismic data volumes by introducing innovative body and seismic trace shape analysis to the interpretation process. This is envisaged to improve the speed and quality of the interpretation process and lead to a more consistent and even more quantifiable 3D seismic interpretation providing more efficient and detailed input into geological models.

The idea of body shape analysis comes from the concept of face recognition techniques used to catch criminals. If sandstone bodies in the subsurface have distinct shapes and these shapes are recognisable in the seismic data then the same technique can be used to identify which depositional environment these bodies belong to and what elements of the sedimentary system they represent. In this thesis a set of body shape parameters that would enable a distinctive description of different turbidite sand bodies are established. The investigation shows that no single parameter is enough to uniquely describe all shapes but a combination of parameters could be used. By introducing body shape analysis to the three-dimensional seismic interpretation process it is envisaged to improve the speed and quality of the interpretation and lead to more consistent and even further quantifiable results providing more efficient and detailed input into geological models. Using this method an interpreter can have an idea of the turbidite (or any other system for that

matter) sand body geometry before even picking any horizons. If somehow we managed to calibrate these bodies to real geology, the whole process of the seismic data interpretation would be revolutionised.

Trace shape analysis, on the other hand, is based on the assumption that changes in lithology, rock properties and fluid content should affect seismic response in the whole shape of the trace. In recent years, many types of seismic attribute analysis techniques have been introduced. Seismic attribute maps have become important tools in the interpretation of seismic data. They have proven to be especially valuable for understanding subtle stratigraphic features and identifying minor structures that are close to or below seismic resolution. However, almost all of these attribute analysis techniques are based on correlation and comparison of a point on one seismic trace to another seismic trace, e.g. amplitude to amplitude. The direct study of the variation of trace shapes has been neglected in hydrocarbon exploration due to the lack of an appropriate tool to accurately map these changes. In the 1990s CGG produced a software package that can cater for such an analysis based on neural network technology. The idea has been slow to gain acceptance due to its unconventionality. In this project the idea and the package are assessed by application to a real seismic dataset volume. The study utilizes the pattern recognition capability of neural network technology to classify seismic traces based on their shapes. Both supervised and unsupervised classifications are applied to the three-dimensional seismic dataset from the Tay turbidite system of Eocene age, Gannet South, Central North Sea (Fig. 1.1). The analysis was constrained by the electrical wireline logs and cores from the 10 exploration wells drilled through the system (see Fig. 1.2 for well locations and the extent of three dimensional seismic survey used in this study). Maps produced reveal subtle geological features only expressed in the shape of the seismic trace and thus substantially enhance the understanding of the sand geometries of the turbidite system and the structural development and evolution of the basin. Furthermore, the results provide clues to the nature, extent and timing of factors controlling the sediment transport pathways in the area, and help in the discovery of hydrocarbon pockets previously gone unnoticed.

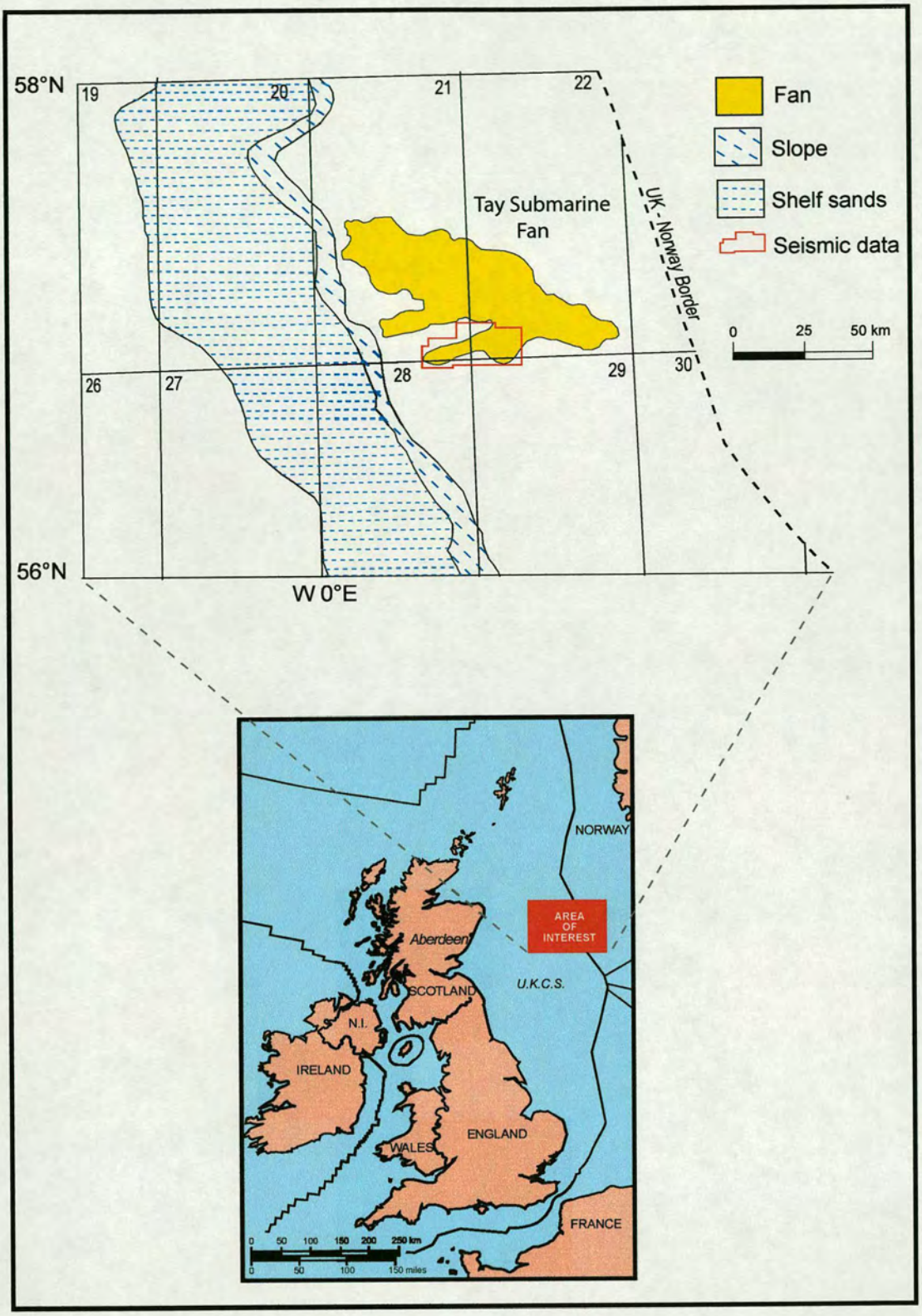

Figure 1.1: Study area location map showing area covered by the seismic data used for this project. (Modified from Den Hartog Jager *et al.*, 1993).

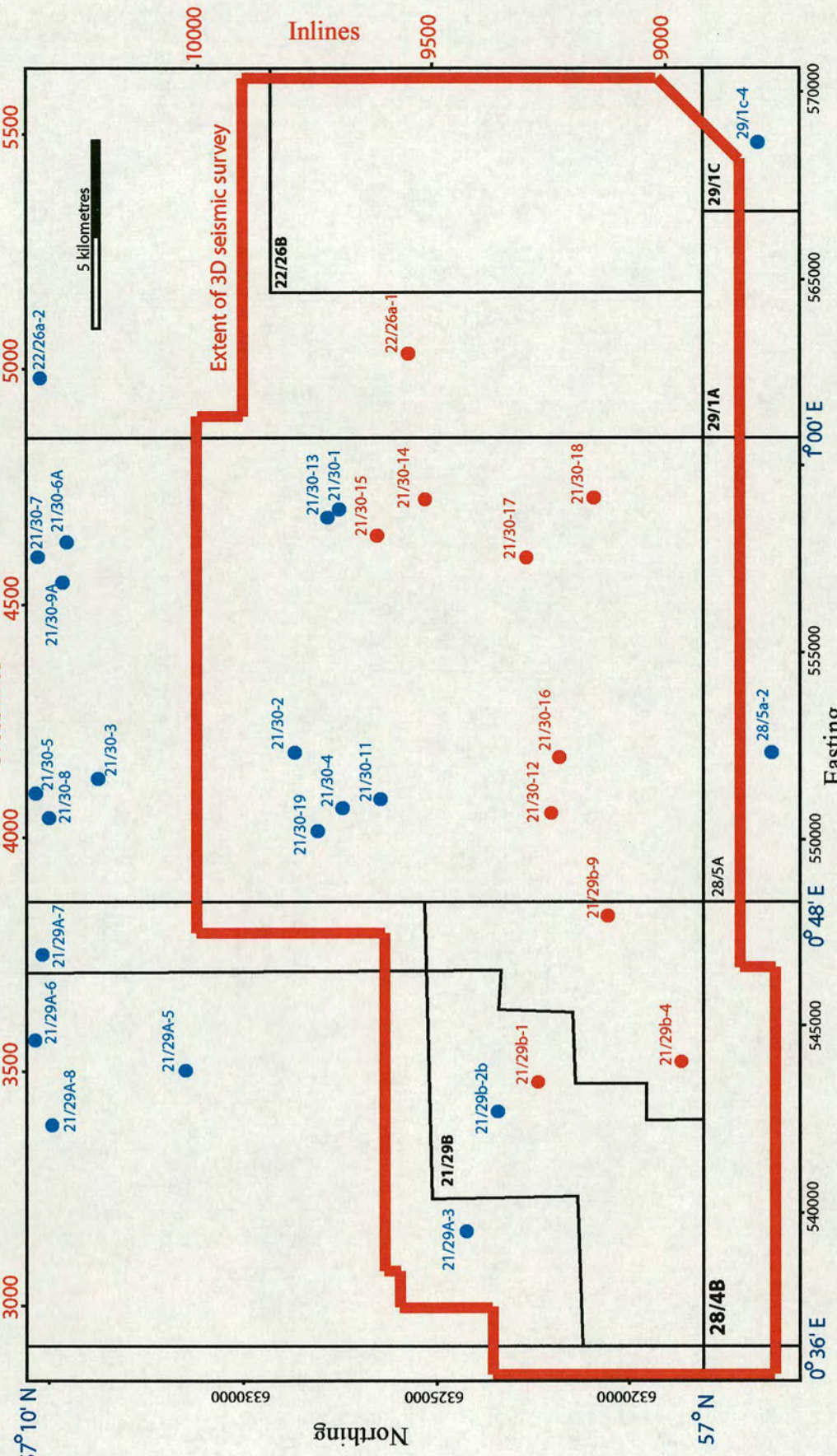

Figure 1.2: Map showing the aerial extent of the 3D seismic survey and well control. Wells available for this project are shown in red.

The Eocene (Ypresian-Lutetian) Tay Sandstone Member of the Central North Sea is a proven highly prospective reservoir in the Gannet area. It has long been interpreted as a deep-water depositional system, comprising deposits of sediment gravity flows and hemipelagites (Armstrong *et al.*, 1987; Milton *et al.*, 1990; Banner *et al.*, 1992; Den Hartog Jagger *et al.*, 1993). In all the previous studies conducted, the Gannet South Tay depositional system was part of a larger regional study. However, none of these studies examined the area in detail. Although they demonstrated that the Tay Fan system, generally speaking, displays a complex distribution, which is restricted to southern parts of UK quadrants 21 and 22 due to syn-depositional salt movement (Armstrong *et al.*, 1987), none of these studies examined in detail the coeval tectonic evolution of the Gannet South area in general and the Tay Sandstone Member in particular or the syn-sedimentary control of salt diapirism on the deposition of the Tay depositional system. Moreover these studies utilized conventional quantitative interpretation of 3D seismic volumes such as extracting maps of amplitude, phase and dip azimuth to emphasise the Tay depositional system extent.

In this study, interpretation of high-quality seismic data using conventional methodology and trace shape analysis, constrained by exploration wells provided insights into controls on the stratigraphic architecture and deep-water sedimentary processes that governed deposition of the Eocene Tay Sandstone Member in the Gannet South area of Central North Sea. This study reveals that salt movement during deposition *is not the only factor* controlling the Tay Sandstone Member distribution but pre-sedimentation salt movement as well as the topographic highs resulting from previous deposition have played an important role in defining the channel pathways and the deposition locus. The evolution of salt induced highs within the basin led to a temporal and spatial variation in the accommodation space generated and a subsequent modification of depocentres which in turn had a direct impact on sediment dispersal patterns and architecture.

The reconstructed depositional model for the Tay turbidite system provides an advance on the four stage fill-and-spill model provided by Sinclair and Tomasso

(2002), which only seems to be adequate for static basins but not for basins that are actively evolving during deposition such as the one in Gannet South area.

1.2 Aims

This thesis has the objective of examining the coeval deposition of the Tay Sandstone Member with basin evolution and Zeschian salt movement and extracting more information from three-dimensional seismic datasets by improved body and seismic trace shape analysis. This will allow more efficient and detailed input to geological models from seismic interpretation and is achieved by:

1) Evaluating the Tay depositional system of the Gannet South area through the interpretation of a three-dimensional seismic dataset aided by the sedimentological analysis of the cores and calibrated with the wireline log data from the wells drilled in the area.

2) Utilizing neural network technology to classify the seismic traces based on their shapes in order to investigate if the seismic trace shape contains any more information that can not be revealed by traditional attributes, e.g. amplitude.

3) Describing the physical properties of a depositional body with a set of parameters that reflect the shapes and interrelationships of petrophysical properties as they vary within and between bodies. The combined set of petrophysical and shape parameters contributes to the seismic image.

1.3 Structure of the Thesis

The thesis is divided into eight chapters. Each chapter examines a particular aspect of the investigation. The research starts by examining geological history of the Central

North Sea then focuses on the specific area of interest as revealed by the seismic data and then zooms in further by examining the wireline logs and core data. Seismic trace shape analysis is then applied to the dataset at the level of interest. The findings from all datasets are then integrated to draw a detailed picture of the Tay Sandstone Member depositional model.

Chapter Two provides a tectono-stratigraphic framework of the Central North Sea area, focusing on the Gannet South prospect, summarised from published literature. Chapter Three details the interpretation method for the high-resolution 3D seismic dataset and presents the results and conclusions of the seismic interpretation. As such, it provides a depositional model for the Tay system in the Gannet South area as well as the necessary surfaces to be used in seismic trace shape analysis. Chapter Four zooms into a higher resolution and gives an evaluation of the sedimentological facies observed in 8 cored exploration wells and calibrates them with the results of the petrophysical analysis of wireline logs. A lithofacies scheme is developed for the Tay depositional system within the Gannet South area. Chapter Five provides the link between the sedimentology described and the seismic volume by performing a seismic to well tie operation. In the process we assess the adequacy of the seismic data to perform attribute analysis on it. Normally seismic attribute analysis is applied to enhance subtle features at the limit of seismic resolution. As such, it is of paramount importance to be sure that these features are real geology and not processing or acquisition artefacts contaminated in the seismic data. Therefore, attribute analysis relies on accurate seismic to well ties. This is further investigated by checking if the seismic source wavelet varies laterally. If it does the attribute analysis will fail (Ziolkowski *et al.*, 1998) since the results will be attributed to processing problems in the data rather than real geology. Chapter Six presents the basic idea and assumption behind the seismic trace shape analysis, provides a review of the published literature relevant to the topic, gives the results of the analysis, discusses them and finally draws some conclusions from them. Chapter Seven presents the basic idea behind the body shape analysis, presents a generalised set of parameters that can describe the geometry of sand bodies in different turbidite depositional systems, provides a review of the published literature relevant to the

topic, gives the results of the analysis, discusses them and finally draws some conclusions from them. Chapter Eight integrates all the data sets, their interpretations and results and draws the key conclusions and implications for hydrocarbon exploration from them and also provides some recommendations for further work.

Chapter Two

Chapter Two

Tectono-Stratigraphic Framework

2.1 Introduction

Submarine fans and turbidite systems constitute major petroleum reservoirs in more than 85 sedimentary basins around the world. Of the 25 largest oil and gas fields in the United States, six occur in turbidite reservoirs (Weimer & Link, 1991). They are also responsible for 89% of the production in offshore Brazil (Bruhn, 1998). In the North Sea, over 22% of the proven petroleum reserves, estimated to be 23 billion barrels (BBO) and 50 trillion cubic feet (TCF) of gas, occur in submarine fan deposits of Late Jurassic, Early Cretaceous, Late Cretaceous, Palaeocene, and Eocene age (Watson, 1984). The North Sea is considered to be a mature petroleum province as it has been explored and developed for more than 35 years, and turbidite reservoirs that occur in both oil and gas fields were among the earliest and largest discovered in the province (Weimer & Link, 1991).

The offshore North Sea area includes three separate basins; Viking, Central, and the Moray Firth grabens. Most of the turbidite production occurs in four different tectonic settings: (1) Late Jurassic early syn-rift basin, (2) Late Jurassic-Early Cretaceous late syn-rift fault-related setting, (3) Late Cretaceous-early Palaeocene post-rift sag basins, and (4) Palaeogene post-rift and/or intracratonic sag basins.

Specific areas of interest for this particular study are the Tertiary fan systems that occur in the Central Graben of the North Sea, in particular, the Gannet- South area, which sits on the eastern edge of western flank of the Central Graben (Fig. 2.1). These Tertiary fan systems represent individual periods of deep-water clastic deposition that punctuated the Tertiary post-rift period of the North Sea. The systems

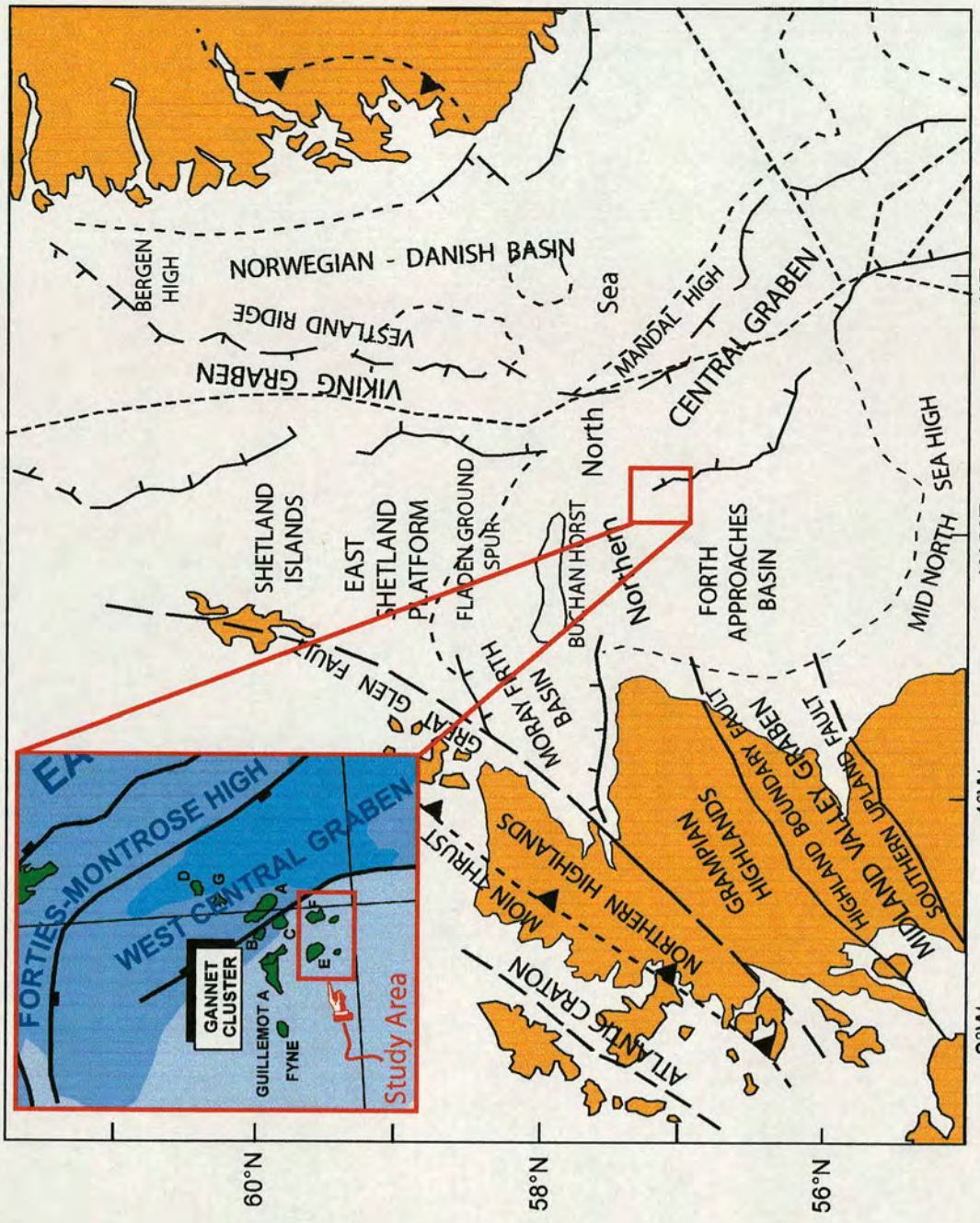

Figure 2.1: Map showing location of the study area. Gannet-South sits on western flank of the Central Graben of UK Central North Sea.

are quite large scale in terms of North Sea distribution but compared to modern deep-water clastic systems are small scale (Johnson and Flint, 1997). The reservoirs are sealed by Tertiary shales and contain hydrocarbon generated from older, underlying Jurassic shales and migrated along fault planes and diapirs.

According to Den Hartog Jagger *et al.* (1993), the large scale Tertiary fan sedimentation started at the end of the early Palaeocene. This was triggered by the onset of rapid thermal doming of the Shetland Platform and the Scottish Highlands. The largest fan (Andrew) was deposited immediately following this uplift and subsequent fans became progressively smaller through Palaeocene and Eocene times. The decrease in the size through time was not gradual and was controlled by relative sea level fluctuation that in turn controlled sand supply and subsequently fan geometry. The relative sea level variations were locally influenced by volcanic activities in the British Thulean Province. The volcanism started in the Maastrichtian and ended in the Middle Eocene (Mussett *et al.*, 1988; Hitchen & Ritchie, 1987). Mussett *et al.* (1988) identified two peak volcanic activity periods. The first was between 59 - 60 Ma and was the cause to trigger the first wave of fan deposition. The second was around 54 - 55 Ma close to the age for the tuffs of the Balder Formation.

Four main sequences were identified by Den Hartog Jagger *et al.* (1993): the Andrew, Forties, Frigg/Tay and Alba sequences. The sand/shale ratio decreased throughout the Palaeocene and Eocene and within each individual sequence. The systems were supplied from the sources to the west and northwest. The rate of sediment supply controlled the resultant sedimentological features. High sand supply created large numbers of small channels with an overall sheet like geometry, whereas low overall sand/shale ratios created isolated, stable long lived channels. Having said that, the rate of sediment supply was not the only factor controlling the resultant sedimentological and geometrical features of the fan systems but, as this study shows, salt movement pre-, syn- and post-deposition have played an important role in the temporal and spatial evolution of these systems (see Fig. 2.2 for the stratigraphic succession of the Central Graben).

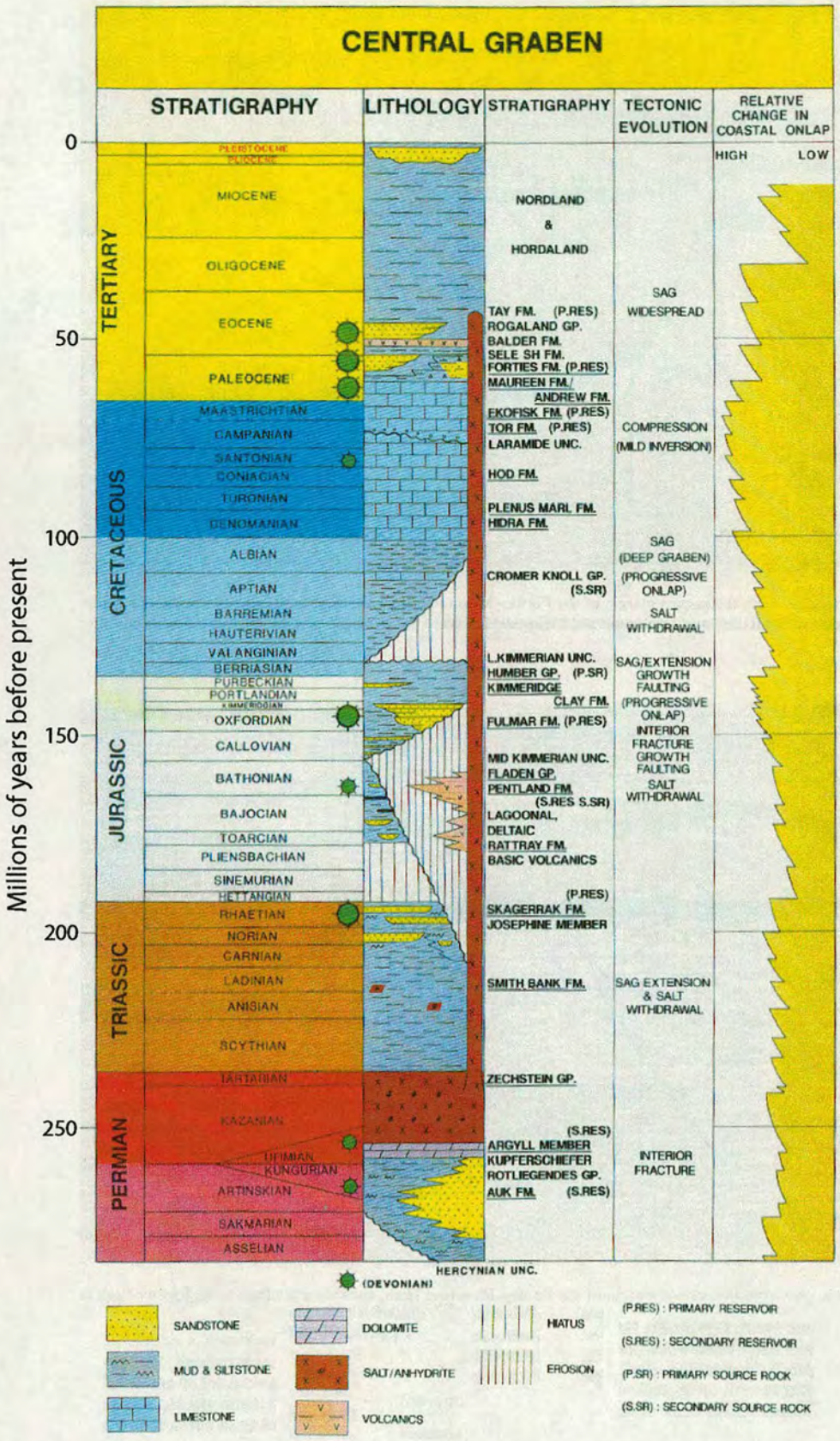

Figure 2.2: Stratigraphic succession of the Central Graben of UK Central North Sea. (From Erratt, 1993)

The aim of this chapter is to provide a brief review of structural and stratigraphic evolution of the Central Graben of the North Sea evidenced from the literature. This area has a long and complex geological history, with the later stages in its structural and stratigraphic development being largely controlled by its earlier history (Glennie & Underhill, 1998). This makes it important to get an appreciation of the wider picture before getting overwhelmed by the details of the zone of interest.

2.2 Structural and Stratigraphic Evolution of the North Sea area

From the Permian to the present day the British Isles and North Sea have largely lain in an intraplate setting (Glennie & Underhill, 1998). Prior to this, major plate tectonic organisation took place starting with the separation of the continental fragments of the supercontinent Pangea and through the Caledonian and Variscan periods of rifting and mountain building. Since this multi-phase tectonic development of the NW area of Europe it has largely been positioned in the resultant intraplate setting. However, it has remained far from quiescent and at least five major regional structural events may be recognised. These have been summarised below using the outline provided by Glennie and Underhill (1998) (Figs. 2.3 & 2.4):

2.2.1 Permo-Triassic rifting and thermal subsidence

Early Permian extension initiated the N-S trending Viking-Central Graben fracture system (Glennie, 1984; Badley *et al.* 1988, Glennie & Underhill, 1998). Two isolated basins were formed (Taylor, 1984; Zeigler, 1988, Glennie & Underhill, 1998): the Northern Permian Basin and the Southern Permian Basin. These were situated between the SW-NE trending Caledonian mountain belt to the north and the east-west trending Variscan fold-belt to the south and were separated by the Mid North Sea High.

The Northern Permian Basin extended across what is now the Central Graben from the Forth Approaches Basin in the west, over the Jæren High to its depocentre in the Norwegian-Danish Basin.

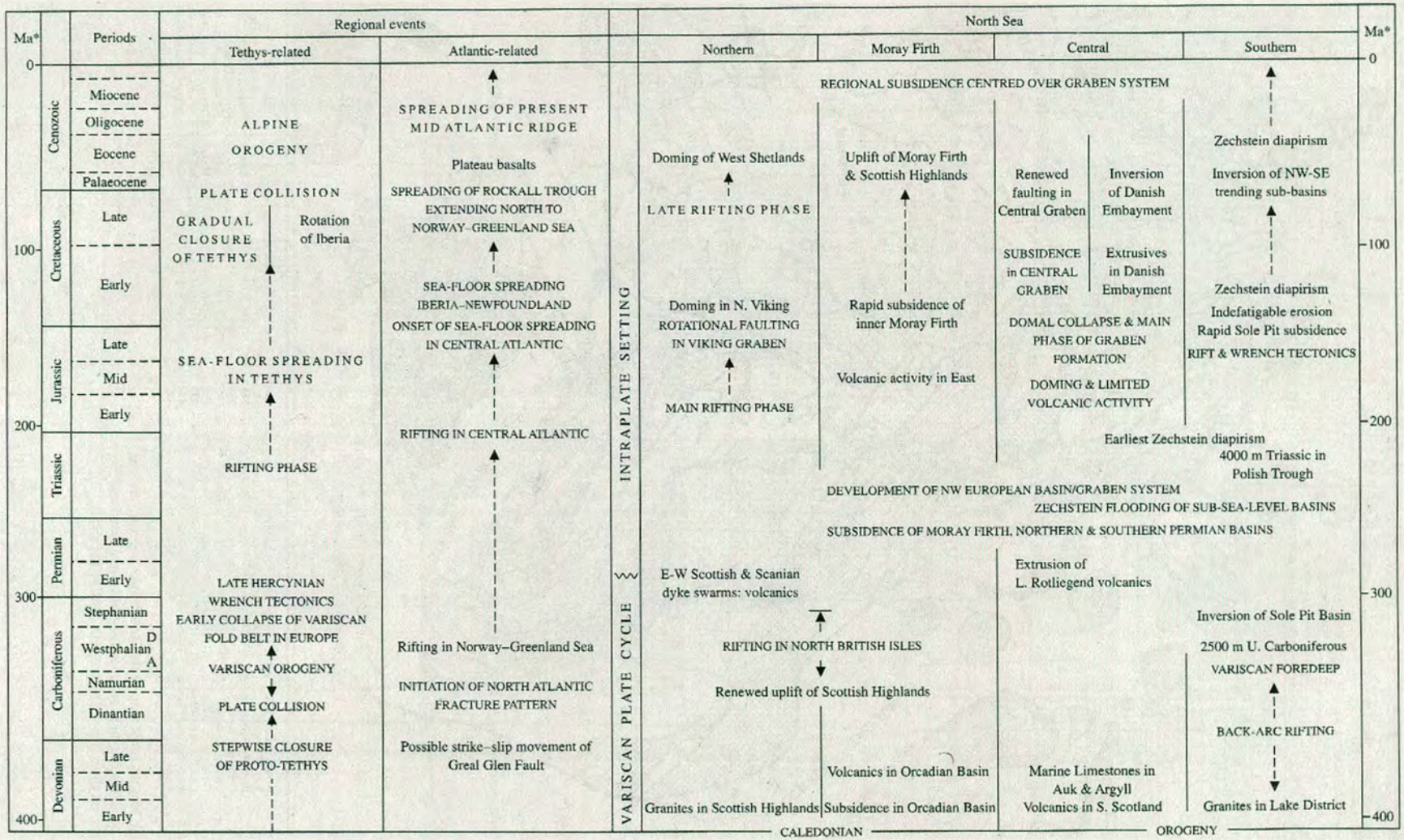

Figure 2.3: Simplified evolution of the Tethys & Atlantic Ocean tentatively related to North Sea post-Caledonian structural events. Note that the time scale is not constant. (From Gelnnie & Underhill, 1998)

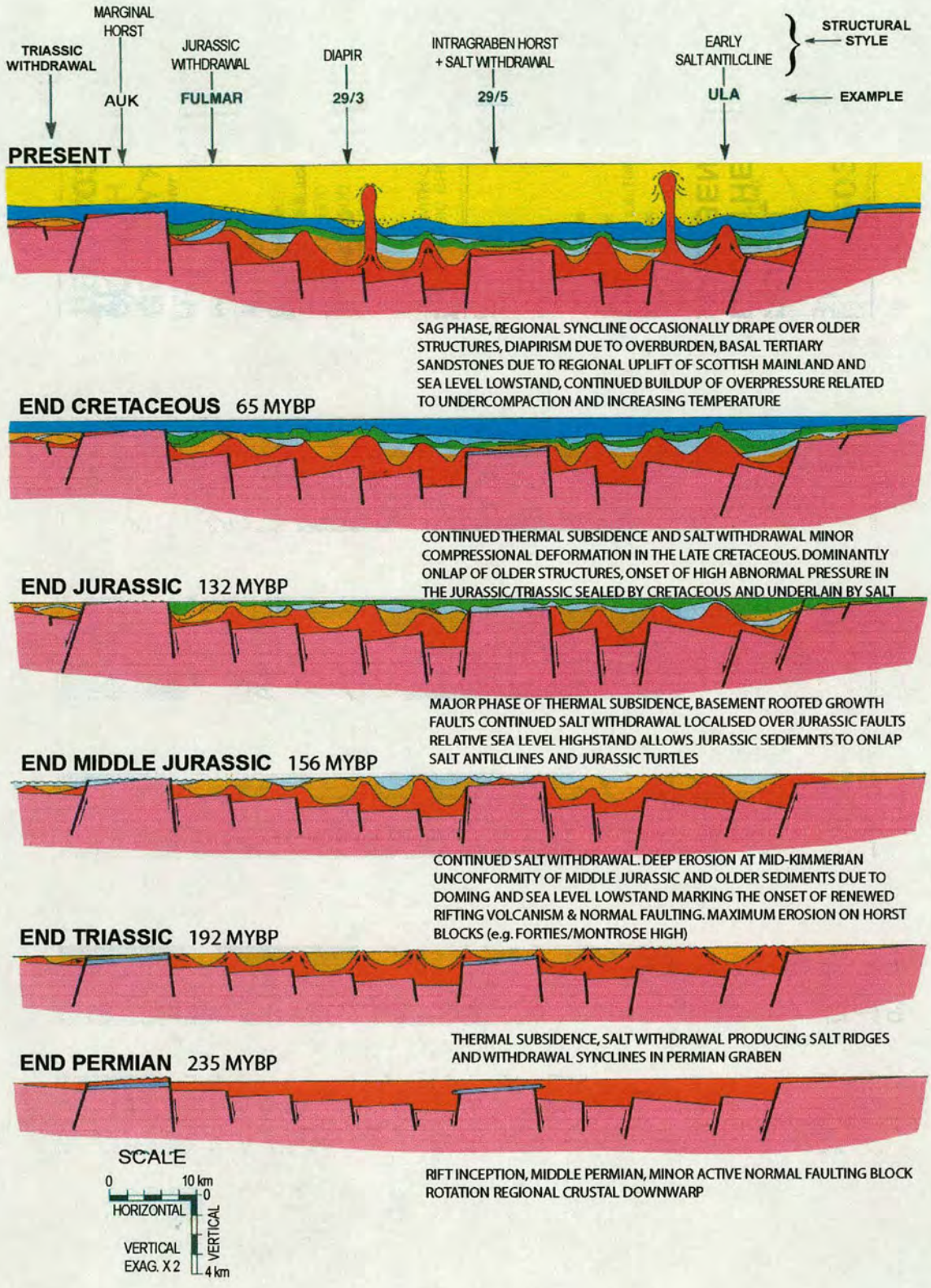

Figure 2.4: Summary of structural evolution of the Central Graben. (From Cayley, 1987)

In the Central Graben, Permian extension resulted in considerable topographic relief (in excess of 3500 ft). However, the rate of subsidence far exceeded the rate of sediment supply (Smith *et al.*, 1993). Consequently, by the time of the Mid-Permian Zechstein transgression, the deepest parts of the basin were occupied by desert lakes whose surfaces were some 600-900 ft below see-level (Ziegler, 1982). Rifting is thought to have ceased by the Late Permian and the basin then underwent a period of thermal subsidence, centred on the Norwegian-Danish Basin.

Following the initial flood of the Zechstein transgression, the Northern Permian Basin became a sediment-starved intra-continental rift. High rates of evaporation were combined with limited access to marine seawater. Periodic transgressions and evaporation of hypersaline water resulted in the basin forming a giant evaporating pan, precipitating vast thicknesses (up to 10 000 ft) of chemical sediments (dominantly halite) (Smith *et al.*, 1993). By the end of Permian these evaporates had infilled the previous rift topography such that the central Graben represented an extensive low-relief basin with little or no topographic expression. Rimmed carbonate shelves developed on the margins of the salt basin during periods when normal marine salinity conditions prevailed following individual transgression events (Taylor, 1984).

A second phase of east-west extension was initiated in the Early Triassic and was centred on the Viking Graben and Norwegian-Danish Basin (Badley *et al.*, 1988). The Central Graben was offset from the axis of the rift and underwent only minor extension. This was accommodated by reactivation of Permian faults, while the Upper Permian salt compensated for the extension by shear and gravity flow (see Fig. 2.5).

The Triassic extension, coupled with gravitational instability, initiated salt movement within the Zechstein sequence (Fig. 2.5) (Smith *et al.*, 1993). Here, the initial salt movement is considered to be a reactive response to localised (extensional related) "thinning" of overlying sediments. The initial movement formed a series of essentially N-S trending salt ridges with "furrows" located in between, above the

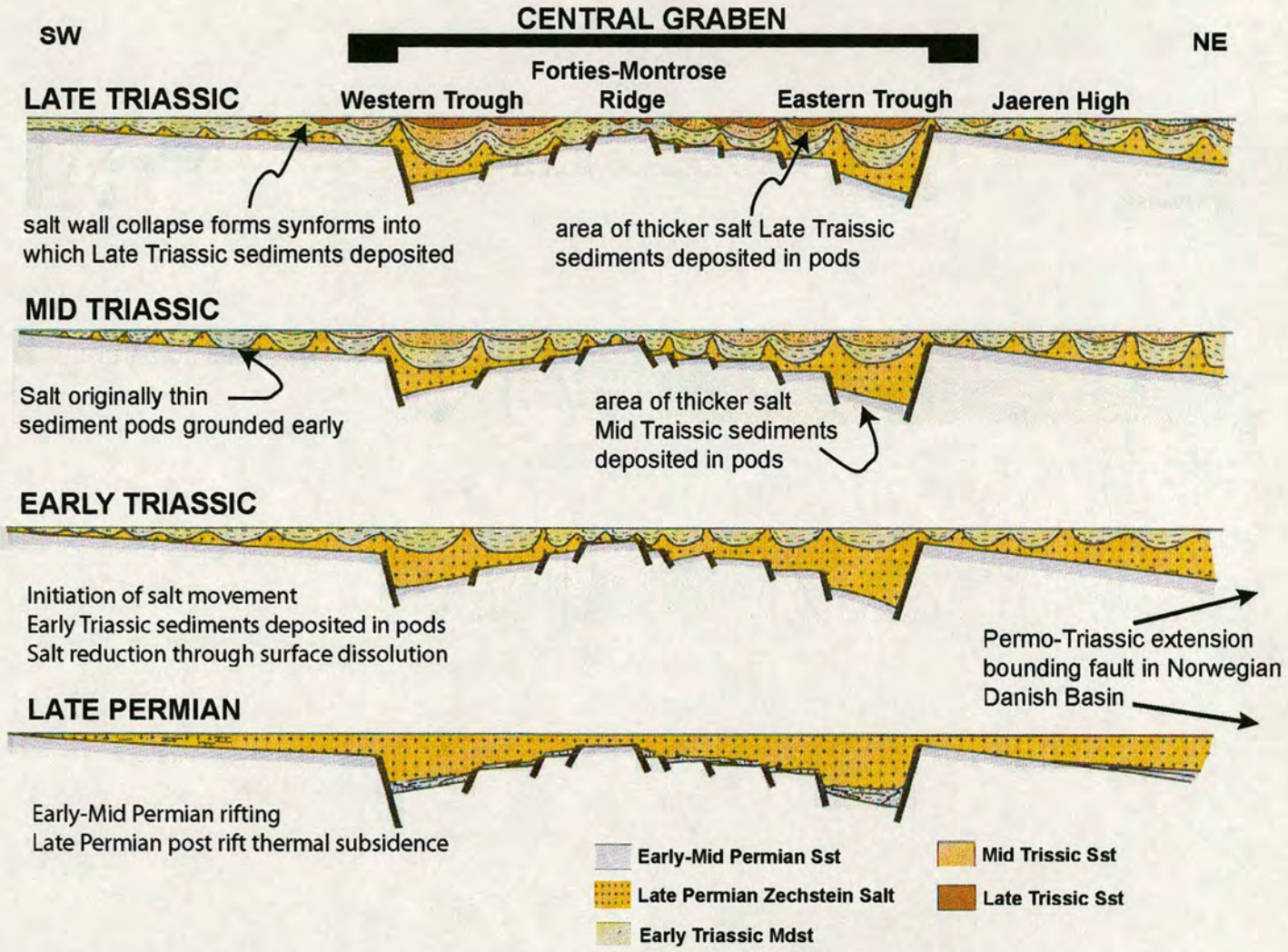

Figure 2.5: Schematic model showing how Zechstein salt deposition and withdrawal started resulting into pod-anti pod structure within the Central Graben. The Triassic extension, coupled with gravitational instability, initiated salt movement within the Zechstein sequence.(Redrawn from Smith *et al.*, 1993).

reactivated Permian faults. These furrows provided the sites for the deposition of the bulk of the continental Triassic (and Middle Jurassic) sediments and were fundamentally controlled by the underlying Permian structural grain. The low initial porosity (higher density), typical of continental deposits, suggests that only a few hundred feet of sediment overburden are required to develop a sufficient density contrast to initiate salt-sediment inversion at the base of each furrow. It is this density contrast which subsequently drives the halokinetic process (Smith *et al.*, 1993).

2.2.2 Middle Jurassic domal uplift

The thermal subsidence initiated in the Permian continued all the way through the Triassic and Early Jurassic and it was not until the Middle Jurassic when this subsidence was abruptly terminated by a phase of Middle Jurassic thermal doming. This occurred in response to the development of a transient mantle-plume head that led to uplift and erosion of the central North area, volcanism and the subsequent development of the Central-Viking-Moray Firth trilete rift system (Glennie & Underhill, 1998).

The boundary between Early and Middle Jurassic sediments is often marked by a widespread stratigraphic break, termed the "Mid-Cimmerian Unconformity", which is apparent from the North Viking Graben to the southern North Sea and from the Moray Firth to the Danish Central Graben and its flank area, where Upper Jurassic and even Upper Cretaceous strata overlie eroded Triassic sequences (Underhill & Partington, 1993, 1994).

2.2.3 Late Jurassic to earliest Cretaceous extensional tectonics

The main structural development of the Central Graben and associated Viking – Moray Firth rift systems did not occur until the Late Jurassic to Early Cretaceous. Subsidence rates accelerated rapidly in the Oxfordian to Volgian under the influence of NW-SE trending extensional fault systems (Rattey & Hayward, 1993). Following active rifting, characteristic of the Late Jurassic development of the North Sea, the Cretaceous records the transition to a gently subsiding basin. Regional subsidence of this nature is attributed to thermal relaxation of the North Sea rift (Wood & Barton,

1983; Ziegler, 1990). Widespread erosion in the Early Cretaceous produced the late Cimmerian unconformity, which may have occurred as a consequence of rotational uplift of footwall fault blocks or eustatic sea level fall (Rawson & Riley, 1982; Rattey & Hayward, 1993).

Rifting in the North Sea had ceased by the Late Cretaceous, and the focus for this mechanism switched to spreading centres west of the British Isles. Late Cretaceous global sea-level rise drastically reduced clastic sediment supply and promoted widespread chalk deposition.

2.2.4 Development of the Iceland hot spot & North Atlantic rifting

In western parts of the UK, tectonic influence was superseded during the Cretaceous by extension linked to the onset of sea-floor spreading in the North Atlantic Ocean. Initially, this was along the line of the Rockall-Fareoes Trough but it shifted to its present axis west of the Rockall Plateau by the mid-Tertiary (Glennie & Underhill, 1998). Opening of the Atlantic Ocean and the development of the Iceland hot spot were major factors in Cenozoic uplift and exhumation of the British Isles. The resultant easterly regional tilt and consequent erosion particularly affected the western rift arm in the North Sea, the Inner Moray Firth (Thomson and Underhill, 1993; Hillis *et al.*, 1994).

In the early Palaeocene, rifting of the Greenland-European plate caused thermal uplift of the Scottish Highlands and the East Shetland Platform, with rejuvenation of older Mesozoic hinterlands and basin margins (Fig. 2.6). This played a major role in controlling the supply of coarse clastic detritus to the North Sea Basin during the Palaeocene. It changed the relatively deep, sediment-starved basins of the Cretaceous into major clastic depocentres, dominated by a complex interplay and mosaic of deltaic and submarine-fan systems (Bowman, 1998). Without these influences, there would be little Cenozoic prospectivity and the early Tertiary would most probably have been a period of largely hemipelagic sedimentation continuing from late Cretaceous time (Bowman 1998).

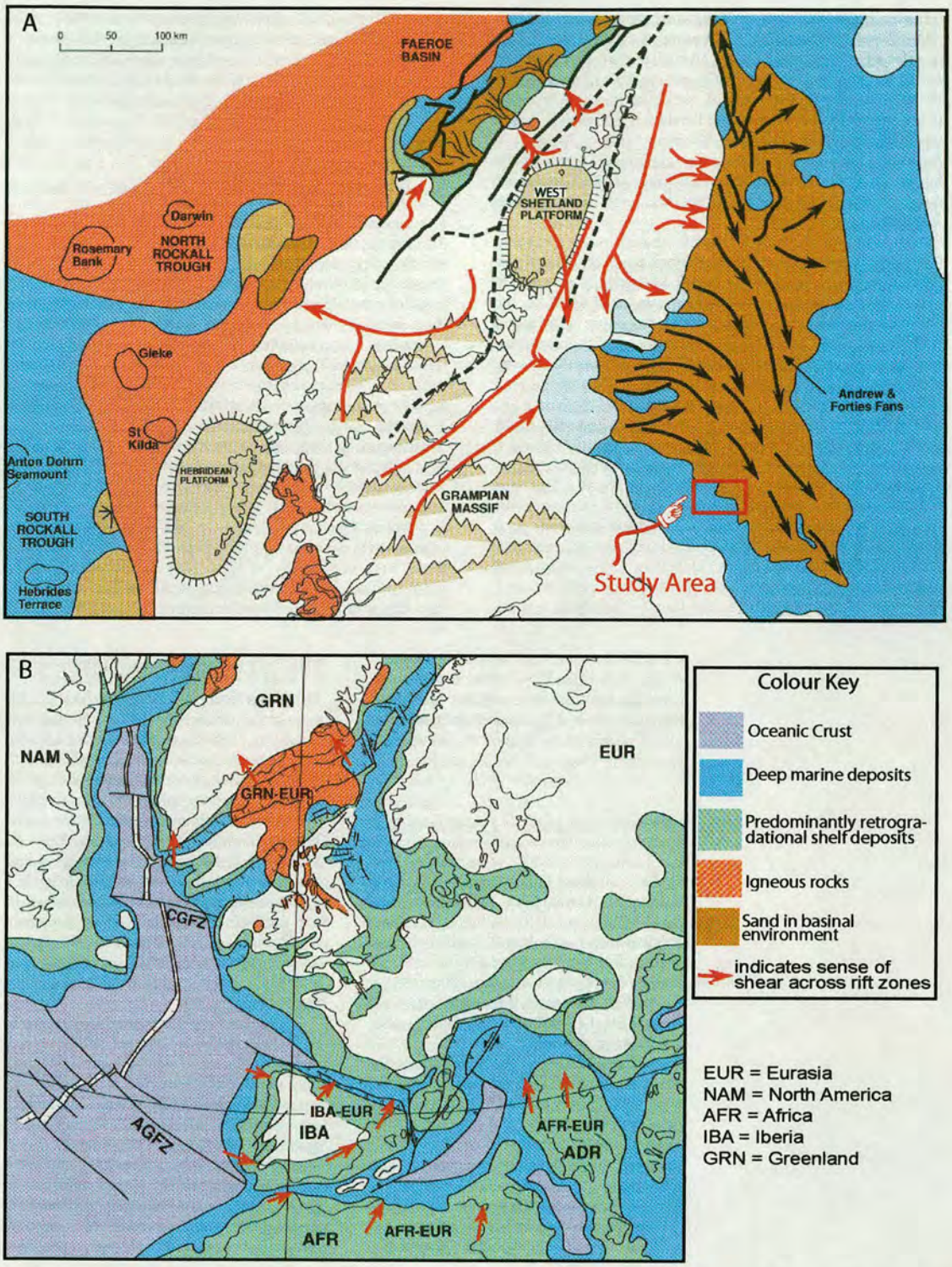

Figure 2.6: (A) Clastic detritus was shed from area of uplift into the North Sea and UKCS Western Margin Tertiary basins.
(B) Paleocene Plate reconstruction. Rifting along the length of the North Atlantic, now situated to the northwest of the Rockall Plateau, was superimposed by major hot spot that initiated in Palaeocene time. (From Knott *et al.*, 1993)

Knox and Morton (1988), White (1988), Milton *et al.* (1990), Morton *et al.* (1993), Anderton (1993), Knott *et al.* (1993) and Bowman (1998) provide a picture of the plate kinematics and their impact on hydrocarbon prospectivity. They distinguished five key events which were summarised by Bowman (1998) as follows and illustrated by Fig 2.6:

1) Danian/Thanetian: major hinterland rejuvenation related to doming around a mantle hot spot centred under East Greenland.
2) Early Palaeocene: volcanic activity, caused by east-west extension, led to the British and Faeroe-Greenland igneous province, with impact in the North Sea exemplified by the Andrew Tuff of the Witch Ground Graben.
3) Late Palaeocene: volcanic activity, associated with the onset of sea-floor spreading in the Norway-Greenland Sea, led to eruption and deposition of widespread tuff marker beds (the Balder Tuff of the Northern North Sea). This is one of the prominent reflectors in the Gannet South area and forms the surface on which the Tay Sandstone Member was deposited.
4) Restriction of the Northern North Sea, due to the thermal doming, leading to the development of an anoxic basin in the North Sea during the late Palaeocene and early Eocene.
5) Minor inversion in the early Eocene caused by the final rupture of the North Atlantic. This was followed by passive subsidence, leading to a clear marine connection of the North Sea with the North Atlantic.

Sedimentation was controlled by a complex interplay between tectonic activity, eustasy and hinterland characteristics. Each operates at both a regional and a local scale, leading to a complex depositional pattern across the basin. The volume and grain size of the clastic detritus increased gradually to a peak in the late Palaeocene (mid-Thanetian). Large volumes of material were fed into the North Sea and Faeroe-Shetland Basins as major submarine-fan systems. Following successful rifting of the North Atlantic, the Eocene and Oligocene are characterised by reduced rates of clastic input along the newly developed passive margin. Sedimentation rates were reduced, the hinterlands gradually denuded, and a more uniform pattern of deposition established across both the North Sea and the Faeroe-Shetland Basins. Relative sea-

level changes became the primary control on sedimentation patterns. In Fig 2.6a, notice the geometry of Forties Fan at the study area. This sedimentary distribution of the Forties Formation had a major role to play in defining the topography on which the Tay Sandstone Member was deposited as will be discussed in the next chapter.

2.2.5 Tectonic inversion of Mesozoic basin

Creation of the Atlantic Ocean caused intraplate compression, leading to the tectonic inversion of former sedimentary basins across north-west Europe during the Late Cretaceous and Tertiary (Ziegler, 1990).

2.3 Role of salt movement in the Central Graben

The structural configuration of the Central Graben is made up of a number of intrabsinal highs (e.g. Forites-Montrose High), terraces and sub-basins. In contrast to the other two rift arms, extension in the Central Graben was more complex, because of the influence of halokenesis. Movement on the basin-bounding faults led to rapid subsidence in the Central Graben, which initiated differential flow of salt at depth (Erratt, 1993; Gowers *et al.*, 1993; Penge *et al.*, 1993). The presence of the underlying Zechstein evaporates allowed shallow detachments to develop. One of the effects of the presence of the salt was to induce regional evacuation from the graben centre, which eventually led to the development of salt pillows and locallised diapiric intrusions during the Cretaceous and Tertiary. Modelling studies conducted by Bishop *et al.* (1995) suggests that salt withdrawal rather than salt injection is the dominant process affecting diapir geometry, excluding the tall diapirs in the vicinity of the Central Graben. Extension of the basement creates regional accommodation space and localised salt withdrawal cells develop in response (Fig. 2.5). The withdrawal cells serve to focus sedimentation, which in turn, exacerbates the withdrawal process and results in down building. The resulting geometry of the salt is one of smooth, sinusoidal swells and basins, where the swells are relatively inactive through time and simply separate regions of active withdrawal.

As observed in the Gannet South area, the diapiric rise of evaporates played an important role in controlling the topography/bathymetry of the basin by defining a series of highs and lows, which influenced the sediment transport pathways and controlled the basin-fill architecture through the spatial variation in the loci, magnitude and rate of accommodation space generation. Thus, it has helped create structural traps for several major fields and discoveries in the Central North Sea.

2.4 Conclusion

The area of interest for this study (Gannet-South of the Central North Sea) has a long and complex geological history, with the later stages in its structural and stratigraphic development being largely controlled by its earlier history. The Central Graben was first initiated in Early Permian, though the main phase of extension did not occur until Late Jurassic to Early Cretaceous.

With onset of the North Atlantic opening a drastic change in the tectonic regime of the area took place during the Cenozoic. This was centred around Scotland and produced a significant tilt of the West Shetland Platform of up to 6° towards the east. This induced gravity driven transportation of coarse clastic material from the uplifted hinterland into the adjacent deep-sea basins. Thick masses of sand accumulated during the Palaeocene and Eocene forming submarine fans. The deposition was controlled by salt movement and diapir formation which were the primary control on the palaeotopography of the receiving basins.

Chapter Three

Chapter Three

Seismic Data Interpretation

3.1 Introduction

As will be discussed in Chapter 6, trace shape analysis integrates seismic horizons together with wireline and core analysis to facilitate the prediction and more accurate mapping of a depositional system and the sediment dispersal patterns and sediment facies distribution. The interpretation of the seismic data underpins this by providing surfaces for this trace shape analysis. Therefore, in this phase of the study, the subsurface seismic dataset aided by petrophysical evaluation of the wireline logs was utilised in order to pick the major horizons in the area.

The Tay Sandstone Member in the Gannet South area of the Central North Sea contains three main depositional units. In addition to yielding the necessary surfaces for trace shape analysis, mapping the tops of these units together with other underlying major reflectors enables a better understanding of the sand geometries of the turbidite system and the structural evolution and development of the basin, and provides clues to the timing, nature and extent of factors controlling the sediment transport pathways in the area.

Detailed three-dimensional seismic data interpretation reveals the importance and control of topography on the spatial distribution of the deepwater depositional system of the Tay Sandstone Member and allows for the reconstruction of temporal evolution of the basin. Pre, syn and post sedimentation salt movement proved to represent the primary control on deflecting sediment pathways and creating accommodation space. Some control was also exerted by highs produced by previous deposits and the original slope of the basin at the onset of deposition.

3.2 Dataset and Research Methods

The turbidite fan system investigated in this study is the Tay sequence of the Gannet South area. The Gannet South area is located some 110 km east of Aberdeen in the British sector of the Central North Sea (Fig. 1.1 & Fig. 2.1). The system outline covers an area of approximately 300 km^2, primarily in Blocks 21/29, 21/30 and 22/26.

The seismic dataset used for the study is relatively new as it was only acquired in 1997. The high-density survey had a bin size of 12.5 by 12.5 m and stack fold of 36 and covered an area of approximately 680 km^2 (Fig. 1.2). However, towards the west, the extent of the dataset does not cover the shelf region, which forms the source area from where the sediments are derived, nor does it go far enough to the east to cover the full fan geometry. This seismic survey has E-W oriented "inlines" and N-S oriented "crosslines" and the polarity convention used is reverse standard Society of Exploration Geophysicists (SEG) polarity, i.e. a positive reflection coefficient (an increase in acoustic impedance) is represented by a trough, a red loop. This is discussed in depth in the seismic data to well tie chapter (Chapter 5).

Interpretation of the seismic data was undertaken using the Landmark Seisworks Software Package and Flagship Geo's Stratimagic Software Package. Volume Viewer of the 123di was also used. The work was carried out within Shell-Expro offices in Aberdeen.

The data is generally of good quality with a vertical resolution of about 10 - 20 ms (*c.* 15 - 35m) over the interval of interest. Mapping the major horizons was conducted with confidence. However, picking the internal horizons within the Tay Sandstone Member was somewhat problematic due to the thin nature of the Formation.

The 3D seismic data was interpreted by identifying key reflectors at well locations and following them through the seismic volume. This process of seismic data to well tie is discussed in detail in Chapter 5. In total, five seismic reflectors were mapped, namely: Top Tay (Upper Tay), Top Middle Tay, Top Basal Tay, Top Balder (Base Tay) and Top Chalk. In addition, on some cross sections, salt induced highs were also mapped. For the major horizons, Top Tay, Top Balder and Top Chalk, initially, inlines and crosslines were interpreted at least every 10^{th} line. The rest of the lines were then auto-picked to cover the area of interest. Due to the enormous variation in the continuity and amplitude of the Top Tay and the internal reflections within the Tay Sandstone Member auto-picking was not very reliable and manual interpretation was carried out on every other line and, in some places, on every inline and crossline. To aid the interpretation, traverses and loops that link the different wells in various orientations, and seismic slices were used. It was noticed that NW-SE oriented diagonal lines (perpendicular to the channel direction) provided the best interpretable view of the sections, as the reflectors seemed more continuous and easier to follow. A horizon map for each reflector in two-way travel times (TWT) was produced. These maps provide the means of studying the basin history and controls on the sediment deposition within it. For the purposes of this thesis, the surfaces interpreted in TWT milliseconds (ms) have not been depth converted. Isochron maps giving the thickness of each interval in TWT (ms) were then produced. These maps play a key factor in determining the location and boundaries of the Tay turbidite system and, hence, the type, the likely nature and geographical distribution of facies across it.

3.2.1 Biostratigraphic Considerations

Milton *et al.* (1990) and Den Hartog Jagger *et al.* (1993) presented sequence stratigraphic interpretations of the North Sea Paleogene. Both identify a second order relative sea-level trend of lowering and then rising sea-level, which is attributed to uplift and subsequent collapse of the Orkney-Shetland axis (Milton *et al.*, 1990) which itself is likely to have been related to the development of the Iceland hotspot (Glennie & Underhill, 1998). Shell "in-house" biostratigraphic analysis on the eight wells that encountered the Tay Sandstone Member in the Gannet South area shows that deposition of the Tay Sandstone Member commenced during a relative sea-level

lowstand following deposition of the Balder Formation during Biozone PT 21, which has *D. oebisfeldensis acme* as the key biomarker.

Biostratigraphically speaking, the Tay Sandstone Member can be divided into four main units. The basal Tay was deposited during a lowstand during biozones PT 22.1 to 22.2, which are marked by the presence of two dynocysts, *Coscinnodiscus and S. linaperta*. This unit is overlain by the Middle Tay unit which started with a relative sea-level rise which was soon lowered resulting in renewed sedimentation of sands during PT 22.3 and it is has *E. ursulae* and *Cenosphaera* as key biomarkers. On top of this comes the Upper Tay B unit which was deposited during PT 22.4. It is recognised by the presence of frequent *H. tenuispinosum* and *W. articulate breviconuta*. The final episode of sea-level fall and then rise occurred during PT 23.1 which resulted in deposition of the Upper Tay A unit sands draped by the mudstone-dominated Horda Formation. *S. aff. Spectabilis* and *Spiniferites* are used as key biomarkers for this unit.

Comparsion with published literature shows that the key biomarkers used here for subdividing the Tay Sandstone Member are not different then the ones used by other workers. However, unlike the lithostratigraphic subdivision of Knox and Halloway, (1992) and biostratigraphic subdivision of Harland et al. (1992), where the Tay Sandstone Member has been divided into Upper and Lower Tay Sandstone Member, here it has been divided into three main units; Upper, Middle and Basal, and the Upper unit has been further subdivided into 2 sub units A and B. The main reason for this difference in subdivision is the difficulty is that unlike the main Tay fairway in other Gannet clusters, Gannet South sands can not be subdivided into discrete Upper and Lower sand packages separated by one extensive shale unit. Sands in Gannet South area occur sporadically within a shale background and are found at all stratigraphic levels. Fig. 3.1 shows the lithostragraphic nomenclature with key biomarkers used for the Tay Sandstone Member. Since the top of each of these units is not always an interface between shale and sand it was not always straightforward to be identified on the seismic section. Seismic to well tie is discussed in details in

Chapter 5 of this thesis. Appendix 1 gives the depth to the top of each of these units as well as the TWT to it.

3.3 Results and Discussion

3.3.1 Top Chalk

The Top Chalk reflector is by far the most prominent reflector over the area. The red trough of the top Chalk is caused by a strong impedance contrast marking the transition from the variably calcareous mudstones and sandstones of the Maureen Formation to the argillaceous chalky limestone of the Ekofisk Formation (see Fig. 3.1 for lithostratigraphic nomenclature scheme of the area). According to Knox and Halloway (1992), the Ekofisk Formation extends throughout the basinal areas of the Central Graben, Outer Moray Firth and South Viking Graben, reaching thicknesses of over 100 m in chalky limestone facies. These facies represent pelagic nannofossil oozes, deposited in an outer shelf to basinal setting, probably in water depths of over 200 m.

The horizon map (in TWT ms) produced for the Top Chalk (Fig. 3.2) clearly shows the structure of the surface. In general, the map emphasises the west-east deepening orientation of the basin with three relatively flat locations (sub-basins), shown in red, green and blue. These sub-basins are separated by two steeply dipping structures parallel to crosslines 3800 and 4900 marked by the transition from red to green and from green to blue. The series of local lows and highs described by the horizon map is associated with the Zechstein salt movement which played an important role in forming the topography of the basin and, hence, controlling the distribution of the Tay sediments as will be discussed in detail later in this chapter. Four such structural highs are apparent on the map; two centred by crossline 4050 and the other two by crosslines 4750 and 5000. The last is clearly marked by the absence of interpretation due to the difficulty in picking the Top Chalk horizon on this high (this is the biggest high of the four). For referencing purposes these salt induced highs are named as A, B, C and D as shown in Fig. 3.2.

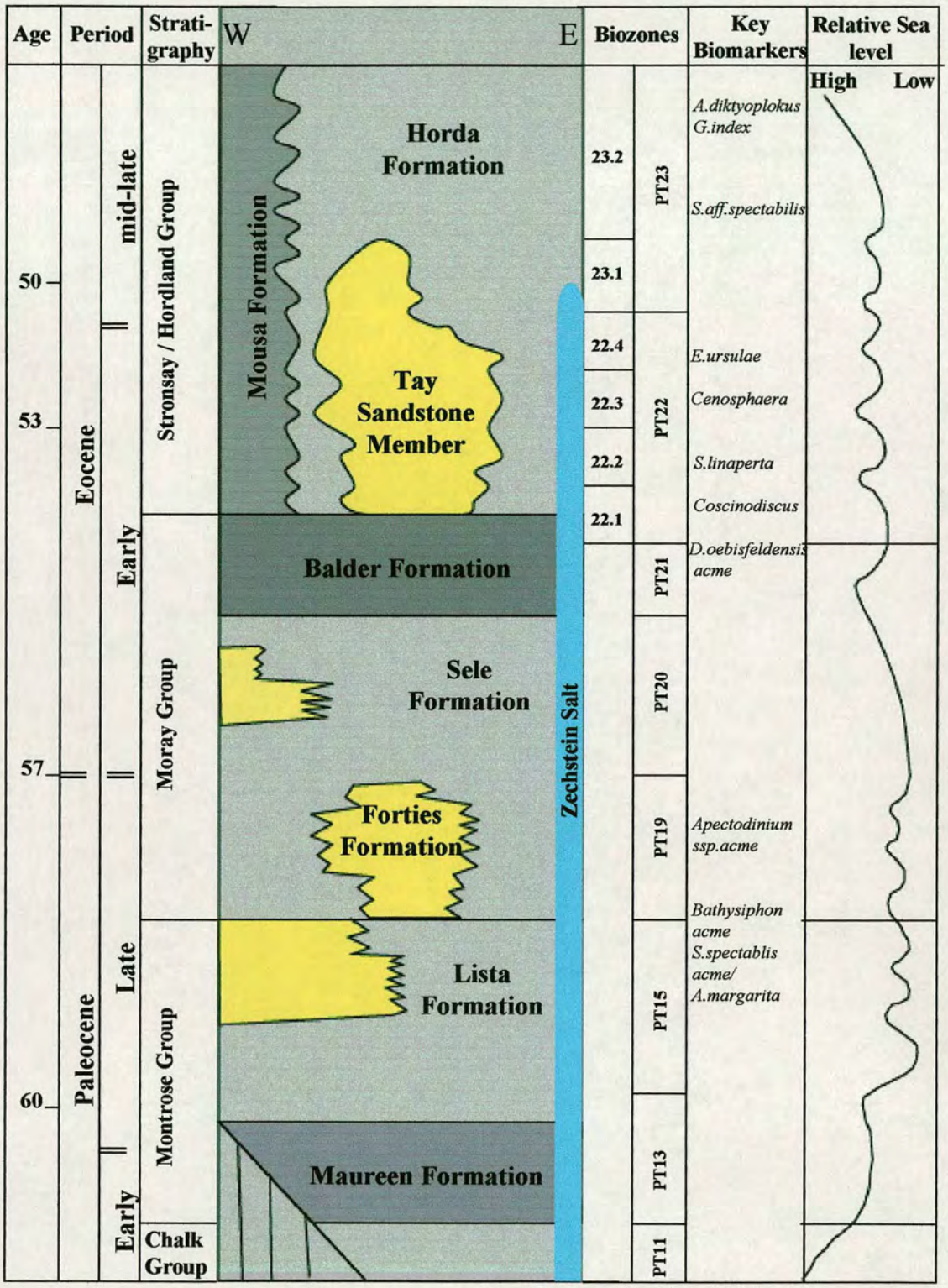

Figure 3.1: Lithostratigraphic nomenclature scheme for the Paleogene of Central North Sea (modified from Knox and Halloway, 1992)

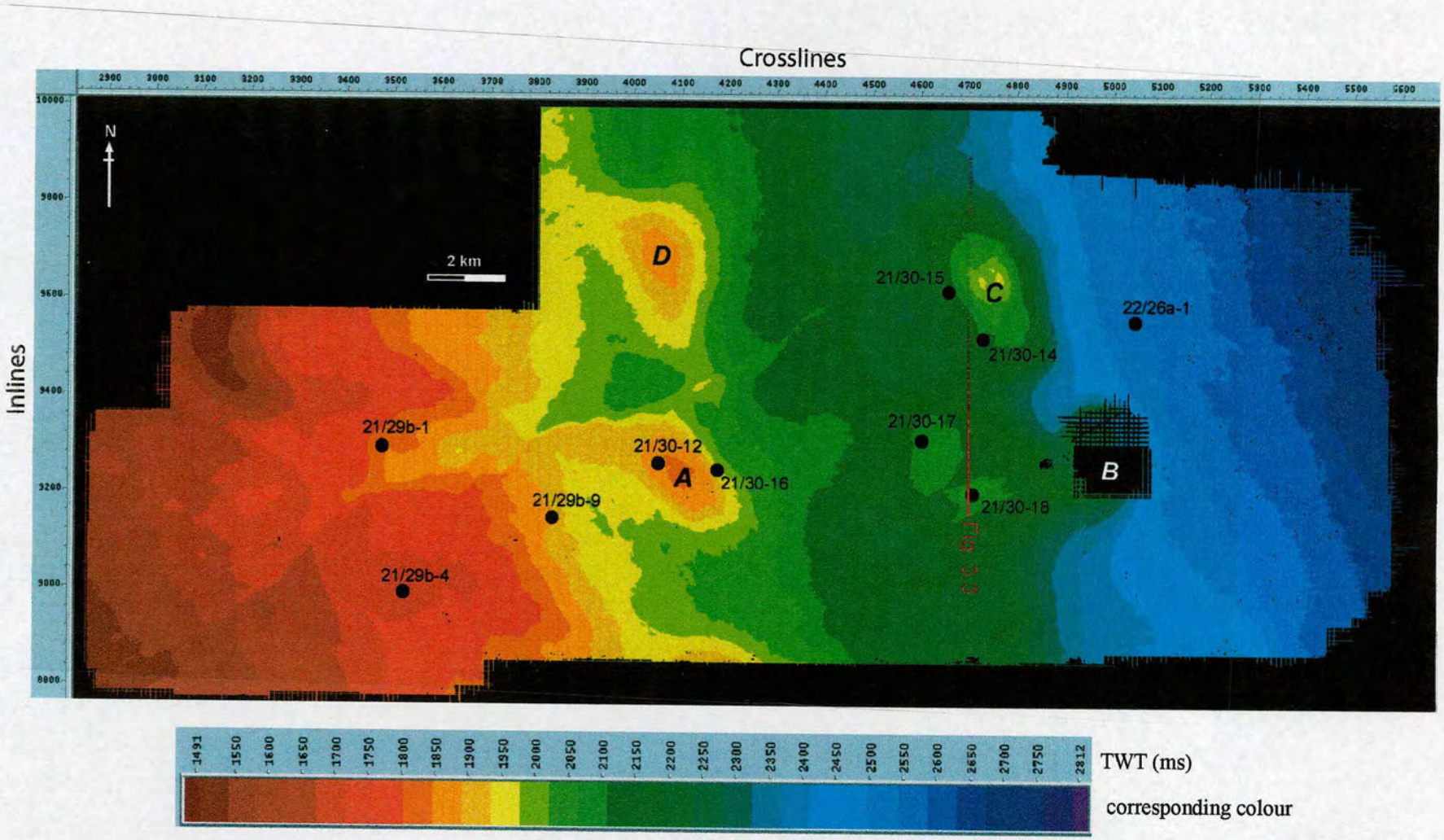

Figure 3.2: Top Chalk TWT map. West-east deepening of the basin with 3 relatively flat locations (sub basins) separated by 2 steeply dipping structures. See text for further details. A, B, C & D indicate the 4 salt domes present in the area. On the overlay note the SW-NE line. Structure to the north of this line is slightly deeper to what lies to the south.

One more important feature to notice in this horizon map is the line running from the lower left hand corner towards the northeast, ending around crossline 4500 as shown by the overlaid transparency. Notice that the structure to the north of this line is slightly lower than that to the south. This will be discussed in more detail later.

There are number of faults imaged at this level but they do not seem to have been active at the time of deposition since there is no thinning or thickening associated with them. One apparent fault is drawn on the transparency overlaid on Fig. 3.2 and a cross-sectional view can be seen in Fig. 3.3, which shows cross line 4700. It is important to know whether this fault had any control on the deposition of the Tay Sandstone Member. This is investigated in the coming sections.

3.3.2 Top Balder

The top of the Balder Formation represents an important surface for the study as it corresponds to the base of the Tay Sandstone Member and, hence, highlights the present day shape of basin onto which the sediments were deposited. Over the greater part of the area widespread Lower Eocene tuff-rich, silica-cemented, high-velocity mudstones produce a strong seismic event known as the "ash marker". This reflector is represented by a peak (blue loop) in the seismic volume and it was mapped with confidence over the whole area, although, in some parts, picking was slightly difficult due to scouring and erosion by the overlying Tay Sandstone Member (see Fig. 3.3). The horizon was also difficult to map over one of the salt induced highs (salt high B), as was the case for Top Chalk.

The Balder Formation is present over most of the Central and Northern North Sea. It is locally absent, however, along the southwestern margin of the Central Graben, as a result of erosion before or during deposition of the Tay Sandstone Member. The mudstones of the Balder Formation were mostly deposited below wave-base and under conditions of bottom water anoxia (Knox and Halloway, 1992).

The Top Balder Formation horizon map seen in Fig. 3.4 shows a pattern of deepening of the basin similar to the one that existed at the beginning of the Tertiary

(increase in TWT towards east). One noticeable development is in the area to the north of the diagonal line drawn on the Top Chalk horizon map. We can see that this area has now become structurally higher than that to the south of the line. Investigation of the area concluded that there were more sediments deposited to the north of this line in the time between Top Chalk and Top Balder as illustrated by the thickness map shown in Fig. 3.5 (also see cross-sectional view in Fig. 3.6). In particular the Forties Formation seems to be very thick on the northern side but it is virtually absent in the south as supported by both seismic and well data. As shown by Fig. 3.6, the reflectors between Top Chalk and Top Balder are clearly down-lapping on to the Top Chalk horizon. Wells 21/29b-4, 21/29b-9, 21/30-16 and 21/30-18 all confirm the absence of the Forties Formation in this southern area, whereas wells 21/30-12, 21/30-14, 21/30-15 and 21/30-17 show very thin layers of the Forties. The main reason for the pinchout of Forties Formation is interpreted to be the underlying Upper Permian Zechstein Group salt ridge that developed parallel to the diagonal line making the Top Chalk structurally high preventing the subsequent sediments to be deposited on top of it. The overburden pressure of the subsequent sediments caused this salt ridge to withdraw and, as a consequence, the four main salt highs were formed. The phenomena of salt withdrawal and development of salt domes is well-known in the North Sea, as discussed in Section 2.3 (Fig. 3.8), and elsewhere around the earth, e.g. Gulf of Mexico. In the Central North Sea, the Zechstein Group salt was deposited in a subsiding basin during Upper Permian times and although it is difficult to make accurate estimates of true salt thickness due to extensive halokinesis and possible dissolution, it may have reached up to 2-3 km in thickness (Allan et al., 1994; Hossack 1995; Davison et al., 2000a). All the diapers are interpreted to have grown by downbuilding from Triassic through Palaeocene times, and were probably triggered by extensional faulting during Triassic times (Hodgson et al., 1992; Smith et al., 1993, Hossack, 1995; Stewart & Clark, 1999; Davison et al., 2000a&b). The continued redistribution and dissolution of salt kept creating accommodation space for new flux of sediments. However, in the Gannet South area there is no clearer evidence for salt dissolution at the Palaeocene-Eocene time. Furthermore, the formation and development of the four diapirs within the area indicates that there has

been "no net loss- no net gain". Fig. 3.9 shows a schematic section for the possible evolution of salt swells and creation of mini-basins providing accommodation space.

From the sedimentary point of view the pinchout of Forties sediments in this area was due to the "sudden death" of the Forties Fan system, which was fed from the northwest by the Dornoch delta. The delta became trapped in a zone of rapid subsidence in the Outer Moray Firth during the latest Palaeocene bringing the sediment supply to the Forties Fan system in the Central Graben area of the North Sea to an end (Bjørslev Neilsen *et al.*, 1986). The geometry and distribution of the Forties Formation is depicted by Fig. 2.6. Since the Tay Sandstone Member at Gannet South sits on the margin of the Forties Formation it is clearly evident that this Formation had an important role in restricting the deposition of the Tay Sandstone Member to the south. The topographic high resulting from the deposition of the thick Forties Formation package in the north had an important role in controlling the sand geometries and the sediment transport pathways in the Gannet South Tay turbidite system as will be discussed in detail later in this chapter.

A Balder to Chalk thickness map shows the reduction in thickness on approaching the salt domes. This means that these domes existed at the time of deposition during the Palaeocene time. Fig. 3.7, which represents an arbitrary seismic line running NW-SE (see Fig. 3.5 for the location of this line), clearly demonstrates the onlapping characteristic of the Forties Formation as it was deposited close to salt dome A. Although this salt dome had some relief at the time of deposition of the Tay Sandstone Member, it was not fully developed to what it is at the present time. This point will be discussed again in more detail when speaking about the depositional model for the Tay Sandstone Member. Some minor faults are also observed at this level but they appear to be post depositional features as no thickness variation is associated with them (see Fig. 3.3).

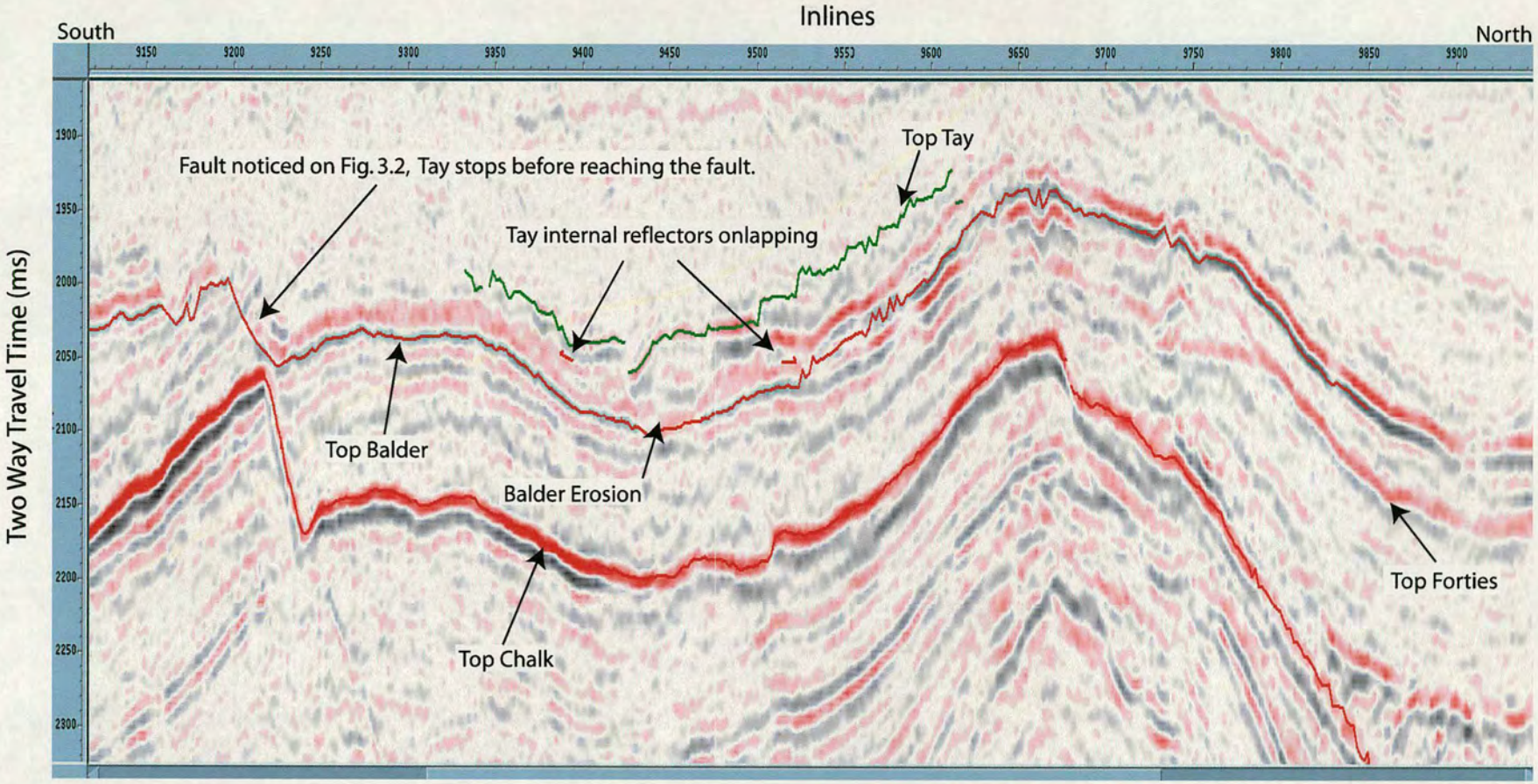

Figure 3.3: Seismic line running perpendicular to the system. For location see Fig. 3.2. Figure shows the main reflectors picked on the seismic survey. One of the salt highs and fault are apparent.

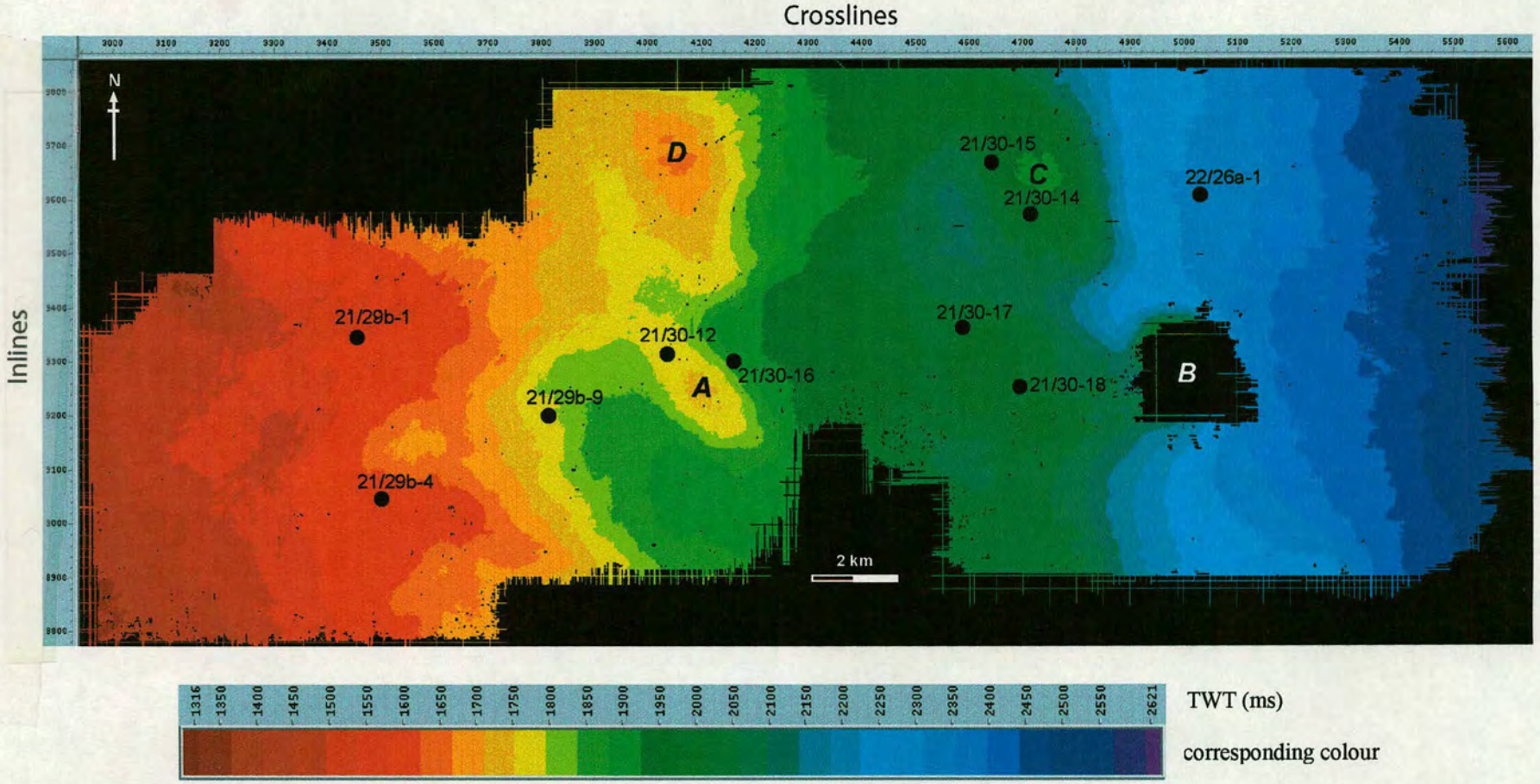

Figure 3.4: Top Balder TWT map. West-east deepening of the basin similar to what was seen at the beginning of the Tertiary (Fig. 3.2). See text for further details. On the overlay note the SW-NE line. Structure to the north of this line has now become higher than what lies to the south.

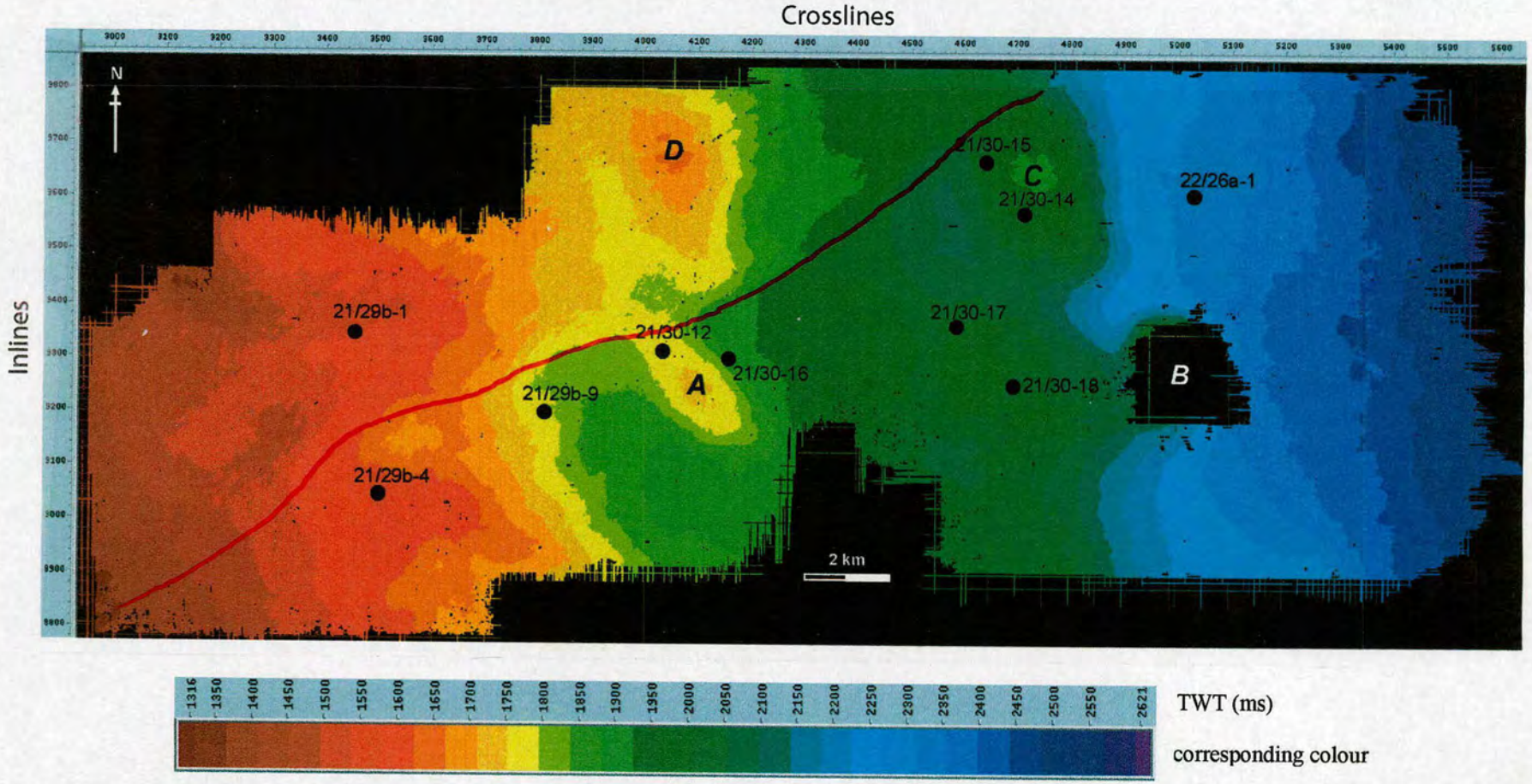

Figure 3.4: Top Balder TWT map. West-east deepening of the basin similar to what was seen at the beginning of the Tertiary (Fig. 3.2). See text for further details. On the overlay note the SW-NE line. Structure to the north of this line has now become higher than what lies to the south.

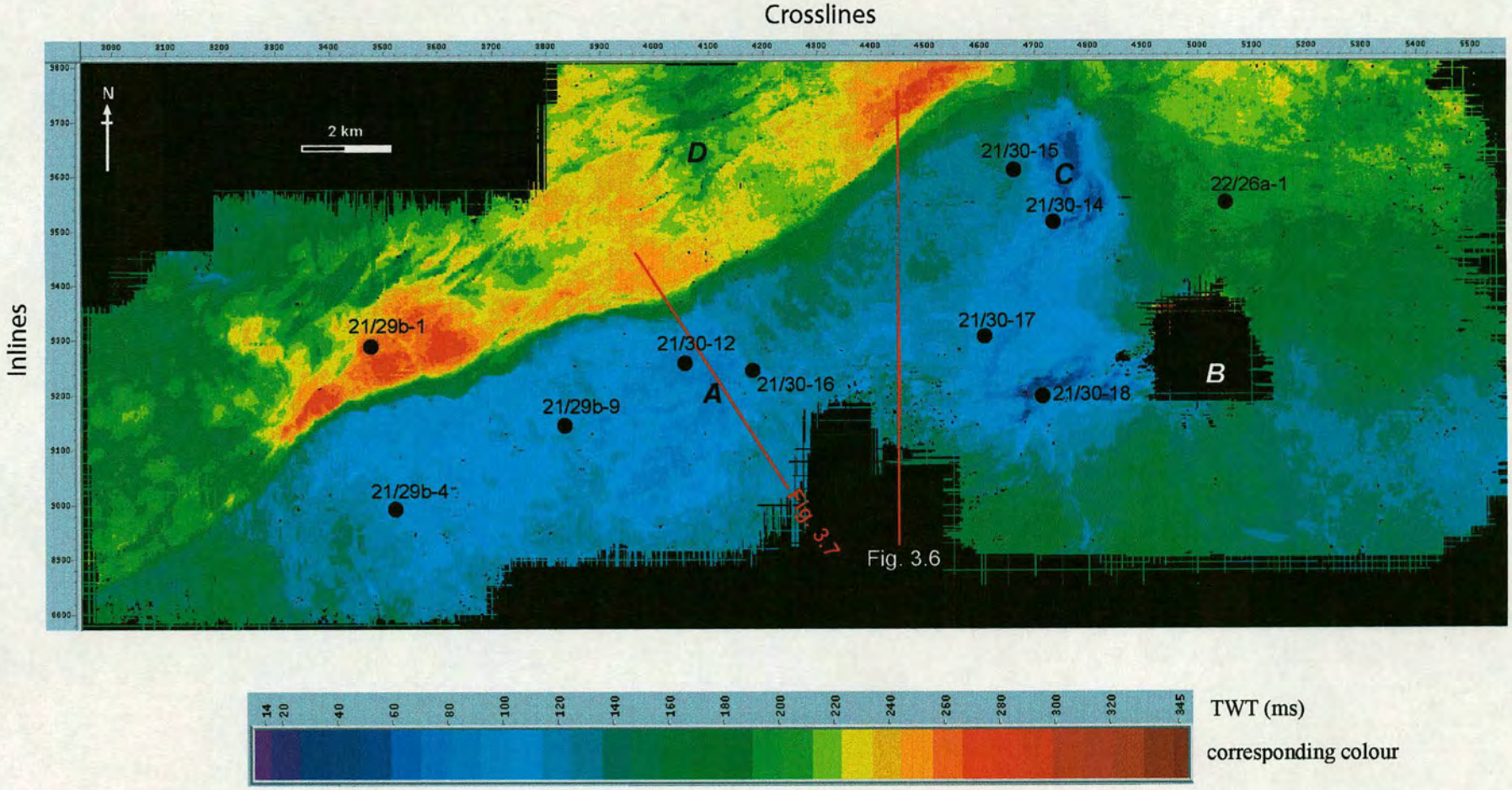

Figure 3.5: Top Balder to Top Chalk thickness map (TWT ms). The package to the north of the SW-NE line drawn on Top Chalk map (Fig. 3.2) is clearly thicker than what lies to the south of the line. See text for a plausible explanation.

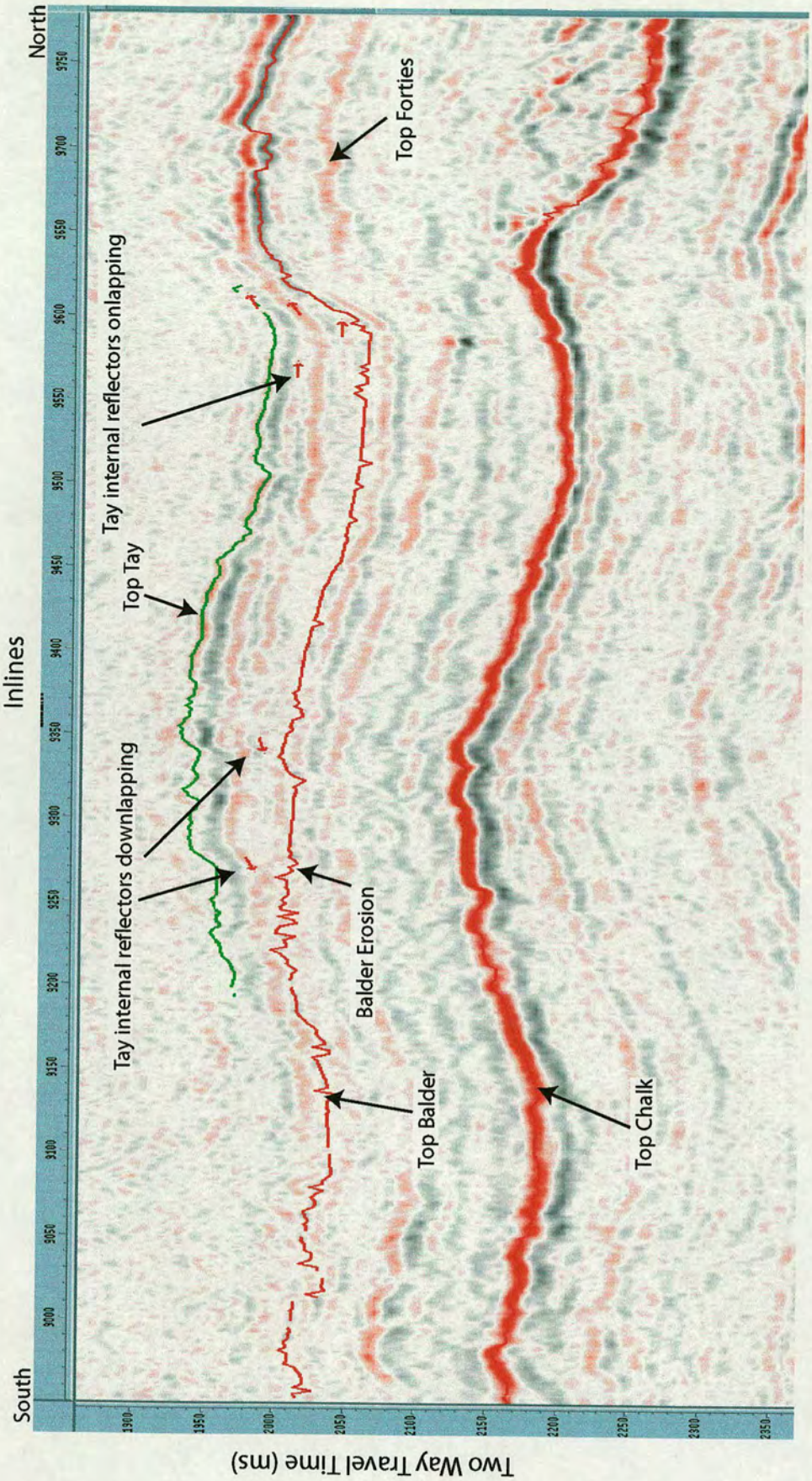

Figure 3.6: Seismic line running perpendicular to the system. For location see Fig. 3.5. Notice the thicker package between Balder and Chalk towards the north. See text for explanation.

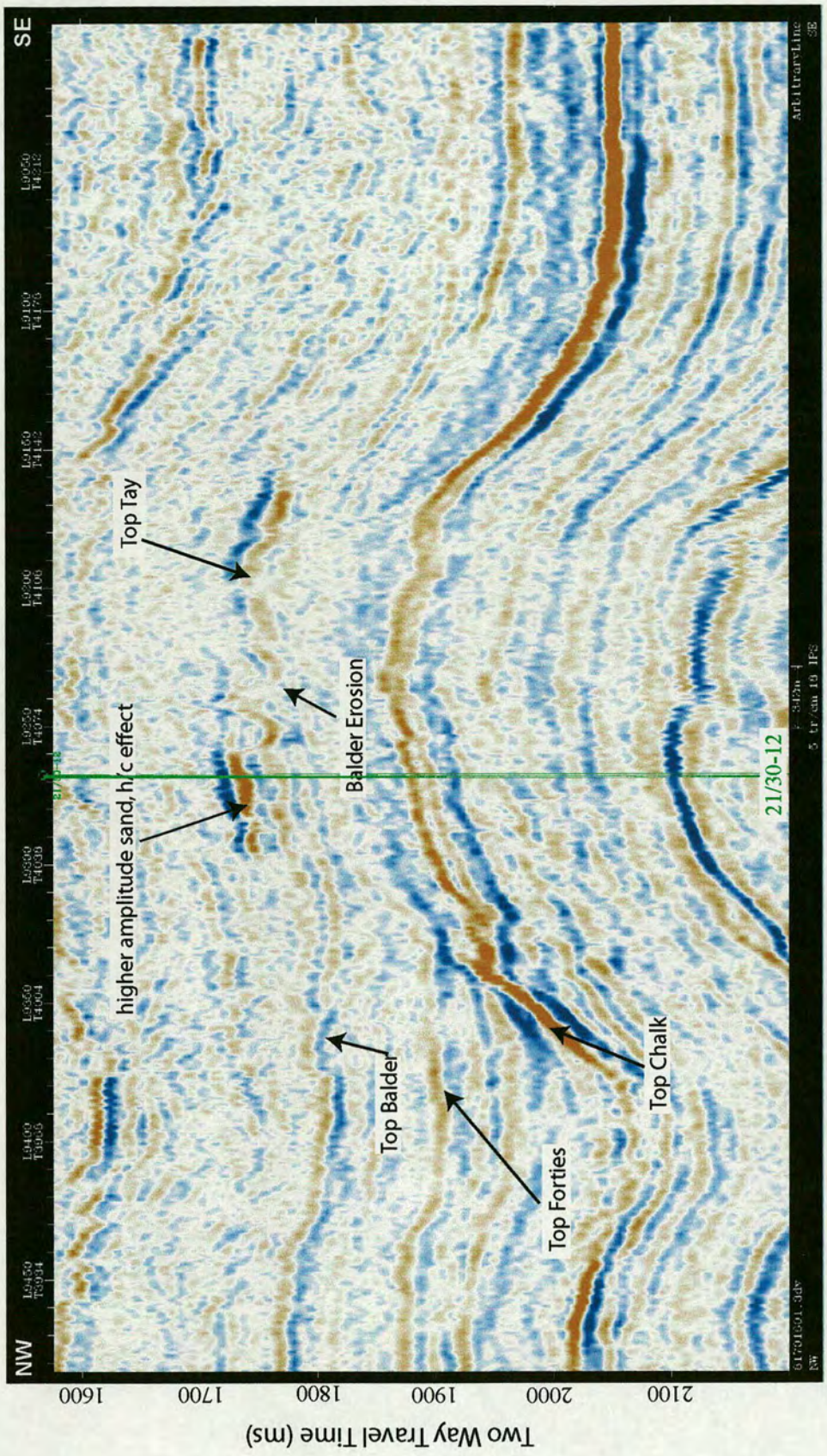

Figure 3.7: Arbitrary seismic line running NW-SE. For location see Fig. 3.5. Forties Formation onlapping onto salt dome A.

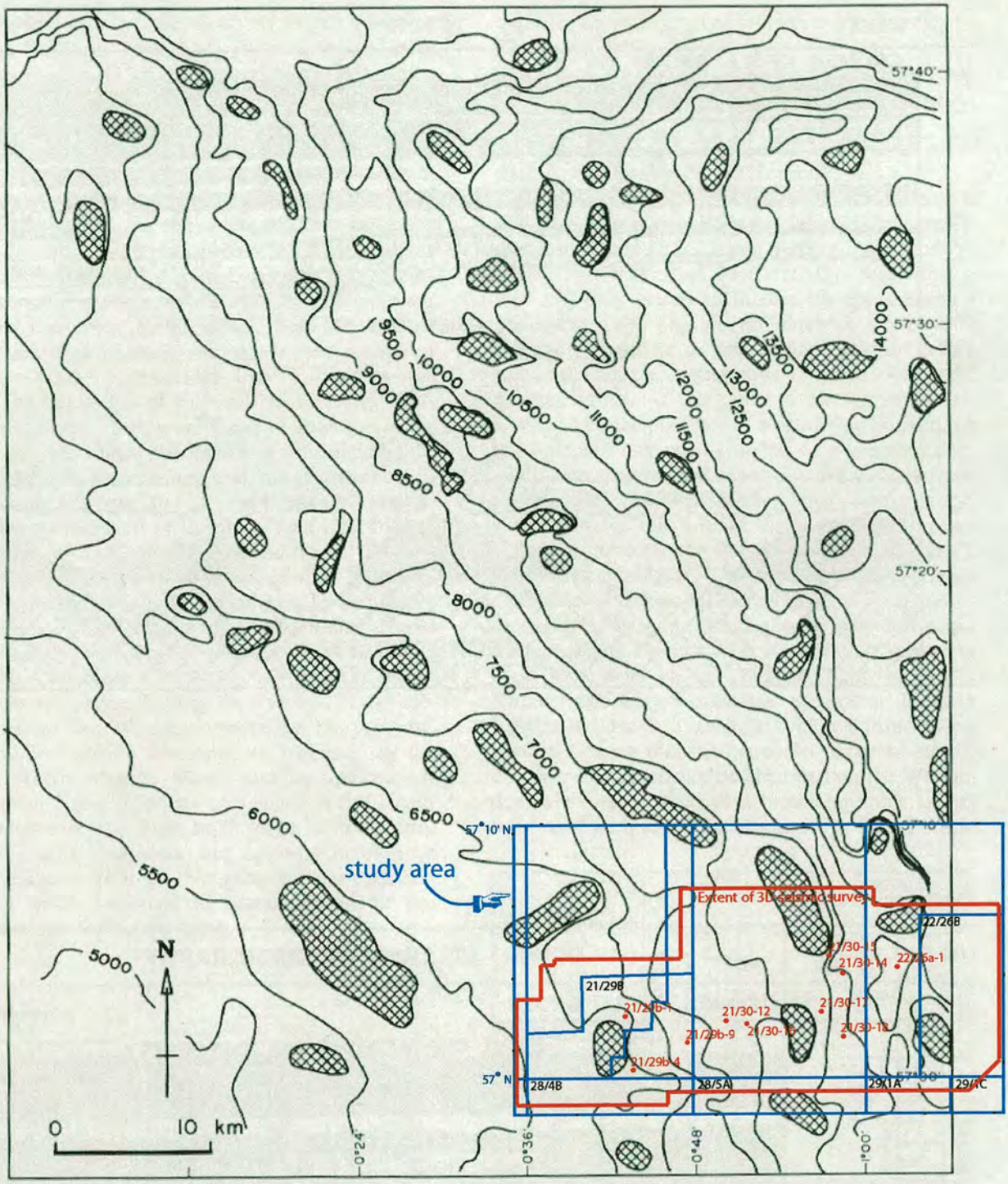

Figure 3.8: Generalised depth contour map (in feet) at base Cretaceous disconformity for Western Central Graben. The regional dip is to the northeast. Distribution of Zechstein salt highs which have moved subsequent to the deposition of the Upper Jurassic are featured as hatched areas. The study area is indicated. (from Wakefield et al., 1993)

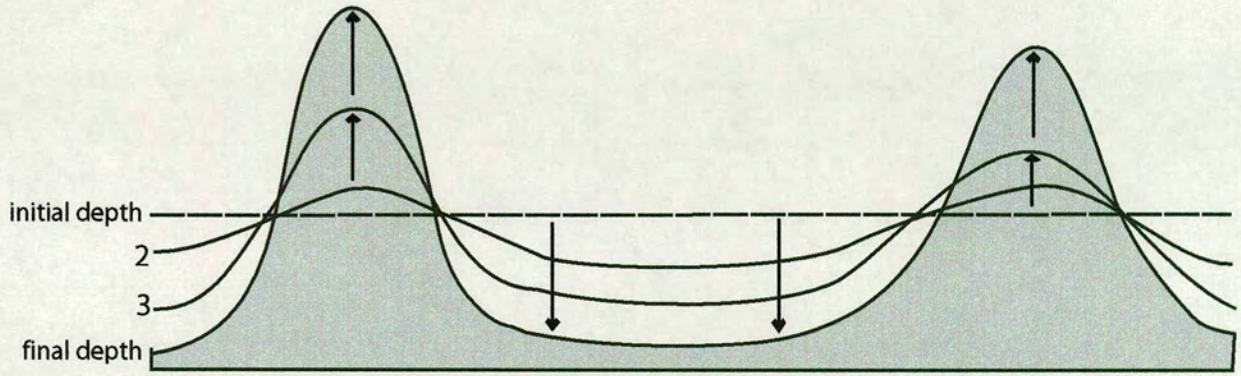

Figure 3.9 : Schematic cross-section showing salt withdrawal resulting in growth of salt diapirs and formation of minibasins. "No net loss - no net gain" in salt volume is assumed.

3.3.3 Tay Sandstone Member

The Tay Sandstone Member is the main objective of this study and was mapped in great detail. The Top Tay sand is uniquely defined as a continuous trough (red loop) resulting from the difference in acoustic impedance between the clean Tay sandstones and the overlying mudstones of the Horda Formation. The definition and tracking of the Top Tay reflector is unequivocal over most of the Gannet South area. However, towards the edges of the system both in the north and south, as the thickness of the Formation gets beyond the limits of the vertical resolution of the seismic data, complication in accurate mapping of the reflector arises making the sand pinch out lines in both north and south uncertain.

The Tay sandstone is a thin to thick-bedded, fine to medium-grained sandstone, interbedded with variably silty, fissile, green-grey to grey mudstones and siltstones. Coarse sands and gravels are completely absent in this area as shown by the cored wells (see Chapter 4 for detailed sedimentological description). Generally speaking, the Tay Fan system displays a complex distribution, which is restricted to the southern parts of UK quadrants 21 and 22. This distribution is attributed to salt movement during sedimentation (Armstrong *et al.*, 1987). The Tay sediments were derived from the West Shetland Platform and accumulated in a submarine fan system (Armstrong *et al.*, 1987; Banner *et al.*, 1992; den Hartog Jager *et al.*, 1993). This study shows, however, that salt movement during deposition is not the only factor controlling the Tay distribution but pre-sedimentation salt movement together with the highs resulted from previous deposition have played a key role in defining the channel pathways as well as locus of deposition.

Fig. 3.10 represents the depth map (in TWT ms) to top of the Tay Sandstone Member. The figure demonstrates a very similar character to the top Balder Formation map in that the surface is generally deepening towards the east. However, the striking characteristic to notice is that the Tay Sandstone Member distribution is restricted to a narrow area oriented WSW-ENE that fans out on the sea floor basin towards the eastern end after going through the passage between salt domes B and C. The surface also has a structural high on salt dome A. It is obvious that the system

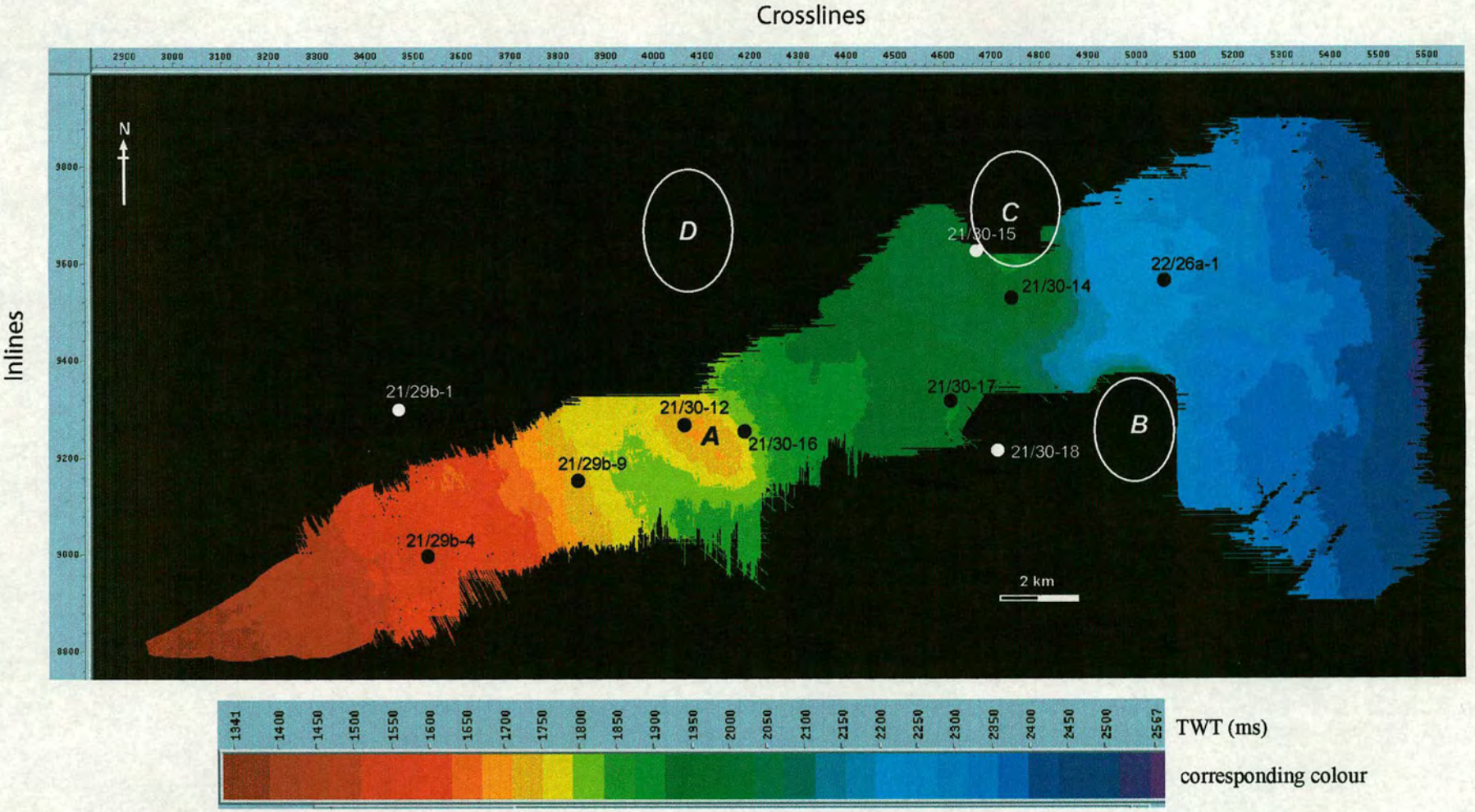

Figure 3.10: Top Tay TWT map. West-east deepening of the basin. Distribution of Tay Sandstone Member is restricted to a narrow area oriented WSW-ENE over salt dome A and between B & C. System is constrained to the south of the line where Forties Formation has abruptly stopped. See text for further details.

has been constrained to the south of the line where Forties Formation deposition had abruptly stopped (as discussed in sections 3.3.1 and 3.3.2).

The Tay Sandstone Member thickness map (in ms) produced by calculating the difference in two way time between Top Tay and Top Balder horizons is shown in Fig. 3.11. The map highlights the three sub basins where accommodation space was available for the sediments to be deposited. It is apparent from this map that the Tay Sandstone Member is relatively thin in this area as the maximum thickness is no more than 141 ms (approximately 700 ft). The thickest Tay package has been deposited on the sea floor basin where the system fans out. The fan has taken an asymmetric lobate shape. Another thick package of the Tay Sandstone Member occurs on the middle subbasin just to the west of salt domes B and C. This subbasin is depicted as green in the Top Tay horizon map (Fig. 3.10). The isochron map also reveals that the Tay Sandstone Member thins and pinches out over salt domes B and C.

The Top Tay Sandstone Member horizon is further analysed by extracting dip azimuth and reflection amplitude maps. The dip azimuth map results from considering the time of each tracked point relative to two neighbouring points in orthogonal directions; the resulting time plane defined by the three points defines a dip vector that has both magnitude and direction. These parameters calculated for every point on the time surface and displayed as map products provide dip magnitude and dip azimuth displays (Brown, 1993). The dip azimuth maps aid in delineating subtle structural and stratigraphic features that are not normally clear on horizon maps. The dip azimuth map for the Top Tay Sandstone Member is given in Fig. 3.12, which shows the structure of the two thick Tay packages already observed on the thickness map. The figure further highlights the most recently active channel between salt domes B and C and continuing westward and also shows some faults mainly on the sea floor basin. The jittering of the surface towards the west of the map is thought to be due to the broken nature of the horizon in this area. In general and since the structure is simple, with little internal faulting, this is an ideal area for applying seismic attribute analysis from 3D seismic data to facies description.

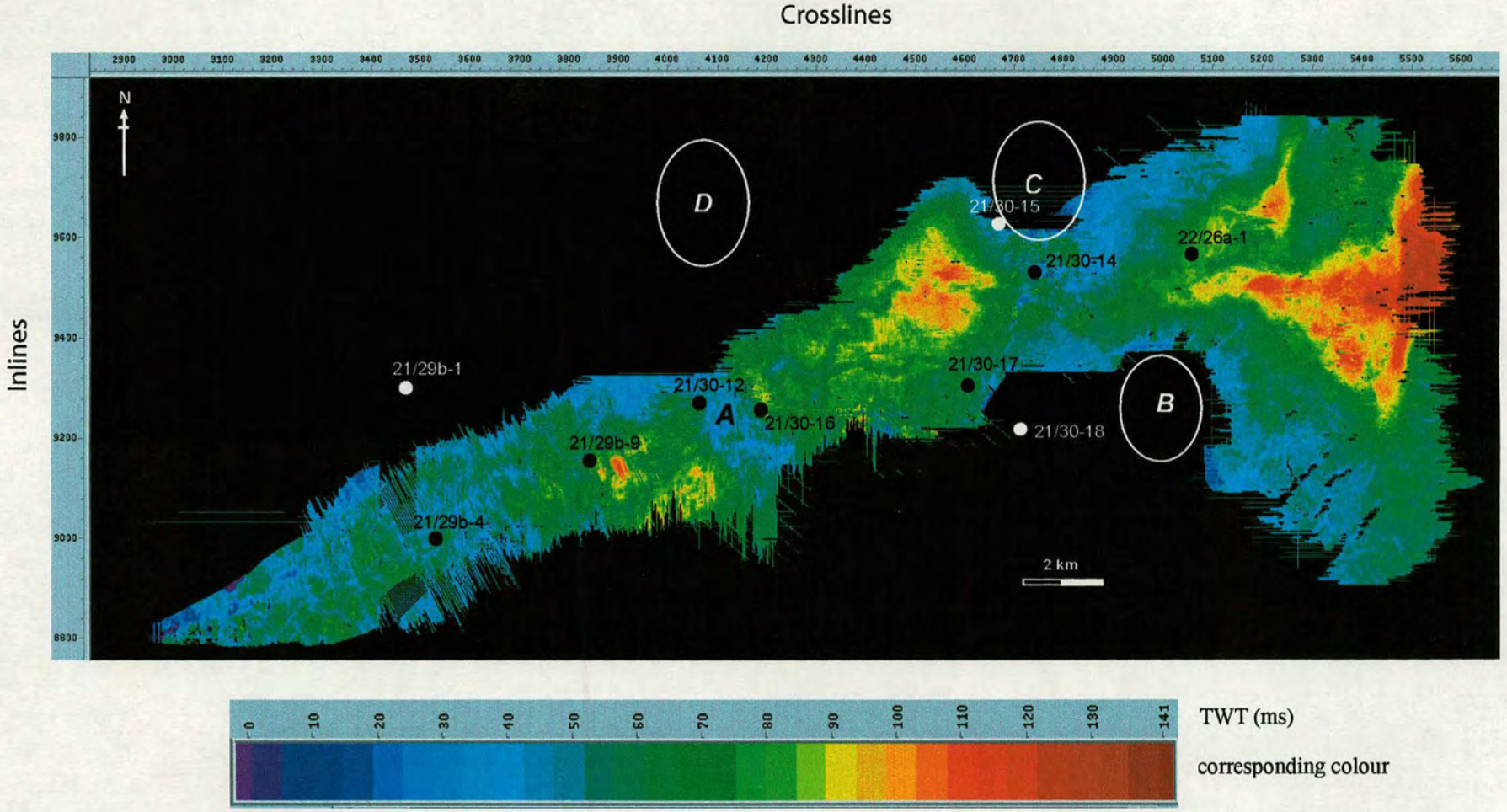

Figure 3.11: Tay Sandstone Member thickness map in TWT. The three sub basins are immdeiately apparent. The system fans out towards the east. Tay Sandstone Member is relatively thin with maximum thickness not more than 141 ms (~ 700 ft).

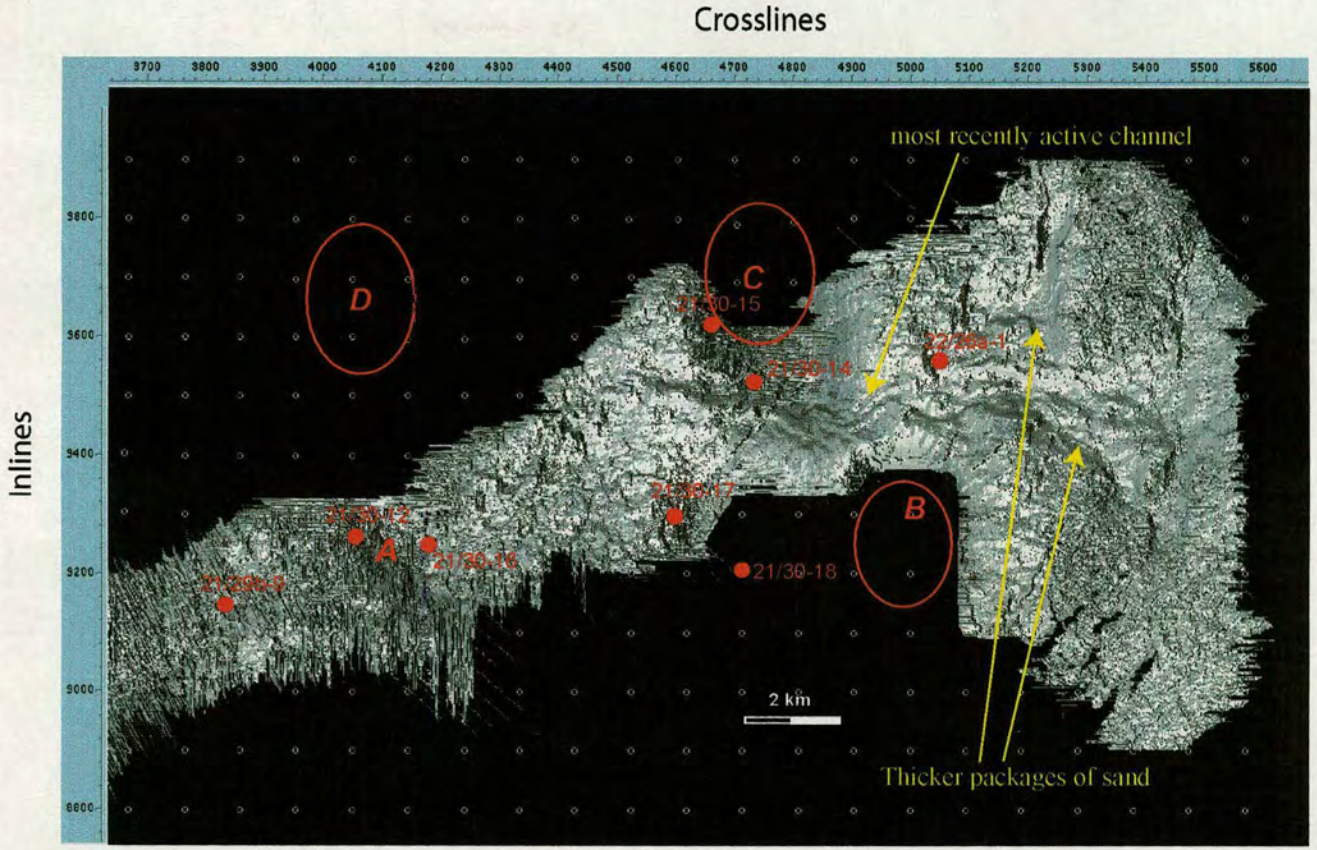

Figure 3.12: Dip Azimuth map for the Top Tay Sandstone Member. Surface structure can be better observed on this map which shows thicker packages of sand as well as the most recently active channel.

Fig. 3.13 shows an amplitude extraction of the Top Tay Sandstone Member reflector. The surface shows quite a variation in amplitude anomalies. The orange to red colours represent higher amplitude sands, whereas the blue colour represents low amplitude siltstones and shales as confirmed by the well data. This is the most useful image so far as it shows more details within the system. The sinuosity of the channel as well as sand distribution is now apparent. The most recently active channel has been preserved in the middle sub basin where the thickness of the Tay Sandstone Member is second highest after the fan itself. The channel is about 200 m wide in an approximately 3 km wide channel belt. Two separate lobes can immediately be distinguished in the fan area.

3.3.4 Tay internal reflectors

Using the higher resolution of wireline logs it was possible to differentiate three distinct depositional units within the Tay Sandstone Member, namely: The Upper Tay, Middle Tay and Basal Tay. The top to each one of these units was mapped and a discussion about each follows starting with the deepest surface;

3.3.4.1 Basal Tay

This is the oldest unit in the Formation. Isolated sand bodies within a shale background occur in this part. The top was mainly picked as the trough (red loop) directly overlying the peak of Top Balder Formation. However, this was mostly discontinuous except in the sea floor basin area where the unit is thicker and the amplitude is higher. The reflector is also continuous in the shallowest sub basin close to salt dome A. This agrees with the well data as both 21/29b-9 and 21/30-12 show the thickest unit of Basal Tay in the area.

Fig. 3.14 shows the Top Basal Tay horizon map. The figure more or less has the same structure as the Top Tay. The thickness map of the Basal Tay unit is given in Fig. 3.15. As shown here, the thickness of this unit does not exceed 45 ms. One reason for this is the progradation nature of the unit as seen in the wells. This could be due to erosion of the upper transgressive deposits by subsequent high-density turbidity currents or sediments not being deposited in the first place.

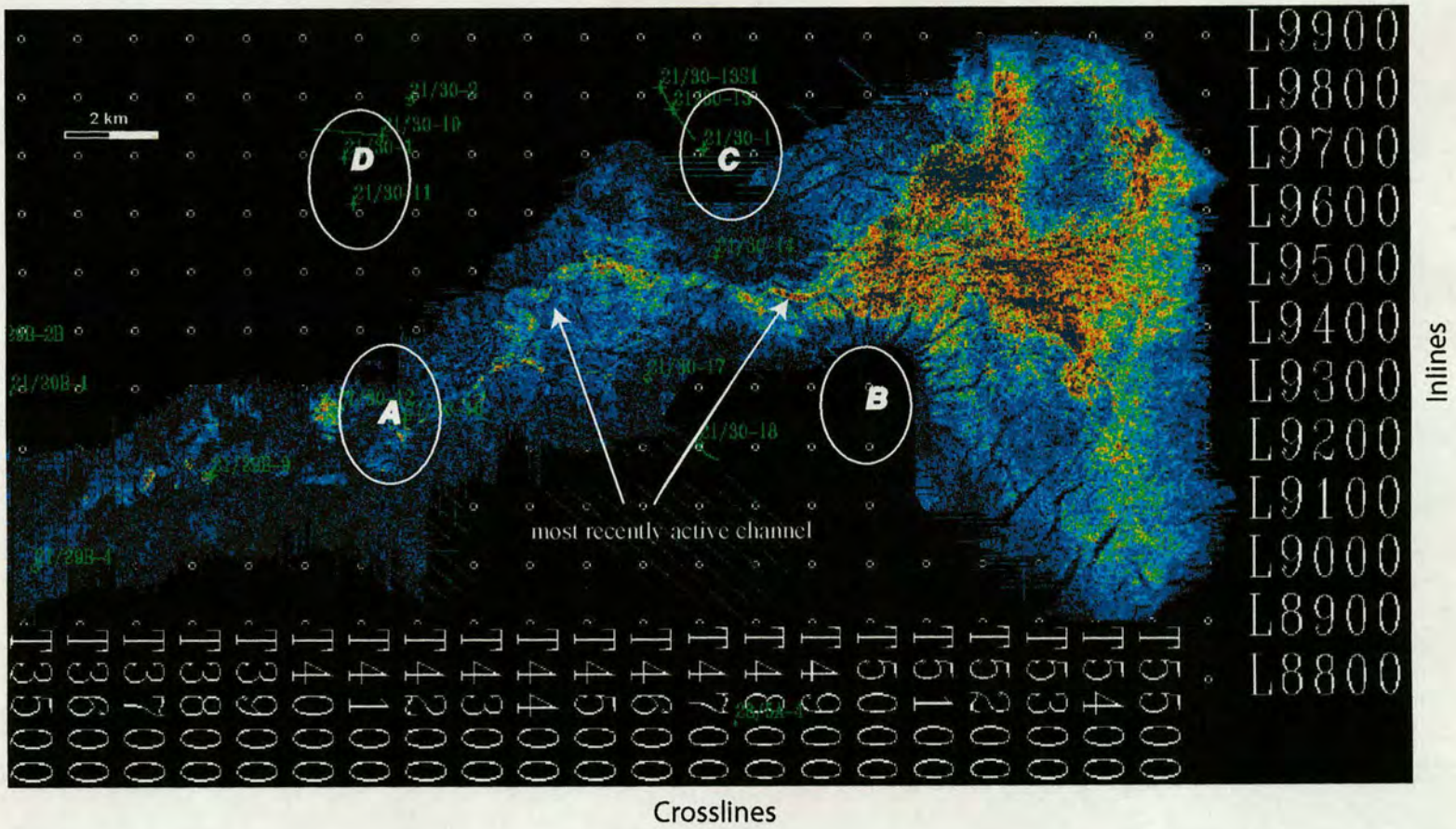

Figure 3.13: Top Tay amplitude map. Orange to red represent high negative amplitudes and blue high positive amplitudes. A, B, C & D indicate the 4 salt domes present in the area.

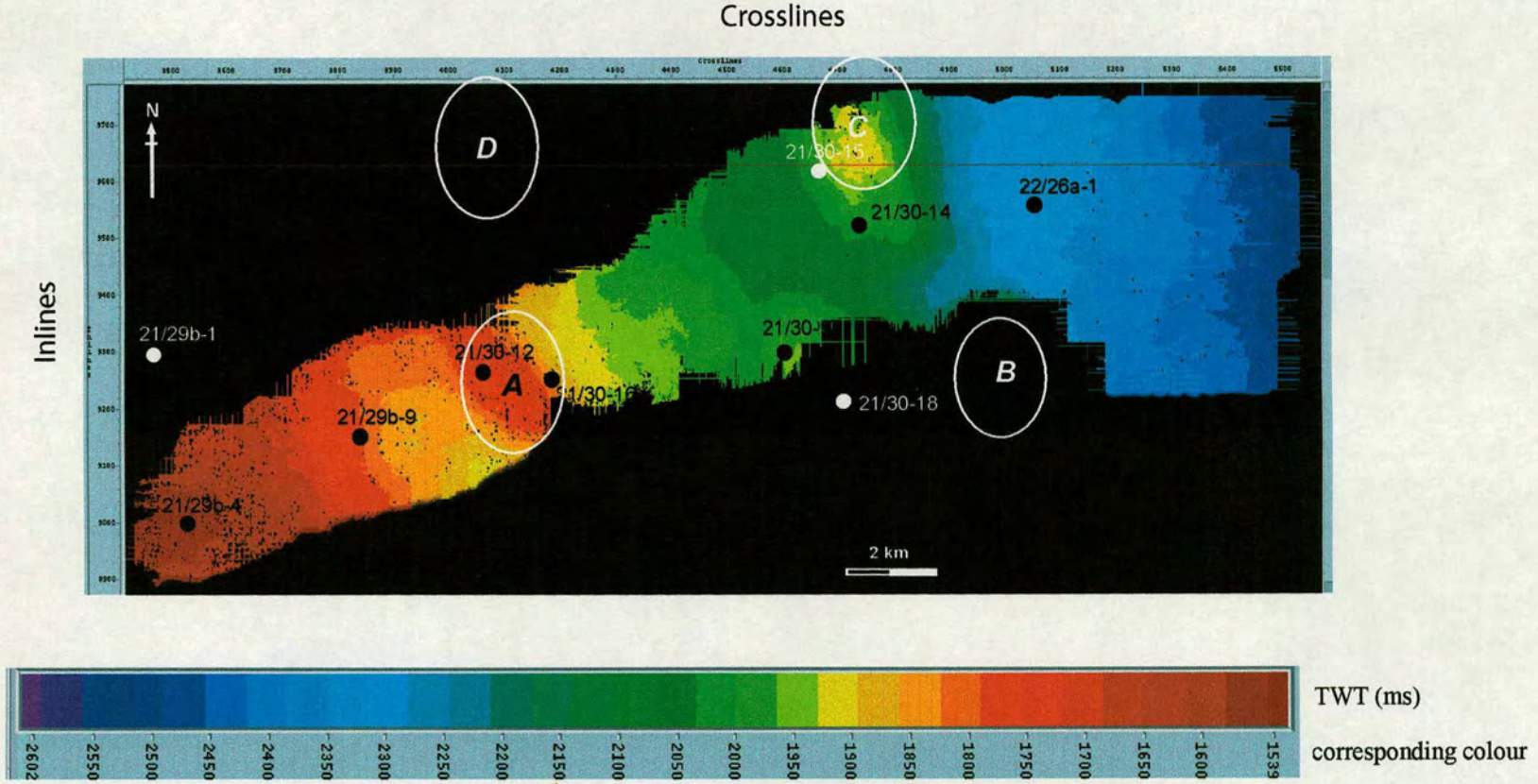

Figure 3.14: Top Basal Tay horizon map in TWT.

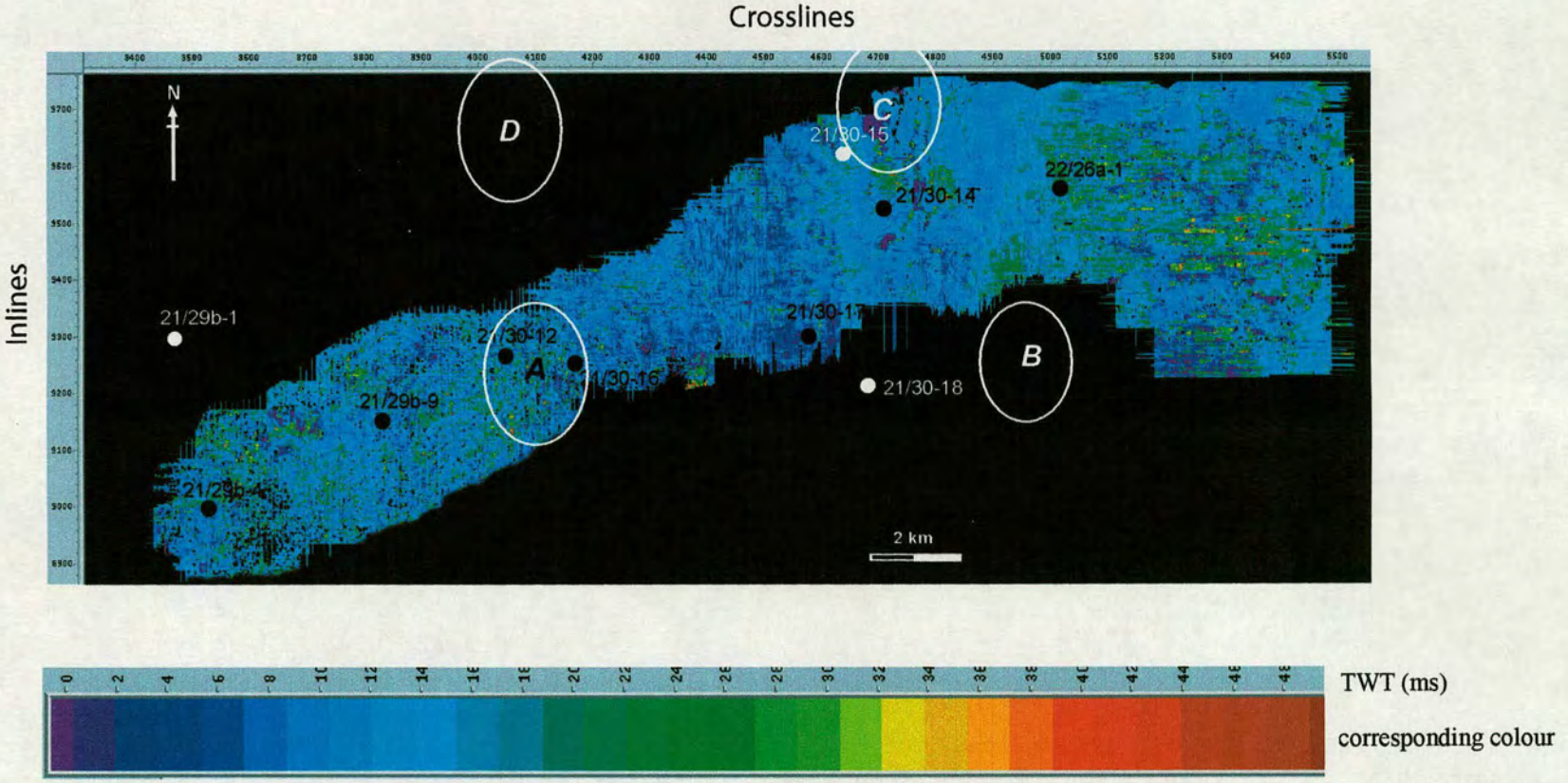

Figure 3.15: Basal Tay thickness map in TWT (ms). Basal Tay is very thin in this area not exceeding a thickness of 45 ms.

3.3.4.2 Middle Tay

This forms one of the main reservoir units in the Tay Sandstone Member in the Gannet South area, as it is sandy and reasonably thick at several locations. The horizon map for Top Middle Tay (Fig. 3.16) shows a very similar surface to the Top Tay. The thickness map (Fig. 3.17) calculated by subtracting the TWT to Top Middle Tay from the TWT to Top Basal Tay, highlights the locations where this unit is thickest. It is illustrated in this map that the Middle Tay is a thicker package in the second sub basin close to well 21/30-17 and within the fan furthest to the east. The map also demonstrates the thinning and eventually pinching out of the Middle Tay unit against the salt highs B and C. Relative thinning is also observed over salt dome A.

3.3.4.3 Upper Tay

This is the youngest unit of all. Top of Upper Tay is the same surface as Top Tay, which has already been described. This unit is the thickest of the three units within the Tay Sandstone Member and specifically in the sea floor basin. As shown in the thickness map in Fig. 3.18, these youngest sands have also been deposited in the area surrounding well 21/29b-9 but seems to have by-passed the area close to wells 21/30-14 and 21/30-15. This observation is consistent with well data.

3.4 Stratigraphic architecture and depositional model

The purpose of this section is to describe and illustrate a number of key features of the Tay Sandstone Member in the Gannet South area as well as to investigate the variation in these features along the system. This is done by taking a number of cross-sections running both parallel and perpendicular to the system as so far we have concentrated on map views of the different horizons.

The amplitude map of the Top Tay reflector shown in Fig. 3.13 clearly demonstrates the single channel system, which can be traced continuously for about 30 km from the toe of the shelf to the fan in the main subbasin. Vining *et al.* (1993) estimated the

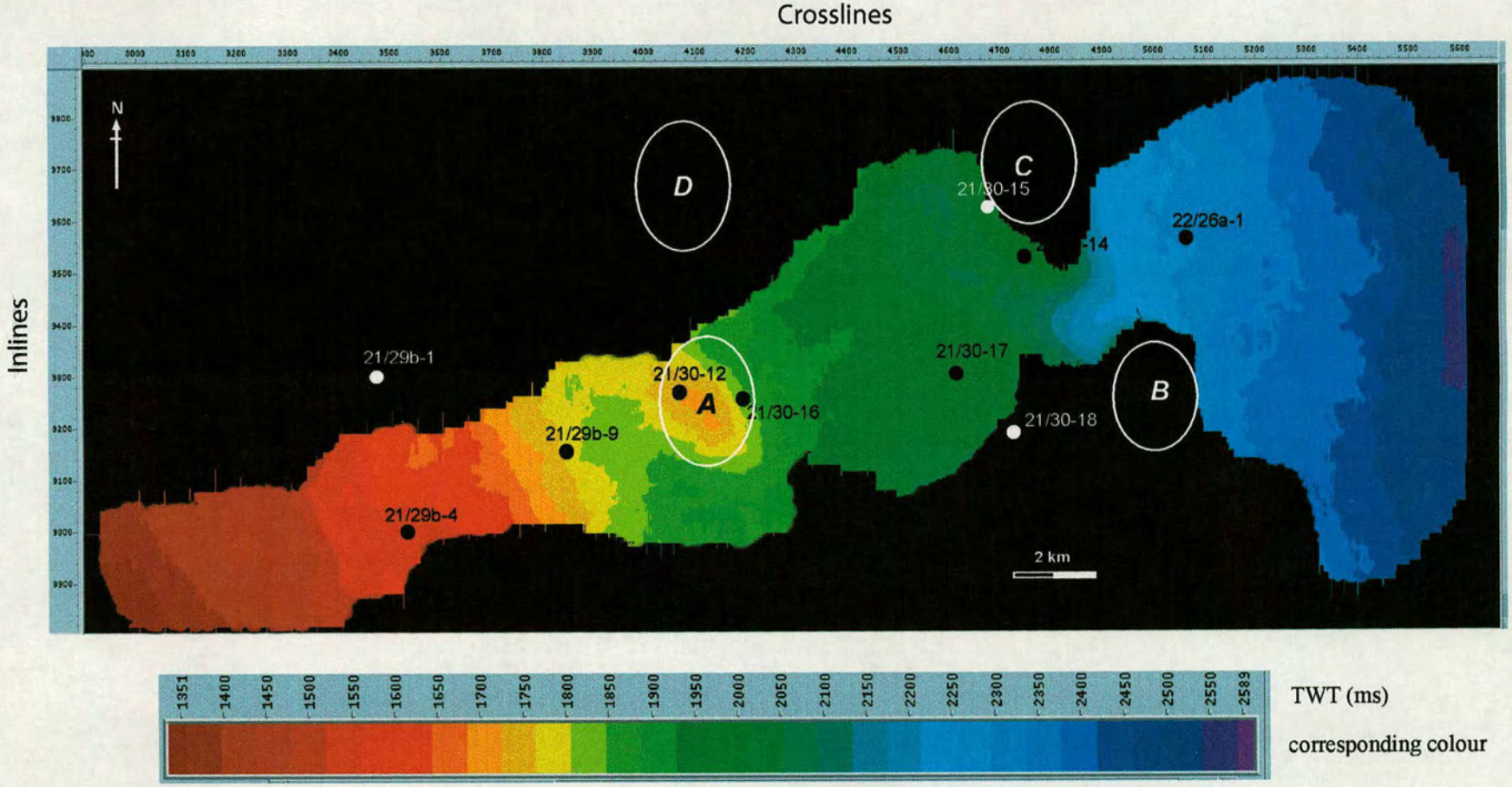

Figure 3.16: To Middle Tay horizon map in TWT (ms).

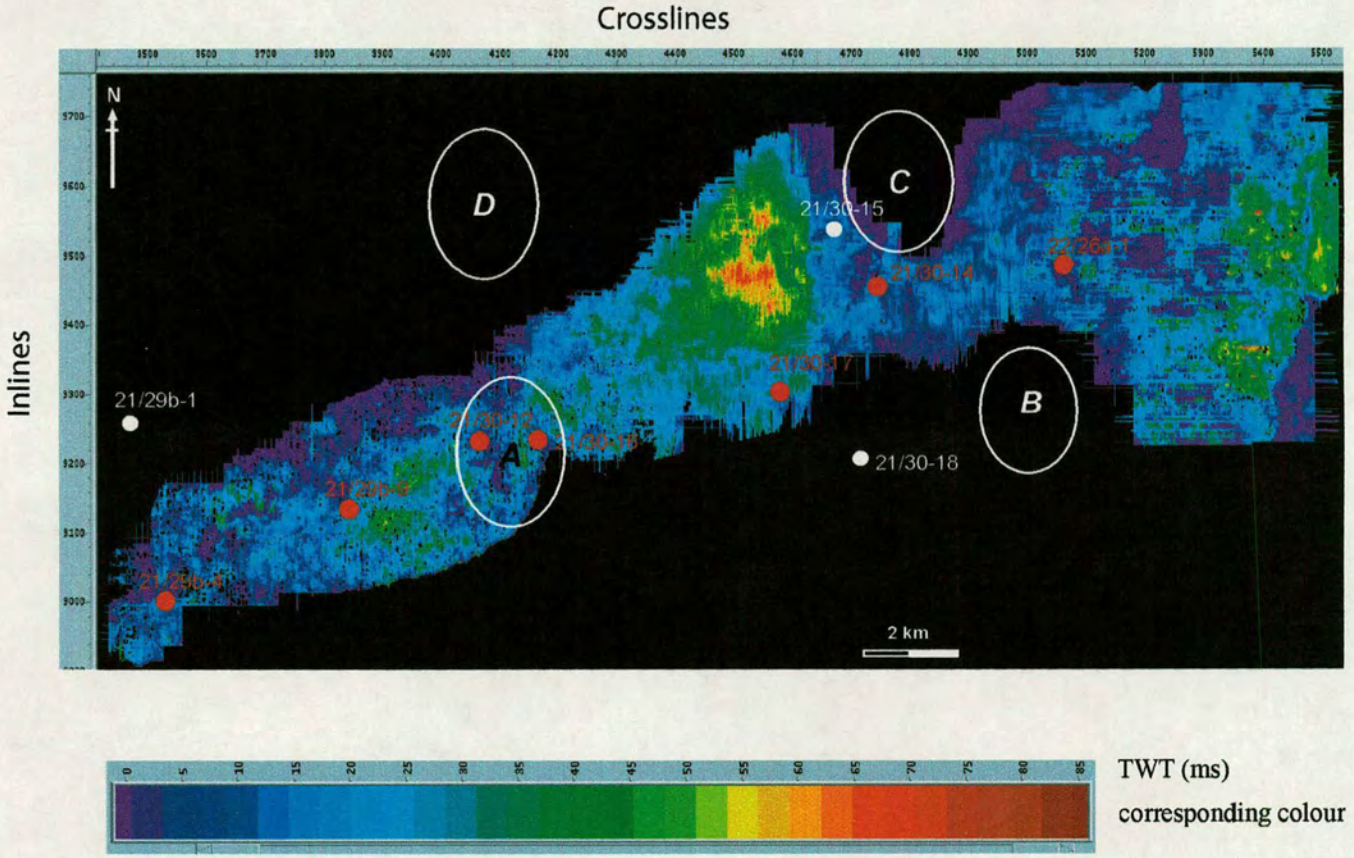

Figure 3.17: Middle Tay thickness map in TWT. Middle Tay appears to be thickest in sub basin II.

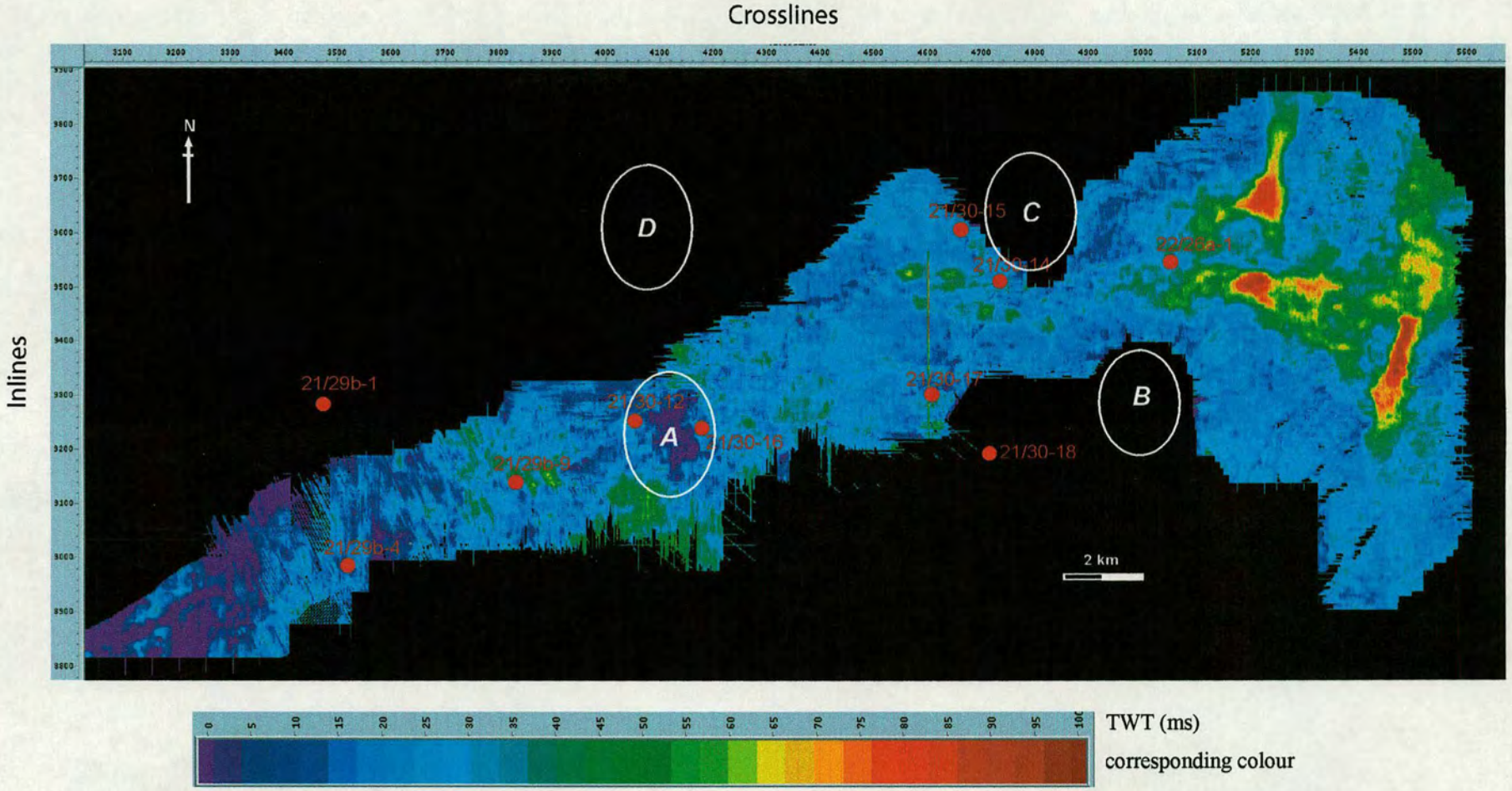

Figure 3.18: Upper Tay thickness map in TWT (ms). Upper Tay is thickest in sub basin III.

water depth during accumulation of the Palaeocene fans to be of the order 200-600 m, based on clinoform geometries and palynofacies. Fig. 3.19 shows a longitudinal depth profile of the system (see Fig. 3.20 for the location of this composite line A-A'). This seismic traverse along the path of the channel shows a system of three intra-slope basins (Basins I, II & III). The overall gradient is approximately 2° (35 m/km) decreasing to less than 0.1° (2 m/km) in basinal areas and going into negative gradients up the structural highs. A key issue to address is the direction of sediment transport within this system. This channel is considered to transport sediment eastwards on the basis of the deepening and broadening of the system in the east. This it is interpreted to represent the channel building into a fan-delta geometry at its terminus. Here we consider the internal and overall architecture of the Tay Sandstone, with the benefit of clearer seismic imaging on the 1997 high-resolution seismic data volume. Seismic continuity appears to be increasing down the slope and within individual basins and gets to its best in the fan area, reflecting better developed sand packages. Having said that, it should be cautioned that not all the beds interpreted on this line are necessarily continuous from the toe of the slope to the basin floor.

The onset of basin filling is interpreted to start first in the basin close to the shelf and progress successively seaward as each basin is filled to a spill point (fill and spill model; Satterfield & Behrens 1990; Winker 1996; Prather *et al.* 1998, Sinclair & Tomasso, 2002). This is why the thickest succession of the youngest Tay sands is observed at the deepest basin (Basin III) in well 22/26a-1. This means the shallower basins were getting filled first with the earliest sands, whereas, finer sands and muds getting spilled to the deeper basins as seen in the lower sections of the well. When accommodation space at the shallower levels got filled the sand started being deposited at deeper levels. This is known as flow ponding (see Sinclair, 2000; Sinclair & Tomasso, 2002) and for it to take place the confining basin must be surrounded by topographic barriers that are sufficient to prevent turbidity currents surmounting them. Flume tank experiments conducted by Muck and Underwood (1990) showed that the flow thickness was the primary control on the ability of turbidity currents to surmount an opposing barrier.

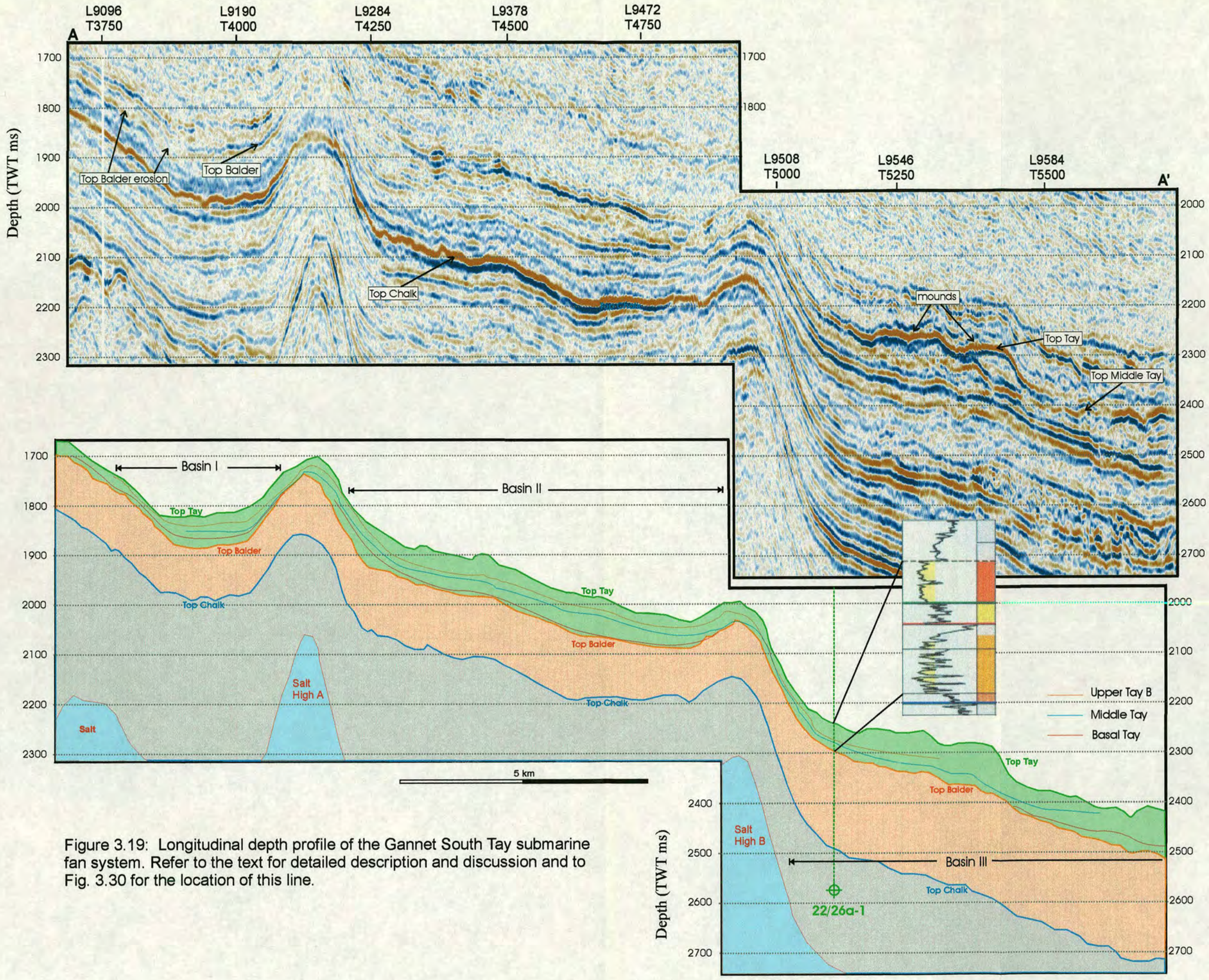

Figure 3.19: Longitudinal depth profile of the Gannet South Tay submarine fan system. Refer to the text for detailed description and discussion and to Fig. 3.30 for the location of this line.

One immediate implication of this barrier being present at the time of deposition is that sediment accumulations will occur immediately upstream of opposing slopes, leaving much thinner deposits accumulating downstream of the topography. This is suggested by the flume tank experiments conducted by Alexander and Morris (1994). However, looking back to Fig. 3.19 and observing sediment accumulation and thickness variation both sides of the structural high between basins I and II demonstrates the opposite of this. Here we have thicker package on the downstream side of the barrier and thinner on the upstream side. One possible explanation for this is that this barrier did not exist at the time of deposition but if this was the case then why were sediments deposited in basin I? The more appropriate interpretation, which also agrees with the well data, is that salt has been moving during deposition and at the time of onset of basin filling this structural high did exist but with a much lower relief. As the sediments started filling the basin, the break of the slope that defined its margin became healed and the high was buried, later sediments bypassed the area and were deposited further down the slope. Meanwhile as salt continued moving the high grew further and started acting as a barrier again creating more accommodation space and making the next episode of deposition once again into basin I.

The fact that salt movement continued after the deposition of the Tay Sandstone Member is demonstrated further by an arbitrary line running perpendicular to the longitudinal line of Fig. 3.19. This is line C-C' as shown in Fig. 3.21 and its location with respect to the system is given in Fig. 3.20. Fig. 3.21 clearly indicates the pinchout of the Tay Sandstone Member towards the edges of the salt dome whereas the thickest package exists right on top of the high. Had this high existed at the time of deposition as it is now the sediment flow would have got deflected away from it following a much easier path around the high. Even if the flow was powerful enough to surmount this high it cannot have deposited that thick a succession of sediments on top of it. Flow deflection at the Tay interval on encountering a salt high has been demonstrated else where in the Central North Sea (e.g. Fyne area northwest of Gannet South, Fig. 1.1, pers. comm. John Underhill, Edinburgh University).

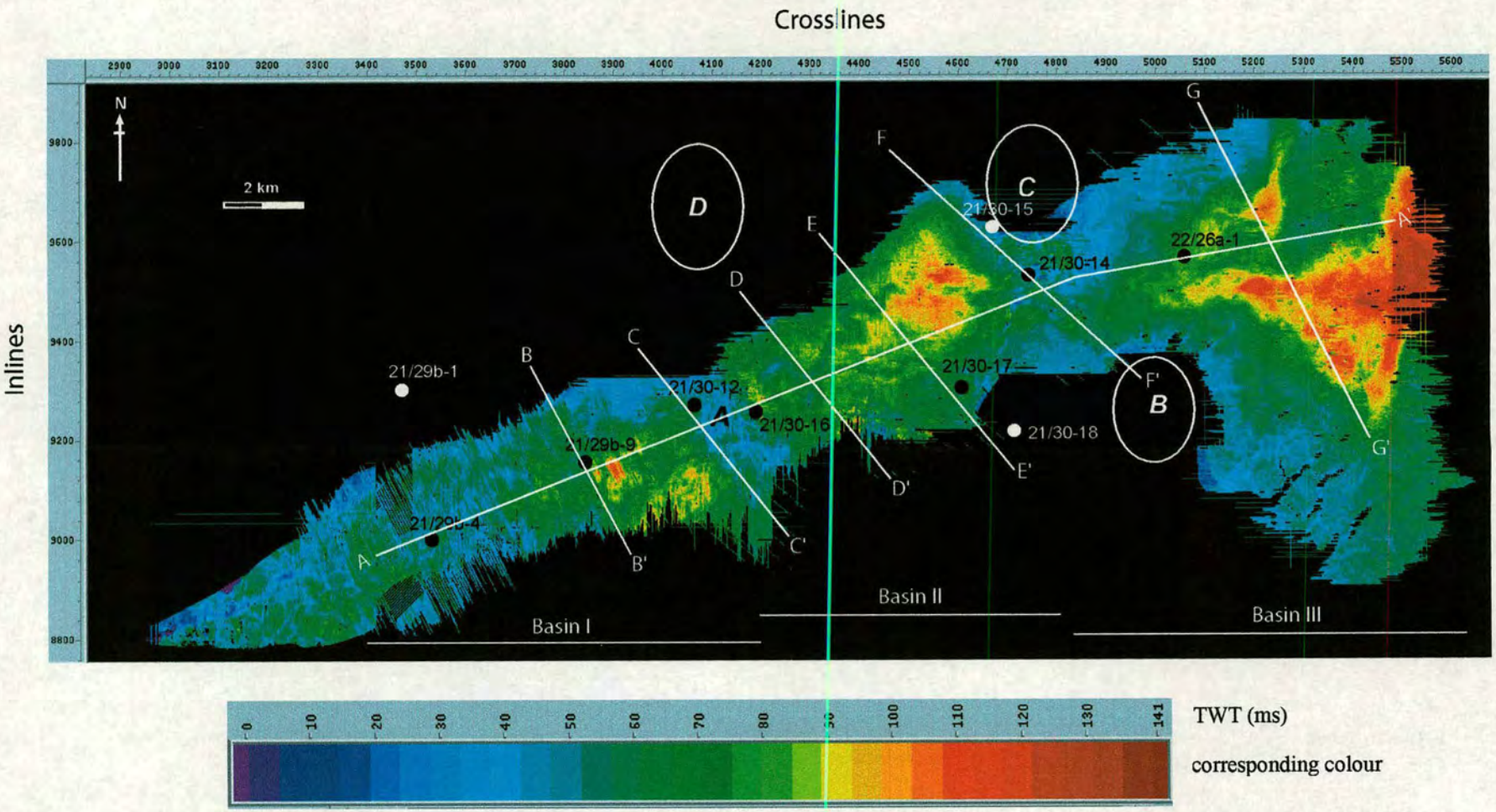

Figure 3.20: Location of cross sectional lines represented by figures 3.19-3.2.6.

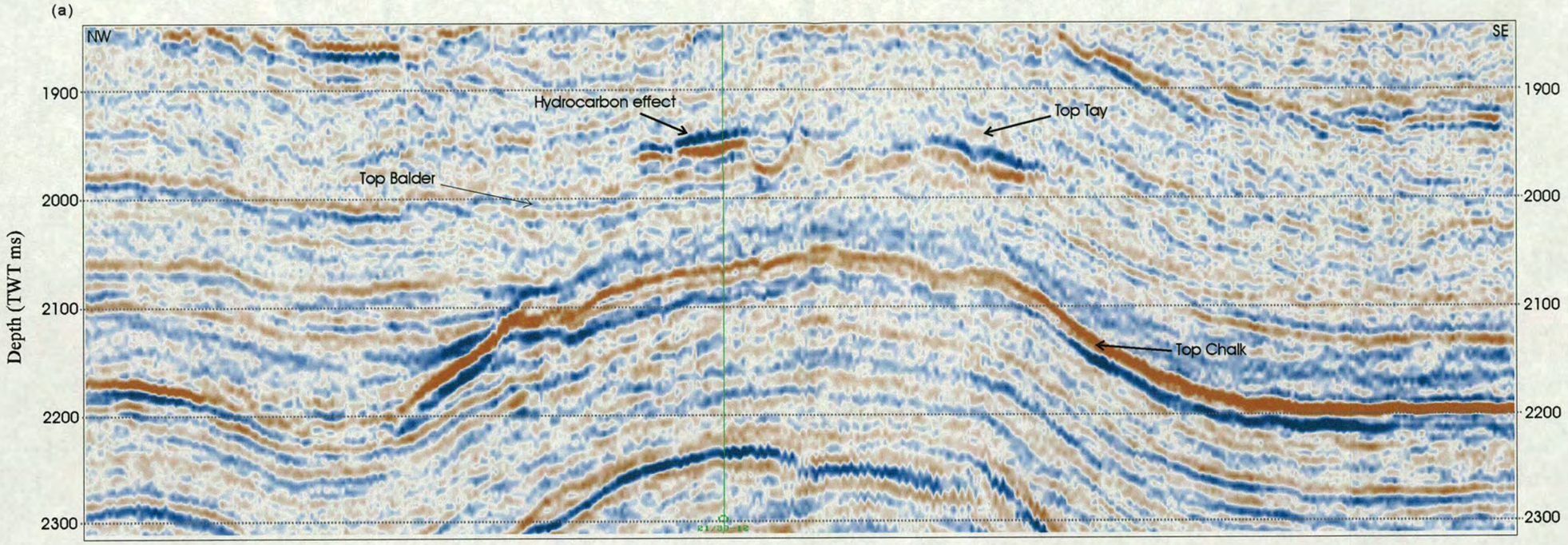

Figure 3.21: Arbitrary seismic line (C-C') running perpendicular to line A-A'. This seismic line illustrates the thick package of Tay Sandstone Member to occur on the crest of the Salt dome and pinching towards the edges. Thus an increase is dome relief must have occurred after deposition of Tay Sandstone Member. For location of the line refer to Fig. 3.20.

Fig. 3.22 shows another arbitrary line running perpendicular to the system but further up the slope then line C-C'. This line B-B', the location of which can be seen in Fig. 3.20, clearly depicts Top Tay onlapping towards the northwest on to Top Balder Formation over the high, which has been produced by previous deposition. It also shows that in the southeastern side Top Tay seems to be downlapping on to Top Balder Formation. The system on this side appears to be unconfined. However, deposition still pinches out. This is thought to be due to the gradient and flow energy which make the sediments travel down the slope rather than being deposited laterally. To this end, the exact edge of the sand distribution is uncertain as the seismic resolution is of insufficient precision to determine this.

Moving further down the slope to the downstream side of the salt high and going into basin II, line D-D' (Fig. 3.23) shows a very similar pattern to what was seen earlier in line B-B' except that the relief of the topography induced by previous sediments has now become less, but still high enough to play an active role in directing the channel pathway. Top Tay Sandstone Member still appears to be onlapping onto Top Balder Formation over this high and downlapping onto it on the southern side of the system.

Line E-E' (Fig. 3.24) provides a cross-sectional view of the Tay sedimentary architecture within basin II. Here we notice the increased continuity of the internal reflectors of the Tay Sandstone Member as well as the Top Tay reflector. Sand packages are better developed especially within the Middle Tay unit. The erosive nature of the Basal Tay can also be seen. Once again topography induced by previous sediments has played a major role in influencing the channel direction, as the formation is pinching-out towards it. In the southeastern part, the deposition has been stopped by faults induced by the salt movement. This salt high is different from the one described on the earlier lines. This is salt high B of Fig. 3.2.

Moving further down the slope in the longitudinal view shown by the composite Line A-A' in Fig. 3.19, the thickness variation at both sides of the salt high can clearly be observed. This agrees with the results from the flume tank experiments conducted by

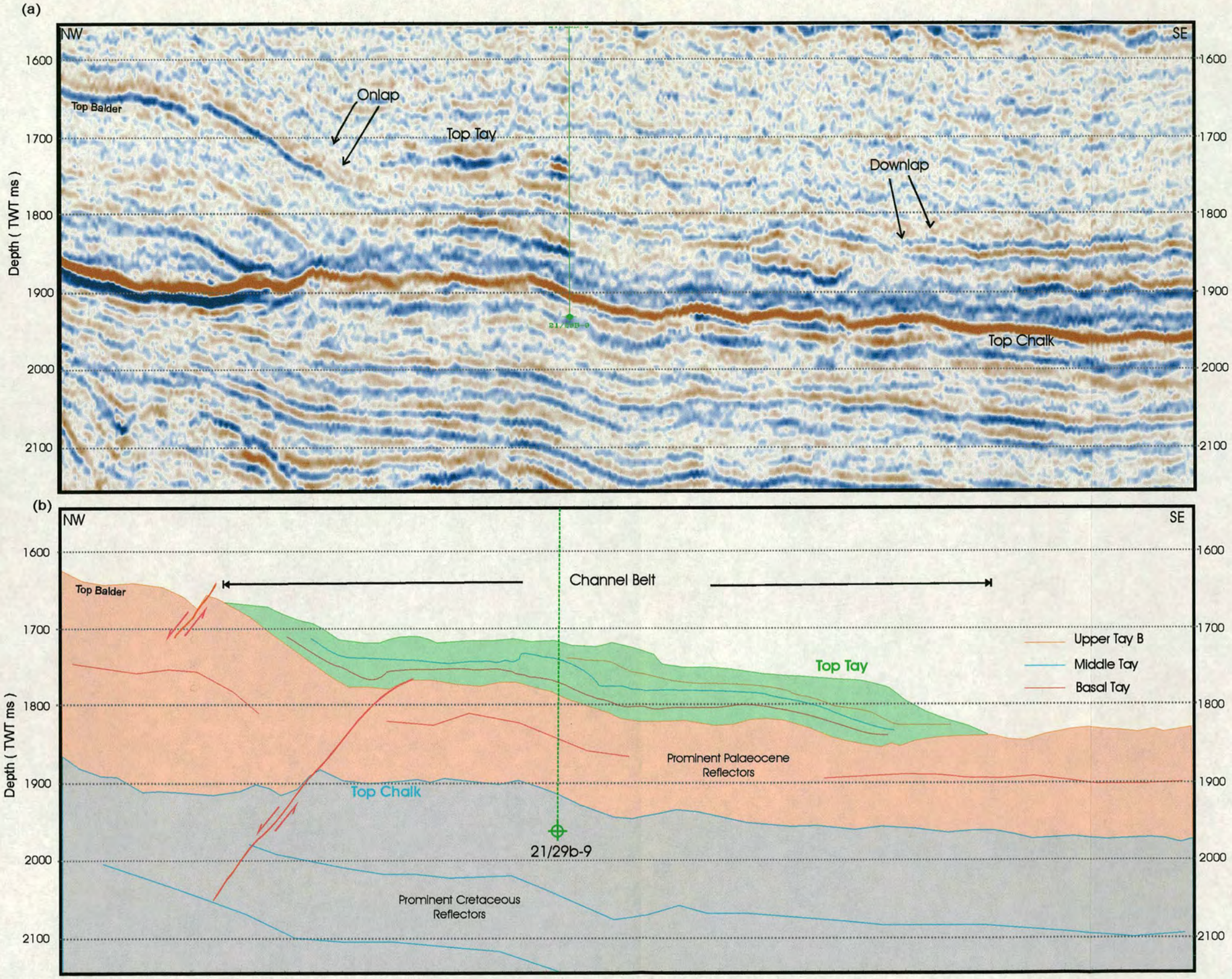

Figure 3.22: Arbitrary seismic line (B-B') running perpendicular to line A-A'. This seismic line is parallel to Fig. 3.21 but further up the slope and illustrates the onlapping of the Tay Sandstone Member onto top Balder Formation to the NW whilst downlapping to the SE. For location of the line refer to Fig. 3.20.

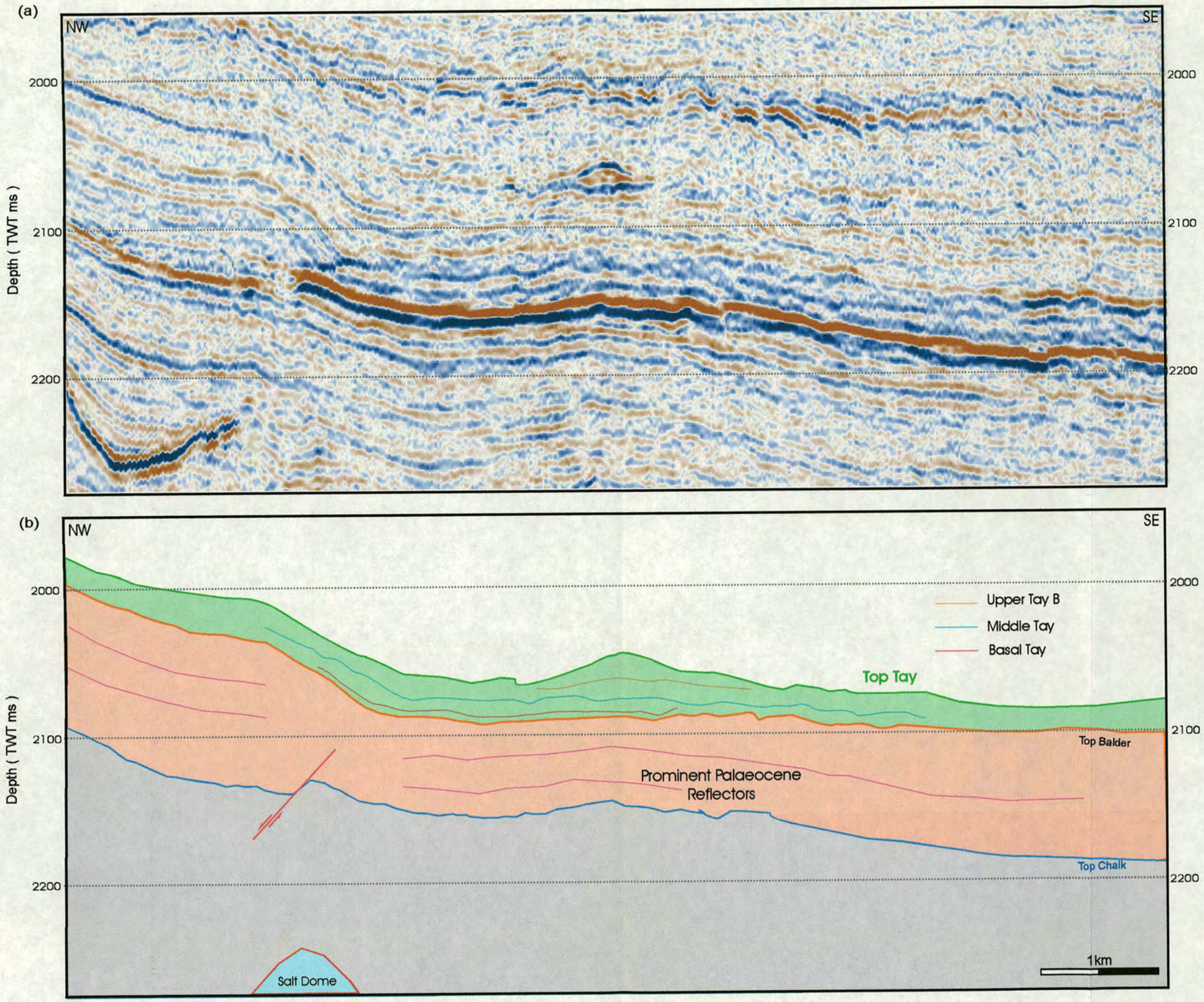

Figure 3.23: Arbitrary seismic line (D-D') further down the slope of the Tay channel. The line illustrates that although the relief of topography to the NW is much reduced, it still plays an active role in confining the channel pathway. For location of the line refer to Fig. 3.20.

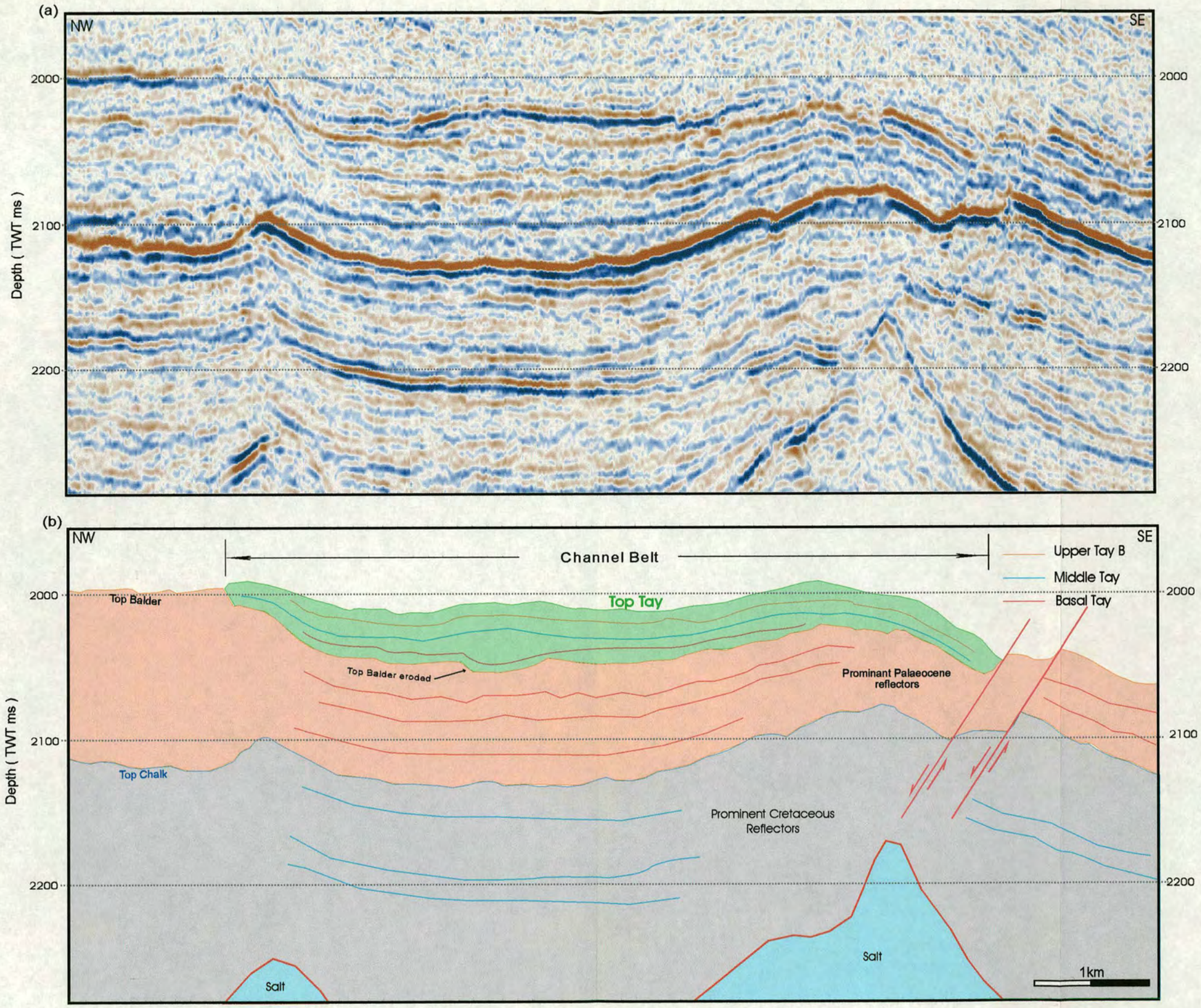

Figure 3.24: Cross sectional view (E-E') of the Tay Sandstone Member sedimentary architecture within basin II. The line shows the increased continuity of internal reflectors of the Tay Sandstone Member with sand packages better developed especially within the Middle Tay unit. For location of the line refer to Fig. 3.20.

Alexander and Morris (1994). The salt dome being present at the time of deposition resulted in sediment accumulating immediately upstream of opposing slopes, leaving much thinner deposits accumulating downstream of the topography. However, this salt high was also developing at the time of deposition as the results from trace shape analysis suggest and this growing of the salt had a major effect on the distribution of the sand in Basin III. This will be discussed in the Trace Shape Analysis chapter. Fig. 3.25 shows Line F-F', which is a perpendicular line close to the salt dome C but not running on top of its highest position. Here we can see some post-deposition faulting which resulted from continuous or reactivated salt movement. These faults are not thought to have existed at the time of deposition as there is no clear thickness variation observed across them.

Moving into Basin III in Fig. 3.19, the better quality of sands resulting in better seismic reflectors is immediately apparent. This seismic response is probably due to the lithologic continuity and high acoustic impedance contrasts characterising the fan internally, as well as the lithologic contacts with overlying and underlying units. The deposition of submarine fan sediments with distinctly different seismic velocity than the pelagic and/or hemipelagic sediments above and below, which usually characterise these deep-water environments, commonly results in a distinctive seismic unit. What is also observable is that there is more than one lobe being deposited. In the longitudinal view, it is only possible to distinguish two separate lobes, however, in the perpendicular cross-section shown on Line G-G' in Fig. 3.26, three such lobes can be distinguished. These are interpreted as different episodes of the Tay Sandstone Member influenced by sea level fluctuations. The top Tay amplitude map shown in Fig. 3.13 depicts the two lobes at this level. In the cross-sectional views, notice the chaotic and bidirectional downlapping nature of the reflectors within each of the mounds. These bidirectionally downlapping seismic reflections are sometimes diagnostic of submarine fans; characterised by reflection terminating in both directions onto a sequence boundary at the base of the fan (Posamentier & Erskine, 1991). The predicted fan intervals are characterised by blocky sandstone as seen in well 22/26a-1 (Fig. 3.19). Posamentier and Erskine (1991) pointed out that basinward-oriented, unidirectional dowlapping seismic

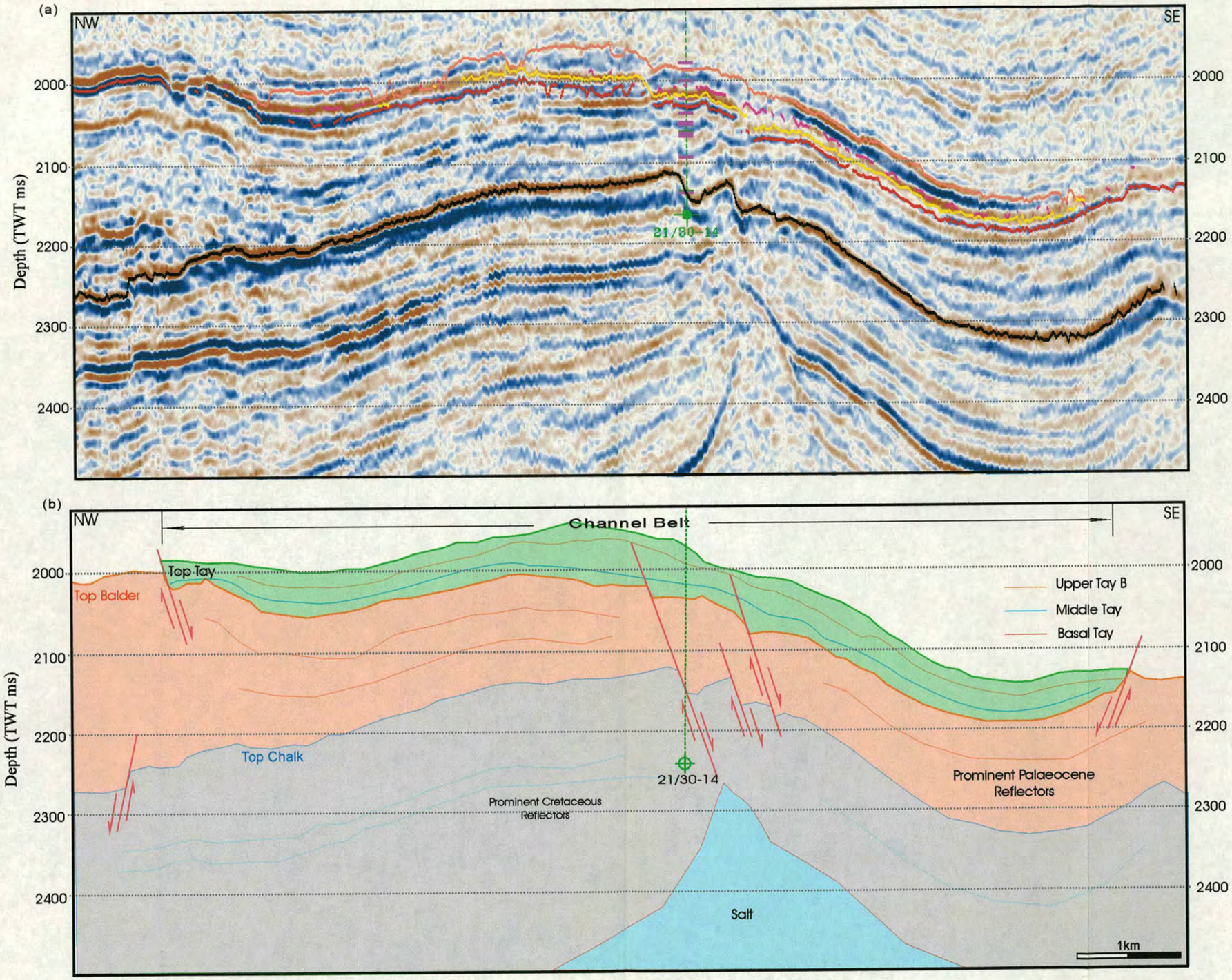

Figure 3.25: Cross sectional view (F-F') of the Tay Sandstone Member in the vicinity of well 21/30-14. Post-deposition faulting which may have resulted from continuous or reactivated salt movement is seen to displace reflectors with the Tay Sandstone Member and all the way to top Chalk Group. For location of the line refer to Fig. 3.20.

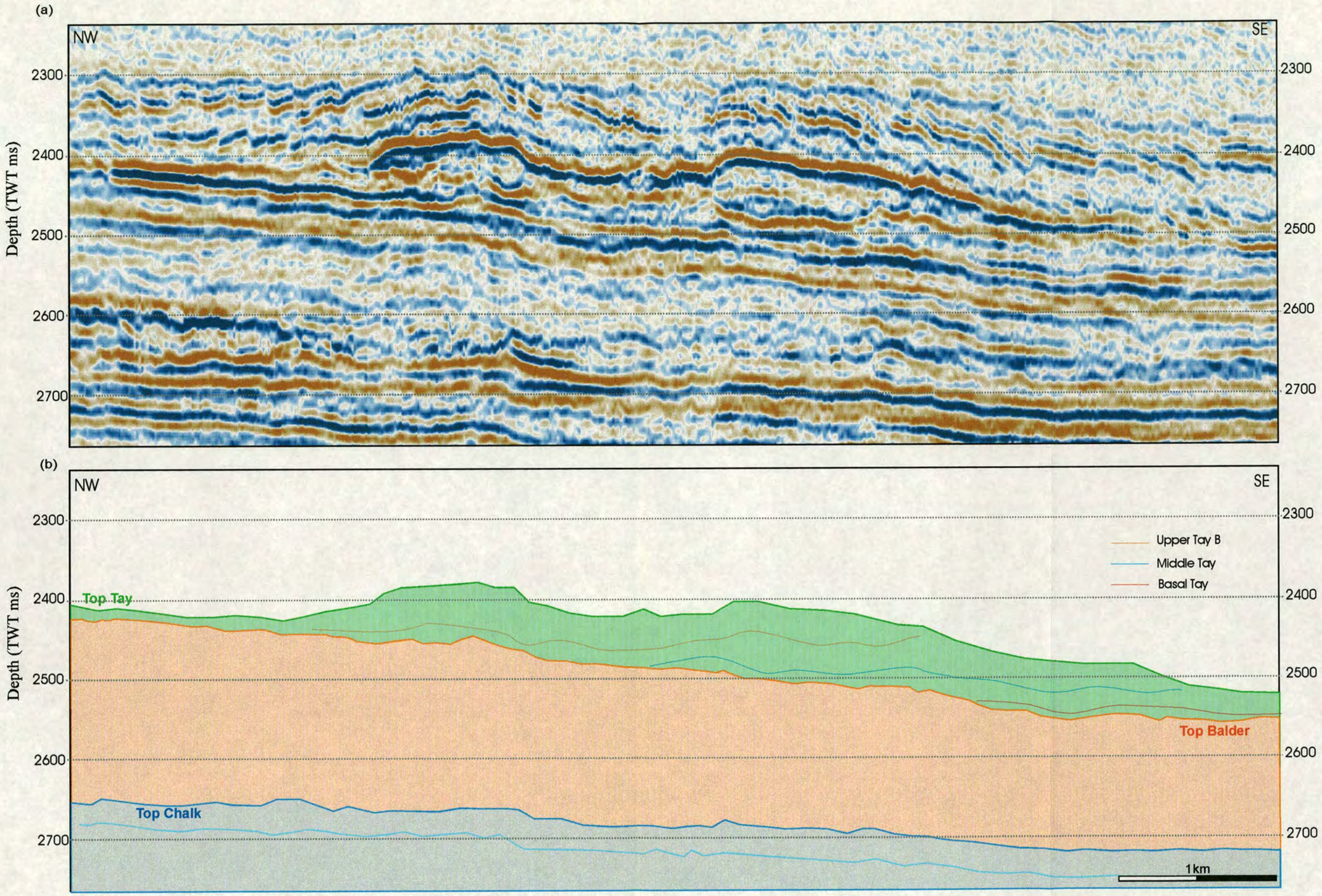

Figure 3.26: Cross sectional view (G-G') of the Tay Sandstone Member sedimentary architecture within basin III. Three depositional lobes may be seen, which are interpreted as different depositional episodes of the Tay Sandstone Member influenced by fluctuations in the sea level. For location of the line refer to Fig. 3.20.

reflection suggestive of progradation are rarely observed within documented submarine fans. The absence of this pattern gives insight to the style of growth of submarine fans. A unidirectional dowlapping pattern would suggest progradation as one might expect in a deltaic setting. A bidirectional dowlapping pattern suggests an aggradational mode of deposition associated with stacking of discrete lobes. Consequently, these observations suggest that the dominant growth style of submarine fan involves an aggradational stacking of fan lobes. The evolution of the three lobes in the Gannet South area will be discussed further in the trace shape analysis chapter as they were first noticed in the results of this analysis.

3.5 Channel Evolution

This was studied using horizon slices. The horizon slices, which show spatial amplitude distribution at time surfaces parallel to the reference horizon, in this case Top Tay horizon, were checked every 4 ms and the main channel was traced on these map views. The results show that there are only minor variations in the channel path and sinuosity throughout the whole period of the Tay deposition. Fig. 3.27 shows the horizon slices used and Fig. 3.28 shows all the traced channels superimposed on each other. The figure also highlights the deposition in basin II as the sinuosity of the channel increased. Changes in sinuosity appear to be closely related to the variations in gradients and well-developed meanders occur where regional gradient reduces. This agrees with outcrop and modern fan observations made by Permiz and Flood, (1995) Flood *et al.*, (1995) Clark and Pickering, (1996) Hiscott *et al.*, (1997) and Permiz *et al.*, (2000). Fig. 3.28 also highlights the sand development in this basin due to flow stripping processes. This sand is highly prospective for hydrocarbon accumulations. Clark and Pickering (1996) point out that these spill-over points develop where flow breaches levees on sharp bends, and where channel gradients decrease cause an increase in flow thickness. This leads to rapid reduction in flow velocity, resulting in deposition of at least part of the coarser fraction from the lower parts of the flow (Normak & Piper 1991).

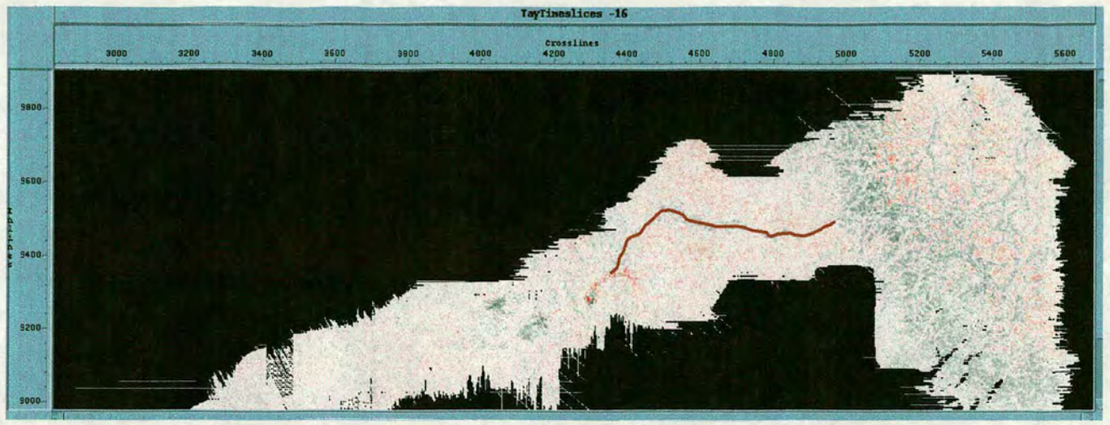

16 ms above Top Tay

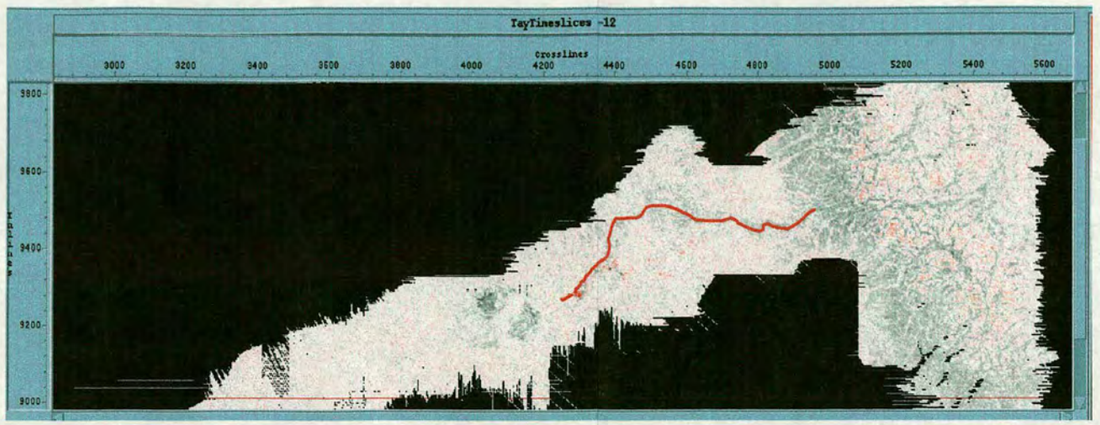

12 ms above Top Tay

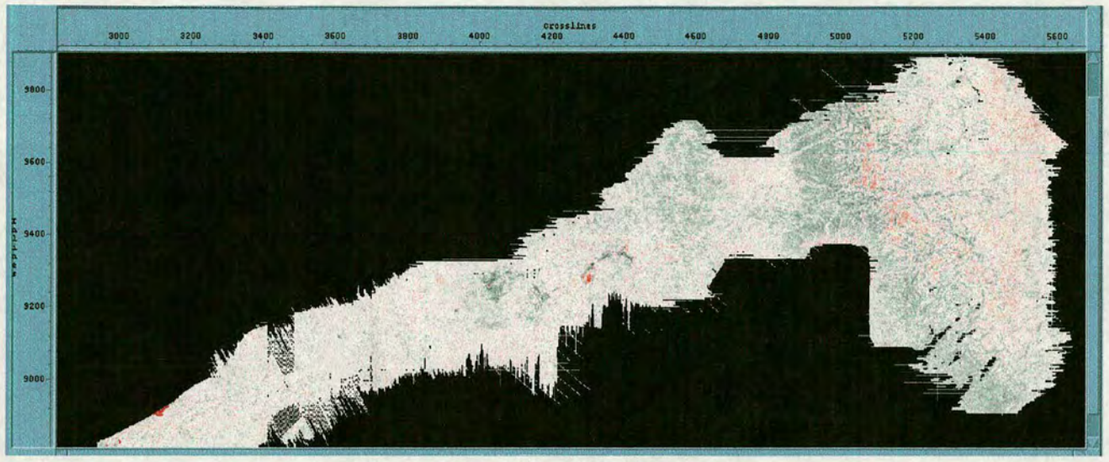

8 ms above Top Tay

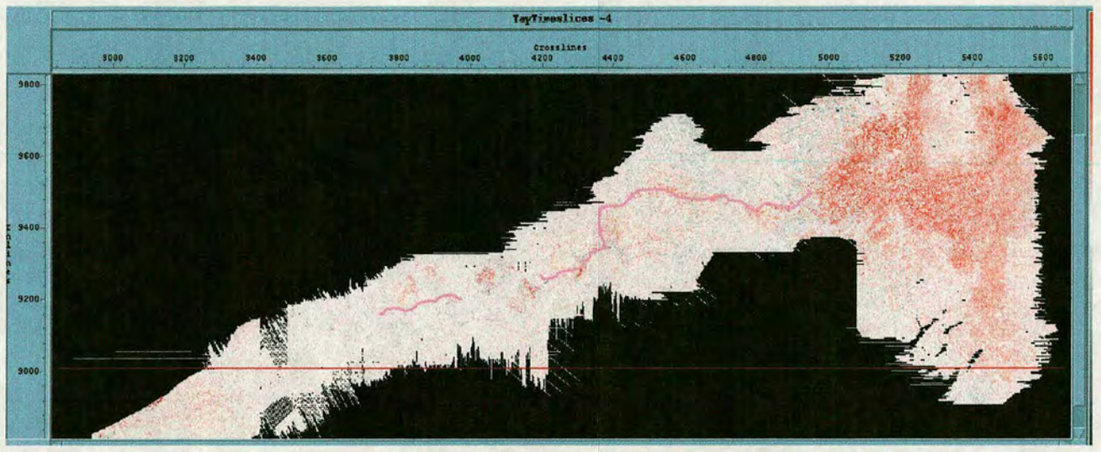

4 ms above Top Tay

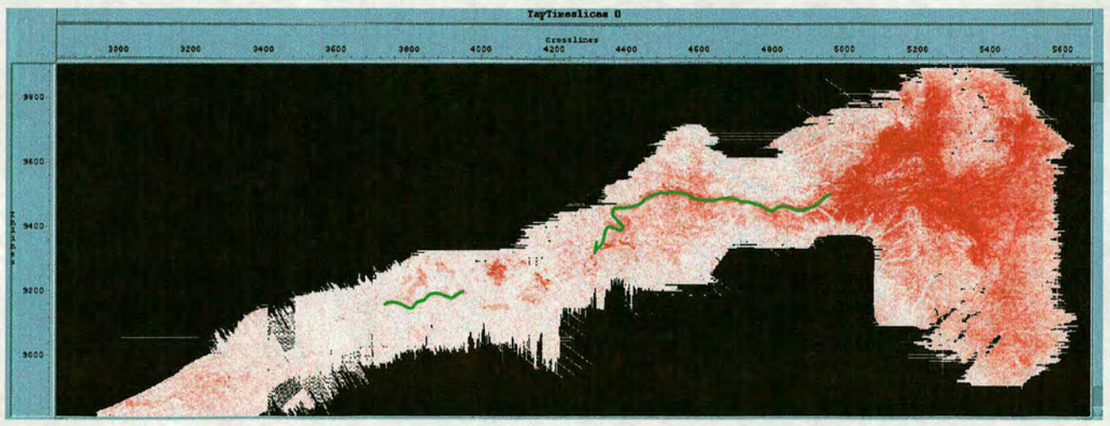

At Top Tay

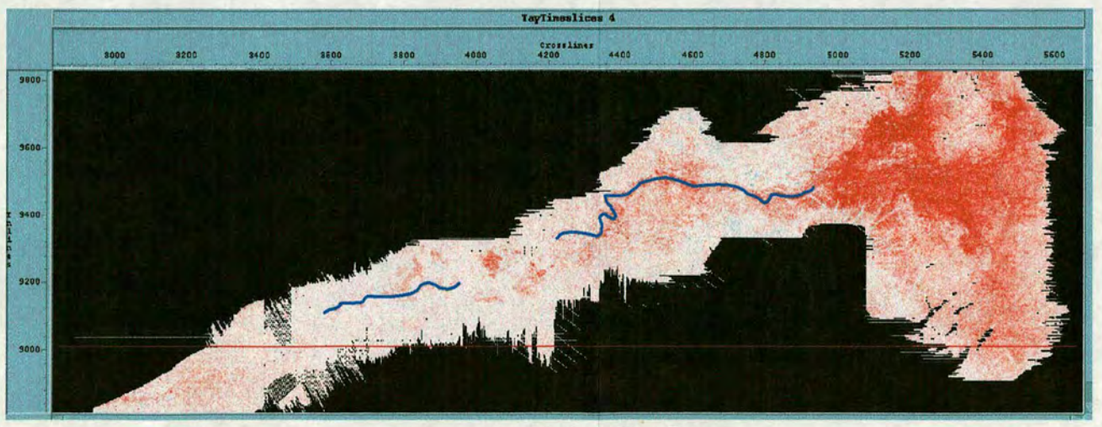

4 ms below Top Tay

Figure 3.27: Channel pathway traced on horizon slices hanging off the Top Tay reflector to evaluate the changes in sinuosity and path of the channel over time. See Fig. 3.28 for the results.

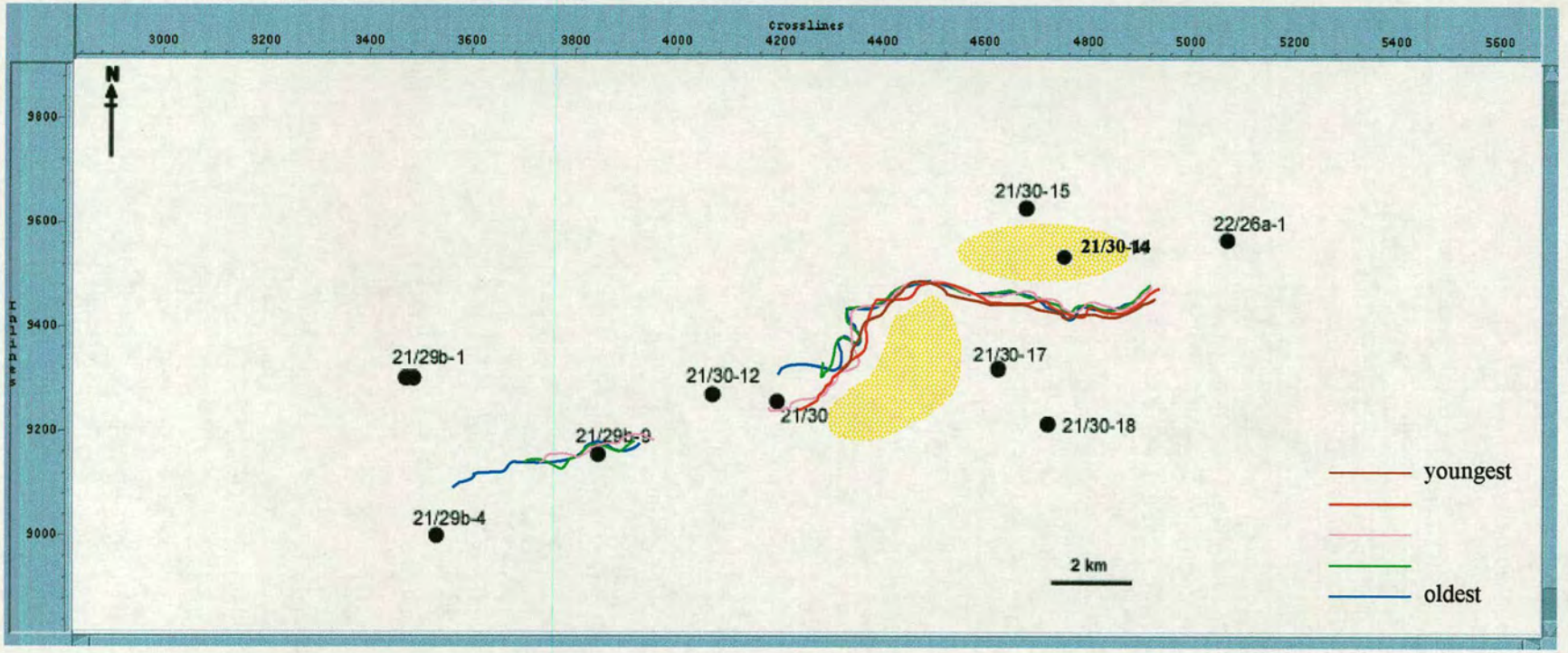

Figure 3.28: Traced channels superimposed on each other to delineate channel evolution over time. Figure highlights there has been no major changes in the channel pathways. It also shows slight increase in sinuosity in basin II with prospective sand deposition. See text for interpretation.

3.6 Conclusions

Interpretation of the high-resolution three-dimensional seismic data within the Gannet South area provides unique insights into controls on the architecture of the Eocene Tay Sandstone Member deposition system. The Tay Sandstone Member deposition system in the Gannet South area represents a single channel system, which was traced continuously for about 30 km from the toe of the shelf to the fan in the main subbasin. This channel is believed to transport sediment northeast-eastwards on the basis of the deepening and broadening of the system in the east, which reflects the channel building into a fan geometry at its terminus. The sheet-like nature of the Tay Sandstone Member within the Gannet South area permits relatively easy correlation. However, there are marked facies changes within the formation, and correlation of individual layers is difficult at some places.

The data presents an excellent example of the geometry and stratigraphic architecture associated with deep-water turbidite sands. Sands are clearly observed interacting with one another and the basin palaeotopography during deposition. It is apparent that the Tay Sandstone Member is relatively thin in this area as the maximum thickness is no more than 141 ms (approximately 700 ft). The thickest Tay package has been deposited on the basin floor where the system fans out. The fan has taken an asymmetric lobate shape.

Interpretation of the seismic data has revealed the important role that topography plays in controlling the spatial geometry and the temporal evolution of the submarine depositional system. In the Gannet South area the factors controlling the topography of the basin in which Tay sands are deposited can be categorised into three main groups; the west-east oriented slope, salt induced highs and highs produced by previous depositions. Although all these factors played a major role, salt induced highs are thought to be principally responsible for controlling the overall locus of the Tay Sandstone Member deposition as they divided the basin into three sub basins separated by salt domes providing accommodation space for the sediments. These salt domes acted as obstacles to the flow and, hence, had an important influence in

controlling channel pathways. Salt movement prior as well as during and after deposition is evident in this area and had an impact on the spatial and temporal distribution of the sediments. The onset of basin filling is interpreted to have started first in the subbasin close to the shelf and progressed successively seaward as each basin is filled to a spill point (fill and spill model). In general, the simplicity of the structure and depositional model for the Tay Sandstone Member presents an ideal depositional system for seismic trace shape analysis using a continuum of data sets from the low resolution three dimensional seismic data to the higher resolution facies description.

Chapter Four

Chapter Four

Sedimentological and Petrophysical Framework

4.1 Introduction

In order to make a meaningful seismic attribute analysis it is crucial to calibrate it with core data. Cores provide us with the only direct view of what the studied subsurface looks like. Therefore, the value of adequate core description cannot be overstated. Detailed sedimentological analysis leading to specific interpretation of depositional processes relies on core material.

In recent years, newer multidisciplinary techniques of high-resolution sequence stratigraphy have increasingly relied on core-derived data to calibrate and explain the attributes of lower-resolution data types such as wireline logs and, more still, 3D seismic datasets. Core-derived petrophysical parameters can be used to calibrate wireline logs and can thus feed into the explanation of different seismic attributes establishing a direct link between the different seismic facies and real subsurface geology.

This chapter is intended to give an evaluation of the sedimentological facies observed in the wells as well as the results of petrophysical analysis of wireline logs. These will provide the means for qualitative correlation to the seismic attributes that will be studied in the following chapters. A lithofacies scheme is developed for the Tay depositional system within Gannet South Field. The scheme consists of seven lithofacies, which are described and then analysed in terms of process and environment of deposition. These lithofacies are then linked to wireline logs to investigate if they have characteristic response specific to each lithofacies. This analysis is also carried out on the depositional units comprising the Tay Sandstone

Member to check if they have characteristic wireline log response specific to each depositional unit. The core description was carried out at DTI's core-store in Edinburgh.

4.2 Datasets and Research Methods

The turbidite fan system investigated in this study is the Tay Sandstone Member in the Gannet South area. To date, 10 wells have been drilled in the area providing some 980 ft of core and different wireline logs. The ten wells are: 21/29b-1, 21/29b-4, 21/29b-9, 21/30-12, 21/30-14, 21/30-15, 21/30-16, 21/30-17, 21/30-18 and 22/26a-1. All wells encountered Tay sands except 21/29b-1 and 21/30-18. However, none of these cored sections cover the whole Tay interval within that well. Fig. 4.10c indicates the cored depths within each well.

Based on lithology, grain size, visually estimated silt/clay content, bed thickness, and the presence or absence of specific primary sedimentary structures, the following seven lithofacies types are designated:

1. **Massive Sandstone**
2. **Thick-Bedded Sandstone**
3. **Medium-Bedded Sandstone**
4. **Thin-Bedded Sandstone**
5. **Parallel Laminated Siltstone**
6. **Bioturbated Siltstone**
7. **Clay and Mud Stone**

The wireline data from the ten wells were then analysed. The lithofacies developed were correlated to wireline data in order to check if there is a typical response from each of the lithofacies. Particular emphasis was given to gamma ray logs, which measure the amount of natural radioactivity of the formation against depth. The primary application of the gamma ray log is lithology identification and will be later

compared with acoustic impedance data to give geological meaning to the seismic. The gamma-ray log is particularly useful in the delineation of shale beds. Sonic and density logs were also checked. There is usually a mismatch between the core depths recorded by the drillers and the wireline logs depth recorded by the wireline tools. Therefore a shift in core depths is needed to match the core to the wireline logs character representing the core facies. Overall, the shift is minimal in most of the wells.

4.3 Core Description

In general the Tay package sampled by the ten wells in Gannet South consists of thin but high quality reservoir sands. The main exception to this is the thick sand package encountered by well 22/26a-1.

A description of the seven lithofacies types designated for the sediments in the Tay depositional system is provided below, along with comments relating to interpretation of the possible depositional processes and typical wireline log responses. The full spectrum of lithofacies is discussed in order of decreasing sand content. In this order they collectively describe the fining downward profile. Codes are indicated in brackets. The lithofacies are then summarised in Fig. 4.8 and typical log responses in Fig. 4.9. The core description logs for each of these wells are available in Appendix 3.

The definition of laminae and bed thicknesses used within the core description are those defined by Pickering *et al.* (1989). Laminae refers to laminations of 1-10mm, very thin beds are 1-3cm, thin beds are 3-10cm, medium thickness beds are 10-30cm, thick beds are 30-100cm and very thick beds are >100cm.

LITHOFACIES 1: Massive Sandstone (MS)

Description: This facies comprises light brownish grey, massive, poorly consolidated, beach like sandstone (Fig. 4.1). The sands are fine-grained and are deprived of any grading. Generally, no sedimentary structures or bed boundaries are evident and mud-clasts and water-escape dish structures and pipes are sparse.

Interpretation: This facies is thought to have been deposited by high-density turbidity currents. The facies is comparable to division A of Bouma's (1962) classic model for turbidity currents and S_3 of Lowe (1982) and was deposited by direct and rapid suspension sedimentation from a high-density turbidity current. Collapse of bed during or after deposition results in the escape of excess pore fluids forming the dish and pipe structures. This facies is typical of amalgamated channels or depositional lobes within the upper fan (Mutti and Ricci Lucchi, 1972)

Log Response: Massive Sands typically display a blocky pattern in gamma ray logs because of their uniform and low clay matrix. Thick, more than 30 feet, of uniform low gamma ray value (40-60 API) is usually observed. There are rare or no high gamma ray interbeds denoting very high net to gross. The log normally has a sharp base and sharp or gradational top. Similarly, density logs are characterised by abrupt decrease and increase in values at top and base of this facies respectively. The density log normally follows the gamma ray log character. The sonic log, on the other hand, goes in the opposite direction to both gamma ray and density logs. It indicates slow velocity for the top and a high sonic velocity for the base. The base of the sonic log is not as sharp as the top. (Fig. 4.9a)

LITHOFACIES 2: Thick-Bedded Sandstone (TBS)

Description: This facies comprises beds of light brownish grey to light grey or light brown, fine to medium-grained, poorly to moderately sorted sandstone. Bed thickness varies from 2 to 5ft. The beds are commonly separated by thin beds of bioturbated siltstone. The sandstone beds have abrupt irregular upper and lower boundaries. Individual beds are ungraded and occasionally poorly developed parallel lamination is observed. (Fig. 4.2)

Interpretation: This facies is interpreted as the deposits of turbidity currents. The mainly massive character of the beds suggests that suspension sedimentation from relatively high-density turbidity currents was the dominant process. The occasional parallel lamination is due to traction sedimentation during lower energy flow conditions (Pickering *et al.*, 1989). The relatively few thin-bedded siltstones, suggests lack of time for accumulation of background sediments, and/or erosion of background sediments by subsequent high-density turbidity currents. The facies are thought to be channel-fill or inner lobe deposits.

Log Response: This facies have uniform gamma ray values and a typical boxy log pattern. Low gamma ray values (20-30 API) are interbedded with very thin high values (70-80 API). The whole unit could be more than 30 feet thick indicating moderate to high net to gross. Sharp tops and bases are commonly seen. There is no typical response from the density logs although in general it displays the same pattern as the gamma ray log. Sonic log indicates slow to high velocity

values with no clear relationship to the lithology observed within the facies (Fig. 4.9b).

LITHOFACIES 3: Medium-Bedded Sandstone (MBS)

Description: This facies comprises light brownish grey to light grey or light to medium brown, fine-grained, moderately sorted sandstone. Bed thickness varies from 0.5 to 2 ft. The beds are commonly separated by bioturbated siltstone beds, which are much thicker intervals than the thin siltstone beds separating the thick-bedded facies. The beds are mostly massive and ungraded. Weak parallel lamination structures are rarely present.

Interpretation: This facies is interpreted as deposits of turbidity currents. The mainly massive charcater of the beds suggests that suspension sedimentation from relatively high-density turbidity currents was the dominant process. The occasional parallel lamination is due to traction sedimentation during lower energy flow conditions. The significant reduction in the thickness of the beds compared to the previous facies is thought to be associated with their depositional location in a more distal part of the system. This is further supported by the thicker intervals of the siltstones separating the medium sandstone beds.

Log Response: Gamma ray response from the medium-bedded sandstones is discrete. 15 to 30 ft thick blocky low (50 API) gamma ray responses from sands are separated by high responses from shales (100 API) of up to 20 ft in thickness. The units normally have sharp tops and bases. Sonic and density logs do not follow any particular character and indicate poor

correlation to the changes in lithology displayed within the facies (Fig. 4.9c).

LITHOFACIES 4: Thin-Bedded Sandstone (ThBS)

Description: This facies comprises thin beds of fine-grained, massive, moderately sorted, light grey sandstones stained brown with hydrocarbons alternating with planar laminated clays. The grain size within an individual sandstone bed is usually invariant and the upper and lower boundaries are abrupt and irregular. Small mud clasts are occasionally present towards the top of the sandstone beds. Bioturbation is absent (Fig. 4.3). The interbedded clays are dark grey and planar laminated resembling Lithofacies 7 described below.

Interpretation: Due to the lack of bioturbation and the massive character of the thin-bedded sandstones, the units are interpreted to result from rapid deposition of suspension sediments from low-density turbidity currents. According to Stow & Shanmugam (1980), this facies occurs closer to channels and on lobes but in a more distal part of the system compared to the previous facies.

Log Response: Overall the gamma-ray pattern for this facies is serrated with rapid alteration between sands and shales. Thin beds of sands, about 15ft thick, form more than 50% of the package. The units normally have sharp tops and bases. Typically, density log is parallel to the gamma ray log. The changes in sonic log do not always occur along with variation in the gamma ray (Fig. 4.9d).

LITHOFACIES 5: Parallel Laminated Siltstone (PLS)

Description: The colour of this facies varies from medium to dark greenish grey to dark grey. Thin, parallel, horizontal lamination is the definitive characteristic of this facies. The grain size is fairly consistent and the upper and lower boundaries are mostly sharp but sometimes transitional to lithofacies 6 or 7 (Fig. 4.4).

Interpretation: This facies is interpreted to have been deposited by low-density flows and from suspensions fed by turbidity currents, in a low energy environment. Traction effects are recognised by the formation of parallel laminations (e.g. Stow & Shanmugam, 1980). Lack of bioturbation in this facies is thought to be attributed to anoxic conditions during deposition.

Log Response: Overall gamma-ray pattern for this facies is serrated. The gamma ray shows slightly spiky character. Density log is also serrated but does not always have the same character as the gamma ray log. Sonic log values are generally high (40 μs/ft) but there are spikes towards the low values (Fig. 4.9e).

LITHOFACIES 6: Bioturbated Siltstone (BS)

Description: This facies comprises medium greenish grey to medium grey or medium reddish brown siltstone, which locally grades to very fine-grained silty sandstone. Occasionally the siltstone is laminated dark grey. No sedimentary structures are apparent due to the extensive bioturbation. Trace fossils (burrows) are recognised. The grain size of the siltstone is mostly invariant or does not appear to change systematically. The top and low boundaries are sharp although irregular (Fig. 4.5).

Interpretation: The evidence for the mechanisms involved in the deposition of this facies has been destroyed by bioturbation. The parallel lamination occasionally present in the finer grained siltstone probably indicates low energy traction and suspension sedimentation. The association with occasional thin-bedded sandstone of turbiditic origin suggests that the siltstone facies may also have a turbidite origin, representing the distal facies deposited by low-density currents and suspension sedimentation. The extent of bioturbation in the siltstone facies indicates that the environment of deposition was highly oxygenated (Pickering *et al.*, 1989).

Log Response: Wireline log response for this facies are very much similar to the one described for parallel laminated Siltsones. The gamma ray pattern is serrated and shows a slightly spiky character. The density log is also serrated but is not always parallel to the gamma ray log. Sonic log values are generally high (120 μs/ft) but there are spikes towards the low values. (Fig. 4.9e)

LITHOFACIES 7: Clay and Mudstone (CMS)

Description: The colour of this facies has a wide spectrum as it varies from medium reddish brown to medium greenish grey to medium to dark grey to black. It is the finest grained of all the facies. Within some sections of the core, the claystone occurs in thick, homogeneous units, where no sedimentary structures are apparent as illustrated in Fig. 4.6. The upper and lower facies boundaries are usually sharp. At other parts, thin, parallel, horizontal lamination is the definitive characteristic of this

facies (Fig. 4.7). It is carbonaceous, slightly pyritic but rarely bioturbated.

Interpretation: The facies is interpreted as the background sedimentation of hemipelagites and/or pelagites. Sediments may have been transported as suspended load in bottom currents. Hence particles or particle aggregates settled from suspension in a protected, low-energy, offshore outer shelf-deeper marine anoxic basin. Anoxic conditions favour the preservation of organic matter and results in a lack of bioturbation (Ravnas & Steel, 1998). This facies is dominant away from the channel axes on levees and interchannel areas, and in the outer fan and abyssal plain environment (Stow & Shanmugam 1980).

Log Response: The hemipelagic muds have the effect of increasing gamma ray and decreasing sonic values. The logs response is generally monotonous without coarsening or fining upward trends. The relatively high gamma ray signature (80-100 API) represents clastic starvation at times of maximum transgression of the shoreline. Density and sonic logs are serrated (Fig. 4.9f).

Figure 4.1: LITHOFACIES 1: Massive Sandstone

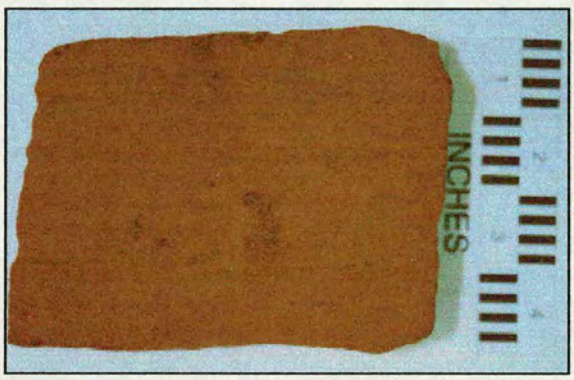

Figure 4.2: LITHOFACIES 2: Thick-Bedded Sandstone (TBS)

Figure 4.3: LITHOFACIES 4: Thin-Bedded Sandstone (ThBS)

Figure 4.4: LITHOFACIES 5: Parallel Laminated Siltstone (PLS)

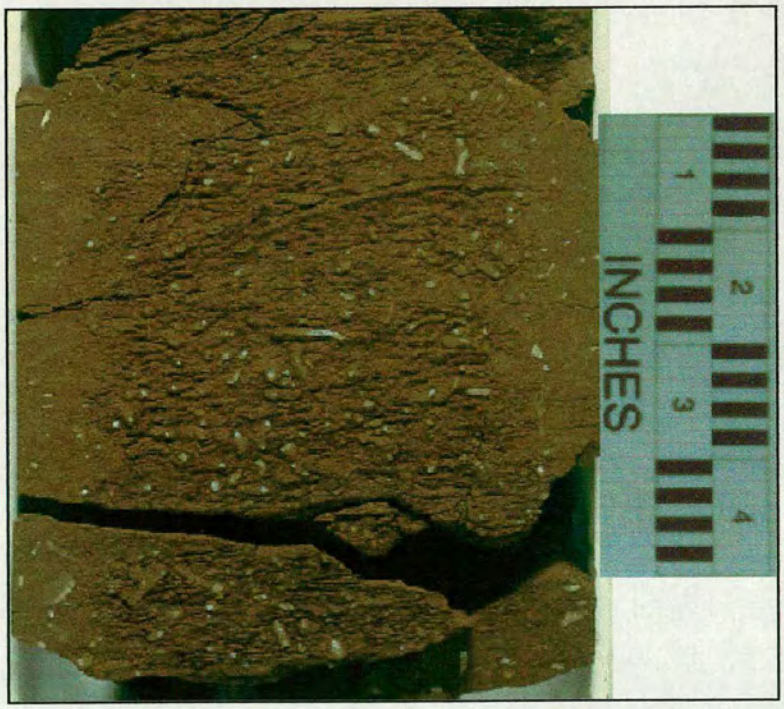

Figure 4.5: LITHOFACIES 6: Bioturbated Siltstone (BS)

Figure 4.6: LITHOFACIES 7: Clay and Mud Stone (CMS)
Homogeneous mud.

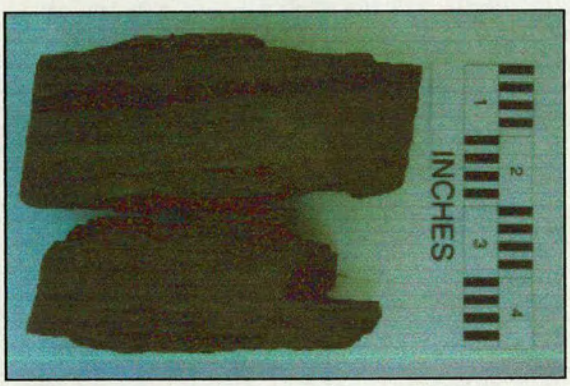

Figure 4.7: LITHOFACIES 7: Clay and Mud Stone (CMS)
Parallel laminated mud.

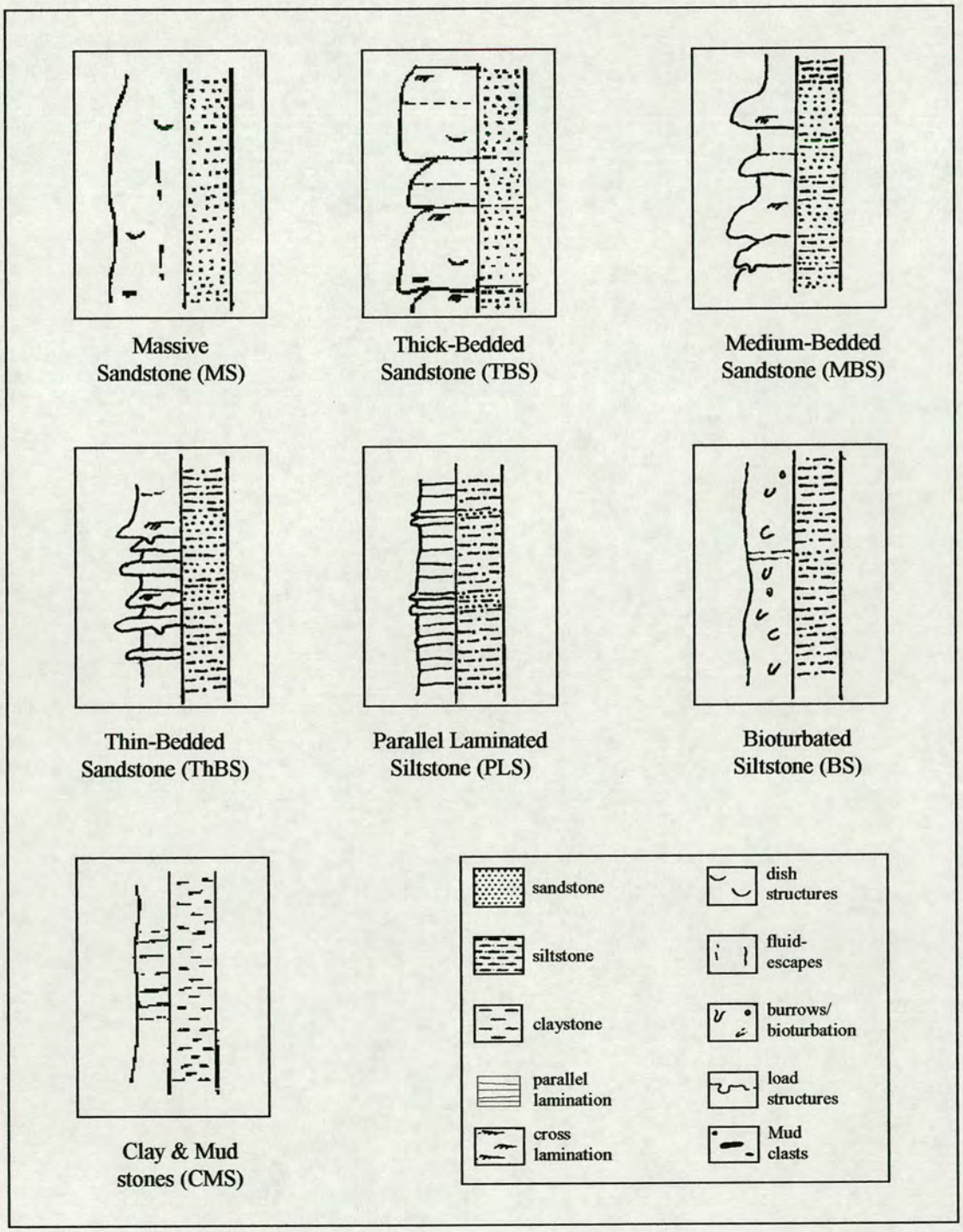

Figure 4.8: Summary of the lithofacies observed within the Tay system of the Gannet South area.

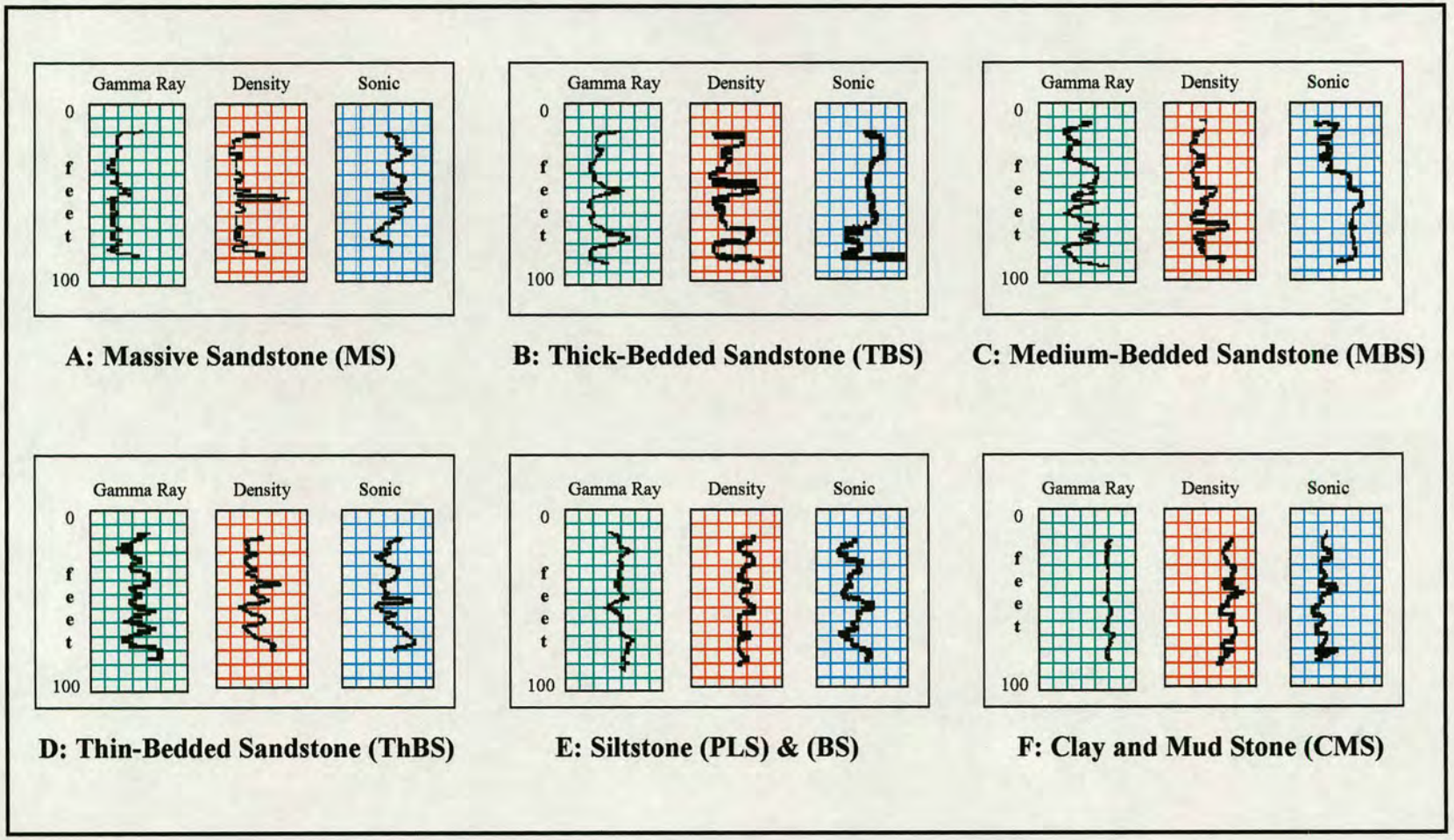

Figure 4.9: Schematic log responses for the different lithofacies observed in the wells. Gamma ray and density increase toward the right whereas sonic increases towards the left. Fig. 4.10 and Fig. 4.11 give complete log responses of the Sandstone Member.

4.4 Facies Associations

In this section the individual lithofacies that are considered to be genetically or environmentally related to each other are grouped into facies associations in order to examine the relationship of one lithofacies to the other. The results provide the basic building blocks for the vertical and lateral variation in depositional environments evident from the well data. The following facies associations are recognised:

4.4.1 Massive sandstone facies association

This facies association comprises all the sediments deposited from the main body of medium to high density turbidity currents. Massive to medium-bedded, amalgamated massive sandstone units, of tens of meters in thickness form this facies association. Lithofacies 1, 2 & 3 can be grouped together to make up this association. Very thin to thin clay intervals may separate the massive sandstone beds. Examples of this facies association are mainly seen in well 22/26a-1 where almost the whole cored section is of amalgamated sandstone beds (see Appendix 3 for the cored section).

These sandstone units are thought to have been deposited by medium to high-density turbidity currents. The facies association is comparable to class B of Pickering *et al.* (1989) and was deposited by direct and rapid suspension sedimentation from a high-density turbidity current. It is typical of amalgamated channel-fills or depositional lobes within the middle to upper fan (Mutti and Ricci Lucchi, 1972). The occasional parallel lamination is due to traction sedimentation during lower energy flow conditions (Pickering *et al.*, 1989). The relatively few thin-bedded siltstones, suggests lack of time for accumulation of background sediments, and/or erosion of background sediments by subsequent high-density turbidity currents. The facies are thought to be channel-fill or inner lobe deposits. Collapse of bed during or after deposition results in the escape of excess pore fluids forming the dish and pipe structures.

4.4.2 Heterolithic facies association

This facies association comprises successions of planar laminated mudstones interbedded with laminations of silt and/or thin bedded turbidite sandstones. Lithofacies 4, 5 & 6 are grouped together to make up this facies association which is observed in almost all the wells (e.g wells 21/29b-9 & 21/30-17, see Appendix 3 for the cored section) within the Gannet South area with the exception of well 22/26a-1. Occasionally the siltstone is extensively bioturbated and trace fossils (burrows) can be recognised.

This facies association can be interpreted as deposits of channel-levee complexes resulting from overbank deposits and/or interchannel or basin plain environment deposition from distal turbidity currents. Overbank deposits can be laterally extensive and occur adjacent to the main channels or confined flows in turbidite systems (Mutti & Normark, 1991). The extent of bioturbation in the siltstone facies indicates that the environment of deposition was highly oxygenated (Pickering *et al.*, 1989).

4.4.3 Mudstone facies association

This facies association consists mainly of lithofacies 7 which is principally clay and mudstones which are hemipelagic to pelagic in nature. It is thought to have been deposited in a protected, low-energy, sediment-starved, marine environment.

4.5 Well Correlation

Based on biostratigraphic data and wireline log response, mainly gamma ray, the Tay Sandstone Member in Gannet South area is generally divided into four Biozones:

- Basal Tay: This is the oldest unit in the Formation. It contains interbedded sands and shales in some parts of the Gannet South area whereas shales dominate other parts. Overall the unit shows a crescent shaped gamma ray log character denoting a start with prograding sequence and ending with a transgression. However, some

wells, e.g. 22/26a-1, only show the progradation part. This could be due to erosion of the upper transgressive deposits by subsequent high-density turbidity currents or the upper part not being deposited in the first place. Fig. 4.12 shows the gamma ray response of this unit taken from the eight wells that encountered the Tay Sandstone Member. The unit is thickest in well 21/29b-9 where the gamma ray log shows several cycles of crescent shaped character. Well 21/30-15 encountered the thinnest unit. The term Basal Tay is used instead of Lower Tay because the latter was used for sands that are now known as Rogaland Sand.

- Middle Tay: This is the thickest of the four units within the Tay Sandstone Member. Although it is thickest in well 21/30-17, the highest net to gross is observed in well 22/26a-1. The rest of the wells display low or moderate sand content within the zone. Fig. 4.13 shows gamma ray response of the eight wells that encountered the unit.

- Upper Tay B: This unit is absent in well 21/29b-9 but present in all other wells that encounter the Tay Sandstone Member. The unit in 22/26a-1 is dominated by sand in contrary to the rest of the wells where it is dominated by shales. As seen in Fig. 4.14, the unit is thickest in well 22/26a-1. This means the flow at the time of lowstand carried all the sediments to the main subbasin (subbasin III) bypassing all the other subbasins but when the basin became sediment starved during sea-level rise shales were deposited at other locations.

- Upper Tay A: This zone encompasses the youngest Tay sand within the Formation. It represents the latest stage of the system development immediately prior to its abandonment. The unit exhibits facies MS described in the previous section and is only observed in cores of wells 21/29b-9 and 22/26a-1. It seems to be thickest within these two wells but based on gamma ray response it is also present in some of the other wells, which have not been cored at its level. See Fig. 4.15.

Based on this subdivision two correlation panels are produced to provide a chronostratigraphic framework for the Tay system. The WSW-ENE correlation panel, seen in Figs. 4.10a, b & c, covers a distance of approximately 30 km. The positions of wells relative to each other are given in the small box. The panel clearly indicates the structural deepening of the Formation towards the ENE. Wells 21/30-12, 21/30-14 and 21/30-17 are structurally higher because they have been drilled on flanks of structural highs induced by salt domes. This is discussed in the seismic interpretation chapter. It is apparent from the seismic interpretation chapter that this correlation panel displays the axial direction of the channel belt, which fans out at the main receiving basin. This basin is penetrated by well 22/26a-1 as discussed earlier. Fig. 4.10c provides a detailed version of the correlation flattened at Top Balder Formation. The detail is based on gamma ray signature as well as lithology observed in the cored sections whenever available and the biostratigraphic subdivision pointed out above.

The second well correlation panel, seen in Figs. 4.11a & b, runs north to south; i.e. perpendicular to the direction of channel flow. This is obvious as the Formation thins towards well 21/30-15 in the north and pinches out towards the south in well 21/30-18. It is better illustrated by Fig. 4.12b where flattening has been applied at the top of the Tay Sandstone Member.

It should be noted that correlation based on biostratigraphy links units of the same age, however, this does not necessarily mean that individual beds within a unit are laterally continuous from one well to the other. Subsurface correlation of stratigraphic intervals can be quite difficult since actual rock geometries and interfingering relationships cannot be visualised. This is particularly true within complex stratigraphic sections that have a degree of lateral and vertical variability.

Evaluating the different wells in terms of the amount of sand to the total thickness of the Tay Sandstone Member, (Net/Gross) values, indicates that the Tay depositional system is relatively sandy (Table 3.1).

Well	Gross (ft)	Net (ft)	N/G (%)	GR-Cut-off
21/29b-1	0	0	0	N
21/29b-4	188	11	6	35
21/29b-9	237	87	37	50
21/30-12	158	46	29	70
21/30-14	194	63	33	70
21/30-15	78	9	12	40
21/30-16	158	57	36	60
21/30-17	277	49	18	55
21/30-18	0	0	0	N
22/26a-1	329	189	57	30

Table 4.1: Summary of the Net-to-Gross values of the ten wells in the Gannet South area.

4.6 Discussion & Conclusions

This chapter provides an evaluation of the sedimentological facies observed in the wells drilled in the Gannet South area as well as the results of petrophysical analysis of wireline logs. Detailed core descriptions led to a seven lithofacies scheme to be developed, which ranged from massive and thick bedded sandstones to monotonous clay and mudstones.

None of the sandstone beds display the typical Bouma sequence. Indeed none of the cross-laminated facies are observed and coarse sand and gravel are completely absent. Beds are fine to medium grained and moderately sorted from top to bottom. They lack clear fining-upwards sequences, probably due to extensive pre-sorting on the shelf. Individual beds are not much thicker than a few feet. They are mostly deprived of any structures with the exception of containing evidence of rapid pore-

fluid dewatering features such as dish and pipe structures. However, the sands are partially consolidated and sedimentary structures are poorly preserved. The beds have abrupt irregular upper and lower boundaries.

Four correlation panels illustrate the variation in character and thickness of the different Tay depositional units within the Gannet South Field. The WSW-ENE correlation panel clearly indicates the structural deepening of the Formation towards the ENE. This panel displays the axial direction of the channel belt, which fans out at the main receiving basin. This basin is penetrated by well 22/26a-1. The N-S panel is perpendicular to the direction of channel flow. This is obvious as the Formation thins towards the north and pinches out towards south as illustrated by Fig. 4.12b where flattening has been applied at the top of the Tay Sandstone Member.

It should be noted that correlation based on biostratigraphy links units of the same age, however, this does not necessarily mean that individual beds within a unit are laterally continuous from one well to the other.

The developed sedimentological facies scheme with the corresponding gamma ray response can now be linked to the seismic attributes once the seismic to well ties are established, which is the task of the next chapter. Based on the success of the seismic to well tie, the usefulness of these facies in terms of their recognition from the attribute analysis can be verified. It has already been demonstrated in this chapter that some of these facies (e.g. Lithofacies 3 & 4) do not have characteristic sonic and density log response, which are principal properties for the generation of seismic response.

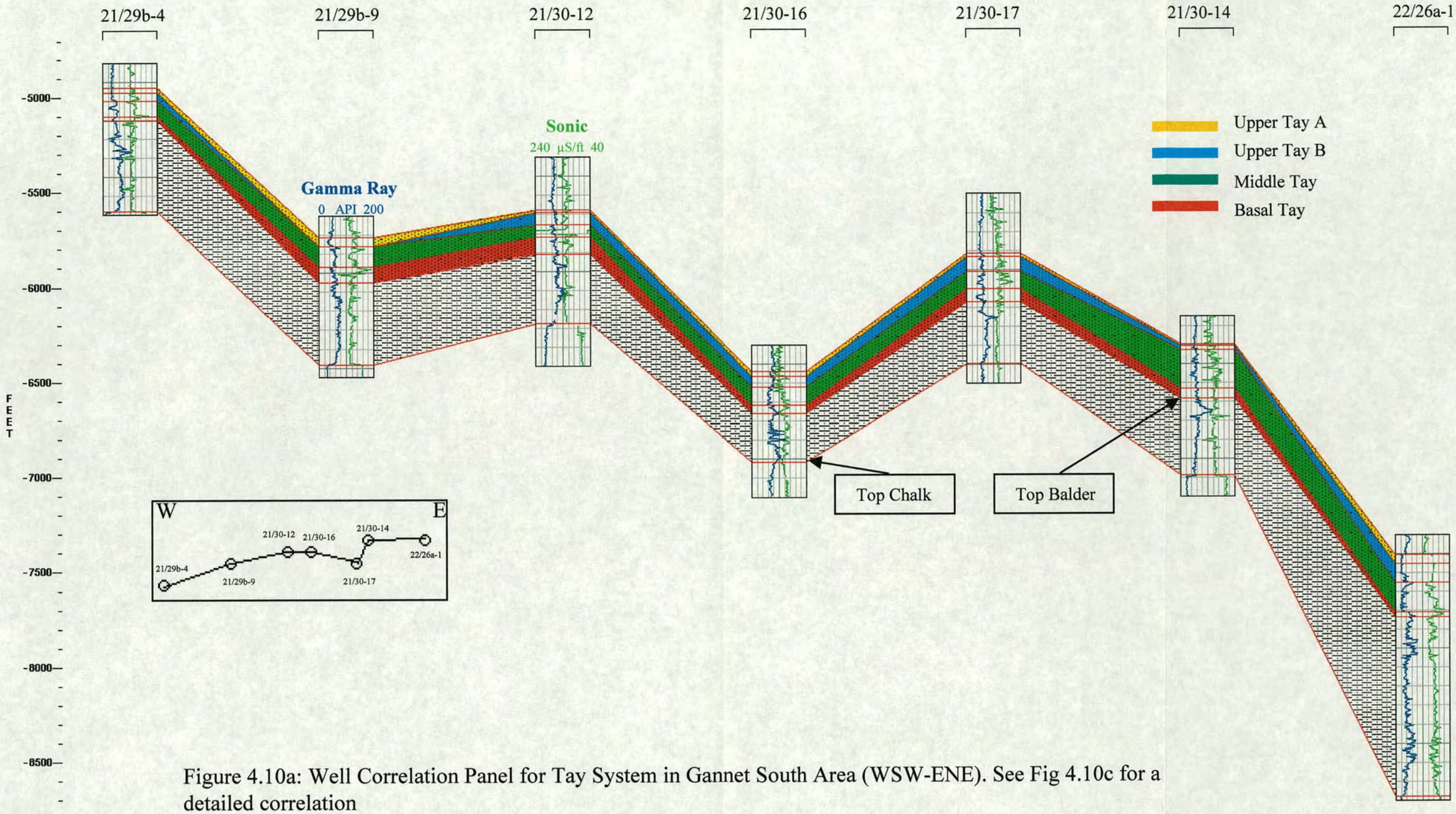

Figure 4.10a: Well Correlation Panel for Tay System in Gannet South Area (WSW-ENE). See Fig 4.10c for a detailed correlation

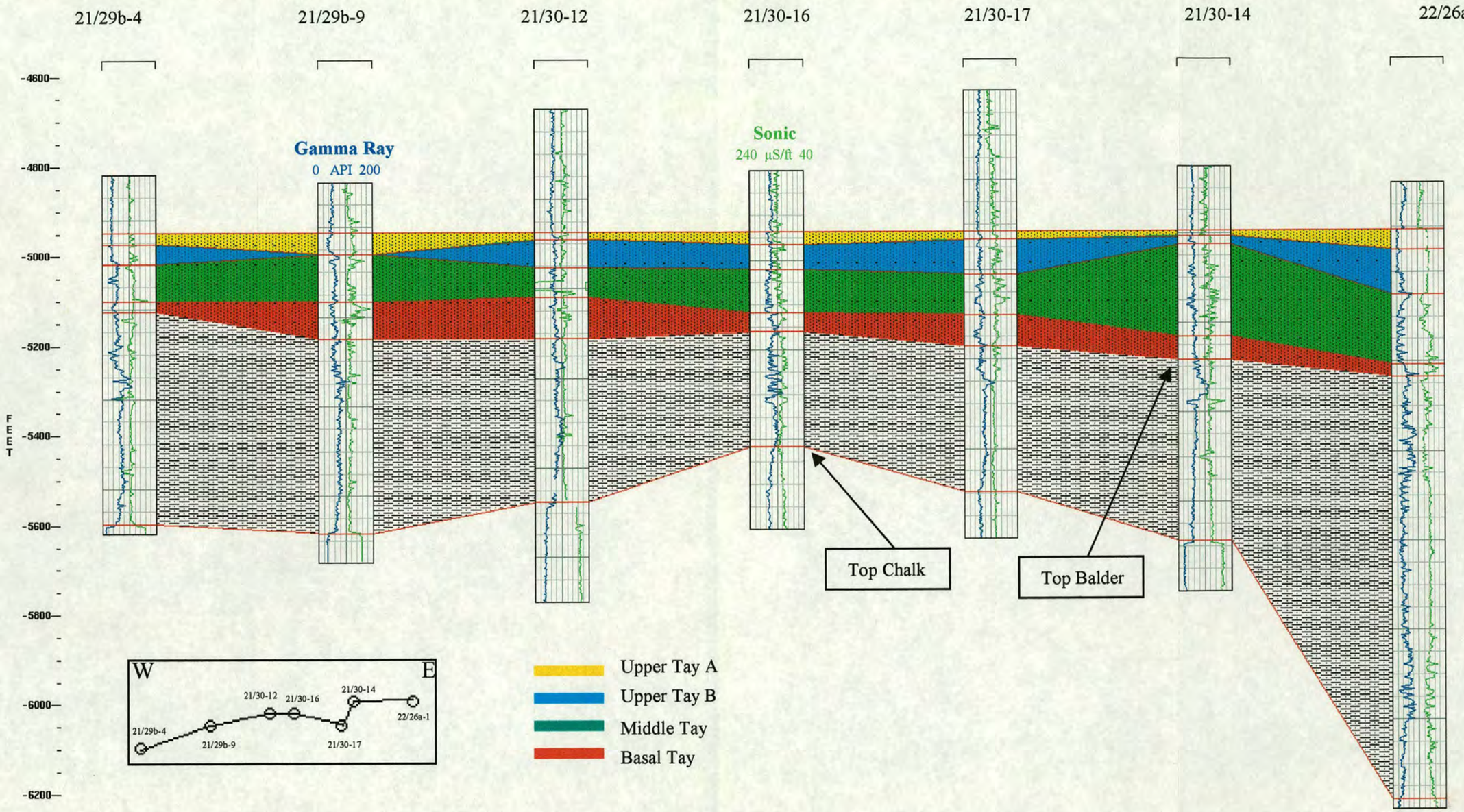

Figure 10b : Well Correlation Panel for Tay System in Gannet South Area (WSW-ENE). Flattened at Top Tay.

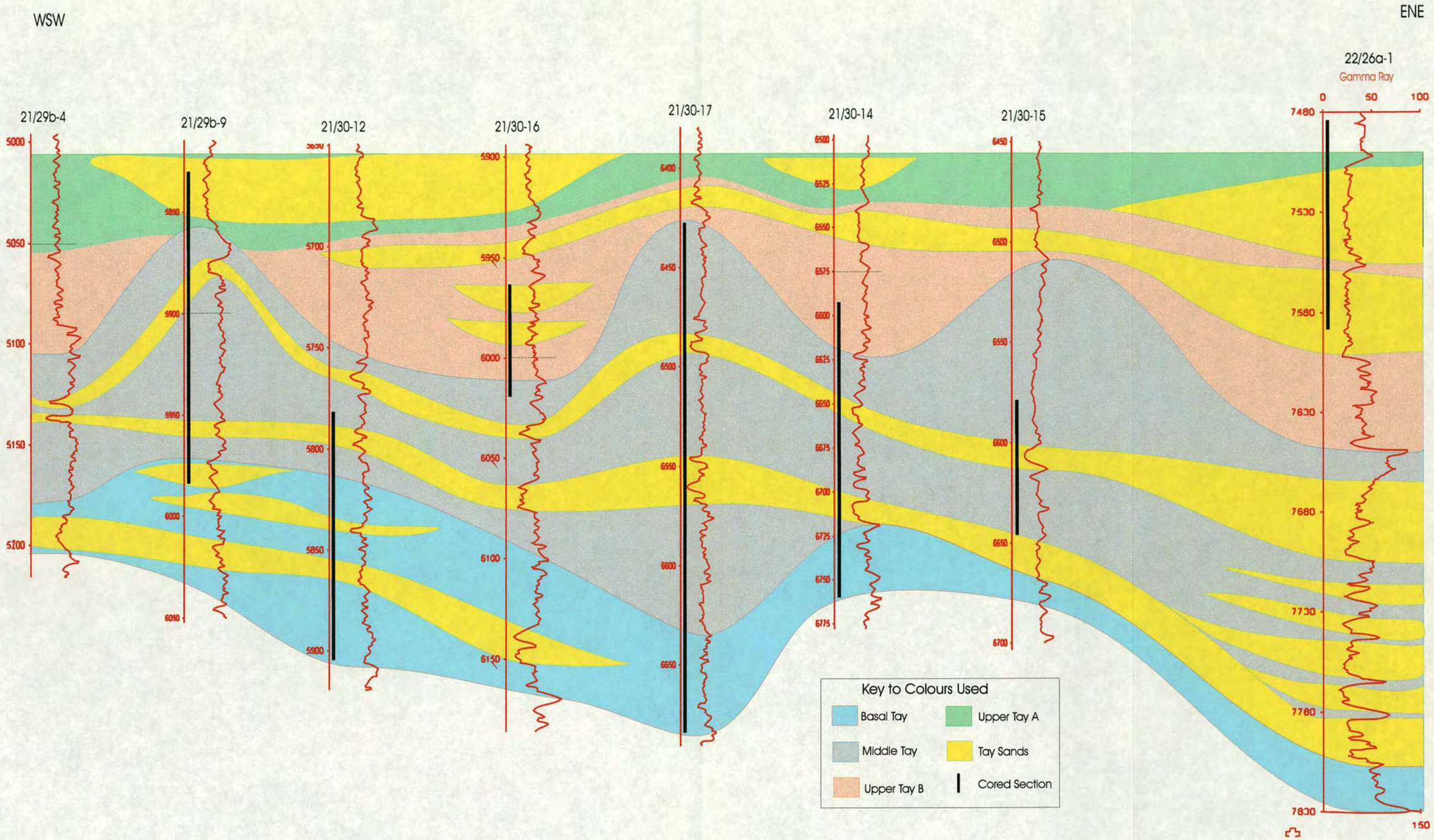

Figure 4.10c: Well correlation panel for Tay System in Gannet South area running WSW-ESE. Flattened at Top Tay and detailed based on Gamma Ray and core data. Tay subdivision is provided by combined wireline log and biostratigraphic data.

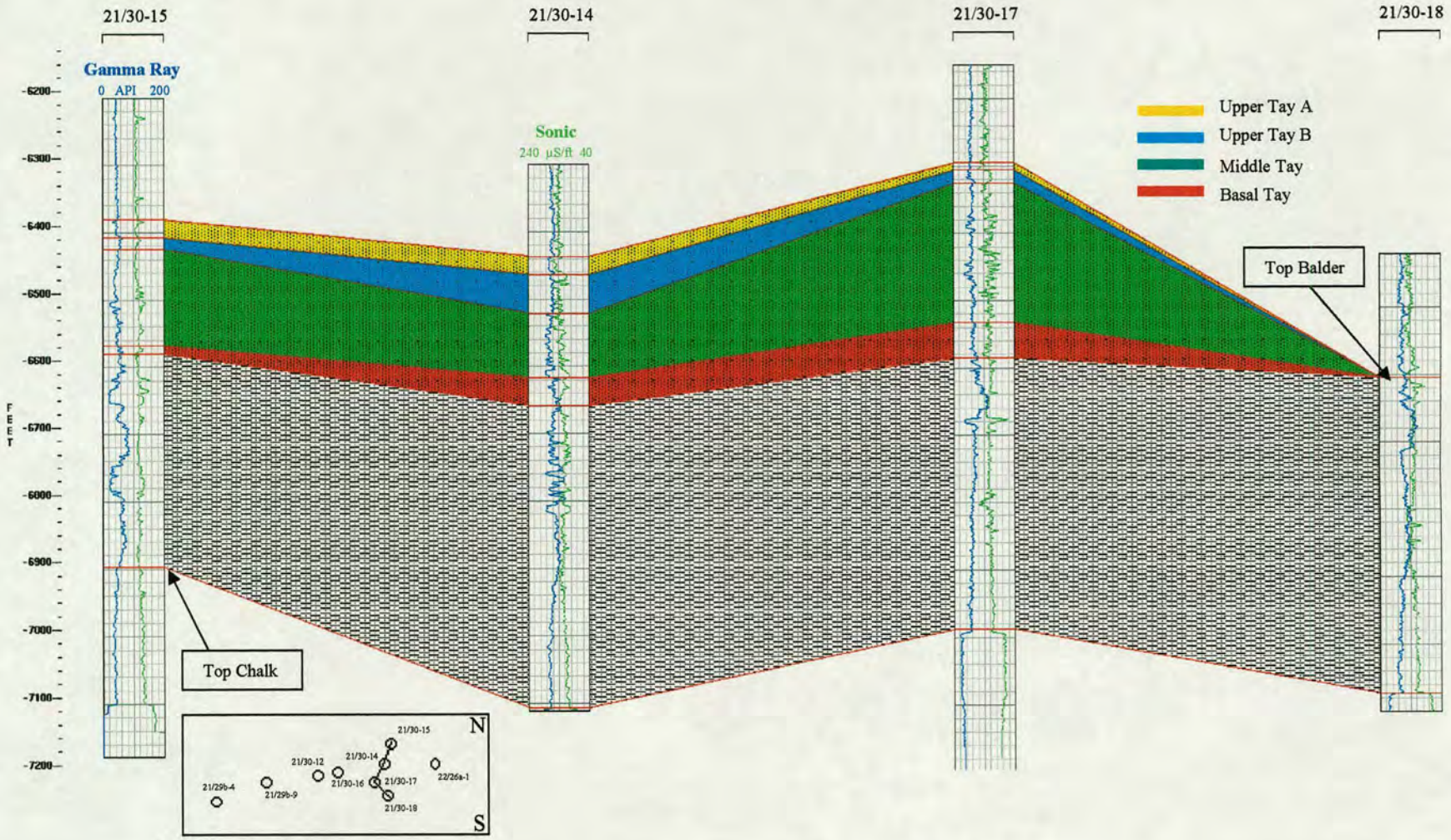

Figure 4.11a: Well Correlation Panel for Tay System in Gannet South Area (N-S)

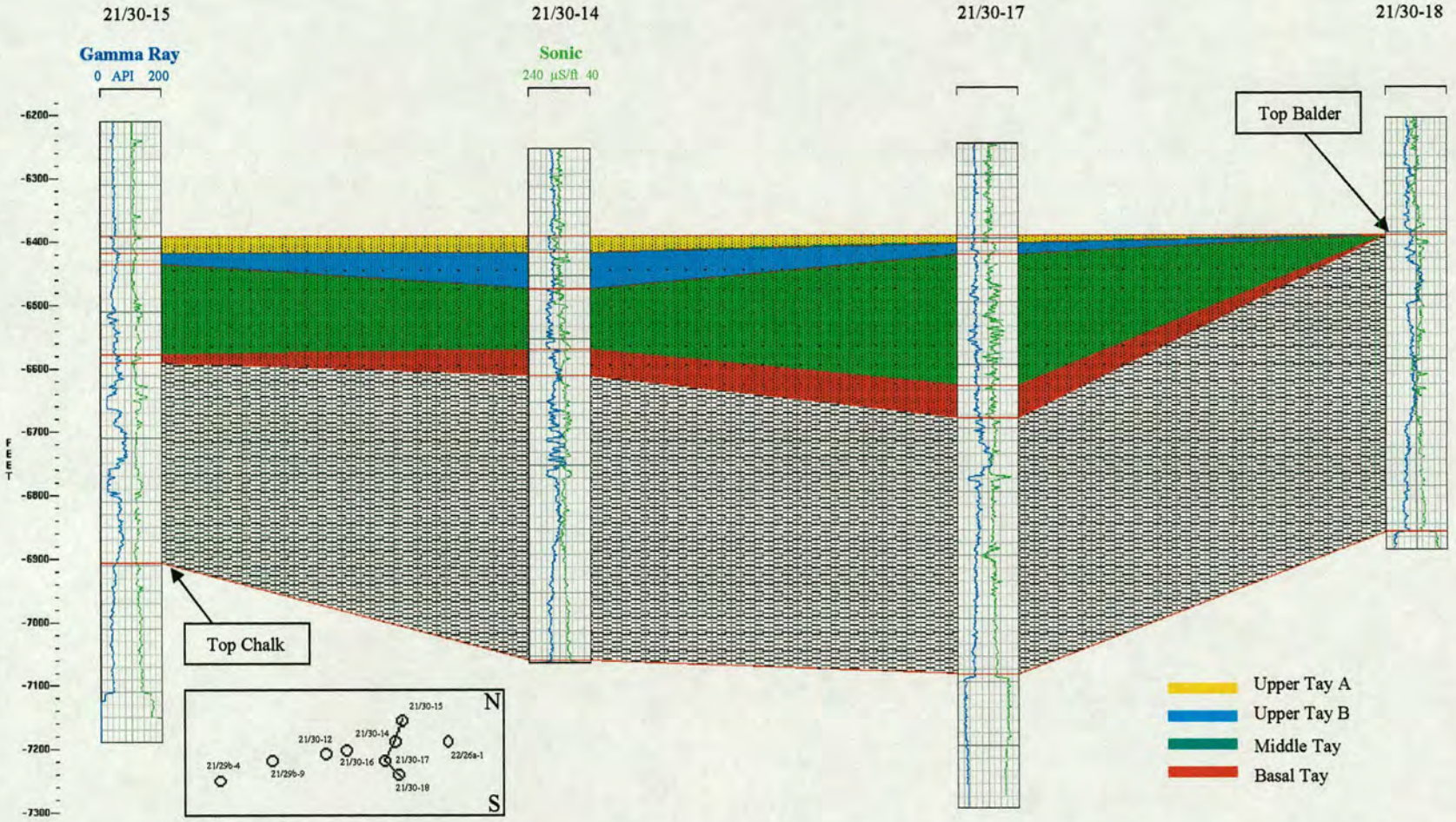

Figure 4.11b : Well Correlation Panel for Tay System in Gannet South Area (N-S) flattened at top Tay.

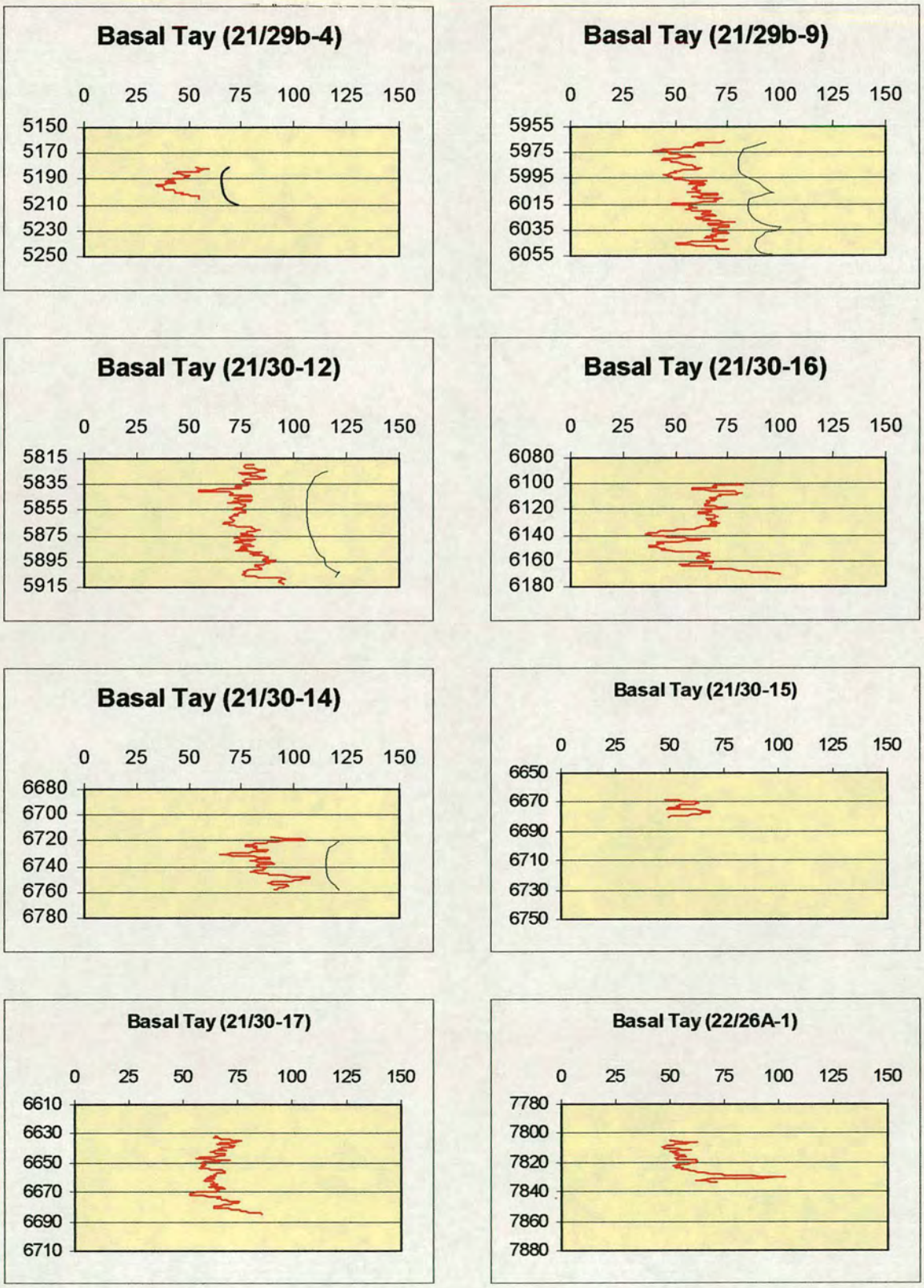

Figure 4.12: Gamma Ray responses of the Basal Tay Unit.

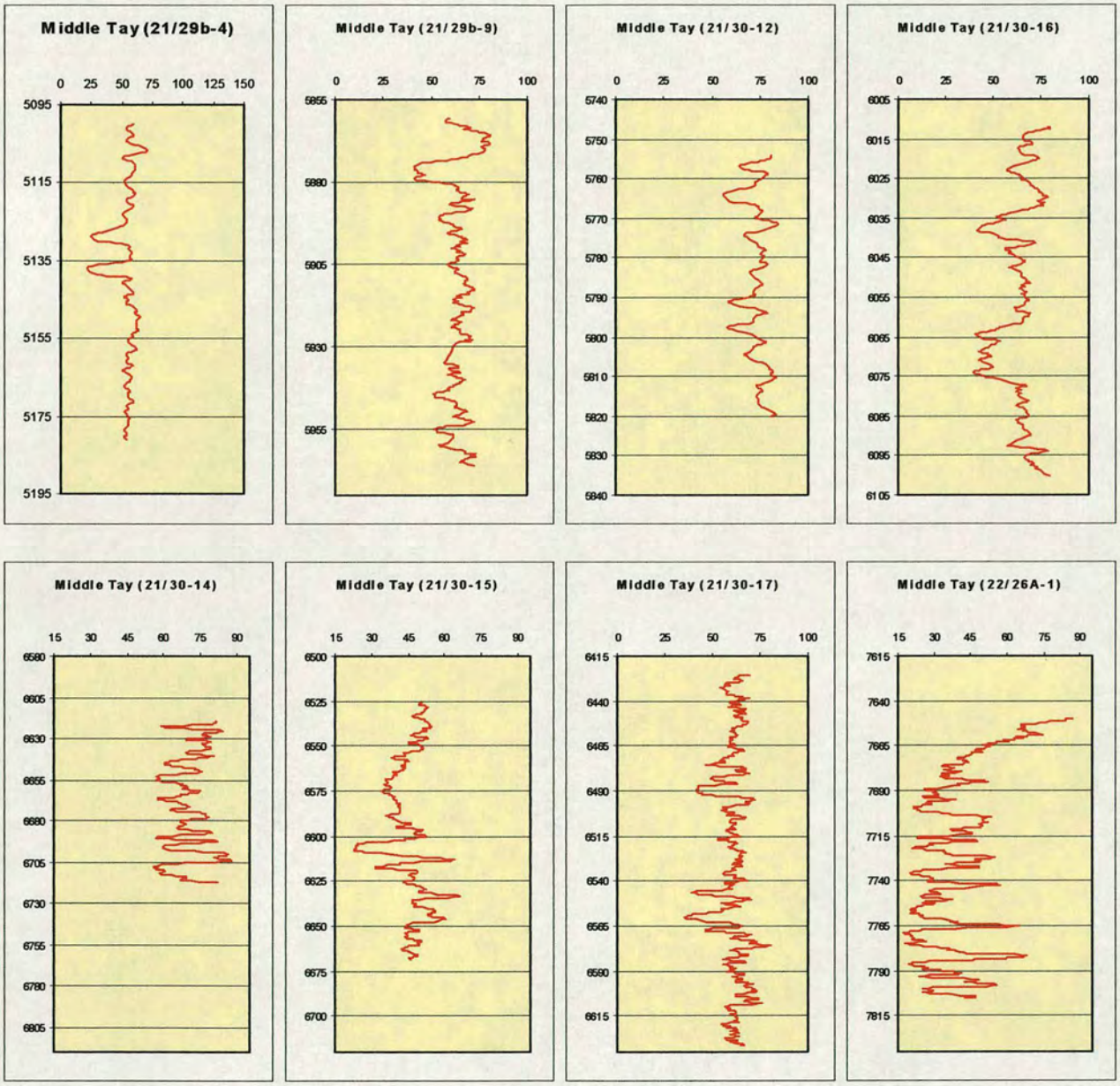

Figure 4.13: Gamma Ray responses of the Middle Tay Unit.

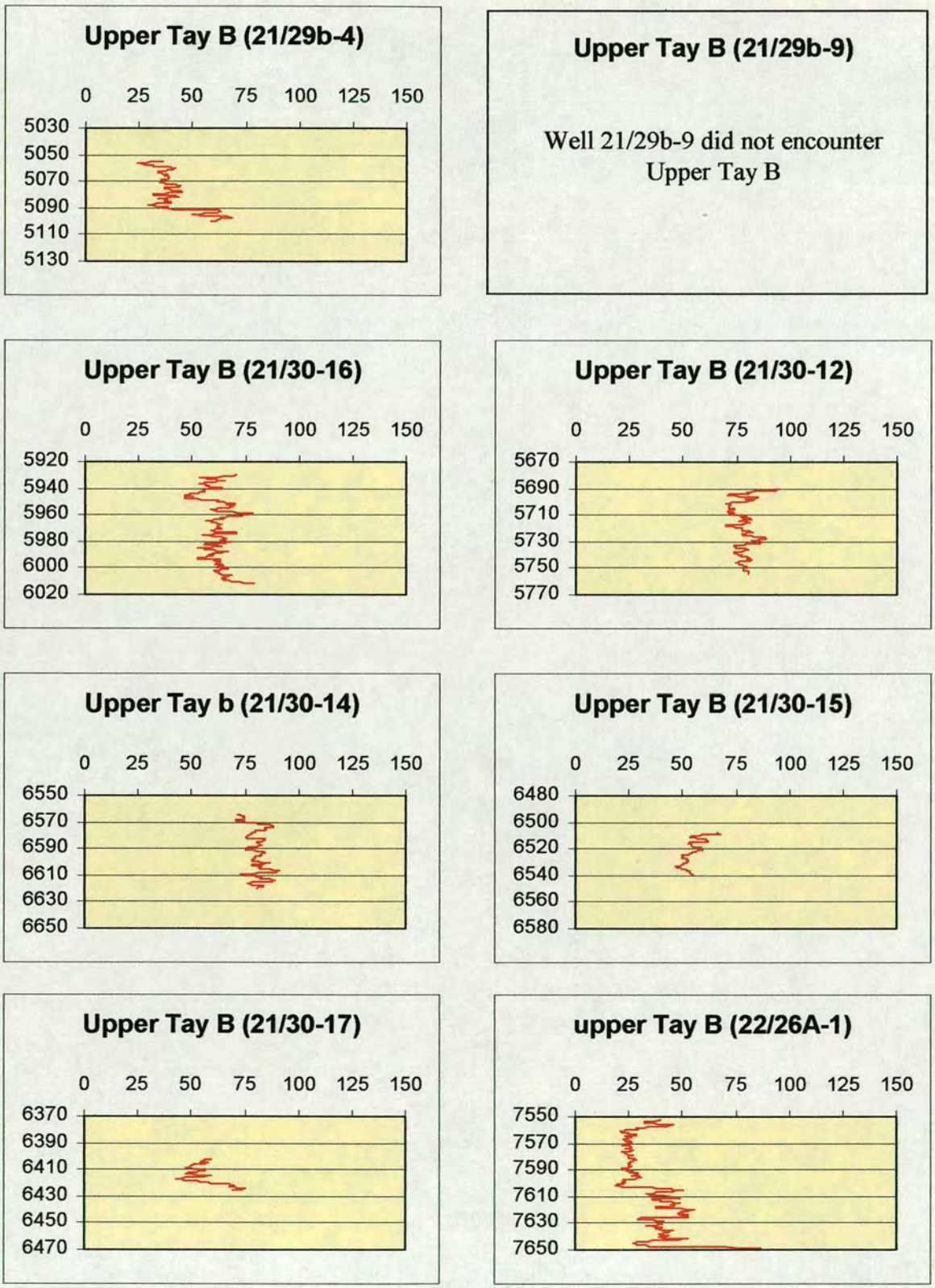

Figure 4.14: Gamma Ray responses of the Upper Tay B Unit.

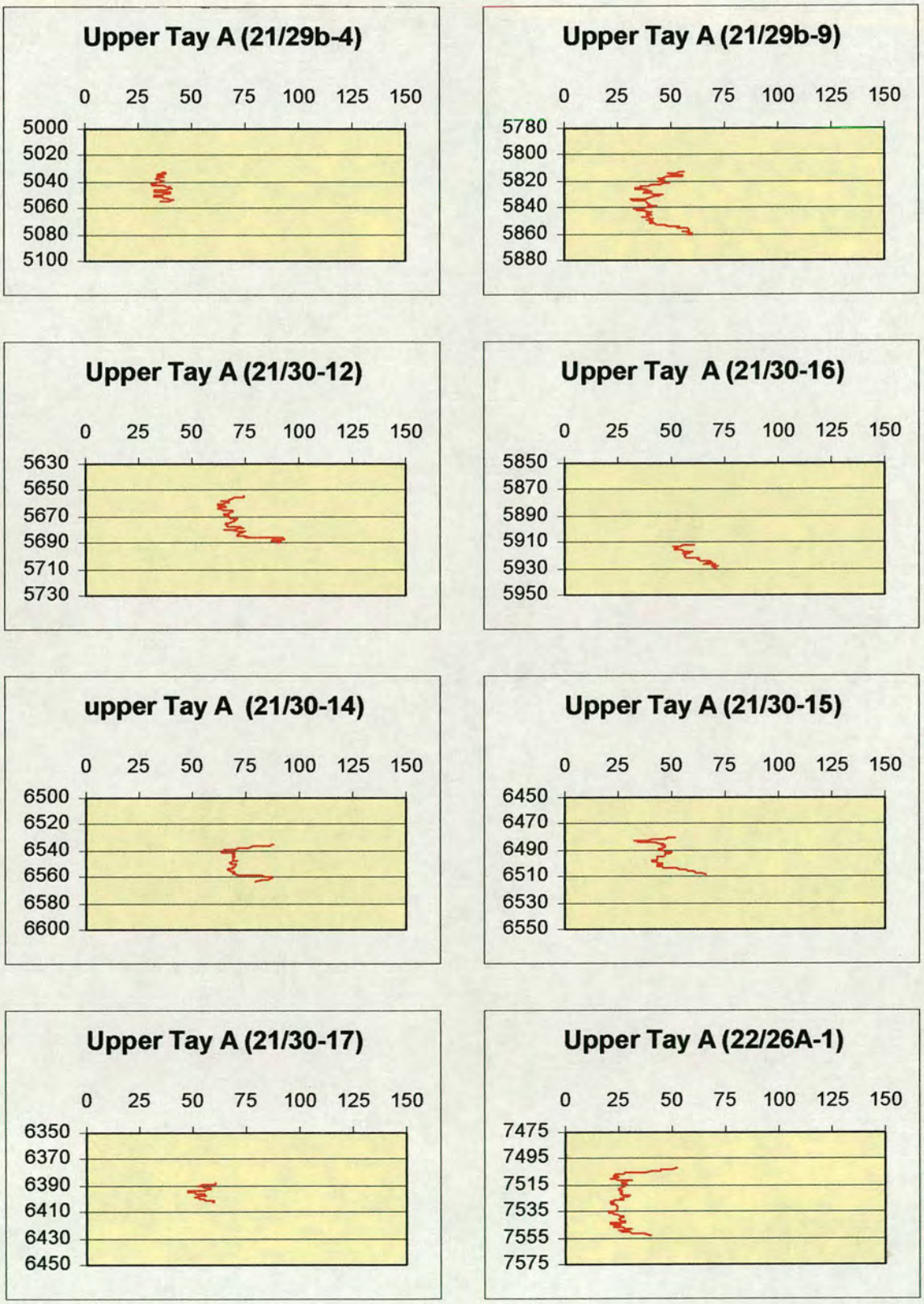

Figure 4.15: Gamma Ray responses of the Upper Tay A Unit.

Chapter Five

Chapter Five

Seismic Data to Well Log Tie

5.1 Introduction

Normally seismic attribute analysis is applied to enhance subtle features at the limit of seismic resolution. As such, it is of paramount importance to be sure that these features are real geology and not processing or acquisition artefacts contaminating the seismic data. Therefore, attribute analysis makes use of accurate seismic data to well ties to confirm the presence of geological features. Well logs and cores provide the only direct contact with the subsurface. From these measurements, we generally get accurate and detailed information about rocks and fluids encountered in the well. Hence, they have a good vertical resolution but very limited lateral resolution. Seismic data, on the other hand, provide good lateral resolution but give only limited vertical resolution. Therefore, to obtain a detailed vertical and lateral description of the subsurface, correlation between seismic and well logs is necessary. However, the two data sets are not in the same format. The seismic data is recorded in time while log data is recorded in depth. Consequently, there is a need to convert data recorded in the depth domain to the time domain before the correlation can be conducted. Furthermore, the resolution difference between to the two datasets (wireline logs having frequencies of 1 kHz, while frequencies of the seismic tools is less than 100 Hz) makes the comparison between the two datasets difficult. Forward modelling is a tool used by geoscientists to construct synthetic seismograms to tie well data with seismic data (Fig. 5.1).

The main objective of this chapter is to link the sedimentology described in the previous chapter to the seismic data that is interpreted in chapter 3. In the process we assess the adequacy of the seismic data to perform attribute analysis on it. Central to this investigation is to check if the seismic wavelet varies laterally. If so then the

attribute analysis will fail (Ziolkowski *et al.*, 1998) as the results will be attributed to processing problems in the data rather than real geology.

Seismic data to well log match was carried out using the SYNTOOL application in the Landmark seismic interpretation package, while wavelet extraction was performed using Jason Geosystems inversion package.

5.2 Dataset and Research Method

5.2.1 Quality Control of the wireline log data

A quality control check of the wireline logs for the 10 wells showed there to be no major problems with the data. The logs were checked for depth mismatches, consistent datum, log units, deviation surveys and locations. A particular emphasis was given to the sonic and density logs since they are the ones used in constructing synthetic seismograms. Both logs are available for all wells apart from 21/29b-1, which does not have a density log. All available sonic and density logs were checked for any errors and borehole effects so that these could be corrected or edited out. Sonic logs can be contaminated with noise caused by unconsolidated formations, formation fractures, gas saturation, cycle skips, or washed out zones. Density logs are particularly affected by washed out zones due to the shallow depth of investigation of the tool. Following are some observations made on the log quality;

1. Within the Tay Sandstone Member there are no major problems with log quality, hence they are reliable for construction of synthetic seismograms apart from the following intervals;

    i) 5165.5 – 5251 in well 21/29b-4, in which sonic log had to be edited.
    ii) 5774 – 5921.5 in well 21/30-12, in which sonic log had to be edited.

2. Generally, over the chalk, there is no complete logging sequence. This means that at the chalk interface, the reflection strength in any calculated synthetic seismograms cannot be relied upon.
3. There is no density log available above the Tay Sandstone Member in Well 21/30-16.
4. Well 21/30-17, due to irregular spikes, has an edited section in the Maureen Formation, which is deeper than the Tay Sandstone Member. This means the seismogram would still be reliable at Tay Sandstone Member.
5. Wells 21/30-16 and 18 are deviated wells. This could make the tie rather problematic.

5.2.2 Acoustic Impedance

The logs are used to derive a reflection coefficient series for the well location, via the intermediate stage of an acoustic impedance series. Acoustic impedance (ρv) is the product of density (ρ) and compressional velocity (v). If both sonic and density logs are available an acoustic impedance series can be produced by simple cross multiplication, after correlation has been made for any discrepancies between the two depth scales and converting them into time domain using check shots and drift curves. Cross multiplication is performed over travel time intervals of equal length, as determined by the integrated sonic log. The result is a series of values at regular intervals in two-way time. It can no longer properly be called a log since the former is defined as a property measured against depth whereas the latter is against travel time.

For deviated wells, sonic and density logs should be scaled against true vertical depth and the integrated sonic log recalculated before the acoustic impedance series is calculated.

The need for re-sampling the logs into travel-time intervals of equal-length arises due to the difference in frequencies of the sonic tool, about 1kHz, and frequencies of the seismic tool, less than 100 Hz. This large difference in resolution makes the comparison of the two measurements difficult (see Fig. 5.2). The new sampling

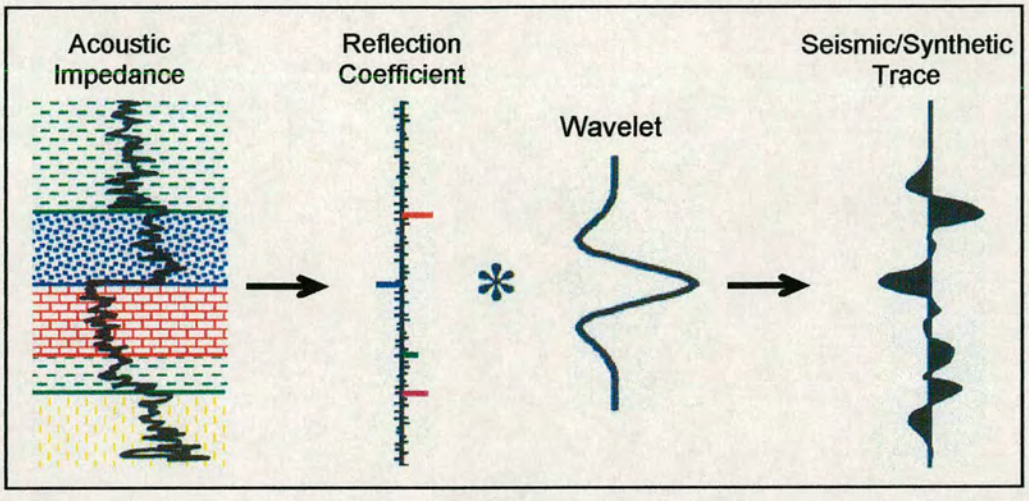

Figure 5.1: Principle of forward modelling. (from Jason Geosystems training Manual)

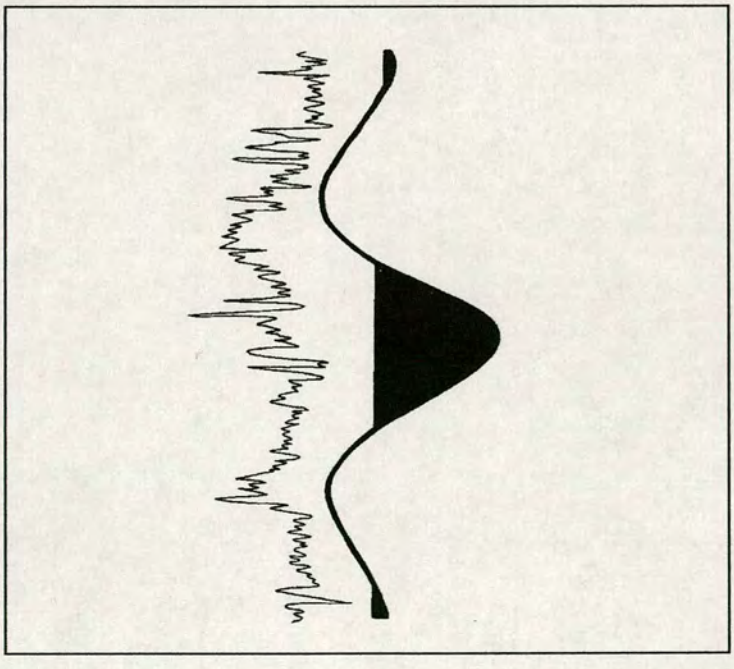

Figure 5.2: Resolution difference between the seismic trace and the well log data. (from Anstey)

interval removes the fine layers within the interval. 2 ms one-way travel time intervals were used. It means, for example, that the reflection coefficients from the top and bottom of thin beds (<2 ms) are ignored. This can be justified by considering the vertical resolution of seismic data. Generally resolution is between one-eighth to one-quarter of the wavelength of the seismic pulse (Sheriff, 1977). The reflections from the upper and lower surfaces of a bed thinner than this will interfere destructively. A seismic pulse with a dominant frequency of 50 Hz would have a period of 20 ms. Most real seismic pulses have lower dominant frequency and therefore longer period than this. Hence it can be seen that a 2 ms one-way time (4 ms two-way time) is almost always less than the limit of seismic resolution. In other words, if the sampling frequency of the seismic data is 2 ms, there is no point in creating synthetic seismograms at higher resolution than that, especially, when this will add to the difficulties in making the comparison between the two datasets.

5.2.3 Reflection Coefficient Series

The reflection coefficient (RC) of an interface is defined as the ratio of the amplitude of the reflected wave to the amplitude of the incident wave when the incident ray path is perpendicular to the interface:

$$RC = \frac{\text{acoustic impedance below - acoustic impedance above}}{\text{acoustic impedance below + acoustic impedance above}}$$

$$RC = \frac{\rho_2 v_2 - \rho_1 v_1}{\rho_2 v_2 + \rho_1 v_1}$$

where v_1 and ρ_1 are the velocity and density of the layer above the interface and v_2 and ρ_2 are the velocity and density of the layer below the interface.

In reality the earth is not usually made up of layers of constant acoustic impedance with sharp transitions between them. Wireline logs show that acoustic impedance is continuously variable in the subsurface. However, in order to be able to calculate a reflection coefficient series, each sample in the acoustic impedance series is assumed

to represent a layer of constant acoustic impedance. The reflection coefficients of the "interfaces" between each of these "layers" can then be calculated using the equation above.

5.2.4 Polarity and phase of the seismic data

Polarity and phase are important considerations in seismic interpretation as they affect the identification of the horizons at well locations and the correlation between wells. The Gannet South seismic dataset is processed by Shell Processing Centre to be zero phase (zero phase seismic data is where the peaks and troughs on the traces are aligned with the acoustic boundary). This was verified by using the knowledge of the prominent reflectors in the Central North Sea and verifying the expected signature for them.

Fig. 5.3 shows the polarity and phase convention used by Shell. It can be seen in this figure that a decrease in velocity is represented by a decrease in the acoustic impedance "soft kick" that gives rise to a negative reflection coefficient and results in a peak (black loop) on the seismic or synthetic trace. On the other hand, an increase in velocity is represented by a "hard kick" in the acoustic impedance that gives rise to a positive reflection coefficient and results in a trough (white or red loop) on the seismic or synthetic trace. It should be noted that this is reverse of the Society of Exploration Geophysicists (SEG) convention (Sheriff & Geldart, 1995).

To verify the polarity and phase of the seismic data, the data polarity was initially calibrated and confirmed using the sea floor seismic signature. The sea floor represents an increase in acoustic impedance due to the increase in velocity as the seismic wavelet goes from seawater to sediments of the seabed, and is represented by a trough in the Gannet South seismic data which agrees with the convention described above. This is further confirmed by checking the seismic signature of the Top Chalk horizon. The Top Chalk reflector is by far the most prominent reflector over the area. The trough of the Top Chalk is caused by a strong impedance contrast marking an increase in velocity due to the transition from the variably calcareous mudstones and sandstones of the Maureen Formation to the argillaceous chalky

limestone of the Ekofisk Formation. Thus, it is confirmed that the seismic dataset used is zero in phase and reverse to SEG polarity convention.

At each well the resultant acoustic impedance was cross plotted against gamma ray. Only well 21/29b-4 shows distinctive clusters for sand (green oval) and shale (red oval). As depicted in Fig. 5.4a, cleaner sandstones have lower gamma ray and acoustic impedance values in comparison to shales. This means a seismic pulse going from shale to sand will result in a negative reflection coefficient (soft kick) i.e. a peak on the seismic or synthetic trace as discussed above and as illustrated by Fig. 5.3. In the cross plot, sandstones with higher impedance values, more or less equal to the shales, were initially thought to contain hydrocarbons. However, since hydrocarbons are less dense than brine, they will always have lower acoustic impedance for a given porosity. Hence, it is now thought that the sandstones with the higher acoustic impedance are compacted sandstones.

Clusters of sand and shale draw closer as we go structurally deeper. This is demonstrated in wells 21/30-16 and 21/30-17 as shown by Fig. 5.4b and Fig. 5.4c. This means that the acoustic impedance contrast between sand and shale is decreasing with depth (e.g. from 750 $g/cm^3 \cdot m/s$ in 21/29b-4, 5000 ft deep, to 500 in 21/30-16, 6000 ft deep, to less than 100 in 21/30-17 which is at depth of 6400 ft) until polarity is reversed in 22/26a-1, 7500 ft deep, as seen in Fig. 5.4d. Now sandstones have higher acoustic impedance values than shales. At this depth the seismic pulse travelling from shale to sand will result in a positive reflection coefficient (hard kick) i.e. a trough on the seismic or synthetic trace.

5.2.5 Seismic Wavelet

An ideal seismic trace would contain only a series of spikes corresponding to subsurface reflectors. However, a real seismic trace departs considerably from this ideal. The source does not emit an ideal sharp pulse, but rather a wavelet. While travelling through the earth it is changed gradually. The seismic trace can be regarded as a convolution of the reflection coefficient series of the earth with a wavelet.

Fig. 5.5 gives a simplified illustration of how each interface produces a reflection proportional in magnitude and sign to the reflection coefficient due to convolution with a wavelet. Individual responses are then summed together to produce the seismic trace.

Therefore, before synthetic seismograms can be produced from the reflection coefficient series an input wavelet is required. To get the best match with real seismic data this should be the same as the "effective wavelet" in the real data. Unfortunately, this is not easy to determine. Unless the source waveform is recorded in the field it must be determined by statistical analysis of the data. Either minimum phase or zero phase may be assumed depending on processing steps applied to the seismic data.

It should be remembered that absorption of sinusoidal components of the seismic wavelet as they pass through the earth is frequency dependent. High frequencies are absorbed more than low frequencies resulting in a longer wavelet. Thus the shape of the effective wavelet changes with increasing travel time. A consequence of this is that several convolutions using different wavelets may need to be performed to obtain the best match with different parts of the real seismic trace. However, at the same time the extraction window has to be long enough for accurate wavelet estimation.

Wavelets were derived using seismic traces in the immediate vicinity of the wells. Four wells that are sparsely spaced were used over a 300 ms time window: wells 21/29b-9, 21/30-14, 21/30-15 and 22/26a-1. The derivation procedure was focussed on the Tay Sandstone Member including Top Balder and Top Chalk reflections, which are marked by significant amplitudes. Fig. 5.6 shows the wavelets extracted at the four wells. Yellow wavelet is extracted in the vicinity of well 21/29b-9 whereas brown, blue and red are at 21/30-14, 21/30-15 and 22/26a-1, respectively. It is obvious that variation in the shape of the wavelet at different well locations is negligible. This means processing has succeeded in reducing the effective wavelet in

the seismic data to zero-phase. In other words, if seismic is tied to one of the wells, and the marker horizon is followed from this well to another well, there would be no or minimal mis-tie at the other well as a result of wavelet shape. As a consequence, the variations seen on attribute maps are most likely to be related to real geology rather than processing artefacts.

Fig. 5.7 shows the smoothed amplitude spectrum for each of the wavelets. Clearly the frequency bandwidth for the four wavelets remains almost the same with a dominant frequency around 35 Hz. The amplitude is very similar for the three eastern wells, 21/30-14, 21/30-15 and 22/26a-1, whereas the western well 21/29b-9 clearly stands out, with lower amplitude. This is pictured through the graphical display of the amplitude spectrum of an arbitrary line through the wells, computed within the time gate 1000-2500 ms. This line can be seen in Fig. 5.8, where the bandwidth appears to be reasonably constant while amplitudes are overall dimming from east to west.

5.2.6 Synthetic Seismograms

Once the reflection coefficient series has been derived and a wavelet decided upon, convolution can take place. The resulting synthetic seismogram may then be compared with the real data. The polarity convention used for the synthetic seismograms and the seismic data is shown in Fig. 5.3. A positive reflection coefficient (an increase in acoustic impedance) is represented by a trough as discussed in Section 5.2.4.

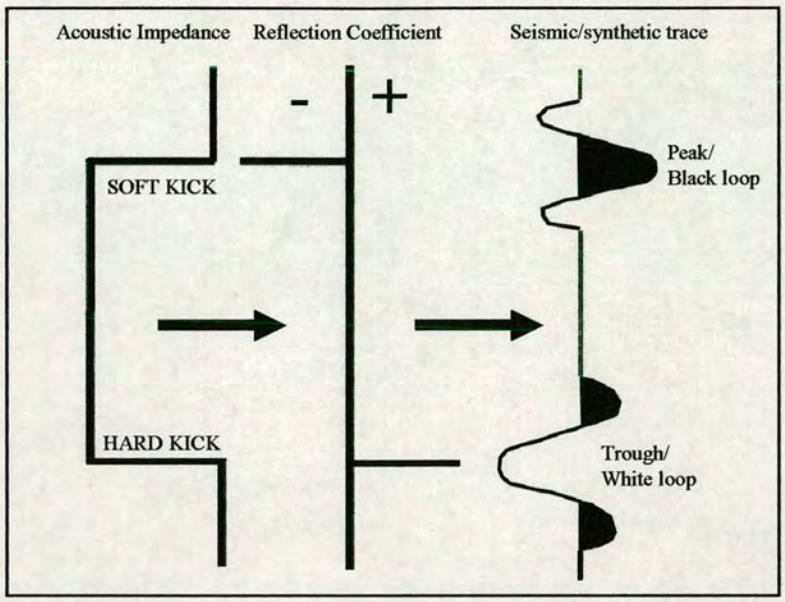

Figure 5.3: Phase convention used for both seismic and synthetic traces.

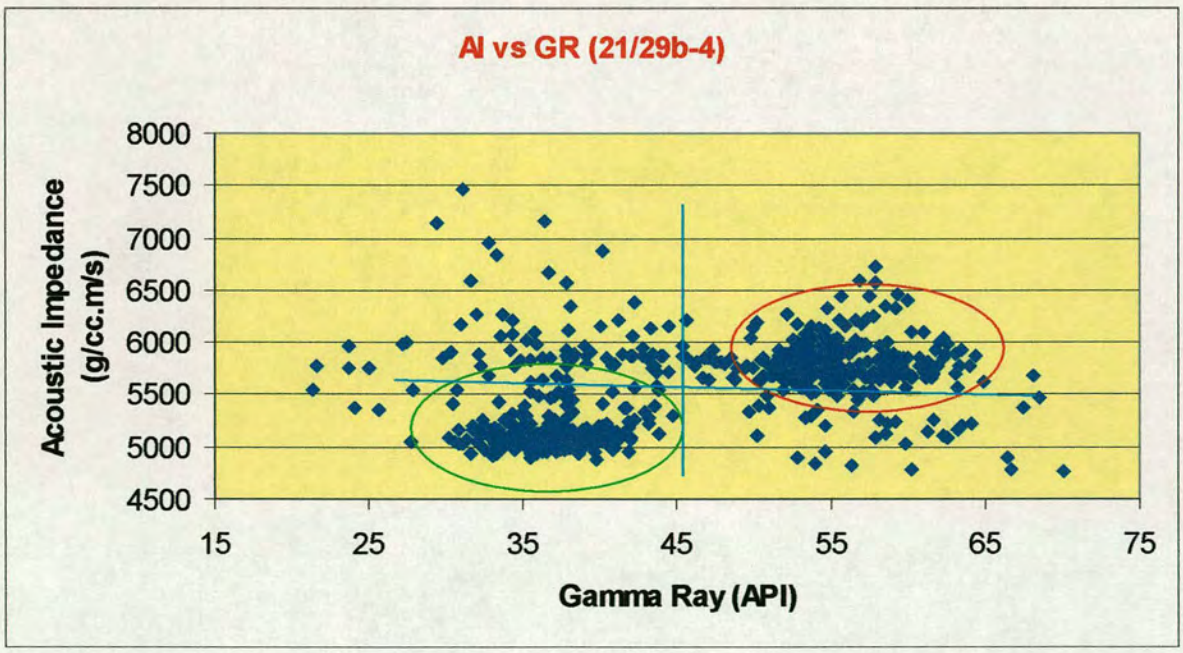

Figure 5.4a: shows distinctive clusters for sand (green oval) and shale (red oval). Cleaner sandstones have lower gamma ray and acoustic impedance values in comparison to shales. This means seismic pulse going from shale to sand will result in a negative reflection coefficient (soft kick) i.e. a peak on the seismic or synthetic trace

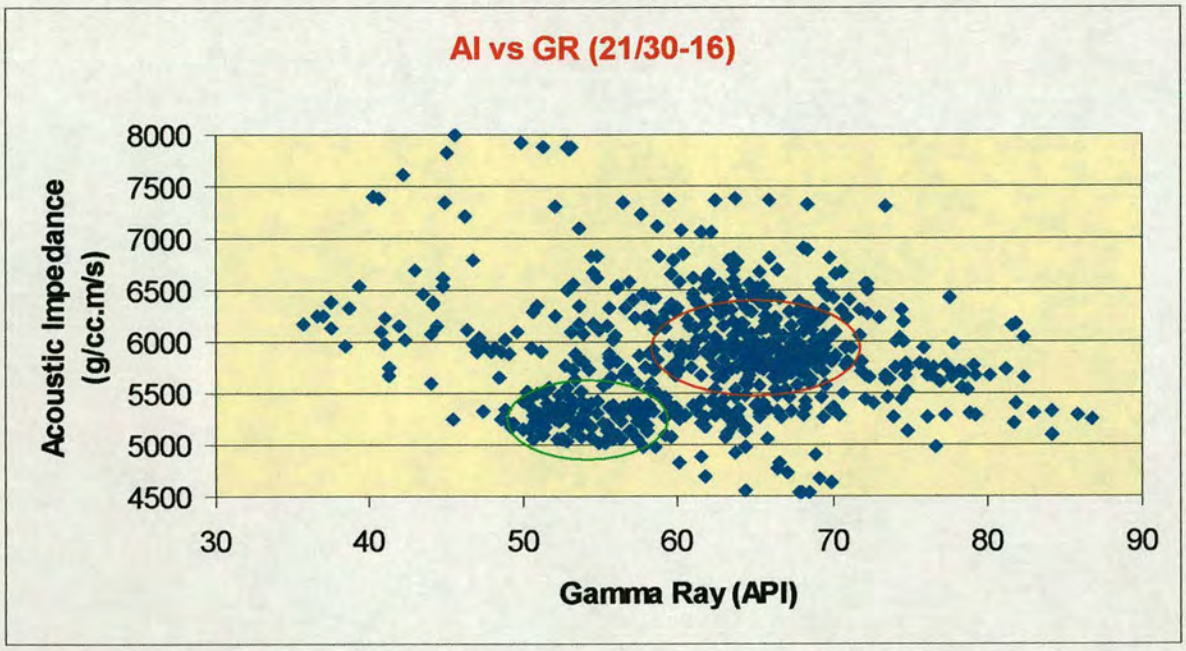

Figure 5.4b: sand and shale clusters have drawn closer making the impedance contrast smaller.

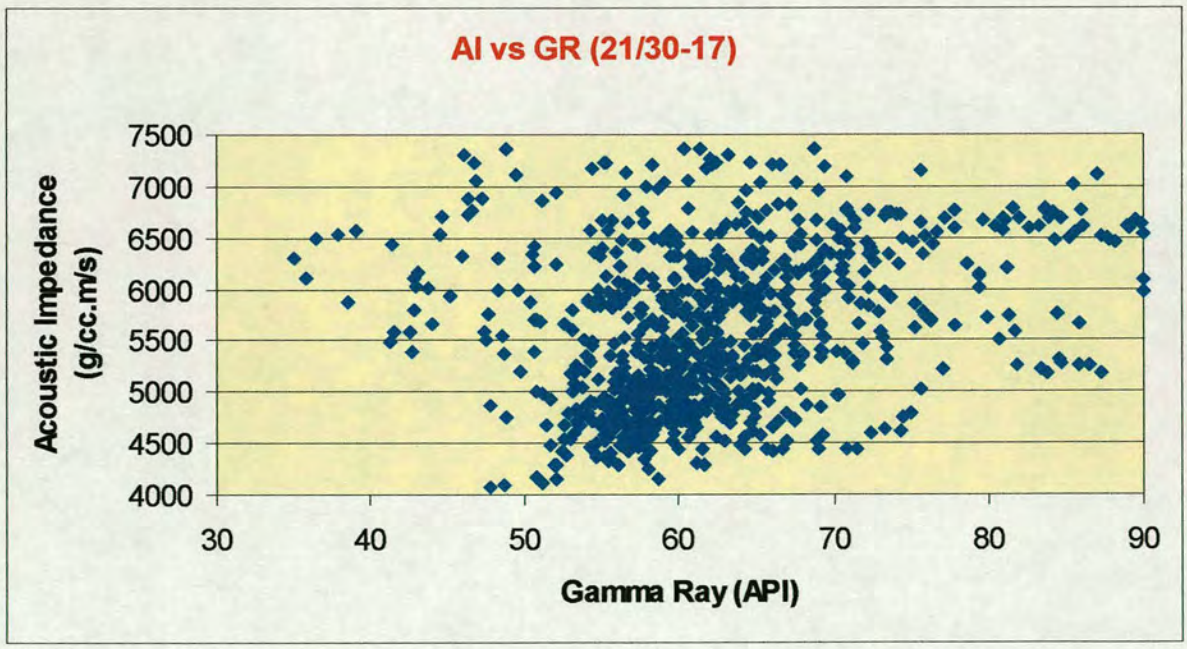

Figure 5.4c: sand and shale clusters have drawn even closer making the impedance contrast smaller.

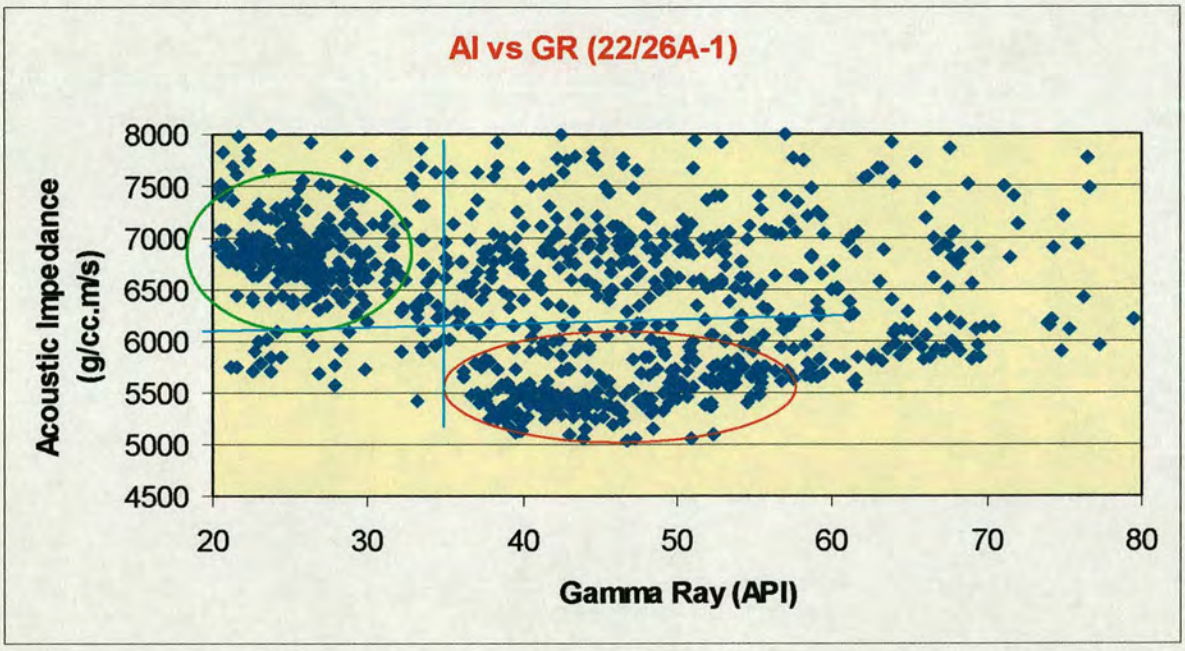

Figure 5.4d: Acoustic impedance contrast has reversed. At this depth seismic pulse travelling from shale to sand will result in a positive reflection coefficient (hard kick) i.e. a trough on the seismic or synthetic trace.

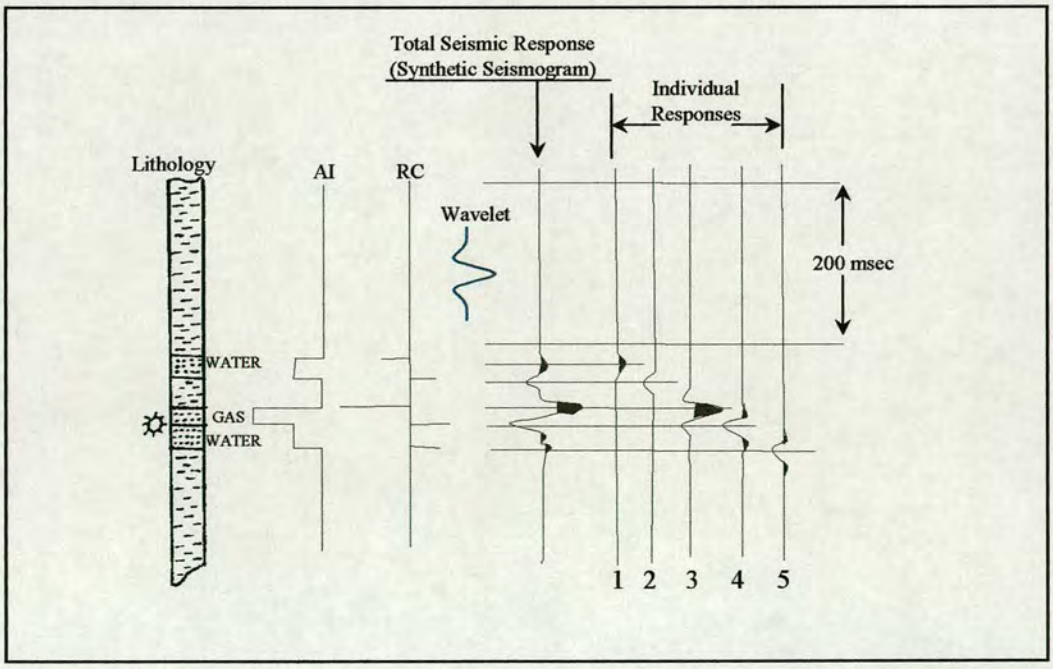

Figure 5.5: Simplified illustration of how each interface produces a reflection due to convolution of reflection coefficient with a wavelet. Individual responses are then summed together to produce the seismic or synthetic trace. Redrawn from Sheriff (1980)

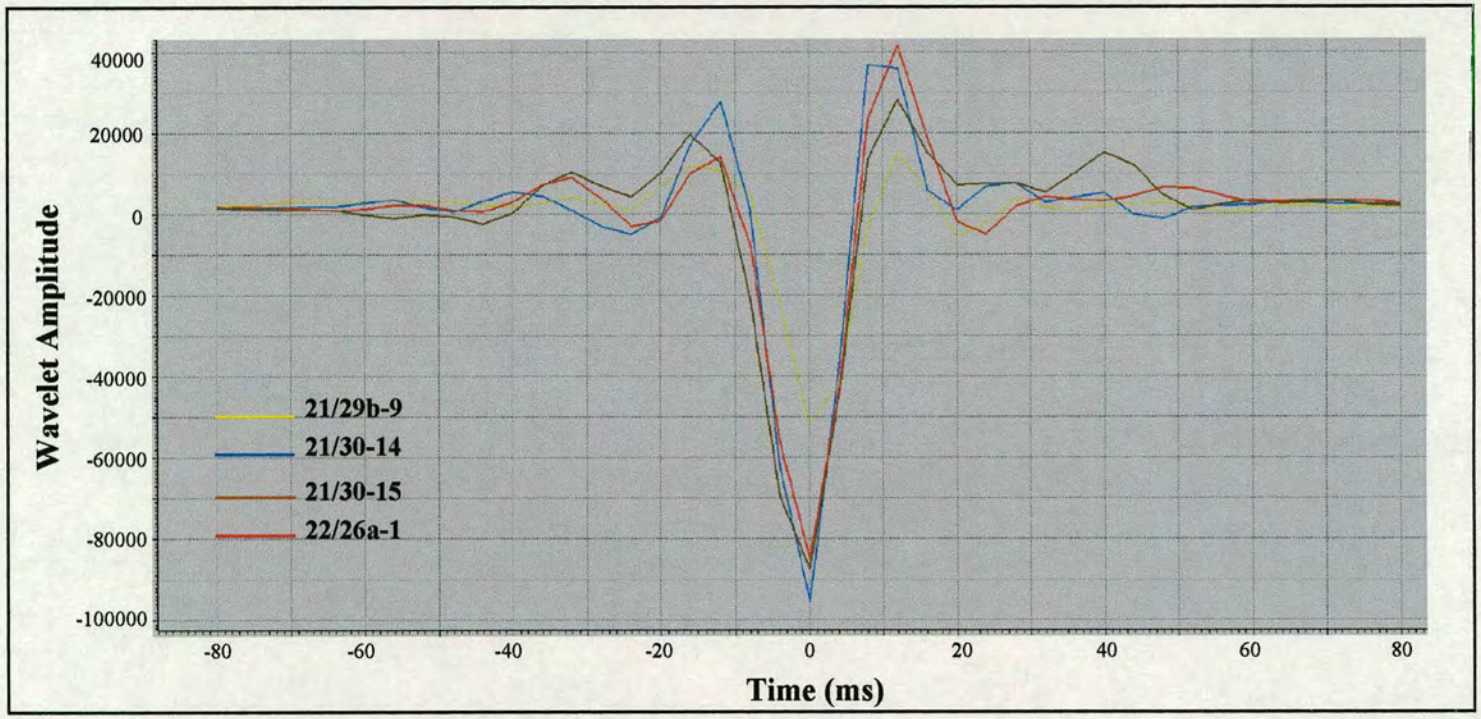

Figure 5.6: Four wavelets derived using seismic traces in the immediate vicinity of the wells over a 300 ms time window. The window included the Tay formation and Top Balder and Top Chalk reflections, which are marked by significant amplitudes. Variation in the shape of the wavelet at different well locations is negligible. This means processing has succeeded in reducing the effective wavelet in the seismic data to zero-phase.

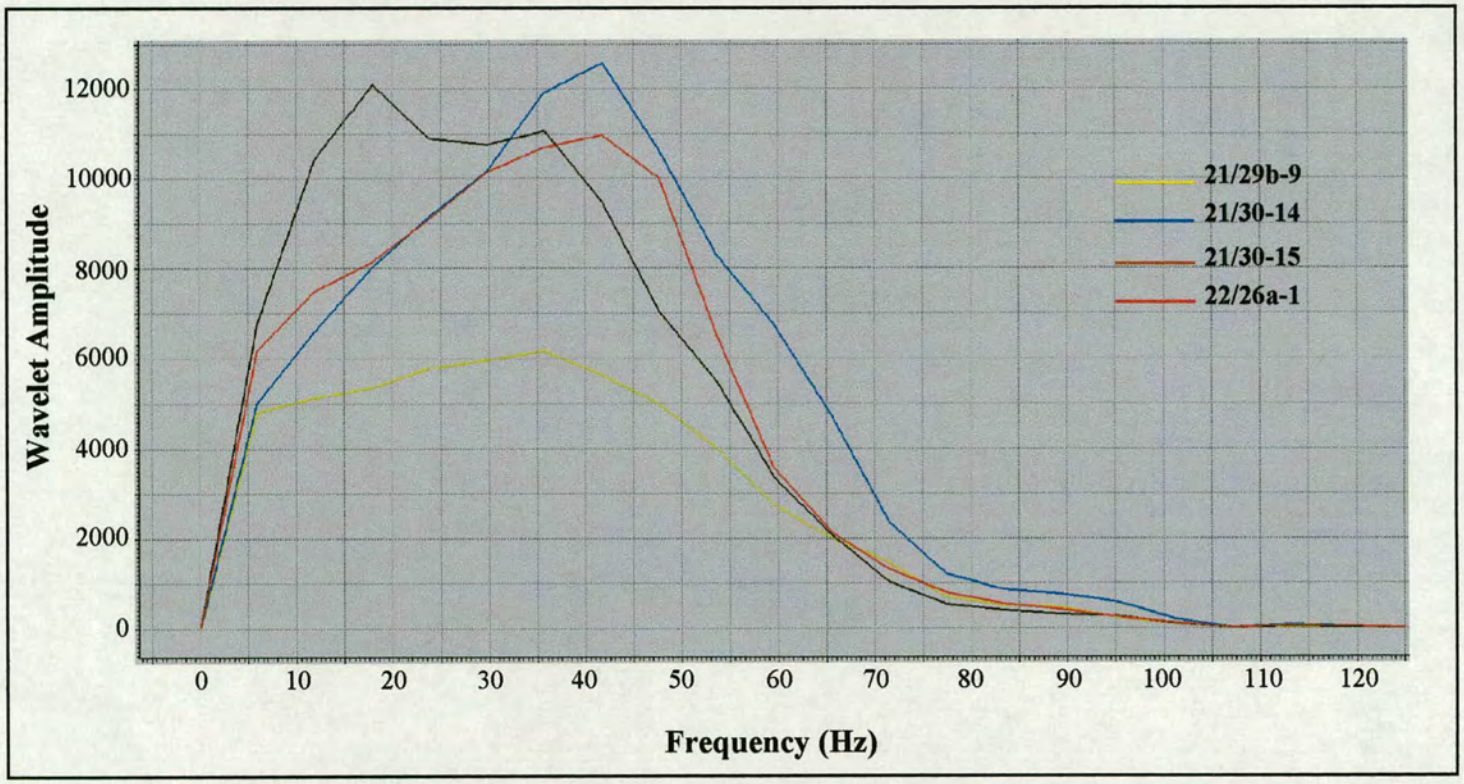

Figure 5.7: shows the amplitude spectrum for each of the wavelet. Frequency bandwidth for the four wavelets remains almost the same with a dominant frequency around 35 Hz. The amplitude is very similar for the 3 eastern wells, 21/30-14, 21/30-15 and 22/26a-1, whereas the western well 22/29b-9 clearly stands out, with lower amplitude.

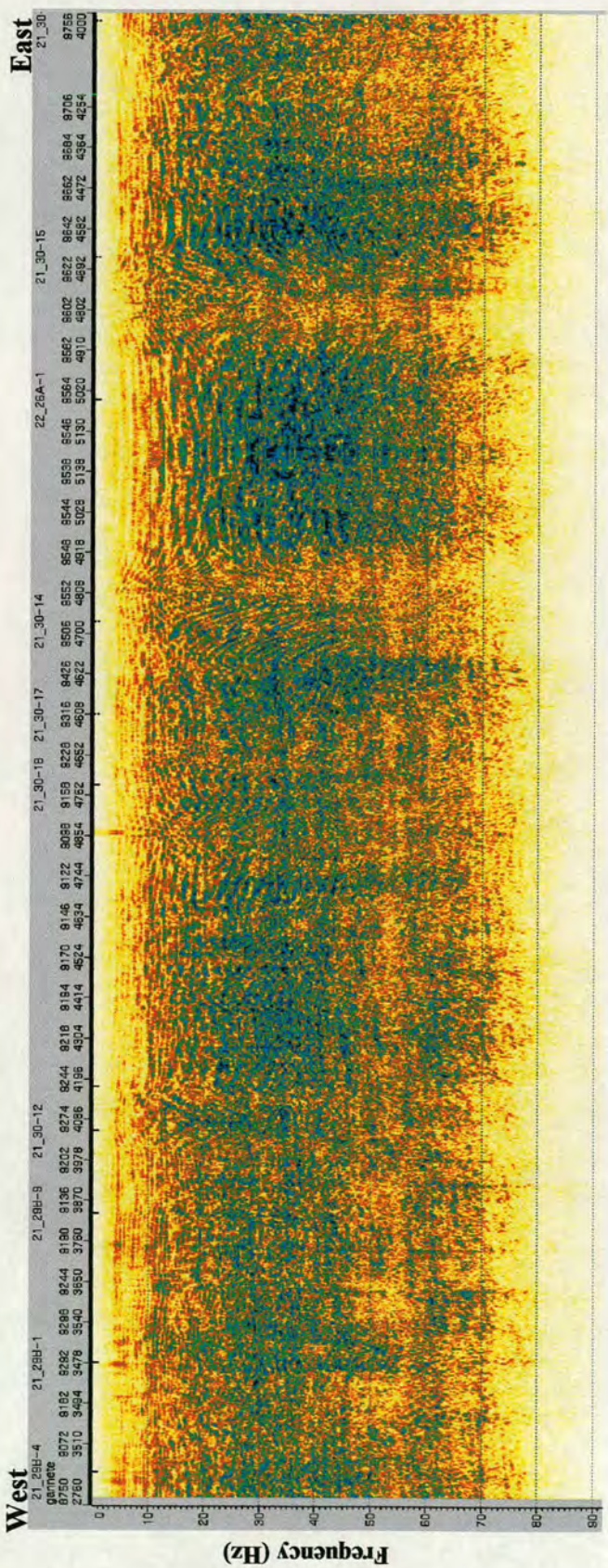

Figure 5.8: amplitude spectrum for an arbitrary line through the wells, computed within the time gate 1000-2500 ms. The bandwidth appears reasonably constant while the amplitude are on overall dimming from the East to the West.

5.3 Well Ties

5.3.1 Results

Each of the ten wells was tied to the 3D depth-migrated seismic data as shown below. For each well a set of panels, measured in true vertical depth subsea (TVSS) and two-way time (TWT) with respect to the sea level datum, were produced. Figs. 5.9a to 5.9j show the match with traces in red colour being measured seismic, while the light blue trace superimposed on them is the synthetic seismogram. Each synthetic trace was matched to both the inline, seismic lines running east-west and denoted "Line" on the panels, and cross line, seismic lines running north-south and denoted "Trace" on the panels. The formation top picks together with gamma ray, sonic, density, and acoustic impedance logs are also included in the figures. General reasons that possibly cause the mis-ties are discussed later.

Well 21/29b-1

Fig. 5.9a shows the result of seismic to well tie for this well. The match seems to be excellent with very good amplitude correlation. There was no time shift required to achieve this match. The correlation coefficients for matching with both inline and cross-line were 0.81 and 0.83 respectively. No Tay Sandstone Member has been deposited at this location. Top Chalk is picked at a trough.

Well 21/29b-4

Fig. 5.9b shows the result of seismic to well tie at this well location. The match appears to be very good with reasonably good amplitude correlation. A time shift of + 2 ms to the synthetic seismogram was required to achieve the best match giving correlation coefficients for matching with both inline and cross-line of 0.79 and 0.81 respectively. The amplitudes at the Tay level are obscured on the synthetic seismogram. As mentioned in Section 5.2.1, the sonic log had to be edited at this level making the synthetic unreliable. The Top Balder pick was also defective as the sonic was also edited at this level. Top Chalk pick was perfect in both time and amplitude.

Well 21/29b-9

Fig. 5.9c shows the result of seismic to well tie at this well location. The match appears to be good with reasonably good amplitude correlation. There was no time shift required to achieve the best match. The correlation coefficients for matching with both inline and cross-line were 0.76 and 0.66 respectively. Top of Upper Tay, Middle Tay, Basal Tay, Balder and Chalk can be confidently tied from this well. However, the seismic on the inline panel shows some exceptionally strong amplitudes left of the synthetic trace that are not seen on the synthetic trace nor on the cross-line panel. These are thought to be caused by hydrocarbon.

Well 21/30-12

Fig. 5.9d shows the result of seismic to well tie at this well location. Time-wise, the match appears to be reasonably good. However, in terms of amplitude, it is rather problematic within the Tay interval as the amplitudes on the synthetics are significantly different from those in the real seismic data. The synthetic is not reliable at this level due to the straight-line edit in the sonic log. Another reason for the difference could be due to fact that logs may have sampled the flushed-zone around the borehole. This will give higher velocity and density readings than would the hydrocarbon-saturated rocks further away from the borehole. Therefore, the acoustic impedance series derived from well logs may be different from the average for the area, which is what real seismic data is affected by. A time shift of – 5 ms was applied to the synthetic seismogram in order to achieve the best match. The correlation coefficients for matching with both inline and cross-line were 0.68 and 0.55 respectively.

Well 21/30-14

Fig. 5.9e shows the result of seismic to well tie at this well location. The match seems to be good with reasonably good amplitude correlation. A time shift of + 5 ms to the synthetic trace was required to achieve the best match. The correlation coefficients for matching with both inline and cross-line were 0.58 and 0.65 respectively.

Well 21/30-15

Fig. 5.9f shows the result of seismic to well tie at this well location. The match seems to be satisfactory bearing in mind the dipping reflector as the well has been drilled on the crest of a structural high. No time shift was applied to achieve the tie. The correlation coefficients for matching with both inline and cross-line were 0.62 and 0.76 respectively.

Well 21/30-16

Fig. 5.9g shows the result of seismic to well tie at this well location. The match seems to be good with reasonably good amplitude correlation. A time shift of + 14 ms was applied to the synthetic seismic trace to achieve the best match. The correlation coefficients for matching with both inline and cross-line were 0.72 and 0.61 respectively. The Tay Sandstone Member is rather thin at this location making the acoustic impedance contrast between the different zones less obvious.

Well 21/30-17

Fig. 5.9h shows the result of seismic to well tie at this well location. The synthetic seismogram at this well has been the most difficult to tie to the seismic reaching a correlation coefficient of only 0.48 for the inline and 0.49 for the cross line. No time shift was applied to achieve this match as top Chalk event tied satisfactory at this location. The possible reasons for the mis-tie are discussed in a later section of this chapter.

Well 21/30-18

Fig. 5.9i shows the result of seismic to well tie at this well location. The match appears to be fairly good with reasonably good amplitude correlation despite the fact that it is a deviated well. A time shift of -16 ms to the synthetic seismogram was required in order to achieve the best match giving correlation coefficients of 0.61 and 0.62 for both inline and cross-line respectively. There was no Tay Sandstone Member deposited at this location.

Well 22/26a-1

Fig. 5.9j shows the result of seismic to well tie at this well location. The synthetic seismogram gave the best match to real seismic data provided that the seismogram was shifted by –18 ms. This well encountered the thickest Tay Sandstone Member package providing good acoustic impedance contrasts between the different units within the formation. The correlation coefficients for matching with both inline and cross-line were 0.83 and 0.85 respectively. Top of Upper Tay, Middle Tay, Basal Tay, Balder and Chalk can be confidently tied from this well.

5.3.2 Reasons for Mis-ties

In general a perfect match in seismic to well tie is very rare for the following reasons:

i) The wavelet used in convolution is rarely exactly the same as the effective wavelet in the seismic data as the shape of the effective wavelet changes with increasing travel time. It has been demonstrated in this chapter that, for the dataset used for this project, the lateral change in shape of the wavelet is not significant.

ii) The logs from which the synthetic seismogram is derived measure only a short distance away from the borehole whereas seismic response is of Fresnel-Zone dimensions (Sheriff, 1977).

iii) The seismic trace at the well location may relate to a different portion of earth from the well unless migration has been performed. The dataset used in this project is 3D depth migrated seismic data.

iv) unless migration is three dimensional, out of plane reflections ("sideswipe") may occur on the seismic data, particularly on lines running along geological strike.

v) In hydrocarbon bearing formations the logging tools may not have sufficient penetration to sample the unaltered formations beyond the flushed zone. This will give higher velocity and density readings than would the hydrocarbon-saturated rocks further away from the borehole. Therefore, the acoustic

impedance series derived from well logs may be different from the average for the area, which is what real seismic data is affected by. This is seen in well 21/30-12.

vi) Both seismic data and well logs are subject to noise of different types. Well logs are subject to borehole size variations, rock alteration by drilling, fluid invasion, cycle skipping etc. Seismic traces, on the other hand, are subject to interference with non-reflection energy, multiples etc.

vii) Either the strata are intensely dipping at the zone of interest, or the wells are intensely deviated near the zone of interest, both of which result in a collapse of the 1D normal incidence assumption crucial to the construction of synthetic seismograms.

5.3.3 Ties with the sedimentology

Once seismic data to well tie was established an attempt was made to calibrate the synthetic and seismic trace to lithology and lithofacies described in Chapter 4. This was done first by comparing the lithofacies to the gamma ray log as shown by the core description log of well 21/30-17 available in Appendix 3, then by reducing the resolution of the cored sections to match the seismic data. Figs. 5.10a to 5.10e illustrate the results achieved by this exercise.

Fig. 5.10a shows the results of lithology to seismic data tie. The effect of the thick sand package observed at the well location is immediately apparent. This is going to be very useful in trace shape analysis.

Fig. 5.10b shows the seismic tie to the lithology at well 21/30-17. Although individual beds of sands observed in this well are relatively thin, not exceeding 10 feet, a combined effect of amalgamated sands with interbedded siltstones is obviously giving a seismic response in the form of a trough in the Middle Tay interval where sands are more frequent.

Fig. 5.10c shows the result of seismic data to lithology tie at well 21/30-14. The effect of thicker sand package at 6690 ft is apparent.

Fig. 5.10d gives the result of lithology to seismic data tie at well 21/30-12. The thin sandstone beds have a dramatic effect on the seismic trace. This thought to be due hydrocarbon as seen in the core at this location. The hydrocarbon are also thought to be the cause of the sonic tool to give unreasonable readings at this location, making the edit for the sonic log necessary to perform forward modelling.

Fig. 5.10e shows the result of lithology to seismic data tie at well 21/29b-9. This well had very variable lithofacies at its location ranging from massive sands to mudstones. The core is at poor condition as most of it is rubble of broken sediments making the exact depth of the consolidated sands uncertain. However, amalgamation of sand and silts shows that the ratio of sand content is relatively high giving rise to a trough in seismic trace.

5.4 Summary and Conclusions

As seismic attribute analysis is applied to enhance subtle features at the limit of seismic resolution, it is very important to be sure that these features are related to real geology and not processing or acquisition artefacts contaminating the seismic data. Confidence in a geological interpretation can be improved by accurate seismic data to well log ties.

The main objective of this chapter was to link the sedimentology described in the previous chapter to the seismic data interpreted in Chapter 3. In particular, to identify reflections, i.e. determining which seismic event relates to which specific geological boundary. In the process we assessed the adequacy of the seismic data to have attribute analysis performed on it.

Routine steps to construct synthetic seismograms at each well were followed. A quality control check of the wireline logs for the 10 wells showed there to be no

major problems with the data. The logs were checked for depth mismatches, consistent datum, log units, deviation surveys and locations.

Acoustic impedance analysis showed that sands in the Tay Sandstone Member are softer than shales at shallower levels, but they become harder than shales at deeper levels. In other words, the seismic pulse traveling from shale to sand will give rise to a peak at shallower levels but a trough at deeper levels. Acoustic impedance cross-plotted against gamma ray also showed that the gamma ray is not always a good discriminator between sand and shale.

Seismic wavelets were derived using seismic traces in the immediate vicinity of the wells. Four wells that are sparsely spaced were used over a 300 ms time window. The results show that variation in the shape of the wavelet at different well locations is minimal. This means processing has succeeded in reducing the effective wavelet in the seismic data to zero-phase. In other words, if seismic is tied to one of the wells, and marker horizon is followed from this well to another well, there would be no or minimal mis-tie at the other well. As a consequence, the variations seen on attribute maps are most likely to be related to real geology rather than processing artefacts.

The resulting synthetic seismograms were then compared to the real data. Each synthetic trace was compared to both inline and cross-line. In general the ties were good and only a minimal time shift was required to attain the optimal match as could be seen in Table 5.1 below. The best tie was provided by well 22/26a-1 which encountered the thickest Tay unit. The match was achieved after applying a time shift of -18 ms to the synthetic seismic trace.

Well	Correlation Coefficient		Time Shift (ms)
	inline	cross-line	
21/29b-1	0.81	0.83	0
21/29b-4	0.79	0.81	+2
21/29b-9	0.66	0.76	0
21/30-12	0.68	0.55	-5
21/30-14	0.58	0.65	+5
21/30-15	0.62	0.76	0
21/30-16	0.72	0.61	+14
21/30-17	0.48	0.49	0
21/30-18	0.61	0.62	-16
22/26a-1	0.83	0.85	-18

Table 5.1: Shows assessment of seismic to well tie applied to the 10 wells.

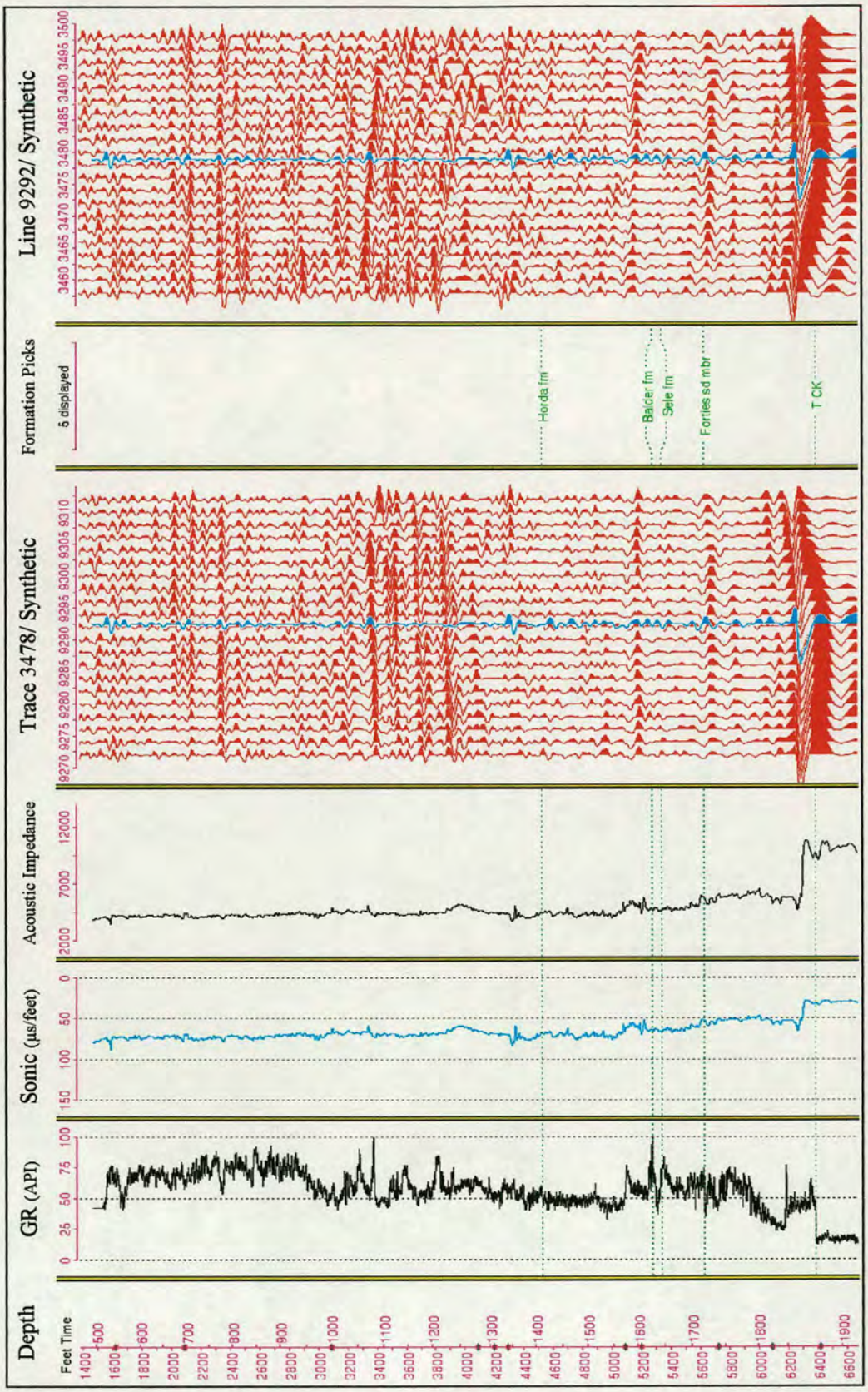

Figure 5.9a: Seismic to Well match for well 21/29b-1. Correlation Coefficients of 0.83 and 0.81 for Trace and Line respectively. No time shift was required for the match. There was no Tay deposited at this location.

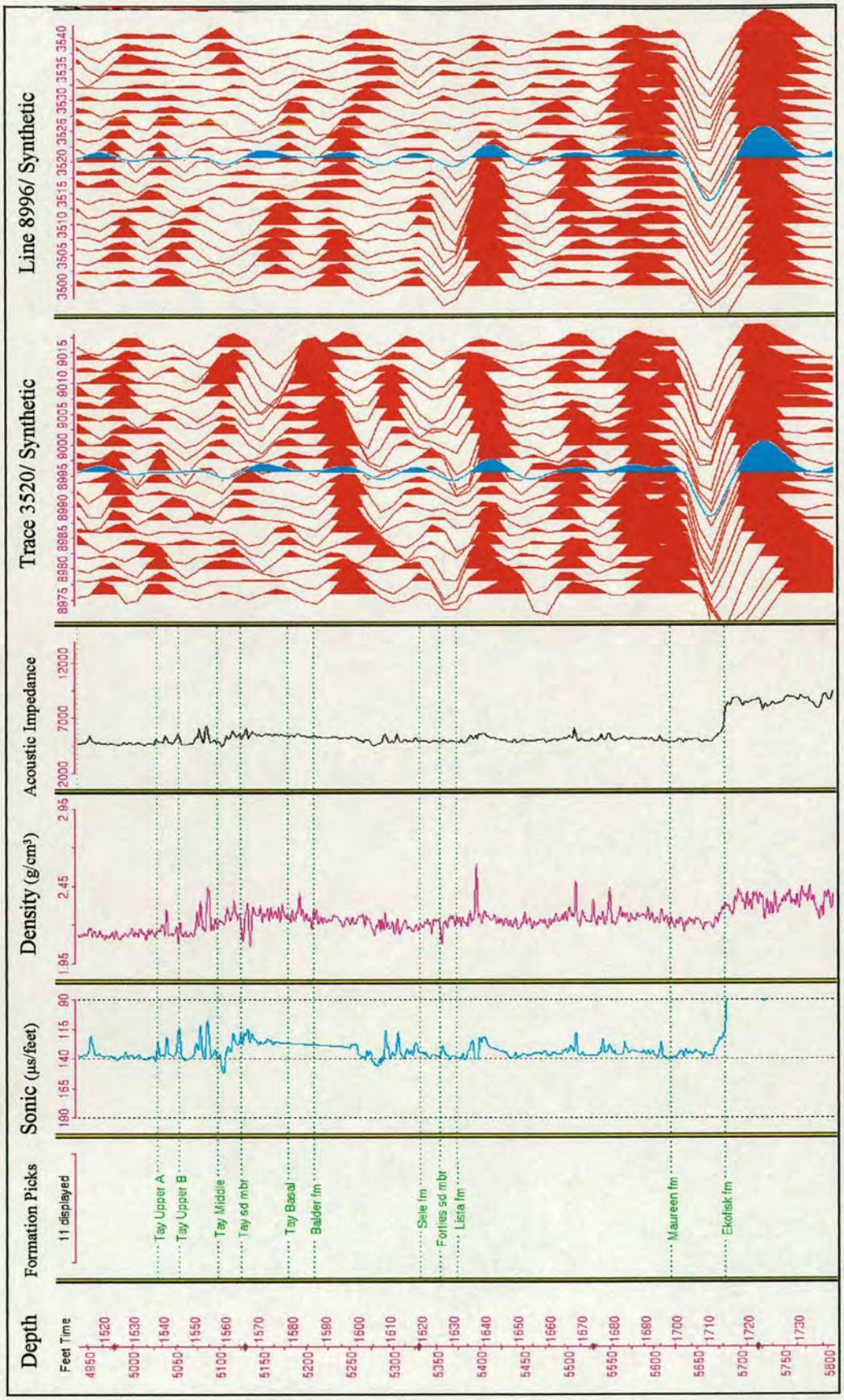

Figure 5.9b: Seismic to Well match for well 21/29b-4. Correlation Coefficients of 0.81 and 0.79 for Trace and Line respectively. + 2 ms time shift was required for the match.

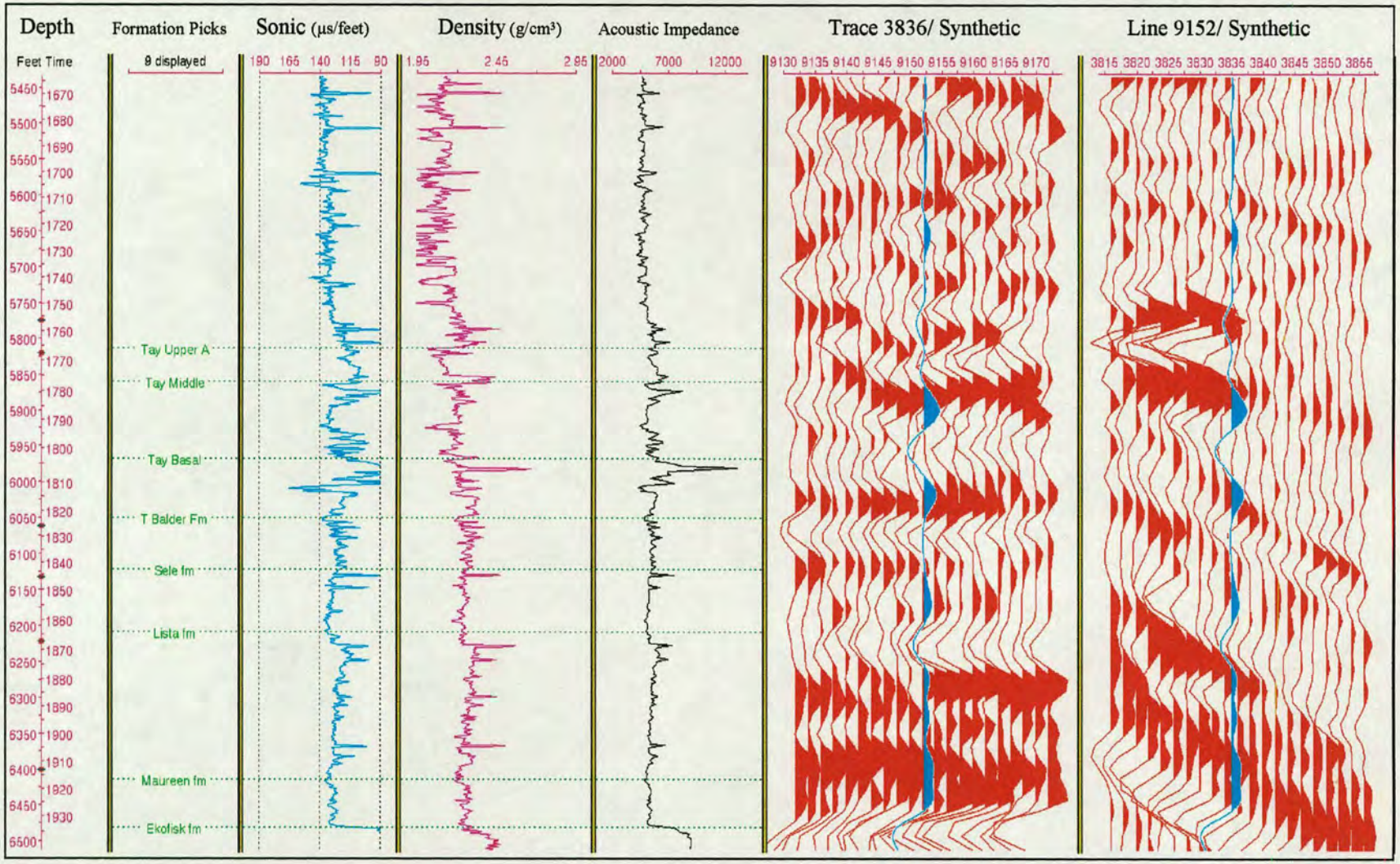

Figure 5.9c: Seismic to Well match for well 21/29b-9. Correlation Coefficients of 0.66 and 0.76 for Trace and Line respectively. No time shift was required for the match. Notice the high amplitudes left of the synthetic on Line.

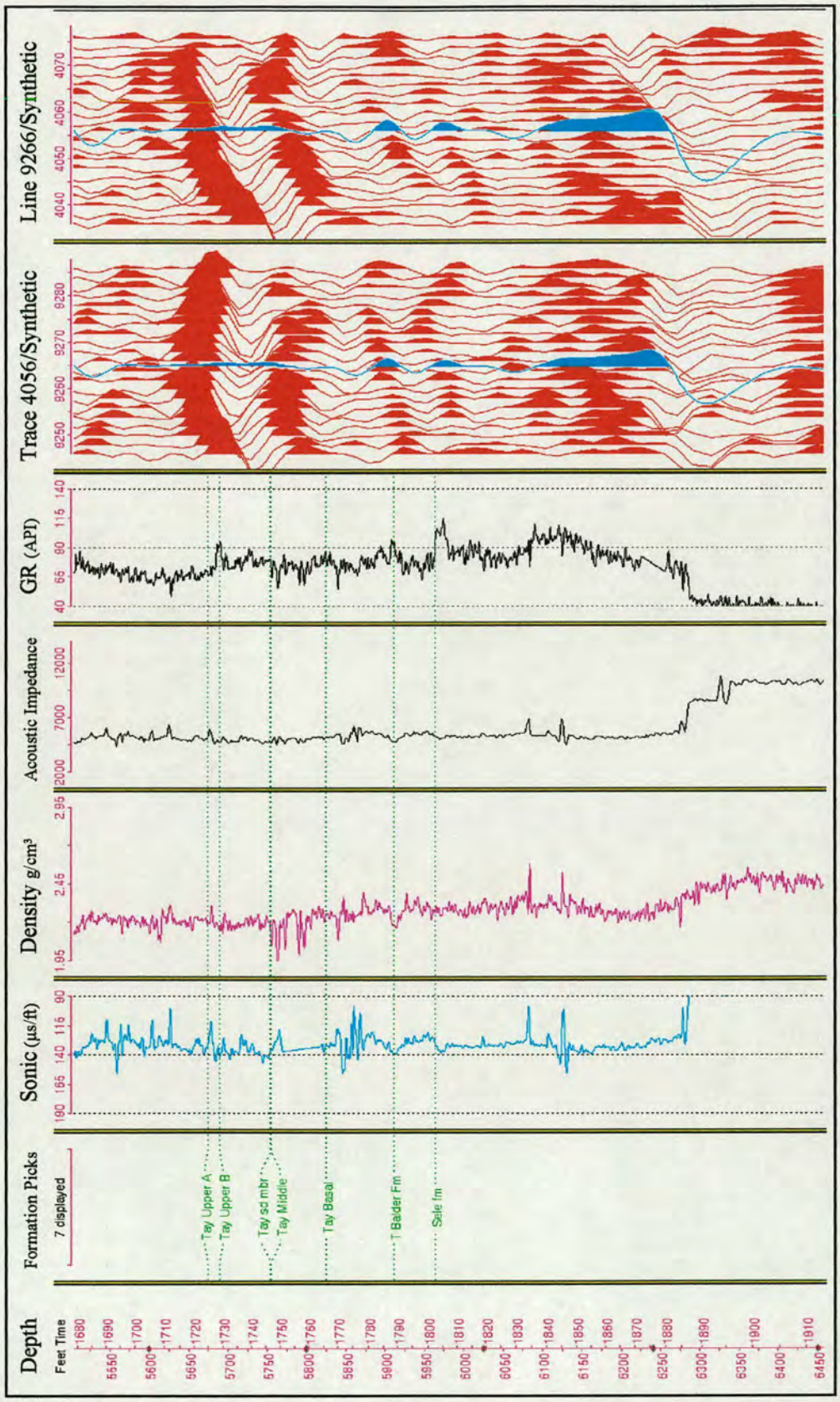

Figure 5.9d: Seismic to Well match for well 21/30-12. Correlation Coefficients of 0.55 and 0.68 for Trace and Line respectively. - 5 ms time shift was required for the match.

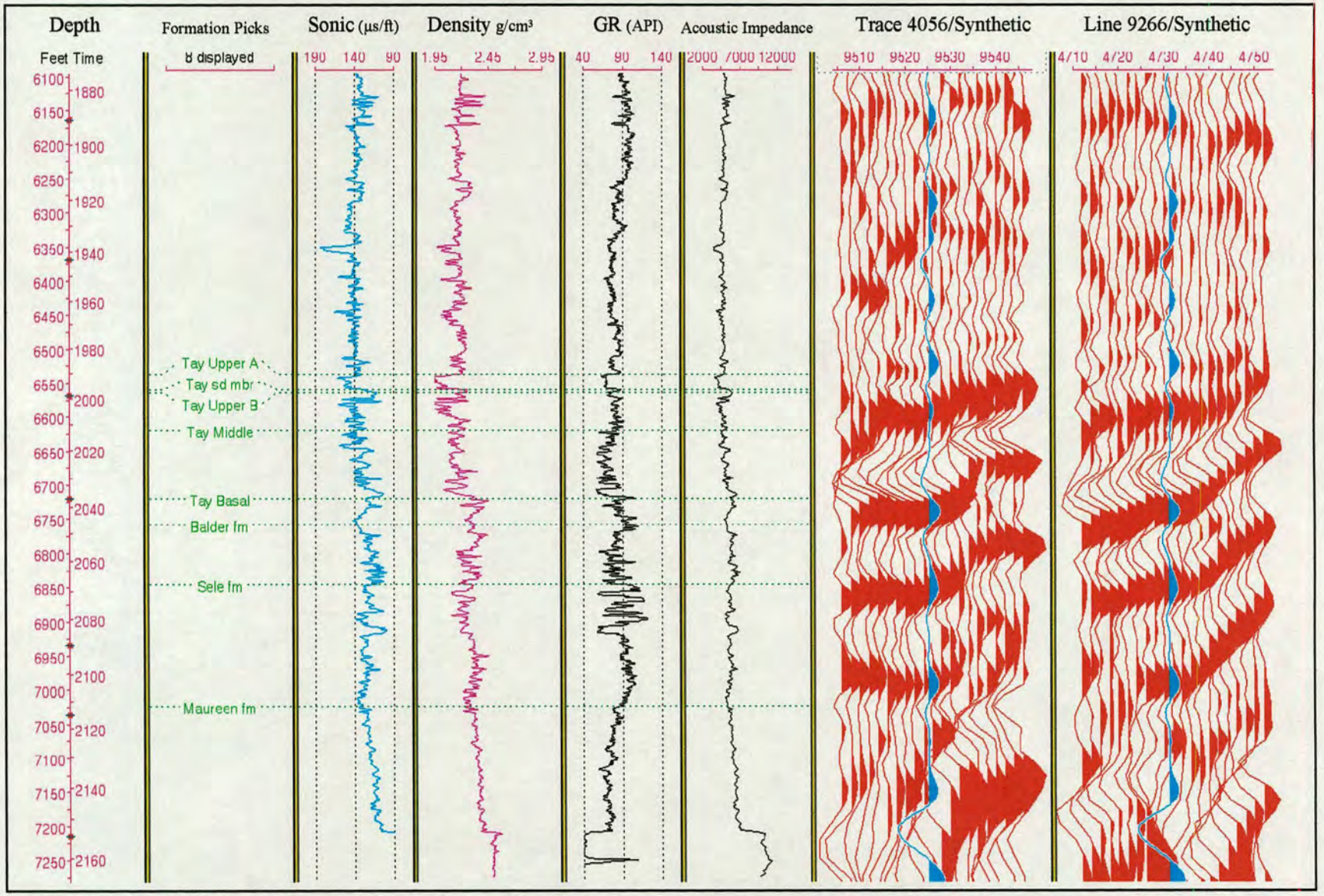

Figure 5.9e: Seismic to Well match for well 21/30-14. Correlation Coefficients of 0.65 and 0.58 for Trace and Line respectively. + 5 ms time shift was required for the match.

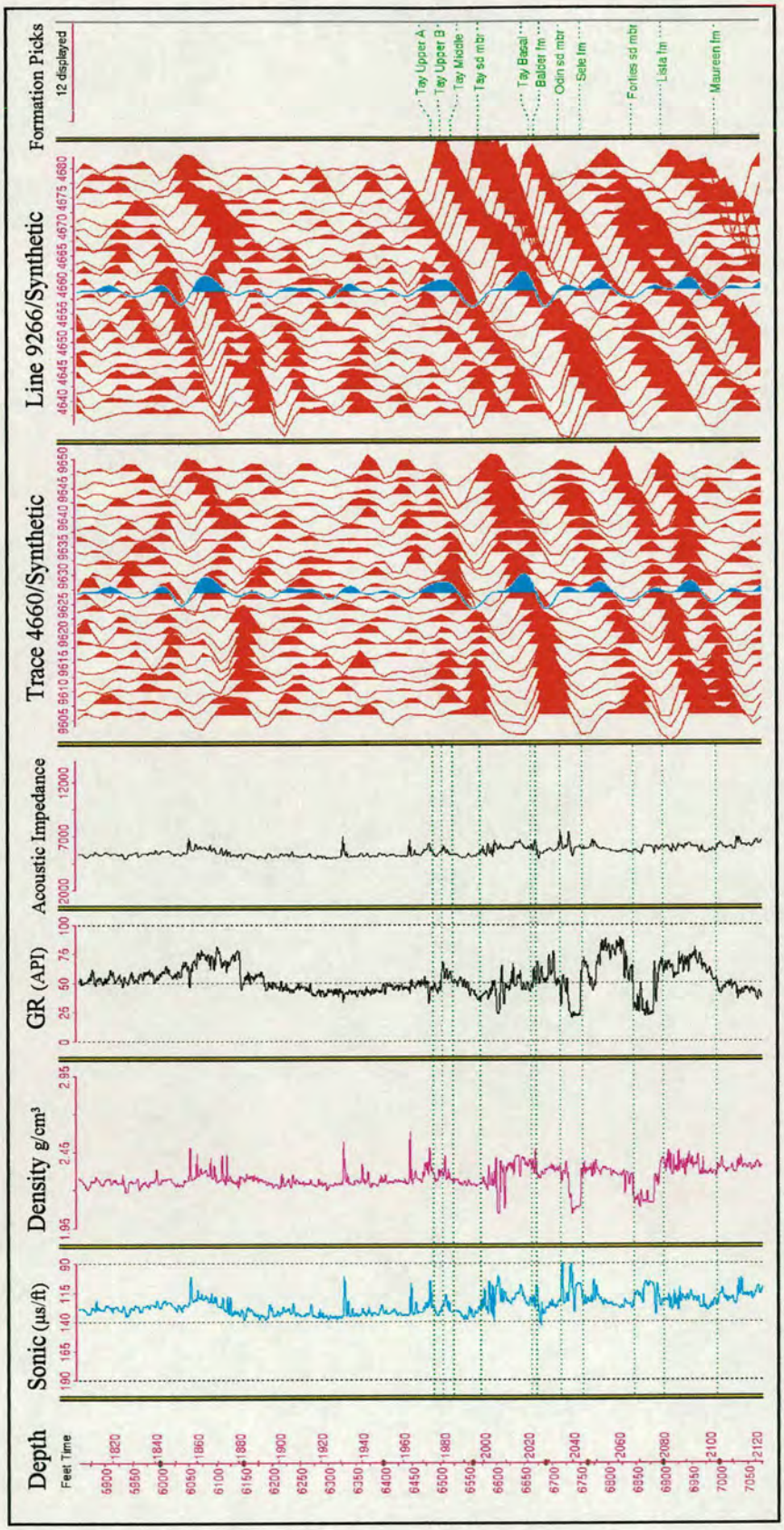

Figure 5.9f: Seismic to Well match for well 21/30-15. Correlation Coefficients of 0.76 and 0.62 for Trace and Line respectively. No time shift was required for the match.

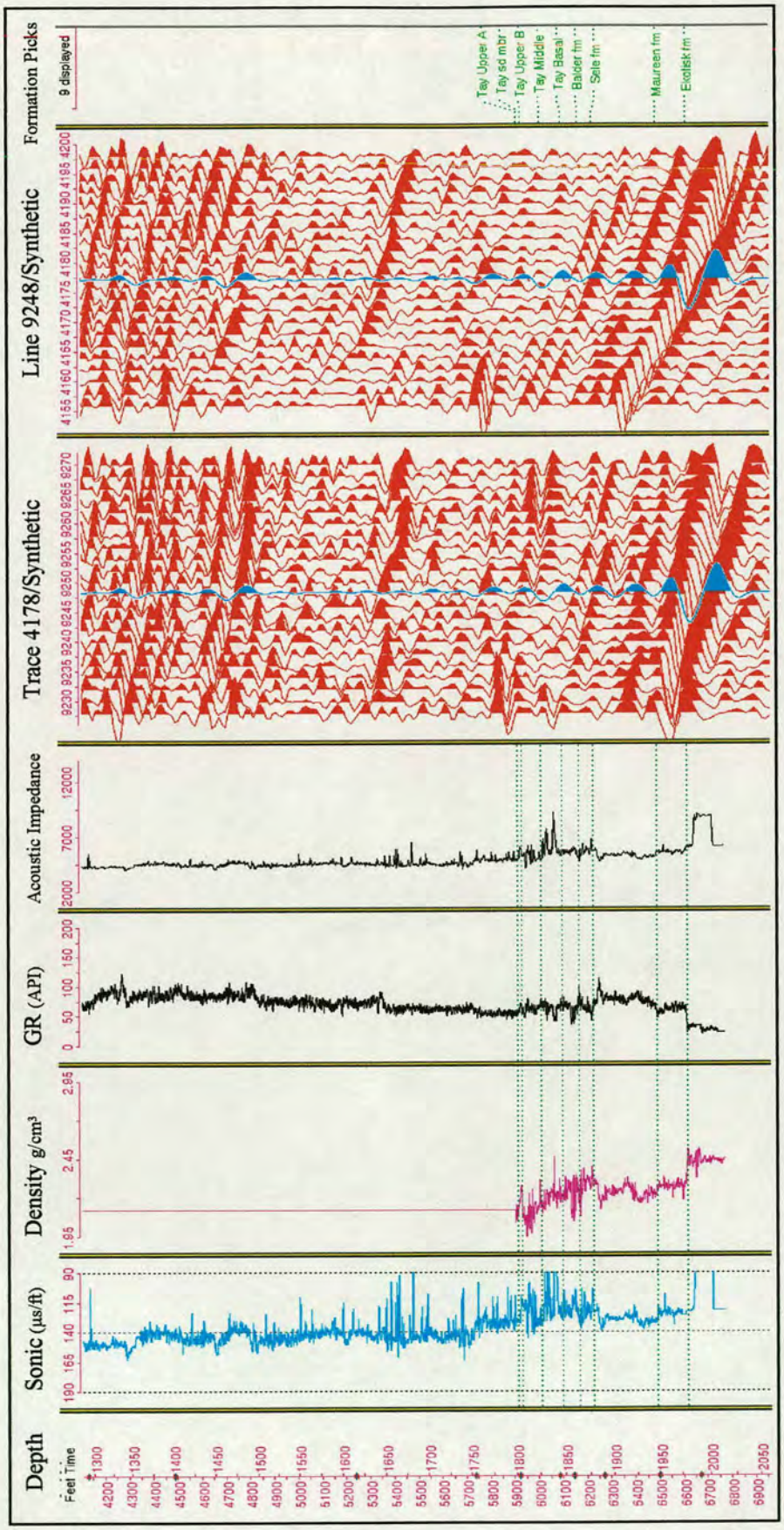

Figure 5.9g: Seismic to Well match for well 21/30-16. Correlation Coefficients of 0.72 and 0.61 for Trace and Line respectively. + 14 ms time shift was required for the match. Note that this is a deviated well.

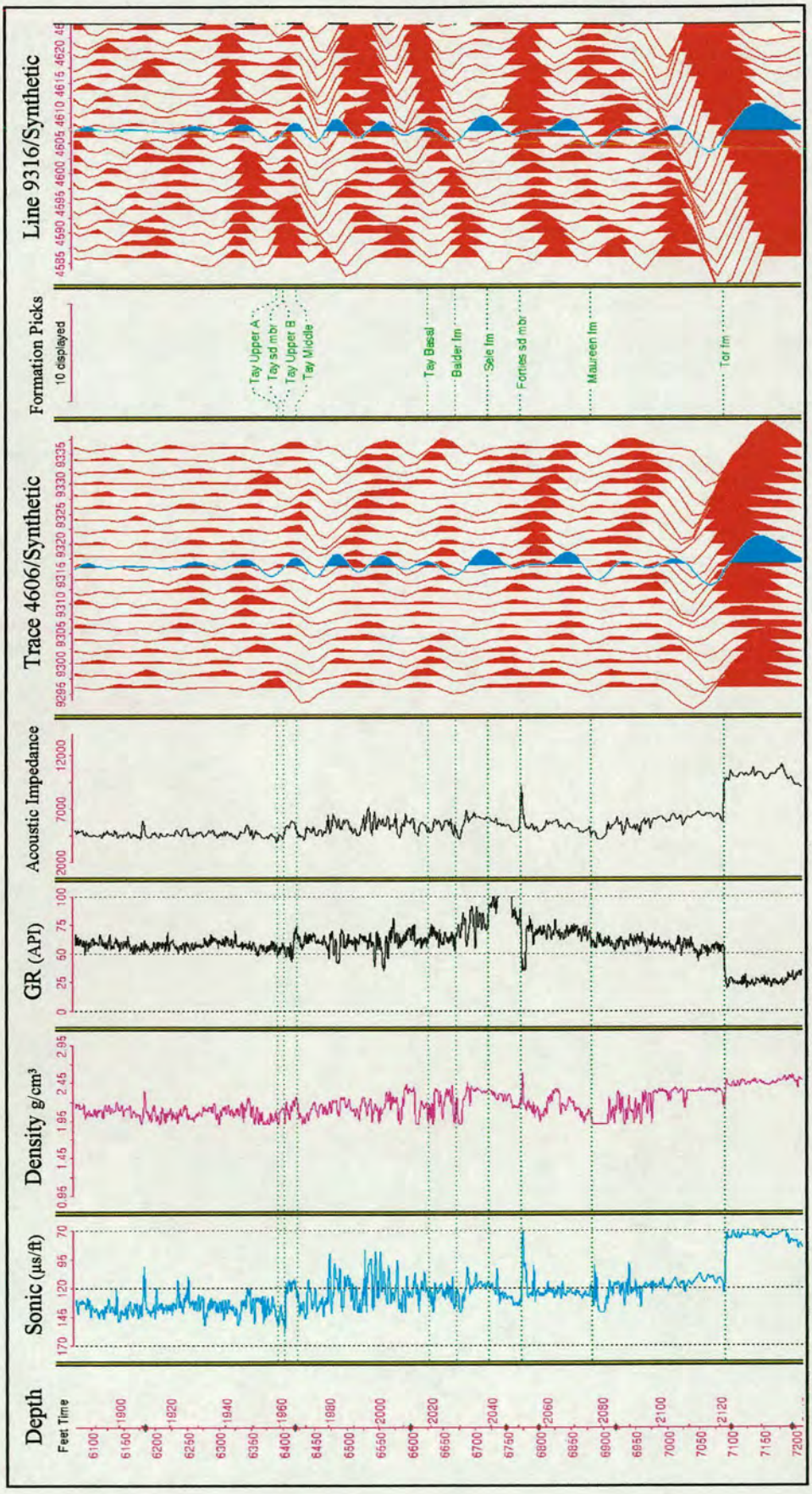

Figure 5.9h: Seismic to Well match for well 21/30-17. Correlation Coefficients of 0.49 and 0.48 for Trace and Line respectively. No time shift was required for the match.

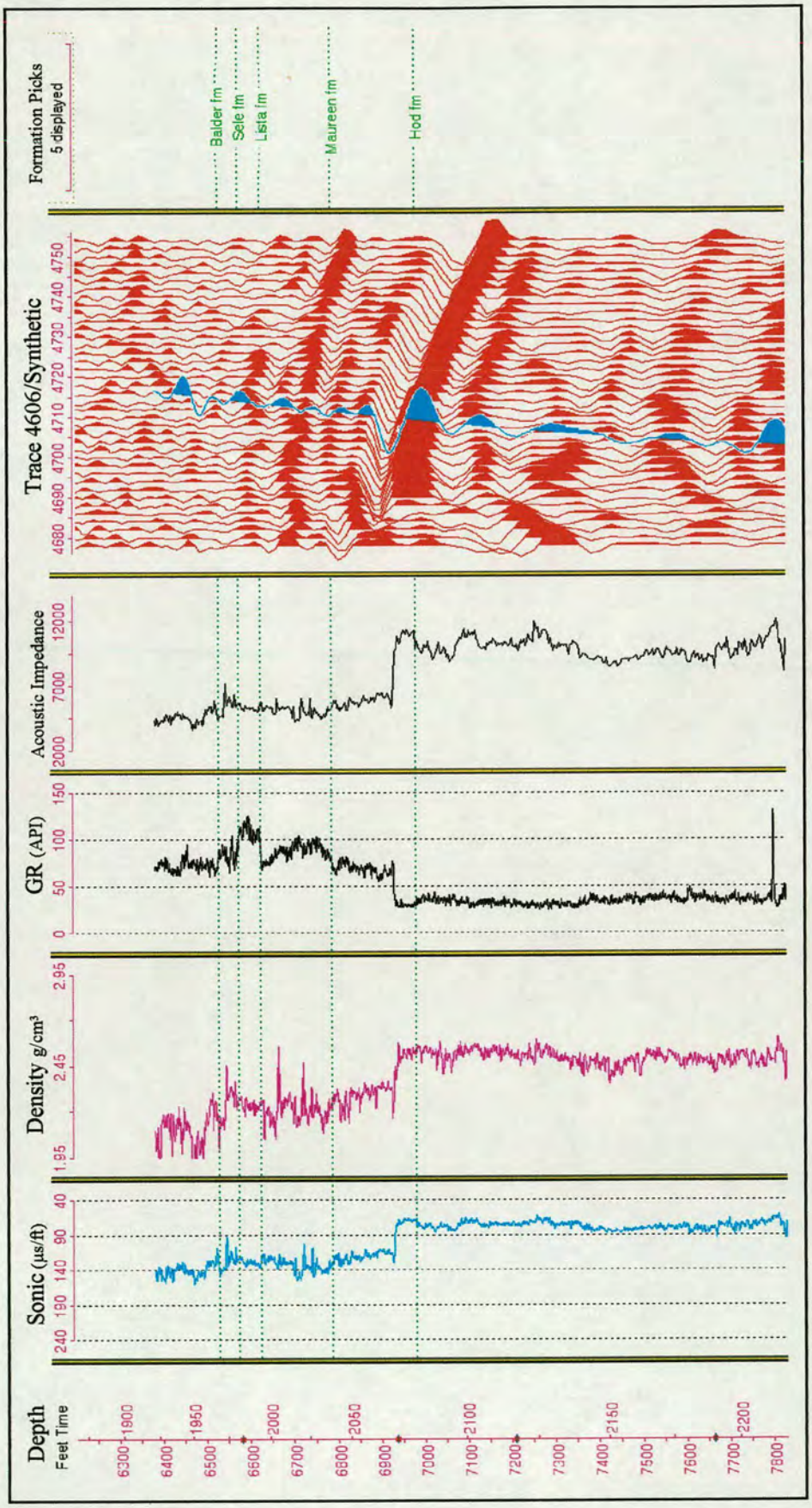

Figure 5.9i: Seismic to Well match for well 21/30-18. Correlation Coefficients of 0.65 and 0.58 for Trace and Line respectively. -16 ms time shift was required for the match. No Tay was deposited at this location.

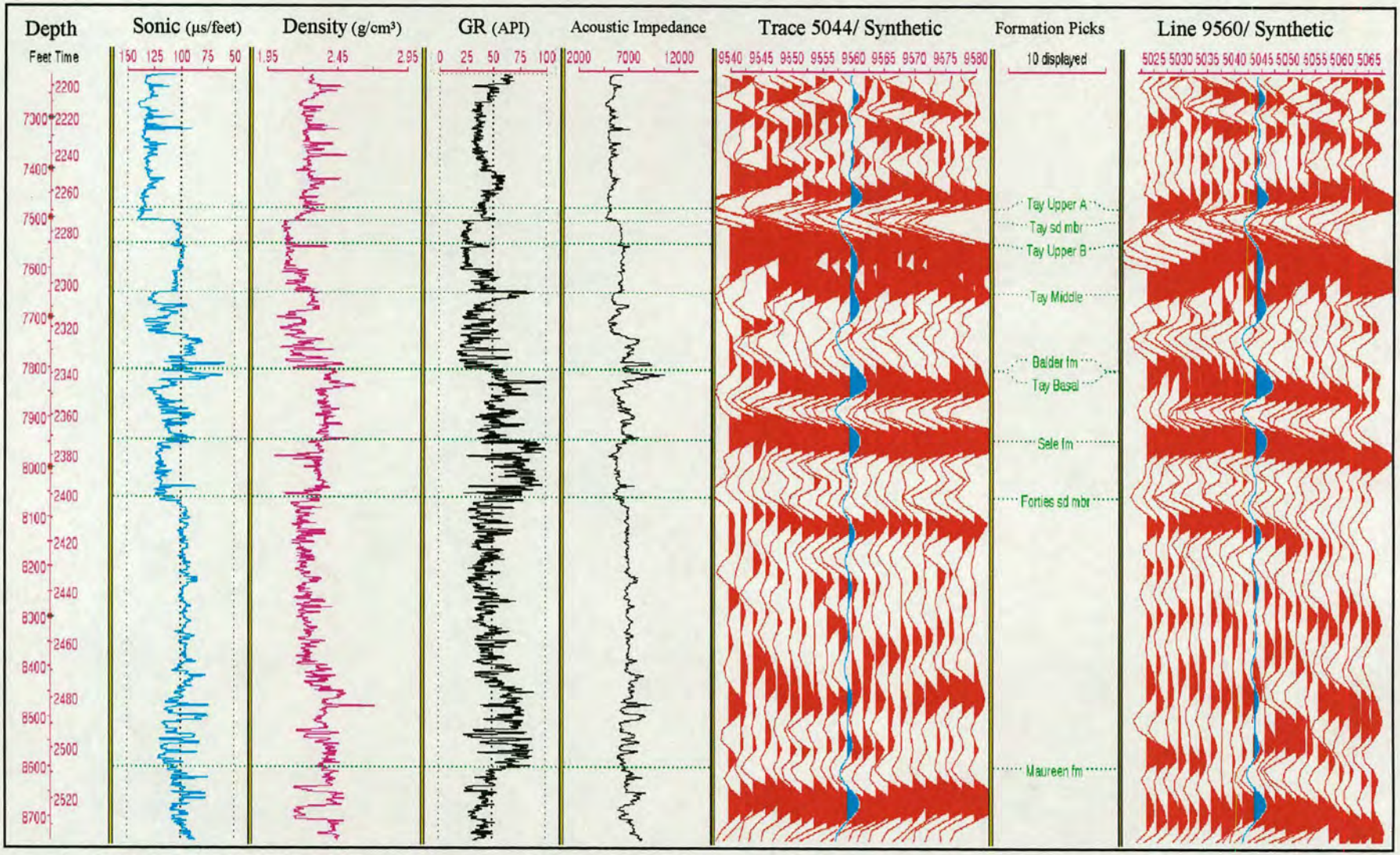

Figure 5.9j: Seismic to Well match for well 22/26a-1. Correlation Coefficients of 0.85 and 0.83 for Trace and Line respectively. Time shift of -18 ms was applied to the synthetic trace.

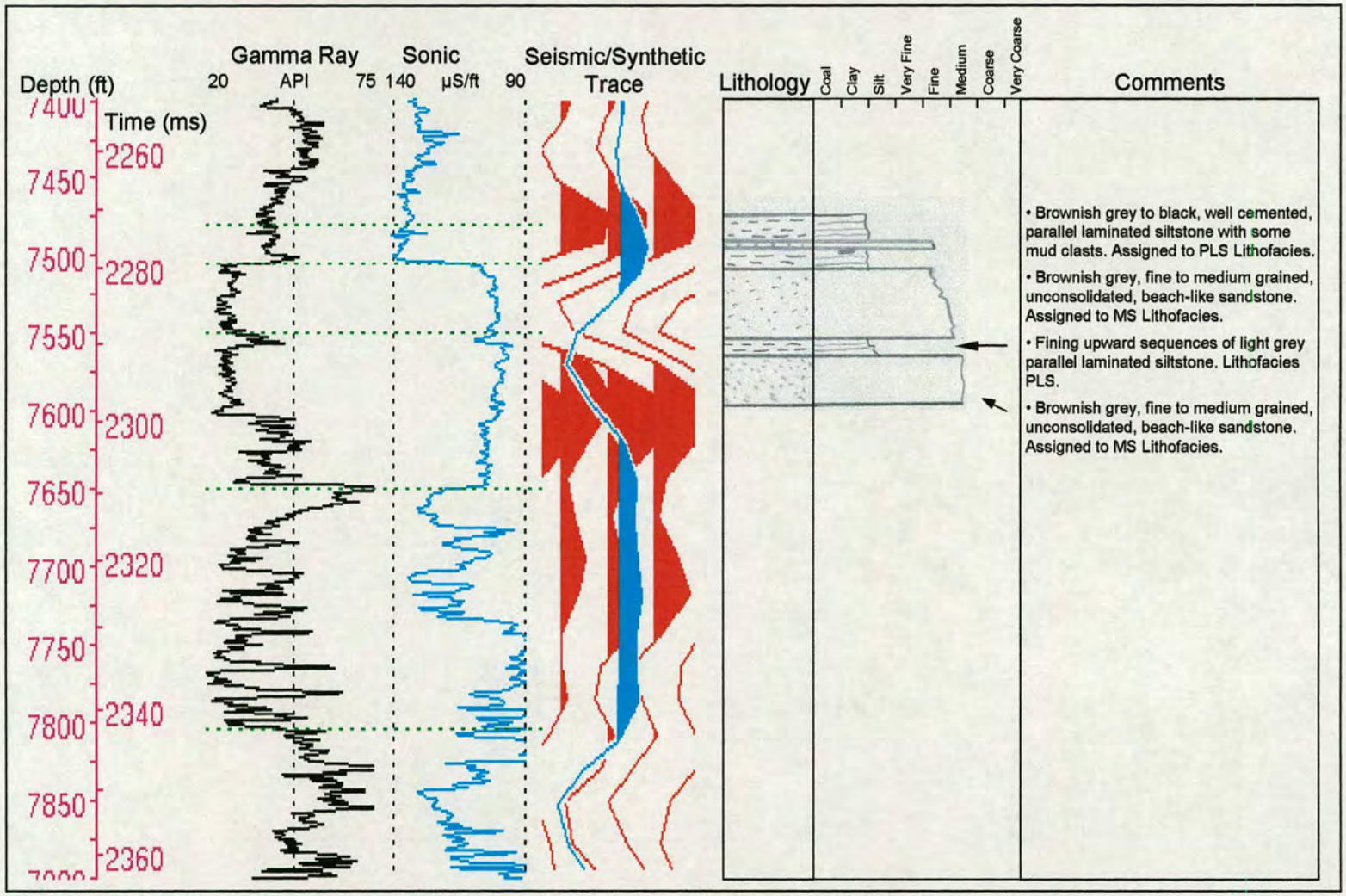

Figure 5.10a: Lithology to seismic data tie at well 22/26A-1. The effect of the thick sand package seen at the well is clearly seen on the seismic traces.

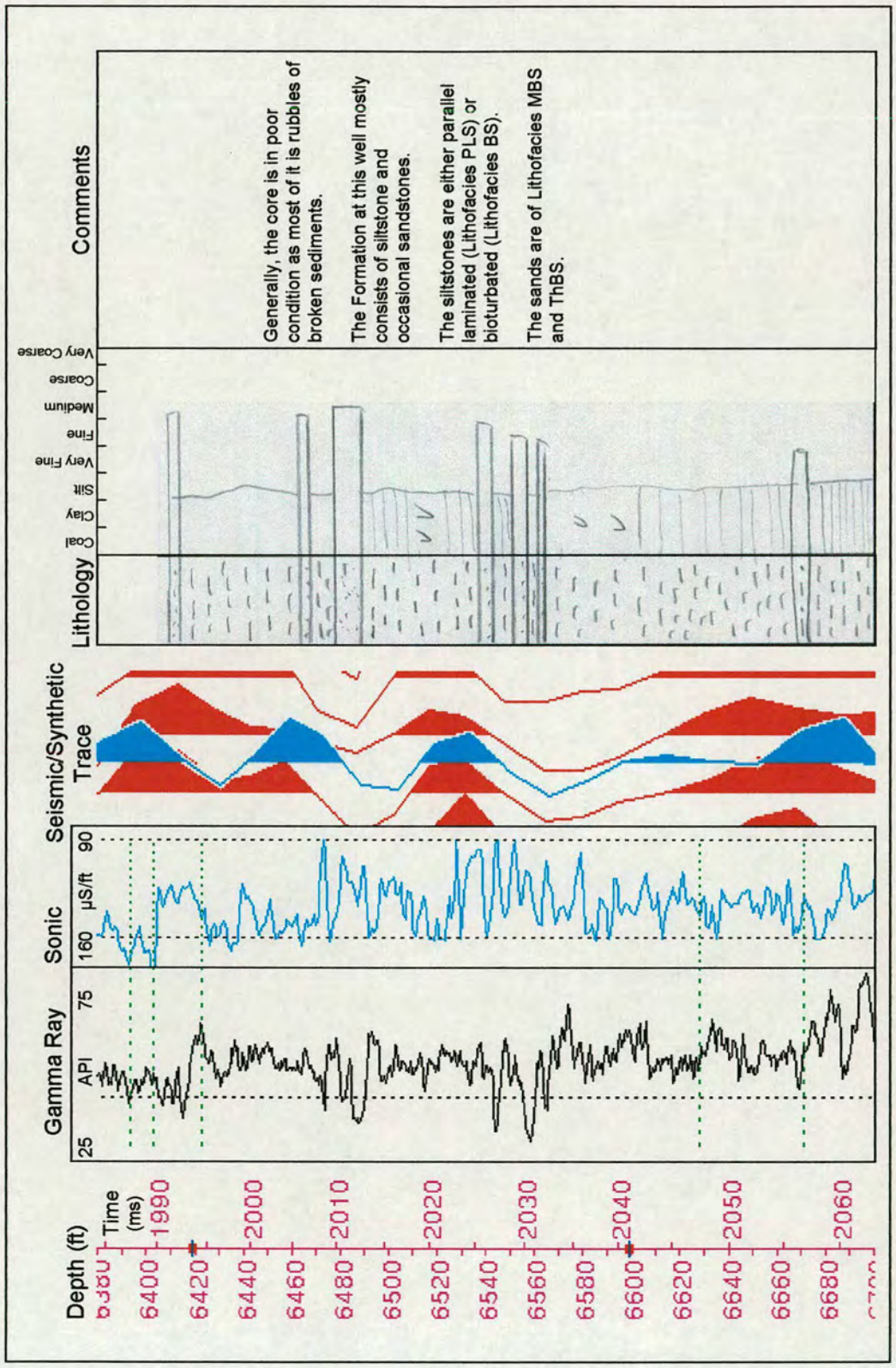

Figure 5.10b: Lithology to seismic data tie at well 21/30-17. Although sand beds are relatively thin but the response in seismic is still apparent.

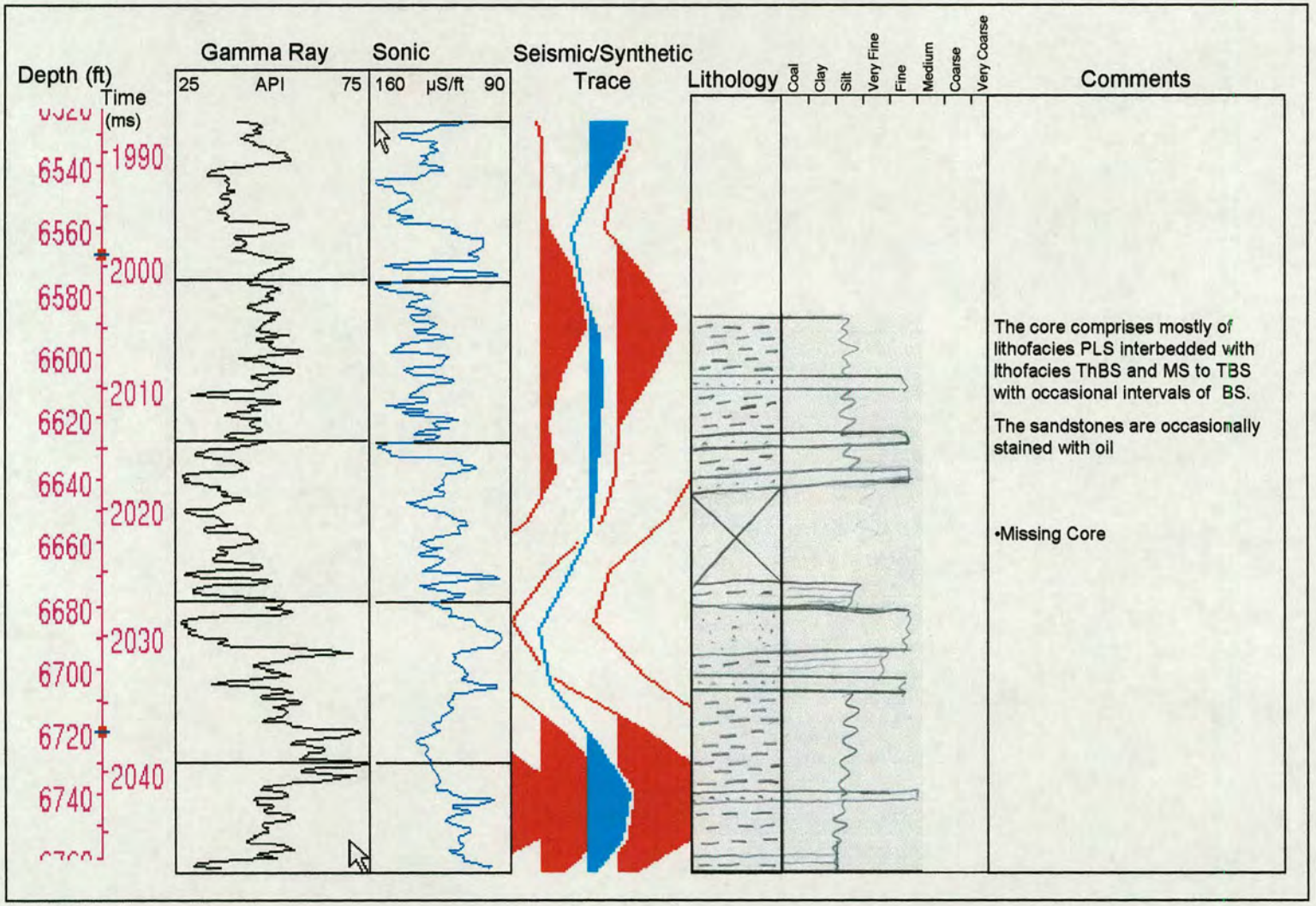

Figure 5.10c: Lithology to seismic data tie at well 21/30-14. The well is mostly consists of siltstone. Sands in this well are oil stained hence the high effect on the seismic despite the thin nature of sands could be due to hydrocarbons

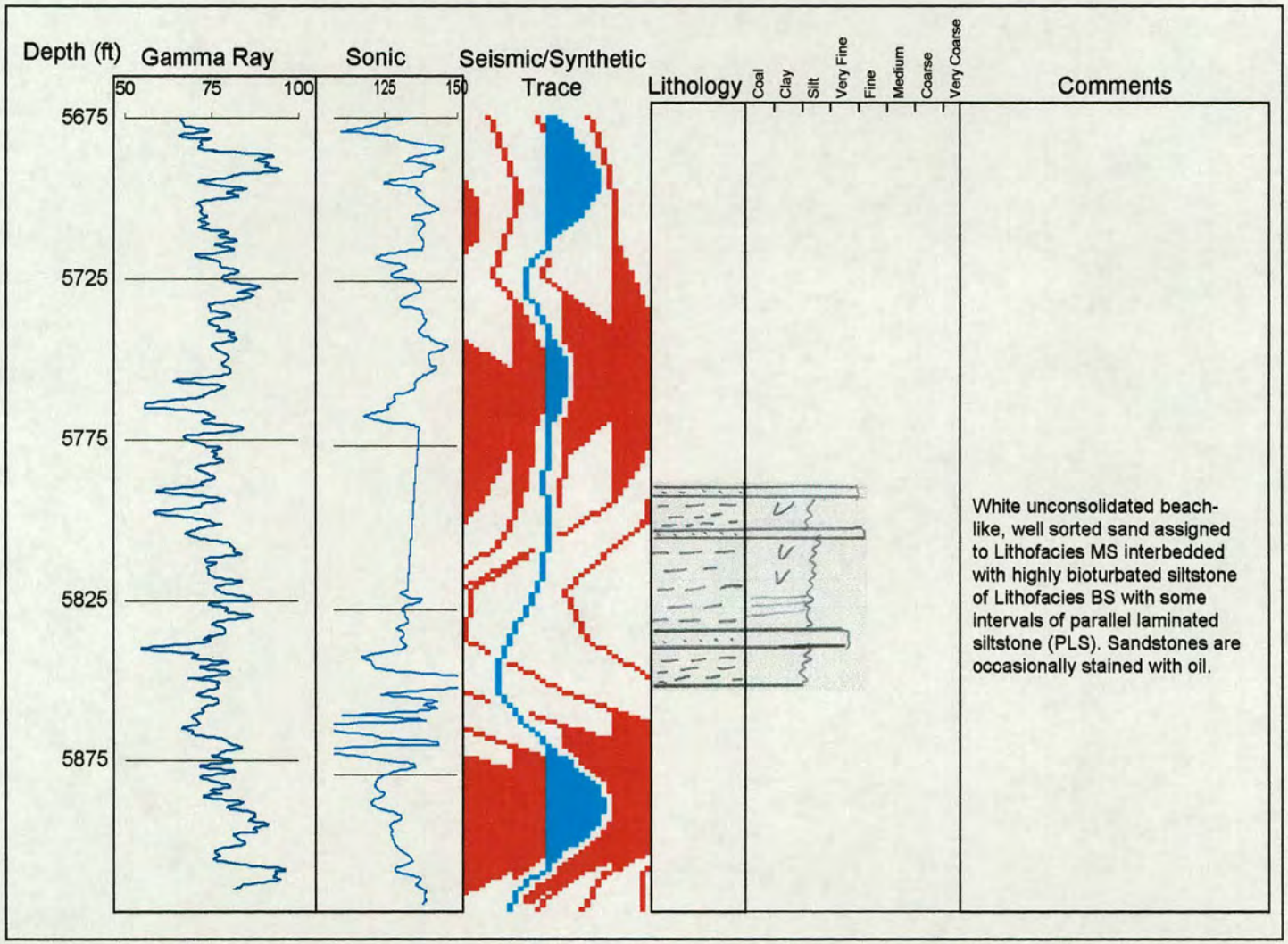

Figure 5.10d: Lithology to seismic data tie at well 21/30-12. Sands in this well are oil stained hence the high effect on the seismic despite the thin nature of sands could be due to hydrocarbons

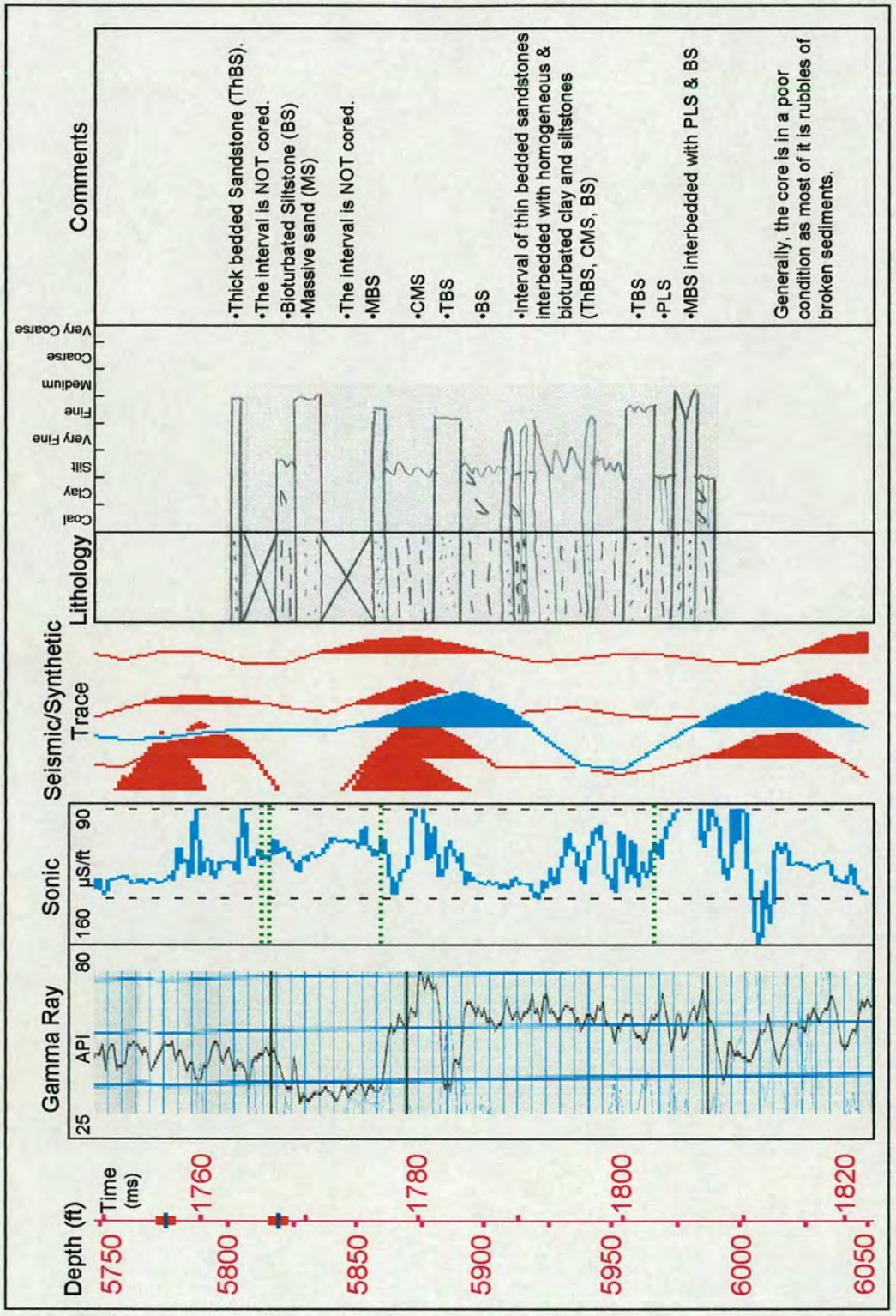

Figure 5.10e: Lithology to seismic data tie at well 21/29b-9

Chapter Six

Chapter Six

Trace Shape Analysis

6.1 Introduction

In recent years, seismic attribute maps have become important tools in the interpretation of seismic data (e.g. Buchanan *et al.*, 1988; Dalley *et al.*, 1989; Rye-Larsen 1994; Dorn *et al.*, 1995; Eggink *et al.*, 1996; Jones & Knipe 1996; Hesthammer & Fossen 1997a,b; Hesthammer 1998; Lanning *et al.*, 2001). The attribute maps have proven especially valuable for understanding subtle stratigraphic features and identifying minor structures such as faults that are close to or below seismic resolution. Such features and structures may have a dramatic effect on reservoir performance. The importance of being able to identify minor features has led to a marked increase in the focus on seismic attribute maps as the interpreter is challenged to provide more accurate and detailed results. However, the increased attention also contains pitfalls that may lead to erroneous interpretation unless the seismic interpreter is aware of the dangers and knows how to quality control the seismic observations, for instance, using well data.

The idea of analysing a seismic data volume based on variation of seismic trace shapes comes from the assumption that changes in lithology, rock properties and fluid content should affect seismic response not only in amplitude but in the whole shape of the trace. Amplitude analysis has always been a key element in hydrocarbon exploration. Although this technique combined with seismic inversion and other attribute analysis has proven successful, it is often time-consuming, requires the expertise of several geoscientists and can mislead the interpreter. The direct study of the variation of trace shapes has been neglected in hydrocarbon exploration due to the lack of an appropriate tool to accurately map these changes. The lack of a tool to

quantify these changes in trace shape controlled by petrophysics was also a major limitation to this technique. This project utilizes the pattern recognition capability of the neural network technology to classify the seismic traces based on their shapes. As a conclusion from the results obtained in the Gannet South area, one can confidently say that seismic trace shape (seismic facies) analysis combined with well data is an accurate, cost-effective and quick methodology. It revealed subtle geological features only expressed in the shape of the seismic trace. This methodology combined with conventional seismic attribute analysis allowed a better understanding of the Gannet South turbidite system. This chapter gives an account of the methodology employed and discusses the results produced. The work was carried out using Flagship Geo's Stratimagic software package based on neural network technology.

6.2 Background to Neural Networks

Eberhart and Dobbins (1990) defined a neural network tool as "an analysis tool that is modelled after the massively parallel structure of the brain: it simulates a highly interconnected, parallel computational structure with many relatively simple individual processing elements or neurons". This definition shows that the term artificial neural network refers to computer systems that are designed to imitate biological processes similar to those that human brain routinely performs. Tasks such as giving expert advice, understanding natural language, speaking, and recognizing complex patterns like handwriting are some of the intelligent actions accomplished by human beings. Similarly, machines or software that can perform some of these tasks are termed intelligent and belong to a group of programmes called artificial intelligence (AI).

Generally neural networks can be classified into two types: supervised and unsupervised neural networks. In a supervised system neural networks exhibit capability to "learn" from examples as the network is presented with a set of inputs and a set of desired outputs. After learning has taken place the network is enabled to predict outputs for a new set of inputs. The other class of networks, however, utilise an unsupervised training procedure. For these systems, only inputs are supplied by

the user; the neural network develops its own classification scheme for the output based on predefined parameters such as number of model classes, number of iteration to find these classes, and correlation coefficient. The idea is based on the "survival of the fittest or the natural selection" rule as the network performs a randomised search using natural selection to find the best representative classes for the entire dataset. This method, which is also called self-organisation, can be very useful for feature extraction in datasets having complex patterns, as it does not employ an "external teacher".

Ali (1994) gave a synopsis of the area of petroleum technology in which neural networks have been used successfully and discussed potential area of application. The current areas of application enumerated include seismic pattern recognition, permeability prediction, and identification of sandstone lithofacies.

Many reasons have been presented by researchers for the application of neural networks for prediction and classification in formation evaluation. The reasons range from the lack of good results using crossplots and correlations to the geological complexity of the formations. Zhou and Wu (1993) argued that conventional log analysis techniques are largely dependent on the initial assumptions about the log analysis parameters. They stated that when using neural networks no assumptions or mathematical models are constructed. The paper pointed out the failure of mathematical formulae or models used in conventional log analysis especially when confronted with complex formations. They explained this failure as being due to the use of simplified equations to express complex correlative relationships between real log reading and formation parameters arising from high heterogeneity and anisotropy of the earth medium. In another paper, Zhou and Yaun (1993) cited the "uncertainty, fuzziness and incompleteness widely existent in reservoir studies" as requiring a powerful tool such as neural networks to deal with them.

Soto *et al* (1997) criticized the application of graphical techniques of prediction and pointed out that neural networks have shown "great potential for generating accurate analysis and results that otherwise seem not to be useful or relevant in the analysis of large amounts of data". Nikravesh (1998) also claimed that conventional mathematical modelling provides simple models that may become inaccurate as

several assumptions are made to simplify the models. In addition Nikravesh mentioned the laborious process involved in complex mathematical analysis and limited human ability to understand and use the information content of the data. The paper listed the potentials of neural networks in modelling from complex and multidimensional data and wide applicability in analysing experimental, industrial and field data. Within similar lines, Trappe & Hellmich (2000) pointed out that neural networks are not domain specific and hence very different data types such as sedimentology or production data can be linked with geological and geophysical information. These features open up the possibility of mapping reservoir properties like facies or permeability that are often only indirectly linked to seismic data and require an analysis of many attributes. Chawathe (1994) indicated the desirability of automating the process of interpretation and hence reduce time and costs associated with the process.

Russell *et al* (1997) described a method for seismic data analysis, which makes use of artificial neural networks to predict log-curves from multiple sets of seismic attributes. Walls *et al* (1999) presented an alternative method for training neural network using model-driven seismic attributes. This trained network is then applied to the seismic data for lithology classification. Schultz *et al* (1994), Trappe *et al* (1995), de Groot *et al* (1998) and Trappe & Hellmich (2000), among others, give examples of the successful application of artificial neural networks in the field of reservoir characterization.

6.3 Dataset and Research methods

6.3.1 Seismic cube extraction

A new project was created in Stratimagic and the 3D seismic data sub-cube for the area of interest was extracted from Landmark software package (N-S oriented "crosslines" from 2820 to 5640 and E-W oriented "inlines" from 8760 to 9910 reducing the original area of the dataset from 680 km^2 to a sub volume covering an area of approximately 500 km^2). All the attribute analysis was conducted on this sub cube.

6.3.2 Horizons transfer

All the horizons interpreted on the seismic data were transferred from Landmark software package to Startimagic. This was done using ASCII format. The horizons were then checked to be on their appropriate signal event i.e. minimum (trough) or maximum (peak). In some cases they had to be shifted to the appropriate event using the adjust option from the toolbar.

6.3.3 Creating a constant time interval

The process of facies classification is performed exclusively on constant intervals, which have both upper and lower boundaries hanging off the same reflector. This is because a neural network needs equal number of samples per wavelet in order to perform the analysis. The interval is defined based upon the reference horizon and where the horizon is not picked, the interval does not exist. The interval should be large enough to capture the entire feature that is being investigated but not so large that other events above or below the feature enter into the analysis. Hence there is no limit for interval size, but it should be more than one half-loop (otherwise, conventional attributes would suffice), and less than 150 ms. Fig. 6.1 shows an example of the main interval used for this study. This is a 30 ms interval as its upper boundary is 10 ms above Top Tay and the lower boundary is 20 ms below Top Tay. Since the definition of the interval is crucial for the seismic facies analysis great care was put into the selection. This interval was determined using horizon slices based upon the reference horizon. The horizon slices, which show spatial amplitude distribution at time surfaces parallel to the reference horizon, were checked every 4 ms and the main channel and lobe features were thought to be prominent within the 30 ms defined as interval of interest as indicated by Fig. 6.2. However, the classification was also run on other intervals, first, to investigate the effect of changing the interval on trace shape analysis results, but more importantly, to understand the change in sand geometries of the turbidite system over time and the structural development and evolution of the basin, hence finding indications to the timing, nature and extent of factors controlling the sediment deposition and transport pathways in the area.

A total of 30 horizon slices were extracted, only three of which are shown in Fig. 6.2 and the rest are given in appendix 4. Table 6.1 below shows the different intervals used for the analysis. Top Upper, Middle and Basal Tay were used as reference horizons. In addition to these horizons and in order to increase the level of detail, the analysis was also run on a zoomed top Tay horizon, which is areally limited to only one area of interest, e.g. just the lobe rather than the lobe and the channel.

Reference Horizon	Upper Boundary	Lower Boundary
Top Tay	- 10 ms	+ 20 ms
	0 ms	+ 30 ms
	+ 10 ms	+ 40 ms
	+ 20 ms	+ 30 ms
	+ 20 ms	+ 50 ms
	+ 30 ms	+ 40 ms
	+ 30 ms	+ 60 ms
Zoomed Top Tay	- 10 ms	+ 20 ms
Middle Tay	- 15 ms	+ 15 ms
	- 10 ms	+ 20 ms
	- 5 ms	+ 15 ms
Basal Tay	- 10 ms	+ 15 ms
	- 10 ms	+ 20 ms

Table 6.1: showing different intervals used for the analysis with reference to each horizon.

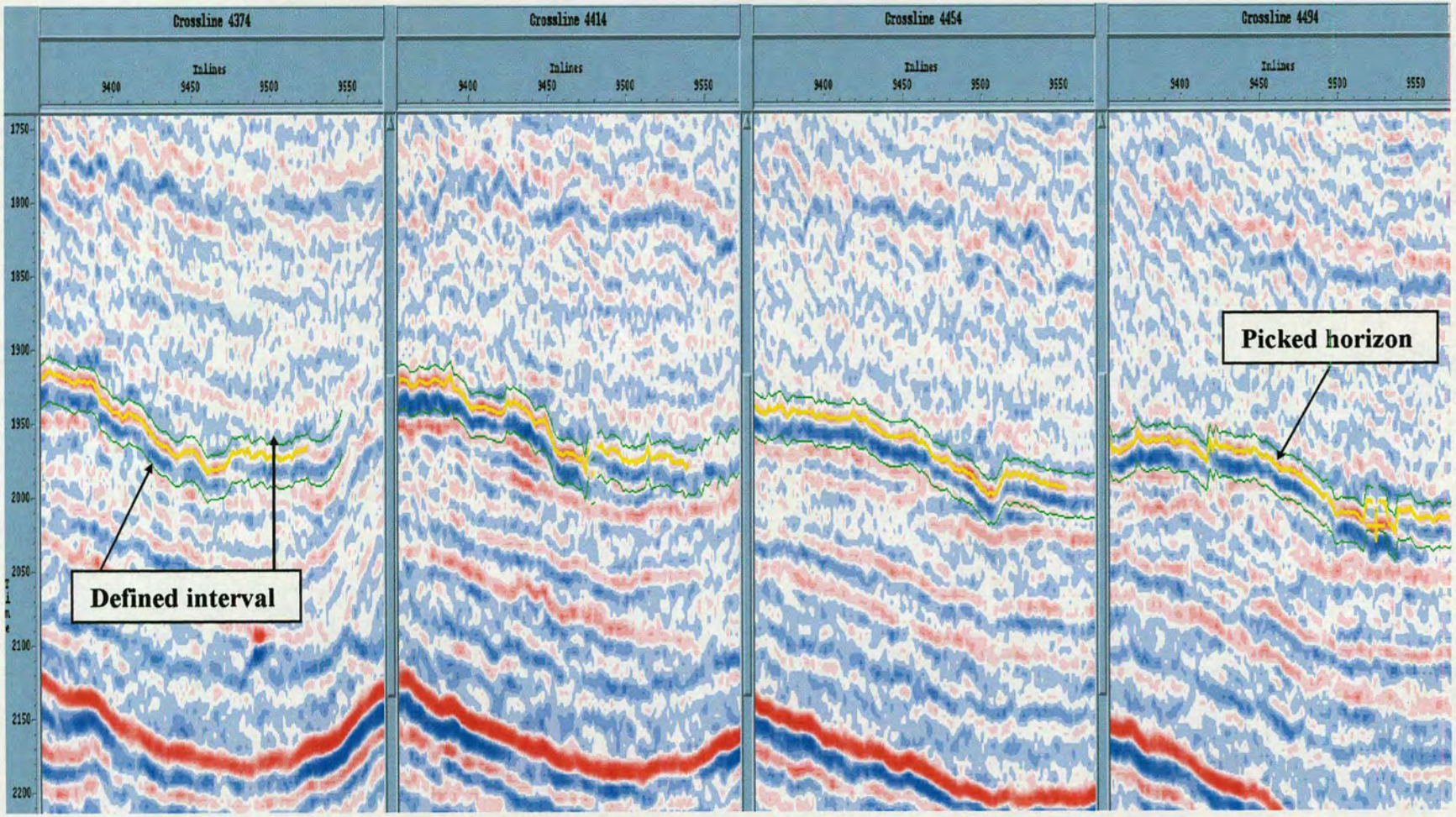

Figure 6.1: Four crosslines showing the picked Top Tay horizon and the 30 ms interval used for trace shape analysis.

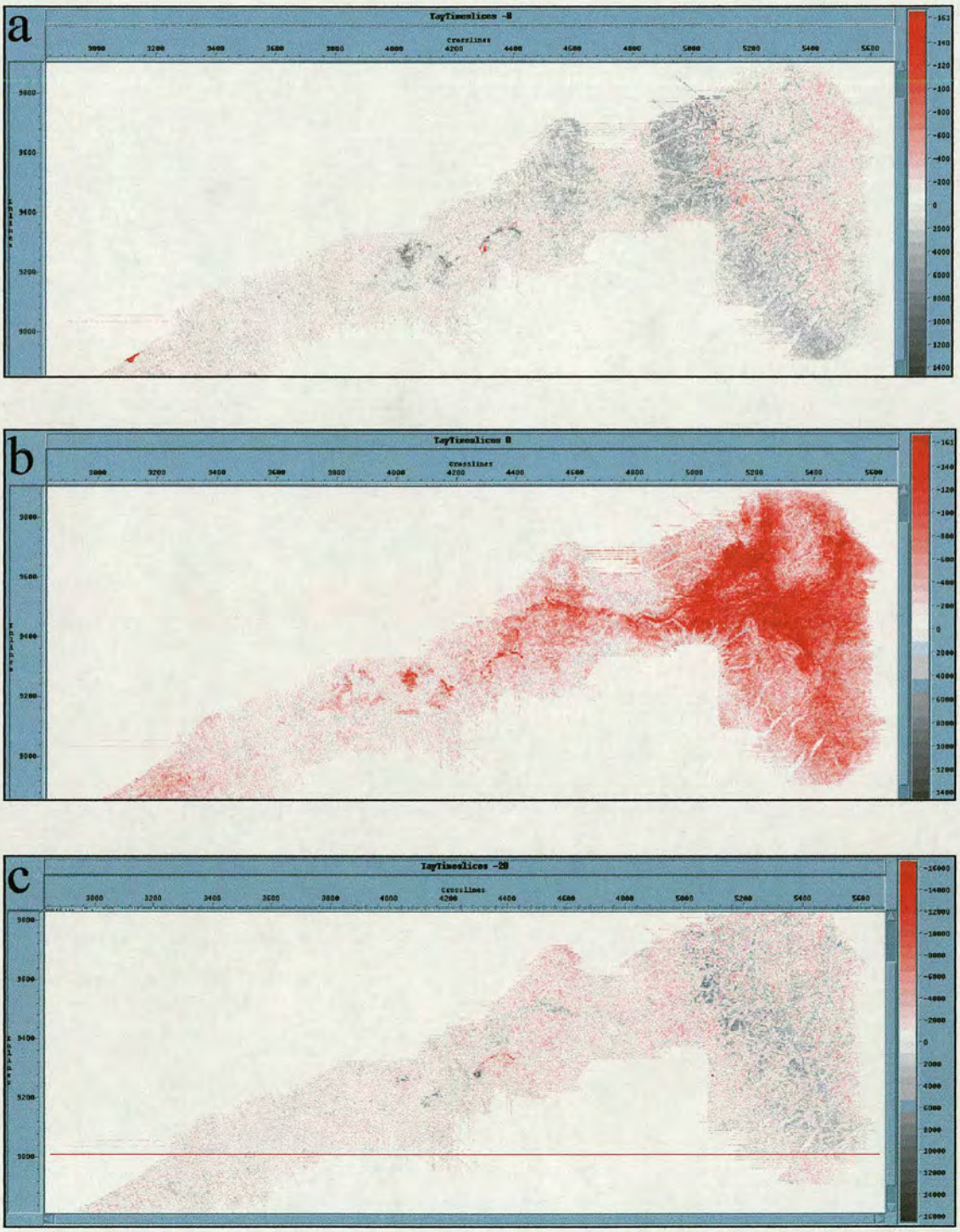

Figure 6.2: Horizon slices used to identify the upper and lower boundary of the interval which is used for trace shape analysis. The main channel and lobe features were thought to be prominent within this 30 ms interval.
a) amplitude distribution at the upper boundary of the interval (Top Tay –8 ms).
b) amplitude distribution at the horizon level (Top Tay).
c) amplitude distribution at the lower boundary of the interval (Top Tay + 20 ms)

6.3.4 Creating facies

Trace shape in Stratimagic is quantified as the change of sample value from sample to sample, i.e. strongly negative, negative, almost nil, positive or strongly positive. The actual amplitude values are not as significant as overall shape. First, a desired number of classes (seismic facies) is identified. This can be based on how many different geological facies giving different seismic response are expected to be found within the interval. However, as a rule of thumb, 10% of the interval size is a good starting number (Stratimagic Manual).

The neural network is then trained on the actual trace shapes within the seismic interval over the whole data set. Through a number of iterations, the neural network constructs synthetic seismic traces according to the number identified at first. Fig. 6.3 shows a series of model traces (facies classes) that were constructed to best represent the diversity of the trace shapes in the seismic data and each trace model was then given a colour. The cyan curve below the facies classes represents the cumulated variation of shapes. In an ideal situation, a linear trend is expected; however, variations in the slope can be a good indicator of different geological environments. The figure shows an increase in the trough amplitude as we go from right to left. Since the interface these traces represent is between the Horda shales and the Tay sands as discussed in the previous chapters, it could be concluded that the impedance contrast increases moving from the purple to the orange and then starts decreasing again towards the brown class. This means for the same fluid content, traces represented by the yellow-orange colours are indicating cleanest sand within the interval. The effect of number of model traces was investigated by running the facies classification using different number of classes as mentioned when the results are discussed. 7, 10, 12, 15, 18, 20 and 25 facies classes were used and analysed both visually and using the correlation threshold option in the software package.

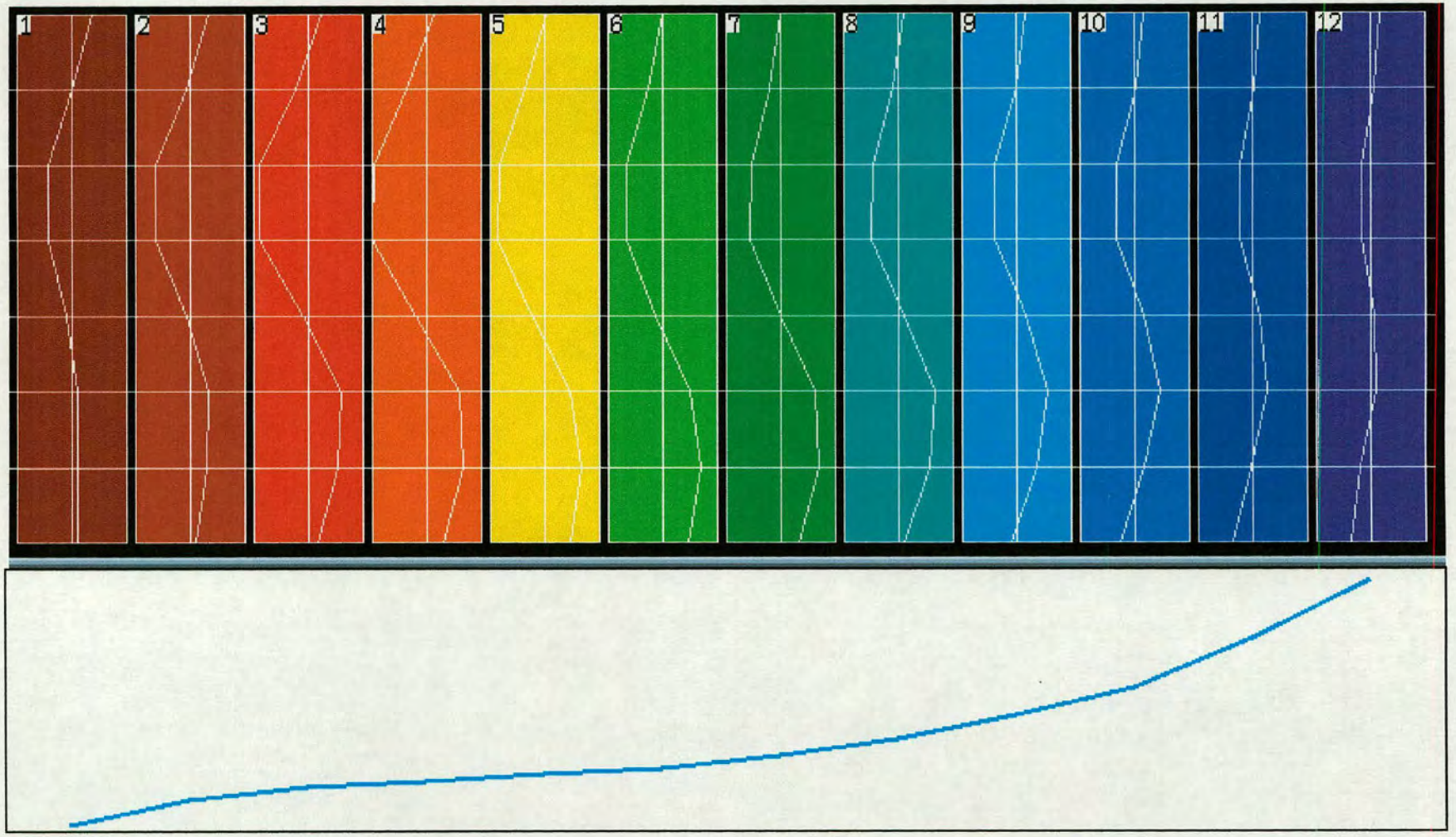

Figure 6.3: Series of model traces that best represent the diversity of the trace shapes within the defined interval of the seismic datase. Each model trace is assigned a representative colour. The cyan coloured line at the lower part of the figure shows the cumulative variation of shapes.

6.3.5 Running facies analysis

Once the model traces that best represent the diversity of trace shapes in the seismic data are constructed and each model trace is given a colour, each seismic trace within the interval is then cross correlated to the model traces and hence it is assigned the colour of the model trace that it best matches. This can be seen in Fig. 6.4. Note that colours have been shifted upward in order to make the interval they represent visible. This way of representation means nothing when seen in the cross-sectional view but observing the distribution of colours in the map view allows the distribution of seismic shapes throughout the interpreted area to be assessed and if these trace shapes are correlated with geological facies, through well information, the map can be a powerful means to study the distribution of these facies over the whole area. In addition to the facies distribution map a correlation map is also produced to allow quality control check on the correlation process. The correlation coefficient provides the degree to which the actual seismic trace matches the model trace.

6.3.5.1 Unsupervised classification

The unsupervised clustering allows zonation of the seismic data into parts with most similar trace patterns. This way a natural grouping of the data can be determined, leading to identification of general trends in the data. The input is the seismic data and the output is a partition of the data in different groups. In the unsupervised classification, model traces that are thought to represent the seismic data are determined automatically based on predefined parameters such as number of model classes, number of iteration to find these classes and correlation coefficient. To refine the analysis one can increase the number of classes as this will increase the level of detail but only up to a point. Alternatively the level of detail can also be increased by areally limiting the classification to cover only the area of interest e.g. only the channel rather than channel and overbank. Below is the list of maps produced using unsupervised classification.

Top Tay Horizon – 10 + 20 ms, 7 classes
Top Tay Horizon – 10 + 20 ms, 10 classes
Top Tay Horizon – 10 + 20 ms, 12 classes

Top Tay Horizon – 10 + 20 ms, 15 classes

Top Tay Horizon – 10 + 20 ms, 18 classes

Top Tay Horizon – 10 + 20 ms, 20 classes

Top Tay Horizon – 10 + 20 ms, 25 classes

Top Tay Horizon 0 + 20 ms, 15 classes

Top Tay Horizon + 20 + 30 ms, 15 classes

Top Tay Horizon + 30 + 40 ms, 15 classes

Top Tay Horizon + 30 + 60 ms, 15 classes

Top Tay Horizon + 20 + 50 ms, 15 classes

Top Tay Horizon + 10 + 40 ms, 15 classes

Zoomed in Top Tay Horizon – 10 + 20 ms, 15 classes

Top Middle Tay Horizon – 5 + 15 ms, 15 classes

Top Middle Tay Horizon – 15 + 15 ms, 15 classes

Top Middle Tay Horizon – 5 + 15 ms, 15 classes

Top Middle Tay Horizon 0 + 15 ms, 15 classes

Top Basal Tay Horizon – 10 + 15 ms, 15 classes

Top Basal Tay Horizon – 10 + 20 ms, 15 classes

6.3.5.2 Supervised Classification

In contrast to unsupervised classification, in this type the model traces are not automatically determined but rather chosen by the user. One can either use synthetic seismic traces calculated from the well data or actual seismic traces at the well location. At this location, taking the knowledge from the well, one can know exactly what the seismic trace represents and hence by studying the extent of similar trace shapes we can envisage the distribution of similar facies. This is thought to be a very powerful tool and was used to determine the extent of different turbidite units within the Gannet South area using facies of the different wells available in the area. Below is the list of maps produced using supervised classification.

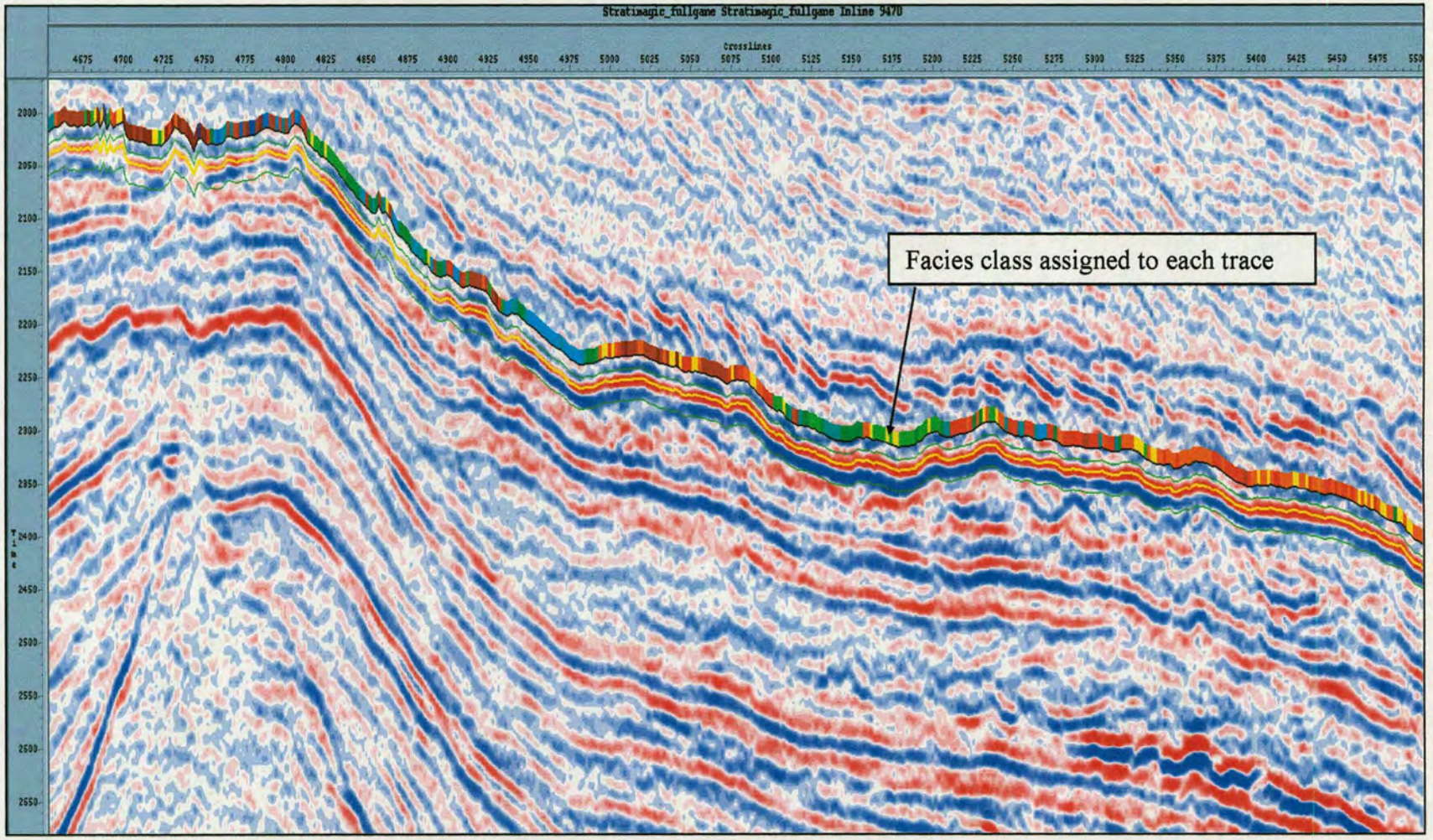

Figure 6.4: Each seismic trace is correlated to the model traces and is assigned the colour of the facies class that it best matches. Note that the colours have been shifted upward to view the interval they represent.

First, using one well at a time:

Upper Tay Unit using well 22/26a-1

Middle Tay Unit using well 22/26a-1

Basal Tay Unit using well 22/26a-1

Upper Tay Unit using well 21/-30-17

Middle Tay Unit using well 21/30-17

Upper Tay Unit using well 21/29b-9

Basal Tay Unit using well 21/29b-9

Using multiple wells:

Upper Tay using wells 21/30-12, 21/30-14, 21/30-15, 21/30-17 and 21/30-18

6.4 Results and Discussion

6.4.1 Unsupervised Classification

6.4.1.1 Effect of number of facies used

Figs 6.5 to 6.9 show the result of unsupervised classification using the same interval but with varying number of classes. The amount of detail added by increasing the number of facies from 10 to 15 is obvious when comparing Figs 6.5 and 6.7 especially in the lobe area. However, the effect of adding any more classes seems to be minimal. Hence 15 facies was assumed to be adequate number of classes to be used for this interval of the seismic data. This exponential effect of increasing the number of facies on the added detail is illustrated by the schematic curve in Fig. 6.10 below. Model traces for each of these maps together with corresponding maps with applied 90% correlation threshold are given in appendix 5.

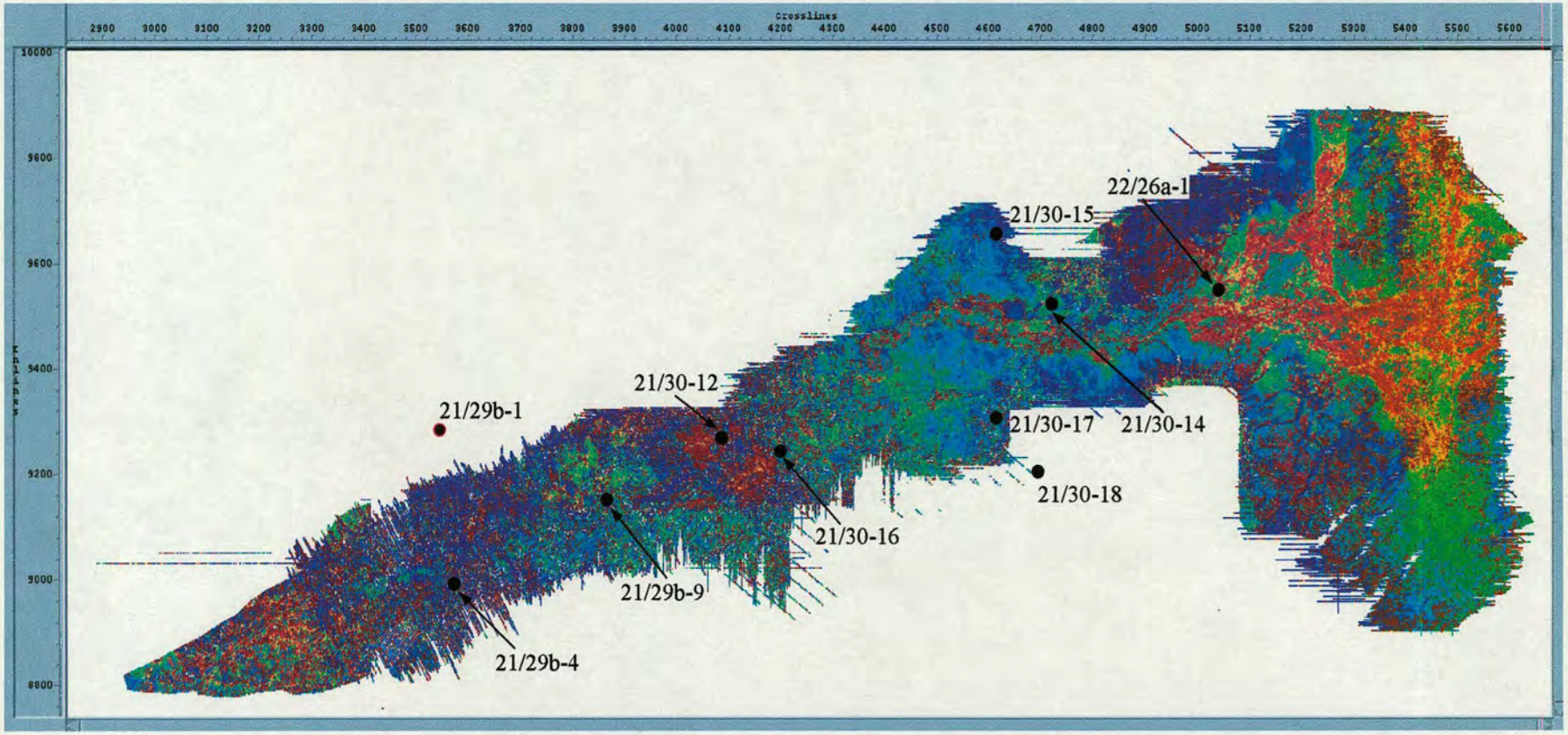

Figure 6.5: Results of unsupervised classification for the 30 ms interval hanging off the Top Tay horizon (-10 and + 20 ms) using 10 facies classes.

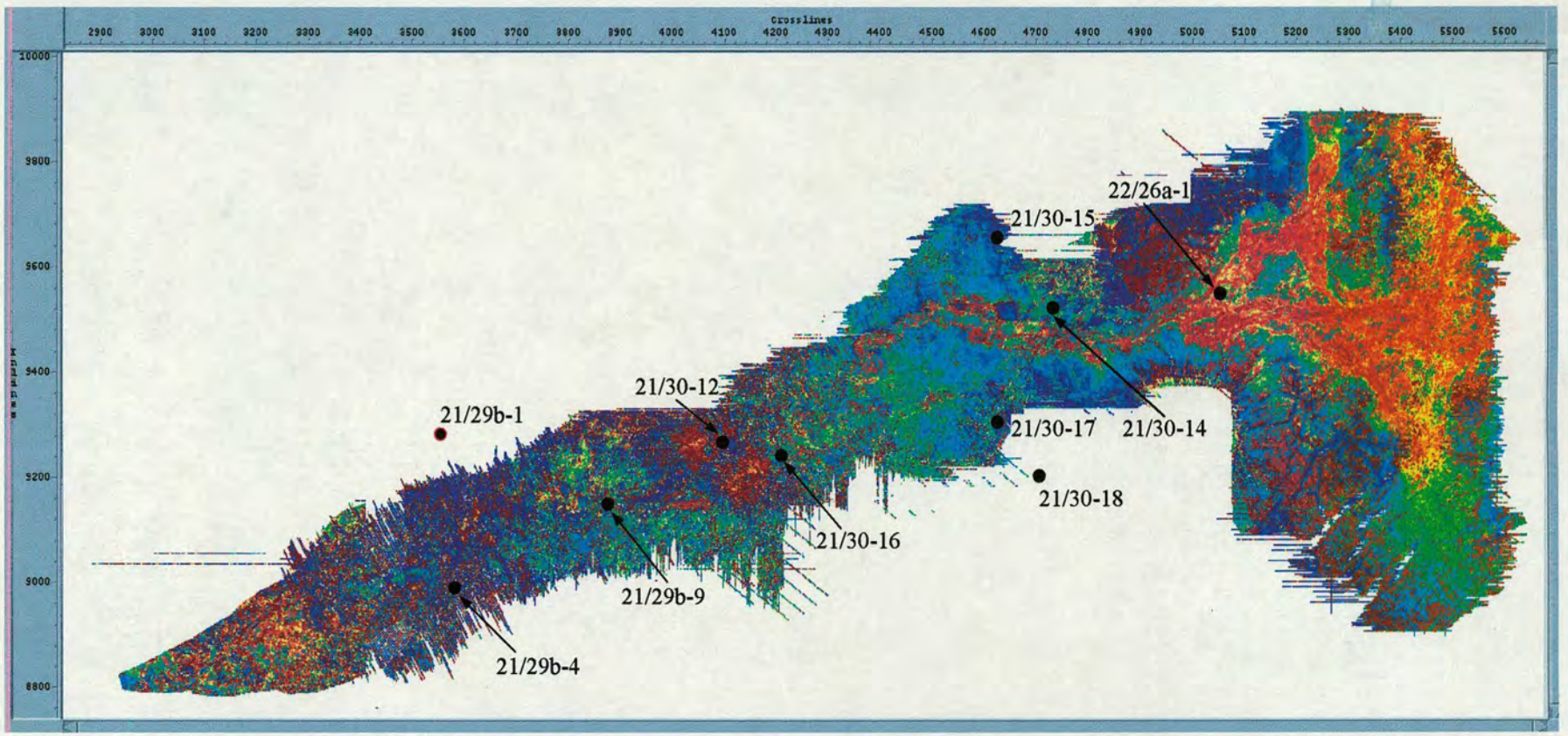

Figure 6.6: Results of unsupervised classification for the 30 ms interval hanging off the Top Tay horizon (-10 and + 20 ms) using 12 facies classes.

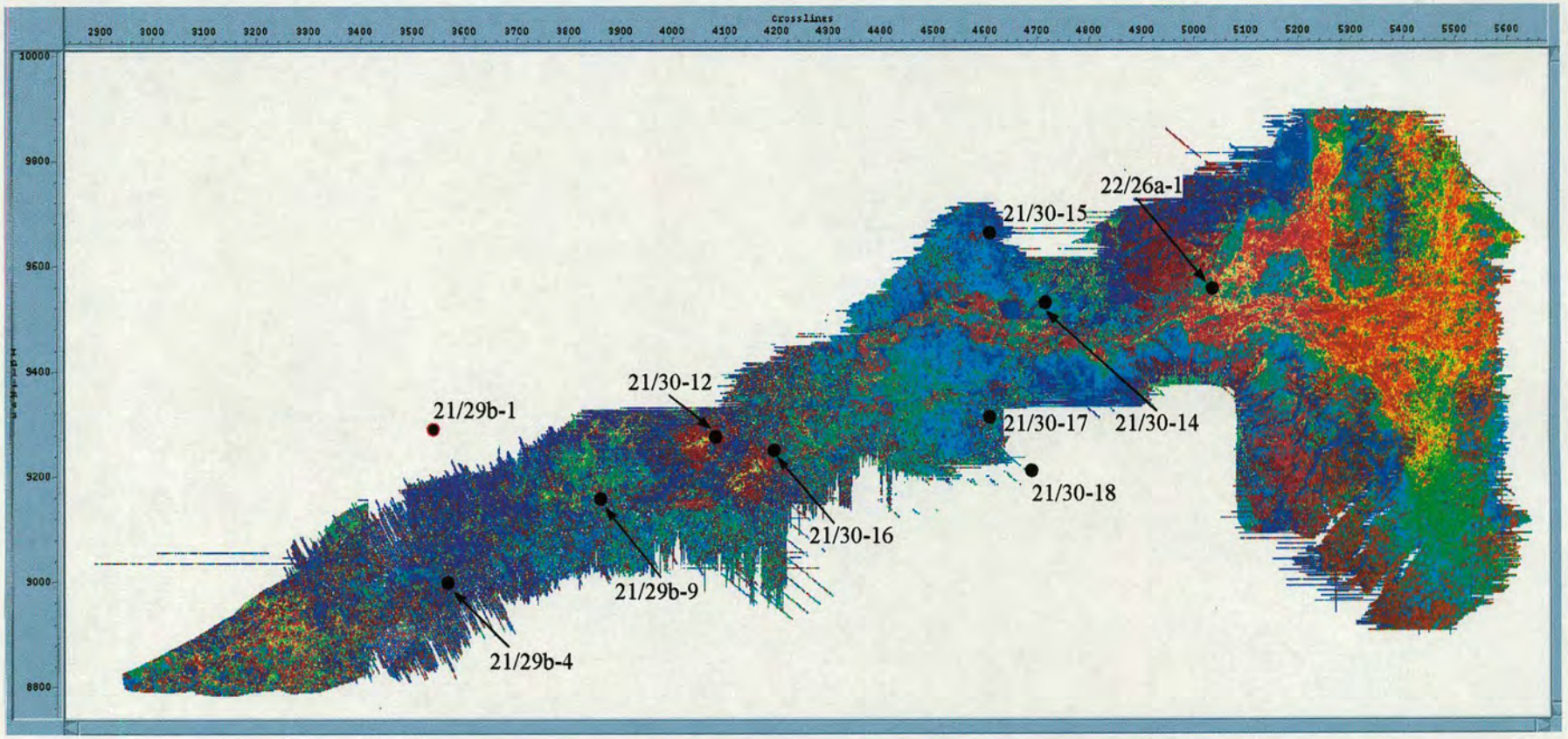

Figure 6.7: Results of unsupervised classification for the 30 ms interval hanging off the Top Tay horizon (-10 and + 20 ms) using 15 facies classes.

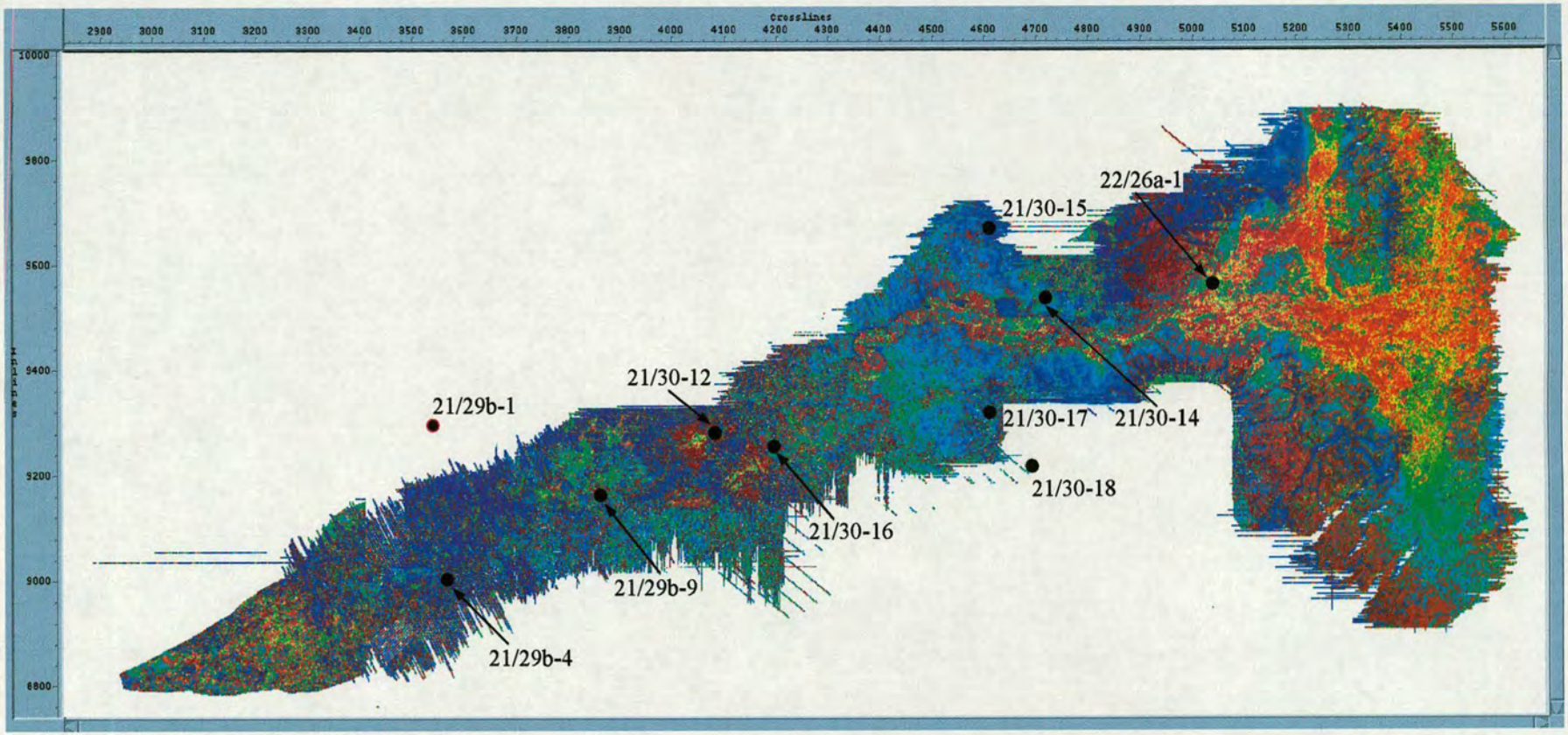

Figure 6.8: Results of unsupervised classification for the 30 ms interval hanging off the Top Tay horizon (-10 and + 20 ms) using 20 facies classes.

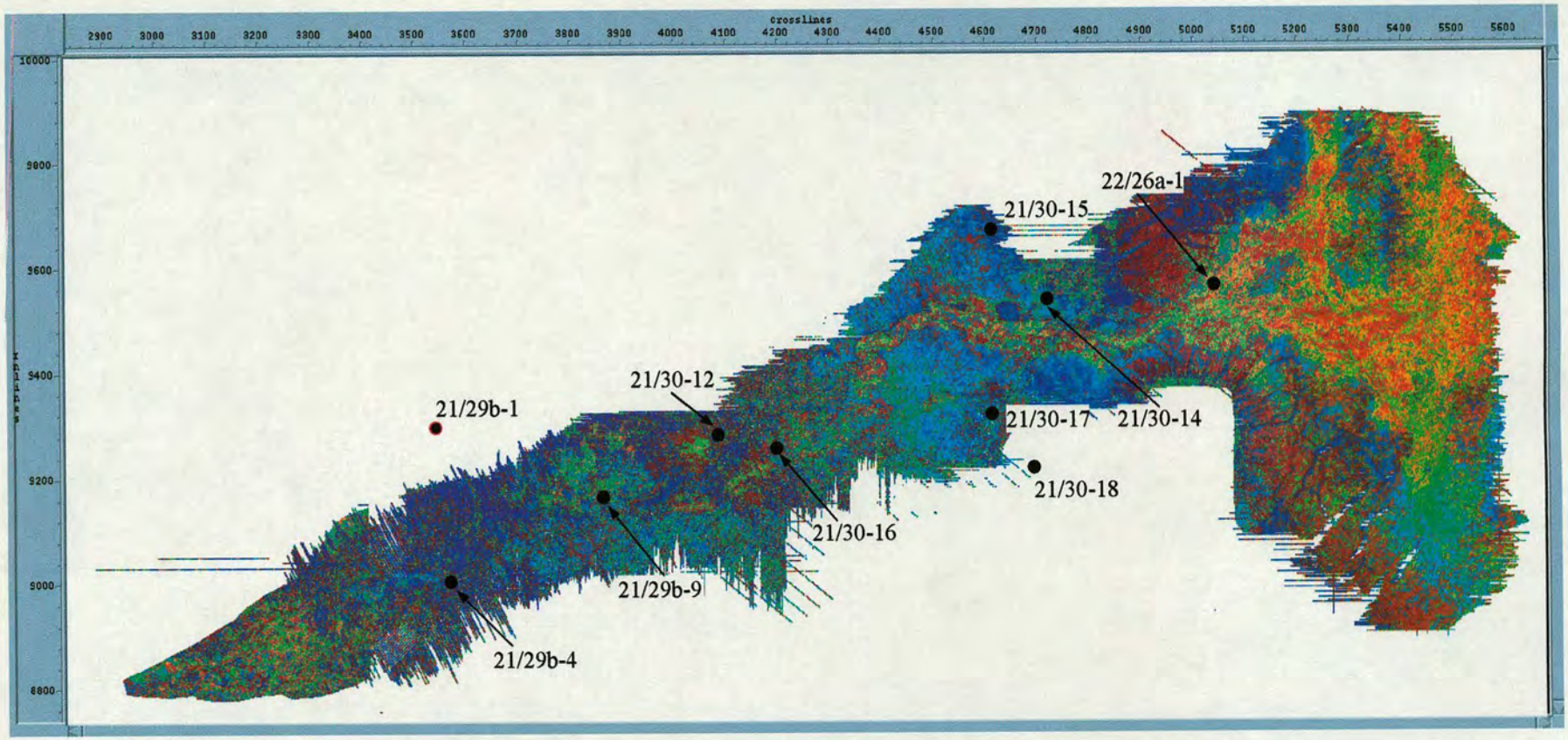

Figure 6.9: Results of unsupervised classification for the 30 ms interval hanging off the Top Tay horizon (-10 and + 20 ms) using 25 facies classes.

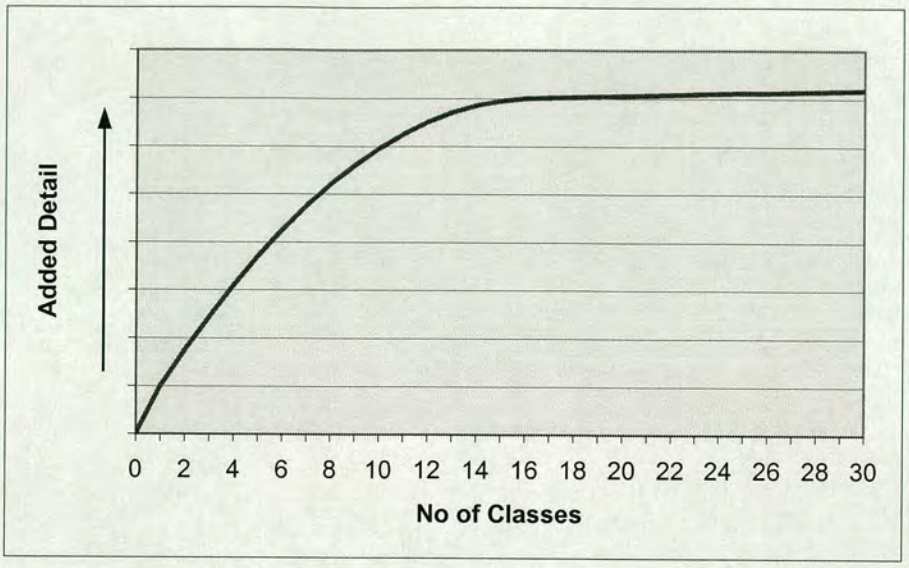

Figure 6.10: A schematic diagram showing the amount of detail added with the increase in number of classes. The amount of detail increases with increasing the number of facies up to a point after which the effect becomes minimal.

6.4.1.2 Classification using Top Tay as the reference horizon

It has been demonstrated in chapter 3 that Top Tay reflection is the strongest within the Tay Sandstone Member in the Gannet South area. The Top Tay is uniquely defined as a continuous trough resulting from the difference in acoustic impedance between the clean Tay sandstones and the overlying mudstones of the Horda Formation. The interpretation of this reflector is the basis for the trace shape analysis conducted on the seismic data. The little structural deformation due to faults on this boundary provided an ideal opportunity for the trace shape analysis.

Fig. 6.11 shows the variation in shape of the seismic traces within the 30 ms interval covering the Top Tay horizon. The figure readily delineates the channel and the lobes. Zooming into the middle subbasin (subbasin II) as depicted by Fig. 6.12 clearly indicates the distribution of the facies within this area. The red colour indicates channel fill sands whereas the green indicate sheet-like sand deposition areas. It is apparent that the sinuosity of the channel has increased. As discussed in chapter 3, this is thought to have been caused by the flow slowing down due to

reduction in the slope angle. Another factor that led to the reduction of flow energy is the bifurcation of the channel, illustrated by Fig.6.12, as sediments followed more than one direction and some were deposited, causing the sediment flow to become even weaker and lose its momentum to follow a straighter path.

Fig. 6.12 also shows a large amount of sand depicted in green colour deposited at the sharp bends of the sinuous channel. According to Clark and Pickering (1996) spillover points develop where flows breach levees on sharp bends, and where channel gradients decrease to cause an increase in flow thickness. If the spillover flow is sandy, then it might accelerate and erode a new channel (e.g. Var Fan, Normak & Piper 1991). If the flow is muddy, however, then the spillover flow will decelerate, resulting in more sheet-like deposition of mud (e.g. turbidity current II on the Navy Fan, Piper & Normak 1983). The amount of flow stripping depends on the competence and capacity, magnitude of velocity change, grain size distribution throughout a flow, and the momentum of turbidity currents with respect to channel depth (Kneller & McCaffrey 1999). Large flows that are an order of magnitude thicker than the height of the levees, are much less affected by the constraints of a channel, and therefore flow stripping has less effect. Flow stripping is also insignificant for flows that are considerably smaller than the channel confines. Intermediate-size flows, however, (e.g. flows twice as thick as the channel depth) may be strongly affected by flow stripping processes. The sandy sediments deposited at the edge of the curves due to the process of flow stripping can be potentially hydrocarbon prospective overbank deposits.

Fig. 6.11 and Fig. 6.12 also show a striking feature in subbasin II. This is the two apparent blue bull's-eyes at crosslines 4550 and 4640 and inline 9530. These two blue areas (acoustically softer) surrounded by red or green (acoustically harder) areas are thought to be hydrocarbon bearing. This was confirmed by applying trace shape analysis on both litho and fluid cubes. Litho-cube is a seismic volume from which hydrocarbon effects have been subtracted, whereas, fluid-cube is a seismic volume from which an attempt is made to subtract the lithology effects. These two cubes were made available by Shell to confirm that the features described above are indeed

caused by the presence of hydrocarbon in this area. Fig. 6.13 shows the results of the trace shape analysis conducted on both data cubes. Indeed the bull's-eyes have totally disappeared from the litho-cube (Fig. 6.13b) but have been further enhanced by the fluid-cube (Fig. 6.13a). This discovery has led to an increase in the reserved hydrocarbon volume of the Gannet-F field penetrated by wells 21/30-14 and 21/30-15 slightly to the north of these features. These half-by-half kilometre and quarter-by-quarter kilometre hydrocarbon pockets that have previously gone unnoticed within the area have been detected by the enhanced benefits of the trace shape analysis.

Fig.6.14 and Fig. 6.15 show a bird's eye view of the Top Tay system enhanced by oblique illumination using 123di volume viewing software package. The figure shows the structure of the Top Tay horizon superimposed by the results from the trace shape analysis. Note that the north is to the right of the map and the green lines represent the well trajectories. This is a spectacular view of the system illustrating the variation in channel sinuosity as it comes down the slope. Schumm *et al.* (1972) and Clark *et al.* (1992) observed in modern fan systems and flume tank experiments that the sinuosity of channel increases at the break of the slope until the channel can no longer hold the energy of the flow and hence takes a much straighter path. This is thought to be the case for the Tay system in Gannet South area when moving from subbasin II to subbasin III. However, because the salt dome (C) was growing at the time of deposition and when flow up the hill became difficult for the channel, it started shifting its path and taking a much easier route. This shift in the path of the channel, shown by a red arrow in both figures, resulted in the deposition of two distinct lobes at the time of the Upper Tay. The lobe on the right of the figures was deposited first then the channel migrated further away from salt dome C to deposit the second lobe to the left of the figures. The two lobes observed here are not separable at the older units as will be discussed in the next section. Fig. 6.16 shows a zoomed in version of Fig. 6.11 at subbasin III. Red and yellow represent best quality sands in the area as observed in well 22/26a-1 with porosity reaching as high as 37%. The green also represents sand but with slightly lower quality. Well 22/26a-1 has penetrated the fan at the slope. This means further down the slope sand packages are

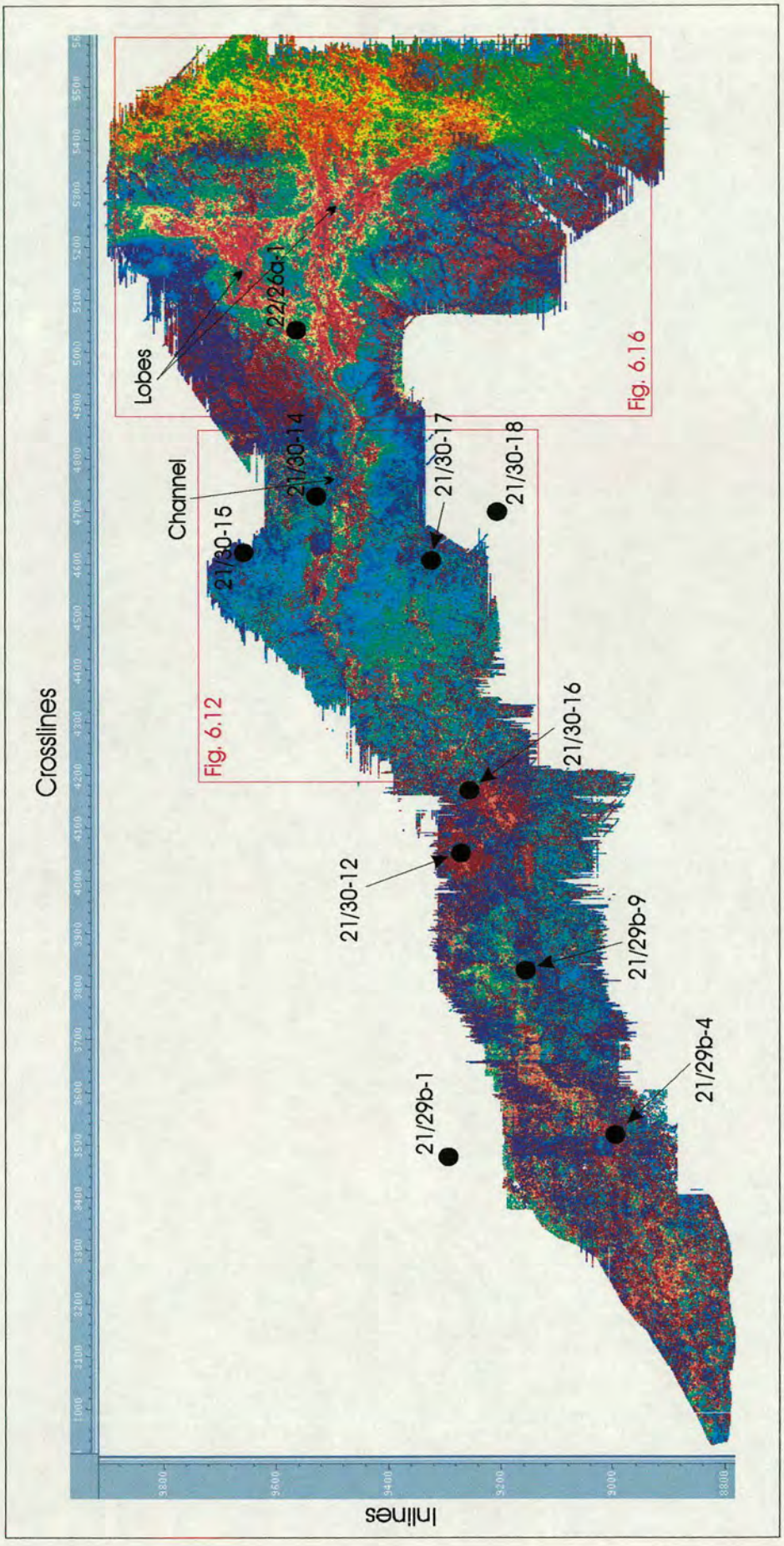

Figure 6.11: shows variation in shape of the seismic traces within the 30 ms interval covering the Top Tay horizon. Variation in facies is clearly delineated and channel and the lobes are apparent.

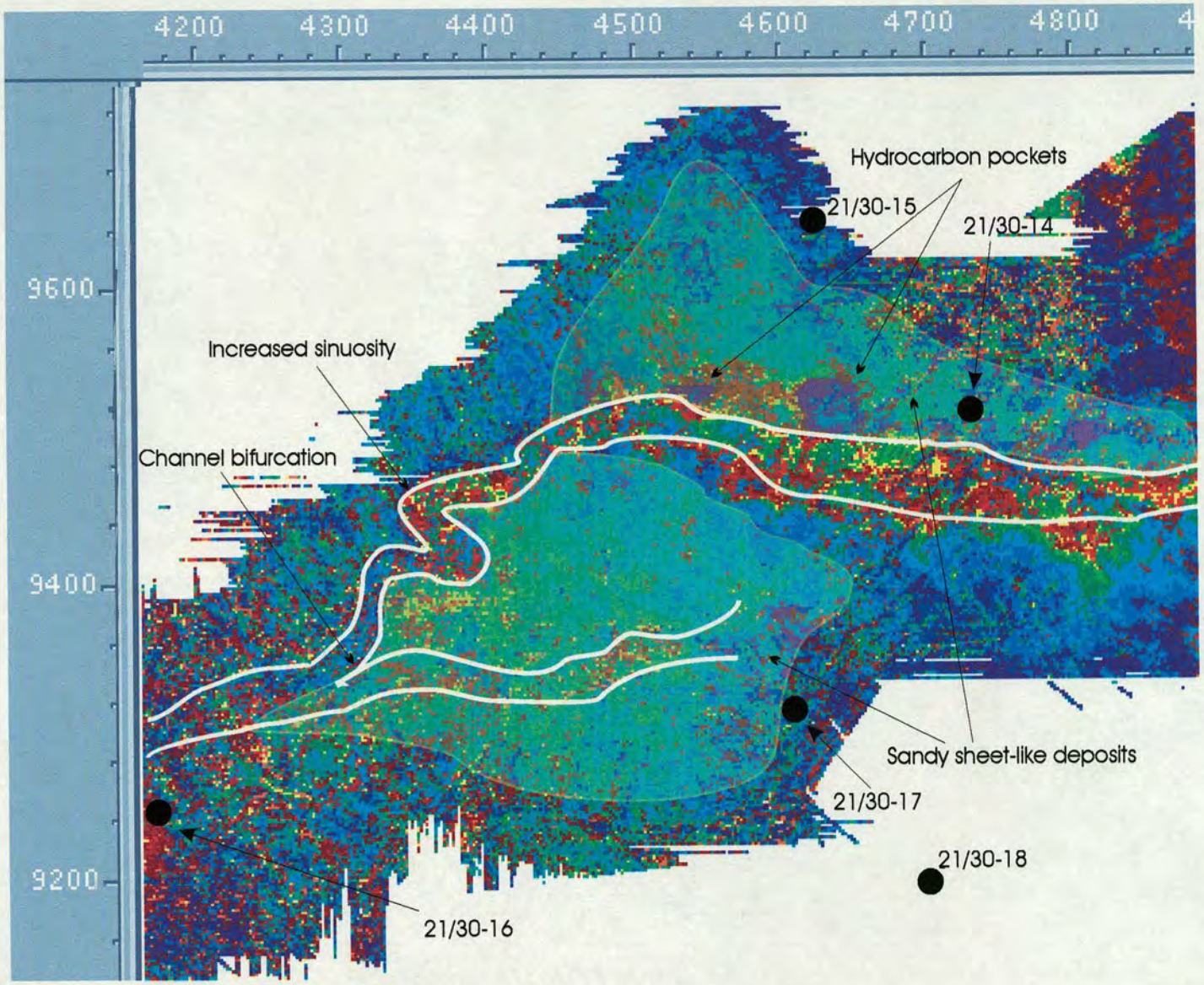

Figure 6.12: Basin II seismic facies distribution showing increased channel sinuosity with sheet like sand deposits and hydrocarbon pockets.

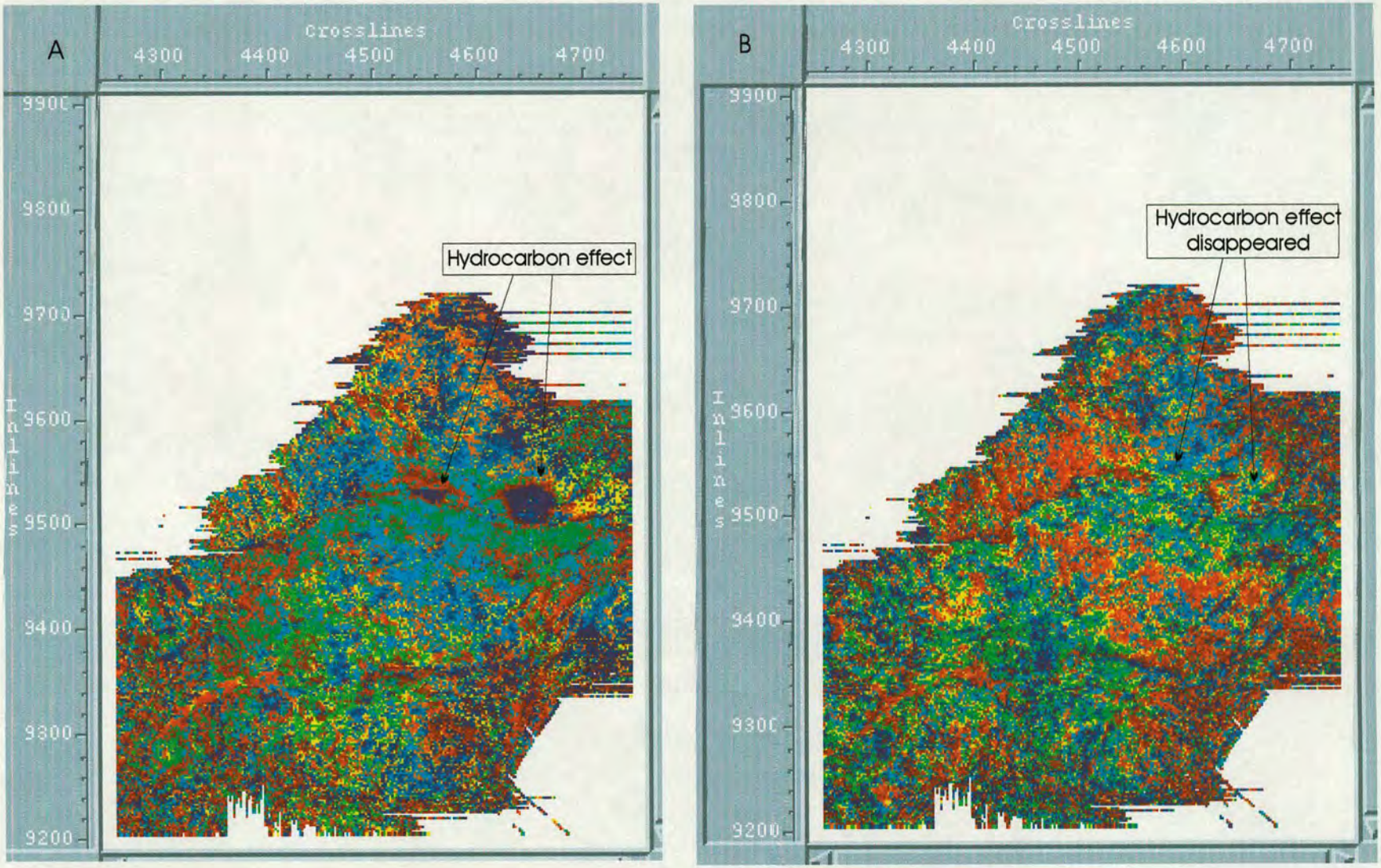

Figure 6.13: Results of trace shape analysis performed on (A) fluid and (B) lithology cube. Hydrocarbon effect enhanced on the fluid map while totally disappeared from the lithology cube map.

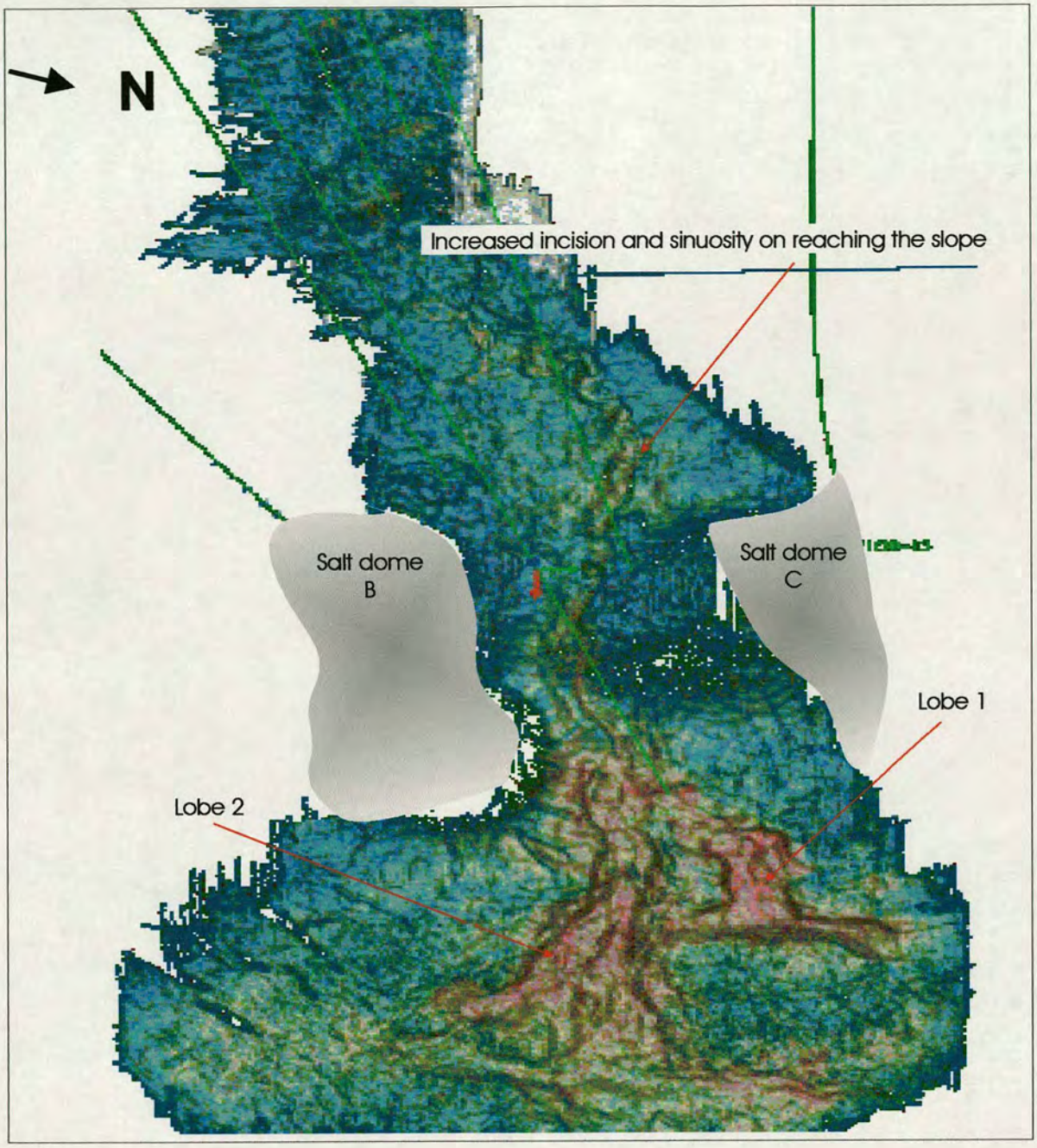

Figure 6.14: Bird's eye view of the Top Tay showing the structure of the surface, superimposed by results of trace shape analysis.

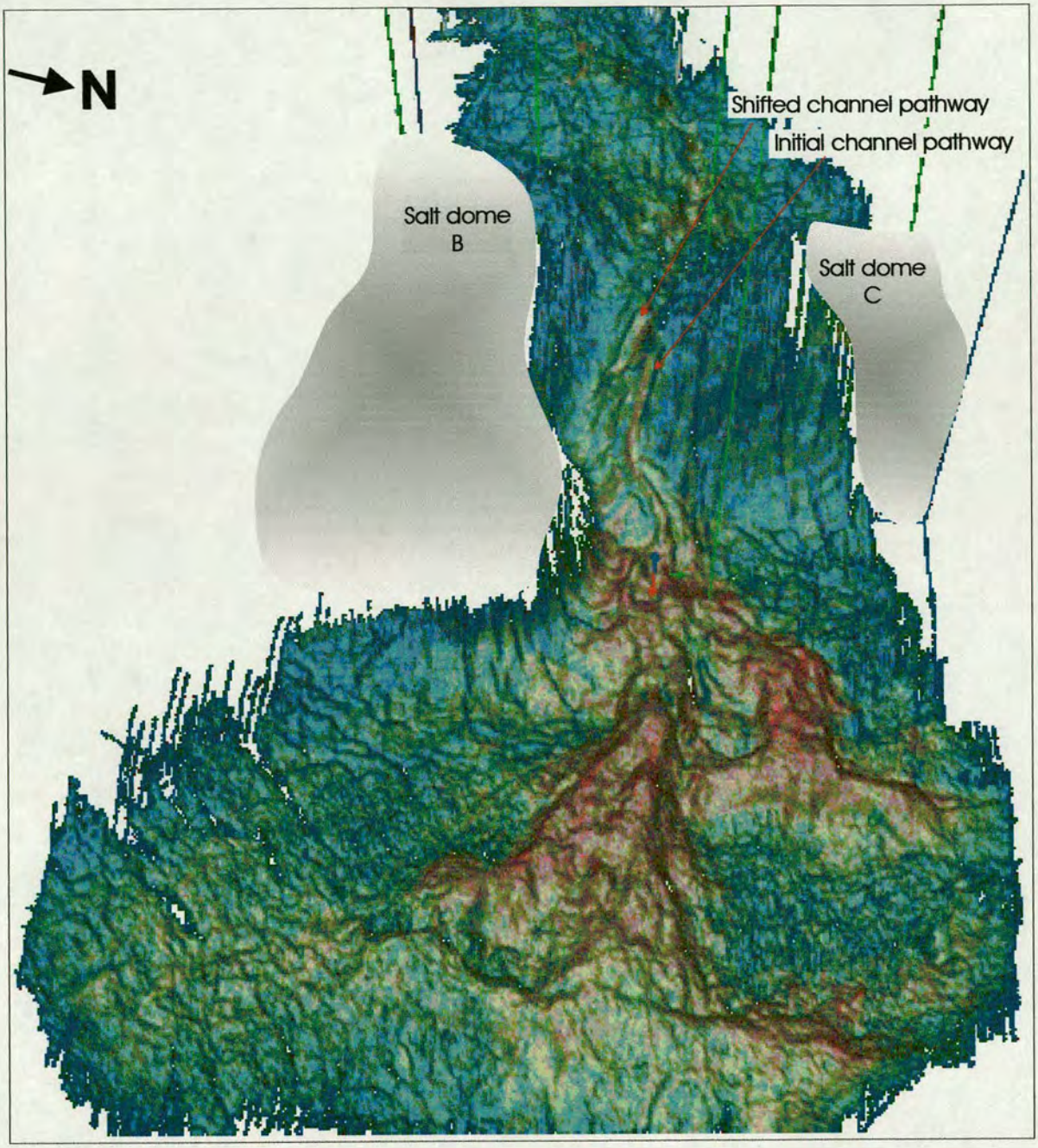

Figure 6.15: Bird's eye view of the Top Tay showing the structure of the surface, superimposed by results of trace shape analysis.

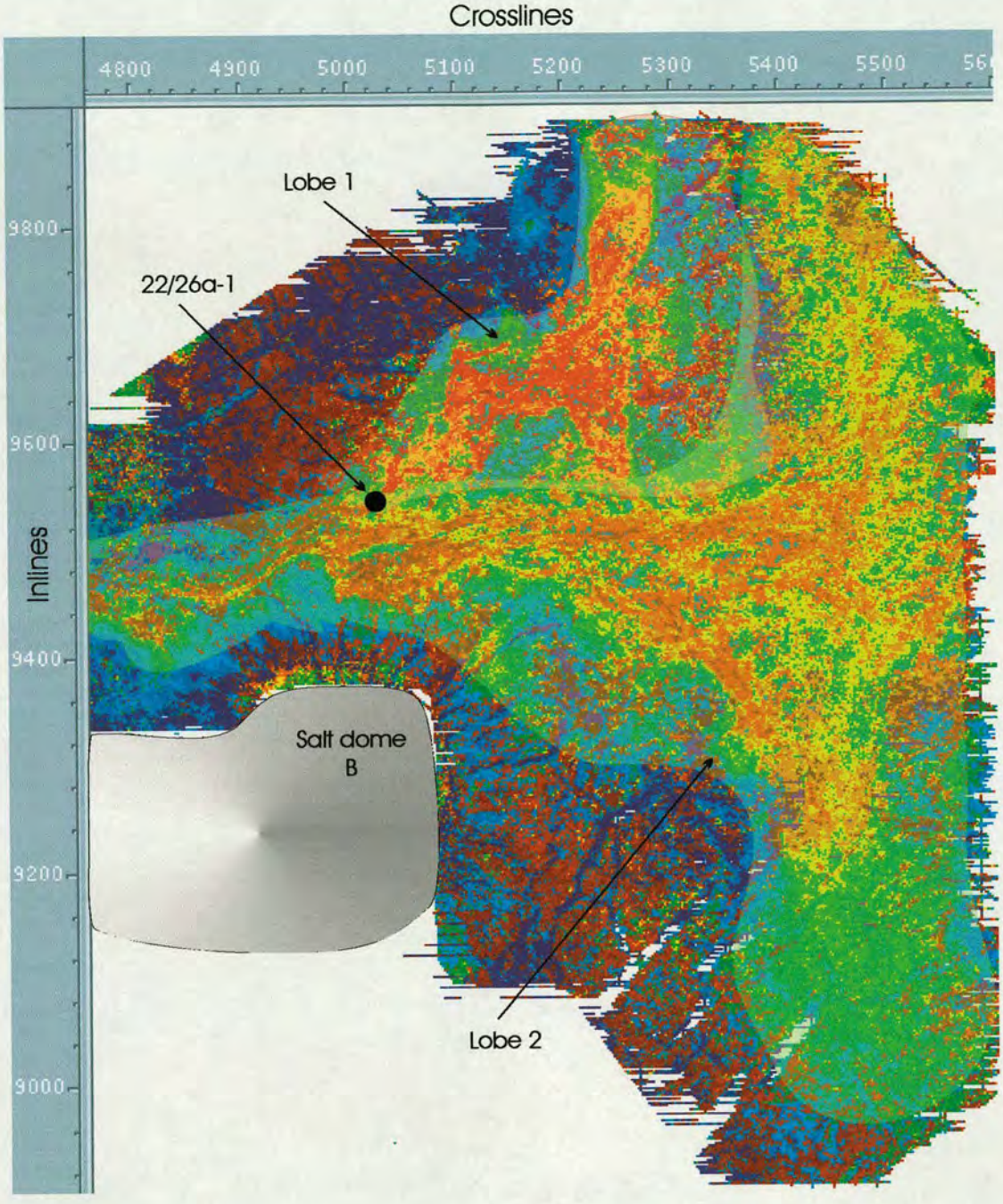

Figure 6.16: Basin III seismic facies distribution allowing distinction of two depositional lobes. Orange/red are better quality sands.

much thicker than what is observed in this well as illustrated by thickness maps discussed in chapter 3.

Trace shape analysis was also made using different intervals hanging off the Top Tay horizon. This was done with the view to investigate the effect of changing the interval on trace shape analysis results, and to understand the change in sand geometries of the turbidite system over time. However, the results from this exercise are not very interesting as it is not empirically easy to compare and contrast these map views due to the fact that different trace shapes have been assigned similar colours within different intervals. Thus, the results of this exercise have been moved to appendix 6.

6.4.1.3 Classification using Top Middle Tay as the reference horizon

Figs. 6.17, 6.18 & 6.19 show the results of the classification using Top Middle Tay as the reference horizon with varying interval thickness. It is immediately obvious from these figures that there are no two distinct lobes at the main sub basin as it was in the upper Tay interval. It is also apparent from these figures that sandier deposits at this level seem to be further to the east (see zoomed in version depicted by Fig. 6.20). This agrees with the Middle Tay thickness map discussed in chapter 3 (Fig. 3.15). Note the red colour at the northern and southern edges of Fig. 6.17. This is thought to be due to the thin nature of the unit and hence the classification interval goes into the lithology that lies below Middle Tay. Fig. 6.18 representing Middle Tay – 15 + 15 ms interval appears to be the best of the three figures as it is finest in delineating the channel and its distributary branches over most of the area. This shows that the deposition of this unit happened over a longer period of time when the energy of the channel was lower and resulted in channel bifurcation. The map also highlights the thick Middle Tay package that occurs in subbasin II as discussed in chapter 3.

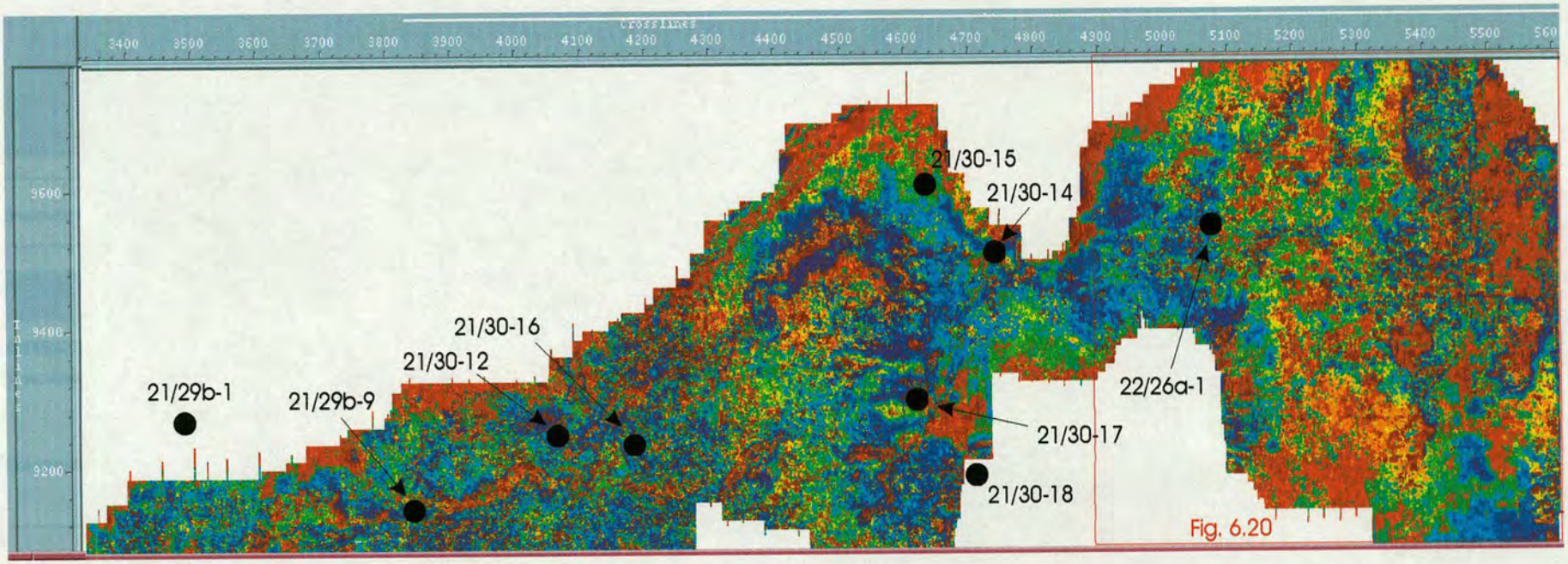

Figure 6.17: Variation in shape of the seismic trace within a 30 ms interval covering Middle Tay horizon (-5 +15). It is not possible to distinguish the two lobes as it was at the Top Tay interval.

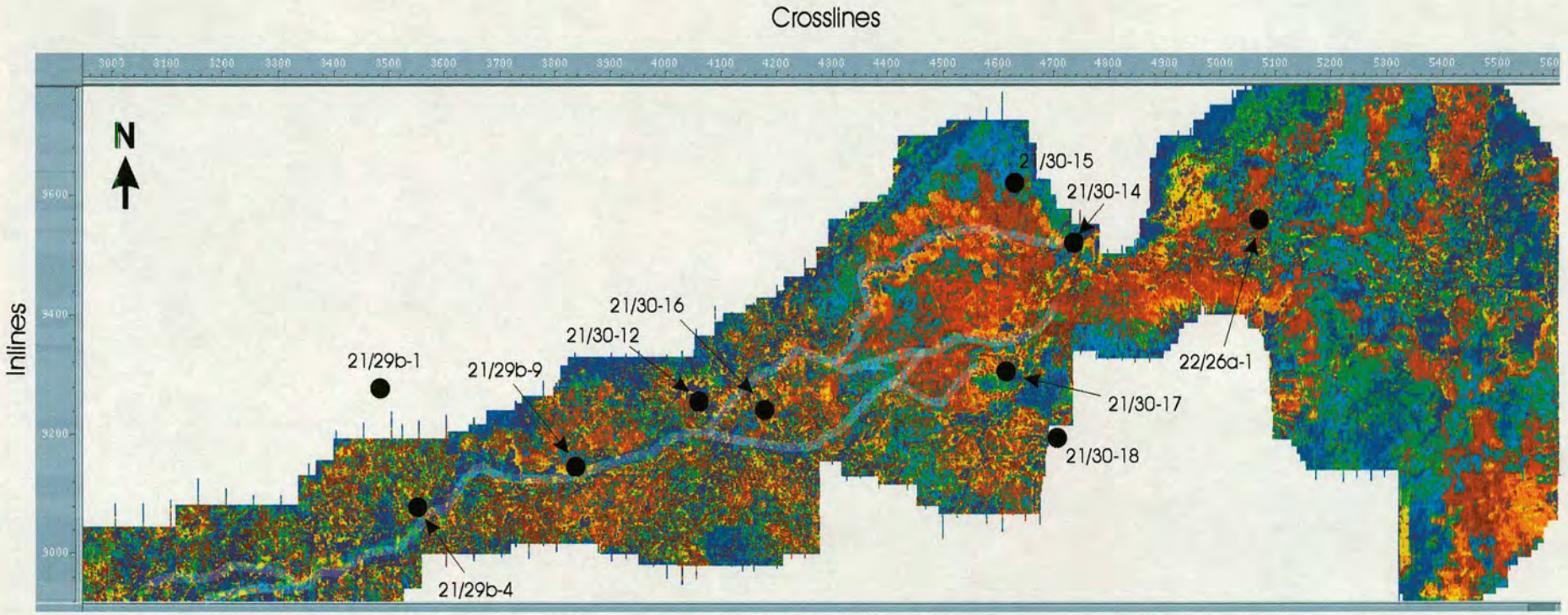

Figure 6.18: Variation in shape of the seismic trace within a 30 ms interval covering Middle Tay horizon (-15 +15). Results delineate the channel pathways across the system.

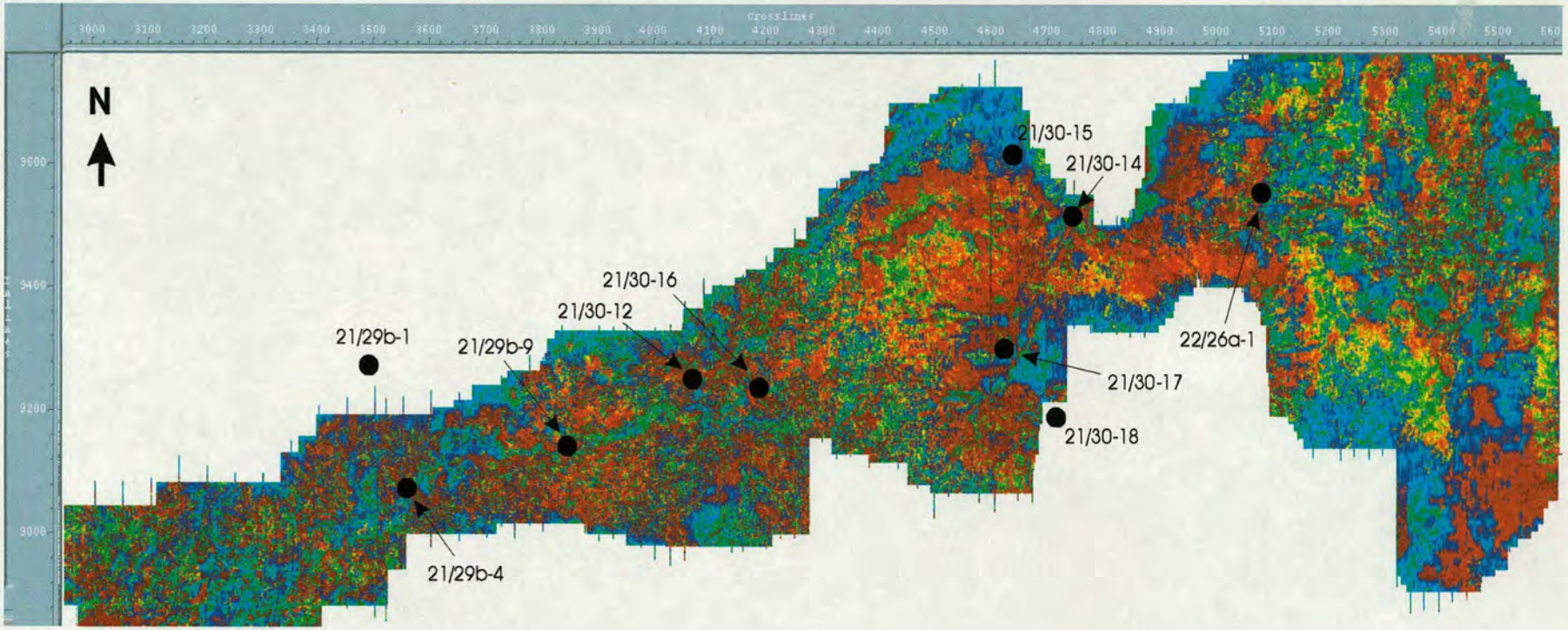

Figure 6.19: Variation in shape of the seismic trace within a 30 ms interval covering Middle Tay horizon (-10 +20).

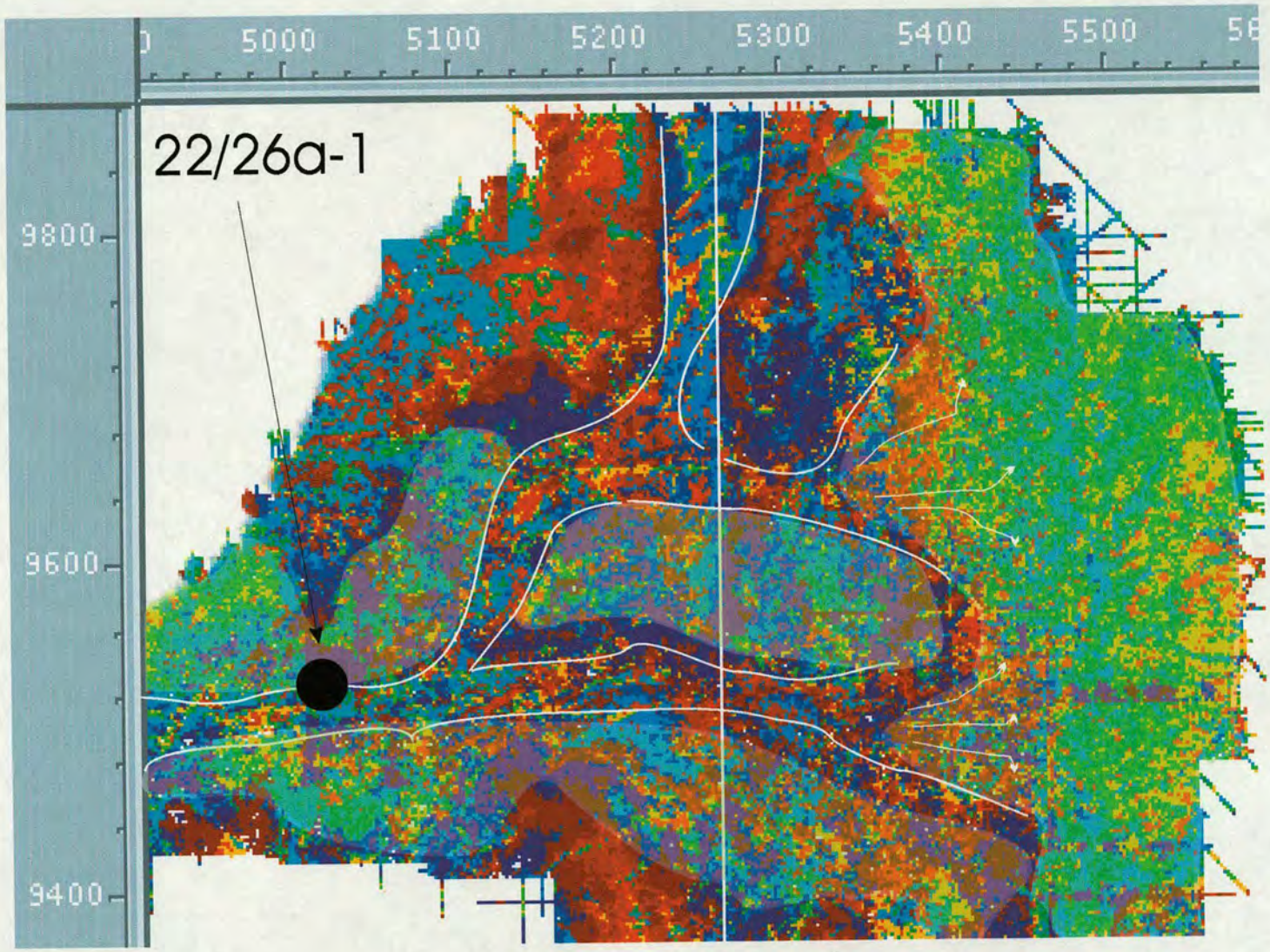

Figure 6.20: Basin III seismic facies distribution using Middle Tay horizon.

6.4.1.4 Classification using Top Basal Tay as the reference horizon

Basal Tay is the oldest unit within the Formation. Isolated sand bodies within a shale background occur in this part. As demonstrated in the seismic data interpretation chapter, the top was mainly picked as the trough (red loop) directly overlying the peak of Top Balder Formation. However, this was mostly discontinuous except in the subbasin III where the unit is thicker and the amplitude is higher. The reflector is also continuous in the shallowest sub basin close to salt dome A. The isochron map of the Basal Tay unit, given in Fig. 3.13, showed that the thickness of this unit does not exceed 45 ms. This has made the analysis difficult as the interval hanging of the Top Basal Tay horizon often included in the analysis lithologies from above and below the actual unit itself. Fig. 6.21 and Fig. 6.22 show the results of the analysis using two different intervals hanging off the Basal Tay horizon. Analysis within the interval Basal Tay -10 + 15 ms (Fig. 6.21) yields better results. The channel in subbasin I is apparent. The thickest package of the unit occurs in this subbasin.

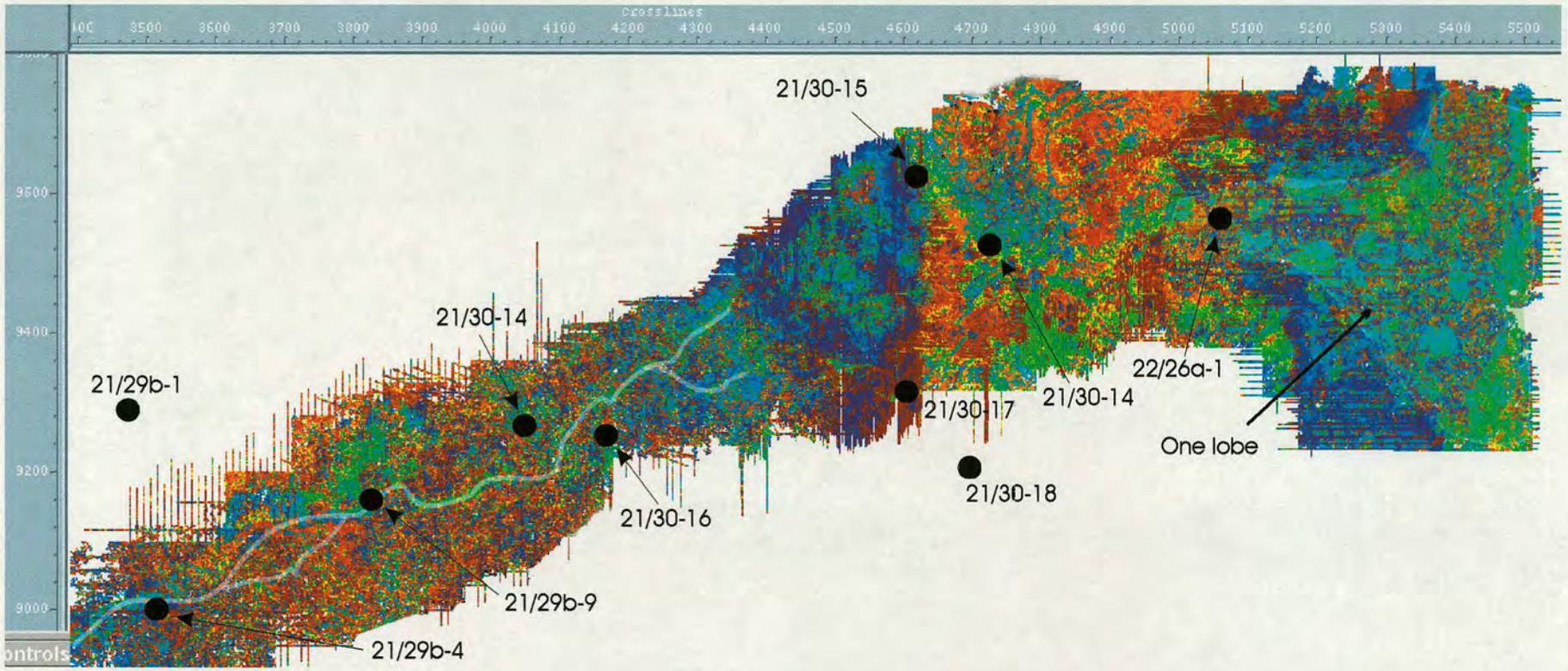

Figure 6.21: Variation in shape of the seismic trace within a 25 ms interval covering Basal Tay horizon (-10 +15). Channel at basin I is apparent but it is not possible to distinguish the two lobes as it was at the Top Tay interval.

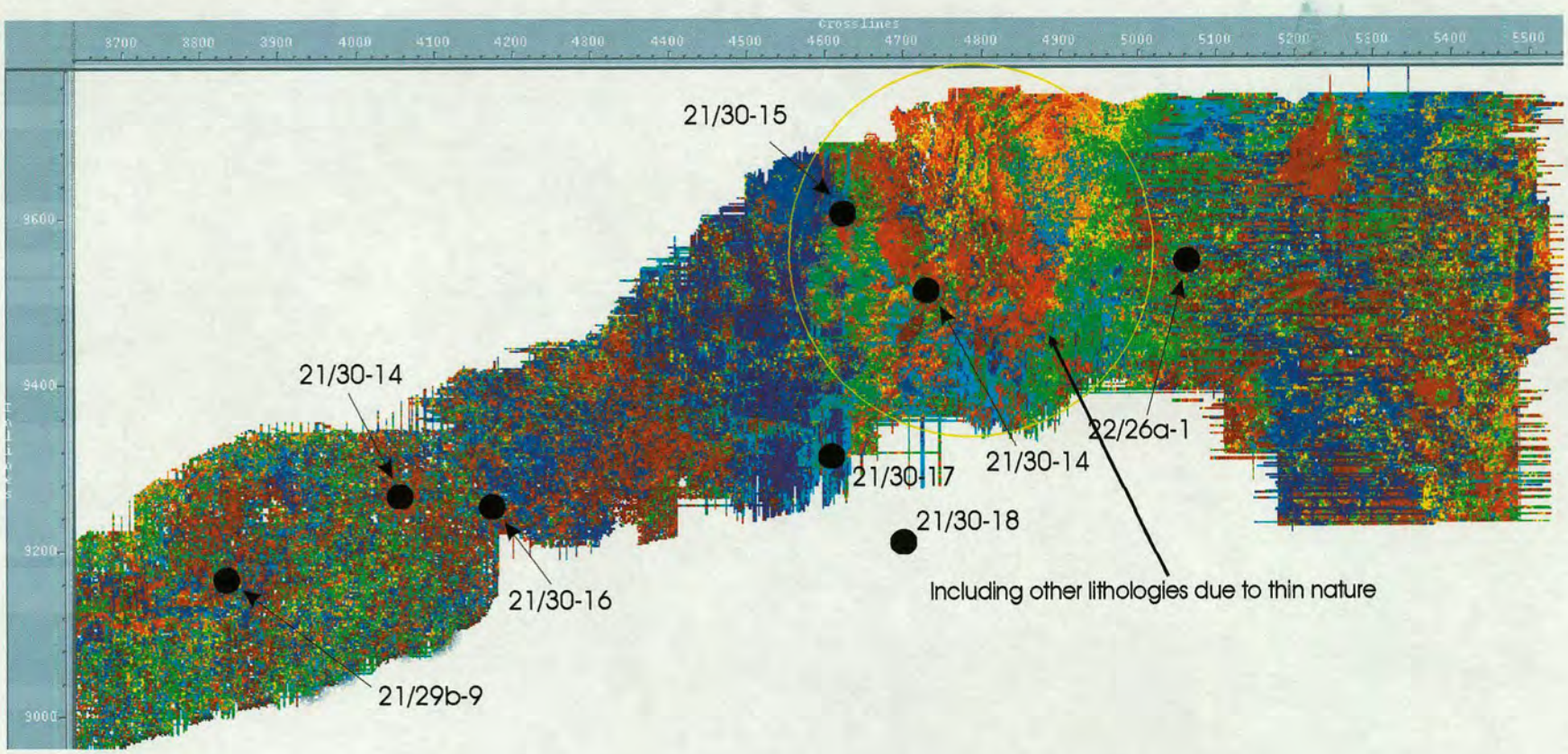

Figure 6.22: Variation in shape of the seismic trace within a 30 ms interval covering Basal Tay horizon (-10 +20). It is not possible to distinguish the two lobes as it was at the Top Tay interval.

6.4.2 Supervised Classification

6.4.2.1 Supervised classification using one well at a time

In contrast to unsupervised classification, in this type the model traces are not automatically determined but rather chosen by the user. At the well location, having the knowledge from the well, we know exactly what the seismic trace represents and hence by studying the extent of similar trace shapes we can envisage the distribution of similar facies. This was carried out using three different wells, namely 22/26a-1, 21/30-17 and 21/29b-9, and at three differrent intervals corresponding to the three units of the Tay Sandstone Member. Below is discussion of the results.

Well 22/26a-1

Fig. 6.23 shows the results produced using the trace representing the Upper Tay unit as seen in well 22/26a-1. Location of the well is shown by the red crosshair. The red colour shows the distribution of this facies within the whole system. All the other trace shapes have been given the green colour. A threshold of 91% was used for the correlation coefficient. Hence everything below 91% confidence of match has been given the white colour. The Upper Tay unit at 22/26a-1 comprises mainly of Lithofacies MS, which consists of poorly consolidated, fine-grained, beach-like massive sandstones. This facies is thought to have been deposited by high-density turbidity currents and it is typical of amalgamated channels or depositional lobes within the upper fan (Mutti and Ricci Lucchi, 1972). Thus, as illustrated by trace shape analysis (Fig. 6.23), this facies is mainly observed in subbasin III. The massive sands of the Upper Tay are encased by parallel laminated siltstones (Lithofacies PLS). With regards to the rest of facies in this basin, it is not possible to establish whether they comprise better sand quality or otherwise since everything other than the facies chosen to guide the analysis is turned into green. However, the unsupervised classification discussed earlier indicated better sand qualities within the fan area since the well has been drilled further up the slope.

Fig. 6.24 shows the results of trace shape analysis using the Middle Tay unit in well 22/26a-1. The orange colour shows the distribution of this facies, whereas the blue

colour represents all the other facies. The white colour corresponds to traces that fall below the threshold used. This interval of the well has not been cored, however, comparison of the wireline logs from this well to core-calibrated logs of the other wells indicates that this unit comprises mainly of thick-bedded sandstones (TBS) interbedded with parallel laminated siltstones (PLS). Hence, the facies has been deposited by direct and rapid suspension sedimentation from a high-density turbidity current, while the interlaying siltstone is thought to have been deposited by low-density flows and from suspensions fed by turbidity currents, in a low energy environment. Traction effects are recognised by the formation of parallel laminations as discussed in detail in chapter 4. Trace shape analysis show that this seismic facies is mainly located on the slope between subbasins II and III. Some low percentage of this facies is also available in subbasin I.

Fig. 6.25 depicts the results of the analysis made using the seismic response from the Basal Tay unit as seen in well 22/26a-1. The Basal Tay unit at this location is less than 20 ms thick and comprises shale and discrete thin sandstones of Lithofacies ThBS. The figure shows that this facies is restricted to the edges of the fan. Due to the thin nature of the unit at the well location, the neural network was not very confident in identifying and correlating the facies class at other locations.

Well 21/30-17

Fig. 6.26 represents the trace shape analysis results using Upper Tay interval at well 21/30-17. The interval at this well location is very thin, as it does not exceed 15 ms making the correlation between seismic traces very difficult. The match at the well location itself was not met even when using a lower correlation threshold of 84%. This section of the well was not cored as indicated by the correlation panel of Fig. 4.10c.

Fig. 6.27 shows the results from correlating the seismic response of the Middle Tay unit at well 21/30-17. The Middle Tay unit at this location comprises mainly of Lithofacies PLS and BS interbedded with ThBS. The package is thickest in subbasin II and the results show that this seismic trace class occurs at the channel overbanks as

well as towards the edges of the ponded sand deposition (e.g. close to the well location).

As the Basal Tay unit at this well location is quite thin, not exceeding 12 ms and has no sandstones deposited, the analysis was not performed at its interval.

21/29b-9

The classification of the Upper Tay unit at this well gives some very interesting results. Fig. 6.28 shows that this same seismic facies form the channel bank over almost the whole system. Looking at the core section at this interval reveals that the Upper Tay unit at this well location consists of massive to thick-bedded sandstones interbedded with bioturbated siltstone (BS). This means that we have a sandy channel in this area. The facies are also available at the fan area, however, here they do not appear to aggregate in any systematic way.

Fig. 6.29 depicts the results of the analysis made using the seismic response from the Basal Tay as seen in well 21/29b-9. The Basal Tay unit at this location is less than 17 ms thick making the correlation between traces difficult even with reduced correlation threshold. This section of the well has not been cored. However, the gamma ray response shows some discrete thin sandstone beds interbedded with thick shale packages.

6.4.2.2 Supervised classification using several wells together

Wells 21/30-12, 21/30-14, 21/30-15, 21/30-16 and 21/30-17 were used to further analyse the Upper Tay facies distribution in subbasins I and II. Because facies observed at well 22/26a-1 are exceptionally thick, the seismic trace shape resulted from them are not thought to be representative of these subbasins. It would be rather difficult to correlate the trace shape formed by the response to these anomalously thick packages to other thinner packages as indicated by the results of supervised analysis using the individual well. To this end, it was decided not to include this well here. Fig. 6.30 illustrates the results of this exercise. The colour assigned to the trace from each well is given in the legend. The hydrocarbon pockets have similar facies to

well 21/30-15, which is hydrocarbon bearing in Gannet-F field. Fig. 6.31 also shows the results of the same analysis but with correlation threshold (white) added to it. These two figures demonstrates that facies of none of the wells dominates the area. This is due to the fact that almost all of these wells have penetrated the Tay Sandstone Member on structurally high areas where the beds are normally thinner than the main fairway. The most laterally spread facies seems to be the one observed in well 21/30-12 despite the fact that this well is right at the pinnacle of salt dome B. This is further evidence that this salt dome continued moving after deposition of the Tay system as discussed in chapter 3. This is also supported by the structural bird's eye view of the dome as shown by the figure in appendix 7. The channel flows right through the dome, a scenario that can not be expected if the dome existed with the present day relief at the time of deposition.

6.4.3 Evolution of the lobes in the main subbasin

Observations about the characteristics of the internal seismic reflections of the mounds seen in subbasin III were made and the corresponding environments of deposition were discussed in Section 3.4, in particular when referring to Fig. 3.17 and Fig. 3.24. The deposition of submarine fan sediments with distinctly different seismic velocity from the pelagic and/or hemipelagic sediments above and below, commonly results in a distinctive seismic unit. The better quality of sands resulting in better seismic reflectors is immediately apparent on the aforementioned figures. What is also evident is that more than one lobe was deposited. In the longitudinal view, it is only possible to distinguish two separate lobes; however, in the perpendicular cross-section shown in Fig. 3.24, three such lobes can be distinguished. These are interpreted as different episodes of the Tay influenced by sea level fluctuations. Possible implications and causes of the chaotic and bidirectional downlapping nature of the reflectors within each of the mounds were also discussed in Section 3.4. These bidirectionally downlapping seismic reflections are sometimes diagnostic of submarine fans, characterised by reflection termination in both directions onto sequence boundary at the base of the fan (Posamentier & Erskine, 1991). A bidirectional dowlapping pattern suggests an aggradational mode

of deposition associated with stacking of discrete lobes. Consequently, these observations suggest that the dominant growth style of the submarine fan involves an aggradational stacking of fan lobes. The trace shape analysis at the different levels of the Tay Sandstone Member enabled the temporal and spatial evolution of the three lobes in the Gannet South area to be assessed. Combining the classification of the seismic traces conducted at Basal, Middle and Upper Tay together with the three-dimensional structural view presented in Fig. 6.14 and Fig. 6.15 revealed that there were four main stages in the development of these lobes. Fig. 6.32 gives a schematic diagram illustrating these stages. The spatial and temporal evolution of subbasin III was controlled by tectonic development in the area as well as sea level fluctuations that controlled the sediment supply. The first episode of deposition (Basal Tay) is thought to have gone furthest to the east. Subsequent lobes have been receding landward until the final influx of sediments (stage 4), which seems to be the highest since it covered almost the whole basin floor. This lobe has taken a different channel path due to syn-depositional salt movement as discussed earlier. The deposition and sediment dispersal patterns in a tectonically active basin cannot be qualified without the understanding of the tectonic evolution of the basin. It has been demonstrated by this analysis that salt induced accommodation spaces are dynamic with the active evolution of the salt highs leading to a variation in the basin structure and, thus, the geometry of submarine fan deposited on it.

The mound structures observed on the axial seismic section of Fig. 3.17 and have been interpreted as depositional lobes are normally thought to have resulted from differential compaction (Armstrong *et al.*, 1987; Den Hartog Jagger *et al.*, 1993; Hiscott *et al.*, 1997). Differential compaction occurs when the sand fills a low area and the top of the sand is a level surface with shales upon deposition. After burial, the shale on the flanks of the sand is compacted more than the sand, which results in a convex-upward geometry for the sand body (Fig. 6.33). However, details of the seismic geometry and the internal architecture in the Gannet South area, as discussed above, suggest that these sand bodies had a positive sea-floor expression upon deposition, prior to deposition of overlying sediments and compaction. It is apparent from the discussion above that each of these lobes is onlapping onto the one below,

suggesting it had a positive sea-floor relief upon deposition (*cf* Shanmugam *et al.* 1997). Hence, it is suggested here that the mounds observed in the Gannet South seismic dataset are not the result of differential compaction as thought by other workers but rather due to depositional geometries.

6.5 Critique of the trace shape analysis

Maps produced by trace shape analysis proved invaluable for obtaining detailed and accurate structural information. They have revealed subtle geological features only expressed in the shape of the seismic trace and thus have substantially enhanced the understanding of the sand geometries of the turbidite system and the structural development and evolution of the basin (Fig. 6.34 provides a direct comparison between the results of trace shape analysis and the amplitude map for the Top Tay horizon). The results also provided clues to the timing, nature and extent of factors controlling the sediment transport pathways in the area, and helped in the discovery of hydrocarbon pockets previously gone unnoticed. However, it should be cautioned that the idea of analysing seismic data based on variation of seismic trace shapes comes from the assumption that changes in lithology, rock properties and fluid content within the analysed interval should affect seismic response and thus the shape of the trace in a systematic predicable way. This is indeed true but are they the only factors controlling the shape of the trace? Below is the list of possible reasons for the variations in the seismic trace shape.

1. Changes in rock properties of the layer overlying the reflector or the interval.
2. Changes in the structure of the layers overlying the reflector or the interval.
3. Changes in the velocity field of the overlying layers.
4. The dip of the reflector itself.
5. Changes in the nature of the interface (sharp contact or gradational).
6. Changes in rock properties below the reflecting interface.
7. Changes in thickness between the reflector and surrounding interfaces (tuning effects).

8. Acquisition artefacts.
9. Processing artefacts.
10. Multiples, noise etc.

The last three points were assessed in the seismic data to well tie chapter and it was concluded that the dataset is of a good enough quality to proceed with the analysis. However, during the analysis it was assumed that the layers above and below the chosen interval remain unchanged and do not affect the shape of the seismic trace. The fixed thickness of the selected interval can lead to erroneous results and interpretations. For example, running the analysis on the Upper Tay interval area in the vicinity of well 21/29b-9 would give wrong results since this well did not encounter any Upper Tay unit. One solution to this is not to have a fixed interval hanging off the same horizon but rather an interval that is bounded by two horizons; e.g. Top Upper Tay and Top Middle Tay. However, we would still remain with the same problem because even if the lithofacies are the same but their thickness has changed, the shape of the seismic trace will change.

It is thought that it was the impressive seismic data quality as well as the thorough line by line interpretation of the horizons within and enveloping the Tay Sandstone Member that led to the success of the trace shape analysis. Although maps produced by trace shape analysis have an advantage over some other attribute maps produced using the same horizons, e.g. amplitude, dip azimuth, we have seen that analysis was not such a success at Basal Tay unit which is the thinnest of the three units comprising the Tay Sandstone Member. As such, it is more important to focus on obtaining a good quality dataset prior to interpretation, by emphasizing better acquisition and processing procedures rather than attribute manipulation after processing. Case examples of attribute analysis from areas of good seismic data quality can be misleading to believe that such exceptional results can also be obtained in areas of poor seismic data quality.

6.6 Conclusions

Deepwater clastic systems and associated turbidite reservoirs are often characterised by very complex sand distributions. With the North Sea becoming an established world class petroleum province in a mature state of development, exploration focus has shifted away from targeting structural traps to more subtle stratigraphic plays. The development of three dimensional seismic imaging and its attribute analysis has given us a unique opportunity to predict sand geometries and properties with improved certainty and in a more efficient way.

Changes in lithology, rock properties and fluid content affect seismic response not only in amplitude but in the whole shape of the trace. The direct study of the variation of trace shapes has been hitherto neglected in hydrocarbon exploration due to the lack of an appropriate tool. Neural network technology using its pattern recognition capability has made such an analysis possible.

Relating lithofacies to rock physics properties and hence to the seismic trace shape allows a direct calibration of seismic response to lithofacies thus enabling an improved interpretation of the turbidite system within a sequence stratigraphic framework. This direct assessment of the lithofacies distribution within the seismic data is tedious and almost not possible in any other way.

Both supervised and unsupervised classification of the seismic trace shapes were performed using the three units comprising the Tay Sandstone Member. 30 ms interval and 15 facies classes were found to be the best parameters for the Upper Tay unit. Results from the analysis provided some spectacular insights into the spatial and temporal development of the Gannet South Tay system and substantially enhanced the understanding of the sand geometries of the turbidite system and the structural development and evolution of the basin. The results also provided clues to the timing, nature and extent of factors controlling the sediment transport pathways in the area, and helped in the discovery of hydrocarbon pockets previously gone unnoticed.

The most striking result of the supervised classification was described by Fig. 6.28, which revealed the lithofacies that form the levee deposits. The levee over almost the whole system consists of massive to thick-bedded sandstones interbedded with bioturbated siltstone (BS). This means that at the Upper Tay level we have a sandy channel in this area.

The analysis demonstrated that the receiving basin at Gannet South has been dynamic throughout the deposition period. The resultant deposition and sediment dispersal patterns in the basin cannot be qualified without an understanding of the tectonic evolution of the basin. This was mainly controlled by salt movement which led to a variation in its structure and geometry and as a result on the geometry and stacking patterns of the sediments deposited on it.

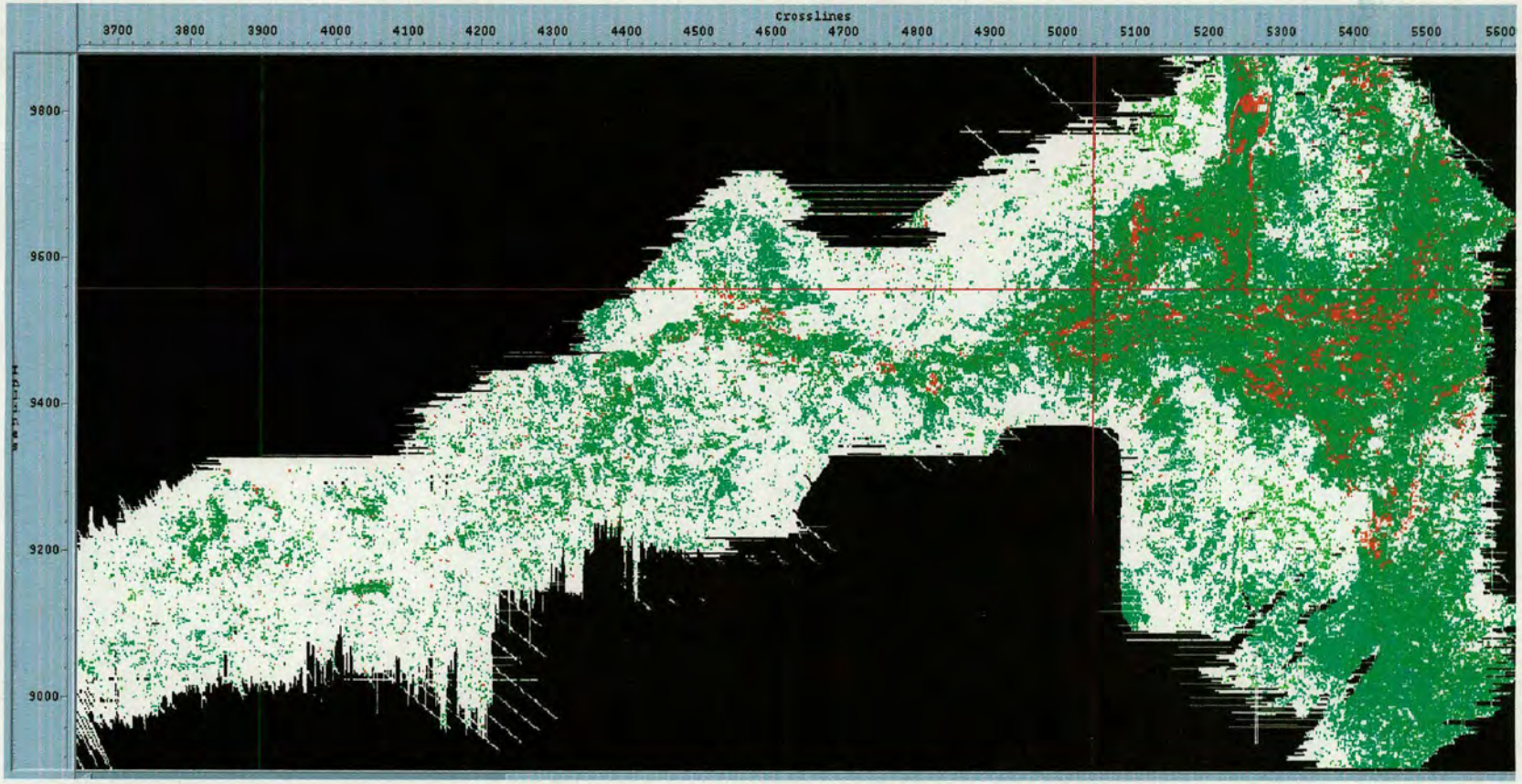

Figure 6.23: Supervised classification of the Upper Tay unit using well 22/26a-1.
Location of the well is where the two red lines cross

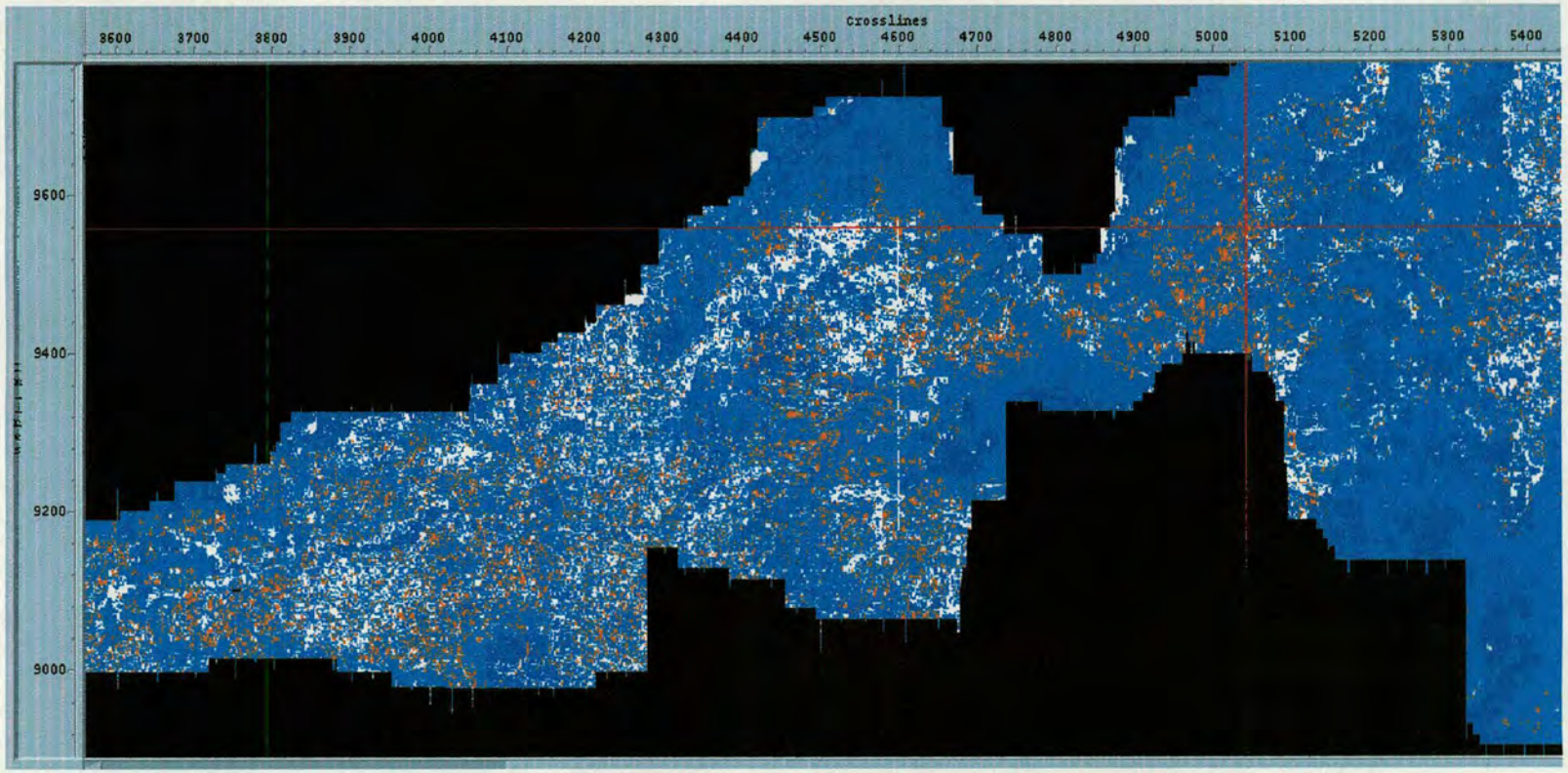

Figure 6.24: Supervised classification of the Middle Tay unit using well 22/26a-1.
Location of the well is where the two red lines cross

Figure 6.25: Supervised classification of the Basal Tay unit using well 22/26a-1.
Location of the well is where the two red lines cross

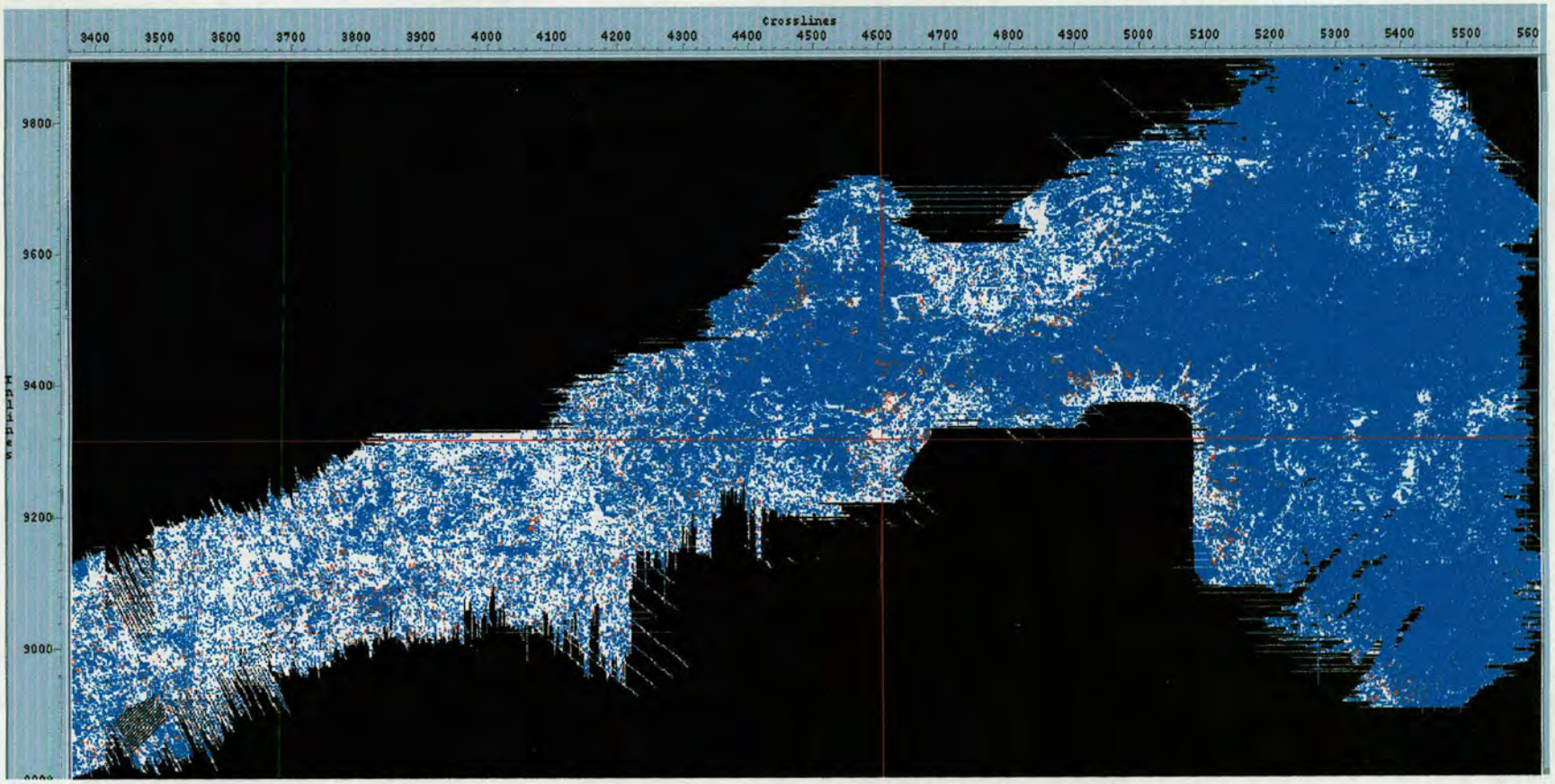

Figure 6.26: Supervised classification of the Upper Tay unit using well 21/30-17.
Location of the well is where the two red lines cross

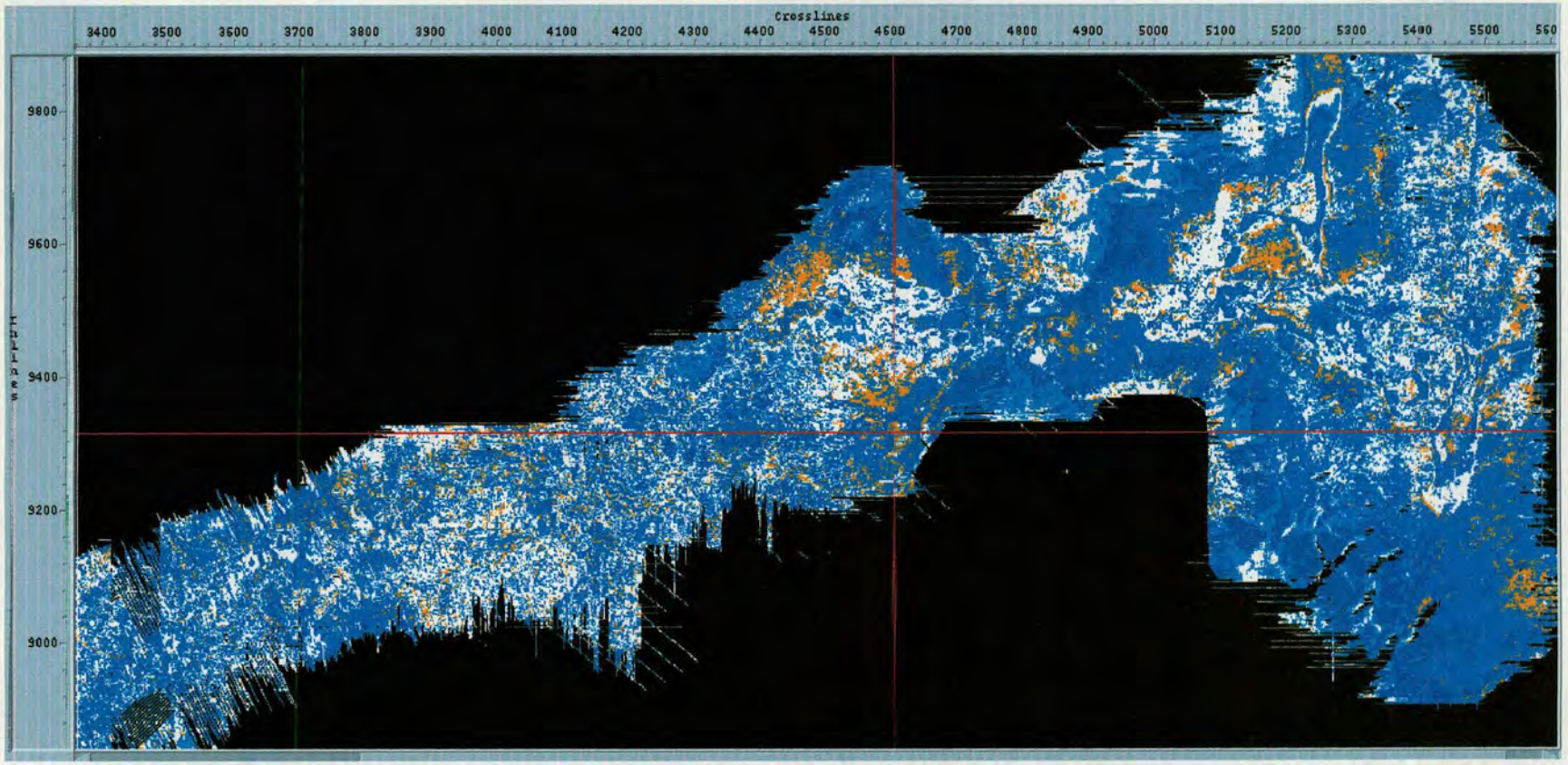

Figure 6.27: Supervised classification of the Middle Tay unit using well 21/30-17.
Location of the well is where the two red lines cross

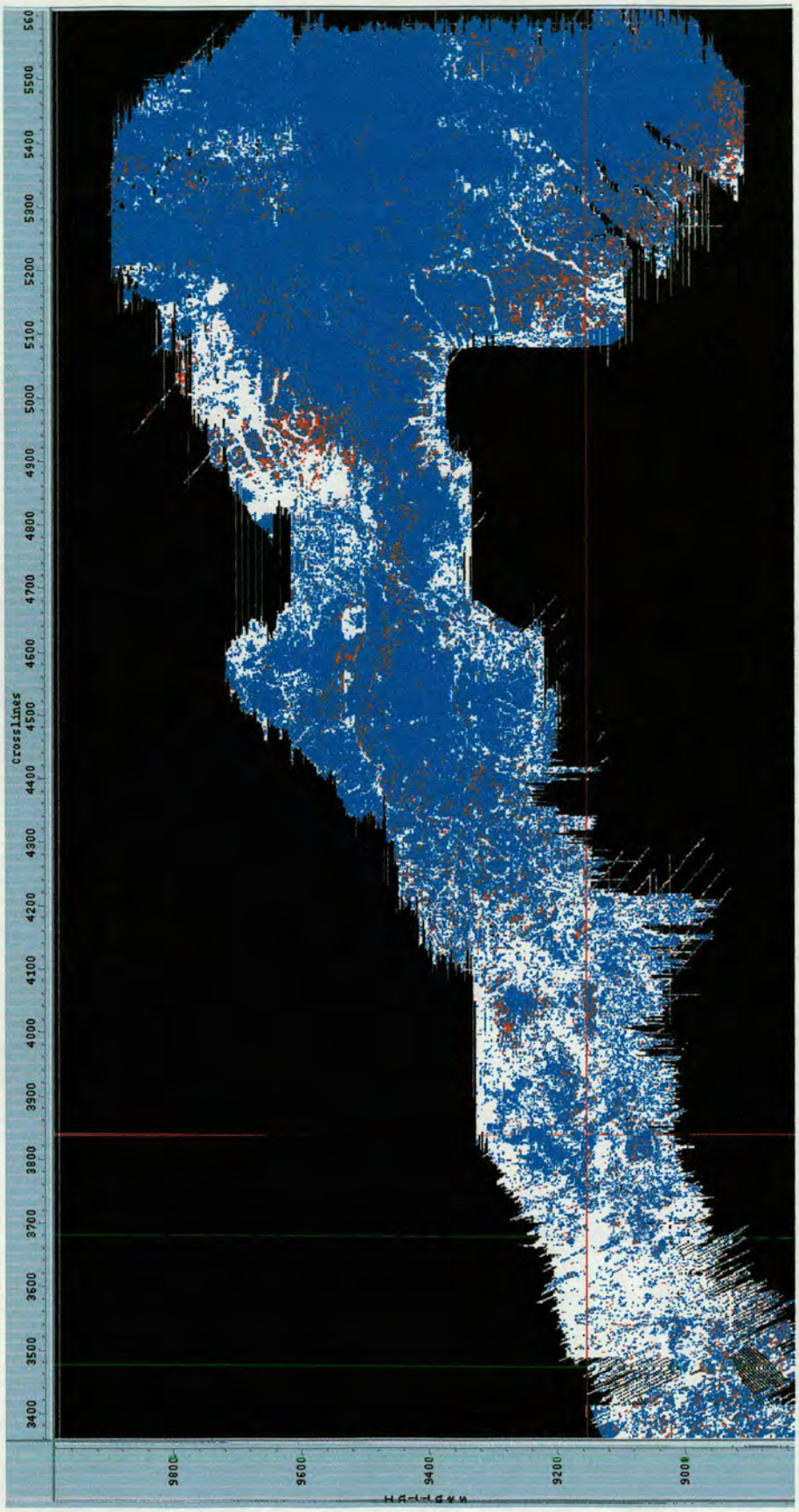

Figure 6.28: Supervised classification of the Upper Tay unit using well 21/29b-9. Location of the well is where the two red lines cross

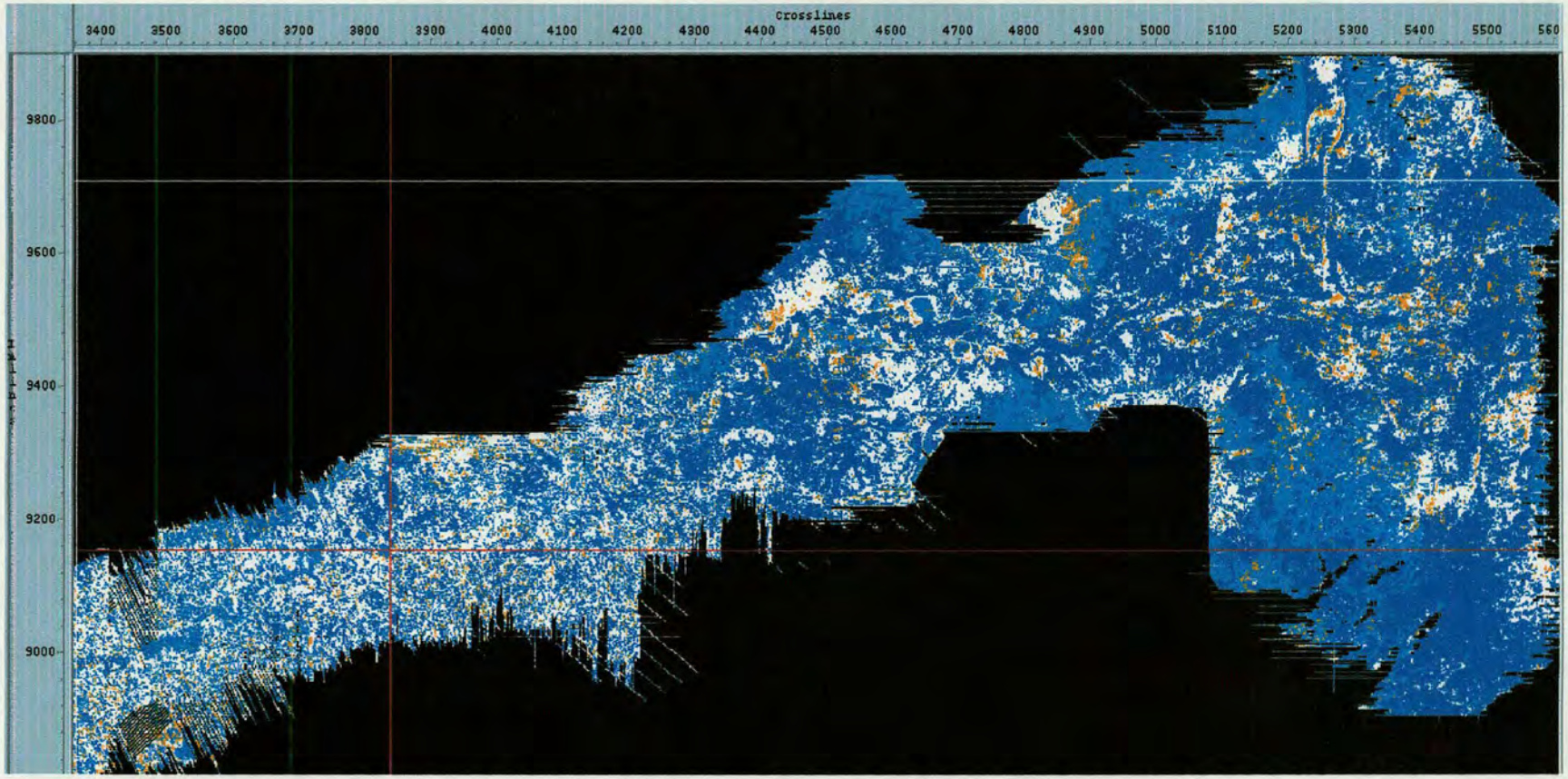

Figure 6.29: Supervised classification of the Basal Tay unit using well 21/29b-9.
Location of the well is where the two red lines cross

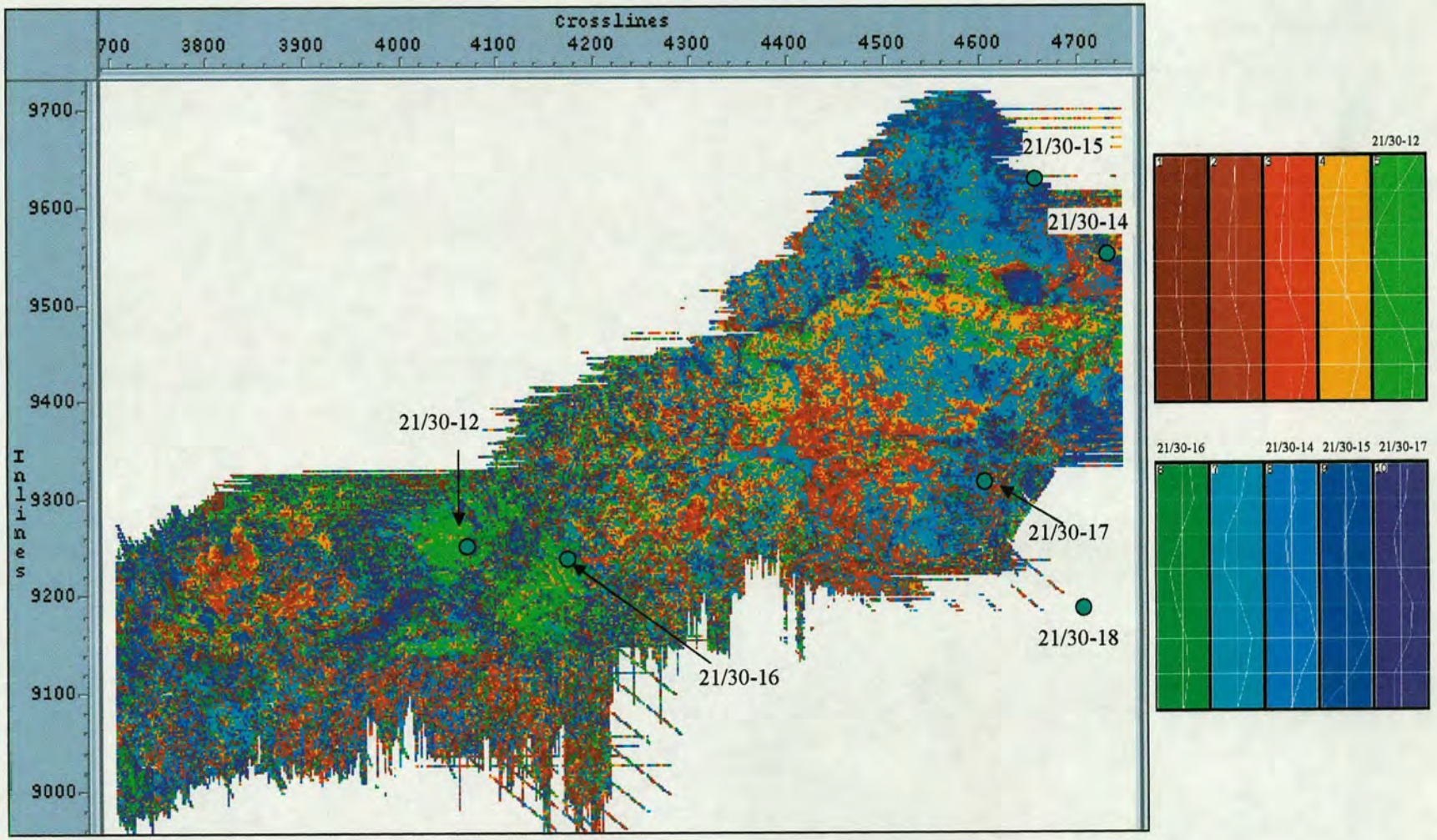

Figure 6.30: Supervised classification using wells 21/30-12, 21/30-14, 21/30-15, 21/30-16 and 21/30-17. See side legend for colour code assigned to each well. Using this method lateral continuity of the facies observed in the wells can be identified.

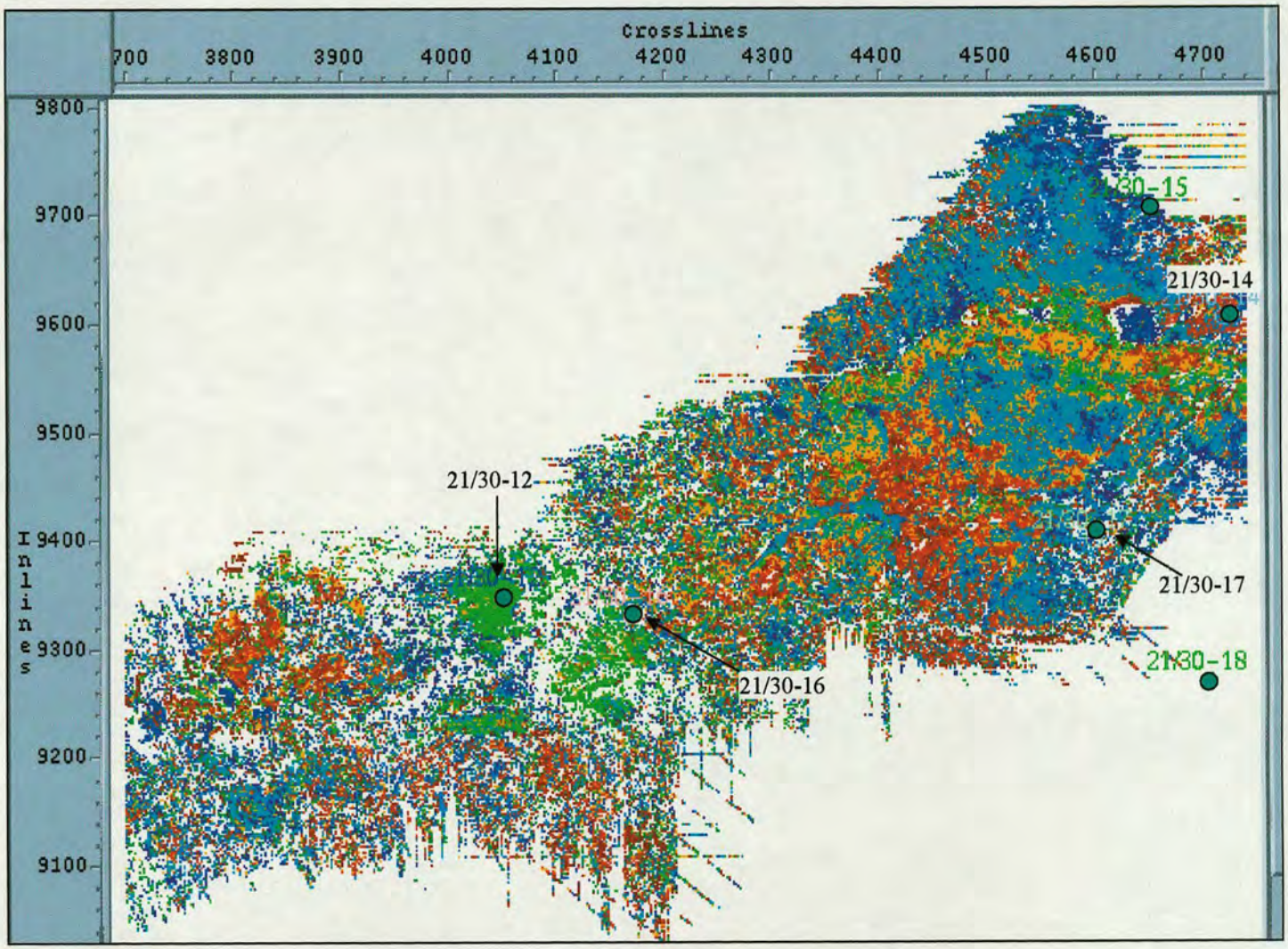

Figure 6.31: Same as Fig. 6.30 but with correlation threshold of 75%. White scatter showing correlation following below the threshold confidence.

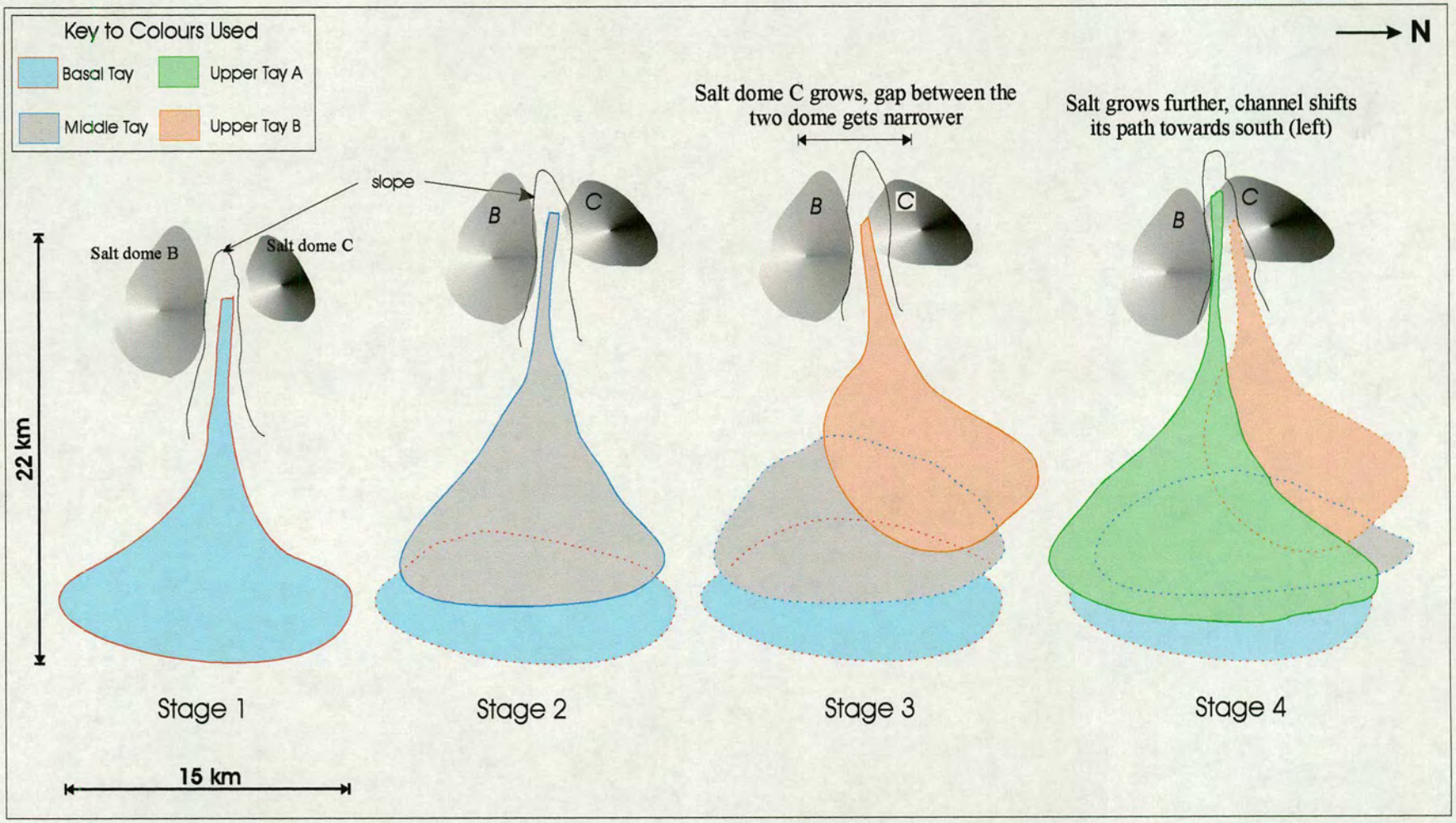

Figure 6.32: Schematic diagram illustrating the evolution of the lobes with structural development within the area.

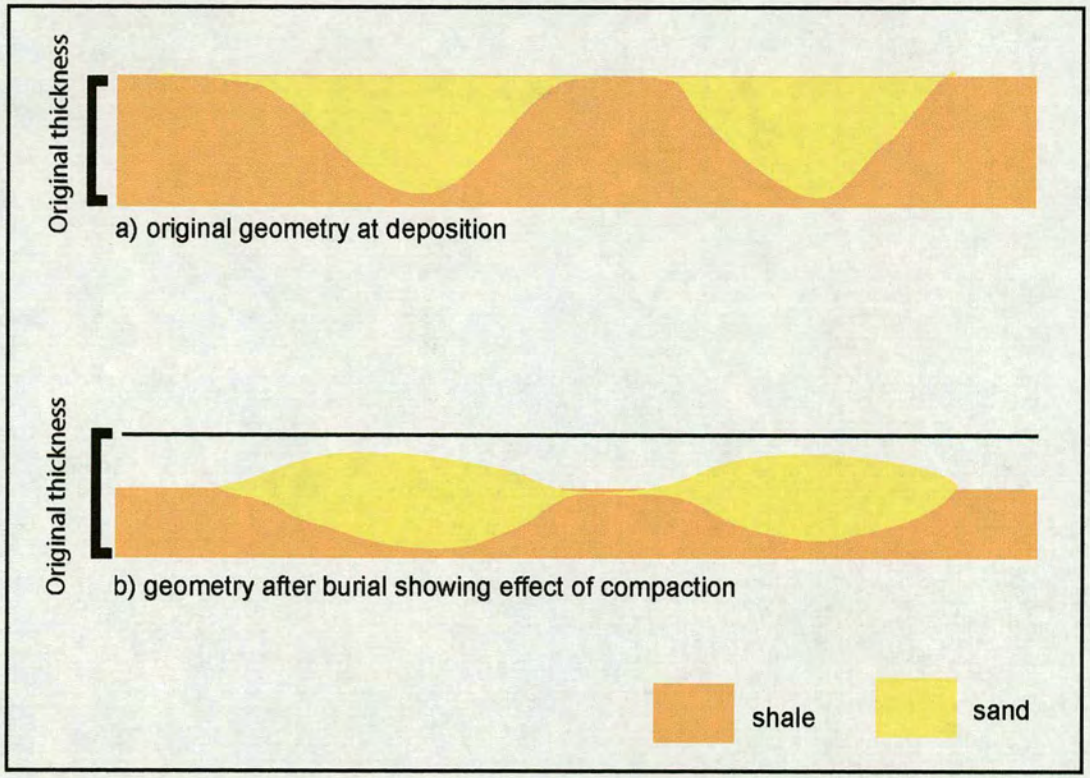

Figure 6.33: A schematic diagram showing the creation of mounded geomtery due to the effect of differential compaction between sand and shale.

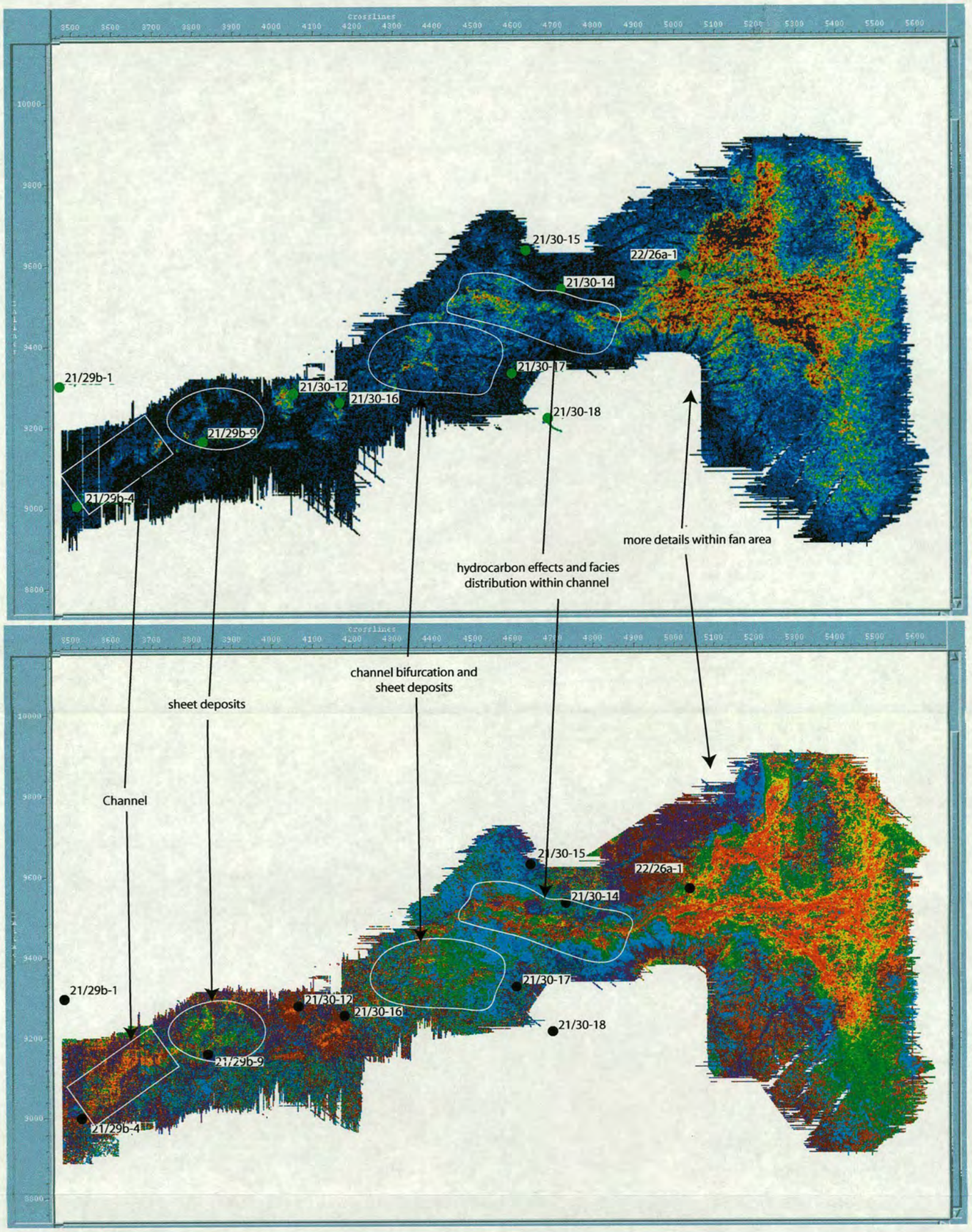

Figure 6.34: A direct comparison between the seismic facies map (lower map) derived from stratimagic and amplitude map (upper map) for the Top Tay horizon. The comparison immediately shows the benefits of trace shape analysis in the bounded areas. Facies variation within the channel and fan area, channel bifurcation, sheet like deposition of the sediments as well as hydrocarbon effects are better resolved in the map produced by seismic trace shape analysis.

Chapter Seven

Chapter Seven

Body Shape Analysis

7.1 Introduction

The human visual system is superb at the qualitative extraction of information. It is good at segmenting a scene or an image into regions that form individual objects. In a split second it can recognize elementary shapes such as triangles, circles and squares. However, it is not so good at counting randomly positioned objects and performing accurate quantitative measurements. It is poor at discriminating objects of nearly the same size or shape. There are many object properties that are represented by a single scalar. Properties that characterize the object are often related to the object size (large, small etc.), shape (regular, irregular etc.), mass (heavy, light etc.), texture (homogeneous, heterogeneous, smooth, rough etc.) or colour. However, many solid objects can be discriminated by shape analysis. In biomedical science shape descriptors have successfully been used in the classification of white cells, morphometry of sperm cells, and many other cytological studies. In meteorological studies shape analysis has been used in discriminating rain clouds and hail clouds, enabling forecasting the movement of clouds and volumes of rain in them (Lovejoy, 1982; Hentschel & Procaccia, 1983; Rys & Waldvogel, 1986).

The development and integration of three-dimensional seismic reflection data in production and exploration geology during the past twenty five years has greatly aided the understanding and mapping of, amongst other things, turbidite sandstone bodies. Typically body information is extracted by eye in a two-dimensional way as the interpreter tracks the horizons seen on an inline or crossline. Moreover, the physical characterisation of bodies is still very much generalised and currently limited to bulk physical properties such as impedance or equivalent porosity.

This project was devoted to the extraction of more quantitative information from the three-dimensional seismic data by introducing body shape analysis to the interpretation process. This is envisaged to improve the speed and quality of the interpretation process and lead to a more consistent and even more quantifiable 3D seismic interpretation providing more efficient and detailed input into geological models. Using this method an interpreter can have an idea of the turbidite (or any other system for that matter) sand body geometry before even picking any horizons.

Nowadays, the incorporation of three-dimensional visualisation application in some seismic data interpretation packages (e.g. VoxelGeo) has allowed complicated reservoir geometries to be isolated from the 3D seismic volume using their seismic expression. This process is called *Body Checking*, which is basically viewing the data with different opacity settings that allows the visual identification of clusters of similar properties (e.g. amplitude, impedance, etc.). VoxelGeo divides the seismic data cube into voxels (unit cubes). When a property (say high amplitude) threshold is picked, the package searches for all the connected voxels that have the high amplitude within the defined threshold and the time window. Thus a separation between the detected voxels, which are highlighted, and the undetected voxels, which are dimmed, can be achieved. The resulting body can now be viewed from different angles and the shape of the body can be analysed. See Fig. 7.1 for the result of this process when applied to the Gannet South area (remember that this result can be achieved prior to picking any horizon). If somehow we managed to calibrate these bodies to real geology, the whole process of the seismic data interpretation would be revolutionalised.

Hence, the objective of this work is three-fold. First, to establish a set of body shape parameters that would enable a distinctive description of different turbidite sand bodies. Second, to know if there are general geological models for turbidite depositional units that have distinctive shapes that reflect the lithological facies variations within them. Third, to investigate by forward modelling and body checking which physical properties influence the geometry and attributes of the bodies in the seismic data. Then, using the combined physical and shape parameters

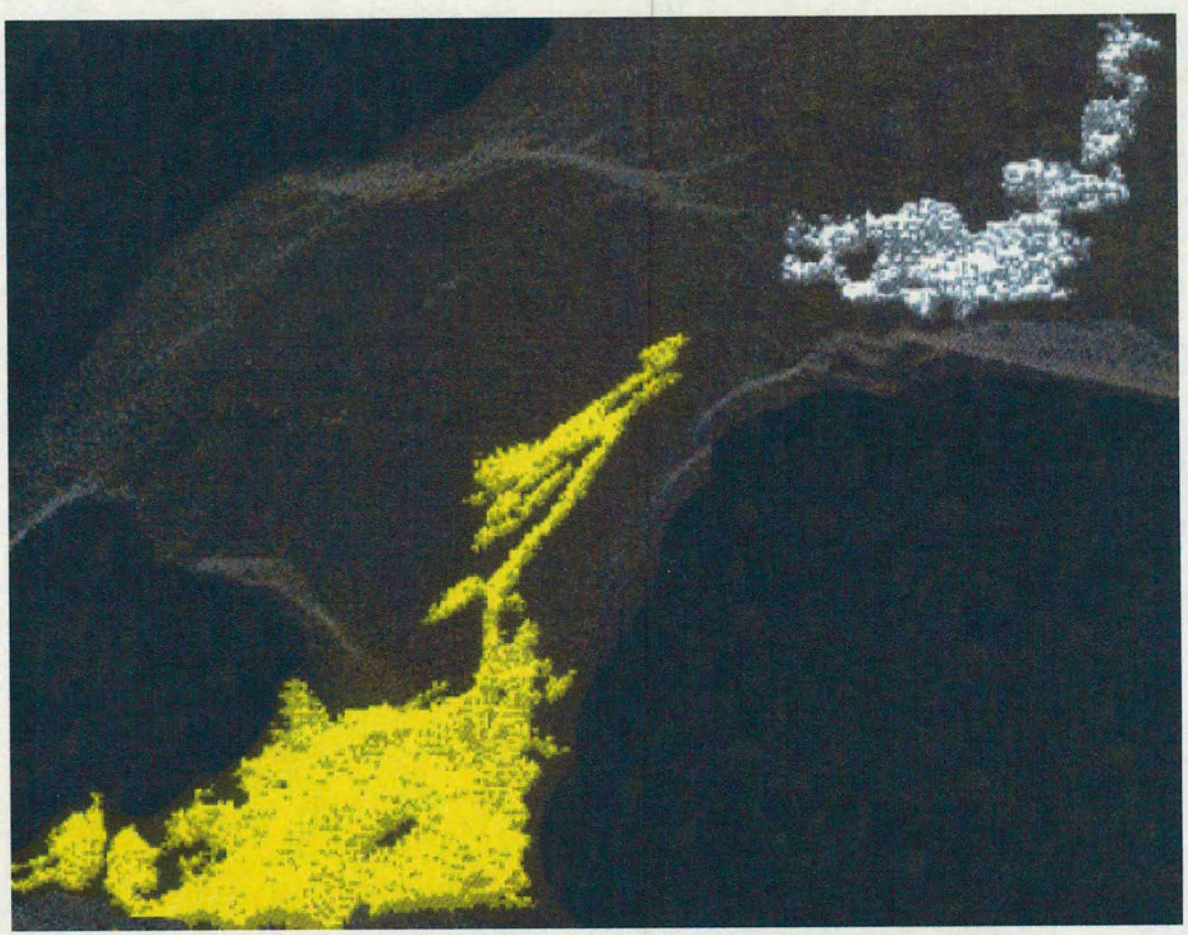

Figure 7.1: Results of body checking in the Gannet South area highlighting the Tay depositional system in sub basins II & III. (from J. Verbeek, pers. comm)

in a predictive way, the validity of the method can be checked. The method needs to be applied on a model dataset and at least one real data example to establish its predictive potential. If the process is successful, the methodology could be automated. However, this task of automating the process is beyond the scope of this thesis and will be considered as one of the recommendations for future work. This chapter gives an account of the methodology employed and discusses the results produced and some of the hurdles faced to achieve the set objectives.

7.2 Shape Parameters

The aim of this section is to find a generalised set of parameters that can describe the geometry of sand bodies in different turbidite depositional system. There are a number of basic parameters that can be derived from any arbitrary shape to provide valuable classification information and, hence, a useful means of checking the identity of the object. These include:

1) Area
2) Perimeter or Circumference.
3) Sphericity
4) Eccentricity
5) Roughness
6) Length verses width

7.2.1 Area and Perimeter (Compactness)

Area and perimeter are the basic parameters of any 2-dimensional shape but are they discriminating descriptors of this shape and can they be measured easily for an irregular shape?

In order to measure the two variables, area and perimeter, of any shape a grid can be used. Below is an illustration as to how this could be done first for simple shapes (a rectangle and a circle) then for a more complicated irregular shape.

To measure the area we use Simpson's Rule (Croft *et al.*, 1992)

$$\text{Area} = d/3\ [(y_0+y_n)+4(y_1+y_3+y_5+\ldots\ldots)+2(y_2+y_4+y_6+\ldots\ldots)]$$

Where d is the width of the grid (the smaller d, the more accurate the results), y is the value of the curve at different x values and n is an even number (maximum number of x).

Example 1

So for the rectangle in Fig.7.2, to calculate the area, Table 7.1 shows the values using 5 mm grid.

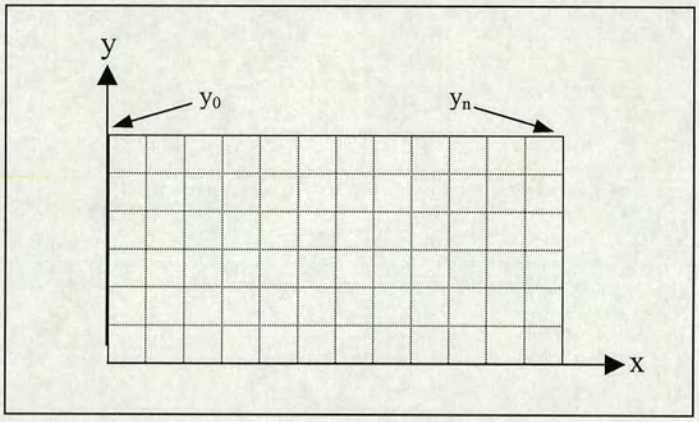

Figure 7.2: A simple grid superimposed on a rectangle to measure its area and perimeter.

y_x	Value (mm)	y_x	Value (mm)
y_0	30	y_1	30
y_2	30	y_3	30
y_4	30	y_5	30
y_6	30	y_7	30
y_8	30	y_9	30
y_{10}	30	y_{11}	30
y_{12}	30		

Table 7.1: x & y values for rectangle in Fig.7.2.

So the area is

$= 5/3\ [(30+30)+4(30+30+30+30+30+30)+2(30+30+30+30+30)]$

$= 5/3(60+720+300)$

$=1800\ mm^2$

Compare this result with the value calculated using the equation for the area of the rectangle,

$$\text{length} \times \text{width} = (12 \times 5)\ (6 \times 5)$$

$$= 60 \times 30 = 1800\ mm^2$$

The perimeter of the rectangle can be measured simply by counting the number of grid boxes the boundary of the rectangle crosses and multiplying that by the length of unit grid (d). In case of the rectangle in Fig.7.2, this is 180 mm, which is exactly the same result we get using rectangle's perimeter equation (2x [length + width]).

Example 2

In the same way we can find the area of a circle. Assume that we have a circle of 25 mm radius as shown in Fig.7.3 below.

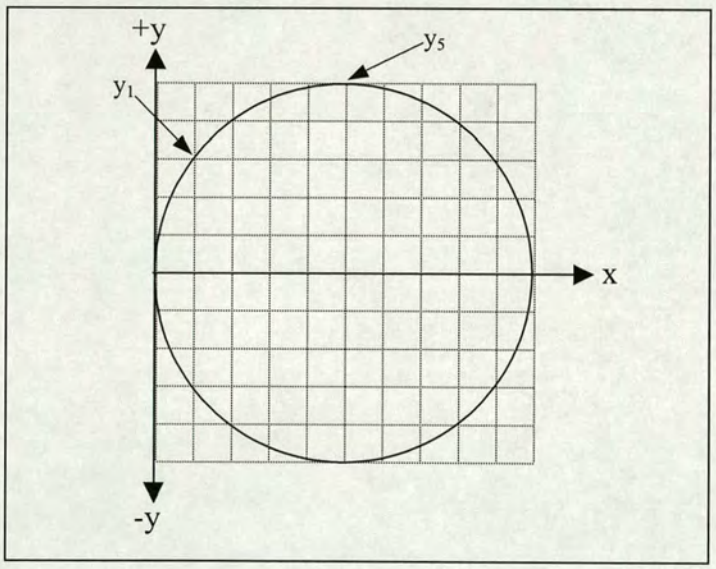

Figure 7.3: a simple grid to measure the area and perimeter of a circle

In order to keep the values for y positive for the simplicity of the calculations, we can divide the circle into two parts; upper and lower. Now to calculate the area above the x-axis, Table 7.2 shows the values using 5 mm grid.

So the area
= 5/3[(0+0)+4(100)+2(89)]
= 5/3 (400+178)
= 5/3 (578)
= 963.33 mm^2

Similarly the area below the x-axis
= 963.33 mm^2

y_x	Value (mm)	y_x	Value (mm)
y_0	0	y_1	15.5
y_2	20	y_3	22.5
y_4	24.5	y_5	25
y_6	24.5	y_7	22.5
y_8	20	y_9	14.5
y_{10}	0		

Table 7.2: x and y values for the upper half of the circle in Fig.7.3.

Hence the total area of the circle = 963.33 + 963.33 = 1926.667 mm^2.

Compare this result with the value calculated using the equation;
Area of a circle = πr^2 where r is the radius of the circle. In our case the radius is 25 mm. Hence area = 3.1415×25^2 = 1963.495 mm^2. The minor discrepancy (~ 1.88 %) between the two results can be improved by increasing the accuracy of the measurement by reducing the grid size.

For perimeter measurement, there are 28 grid boxes crossed by the boundary of the circle. Hence the perimeter equals 28 x 5 (140 mm). The result using the circle perimeter equation is 157.08 mm (circumference of a circle = $2\pi r$).

In this way we can measure the area of any irregular shape using the grid and Simpson's formula. The shape can also be divided in more than one part to measure its area, just as we divided the circle in upper and lower areas.

Example 3

Fig.7.4 shows an irregular body for which we want to measure its area and perimeter. The body can be divided into upper and lower parts and the measurements can be conducted in the same way as above.

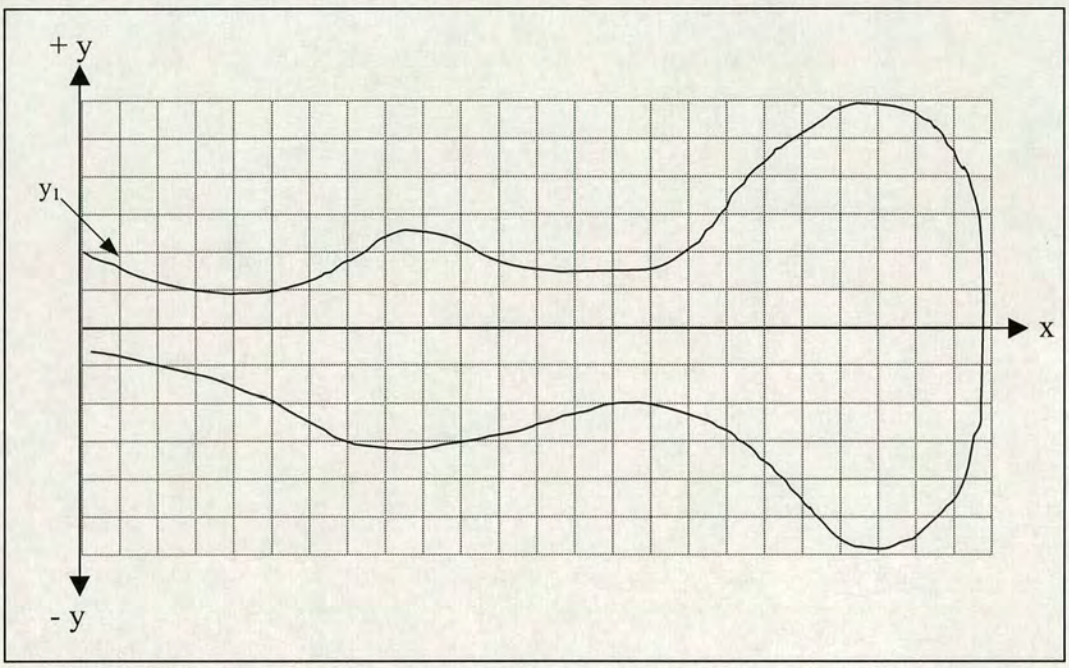

Figure 7.4: A simple (5mm) grid superimposed on an irregular shape to measure its area and perimeter.

y_x	Value (mm)		y_x	Value (mm)	
	Upper	Lower		Upper	Lower
y_0	10	3	y_1	8	3.5
y_2	6	5	y_3	5	6
y_4	4.5	7.5	y_5	5	9.5
y_6	6.5	12.5	y_7	9	15
y_8	12.5	15.5	y_9	12.5	15.5
y_{10}	11.5	15	y_{11}	9	14
y_{12}	8	12.5	y_{13}	7.5	11
y_{14}	7.5	10	y_{15}	8	10
y_{16}	10.5	11	y_{17}	16	13.5
y_{18}	22	17.5	y_{19}	25.5	22.5
y_{20}	29	28	y_{21}	29.5	29
y_{22}	29	27.5	y_{23}	23.5	22

Table 7.3: x & y values for the irregular shape in Fig.7.4. Upper and Lower denotes above and below the x-axis.

So the area above the x-axis

$= 5/3\ [(10+23.5)+4(135)+2(147)]$
$= 5/3\ (578)$
$= 1445.833\ mm^2$

Similarly the area below the x-axis

$= 5/3[(3+22)+4(149.5)+2(162)]$
$= 5/3(922)$
$= 1578.333\ mm^2$

So the total area of the shape is 3024.166 mm^2.

For perimeter measurement, there are 58 grid boxes crossed by the boundary of the circle. Hence the perimeter equals 58 x 5 (290 mm).

Hence, it has been illustrated the perimeter and area of any irregular closed shape can be measured. For computer images Fairhurst (1988) showed that in an automated way area, perimeter and width of any shape can be quite easily obtained from the boundary representations based on chain code; perimeter, for example, is given by

$p = \sqrt{2} \cdot m + n$ (m and n are the numbers of odd and even direction codes, respectively).

However, area and perimeter separately cannot be distinctive shape indicators. For example, both a square and a circle can have exactly the same area. But these two parameters can be joined together to give a third more descriptive parameter. This is known as the *shape factor* or *compactness* since it is the measurement of the efficiency with which a boundary encloses an area. This can be calculated simply by the following equation;

$$\text{Compactness } C = \frac{4\pi A}{p^2} \qquad (A \text{ is area and } p \text{ is perimeter})$$

For any shape (circle, triangle, hexagon, etc.) the compactness is always the same regardless of the size of the shape. Fig. 7.5 shows some examples of this. A circle encloses the maximum area for a given perimeter, and hence it has the maximum C (=1). Other shapes will be characterised by smaller values of C. Addison (1997) illustrated that for islands with similar shapes, C is always the same regardless of the size of the islands. This area-perimeter relationship has been intensively and successfully used in different scientific fields to characterise different objects: Mandelbrot *et al.* (1984) and Mu and Lung (1988) to characterise the contours of fracture surfaces of steel; Nikora *et al* (1993) and Wu and Lai (1994) to investigate river channels and drainage areas; Lovejoy (1982), Hentschel and Procaccia (1983), and Rys and Waldvogel (1986) to characterise rain and hail clouds; and Cheng (1995) to investigate the distribution of different chemical elements using geochemical data.

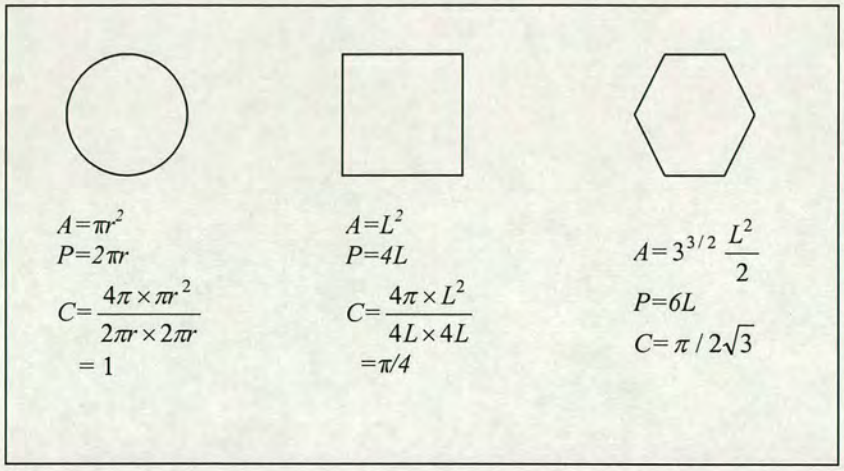

Figure 7.5: Compactness of some simple shapes.

7.2.2 Sphericity and Eccentricity (or rectangularity)

Although compactness is a useful discriminator for the shape of many objects, it is not sufficient alone for distinguishing many others. Fig.7.6 shows two such shapes. Both shapes have an area of 30 mm^2 and perimeter of 14 mm and hence the same compactness. This ambiguity can be resolved by employing additional shape measures. Sphericity and Eccentricity (or rectangularity) are two such parameters. Sphericity measures how close is the object to a sphere and can be calculated using the simple ratio

$$\text{Sphericity} = \frac{(R_i)}{(R_c)}$$

Where R_i is radius of the inscribed circle and R_c is radius of the circumscribed circle (Fig. 7.7).

Eccentricity or Rectangularity of a shape is a feature related to the length and width of the shape (major and minor axis) and can be measured by identifying the minimum bounding rectangle i.e. the smallest rectangle which can completely enclose the object. The main axis of this rectangle is in fact the principal axis of the object itself and, hence, the dimensions of the minimum bounding rectangle

correspond to the features of length and width (Fig. 7.8). Therefore, Eccentricity or Rectangularity of a shape can be measured by taking the ratio of the width to the length of the rectangle and, hence, the values will always be between 0 and 1.

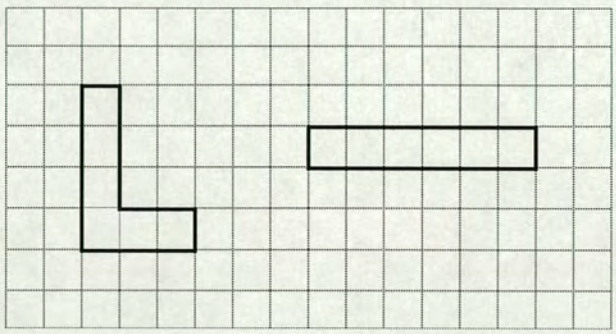

Figure 7.6: Compactness fails to distinguish the two shapes since both have the same area and perimeter values.

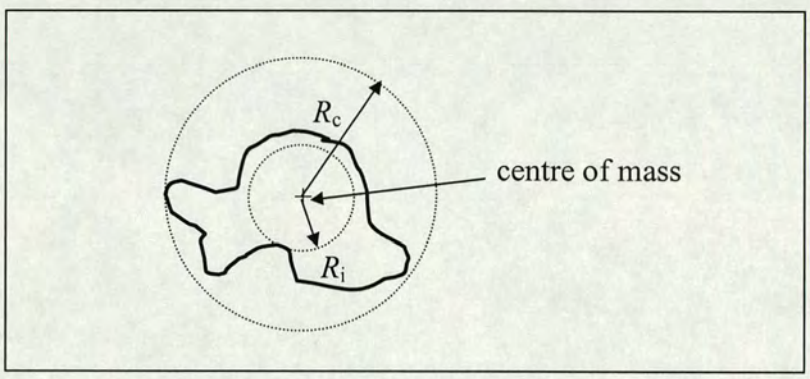

Figure 7.7: Sphericity of an object.

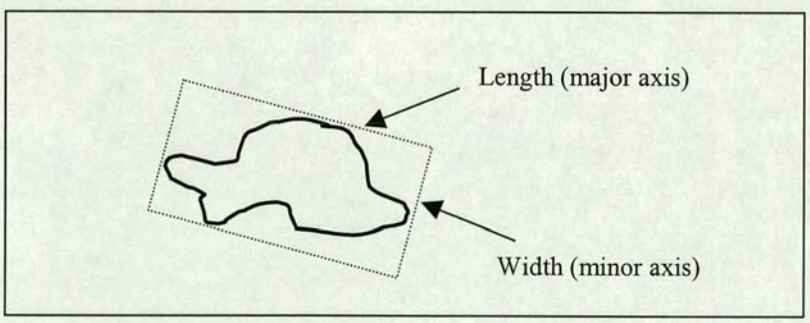

Figure 7.8: Eccentricity or Rectangularity of an object.

7.2.3 Spread and Elongation

Using statistical methods Wilf (1981) showed that raw moments and central moments of a shape can be readily computed from its boundary, and from these two new parameters the spread and the elongation can be obtained.

The spread measures how unevenly an object's mass is distributed about a centroid and it can be calculated using the formula

$$S = (\mu_{20} + \mu_{02}) / m_{00}^2$$

where S is spread, m_{00} is the central moment of the shape and μ_{20} and μ_{02} are the second order moments of the shape.

The elongation measures the degree to which mass is concentrated along a particular axis and it can be calculated using the equation

$$E = 2m_{00}^2[4\mu_{11}^2 + (\mu_{20} + \mu_{02})^2]^{1/2} / (\mu_{20} + \mu_{02})$$

where E is elongation, m_{00} is the central moment of the shape, μ_{11} is first order moment and μ_{20} and μ_{02} are the second order moments of the shape.

7.2.4 Normalised polar representation of the shape

In all the previous methods we were trying to represent the shape of an object by a single dimensionless number. This section provides the means of representing the shape by another unique shape that will be the same even if the size, orientation or position of the object has changed. Here the distance from the centre of mass to the edge of the shape is measured at a regular interval of angle ($\delta\theta$) and a cross plot is produced. In order to have scale invariant results each distance (d) is divided by the maximum distance (D), hence, all the results lie between 0 and 1. In order to have rotation invariant results the plot is always started from the maximum distance i.e. the shape is rotated until the maximum length lies on 0°. It is obvious that for a circle of any size the result will always be a straight line having a y-value of 1 as shown by Fig. 7.9. This figure also shows the polar representation for any square and any

hexagon. Calculations and values used for plotting this figure are given in appendix 8.

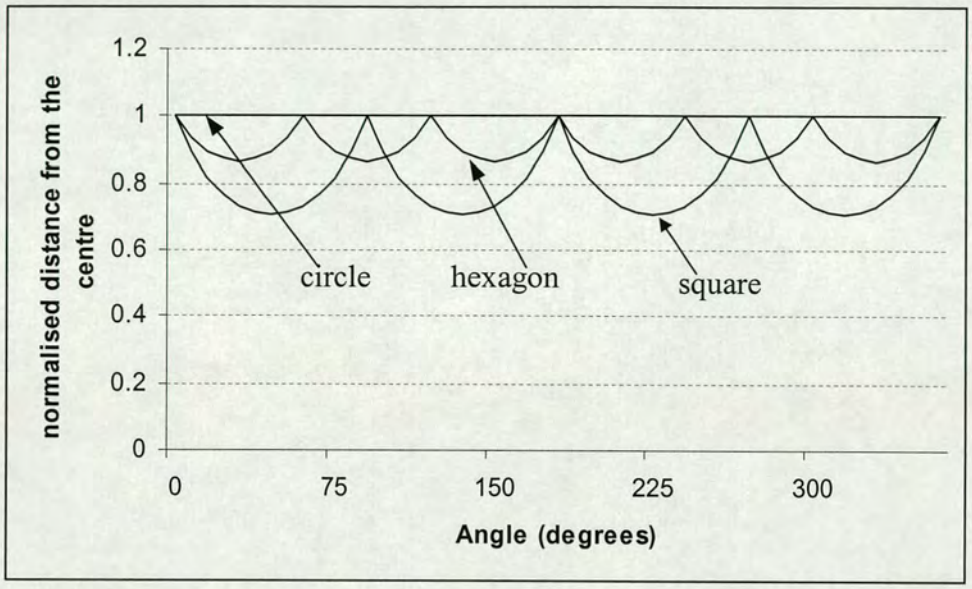

Figure 7.9: Polar representation of some simple shapes. Results show that each shape has a unique representation.

For the irregular shapes in Fig. 7.4 and Fig. 7.8, Table 7.4 and Table 7.5 show the distances from the centre to the edge of each shape using 10° for $\delta\theta$. All the distances were then divided by the maximum value to normalise the results and, hence Fig. 7.10 shows the resultant polar representation of these two irregular shapes. Fig. 7.9 and Fig. 7.10 both illustrate that polar representation of any shape can be quite useful as a discriminating method.

Normalised polar representation of shapes can also be used for matching purposes, as it is scale and rotation invariant. One further advantage of this method is whereas the results from all the previous methods could not be used to reconstruct the original shape, if we had the polar representation of the shape it can be reconstructed accurately. The smaller the $\delta\theta$, the more accurate the reconstructed shape.

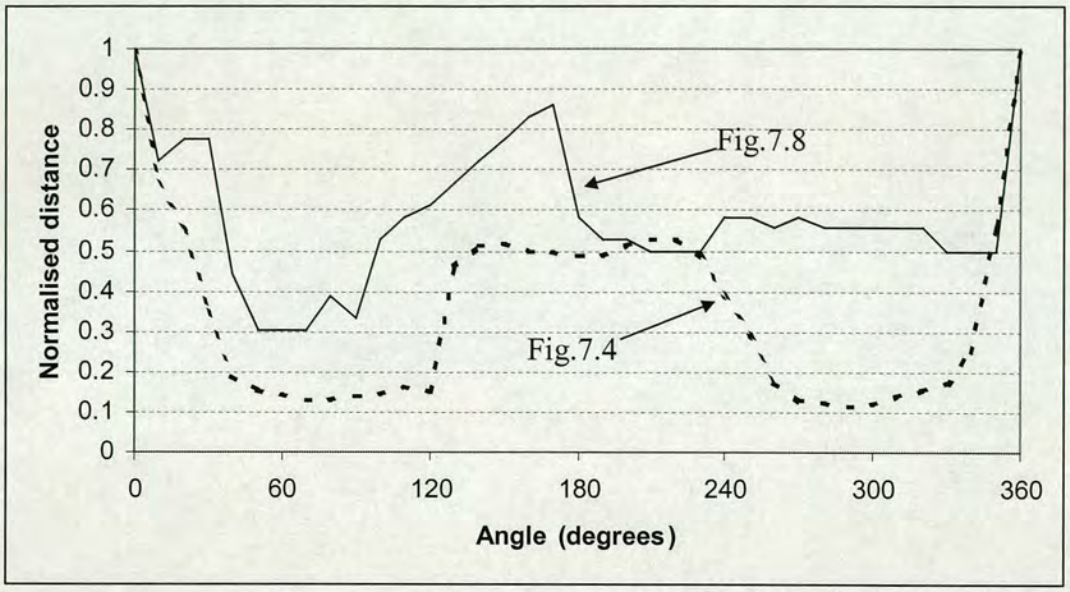

Figure 7.10: Polar representation of the irregular shapes shown in Fig 7.4 and Fig.7.8.

Angle (Degrees)	Distance (cm)	Normalised Distance	Angle (Degrees)	Distance (cm)	Normalised Distance
0	1.8	1	190	0.95	0.5278
10	1.3	0.7222	200	0.95	0.5278
20	1.4	0.7777	210	0.9	0.5
30	1.4	0.7777	220	0.9	0.5
40	0.8	0.4444	230	0.9	0.5
50	0.55	0.3055	240	1.05	0.5833
60	0.55	0.3055	250	1.05	0.5833
70	0.55	0.3055	260	1	0.5556
80	0.7	0.3889	270	1.05	0.5833
90	0.6	0.3333	280	1	0.5556
100	0.95	0.5278	290	1	0.5556
110	1.05	0.5833	300	1	0.5556
120	1.1	0.6111	310	1	0.5556
130	1.2	0.6667	320	1	0.5556
140	1.3	0.7222	330	0.9	0.5
150	1.4	0.7778	340	0.9	0.5
160	1.5	0.8333	350	0.9	0.5
170	1.55	0.8611	360	1.8	1
180	1.05	0.5833			

Table 7.4: Distances from the centre to the edge of the shape in Fig.7.8 using 10° for $\delta\theta$. The maximum distance from the centre is 1.8 cm and, hence, all the distances are divided by this value to normalise the results.

Angle (Degrees)	Distance (cm)	Normalised Distance	Angle (Degrees)	Distance (cm)	Normalised Distance
0	8	1	190	3.9	0.4875
10	5.3	0.6625	200	4.1	0.5125
20	4.4	0.55	210	4.2	0.525
30	2.8	0.35	220	4.2	0.525
40	1.5	0.1875	230	3.9	0.4875
50	1.25	0.15625	240	3.1	0.3875
60	1.15	0.14375	250	2.3	0.2875
70	1.05	0.13125	260	1.4	0.175
80	1.05	0.13125	270	1.05	0.13125
90	1.1	0.1375	280	1	0.125
100	1.15	0.14375	290	0.9	0.1125
110	1.3	0.1625	300	0.95	0.11875
120	1.2	0.15	310	1.1	0.1375
130	3.7	0.4625	320	1.25	0.15625
140	4.1	0.5125	330	1.4	0.175
150	4.15	0.51875	340	2	0.25
160	4	0.5	350	4.5	0.5625
170	4	0.5	360	8	1
180	3.9	0.4875			

Table 7.5: Distances from the centre to the edge of the shape in Fig.7.4 using 10° for $\delta\theta$. The maximum distance from the centre is 8 cm and, hence, all the distances are divided by this value to normalise the results.

7.3 General models for turbidites

The aim of this section is to produce a review of the literature and investigate if there are general geological models for turbidite depositional units that have distinctive shapes that reflect the lithological facies variations within them in order to apply to them the shape parameters just discussed.

7.3.1 Complexity of turbidite systems

Due to their importance as source and host rocks of hydrocarbons, deep-water siliciclastic systems have been extensively investigated over the past 50 years through outcrop and laboratory studies, acoustic imaging of modern fans and deep-penetration seismic profiling of buried systems. These investigations have provided a wealth of information which has been summarised in special publications such as

those edited by Berg and Woolverton (1985), Bouma *et al.* (1985), Clark and Pickering (1996), Hartley and Prosser (1995), Mutti (1992), Pickering *et al.* (1989), Pickering *et al.* (1995), Reading (1996) and Weimer and Link (1991), as well as in specific papers (e.g. Damuth *et al.*, 1988; Galloway, 1998; Kolla & Macurda, 1988; Manley & Flood, 1988; Reading & Richards, 1994; Sanders & Friedman, 1997; Shanmugam, 2000 and Weimer, 1989).

These and other publications have demonstrated that deep-water systems are quite complex in terms of depositional processes, geometries and stacking patterns. Despite the many attempts to develop a single facies model (e.g. Normark, 1970, 1978; Mutti & Ricci Lucchi, 1972; Walker, 1978; Stow & Shanmugam, 1980; Lowe, 1982), no single facies model has been found that can adequately represent all deep-water systems (Shanmugam, 1990 & 2000; Mutti, 1992). Shanmugam (2000) argues that unlike fluvial and deltaic environments, it is not practical to observe and analyse features and processes directly in deep-water environments. We are also hampered by our inability to emulate deep-water conditions realistically in laboratory experiments. This is further complicated by the problems of comparing modern and ancient deep-water systems (Shanmugam *et al.*, 1985; Mutti & Normark, 1987 & 1991; Normark *et al.*, 1993; Pickering *et al.*, 1989). As a result, deep-water facies models are mostly based on incomplete observation made on modern and ancient systems (Shanmugam, 2000). Fig. 7.11 shows a number of fan models that have been developed in an attempt to better understand fan growth and the pattern of facies distribution. There is no real consensus with regards to these models. Anderton (1995) believes that facies models are ephemeral, and that each facies model is unique, because each facies model is unique to a certain environment. He argues that since a facies model is developed from a local example, it should not be expected to encompass all possible variabilities. Furthermore, he notes that there is no fundamental reason why there should be a relationship between the vertical succession of beds in a submarine fan deposit and their three dimensional geometry, particularly in the mid-fan region, where random processes will dominate. Bouma (2000) warns about the danger of not applying the models selectively and critically. He points out that it should be understood that no two deposits are mirror images but may have several characteristics in common. Clark *et al.* (1992) concluded that using

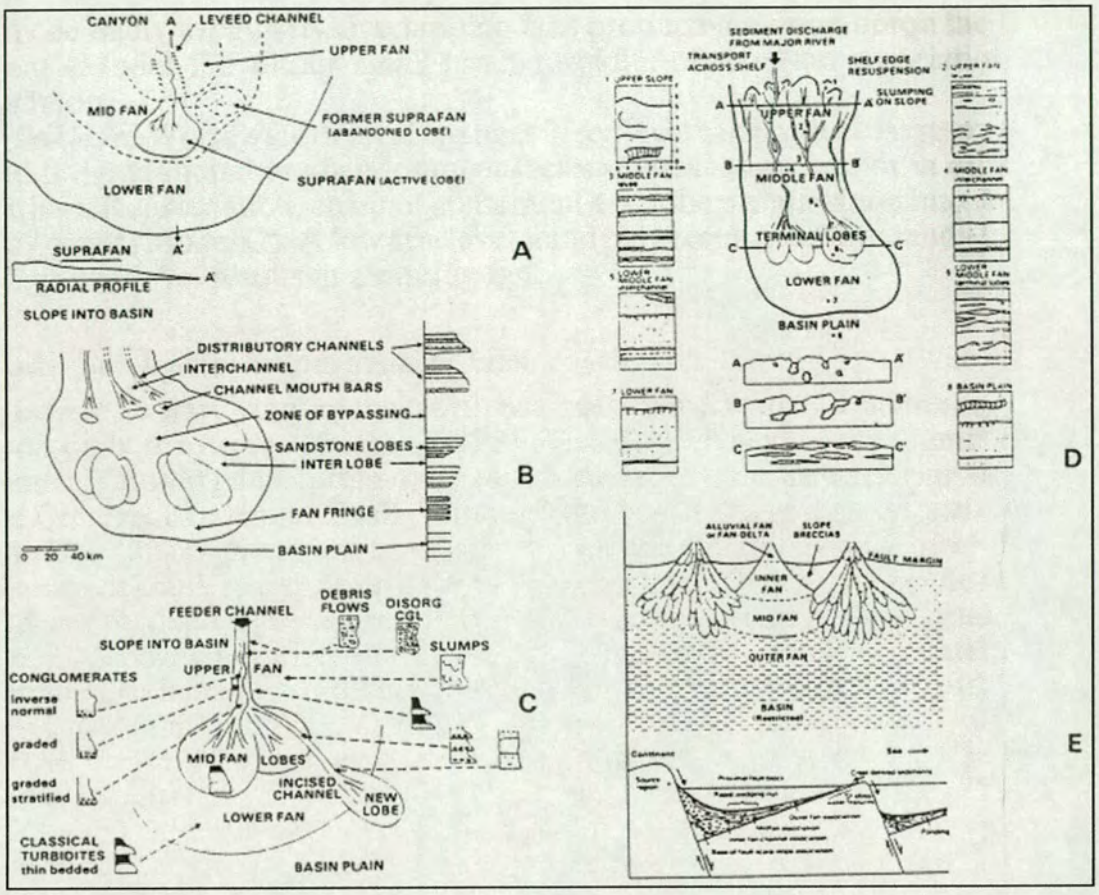

Figure 7.11: Deep-Water Fan Models. A) model after Normark (1978); B) model after Mutti & Ricci Lucchi (1972); C) model after Walker (1978); D) model after Stow (1981); E) model after Surlyk (1978). (Figure taken from Stow *et al.*, 1982)

data from 16 modern submarine fans, a graph of sinuosity versus width/depth ratio reveals no obvious trends. This is thought to be due to the fact that, unlike in the fluvial systems, many turbidity currents overspill the confines of their channels by height and widths much greater than the bankfull cross-sectional area. All of that is inter-related to sinuosity and gradient. Therefore, even if we can estimate sinuosity of a turbidite channel, we cannot use this to establish a width/thickness ratio.

7.3.2 Turbidite Elements

As a result of the aforementioned difficulties Mutti (1985) and Mutti and Normark (1987, 1991) introduced the concept of elements in turbidite systems. They defined a turbidite system as a genetic unit, i.e. a stratigraphic unit that records a series of genetically linked erosional and depositional events that occurred in virtual stratigraphic continuity and are expressed by erosional and depositional elements respectively. They proposed that since turbidite systems differ from each other in terms of size, geometry, and sediment types, as well as in terms of vertical and lateral stratigraphic relationships between facies and facies associations, the idea of elements can serve as a natural bridge between different types of datasets. Elements are the basic mappable components of both modern and ancient turbidite systems that can be recognised in marine, outcrop and subsurface studies. This method of using the concept of elements in describing turbidite systems is similar to the elements of a face used in face recognition; instead of describing the whole face, we describe and classify the nose on its own, and so we do for the eyes, mouth etc. The combined classification of these elements results in the description of the face. The following section gives a summary of these elements as described by Mutti and Normark (1987, 1991); Mutti (1992) and Normark *et al.* (1993).

7.3.2.1 Major Erosional Features

This element includes a number of large-scale negative relief features. Due to their size they commonly have clear seismic expressions. However, their recognition in outcrop studies requires careful mapping and detailed stratigraphic and facies analysis. These features include:

- Shelf edge failures,
- Slope failures,
- Intrabasinal failures, and
- Canyons.

All of these erosional features can provide pathways for coarse sediment to move directly into deeper water thus bypassing the outer shelf and upper slope environments. Most failures act as a main source for turbidite accumulations in a basinward direction. Some failures may involve huge volume of sediment (up to 5000 km^3) removed in extremely short periods of time.

The fill of these large-scale erosional features is highly variable and generally quite complex because they are related to repeated periods of erosion and sedimentation. Most commonly, chaotic deposits and thin-bedded turbidites with local development of coarse grained and usually lenticular bodies could be found, particularly in the basal part of the fill.

7.3.2.2 Channels

Channels are elongate negative relief features produced by turbidity current flow and hence they represent major, relatively long-term pathways for sediment transport. Channel shape and position within a turbidite system are controlled either by depositional processes in the case of those associated with large levee wedges or by erosional down-current cutting.

Channels and channel-levee complexes can be observed on multichannel seismic reflection data in areas where sufficiently high sediment flux permits resolution of these features. Mitchum (1985) describes some channel-levee complexes observed in the early Eocene fans of the North Sea.

Most channel-fill deposits form depositional elements bounded by a basal erosional surface. They reflect stages of deposition in a system during which a decrease in the energy of flows forces many of the turbidity currents to deposit their sediment load

directly in the channel rather than further basinward. Three main types of channel-fill deposits are commonly observed in ancient turbidite systems in both outcrop and subsurface studies (Fig. 7.12):

- Erosional channel-fill deposits are those in which basal, coarse grained residual facies are overlain by fine grained channel-abandonment deposits.
- Depositional channel-fill deposits are primarily made-up of depositional facies that infilled the channel after its main phase of activity as a pathway for sediment transport.
- Mixed channel-fill deposits are transitional between the above two types or result from a switch between types.

7.3.2.3 Overbank/Levee Deposits

Overbank deposits are generally fine-grained, thin-bedded turbidite sediments that can be laterally extensive and are adjacent to the main channels in a turbidite system. The areas of overbank deposition on most systems can be subdivided into two parts:

- Channel related overbank deposits: these include a variety of thin bedded and fine-grained turbidite sandstone facies that occur within the channel, along the edges of the channel, or within interchannel areas.
- Overbank wedges: these are characterised by a thick wedge of fine-grained, mainly muddy turbidite beds that are as much as several 100 m's thick near the margins of the basin and gradually wedge-out in a basinward direction over distances of 10's of kilometres into thin mudstone units that are probably of basin-wide extent.

Because these overbank wedges are relatively thin, their internal reflection geometries are not well imaged due to resolution problems. Hence, internal reflection configurations are characterised by a low to moderate amplitude, continuous to discontinuous seismic response.

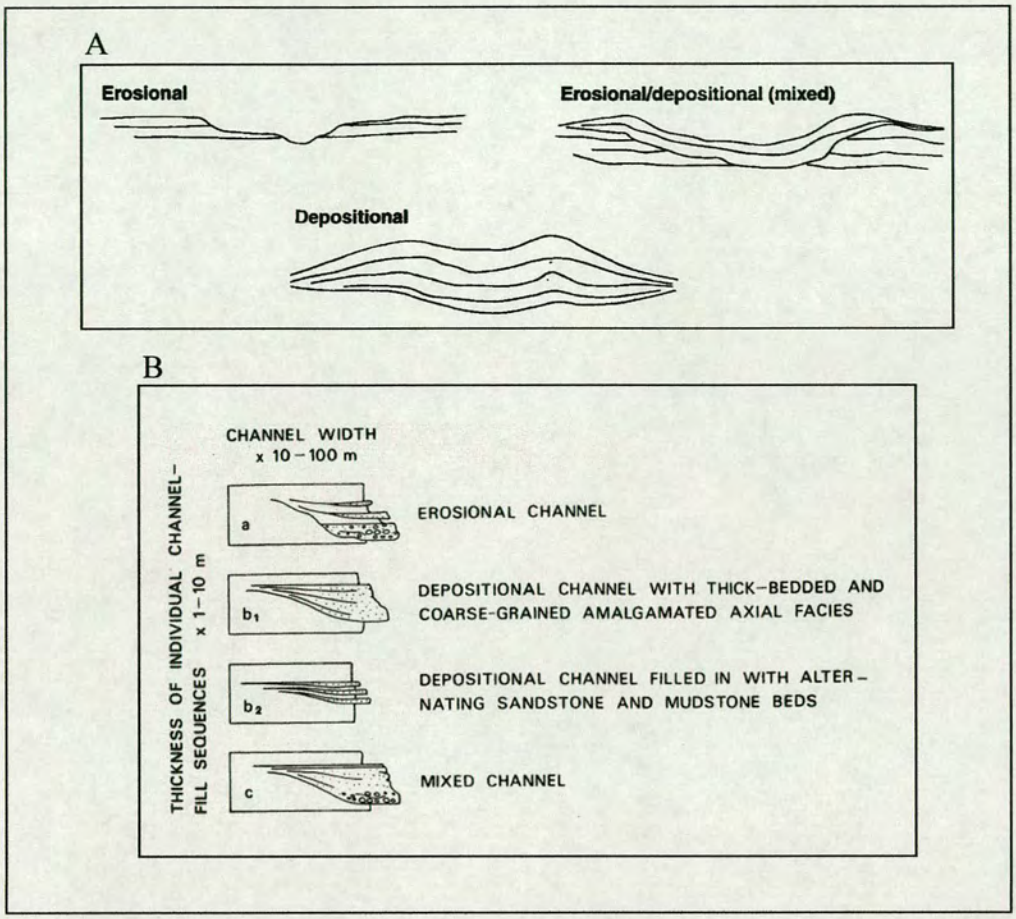

Figure 7.12. Main types of channels and channel fills commonly observed in ancient turbidite systems in both outcrop and subsurface studies. A) Main channel types. B) Main types of channel fill deposits. (Mutti and Normark, 1987).

7.3.2.4 Depositional Lobes

Despite the fact that turbidite lobes are probably the most prominent element in deep water turbidite systems from both stratigraphic and exploration standpoints, as they represent the environment where most systems develop thicker and more laterally extensive sandstone bodies, this element is least compatible in usage between different turbidite systems. The down current extent of sandstone lobe packages depends on the size of the system and on basin size and configuration and is primarily controlled by the volume of the individual turbidity currents. The thickness of individual sand lobes on modern fans is difficult to resolve with standard seismic techniques unless the lobes are exceptionally thick. The consequence is that lobes on modern fans cannot be defined using any of the characters used for identifying lobes of the ancient systems. A seismically defined lobe can be described as a relatively conformable succession of reflections bounded at its base and top by stratal discontinuities (Fig. 7.13).

Although lobes may differ considerably from one system to another in terms of overall geometry, facies types, and stacking patterns, depositional sandstone lobes are characteristically tabular bodies with individual thickness generally between 3-15 m and made up of medium to thick-bedded sandstone. Small and sand-rich systems generally have poorly-developed sandstone lobes which grade upsystem into extensively scoured and channelled sandstones and pebbly sandstones. Large and mud rich systems have the greatest development of depositional sandstone lobes which are detached from their feeder features. Particularly in these systems, sandstone lobes and similar thick units made up of mudstones with thinner-bedded and fine-grained sandstone stack to form spectacularly cyclic successions up to some hundreds of metres in thickness.

Depending on many factors, mainly related to basin configuration and to the different stages of growth that characterised most turbidite systems, the deposits that comprise the lobe element can include;

- Sheet-like bodies that in some cases have virtual basinwide extent.

- Slightly mounded bodies that can occur at the terminus of basin margin channels (as seen in the Tay Sandstone Member discussed in the seismic interpretation chapter).
- Confined bodies that formed as the fill of variety of both structural and erosional depressions

Pickering *et al.* (1995) provided a scale-independent classification of two-dimensional architectural geometries both in cross-sectional and plan view, as shown in Fig. 7.14 and Fig. 7.15 respectively. They also provided the different stacking patterns for channel complexes. This is shown in Fig. 7.16. These cross-sectional and stacking patterns have been used in this study for forward modelling purposes in order to investigate their seismic response as will be discussed later in this chapter.

7.3.3 Classification based on grain size and feeder system

According to Reading and Richards (1994) depositional systems in deep-water basin margins can be classified on the basis of grain size and feeder system. As grain size decreases there is an increase in the size of the source, the size of the depositional system, the down-current length, the persistence and size of flows, fan channels, channel-levee systems, and in the tendency to meander and for the major slumps and sheet sands to reach the lower fan and basin plain. Four classes are identified based on grain size:

- Gravel rich systems;
- Sand rich systems;
- Mud rich systems; and
- Sand/mud mix systems.

Similarly, the size and stability of channels and the organisation of the depositional sequences decreases toward a linear source, as does the length to width ratio of the system. Hence, each of the classes above is further subdivided based on feeder system:

- Point (or single) source fans;
- Multi source submarine ramps; and

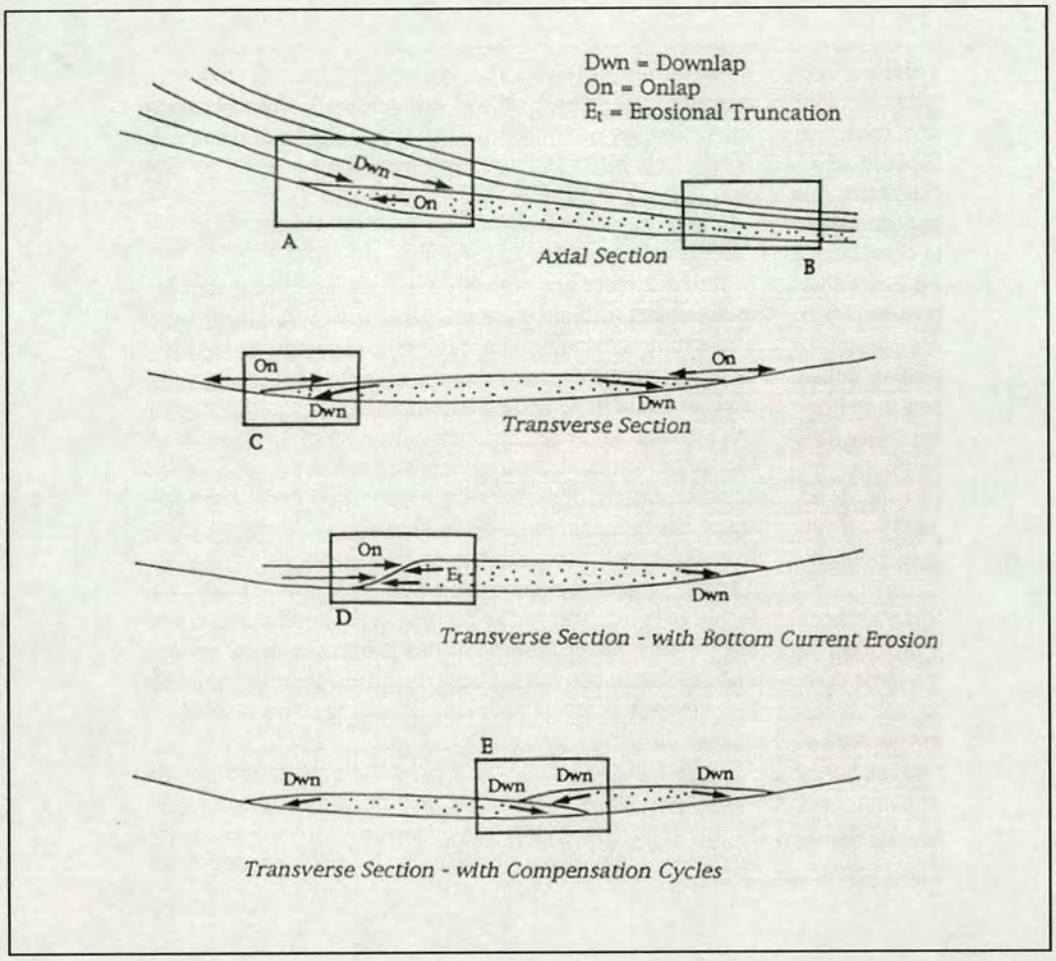

Figure 7.13: Schematic depiction of stratal geometries that define the upper and lower bounding surfaces of deepwater turbidite deposits. Small arrows indicate terminations. **A**) Axial section illustrating stratal onlap against updip basin margins; onlap defines base of the unit whereas downlap of later progradational deposits define top of the unit. **B**) In distal settings, both the top and the base of the unit can be characterized by conformable surfaces. **C**) Transverse section wherein submarine fan lobe develops external mounding as a result of original depositional relief later enhanced by differential compaction and/or relief related to bottom current erosion. Note that the base of the unit in C is defined by onlapping geometry. **D**) Transverse section wherein onlap of later deposited sediments can define the top unit. Where bottom current erosion occurs, the stratal geometry internal to the unit may be characterized by erosionally truncated horizons. **E**) Transverse section wherein compensation cycles may result in bounding stratal geometries characterized by downlap. (Normark *et al.*, 1993)

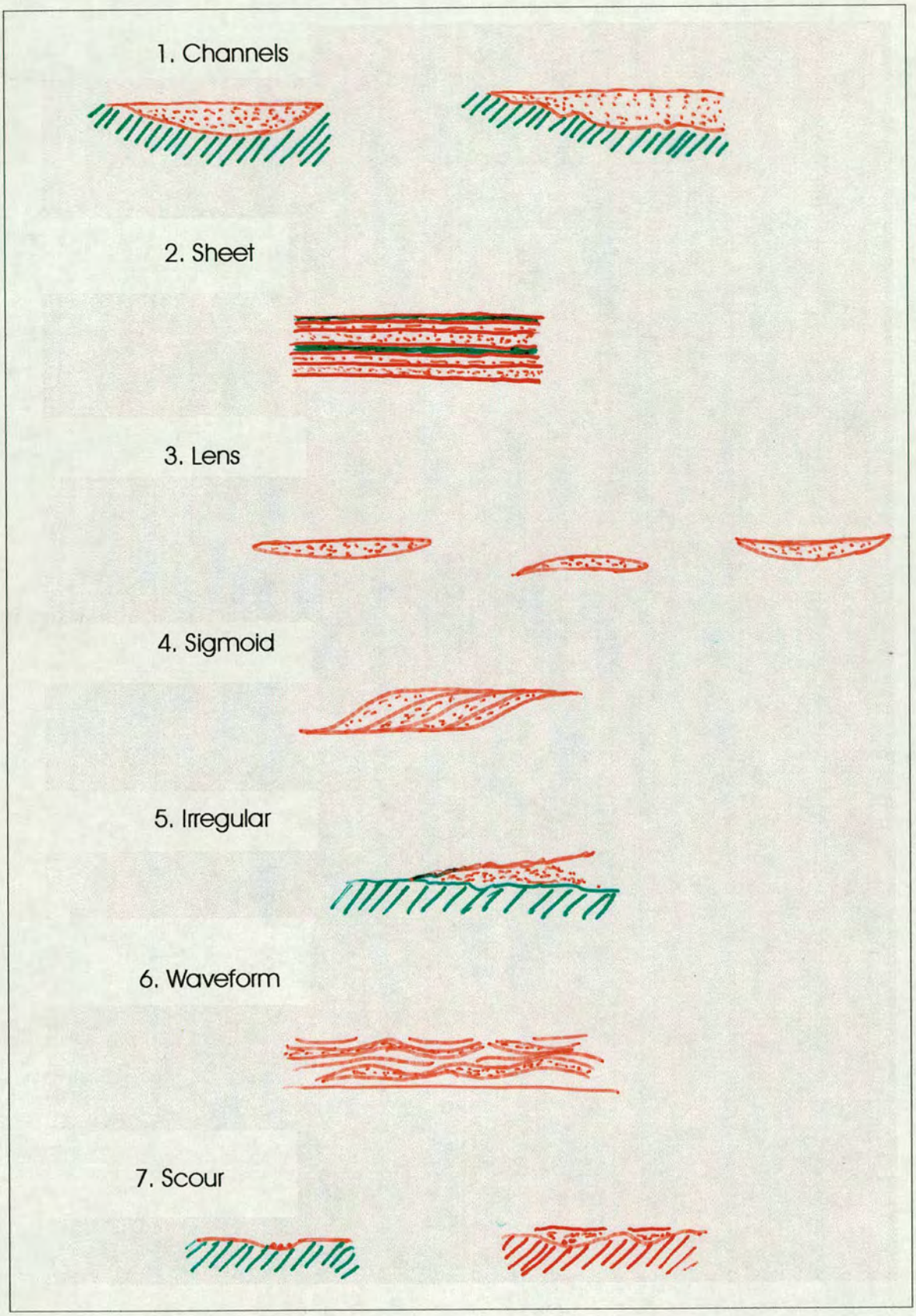

Figure 7.14: Scale-independent classification of 2D architectural geometries in cross-sectional view. (From Pickering *et al.*, 1995)

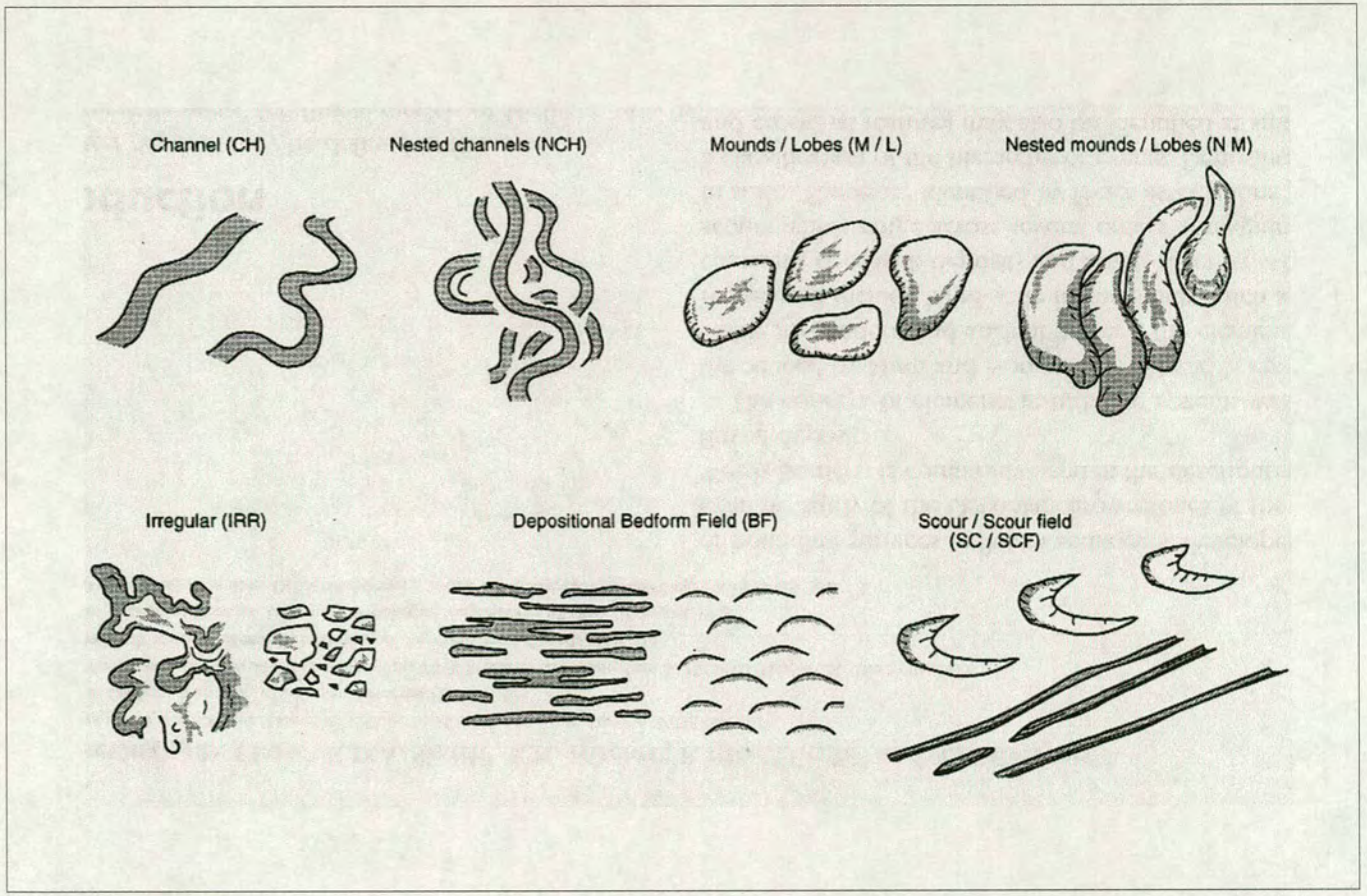

Figure 7.15: Planform classification of deepwater architectural geometry, applicable over wide range of scales. (From Pickering *et al.*, 1995)

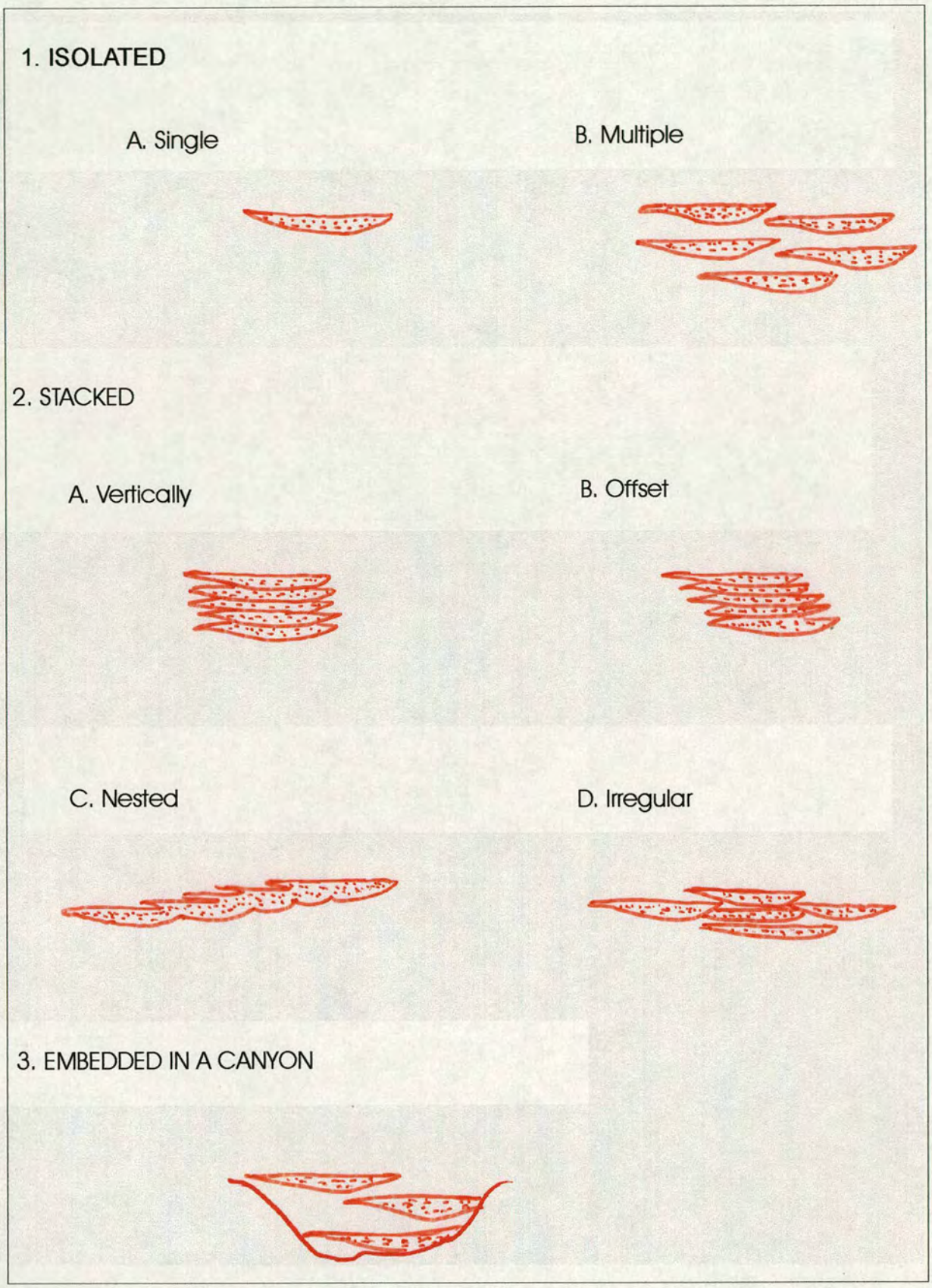

Figure 7.16: Scale independent stacking pattern for channel complexes. (From Pickering *et al.*, 1995)

- Linear source slope aprons.

As a result we have 12 types of models for the turbidite systems as shown in Fig. 7.17. For detailed description of these systems refer to Reading and Richards (1994). It is important to point out that these are just conceptual models and there is a lot of debate and dispute in the literature about their validity to serve as general models for turbidite systems (see Shanmugam, 2000). Clark *et al.* (1992) regard classifications of submarine fans concentrating on relating fan shape to grain size and sediment calibre to be inadequate, principally because the shape of the fan is strongly controlled by the shape of the receiving basin, which in turn is dependent upon parameters such as tectonics and diapirism as we have seen in the Gannet South area of the Central North Sea (see seismic interpretation chapter and trace shape analysis chapter).

7.4 Generating synthetic seismic data and body checking

The final task of this chapter is to investigate by forward modelling and body checking which physical properties influence the geometry and attributes of the bodies in the seismic data. Then, using the combined physical and shape parameters in a predictive way on a model dataset as well as at least one real data example the validity of the method can be checked.

The following methodology was proposed. Using the classification proposed by Reading and Richards (1994) we have 12 different types of turbidite systems. By combining the turbidite elements of Mutti and Normark (1987, 1991), the different architectural geometries provided by Pickering *et al.* (1995), and the grain size analysis conducted by Bruhn (1998), several two-dimensional geological cross sections along the 12 types of systems can be constructed. These two-dimensional synthetic seismic lines can then be combined by interpolating between them to produce a three-dimensional synthetic seismic cube for each of these scenarios. These datasets can then be analysed by body checking and application of shape

parameters discussed earlier. By an iterative forward modelling process, an investigation will be carried-out as to which petrophysical properties influence the geometry of the bodies in the seismic data as revealed by the body checking process.

Fig. 7.18 shows the geological cross sections along the sand rich turbidite fan system. This system was chosen particularly to start with because the Gannet South is of this category as discussed earlier. Hence, the petrophysical values allocated for each lithology in the cross section were taken from the different litholigies observed in the Gannet South area and specifically from well 22/26a-1.

These geological cross sections together with the associated petrophysical values were loaded into the forward modelling package (GMAplus) and two-dimensional synthetic seismic data were generated. Fig. 7.19 and Fig. 7.20 show the synthetic seismic for the different sectional classification and channel stacking patterns provided by Pickering *et al.* (1995) and Fig. 7.21 shows the effect of varying the channel thickness. It must be noted that, these were the first results produced in order to become familiar with the functionality of the modelling package and rather high values for geophysical and petrophysical parameters were assumed. Fig. 7.22 shows the 2D synthetic seismic sections for the slope channel and channel complex at the toe of the slope (lines 2 and 3 of Fig. 7.18 respectively).

7.5 Obstacles in the way

At the outset of this project usage of a high-resolution, three-dimensional seismic dataset with an appropriately dense well dataset was proposed in order to constrain the three-dimensional forward modelling of turbidite systems. It will not be possible to find out what, geologically, lies behind the seismic expression of turbidites unless a coincident three-dimensional seismic and equally dense geological well dataset is available. The hypothetical models developed are not adequate because they do not have a coincident seismic expression. It is also important to have a feeling for the range of physical properties that is acceptable for different components of a turbidite system and any relationships between them. This will allow quantitative constraints

to be placed on the forward models and, ultimately, on inversions, once it is known how the range available is expressed in the seismic data. This information can be gleaned from the literature, but also from well sampled fields/reservoirs where porosity and density measurements (*in situ* or on samples) have been made on known elements of a turbidite system. To this end, the Nelson Field dataset which has both a very good seismic quality and well spacing of less than 0.5 km was thought to be ideal for the project. The Gannet-South dataset was chosen to be an example where the developed body shape parameters would have been applied in a predictive way to assess and confirm their validity as a tool for identifying turbidite sand bodies and their corresponding depositional environments. This was accepted by Shell-UK together with the initial project proposal. However, the other partners of Shell and the field operator did not permit access to the dataset for the study. The loss of the dataset was unfortunate and it was not possible for Shell to replace it with another equally adequate dataset. Using Gannet-South as an alternative was not feasible because the density of the wells within the area is not thought to be adequate. The shortest distance between any two wells is approximately 2.5 km and the longest is 11 km. Deepwater clastic systems and associated turbidite reservoirs are often characterised by very complex sand distributions. In areas of high heterogeneity where fine details of the horizons are required, logging tools do not have adequate spatial resolution. They can only measure up to a distance of one metre from the borehole (Al-Aufi, 1996). Fig. 7.24 from Al-Aufi (1996) summarises the effect of well spacing on the actual spatial resolution induced from the wells.

The previous review of the literature has illustrated the on going debate between geologists with regards to the existence of general depositional models for turbidite systems. This made the task of the project more difficult to achieve. It was not easy to decide which depositional model is best to follow. The literature-based simple three-dimensional models of stacked turbidites (from Mutti, Reading & Richards, Pickering and flume tank experiments at Leeds University and others) were used to assess sensitivity of seismic synthetics to changes in sediment body shape and properties. During model development to greater complexity quantitative and semi-quantitative relationships between parameters was required in order to constrain

model options. Initially, the synthetic seismic models were built in two-dimensions with the view of transferring them into three-dimensional synthetic seismic data cube using a package that can interpolate between the two-dimensional lines. The author was under the impression that such a technology did exist, but was soon to find out that it did not. What further exacerbated the problem is that the supervisor (Dr. John Verbeek) with whom this project was initiated left the UK for his next posting within the first year of the project.

7.6 Conclusions

At the outset of this chapter its objective was defined to be three-fold. First, to establish a set of body shape parameters that would enable a meaningful and distinctive description of different turbidite sand bodies. Investigation has concluded that there are a number of basic parameters that can be derived from any arbitrary shape to provide valuable classification information and, hence, a useful means of checking the identity of the object. A total of seven such parameters were examined first on simple shape like squares, circles and hexagons, then on more complex arbitrary shapes. Results demonstrated that no single parameter is enough to uniquely describe all shapes on its own but a combination of parameters could be used. The study also showed that the normalised polar representation of any shape can be significant for its recognition as well as for matching purposes.

The second part of the objective of this chapter was to do a literature search for accepted general geological models for turbidite depositional units with distinctive shapes that reflect the lithological facies variation within them. Literature review concluded that deepwater systems are quite complex in terms of depositional processes, geometries and stacking patterns. Despite the many attempts to develop a single facies model, no single facies model has been found that can adequately represent all deepwater systems (Shanmugam, 1990 & 2000; Mutti, 1992). Review of the literature illustrated the on going debate between geologists with regards to the existence of general depositional models for turbidite systems.

The third component of the objective was to investigate by three-dimensional forward modelling and body checking which physical properties influence the geometry and attributes of the bodies in the seismic data. Then, assess the validity of the method by using the combined physical and shape parameters in a predictive way on a model dataset and at least one real dataset example. To this end, a number of simple two-dimensional synthetic seismic sections were constructed using literature based models. For model development to greater complexity quantitative and semi-quantitative relationships between parameters was required in order to constrain model options. It will not be possible to find out what, geologically lies behind the seismic expression of turbidites unless a coincident three-dimensional seismic and appropriately dense geological well dataset is available. It is also important to have a feeling for the range of physical properties that are acceptable for different components of a turbidite system and any relationships between them. In the event, such a dataset did not become available for this project. Furthermore, the synthetic seismic models were built in two-dimensions with the view of transferring them into three-dimensional synthetic seismic data cube using a package that can interpolate between the two-dimensional lines. Such a tool was not found to be available when this work was being conducted bringing the idea of body shape analysis to a halt.

As a suggestion for future work it is recommended here to make a database in which the results of bodychecking from different turbidite system components are gathered from different seismic datasets. Once this is done and a substantial amount bodies calibrated with well data is available, body shape parameters established in this chapter can be applied on them to investigate if there is a unique relationship between petrophysical properties, turbidite components and the shape of the sand body as extracted by bodychecking process. This is not a simple task and requires resources and several man years to achieve but the results could be worthwhile.

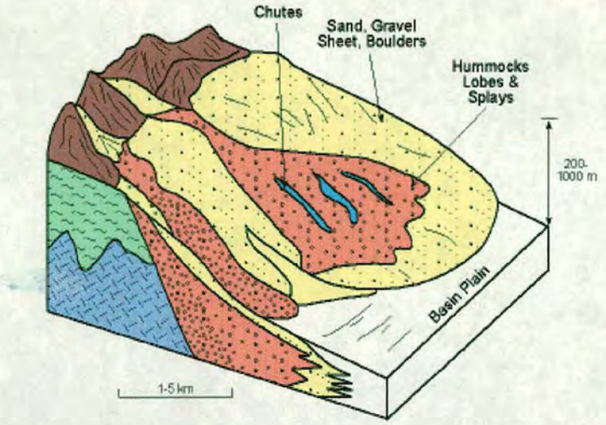

(a) Gravel-rich systems: Mostly coarse grained fans with radii 1-10 km and Much larger in tectonically active basins. Slopes from 1 to 14.

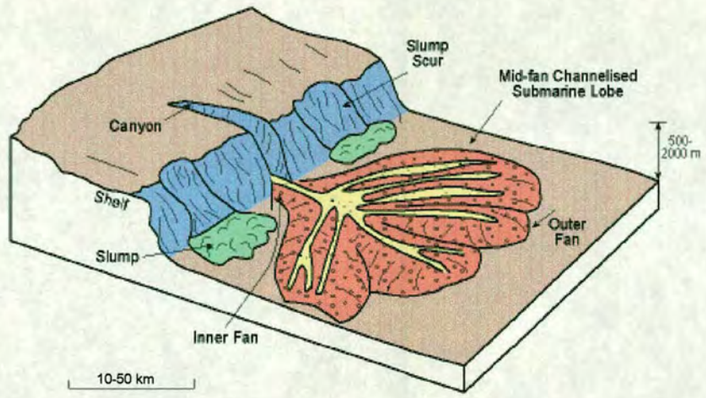

(b) Sand-rich systems: moderate in size with radii 5-10 km and tend to be radial rather than lobate in shape.

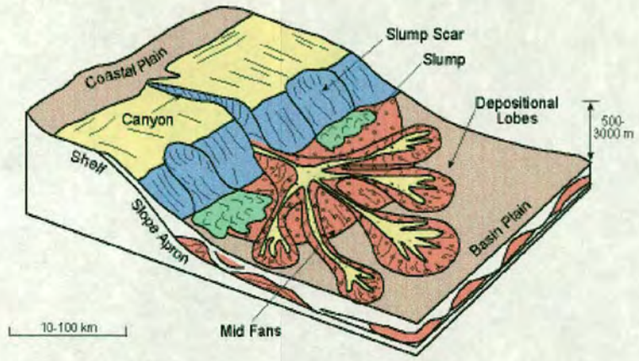

(c) Sand/mud mix systems: moderate in size and their shape is lobate rather than elongate.

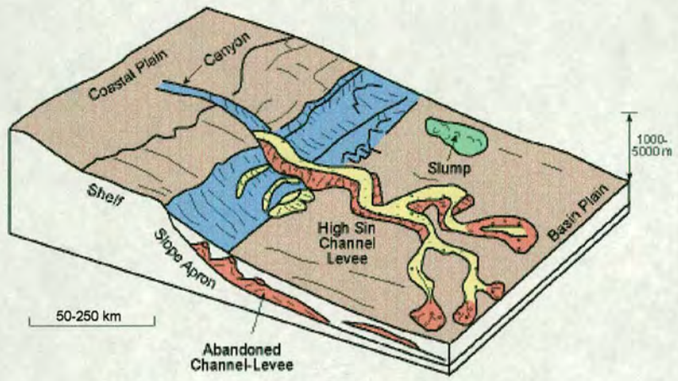

(d) mud-rich systems: modern systems include all the large, elongate, high efficiency major deep sea fans of the present day. Radii range from 100- 3000 km. Slope are relatively low.

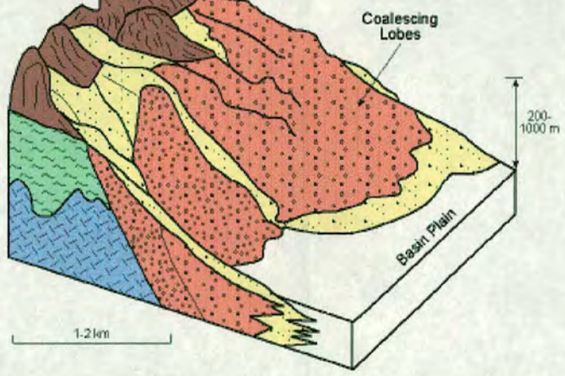

(e) Gravel-rich systems: normally very small in size but very high in gradient.

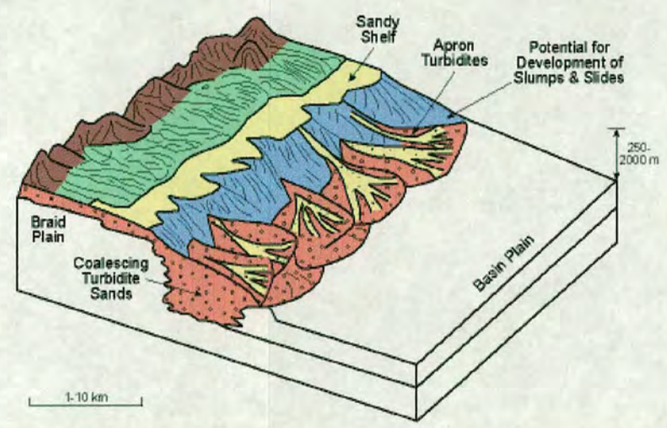

(f) Sand-rich systems: consist of small scale fans that coalesce to form a complex linear sheet of sandstones not extending far into the basin.

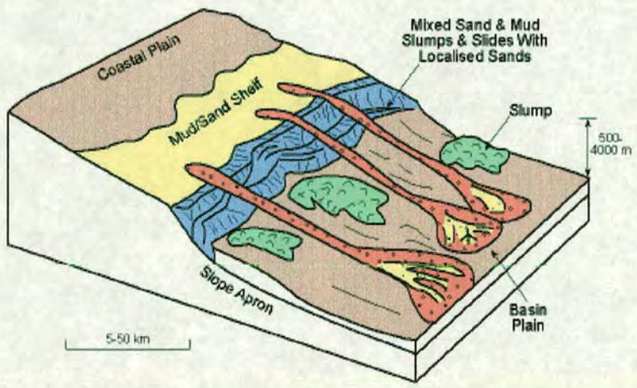

(g) Sand/mud mix systems: associated with low-gradient basin margins that form either at passive margins or at times of relatively inactive fault movements in pre- or post- rift stages.

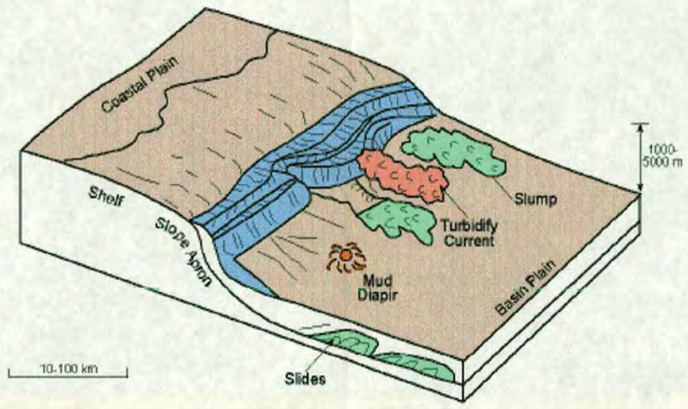

(h) Mud-rich systems: relative absence of turbidites. They extend 10-100 km into basins with relatively high gradients.

Figure 7.17: Depositional systems in deep-water basin margins classified based on grain size and feeder system. Figure shows 8 out of the 12 types classified by Reading and Richards (1994). a-d represent submarine fans, while e-h are slope aprons

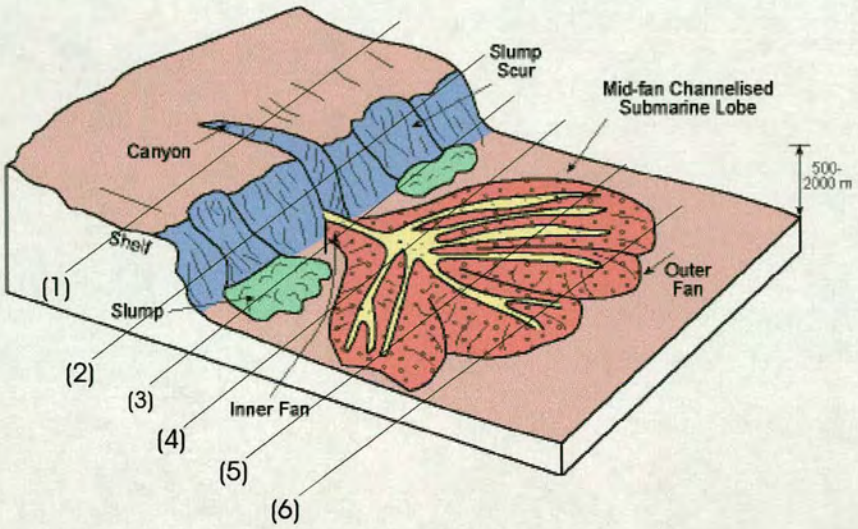

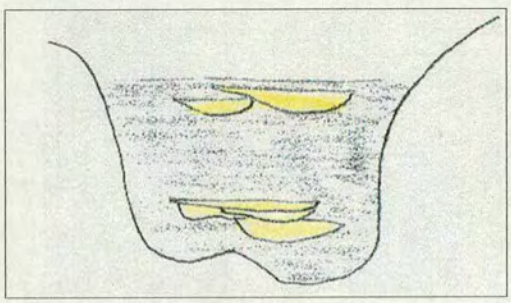

(1) Submarine canyon

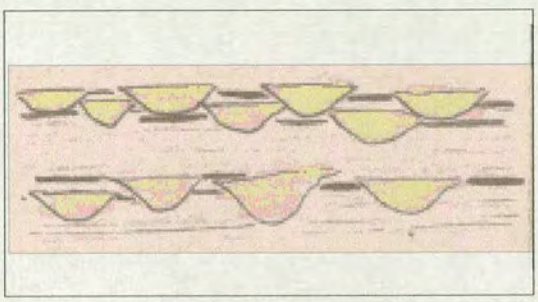

(4) Proximal basin floor

(2) Slope channels

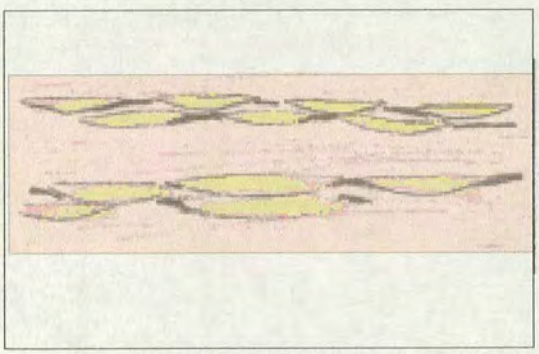

(5) Medial basin floor

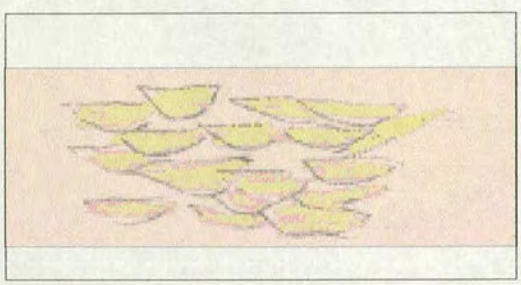

(3)Toe of slope complex

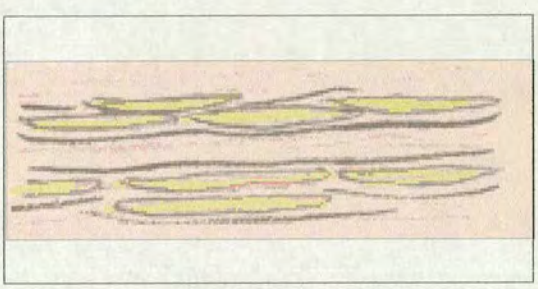

(6)Distal basin floor

Figure 7.18: model cross-sections along the sand-rich submarine fan

1. Isolated

a. single

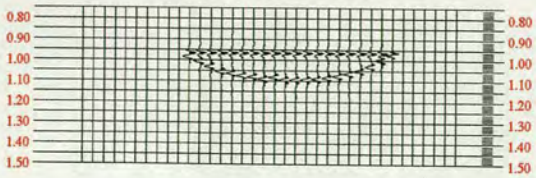

b. multiple

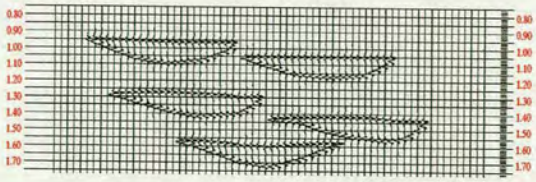

2. Stacked

a. vertically

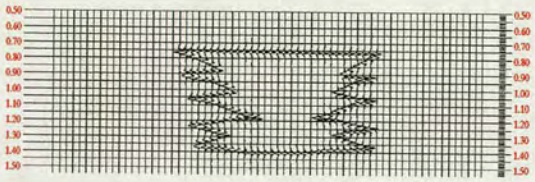

b. offset

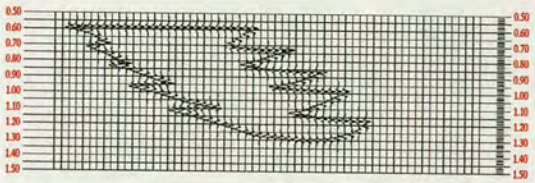

c. nested

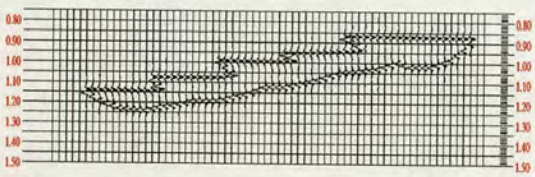

d.irregular

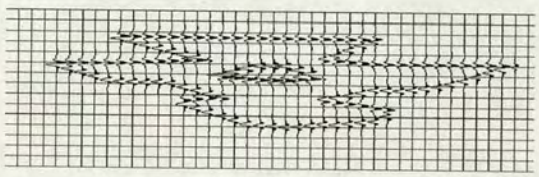

3. Imbedded in a canyon

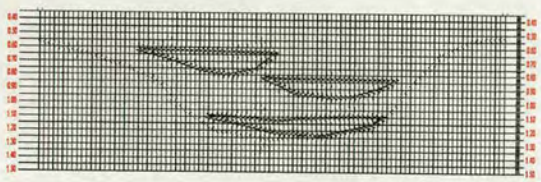

250 m

500 m

Parameters used:

Wavelet Ormsby

Frequency 1 = 10 Hz

Frequency 2 = 20 Hz

Frequency 3 = 50 Hz

Frequency 4 = 70 Hz

Phase = 0 degrees

Sampling rate = 2

Trace amplitude 1

Trace increment = 1

No Flattening

Figure 7.19: Seismic response of different stacking patterns shown in Fig. 7.16

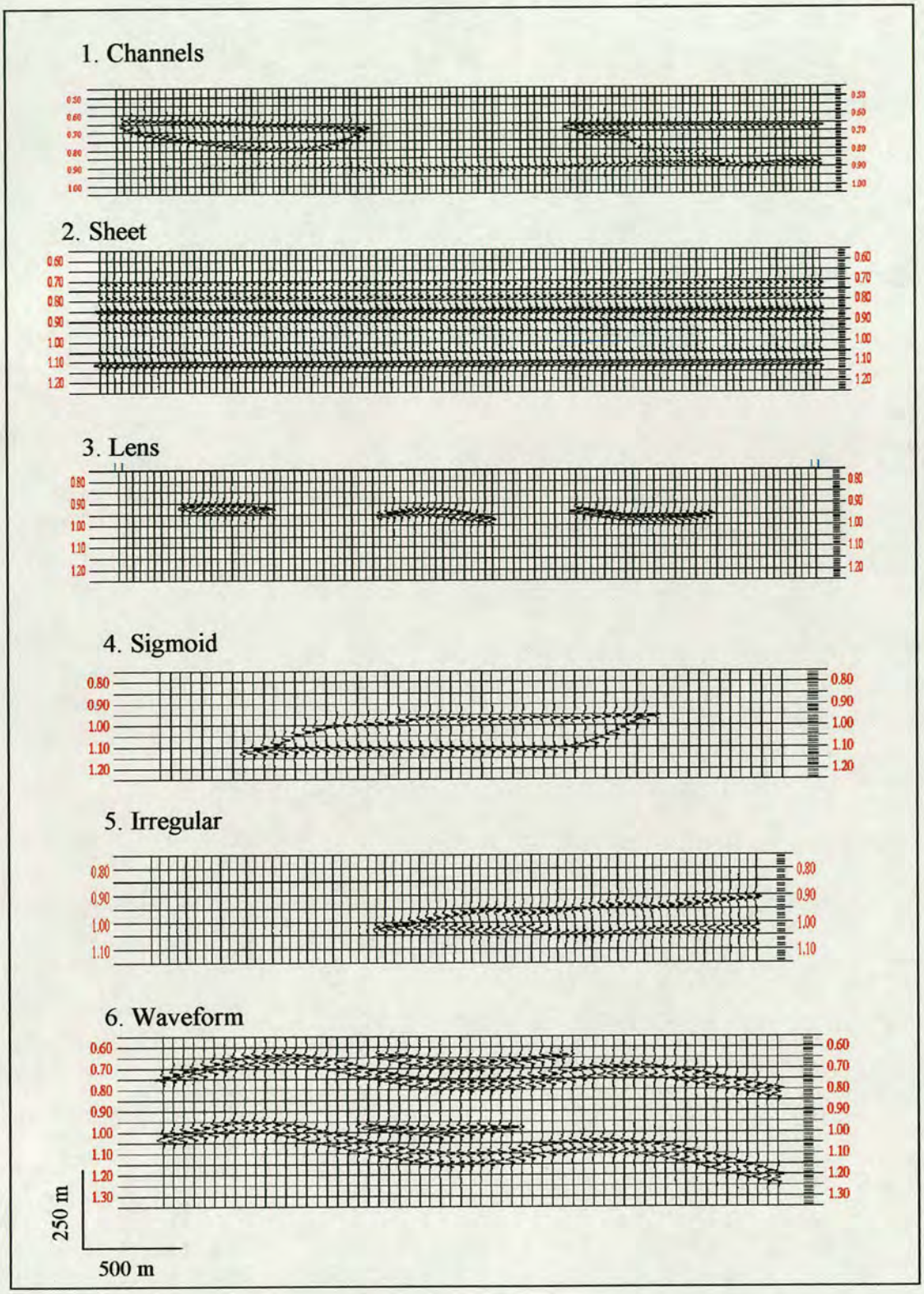

Figure 7.20: Seismic response from different sectional classes of Pickering *et al.* (1995) shown in Fig.7.14

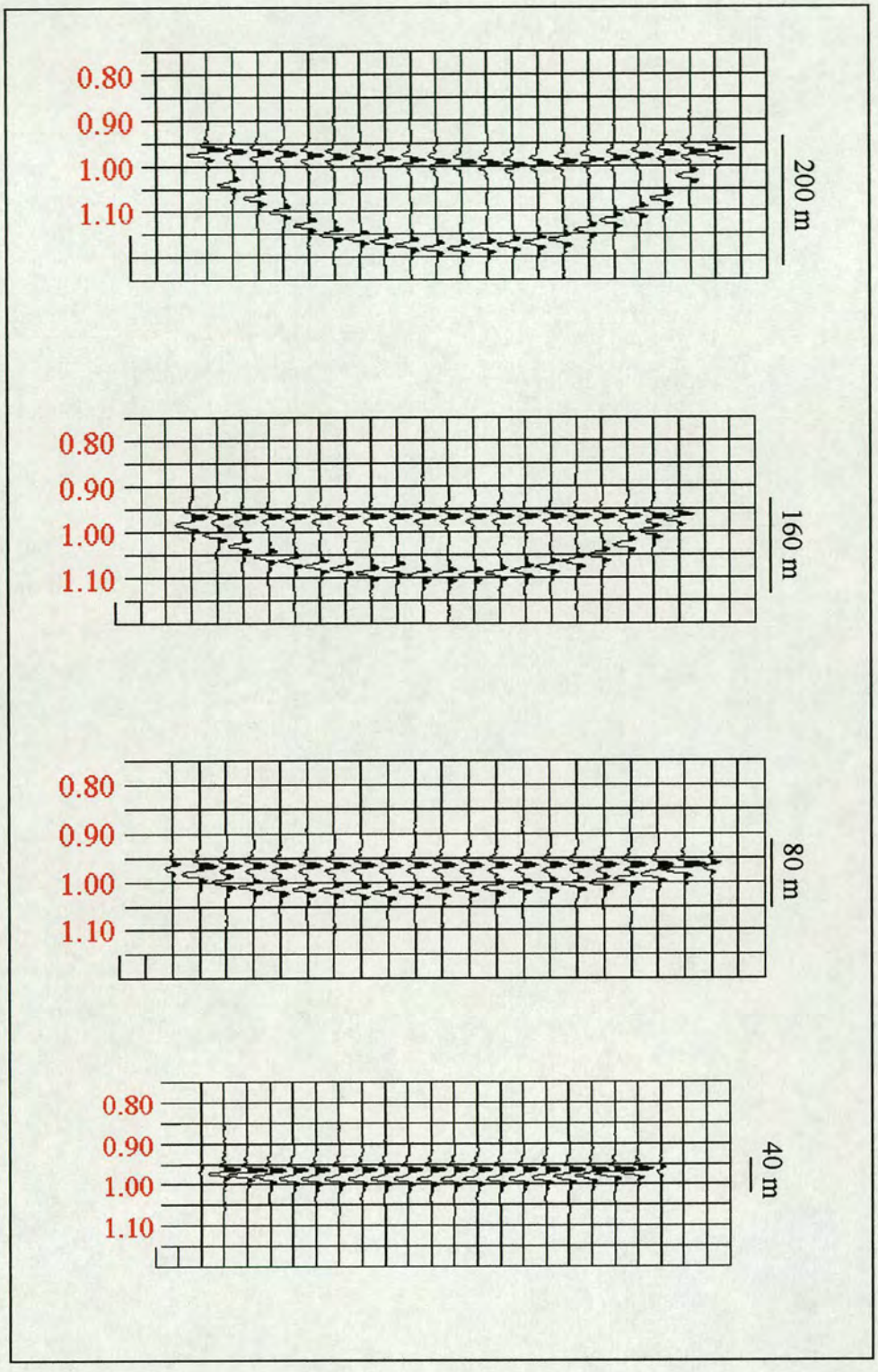

Figure 7.21: Effect of thickness variation of single channel on its seismic response.

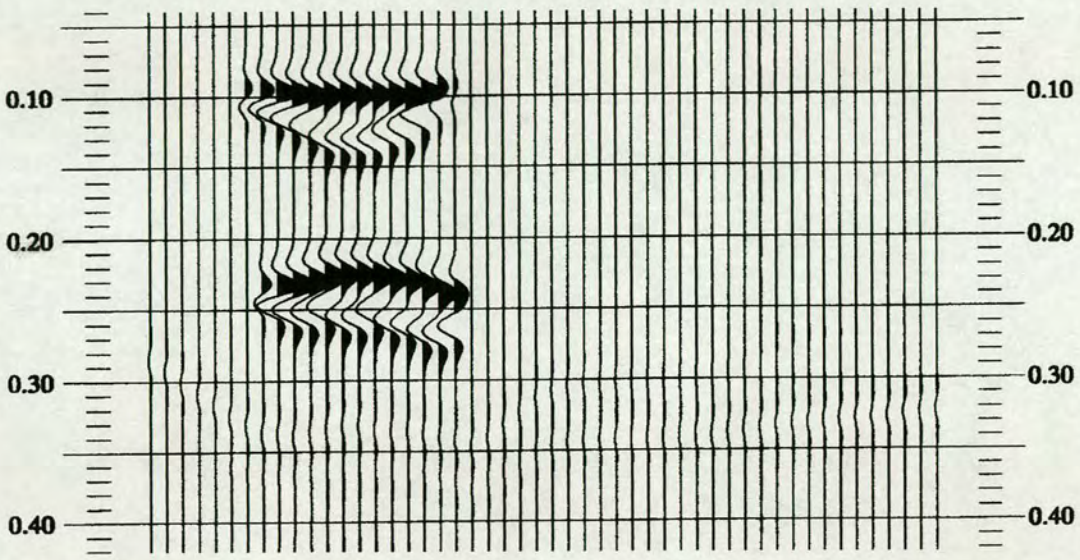

(a) slope channels

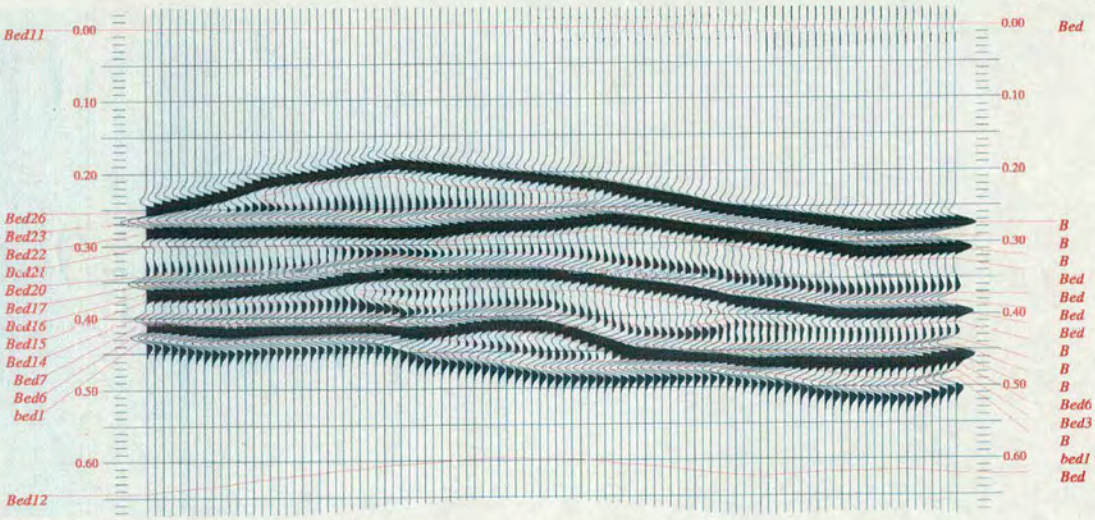

(b) channel complex at the lobe area

Figure 7.22: 2D synthetic seismic for two of the model cross-sections along the sand-rich submarine fan shown in Fig. 7.18

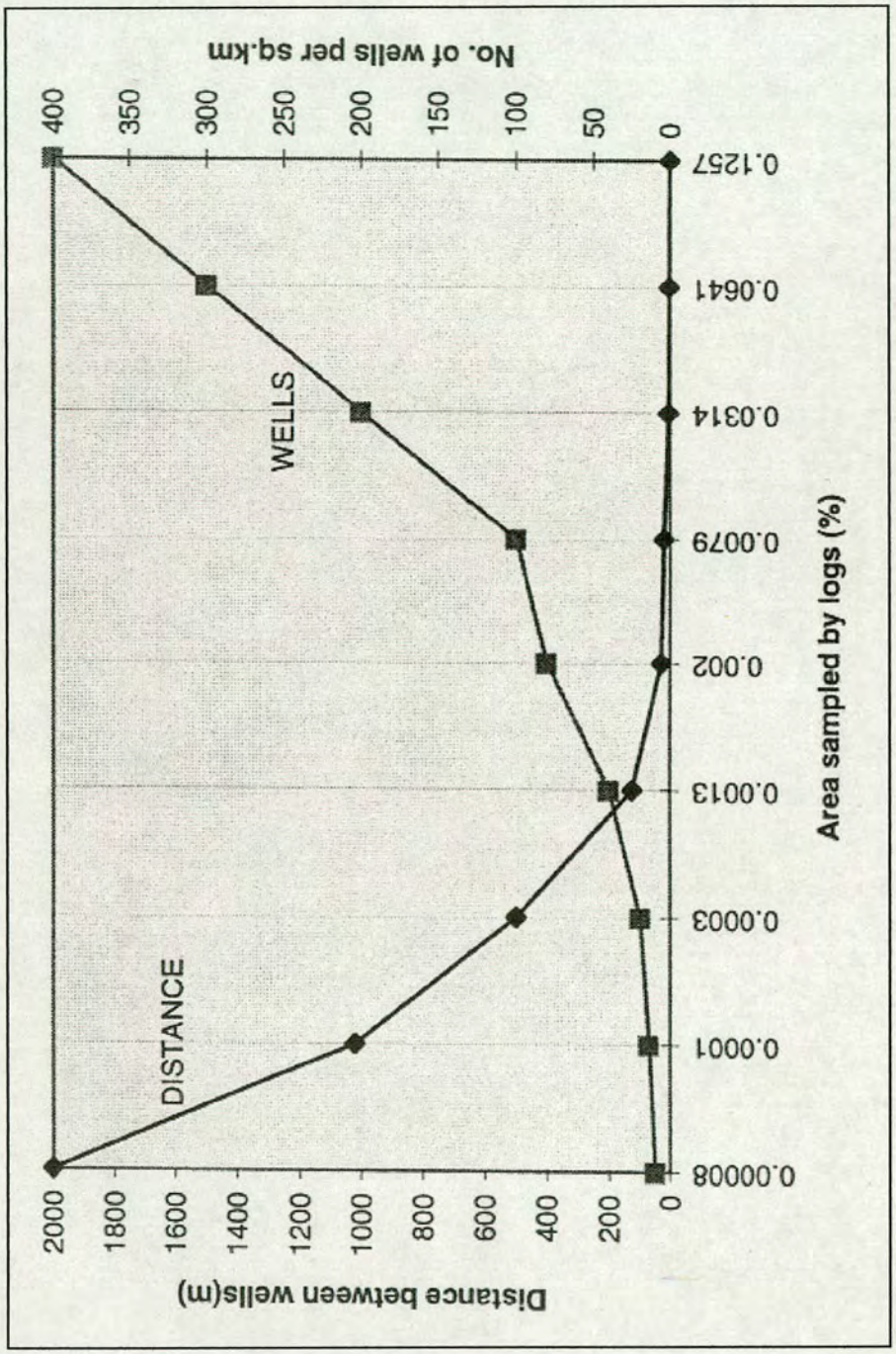

Figure 7.23: Shows variation of spatial resolution induced from wells with the increase in number of wells per squared kilometer and distance between wells (from Al-Aufi, 1996).

Chapter Eight

Chapter Eight

Synthesis and Conclusions

8.1 Introduction

The success of an exploration or production project hinges on the knowledge of the subsurface. Understanding the subsurface geology is very important in order to optimise exploitation, such as minimising the number of wells required in a hydrocarbon field. Geoscientists are normally asked to estimate the petrophysical properties of lithologies and the uncertainties involved. However, the success of exploration or production ventures does not depend only on the geologists getting it right, but on what is technically achievable. The development of three-dimensional seismic imaging combined with major advancement in wireline log technology has given us a unique opportunity to predict reservoir geometries and properties with improved certainty and in a more efficient way. However, despite these advances in the subsurface imaging methods and tools, they are still not able to lead to a full description of the subsurface. All that they are capable of is to give a prediction of what could be found. Furthermore, now that most of the established world class petroleum provinces, e.g. North Sea basin, have reached a mature state of development, exploration focus has shifted away from targeting structural to more subtle stratigraphic plays making the challenge of providing more accurate maps even greater than at any other time.

This project was devoted to the extraction of more quantitative information by integrating the high-resolution (12.5 by 12.5 m) three-dimensional seismic data with the electrical wireline logs and cores from 10 exploration wells drilled through the Tay system, Gannet South, Central North Sea and by introducing innovative body and seismic trace shape analysis to the interpretation process.

In recent years, seismic attribute maps have become important tools in the interpretation of seismic data. The attribute maps have proven especially valuable for understanding subtle stratigraphic features and identifying minor structures that are close to or below seismic resolution. However, the increased attention also contains pitfalls that may lead to erroneous interpretation unless the seismic interpreter is aware of the dangers and knows how to quality control the seismic observations, for instance, by using well data.

In this study, interpretation of high-quality seismic data using conventional methodology and trace shape analysis, constrained by exploration wells provided insights into controls on the stratigraphic architecture and deep-water sedimentary processes that governed deposition of the Eocene Tay Sandstone Member in the Gannet South area of Central North Sea. Maps produced by trace shape analysis revealed subtle geological features only expressed in the shape of the seismic trace and thus substantially enhanced the understanding of the sand geometries of the turbidite system and the structural development and evolution of the basin. Furthermore, the results also provided clues to the timing, nature and extent of factors controlling the sediment transport pathways in the area, and helped in the discovery of hydrocarbon pockets previously gone unnoticed.

The study suggests a modified depositional model with an added dynamic dimension to the classic fill-and-spill model. The classic model assumes a static basin where the history of fill and subsequent spill and abandonment of intra-slope basins passes through four dominant processes starting with flow ponding, followed by flow stripping, then flow-by pass and ending with backfilling (Sinclair & Tomasso, 2002). This model is true for a static basin where the basin is only receiving sediments. However, this study shows that for a dynamic basin where the shape of the basin continues to change during deposition, due to evolution of the basin bathymetry with the underlying salt movement, the order of processes described by Sinclair & Tomasso (2002) requires modification. Basing the interpretation of a dynamic basin on this static model can lead to erroneous interpretation of sand body thickness variations.

This study also demonstrates that salt movement during deposition is not the only factor controlling Tay distribution as it has hitherto been thought (Armstrong *et al.*, 1987; Den Hartog Jagger *et al.*, 1993). Pre-sedimentation salt movement as well as the topographic highs resulting from previous deposition have played an important role in defining the channel pathways and deposition locus. The evolution of salt induced highs within the basin lead to a temporal and spatial variation in the accommodation space generated and a subsequent modification of depocentres which in turn had a direct impact on sediment dispersal patterns and architecture.

This chapter synthesises interpretations from the previous seven chapters, puts forward a temporal and spatial depositional model for the Tay Sandstone Member system and presents key conclusions for the usage of body and trace shape analysis for evaluating three-dimensional seismic datasets.

8.2 Structural context

The Gannet South area sits on the western flank of Central Graben, Central North Sea. The cause for the deposition of submarine fans in the Palaeocene and Eocene in this basin margin setting was regional uplift and erosion of the Shetland Platform and the Scottish Highlands (Den Hartog Jagger *et al.*, 1993). During the Jurassic, the North Sea was dominated by E-W extension and rifting. This defined the North Sea trilete graben system and by the Upper Jurassic subdivided it into the Viking Graben, the Central Graben and the Moray Firth Graben (Glennie & Underhill, 1998). The Cretaceous was a period of transition from extension to compression. Around the British mainland, the Late Cretaceous was generally a period of relative tectonic quiescence. Nearly all of England and Wales, and a large part of Scotland, were blanketed with Chalk, without the presence of significant land masses (Zeigler, 1990). The main phase of uplift started at the Early/Late Palaeocene boundary, as indicated by apatite fission track studies (Green, 1986; Giles *et al.*, 1989). The onset of the major uplift is associated with the development of the Thulean Volcanic

Province. The volcanism started in the Maastrichtian and ended in the Middle Eocene (Hitchen & Ritchie, 1987; Mussett *et al.*, 1988). Four main depositional sequences were identified by Den Hartog Jagger *et al.* (1993): the Andrew, Forties, Frigg/Tay and Alba sequences. The sand/shale ratio decreased throughout the Palaeocene and Eocene and within each individual sequence.

8.3 Control of topography on deposition

This study demonstrated that the diapiric rise of Permo-Triassic evaporates played an important role in controlling the topography/bathymetry of the basin by defining a series of highs and lows, which influenced the sediment transport pathways and controlled the basin-fill architecture through the spatial variation in the loci, magnitude and rate of accommodation space generation. The detailed three-dimensional seismic data interpretation aided by trace shape analysis revealed the importance and control of topography on the spatial distribution of the deepwater depositional system of the Tay Sandstone Member and allowed the reconstruction of the temporal evolution of the basin. There were three main factors controlling the paleobathymetry of the basin:

1. A regional tectonic tilt of up to 6° towards the east (Buchanan *et al.*, 1996). This slope was a result of a drastic change in the tectonic regime of the area due to the North Atlantic opening during the Cenozoic. This controlled the transport direction of the sediments from Scottish Highlands and Shetland Platform in the west to the receiving basin in the east. Although the gradient in the study area does not exceed 2°, it seems to provide sufficient slope for the flow to continue and limits the development of lateral or radial depositional patterns normally associated with lobes (Normark, 1970; Mutti & Ricci Lucchie, 1972).
2. Salt induced highs which subdivided the basin into three minibasins and played an active role during deposition.

3. A topographic/bathymetric high created due to the deposition of previous sedimentation. This restricted the deposition of the Tay to the south of the high.

8.4 Depositional Environment & Sedimentary Facies Distribution

Detailed description of the available core allowed subdivision of the observed sedimentary facies into seven lithofacies. These lithofacies do not individually form mappable units as several of these facies should stack before the resulting sandstone mudstone, or sand-mud mix body can reach a mappable size. None of the sandstone beds display the typical Bouma sequence. Indeed none of the cross-laminated facies, characteristic of flow reversals (Pickering & Hiscott, 1985), are observed and coarse sand and gravel are completely absent. Beds are fine to medium grained and moderately sorted from top to bottom. They lack clear fining-upwards sequences, probably due to extensive pre-sorting on the shelf. Individual beds are not much thicker than a few feet. They are mostly deprived of any structures with the exception of containing evidence of rapid pore-fluid dewatering features such as dish and pipe structures. However, the sands are partially consolidated and sedimentary structures are poorly preserved. The beds have abrupt irregular upper and lower boundaries.

Detailed biostratigraphic analysis provided by Shell "in house" studies allowed chronostratigraphic subdivision of the Tay Sandstone Member into four main units. Based on clinoform geometries and palynofacies Vining *et al.* (1993) suggest that Tay sandstones were deposited in a deep-water marine environment and estimated the water depth during accumulation of the Palaeocene fans to be of the order 200-600 m.

Most of the cores, with the exception of well 22/26a-1, are dominated by siltstones and mudstones. The association of siltstones with occasional thin-bedded sandstone of turbiditic origin suggests that the siltstone facies may also have a turbidite origin, representing the distal facies deposited by low-density currents and suspension

sedimentation. The facies interchange between parallel laminated and bioturbated. Parallel lamination is due to traction effects as sediments settle from suspensions (Stow & Shanmugam, 1980), while the extent of bioturbation in the siltstone facies indicates that the environment of deposition was highly oxygenated (Pickering *et al.*, 1989).

The developed sedimentological facies scheme with the corresponding gamma ray response was linked to the seismic attributes once the seismic to well ties were established. Some of these lithofacies (e.g. Lithofacies 3 & 4) do not have characteristic sonic and density log response, which are principal properties for the generation of a seismic response. Nevertheless, both supervised and unsupervised classification of the seismic trace shape enabled assessing the lithofacies distribution over the whole area. Fig. 8.1 a, b & c show the facies distribution map based on core analysis, wireline log analysis, seismic interpretation and trace shape analysis for the three main units of the Tay Sandstone Member.

8.5 Stratigraphic Architecture

The high-resolution three-dimensional seismic data enabled the Top Tay Sands to be uniquely defined as a continuous trough (red loop) resulting from the difference in acoustic impedance between the clean Tay sandstones and the overlying mudstones of the Horda Formation. The definition and tracking of the Top Tay reflector is unequivocal over most of the Gannet South area. However, towards the edges of the system both in the north and south, as the thickness of the Formation gets beyond the limits of the vertical resolution of the seismic data, complication in accurate mapping of the reflector arises making the sand pinch out lines in both north and south uncertain.

Generally speaking, the Tay Sandstone Member turbidite system displays a complex distribution, which is restricted to the southern parts of UK quadrants 21 and 22. The distribution is restricted to a narrow area oriented WSW-ENE that fans out on the

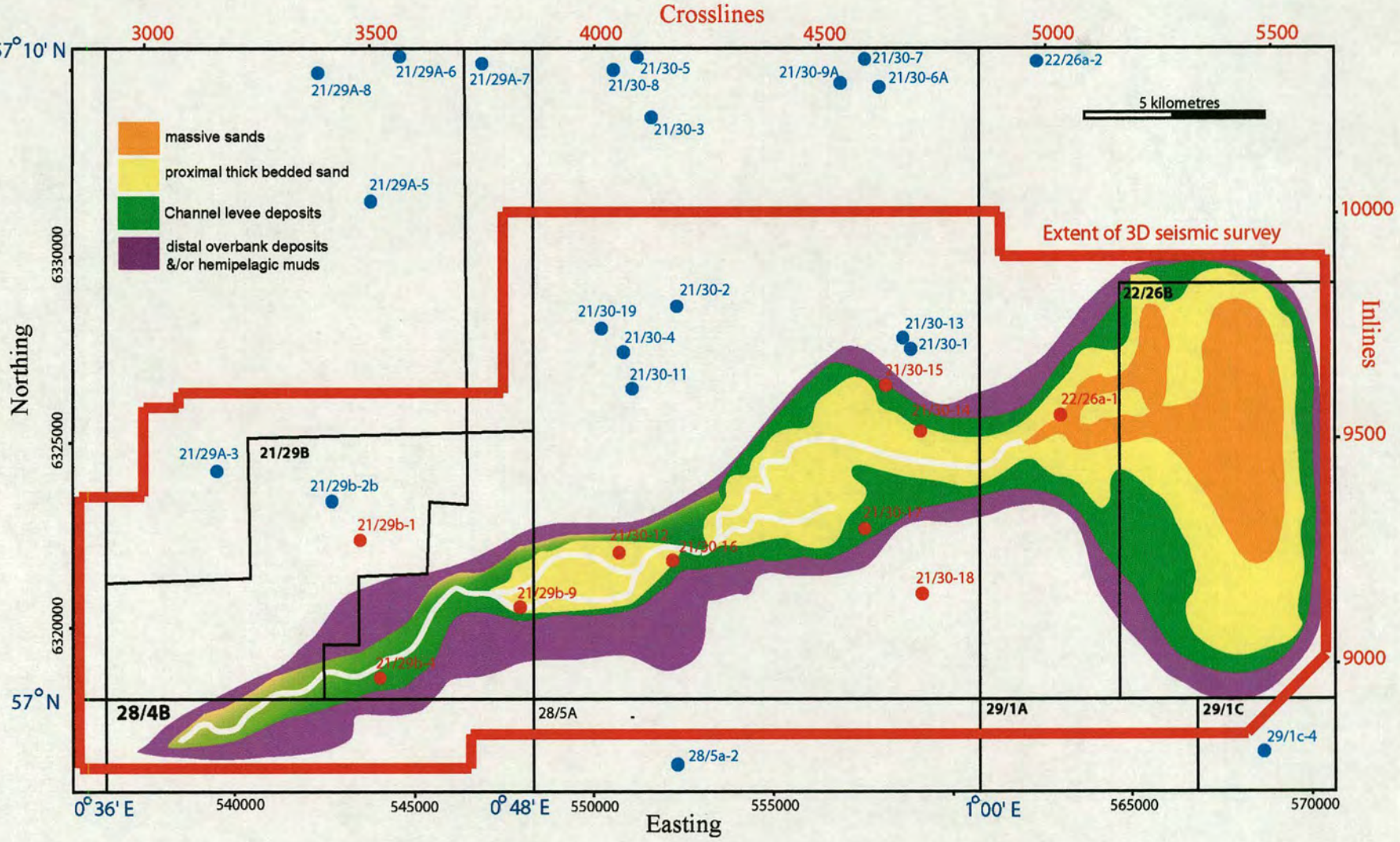

Figure 8.1a: Upper Tay facies distribution map based on core analysis, wirelilne log analysis, seismic interpretation and trace shape analysis.

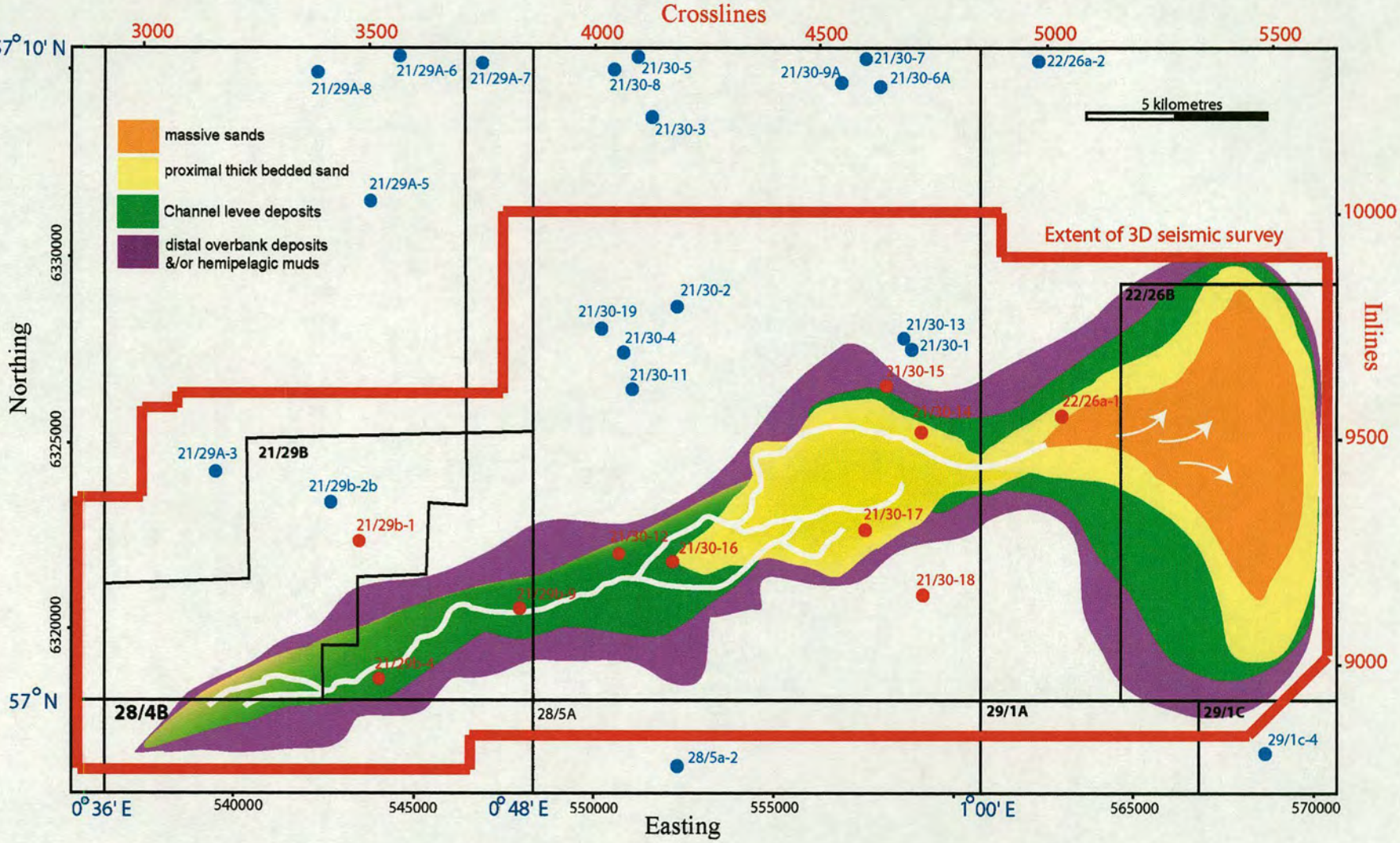

Figure 8.1b: Middle Tay facies distribution map based on core analysis, wirelilne log analysis, seismic interpretation and trace shape analysis.

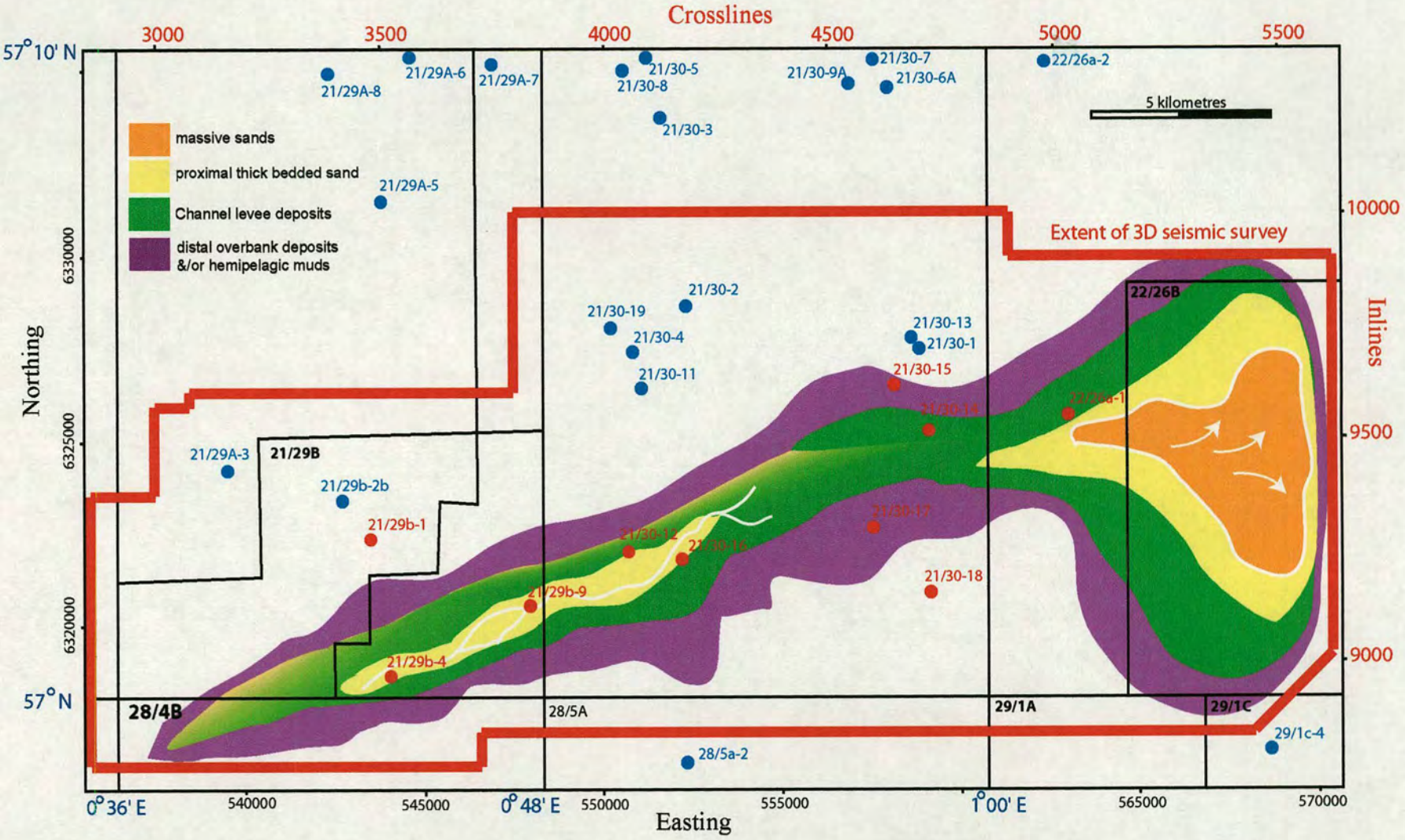

Figure 8.1c: Basal Tay facies distribution map based on core analysis, wirelilne log analysis, seismic interpretation and trace shape analysis.

basin floor towards the eastern end after going through the passage between two salt domes that were actively growing at the time of deposition.

A seismic section along the path of the channel showed a system of three intra-slope basins (Basins I, II & III). This is depicted by Fig. 8.2. The overall gradient is approximately 2° (35 m/km) decreasing to less than 0.1° (2 m/km) in basinal areas and going into negative gradients up the structural highs. Seismic continuity appears to be increasing down the slope and within individual basins and gets to its best in the fan area, reflecting better developed sand packages. It was noticed that NW-SE oriented diagonal lines (perpendicular to the channel direction) provided the best interpretable view of the sections, as the reflectors seemed more continuous and easier to follow. In addition to the structural evidence discussed in Section 8.2 and Section 8.3, the direction of sediment transport within this fairway is considered to be eastwards on the basis of the deepening and broadening of the system in the east. This is interpreted as the channel building into a fan geometry at its terminus.

The Tay thickness map shown in Fig. 8.3 highlighted the three sub basins where accommodation space was available for the sediments to be deposited. It is apparent from this map that the Tay Sandstone Member is relatively thin in this area as the maximum thickness is no more than 141 ms (approximately 700 ft). To the north the sands laterally onlap onto the topography created by the previous sediments. The southern margin of this sand body abruptly pinches-out onto a subtle basinal slope. The beds also appear to be onlapping onto the salt dome B in the south and salt dome C in the north. In the fan area it was possible to delineate four distinct lobes. Each of these lobes appears to be onlapping onto the one older than it as illustrated by the schematic diagram of Fig. 8.5.

8.5.1 Topography and channel evolution

Analysis of horizon slices over the whole system indicated that in basins I and II there has been little or no lateral migration of channel pathways throughout the history of deposition of the Tay Sandstone Member. This is clearly evident in Fig. 8.4, which shows channel pathways traced from horizon slices and superimposed on

each other. The figure also highlights the deposition in basin II as the sinuosity of the channel increased. Changes in sinuosity appear to be closely related to the variations in gradients and well-developed meanders occur where regional gradient reduces. This agrees with outcrop and modern fan observations made by Permiz and Flood (1995) Flood *et al.*, (1995), Clark and Pickering, (1996) Hiscott *et al.*, (1997) and Permiz *et al.*, (2000). Fig. 8.4 also highlights the sand development in this basin due to flow stripping processes. This sand has high potential for hydrocarbon accumulations. Clark and Pickering (1996) point out that these spill-over points develop where flow breaches levees on sharp bends, and where channel gradient decrease causes an increase in flow thickness. This leads to rapid reduction in flow velocity, resulting in deposition of at least part of the coarser fraction from the lower parts of the flow (Normak and Piper 1991).

8.5.2 Lobe evolution & mound structures

There was one important variation in the channel pathway that was not detected by the horizon slices but was nicely picked by the trace shape analysis. This change in the channel pathway produced by salt dome C had a key role in defining the resultant lobe geometry in basin III. The salt was clearly growing at the time of deposition. Combining the classification of the seismic traces conducted at Basal, Middle and Upper Tay together with the three-dimensional structural view presented in Fig. 6.14 revealed that there were four main stages in the development of these lobes. Fig. 8.5 gives a schematic diagram illustrating these stages. The spatial and temporal evolution of subbasin III was controlled by tectonic development in the area as well as sea level fluctuations that controlled the sediment supply. The first episode of deposition (Basal Tay) is thought to have gone furthest to the east; subsequent lobes have been receding landward until the final influx of sediments (stage 4), which seems to be the greatest in volume since it covered almost the whole basin floor. This lobe has taken a different channel pathway due to syn-depositional salt movement as discussed earlier. A key conclusion from this is that the deposition and sediment dispersal patterns in a tectonically active basin can not be qualified without the understanding of the tectonic evolution of the basin. It has been demonstrated by this analysis that salt induced accommodation spaces are dynamic with the active

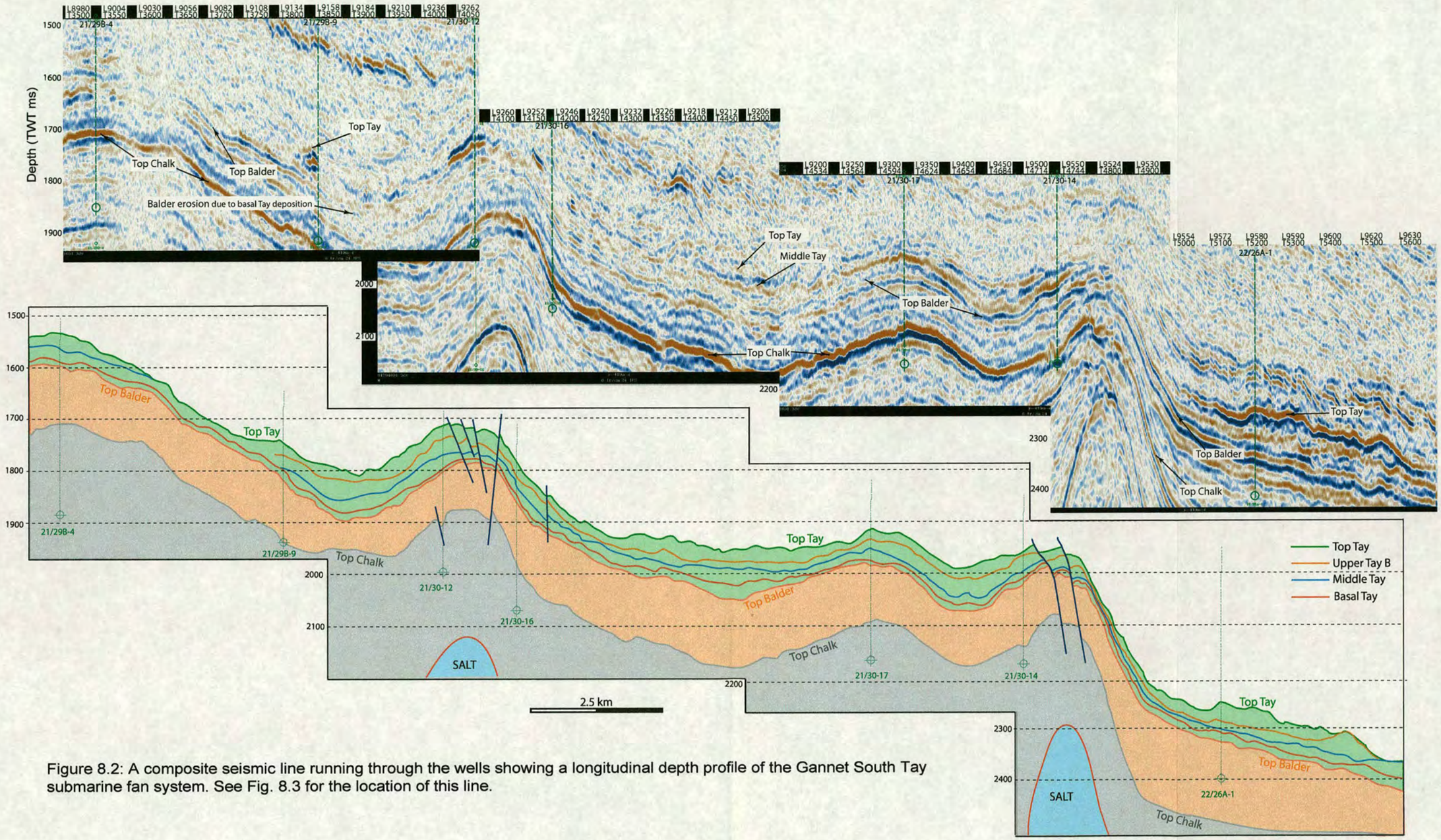

Figure 8.2: A composite seismic line running through the wells showing a longitudinal depth profile of the Gannet South Tay submarine fan system. See Fig. 8.3 for the location of this line.

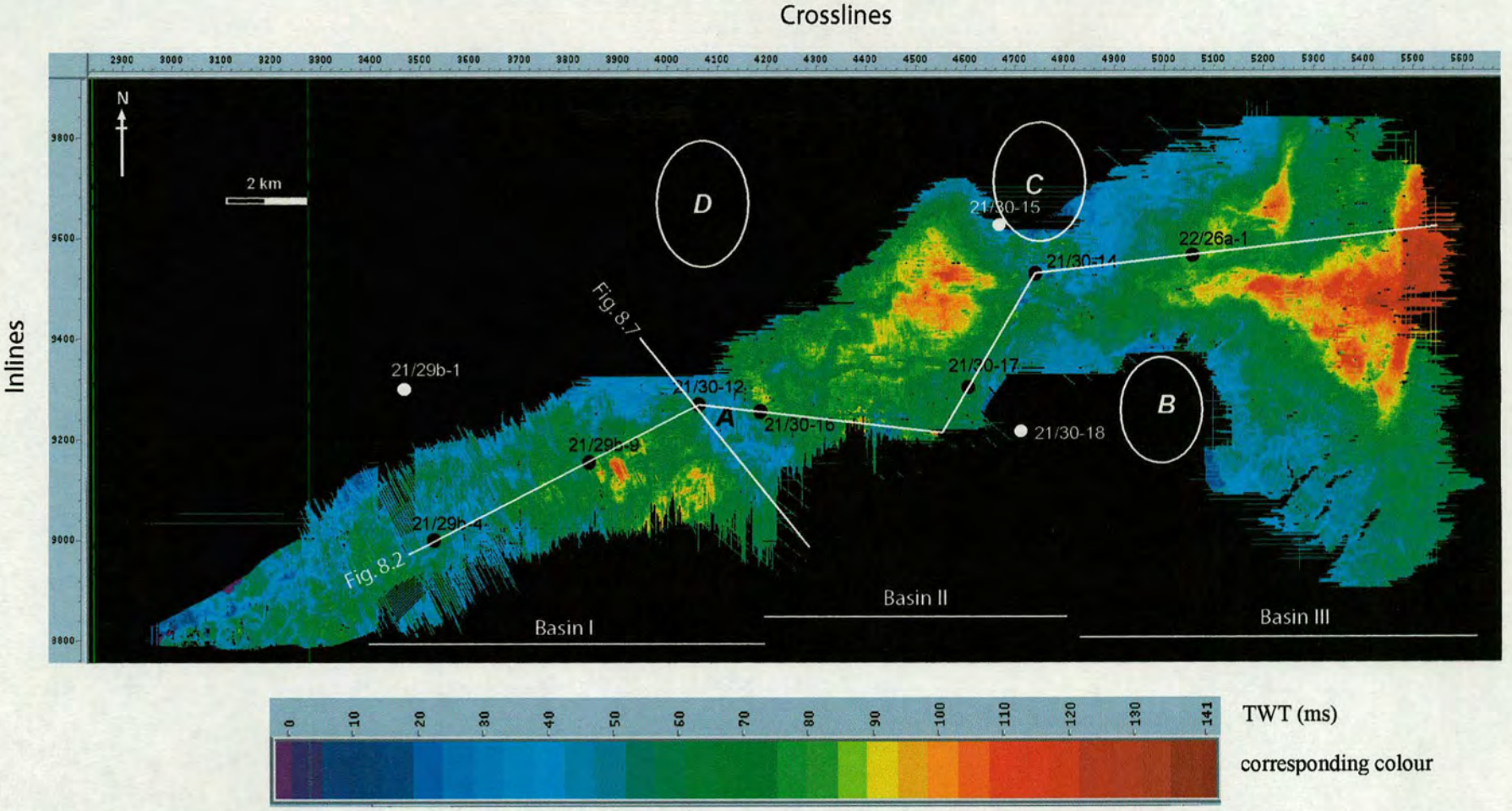

Figure 8.3: Tay Sandstone Member thickness map in TWT. The three sub basins are immdeiately apparent. The system fans out towards the east. Tay Sandstone Member is relatively thin with maximum thickness not more than 141 ms (~ 700 ft).

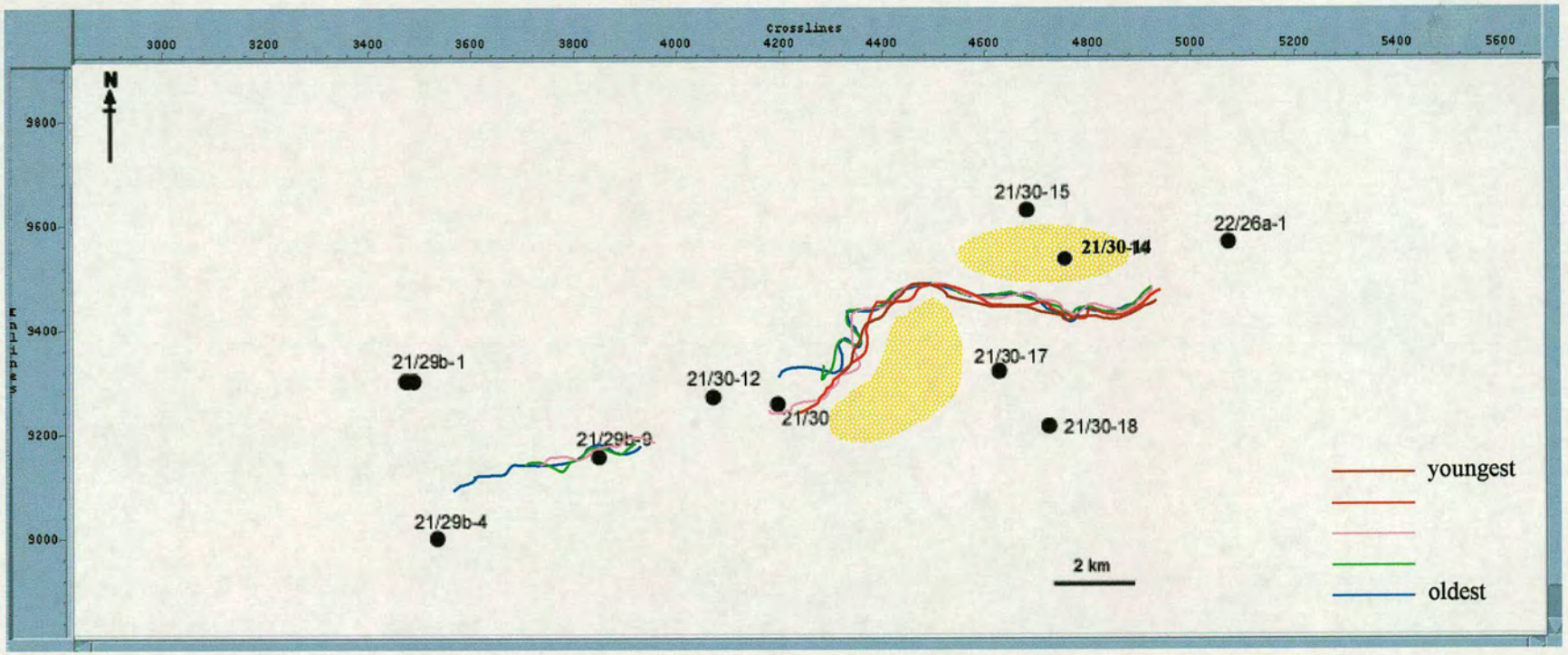

Figure 8.4: Traced channels superimposed on each other to delineate channel evolution over time. Figure highlights there has been no major changes in the channel pathways. It also shows slight increase in sinuosity in basin II with prospective sand deposition.

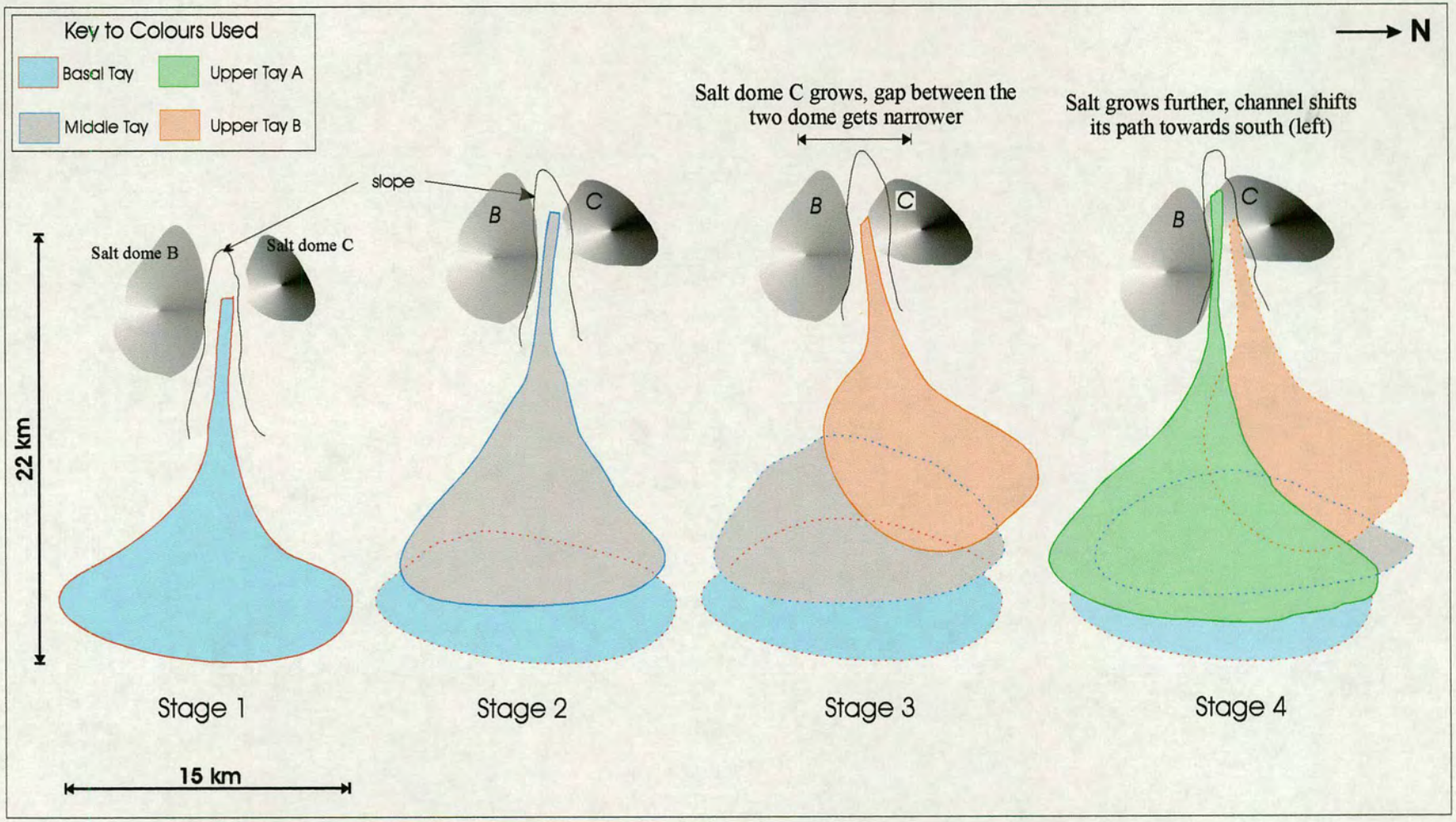

Figure 8.5: Schematic diagram illustrating the evolution of the lobes with structural development within the area.

evolution of the salt highs leading to a variation in the basin structure and, thus, the geometry of submarine fan deposited on it.

The mound structures observed on the axial seismic section of Fig. 8.2 and interpreted as depositional lobes are normally thought to have resulted from differential compaction (Armstrong *et al.*, 1987; Den Hartog Jagger *et al.*, 1993; Hiscott *et al.*, 1997). Differential compaction occurs when the sand fills a low area and the top of the sand is a level surface upon deposition. After burial, the shale on the flanks of the sand is compacted more than the sand, which results in a convex-upward geometry for the sand body (Fig. 6.33). However, details of the seismic geometry and the internal architecture, discussed in Section 3.4 and Section 6.4.3, suggest that these sand bodies had a positive sea-floor expression upon deposition, prior to deposition and compaction. It is apparent from the discussion above that each of these lobes is onlapping onto the one below, suggesting it had positive sea-floor relief upon deposition (*cf* Shanmugam *et al.* 1997).

8.6 Depositional Model

Detailed structural and stratigraphic interpretation through the integration of high-quality three-dimensional seismic data, core description, wireline log analysis and trace shape analysis has demonstrated that the Eocene Tay Sandstone Member evolved in multiple but arguably predictable phases of deposition and basin evolution.

As discussed earlier, NW-SE trending (strike-parallel) salt-induced highs have subdivided the basin into three mini-basins. The onset of basin filling is interpreted to start first in the basin close to the shelf and progress successively seaward as each basin is filled to a spill point (fill and spill model; Satterfield & Behrens 1990; Winker 1996; Prather et al. 1998, Sinclair & Tomasso, 2002). This provides an attractive explanation of why the thickest succession of the youngest Tay sands is observed at the deepest basin (Basin III) in well 22/26a-1. This means the shallower

basins were getting filled first with the earliest sands, whereas finer sands and muds were spilled to the deeper basins, as seen in the lower sections of the well. When accommodation space at the shallower levels got filled (flow ponding, *sensu* Sinlcair & Tomasso, 2002), the sand started being deposited at deeper levels. In order for flow ponding to take place, the confining basin must be surrounded by topographic barriers that are sufficient to prevent turbidity currents surmounting them. One immediate implication of this barrier being present at the time of deposition is that sediment accumulations will occur immediately upstream of opposing slopes, leaving much thinner deposits accumulating downstream of the topography. This is suggested by the flume tank experiments conducted by Alexander and Morris (1994). However, a look back to Fig. 8.2 and the well correlation panel of Fig. 4.10c and observing sediment accumulation and thickness variation both sides of the structural high between basins I and II *demonstrates the opposite of this*. Here we have a thicker package on the downstream side of the barrier and thinner on the upstream side. One possible explanation for this is that this barrier did not exist at the time of deposition, but if this was the case then why were sediments deposited in the proximal basin I at all? The more appropriate interpretation, which is also supported by well data, is that salt has been moving during deposition and at the time of onset of basin filling this structural high did exist *but with a much lower relief*. As the sediments started filling the basin, the break of the slope that defined its margin became healed and the high was buried. Later sediments bypassed the area and were deposited further down the slope. Meanwhile as salt continued moving the high grew further and started acting as a barrier again creating more accommodation space and making the next episode of deposition once again in basin I. Hence, the system went back to flow ponding phase without completing the rest of the phases described by Sinclair & Tomasso (2002) as shown in Fig. 8.6, and started all over once again.

The fact that salt movement continued after Tay deposition is demonstrated further by an arbitrary line running perpendicular to the longitudinal line of Fig. 8.7 right on top of the salt high. The line clearly indicates the pinchout of the Tay Sandstone Member towards the edges of the salt dome whereas the thickest package exists right on top of the high. Had this high existed at the time of deposition as it is now the

sediment flow would have got deflected from it and found a much easier path for itself. Even if the flow was powerful enough to surmount this high it cannot have deposited its sediment on top of it. Flow deflection at the Tay interval on encountering a salt high has been demonstrated elsewhere in the Central North Sea (e.g. Fyne area northwest of Gannet South, pers. comm. John Underhill, Edinburgh University).

The study suggests a modified depositional model with an added dynamic dimension to the classic fill-and-spill model. The classic model assumes a static basin where the history of fill and subsequent spill and abandonment of intra-slope basins passes through four dominant processes starting with flow ponding, followed by flow stripping, then flow by pass and ending with backfilling (Sinclair & Tomasso, 2002). This model is true for a static basin where the shape and geometry of the basin remains the same throughout the period of deposition. However, this study shows that for a dynamic basin where the shape of the basin continues to change during deposition, due to evolution of the basin bathymetry with the underlying salt movement, the order of processes described by Sinclair & Tomasso (2002) requires modification. Applying the static model on a dynamic basin can lead to erroneous interpretation of sand body thickness variations. Fig. 8.8 provides a modified version for the deposition of the Tay Sandstone Member within the Gannet South area.

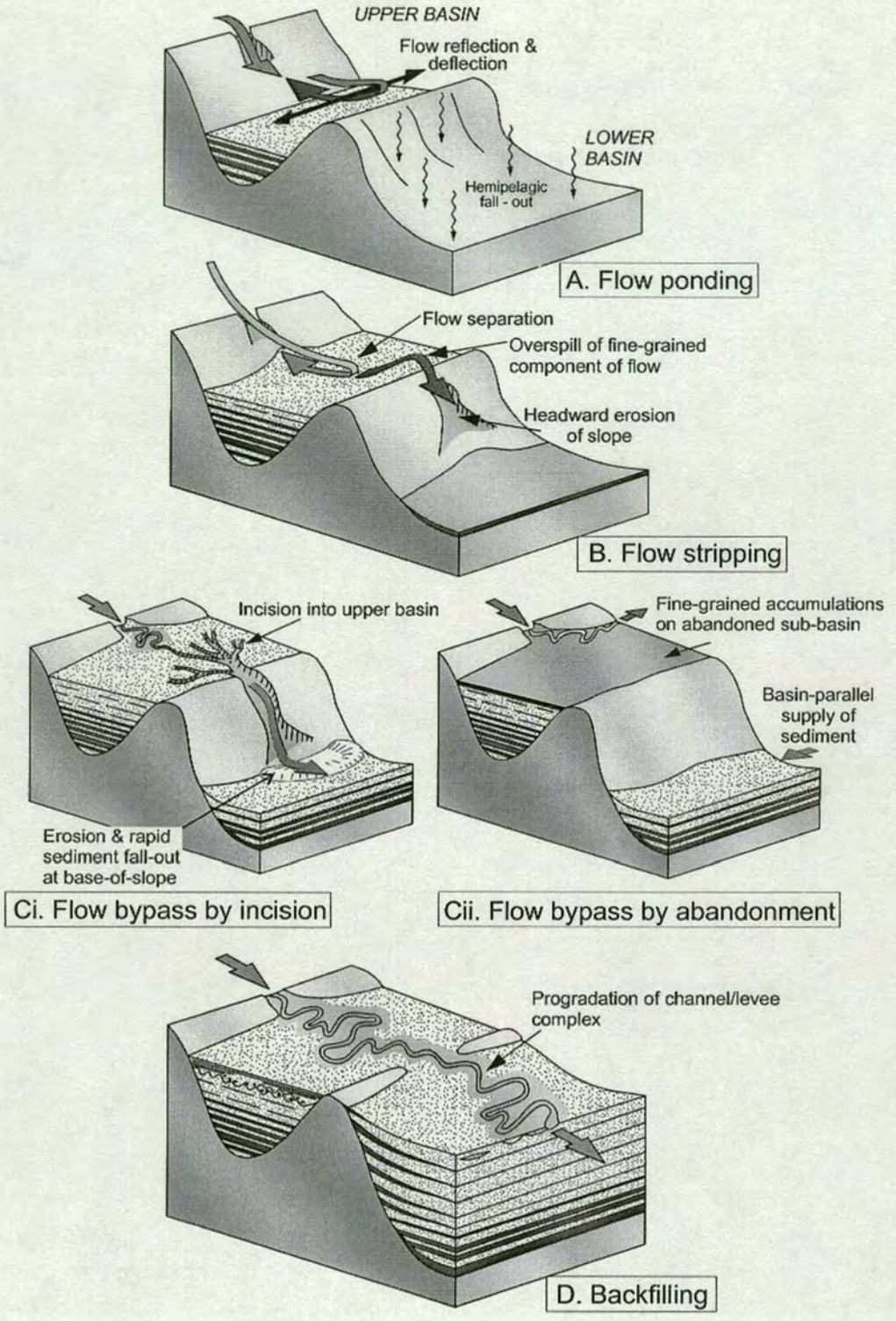

Figure 8.6: Depositional model for the fill and spill development of perched sub-basins. The figure illustrates the different processes and facies expected from a) Flow ponding followed by b) Flow stripping then c) Flow bypass and ending with d) Backfilling.
(From Sinclair & Tomasso, 2002)

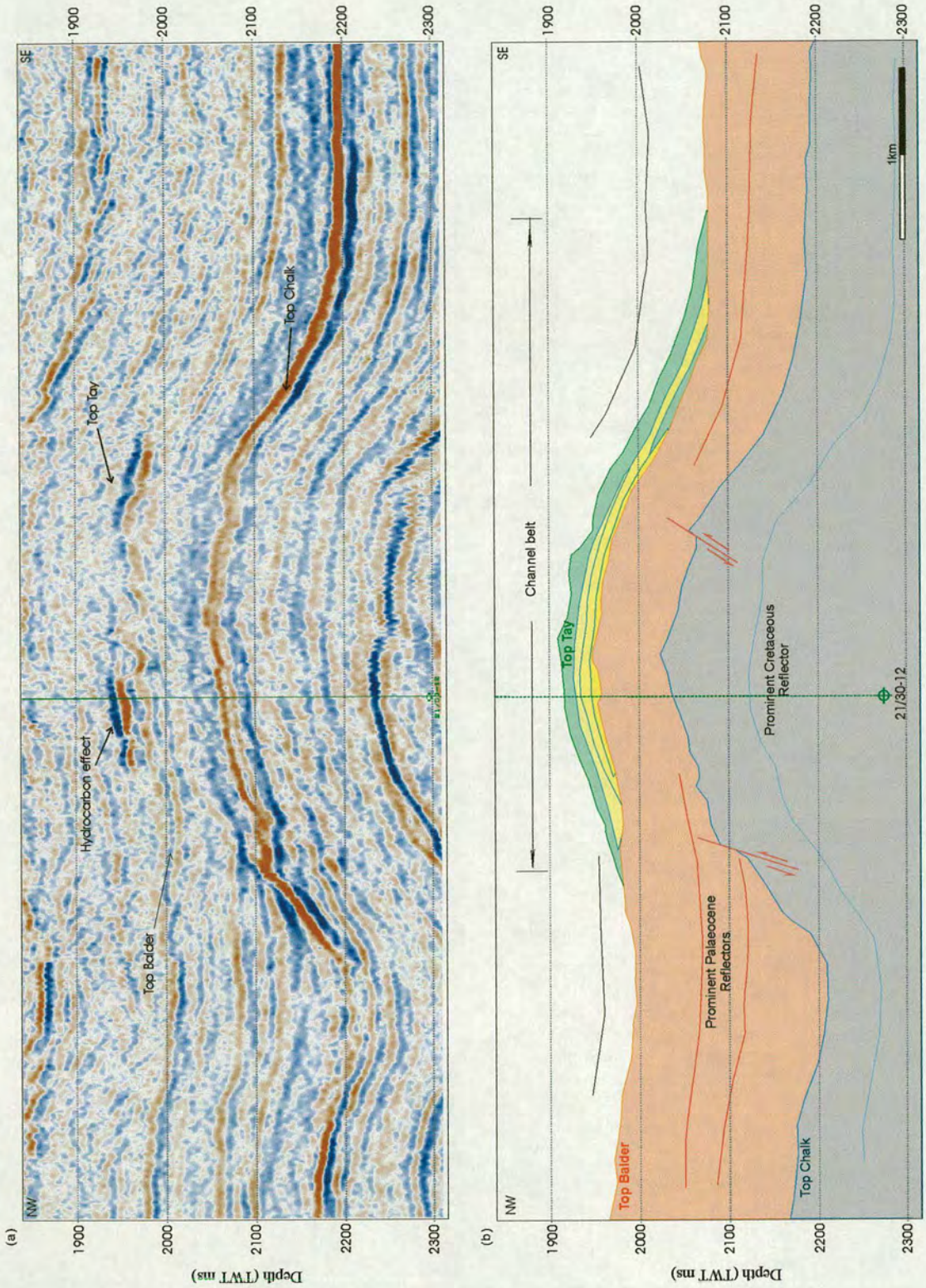

Figure 8.7: Arbitrary seismic line over the salt high illustrating movement of salt after deposition of the Tay Sandstone Member. Location of the line is given in Fig. 8.3.

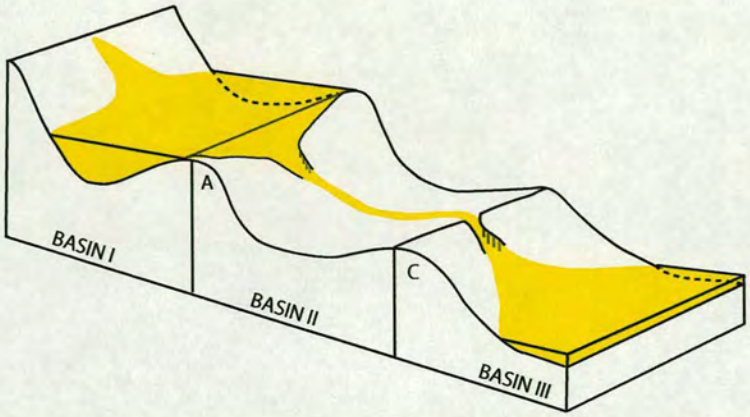

Stage 1: initial relief of salt high A leads to deposition of parts of the sediments in basin I. As the high heals it becomes possible for for the flow to surmount it and carry the sediments to the deeper basins. The energy of the flow is high enough, possibly due to the momentum gained from the slope, to bypass basin II and deposit rest of the sediments in basin III.

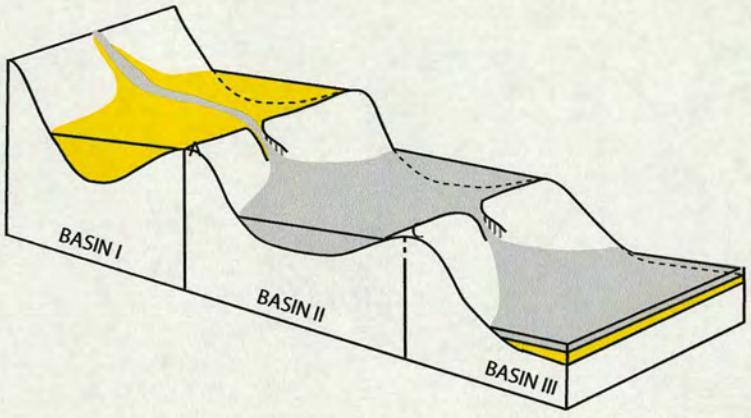

Stage 2: Since A is levelled the next flux of sediments are deposited in basin II and III. Growth of C creates more accommodation space for the episode.

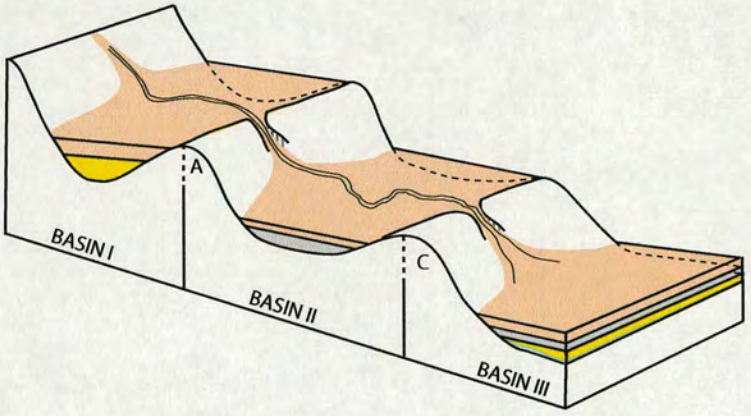

Stage 3: Continous growth of A and C provide more accommodation space in basins I & II taking them back to the ponding stage (*sensu* Sinclair & Tomasso,2002)

Figure 8.8: Depositional model for the fill and spill development with the salt high growth as interpreted in Gannet South area.

8.7 Trace Shape Analysis

Changes in lithology, rock properties and fluid content affect seismic response not only in amplitude but in the whole shape of the trace. The direct study of the variation of trace shapes has been hitherto neglected in the hydrocarbon exploration due to the lack of an appropriate interpretation tool. Neural network technology, using its pattern recognition capability, has provided the opportunity to conduct such an analysis.

Relating lithofacies to rock physics properties and hence to the seismic trace shape allowed a direct calibration of seismic response to lithofacies, thus enabling an improved interpretation of the turbidite system within a sequence stratigraphic framework.

Both supervised and unsupervised classification of the seismic trace shapes were performed using the three units within the Tay Sandstone Member. Results from the analysis provided some spectacular insights into the spatial and temporal development of the Gannet South Tay system and substantially enhanced the understanding of the sand geometries of the turbidite system and the structural development and evolution of the basin. The results also provided clues to the timing, nature and extent of factors controlling the sediment transport pathways in the area, and helped in the discovery of hydrocarbon pockets previously gone unnoticed.

The most striking result of the supervised classification was described by Fig. 6.28, which revealed the lithofacies that form the levee deposits. The levee over almost the whole system consists of massive to thick-bedded sandstones interbedded with bioturbated siltstone. This means that at the Upper Tay level we have a sandy channel in this area.

The analysis demonstrated that the receiving basin at Gannet South has been dynamic throughout the deposition period. The resultant deposition and sediment

dispersal patterns in the basin can not be qualified without an understanding of the tectonic evolution of the basin. This was mainly controlled by salt movement which led to a variation in its structure and geometry and, as a result, in the geometry and stacking patterns of the sediments deposited on it.

8.8 Body Shape Analysis

A set of body shape parameters that would enable a meaningful and distinctive description of different turbidite sand bodies was established. Investigation has concluded that there are a number of basic parameters that can be derived from any arbitrary shape to provide valuable classification information and, hence, a useful means of checking the identity of the object. A total of seven such parameters were examined first on simple shape like squares, circles and hexagons, then on more complex arbitrary shapes. Results demonstrated that no single parameter is enough to uniquely describe all shapes on its own but a combination of parameters could be used. The study also showed that the normalised polar representation of any shape can be significant for its recognition as well as for matching purposes.

Unfortunately, application of these parameters to turbidite sand bodies was brought to a halt due the lack of accepted general geological models for turbidite depositional units that have distinctive shapes that reflect the lithological facies variation within them. No single facies model has been found that can adequately represent all deepwater systems (Shanmugam, 1990 & 2000; Mutti, 1992). Review of the literature illustrated the on going debate between geologists with regards to the existence of general depositional models for turbidite systems. Research was further cut short by withdrawal of the originally proposed seismic dataset which had a coincident dense well data distribution.

8.9 Recommendations for further studies

Body shape parameters established in this research are thought to be useful in describing and, hence, delineating different sand or shale bodies. Therefore, it is recommended to facilitate these parameters in two different ways. First, by creating a database from the results of body checking performed on different elements of turbidite systems and then applying body shape parameters on them to verify that each of these elements has a distinct shape. As such, when a new dataset will become available a correlation exercise can be carried by an automated process, possibly using neural network, to delineate the different shapes in the new dataset. This is comparable to the method used in recognising the face of a criminal from the database available.

The second possible line for future research can be the application of the established set of body shape parameters on a depositional environment that is less complicated than the deep-marine environment and one that has better accepted models in the literature (e.g. fluvial or deltaic systems).

As for the trace shape analysis, it is recommended to create a database of traces gathered from different wells. A research on seismic traces at wells that have exactly the same lithological facies and fluid contents can help to identify how and what exactly affects the shape of the seismic trace. Again this database can be used in applying supervised classification in new areas and hence delineating the different lithofacies that lie behind the seismic response.

8.10 Conclusions

Detailed structural and stratigraphic interpretation through the integration of high-quality three-dimensional seismic data, core description, wireline log analysis and trace shape analysis in the Gannet South area provided insights into controls on the stratigraphic architecture and deep-water sedimentary processes that governed

deposition of the Eocene Tay Sandstone Member in the Gannet South area of Central North Sea. Maps produced by trace shape analysis revealed subtle geological features only expressed in the shape of the seismic trace and thus substantially enhanced the understanding of the sand geometries of the turbidite system and the structural development and evolution of the basin. Furthermore, the results also provided clues to the timing, nature and extent of factors controlling the sediment transport pathways in the area, and helped in the discovery of hydrocarbon pockets previously gone unnoticed.

Although attribute analysis may enhance the understanding for a particular study area, it is more important to focus on obtaining a good quality dataset prior to interpretation, by emphasizing better acquisition and processing procedures rather than attribute manipulation after processing. Case examples of attribute analysis from areas of good seismic data quality can be misleading, leading to the belief that such exceptional results can also be obtained in areas of poor seismic data quality.

The study suggests a modified depositional model with an added dynamic dimension to the classic fill-and-spill model. The classic model assumes a static basin where the history of fill and subsequent spill and abandonment of intra-slope basins passes through four dominant processes starting with flow ponding, followed by flow stripping, then flow by pass and ending with backfilling. The analysis of stratigraphic deposition and dispersal patterns with reference to tectonic evolution of the basin therefore presents an advance on just applying the classic model as it predicts the facies distribution within the system, which is controlled by the basin's tectonically evolving bathymetry.

Sediment dispersal patterns and deposition in a deepwater basin are only fully understood with an understanding of the evolution of the basin. This study demonstrated that active basins that evolve throughout the period of deposition lead to a variation in the basin structure and geometry through time. Therefore, when exploring for hydrocarbons in deep-marine sediments studies must include detailed analysis of the tectono-stratigraphic evolution of the individual basins.

References

References

- Addison, P. S. 1997. Fractals and chaos: an illustrated course. The Institute of Physics, London, 262pp.

- Al-Aufi, Y. M. R. 1996. Technological limitations to geological success. *Unpublished report part of Petroleum Geosciences MSc Course*, University of Aberdeen, 11pp.

- Alexander, J. & Morris, S. 1994. Observations on experimental, non-channelised, high-concentration turbidity currents and variations in deposits around obstacles. *Journal of Sedimentary Research*, v. 64, pp. 899-909.

- Ali, J. K., 1994. Neural Networks : A new tool for petrology? *SPE paper* no. 27561.

- Anderton, R. 1993. Sedimentation and basin evolution in the Palaeogene of the Northern North Sea and Faeroe-Shetland Basins. Abstract. *In*: Parker, J. R. (ed.) *Petroleum Geology of Northwest Europe: Proceedings of the 4th Conference*: Geological Society, London, p. 31

- Allan, P., Anderton, R., Davies, M., Marshall, A., Pooler, J. & Vaughan, O. 1994. Structural development of the ETAP diapirs, central North Sea. Salt Tectonics meeting, Petroleum Group of the Geological Society, 14-15th Sep, (Abstract volume, unnumbered pages).

- Anderton, R. 1995. Sequences, cycles and other nonsense: are submarine fan models any use in reservoir geology? *In*: Hartley, A. J. & Prosser, D. J. (eds.), *Characterisation of deep marine clastic systems*. Geological Society Special Publication, No. 94, pp. 5- 11

- Anstey, N. A. 1977. Seismic interpretation; the physical aspects. International Human Resources Development Corporation, Boston, 635pp.

- Anstey, N. A. Simple Seismics for the petroleum geologist, the reservoir engineer, the well-log analyst, the processing technician, and the man in the field. International Human Resources Development Corporation, Boston, 168pp.

- Argent, J. D. Stewart, S. A. & Underhill, J. R. 2000. Controls on the Lower Cretaceous Punt Sandstone Member, a massive deep-water clastic deposystem, Inner Moray Firth, UK North Sea. *Petroleum Geoscience*, v. 6, pp. 275-285.

- Armstrong, L. A., Ten-Have, A. & Johnson, H. D. 1987. The geology of the Gannet fields, Central North Sea. *In*: Brooks, J. & Glennie, K. (eds.), *Petroleum Geology of North West Europe*, Graham and Trotman, pp. 533-548.

- Badley, M. E., Price, J. D., Rambech Dahl, C. & Agdestein, T. 1988. The structural evolution of the northern Viking Graben and its bearing upon extensional modes of basin formation. *Journal of the Geological Society*, v. 145, pp. 455-472.

- Bally, A. W. 1983. Seismic expression of structural styles. Vol. 3. *AAPG Studies in Geology*, 15, Tulsa, Oklahoma.

- Bally, A. W. 1988. Atlas of seismic stratigraphy. Vol. 2. *AAPG Studies in Geology*, 27, Tulsa, Oklahoma.

- Banner, J. A., Chatellier, J. Y., Feurer, J. R. & Neuhaus, D. 1992. Guillemot D: a successful appraisal through alternative interpretation. *In:* Hardman, R. F. P. (eds.), *Exploration Britain: Geological insights for the next decade*. Geological Society Special Publication, no. 67, pp. 129-149.

- Berg, O. R. & Woolverton, D. J. 1985. Seismic stratigraphy II: An integrated approach to hydrocarbon exploration. *AAPG Memoir,* No. 39.

- Bishop, D. J. 1996. Regional distribution and geometry of salt diapirs and supra-Zechstein Group faults in the western and central North Sea. *Marine and Petroleum Geology,* v. 13, no. 4, pp. 355-364.

- Bishop, D. J., Buchanan, P.G. & Bishop, C. J. 1995. Gravity-driven thin-skinned extension above Zechstein Group evaporates in the Western Central North Sea: an application of computer-aided section restoration techniques. *Marine & Petroleum Geology*, v. 12, pp. 115-135.

- Bjørslev Neilsen, O., Sørensen, S., Thiede, J., and Skarbø, O., 1986. Cenozoic differential subsidence of North Sea. *AAPG- Bulletin*, v. 70, No. 3, pp. 276-298.

- Bouma, A. H. 1962. Sedimentology of some flysch deposits: A graphic approach to facies interpretation. Elsevier Scientific Publishing Co, Amsterdam, 168pp.

- Bouma, A. H. 2000. Coarse-grained and fine-grained turbidite systems as end member models: applicability and dangers. Marine and Petroleum Geology, v. 17, pp. 137-143

- Bouma, A. H., Normark, W. R. & Barnes, N. E. 1985. Submarine fans and related turbidite sequences. Springer-Verlag, New York, 351pp.

- Bowman, M. B. J. 1998. Cenozoic. *In*: Glennie, K. W. (eds.) *Petroleum Geology of the North Sea: Basic concepts and recent advances*, 4th edition, pp. 350- 375, Blackwell Science publication.

- Brown, A. R. 1993. Interpretation of three dimensional seismic data. *AAPG Memoir* No 42

- Bruhn, C. H. L. 1998. Petroleum Geology of rift and passive margin turbidite systems: Brazilian and worldwide examples. Course 12-13/11/1998, Rio de Janeiro, Brazil. AAPG International Conference.

- Buchanan, P.G., Bishop, D. J. & Hood, D. N. 1996. *In:* Alsop, G. I., Blundell, D. J. & Dividson, I. (eds.), *Salt Tectonics*, Geological Society Special Publication, No. 100, pp. 111-128.

- Buchanan, J. G. & Buchanan, P. G. 1995. Basin Inversion. Geological Society Special Publication No. 88.

- Buchanan, R., Marke, P. A. B. & Ruijtenberg, P. A. 1988. Application of 3D seismic to detail reservoir delineation. *Society of Petroleum Engineers International Meeting Proceedings*, pp. 91-97.

- Cartwright, J., Stewart, S. & Clark, J. 2001. Salt dissolution and salt-related deformation of the Forth Approaches Basin, UK North Sea. *Marine and Petroleum Geology,* no. 18, pp. 757-778.

- Cayley, G. T. 1987. Hydrocarbon migration in the Central North Sea. *In*: Brooks, J. & Glennie, K. (eds.), *Petroleum Geology of North West Europe*, Graham and Trotman, pp. 549-555.

- Chapin, M. A., Davies, P., Gibson, J. L. & Pettingill, H.S. 1994. Reservoir architecture of turbidite sheet sandstones in laterally extensive outcrops, Ross Formation, Western Ireland. *GCSSEPM Foundation, 15th Annual Research Conference Submarine Fans and Turbidite Systems,* pp. 53- 68.

- Chawathe, A., 1994. The application of Kohonen type self organisation algorithm to formation evaluation. *SPE paper,* no. 29179.

- Cheng, Q. 1995. The perimeter-area fractal model and its application to geology. Mathematical Geology, v. 27, no.1, pp. 69-82.

- Clark, J. A., Cartwright, J. A. & Stewart, S. A. 1999. Mesozoic dissolution tectonics on the West Central Shelf, UK Central North Sea. *Marine and Petroleum Geology,* no. 16, pp. 283-300.

- Clark, J. D., Kenyon, N. H. & Pickering, K. T. 1992. Quantitative analysis of the geometry of submarine channels: implications for the classification of submarine fans. *Geology*, no. 20, pp. 633-636.

- Clark, J. D. & Pickering, K. T. 1996. Architectural Elements and Growth Patterns of Submarine Channels: Application to Hydrocarbon Exploration. *AAPG Bulletin*, v. 80, No. 2, pp. 194-221.

- Clark, J. D. & Pickering, K. T. 1996. Submarine Channels: Processes and Architecture. Vallis Press, London, 231pp.

- Dalley, R. M., Gevers, E. C. A., Stampfli, G. M., Davies, D. J., Gastaldi, C. N., Ruijtenberg, P. A. & Vermeer, G. J. O. 1989. Dip and azimuth displays for 3D seismic interpretation. *First Break*, v. 7, pp. 86 – 95.

- Damuth, J. E., Flood, R. D., Kowsmann, R. O., Belderson, R. H. & Gorini, M. A. 1998. Anatomy and growth pattern of Amazon deep-sea fan as revealed by long-range side-scan sonar (Gloria) and high-resolution seismic studies. *AAPG-Bulletin*, v. 72, pp. 885-911.

- Davison, I., Alsop, I.,Birch, P., Elders, C. Evans, G., Nicholson, H., Rorison, P., Wade, D., Woodward, J. & Young, M. 2000a. Geometry and late-stage structural evolution of Central Graben salt diapirs, North Sea. *Marine and Petroleum Geology,* No. 17, pp. 499-522.

- Davison, I., Alsop, G. I., Evans, N. G. & Safaricz, M. 2000b. Overburden deformation patterns and mechanisms of salt diapir penetration in the Central Graben, North Sea. *Marine and Petroleum Geology,* No. 17, pp. 601-618.

- de Groot, P., Krajewski, P. and Bischoff, R., 1998. Evaluation of remaining oil potential with 3D seismic using neural networks, *EAGE 60th Conference and Exhibition 1998*, Extended Abstract.

- Deegan, C. E. & Scull, B. J. 1977. A standard lithostratigraphic nomenclature for the central and northern North Sea. *Institute of Geological Sciences*, Report 77/25, pp. 1-33.

- Den Hartog Jager, D. G., Giles, M. R., & Griffiths, G. R. 1993. Evolution of Palaeogene submarine fans of the North Sea in space and time. *In*: Parker, J.R. (eds) *Petroleum Geology of Northwest Europe: Proceedings of the 4th Conference.* The Geological Society, London, 59-71

- Dorn, G. A., Cole, M. J. & Tubman, K. M. 1995. Visualisation in 3D seismic interpretation. *The Leading Edge*, v. 14, pp. 1045 – 1049.

- Elberhart, R. C. & Dobbins, R. W., 1990. Neural networks PC tools- A practical guide. Academic Press, London.

- Eggink, J. W., Riegstra, D. E. & Suzanne, P. 1996. Using 3D seismic to understand the structural evolution of the UK Central North Sea. *Petroleum Geoscience*, v. 2, pp. 83 – 96.

- Erratt, D. 1993. Relationships between basement faulting, salt withdrawal and Late Jurassic rifting, UK Central North Sea. *In*: Parker, J. R. (ed.), *Petroleum Geology of Northwest Europe: Proceedings of the 4th Conference.* Geological Society, London, pp. 1211-1220.

- Fairhurst, M. C. 1988. Computer vision for Robotic Systems. Prentice-Hall International (UK) Ltd. 193pp.

- Flood, R. D., Piper, D. J. & Klaus, A. 1995. *Proc. ODP, Init. Repts,*. v. 155, Ocean Drilling Program, College Station, TX, pp. 23-45.

- Galloway, W. E. 1989. Genetic sequence stratigraphic sequences in basin analysis I: genesis of flooding-surface bounded depositional units. *AAPG Bulletin,* v. 73, pp. 125-142.

- Galloway, W. E. 1998. Siliciclastic slope and base-of-slope depositional systems: component facies, stratigraphic architecture, and classification. *AAPG-Bulletin*, no. 82, pp. 569-595.

- Glennie, K. W. 1984. Structural framework and pre-Permian history of the North Sea area. *In*: Glennie, K. W. (eds.) Introduction to the *Petroleum Geology of the North Sea.* Blackwell Science publication, pp. 17- 40.

- Glennie, K. W. & Underhill, J. R. 1998. Origin, development and evolution of structural styles. *In*: Glennie, K. W. (eds.) *Petroleum Geology of the North Sea: Basic concepts and recent advances*, 4th edition, pp. 42- 84, Blackwell Science publication.

- Gowers, M. B., Holter, E. & Swensson, E. 1993. The structure of the Norwedgian Central Trough (Central Graben area). *In*: Parker, J. R. (ed.), *Petroleum Geology of Northwest Europe: Proceedings of the 4th Conference.* Geological Society, London, pp. 1245-1254.

- Hampton, M.A. 1972. The role of subaqueous debris flow in generating turbidity currents. *Journal of Sedimentary Petrology*, v. 42, pp. 834-844.

- Hampton, M.A. 1975. Competence of fine-grained debris flows. *Journal of Sedimentary Petrology*, v. 45, pp. 775-793.

- Harland, R. Hine, N. M. & Wilkinson, I. P. 1992. Paleogene biostratigraphic markers. *In:* Knox, R. W. & Cordey, W. G. (eds.), *Lithostratigraphic Nomenclature of the UK North Sea*. BGS, Nottingham, Appendix.

- Hartley, A. J. & Prosser, D. J. 1995. Characterisation of deep marine clastic systems. Geological Society Special Publication No. 94, 247pp.

- Haughton, P. D. W. 1994. Deposits of deflected and ponded turbidity currents, Sorbas Basin, southeastern Spain. Journal of Sedimentary Research, v. A64, pp. 223-246.

- Haughton, P. D. W. 2000. Evolving turbidite systems on a deforming basin floor, Tabernas, SE Spain. Sedimentology, v. 47, pp. 497-518.

- Hentschel, H. G. E. & Procaccia, I. 1983. The infinite number of generalised dimensions of fractals and strange attractors. *Physica*, v. 8, pp. 435-444.

- Hesthammer, J. & Fossen, H. 1997a. Seismic attribute analysis in structural interpretation of the Gullfaks Field, northern North Sea. *Petroleum Geoscience*, v. 3, pp. 13 – 26.

- Hesthammer, J. & Fossen, H. 1997b. The influence of seismic noise in structural interpretation of seismic attribute maps. *First Break*, v. 15, pp. 209 – 219.

- Hesthammer, J. 1998. Evaluation of the timedip, correlation and coherence maps for structural interpretation of seismic data. *First Break*, v. 16, pp. 151 – 167.

- Hillis, R. R., Thomson, K. & Underhill, J. R. 1994. Quantification of Tertiary erosion in the Inner Moray Firth usinf sonic velocity data from the Chalk and the Kimmeridge Clay. *Marine and Petroleum Geology*, no. 11, pp. 283-293.

- Hiscott, R., Pickering, K., Bouma, A. Kneller, B., Postma, G. & Soh, J. 1997. Basin-floor fans in the North Sea: sequence stratigraphic models vs sedimentary facies: Discussion. *AAPG-Bulletin*, v. 81, pp. 661-665.

- Hodgson, N. A., Farnsworth, J. & Fraser, A. J. 1992. Salt-related tectonics, sedimentation and hydrocarbon plays in the Central Graben, North Sea, UKCS. *In:* Hardman, R. F. P. (eds) Exploration Britain, Special Publication of the Geological Society. London. No. 67, pp. 31-63.

- Hossack, J. 1995. Geometric rules of section balancing for salt structures. In: Jackson, M. P. A., Roberts, D. J. & Snelson, S. Salt Tectonics: a global perspective. *AAPG-Memoir,* no. 65, pp. 29-40.

- Johnson, S. & Flint, S. 1997. Stratigraphic studies of deepwater clastic systems.

- Jones, G. & Knipe, R. J. 1996. Seismic attribute maps; application to structural interpretation and fault seal analysis in the North Sea Basin. *First Break*, v. 14, pp. 449 – 461.

- Kneller, B.C., 1995. Beyond the turbidite paradigm: physical models for deposition of turbidites and their implications for reservoir prediction. *In:* Hartley A.J. & Prosser D.J. (eds) Characterisation of Deep Marine Clastic Systems. Special Publication of the Geological Society. London. No. 94, pp. 29-46.

- Kneller, B.C., Edwards, D.A., McCaffrey, W.D. & Moore, R.M. 1991. Oblique reflection of turbidity currents. *Geology*, v. 19, pp. 250-252.

- Kneller, B.C. & McCaffrey, W.D. 1999. Depositional effects of flow non-uniformity and stratification within turbidity currents approaching a bounding slope: deflection, reflection and facies variation. *Journal of Sedimentary Research*, v. 69, pp. 980-991

- Knot, S. D., Burchell, M. T., Jolley, E. J. & Fraser. 1993. Mesozoic to Cenozoic plate reconstructions of the North Atlantic and hydrocarbon plays of the Atlantic margins. *In*: Parker, J. R. (ed.), *Petroleum Geology of Northwest Europe: Proceedings of the 4th Conference.* Geological Society, London, pp. 953-974.

- Knox, R. W. & Halloway, S. 1992. Palaeogene of the Central and Northern North Sea. *In:* Knox, R. W. & Cordey, W. G. (eds.), *Lithostratigraphic Nomenclature of the UK North Sea*. BGS, Nottingham, 133pp.

- Knox, R. W. & Morton, A. C. 1988. The record of Early Tertiary N. Atlantic volcanism in sediments of the North Sea Basin. *In:* Morton, A. C. & Parson, L. M. (eds), *Early Tertiary Volcanism and the opening of the NE Atlanting*. Geological Society Special Publication, no. 39, pp. 407-419.

- Kolla, V. & Macurda, D. B. Jr. 1988. Sea level changes and timing of turbidity current events in deep-sea fan systems. *In*: Wilgus, C. K., Hastings, B. S. Kendall, C. G. St. C., Posamentier, H. W., Ross, C. A. & Van Wagoner, J. C. (eds.), *Sea level changes: an integrated approach*. SEPM Special Publication, no. 42, pp. 381-392.

- Lanning, K., Cambois, G. & Hallin, J. 2001. Case study of Elkhorn Slough Field, Solo County, and Grand Island Field, Sacramento County, California: Pre-3D versus post 3D field development. *The Leading Edge*, v. 20, pp. 596 – 599.

- Leeder, M. R. 1993. Tectonic controls upon drainage basin development, river channel migration and alluvial architecture: implications for hydrocarbon reservoir development and characterization. *In:* North, C.P. & Prosser, D.J. (eds.), *Characterization of Fluvial and Aeolian Reservoirs.* Geological Society Special Publication, No. 73, pp. 7-22.

- Leeder, M. R., Harris, T. & Kirkby, M. J. 1998. Sediment supply and climate change: Implications for basin stratigraphy. *Basin Research,* v. 10, pp. 7-18.

- Lovejoy, S. 1982. Area-perimeter relationship for rain and cloud areas. *Science*, v. 216, pp. 185-187.

- Lowe, D.R. 1975. Water escape structures in coarse-grained sediments. *Sedimentology*, v. 22, pp. 157-204.

- Lowe, D.R. 1976. Grain flow and grain flow deposits. *Journal of Sedimentary Petrology*, v. 46, pp. 188-199.

- Lowe, D. R. 1982. Sediment gravity flows: Depositional models with special reference to the deposits of high-density turbidity currents. *Journal of Sedimentary Petrology*, v. 52, pp. 279-297.

- Lowe, D.R. & LoPiccoio, R.D. 1974. The characteristics and origins of dish and pillar structures. *Journal of Sedimentary Petrology*, v. 44, pp. 484-501.

- Mandelbrot, B. B., Passoja D. E. & Paullay, A. J. 1984. Fractal character of fracture surfaces of metals. *Nature*, v. 308, pp. 721-722.

- Manley, P. L. & Flood, R. D. 1988. Cyclic sediment deposition within Amazon deep-sea fan. *AAPG-Bulletin*, v. 72, no. 8, pp. 912-925.

- McCaffrey, W.D. & Kneller. B.C. 2001. Process controls on the development of stratigraphic trap potential on the margins of confined turbidite systems, and aids to reservoir evaluation. *AAPG Bulletin*, v. 85, pp. 971-988

- McKenzie, D.P. 1978. Some remarks on the development of sedimentary basins. *Earth and Planetary Science Letters,* v. 40, pp. 25-32.

- Middleton, G. V. 1967. Experiments on density and turbidity currents. III. Deposition of sediment. *Canadian Journal of Earth Science*, v. 4, pp. 475-505.

- Middleton, G. V. & Hampton, M. A. 1973. Sediment gravity flows: mechanisms of flow and deposition. SEPM, Pac. Section, Short Course Lecture Notes. Turbidity and Deep-water sedimentation.

- Middleton, G. V. & Hampton, M. A. 1976. Subaqueous sediment transport and deposition by sediment gravity flows. *In*: Stanley, D. J. & Swift, D. J. (ed.), *Marine Sediment Transport and Environmental Management*, Wiley, New York, pp. 197-218.

- Middleton, G. V. & Southards, J. B. 1984. Mechanics of sediment movement. SEPM Short course No. 3, Tulsa.

- Milton, N. J., Bertram, G. T. & Vann, I. R. 1990. Early Palaeogene tectonics and sedimentation in the Central North Sea. *In:* Hardman, R. F. P. & Brooks, J. (eds.), *Tectonic Events Responsible for Britain's Oil and Gas Reserves.* Geological Society Special Publication No. 55, pp. 339-351.

- Mitchum, R. M. Jr. 1985. Seismic stratigraphic expression of submarine fans. *In:* Berg, O. R. & Woolverton, D. J. Seismic *stratigraphy II: An integrated approach to hydrocarbon exploration. AAPG Memoir,* no. 39. pp. 117-136.

- Morton, A. C., Hallsworth, C. R. & Wilkinson, G. C. 1993. Stratigraphic evolution of sand provenance during Palaeocene deposition in the Northern Nroth Sea area. *In*: Parker, J. R. (ed.), *Petroleum Geology of Northwest Europe: Proceedings of the 4th Conference.* Geological Society, London, pp. 73-84.

- Mu, Z. Q. & Lung, C. W. 1988. Studies on the fractal dimension and fracture toughness of steel. J. Phys. D: Appl. Phys., v. 21, pp. 848-850.

- Muck, M.T., and Underwood, M.B., 1990, Upslope flow of turbidity currents: A comparison among field observations, theory, and laboratory models. *Geology*, v. 18, pp. 54-57.

- Mutti, E. 1977. Distinctive thin bedded turbidite facies and related depositional environments in the Eocene Hecho Group, South Central Pyrenees, Spain. *Sedimentology*, v. 24, pp. 107- 131.

- Mutti, E. 1985. Turbidite systems and their relations to depositional sequences. In Zuffa, G. G. Provenance of Arenites, NATO-ASI Series, D. Reidel Publishing Co., pp. 65-93.

- Mutti, E. 1992. Turbidite Sandstones. Agib and the Institute di Geologia, University di Parma. 275pp.

- Mutti, E. & Normark, W. R. 1987. Comparing examples of modern and ancient turbidite systems: Problems and concepts. *In*: Leggett, J. K. and Zuffa, G. G. (eds.), *Marine clastic sedimentology: Concepts and case studies*. Graham & Trotman, London, pp. 1- 38.

- Mutti, E. & Normark, W. R. 1991. An integrated approach to the study of turbidite systems. *In*: Weimer, P. & Link, M. H. (eds.), *Seismic facies and sedimentary processes of submarine fans and turbidite systems*. Springer-Verlag New York, Inc, pp. 75- 106.

- Mutti, E. & Ricci Lucci, F. 1972. Le torbiditi dell' Appenniono Settentrionale: introduzione all'analisi di facies. *Geological Society of Italy*.

- Mutti, E. & Ricci Lucci, F. 1975. Turbidite facies and facies associations. *In*: Examples of turbidite facies and facies associations from selected formations of the Northern Apennines. Field trip Guidebook A-11. International Sediment. Cong., Nice IX, pp. 21- 36.

- Nikora, V. I., Sapozhnikov, V. B. & Noever, D. A. 1993. Fractal geometry of individual river channels and its computer simulation. Water Resources Res., v. 29, pp. 3561-3568.

- Normark, W. R. 1970. Growth patterns of deep-sea fans. *AAPG Bulletin*, no. 54, pp. 2170-2195.

- Normark, W. R. 1978. Fan valleys, channels, and depositional lobes on modern submarine fans: characters for recognition of sandy turbidite environments. *AAPG Bulletin*, no. 62, pp.912-931.

- Normark, W. R. & Piper, D. J. W. 1991. Initiation processes and flow evolution of turbidity currents: implications for depositional record. *In*: Osborne, R. H. (eds.), *From Shoreline to Abyss*. SEPM Special Publication, no. 46, pp. 207-230.

- Normark, W. R., Moore, J. G. & Forresan, M. E. 1993. Giant volcano-related landslides and the development of the Hawaiian Islands. *In:* Schwab, W. C., Lee, H. J. & Twichell, D. C. *Submarine landslides: selected studies in the US Exclusive Economic Zone*, US Geological Survey Bulletin, no. 2002, pp. 184-196.

- Oakman, C. D. Martin, J. H. & Corbett, P. W. M. (eds.), 1997. Cores from the Northwest European Hydrocarbon Province: An illustration of geological applications from exploration to development. Geological Society Publication. 232pp.

- Peakall, J., McCaffrey, B. & Kneller, B. 2000. A process model for the evolution, morphology, and architecture of sinuous submarine channels. *Journal of Sedimentary Research,* v. 70, No. 3, pp. 434- 448.

- Penge, J., Taylor, B., Huckerby, J. A. & Munns, J. W. 1993. Extension and salt tectonics in the east Central Graben. *In*: Parker, J. R. (ed.), *Petroleum Geology of Northwest Europe: Proceedings of the 4th Conference.* Geological Society, London, pp. 1197-1210.

- Permiz, C., Beaubouef, R. T., Friedmann, S. J. & Mohrig, D. C. 2000. Equilibrium profile and baselevel in submarine channels: examples from Late Pleistocene systems and implications for the architecture of deepwater reservoirs. *GCSSEPM Foundation 20th Annual Research Conference*, Deep-water Reservoirs of the World, December 3-6, 2000, pp. 782-805.

- Permiz, C. & Flood, R. D. 1995. Morphology and structure of Amazon channel. *In:* Flood, R. D., Piper, D. J. & Klaus, A. *Proc. ODP, Init. Repts,*. v. 155, Ocean Drilling Program, College Station, TX, pp. 23-45.

- Pickering, K. T. 1982. Middle fan deposits from the late Precambrian Kongsfjord Formation submarine fan, northeast Finnmark, northern Norway. *Sedimentary Geology*, v. 33, pp. 79- 110.

- Pickering, K. T. 1983. Small scale syn-sedimentary faults in the Upper Jurassic "Boulder Beds". *Scottish Journal of Geology*, v. 19, pp. 169- 181.

- Pickering, K. T. 1984. The Upper Jurassic "Boulder Beds" and related deposits: a fault controlled submarine slope, NE Scotland. *Journal of Geological Society*. London, v. 141, pp. 357- 374.

- Pickering, K. T., Clark, J. D., Ricci Lucchi, F., Smith, R. D., Hiscott, R. N. & Kenyon, N. H. 1995. Architectural element analysis of turbidite systems, and selected topical problems for sand-prone deep-water systems. *In*: Pickering, K. T., Hiscott, R. N., Kenyon, N. H., Ricci Lucchi, F. & Smith, R. D. (eds.), *Atlas of deep-water environments: architectural style in turbidite systems*. London, Chapman & Hall. pp. 1-10.

- Pickering, K.T., & Hiscott, R.N., 1985, Contained (reflected) turbidity currents from the Middle Ordovician Cloridorme Formation, Quebec, Canada: An alternative to the antidune hypothesis. *Sedimentology*, v. 32, pp. 373-394.

- Pickering, K. T., Hiscott, R. N., Kenyon, N. H., Ricci Lucchi, F. & Smith, R. D. (eds.), *Atlas of deep-water environments: architectural style in turbidite systems*. London, Chapman & Hall. 329pp.

- Pickering, K. T., Hiscott, R. N. & Hein, F. J. 1989. Deep marine environments: Clastic sedimentation and tectonics. 2nd edition, Unwin Hayman publications. 416pp.

- Pickering, K.T., Underwood, M.B. & Taira, A. 1992. Open ocean to trench turbidity-current flow in the Nankai Trough: Flow collapse and reflection. *Geology*, v. 20, pp. 1099-1102.

- Piper, D. J. W. 1978. Turbidite muds and silts in deep sea fans and abyssal plains. *In*: Sedimentation in submarine canyons, fans and trenches sedimentation. Stanley, D.J. & Kelling, G. (eds.),. Dowden, Hutchinson and Ross, Stroudsburgh, pp. 163- 176.

- Piper, D. J. & Normark, W.R. 1983. Turbidite depositional patterns and flow characteristics, Navy submarine fan, California Borderland. *Sedimentology*, v. 30, pp. 681-694.

- Posamentier, H. W. & Erskine, R. D. 1991. Seismic expression and recognition criteria of ancient submarine fans. *In:* Weimer, P. & Link, M. H. (eds.), *Seismic facies and sedimentary processes of submarine fans and turbidite systems*. Springer-Verlag, New York, pp. 197-222.

- Posamentier, H. W., Jervey, M. T. & Vail, P. R. 1988. Eustatic controls on clastic deposition I - conceptual framework. *In:* Wilgus, C. K., Bastings, B. S., Ross, C. A., Posamentier, B. W., Van Wagoner, J. & Kendall, C.G.St C. (eds.), *Sea-level changes: An integrated approach.* SEPM Special Publication, No. 42, pp. 109-124.

- Posamentier, H. W. & Vail, P. R. 1988. Eustatic controls on clastic deposition II – Sequence and systems tract models. *In:* Wilgus, C. K., Bastings, B. S., Ross, C. A., Posamentier, B. W., Van Wagoner, J. & Kendall, C.G.St C. (eds.), *Sea-level changes: An integrated approach.* SEPM Special Publication, No. 42, pp. 125-154.

- Prather, B. E., Booth, J. R., Steffens, G. S. & Craig, P. A. 1998. Classification, lithologic calibration and stratigraphic succession of seismic facies of intra-slope basins, deep-water Gulf of Mexico. *AAPG-Bulletin*, v. 82, pp. 701-728.

- Rattey, R. P. & Hayward, A. B. 1993. Sequence stratigraphy of a failed rift system: the Middle Jurassic to Early Cretaceous basin evolution of the Central and Northern North Sea. *In*: Parker, J. R. (ed.), *Petroleum Geology of Northwest Europe: Proceedings of the 4th Conference.* Geological Society, London, pp. 215-249.

- Rawson, P. F. & Riley, L. A. 1982. Late Jurassic-Early Cretaceous events and the "Late Cimmerian Unconformity" in the North Sea area. *AAPG-Bulletin*, v. 66, pp. 2628-2648.

- Ravnås, R. & Steel, R. J. 1998. Architecture of marine rift-basin successions. *AAPG Bulletin,* v. 82, pp. 110-146.

- Reading H. G. 1996. Sedimentary Environments: Processes, Facies and Stratigraphy. 3rd edition, Blackwell Science Publication. 688pp.

- Reading, H. G. & Richards, M. 1994. Turbidite systems in deep-water basin margins classified by grain size and feeder system. *AAPG Bulletin,* v. 78, pp. 792-822.

- Richards, P.C. 1990. The early to mid-Jurassic evolution of the northern North Sea. *In:* Hardman, R. F. P. & Brooks, J. (eds.), *Tectonic Events Responsible for Britain's Oil and Gas Reserves.* Geological Society Special Publication No. 55, pp. 191-205.

- Russell, B., Hampson, D., Schuelke, J. & Quirein, J. 1997. Multi-attribue seimic analysis, *The Leading Edge,* v. 10, pp. 1439-1443.

- Rye-Larsen 1994. The Balder Field: refined reservoir interpretation with the aid of high resolution seismic data and seismic attibute mapping. *In:* Aasen, J. O., Berg, E., Buller, A. T., Hjelmeland, O., Holt, R. M., Kleppe, J. and Torster, O. (eds), *North Sea Oil and Gas Reservoirs* The Norwegian Institute of technology/Kluwer, London. No. 3, pp. 115 – 124.

- Rys, F. S. & Waldvogel, A. 1986. Fractal shape of hail clouds. *Phys. Rev. Lett*, no. 45, pp. 784-787.

- Sanders, J. E. & Friedman, G. M. 1997. History of petroleum exploration in turbidites and related deep-water deposits. *Northeastern Geology and Environmental Sciences*, no. 19, pp.67-102.

- Satterfield, W. M. & Behrens, E. W. 1990. A late Quaternary canyon/channel system, northwest Gulf Mexico continental slope. *Marine Geology*, v. 92, pp. 51-67.

- Scheck, M., Bayer, U. & Lewerenz, B. 2003. Salt redistribution during extension and inversion inferred from 3D backstripping. *Tectonophysics*, no. 373, pp. 55-73.

- Schultz , 1994 Part2: Using artificial neural networks for nonlinear attribute calibration. *The Leading Edge*, June.

- Schumm, S. A. & Khan, H. R. 1972. Experimental study of channel patterns. Geological Society of America Bulletin, v. 88, pp. 1755-1770.

- Schumm, S. A., Khan, H. R., Winkley, B. R. & Robins, L. G. 1972. Variability of river patterns. *Nature; Physical Sciences*, no. 237, pp. 75-76.

- Shanmugam, G. 1990. Deep marine facies models and the interrelationship of depositional components in time and space. *In*: Brown, G. C. Gorsline, D. S. & Schweller, W. J. *Deep-marine sedimentation: depositional models and case histories in hydrocarbon exploration and development*. Soc. Econ.Paleon. & Min. San Francisco. pp. 199-246.

- Shanmugam, G. 1996. High-density turbidity currents: are they sandy debris flows? *Journal of Sedimentary Research,* v. 66, No. 1, pp. 2- 10.

- Shanmugam, G. 2000. 50 years of the turbidite paradigm (1950s-1990s): deep-water processes and facies models- a critical perspective. *Marine & Petroleum Geology*, no. 17, pp. 285-342.

- Shanmugam, G., Bloch, R., Damuth, J. & Hodgkinson, R. 1997. Basin-floor fans in the North Sea: sequence stratigraphic models vs sedimentary facies: Reply. *AAPG-Bulletin*, v. 81, pp. 666-672.

- Sheriff, R. E. 1977. Limitations on resolution of seismic reflections and geologic detail derivable from them. *AAPG Memoir,* no. 26, pp. 3-14

- Sheriff, R. E. 1980. Seismic Stratigraphy. International Human Resources Development Corporation, Boston.

- Sheriff, R. E. & Geldart, L. P. 1995. Exploration Seismology, 2nd edition. Cambridge University Press, New York, USA, 592pp.

- Sinclair, H.D. 2000. Delta-fed turbidites infilling topographically complex basins: A new depositional model for the Annot Sandstone, SE France. *Journal of Sedimentary Research*, v. 70, No. 3, pp. 504- 519.

- Sinclair, H.D. & Tomasso, M. 2002. Depositional evolution of intra-slope turbidite sub-basins. *Journal of Sedimentary Research.* v. 85 pp.

- Smith, R. I., Hodgson, N. & Fulton, M. 1993. Salt control on Triassic reservoir distribution, UKCS Central North Sea. *In*: Parker, J.R. (eds) *Petroleum Geology of Northwest Europe: Proceedings of the 4th Conference.* The Geological Society, London, pp. 547-557.

- Soto, B. R. 1997. Use of neural networks to predict the permeability and porosity of zone C of the Cantagallo Field in Colombia. *SPE paper,* no. 38134.

- Stewart, I. J. 1987. A revised stratigraphic interpretation of the Early Palaeogene of the Central North Sea. 557-576.

- Stewart, S. A. & Clark, J. A. 1999. Impact of salt on the structure of the Central North Sea hydrocarbon fairways. *In*: Fleet, A. J. & Boldy S. A. R. (eds) *Petroleum Geology of Northwest Europe: Proceedings of the 5th Conference.* The Geological Society, London, pp. 179-200.

- Stewart, S. A., Ruffel, A. H. & Harvey, M. J. 1997. Relationship between basement-linked and gravity-driven fault systems in the UKCS salt basins. *Marine and Petroleum Geology*, v. 14, no. 5, pp. 581-604.

- Stow, D. A. V. 1985. Deep-Sea clastics: where are we and where are we going? *In*: Brenchley P. J., & Williams, B. P. J. (eds.), *Sedimentology: Recent Developments and Applied Aspects.* Geological Society Special Publication No. 18, pp. 67- 93.

- Stow, D. A. V., Bishop, C. D., & Mills, S. J. 1982. Sedimentology of the Brae oil field, North Sea: fan models and control. *Journal of Petroleum Geology*, v.5, pp. 129-148.

- Stow, D. A. & Bowen, A. J. 1978. Origin of lamination in deep-sea fine-grained sediments. *Nature*, v. 274, pp. 324-328.

- Stow, D. A. & Piper, D. J. W. 1984. Deep-water fine-grained sediments: history methodology and terminology. *In*: Stow, D. A. & Piper, D. J. W. (eds.), *Fine-grained Sediments: Deep-water Processes and Facies*. Geological Society Special Publication No. 15, pp. 3-14.

- Stow, D. A. V., Reading, H. G. & Collinson, J. D. 1996. Deep seas. *In;* Reading, H.G. (ed.), *Sedimentary environments; processes, facies and stratigraphy.* Blackwell Science, London, pp. 395-453.

- Stow, D. A. V. & Shanmugan, G. 1980. Sequence of structures in fine-grained turbidites: comparison of recent deep-sea and ancient flysch sediments. *Sedimentary Geology,* v. 25, pp. 23-42.

- Syrlyk, F. 1978. Submarine fan sedimentation along fault scarps on tilted fault blocks (Jurassic/Cretaceous boundary, East Greenland) Bull. Grønlands Geologiske Undersøgelse, no. 128, 108pp.

- Taylor, J. C. M. 1984. Late Permian Zechstein. *In*: Glennie, K. W. (eds.) Introduction to the *Petroleum Geology of the North Sea.* Blackwell Science publication, pp. 17- 40.

- Thomson, K. & Underhill, J. R. 1993. Controls on the development and evolution of structural styles in the Inner Moray Firth Basin. *In*: Parker, J.R. (eds) *Petroleum Geology of Northwest Europe: Proceedings of the 4th Conference.* The Geological Society, London, pp. 1167-1178.

- Trappe, H. Kraft, T., & Schweitzer, C. 1995. Neurale Netzwerke zur permeabilitatsbestimmung in Rotliegendsandsteinen (Neural Networks for permeability determination in Rotliegend sandstones). *Erdol Erdgas Kohle*, no. 111.4, pp. 159-162.

- Trappe, H. & Hellmich, C. 2000. Using neural networks to predict porosity thickness from 3D seismic. *First Break*, v. 18 no. 9 pp. 377-384.

- Underhill, J. R. 1998. Jurassic. *In*: Glennie, K. W. (ed.) *Petroleum Geology of the North Sea: Basic concepts and recent advances*", 4th edition, pp. 245-293, Blackwell Science publication.

- Underhill, J. R. & Partington, M. A. 1993. Jurassic thermal doming and deflation in the North sea: implication of the sequence stratigraphic evidence. *In*: Parker, J. R. (ed.), *Petroleum Geology of Northwest Europe: Proceedings of the 4th Conference.* Geological Society, London, pp. 337-345.

- Underhill, J. R. & Partington, M. A. 1994. Use of genetic sequence stratigraphy in defining and determining a regional tectonic control on the 'Mid-Cimmerian Unconformity': implications for North Sea basin development and the global sea-level chart. *In:* Weimer, P.1. & Posamentier, H. W. (eds.), *Siliciclastic sequence stratigraphy.* AAPG Memoir 58, pp. 449-484.

- Vail, P. R. 1987. Seismic stratigraphy interpretation procedure. *In*: Bally, A. W. (eds.), *AAPG Atlas of seismic stratigraphy.* AAPG Studies in Geology, No. 27, pp. 1- 10.

- Van Wagoner, J. C., Mitchum, R. M., Campion, K. M. & Rahmanian, V. D. 1990. Silicic1astic sequence stratigraphy in well logs, cores and outcrops: Concepts for high-resolution correlation of time and facies. *AAPG methods in exploration series*, No. 7, 55pp.

- Walkfield, L. L., Droste, H., Giles, M. R. & Janssen, R. 1993. Late Jurassic plays along the western margin of the Central Graben. *In*: Parker, J. R. (ed.), *Petroleum Geology of Northwest Europe: Proceedings of the 4th Conference.* Geological Society, London, pp. 459-468.

- Walker, R. G. 1965. The origin and significance of the internal sedimentary structures of turbidites. *Proceedings of Yorkshire Geological Society*, No. 35, pp. 1-32.

- Walker, R.G. 1967. Turbidite sedimentary structures and their relationship to proximal and distal depositional environments. *Journal of Sedimentary Petrology,* v. 37, p. 25-43.

- Walker, R. G. 1978. Deep-water sandstone facies and ancient submarine fans: models for exploration for stratigraphic traps. *AAPG Bulletin*, v. 62, pp. 932-966.

- Walker, R. G. 1984. Facies models. Geoscience Canadian Reprint Series 1. Geological Society Canada, Waterloo. Ontario. 364pp.

- Walker, R. G. & Mutti, E. 1972. Turbidite facies and facies associations. *In*: Bouma, A. H. & Middelton, G. V. (eds.), *Turbidites and deep water sedimentation*. SEPM Pacific Section, pp. 119-157.

- Walls, J., Derzhi, N., Dumas, D., Guidish, T., Taner, M. & Taylor, G. 1999. North Sea reservoir characterisation using rock physics, seismic attributes, and neural networks: a case history. *Annual Meeting Abstracts*, Society of Exploration Geophysicists, pp. 1572-1575.

- Watson, M. P. 1984. Submarine fans in a developing extensional regime: their significance in the North Sea hydrocarbon province. Abstract in *AAPG-Bulletin*, v. 68, p. 538.

- Weimer, P. 1989. Sequence stratigraphy of the Mississippi Fan (Plio-Pleistocene), Gulf of Mexico. *Geo-Marine Letters*, v. 9, pp.185-272.

- Weimer, P. & Link, M. H. 1991. Global petroleum occurrences in submarine fans and turbidite systems. *In:* Weimer, P. & Link, M. H. (eds.), *Seismic facies and sedimentary processes of submarine fans and turbidite systems*. Springer-Verlag, New York, pp. 9-67.

- Weimer, P. & Link, M. H. 1991. Seismic facies and sedimentary processes of submarine fans and turbidite systems. Springer-Verlag, New York, 447pp.

- White, R. S. 1988. A hot spot model for the Early Tertiary volcanism in the North Atlantic. *In:* Morton, A. C. & Parson, L. M. (eds), *Early Tertiary Volcanism and the opening of the NE Atlanting*. Geological Society Special Publication, no. 39, pp. 3-13.

- Wilf, J. M. 1981. Chain Code. *Robotics Age*, v. 3, no. 2, pp. 12-19.

- Winker, C. D. 1996. High resolution seismic stratigraphy of a late Pleistocene submarine fan ponded by salt-withdrawal on the Gulf of Mexico Continental slope. *Proceedings from 1996 Offshore Technology Conference*, paper OTC 8024, May 6-9, 1996, Houston Texas, pp. 619-628.

- Wood, R & Barton, P. 1983. Crustal thinning and subsidence in the North Sea. *Nature*, no. 302, pp. 134-136.

- Wu, R-S. & Lai, Y-S. 1994. An observation on the fractal characteristics of individual river plan forms. *Fractals Natural Appl. Sci.*, v. 41, pp. 441-451.

- Zhou, C. & Wu, X., 1993. Neural network-based formation parameters estimation from well logs in quantitative log analysis: a comparative study. *SPE paper*, no. 25359

- Ziegler, W. H. 1982. Geological Atlas of Western and Central Europe. Elsevier Scientific Publishing Co, Amsterdam.

- Ziegler, W. H. 1990a. Geological Atlas of Western and Central Europe. Elsevier Scientific Publishing Co, Amsterdam.

- Ziegler, W. H. 1990b. Tectonic and palaeogeographic development of the North Sea rift system. *In*: Blundell, D.J. & Gibbs, A.D. (eds.), *Tectonic evolution of the North Sea Rifts*. Oxford Science Publications, pp. 1-36.

- Ziolkowski, A. 2000. Simplified wavelet estimation using source-signature measurements. *The Leading Edge*, no. 1, pp. 61-67.

- Ziolkowski, A. & Fokkema, J. T. 1986. Tutorial: The progressive attenuation of high-frequency energy in seismic reflection data. *Geophysical Prospecting*, v. 34, pp. 981-1001.

- Ziolkowski, A., Underhill, J. R. & Johnston, R. G. 1998. Wavelets, well ties, and the search for subtle stratigraphic traps. *Geophysics*, v. 63, No. 1, pp. 297-313.

Appendices

Appendix 1

Well Parameters and Formation Tops

			21/29b-1	21/29b-4	21/29b-9	21/30-12	21/30-14	21/30-15	21/30-16	21/30-17	21/30-18	22/26a-1
Well Location	Easting		543486.6	544009	547944	550706	559142	558236	552190	557571	559173	563066
	Northing		6322372	6318669	6320624	6322036	6325290	6326558	6321830	6322657	6320931	6325720
	Inline		9292	8996	9152	9266	9526	9626	9248	9316	9206	9560
	Crossline		3478	3520	3836	4056	4732	4660	4178	4606	4712	5044
Tops / Horizons												
Tay Sandstone Member	Upper Tay	AHD (ft)	Nil	5006	5813	5652	6508	6460	5895	6395	Nil	7505
	(PT 23.1)	TVD (ft)	Nil	4924	5738	5570	6418	6370	5808	6309	Nil	7425
		TWT (ms)	Nil	1539	1766	1725	1991	1978	1800	1959	Nil	2269
	Middle Tay	AHD (ft)	Nil	5100	5861	5753	6620	6525	6012	6425	Nil	7650
	(PT 22.3)	TVD (ft)	Nil	5018	5786	5673	6530	6435	5925	6339	Nil	7570
		TWT (ms)	Nil	1557	1777	1746	2012	1985	1827	1968	Nil	2303
	Basal Tay	AHD (ft)	Nil	5182	5967	5825	6720	6668	6100	6631	Nil	7806
	(PT 22.1)	TVD (ft)	Nil	5100	5892	5743	6630	6578	6013	6545	Nil	7726
		TWT (ms)	Nil	1579	1804	1765	2038	2022	1849	2019	Nil	2338
Balder Formation		AHD (ft)	5280	5205	6050	5912	6758	6680	6170	6684	6540	7834
		TVD (ft)	5198	5123	5975	5830	6668	6590	6083	6598	6450	7754
		TWT (ms)	1622	1587	1822	1789	2047	2027	1857	2029	1973	2338
Chalk Group		AHD (ft)	6395	5662	6474	6282	7240	7202	6617	7097	6930	8772
		TVD (ft)	6313	5580	6420	6218	7150	7112	6529	7011	6840	8692
		TWT (ms)	1872	1714	1934	1887	2155	2102	1978	2121	2070	2490

AHD = Along-hole depth (below rotary table) TVD = True vertical depth (subsea) TWT = Two way travel time (subsea)

Appendix 2

Completion Logs

SHELL/ESSO 22/26a-1

SHELL U.K. EXPLORATION AND PRODUCTION

COMPLETION LOG

PRODUCTION LICENCE P ROUND

22/26a - 1

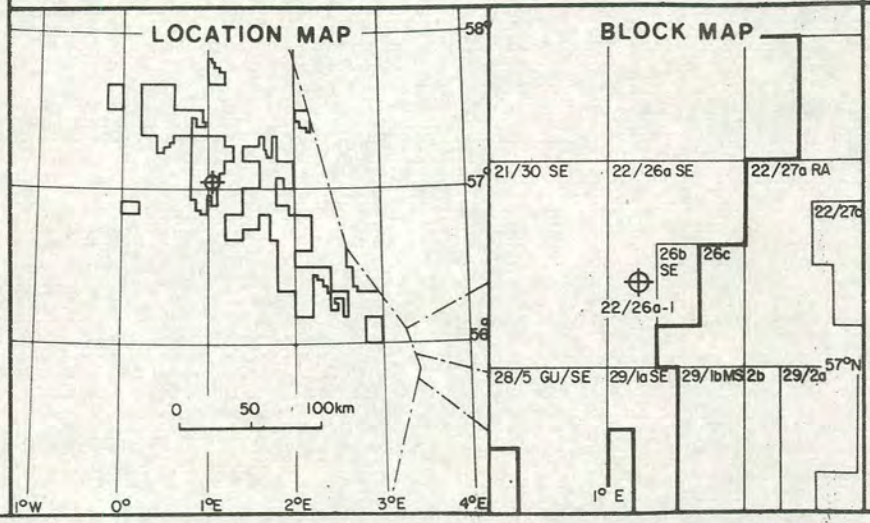

LOCATION COORDINATES

Latitude 57°04'10·16"N

Longitude 01°02'24·60"E

RIG SEDCO 709

DF ELEVATION 80 AMSL

WATER DEPTH 294 BMSL

TOTAL DEPTH 8875' BDF

8795' SS

UTM

OPERATED BY SHELL EXPRO

ARRIVED ON LOC. 27·9·81

SPUD DATE 1·10·81

ABANDON DATE 4·11·81

RIG RELEASE DATE

WELL STATUS PLUGGED AND ABANDONED

MUDLOGGING BY GEARHART OWEN

LOGGING SCHLUMBERGER

INTERESTS

SHELL 50%

ESSO 50%

PREPARED DATE

TERTIARY

MIDDLE EOCENE

PT 22 - PT 27/29

PT 23

Upper part)

7624' 7606' 7560' 7505'

HORDALAND GROUP

CLST: dk. gy. - med. gn. - gy. sft. - mod. hd, non swelling, non calc.

TAY FM. (7505' - 7834')

PETROPHYSICAL EVALUATION			
7505' - 7834'			
163' NS			
		Ø	Sw
7505' - 7520'		36·3%	74·6%
7520' - 7834'		32·9%	100%

SST: fSL - crs SL., av. fSU, (srt.), (ang.), - ang., lt. yel. gy. - po. gy. brn., mic. - (mic.), glc. - (glc.), carb., non calc., lse, from 7650' - 7824', freq. interbedded with CLST, sft., med. - dk. gy., (micro mic.) occas. (micro-py.) and glc., brit. - mod hd., non calc.

7700 7600 7500 7400

MG 0·58 psi/ft. MG 0·640 psi/ft.

CORE 1 7440·6" - 7490'

CORE 2 7490' - 7528'

CORE 3 7528' - 7560'

CORE 4 7560' - 7591'

SH SS SH SS SS SH SH SH

7351' 9⅞"

3421 psi 3381 psi 3374 psi (ran 2)

MIDDLE EOCENE

PT 22 - PT 27/29

PT 23

PT 35

7250'
7230'
7200'

CLST: dk gy - med. gn - gy. sft. - mod. hd., non swelling, non calc.

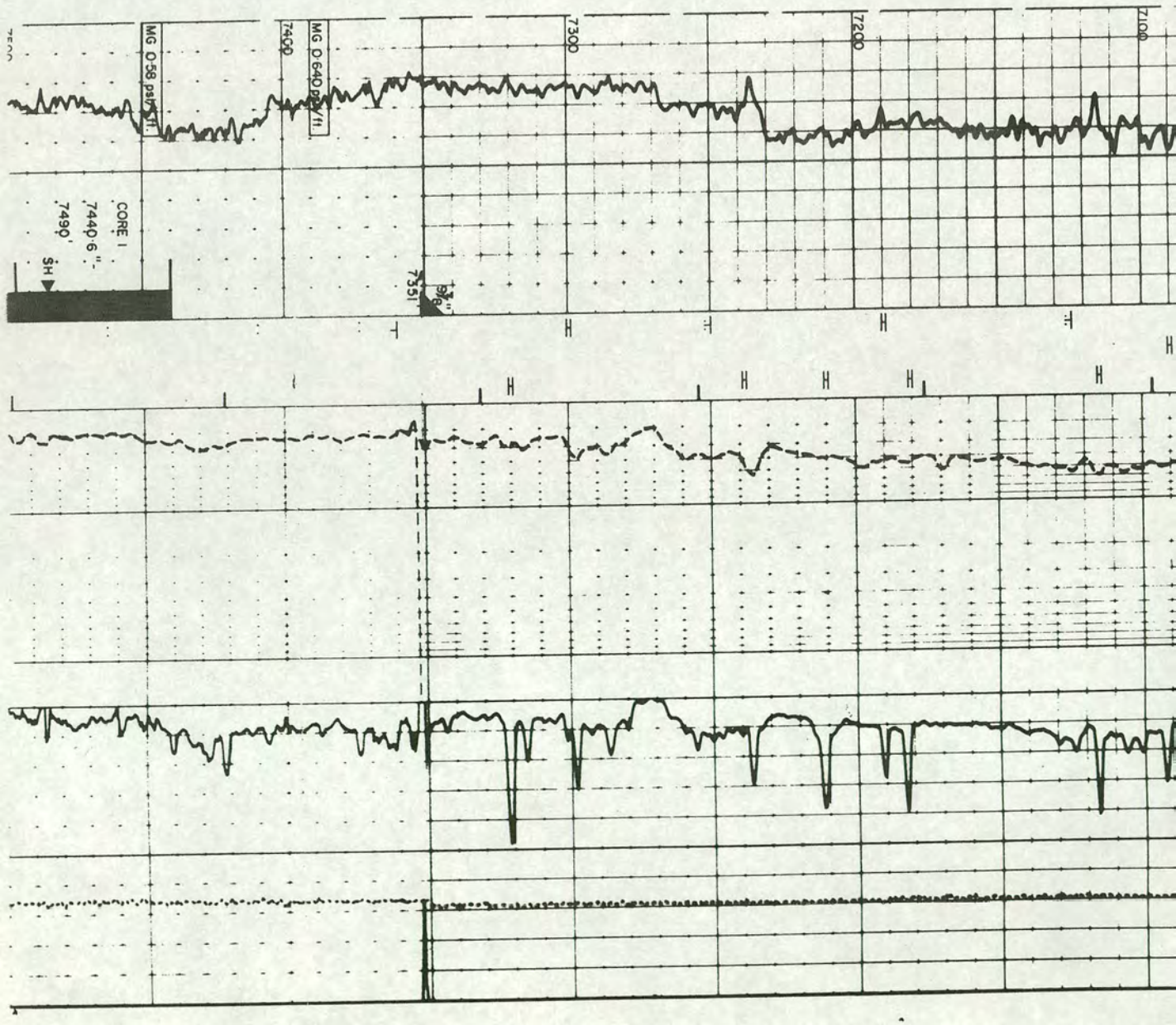

LOWER EOCENE

PT21

PT 21 | PT 22(Upper part)

7970' 7952' 7845' 7840' 7834' 7782' 7624' 7606'

ALAND GROUP | HORDALAND

7520'-7834' 32.9% 100%

SST: fSL- crs SL, av. fSU, (srt.), (ang.), - ang., lt yel. gy. - pa. gy. brn., mic.-(mic.), glc.-(glc.), carb., non calc., lse, from 7650'-7824' freq. interbedded with CLST, slt., med.-dk. gy., (micro mic.) occas. (micro-py.) and glc., brit.-mod hd., non calc.

SELE FM (7952'-8069')

SST & CLST: SST, crg-arg, fSL-mSL, (srt.)-srt., (rnd.), lt. yel. gy.-wh., cmt., hd., fractures, occ. glc.,

BALDER FM (7834'-7952')

SH: (slt.), dk. gy-gy, subfissile hd., non calc.-(calc.)

7900 7800 7700 7600

SH SH SH SH CLST(SL) CLST(SL) 6S SS SH SH SS SH SH 6S SH SS SS

CORE 4 7560'-7591'

3471 psi 3421 psi

UPPER PALEOCENE

T19

PT 19

PT20

8069'

8056'

8008'

7970'

7952'

ROGALAND

SELE FM (7952' - 8069')

SST & CLST: SST, arg - arg, fSL - mSL, (srt.) - srt., (rnd.), lt. yel. gy - wh., cmt., hd., fractures, occ. glc., CLST., sil., lt - dk. gy., mod. hd - hd., non calc.

N.B. The base Sele Fm. has been defined as coinciding with top of massive sand (Forties Fm.) at 8098' according to I.G.S. standards.

A correlative log marker would rather define it at 8037'.

FORTIES FM (8069' - 8396')

SST & CLST: SST., fSL - crsSU, (srt.) - srt., arg., (ang.) - (rnd.), lt. yel. gy., mod. hd - fri., mic., (glc.) - ((glc.)), non calc. CLST., slt., med. - dk. gy., mod. hd., non calc.

PETROPHYSICAL EVALUATION
7834' - 8772'
8069' - 8396', 292' NS
Ø 27.3% Sw 100%
8396' - 8772'
Ø 25.7% Sw 100%

8300 8200 8100 8000

MG 0.58 psi/min

SS CLST(SL) SS(CL) SLST CLST SS CLST SS SH SH SH SH

3737 psi

3632 psi

TERTIARY

MIDDLE PALEOCENE — UPPER

NP4A

PT15? — PT 15 — PT15? — NF — PT19

8650' 8652' 8633' 8600' 8500' 8466' 8450' 8410' 8396'

MONTROSE GROUP

CLST: gn-gy. to pa.gy., sft.-mod. hd., calc. i/p.

CLST: dk.gy.-brn. to dk.gy.-gn., mod hd., silty, calc. i/p.

CLST: dk.gy.-blk., hd., slt., (fiss.)

MAUREEN FM (8396' - 8772')

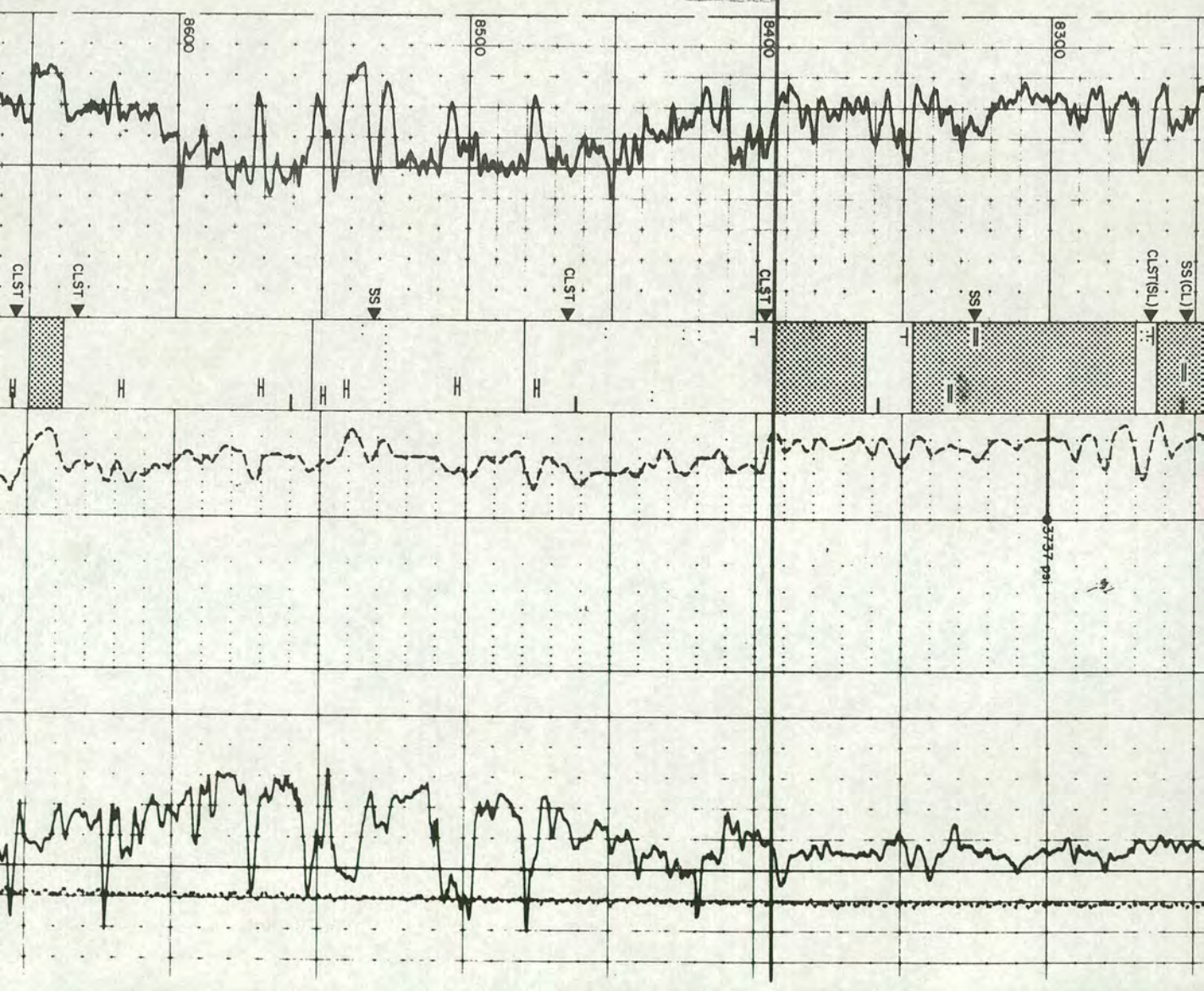

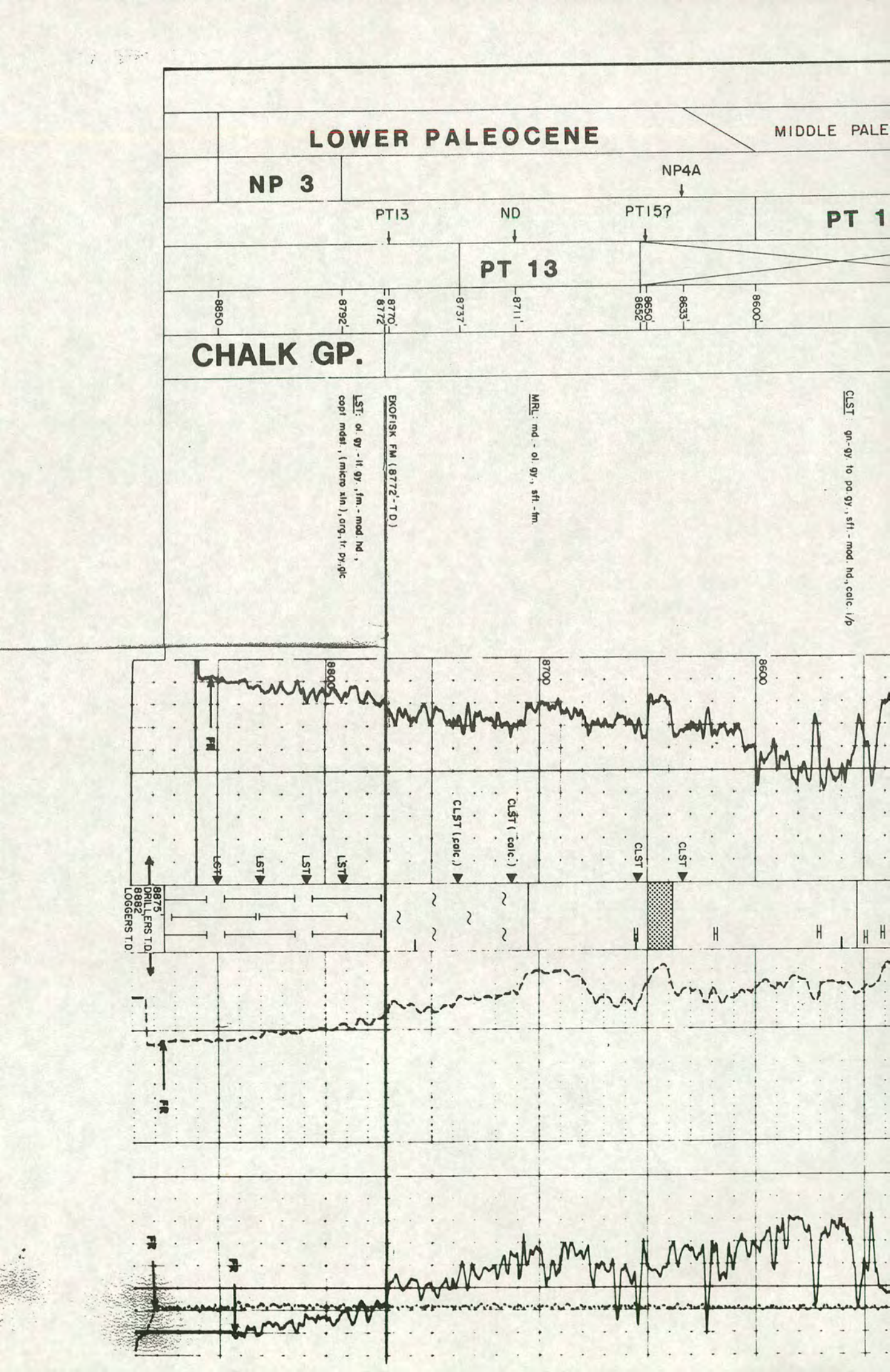
LOWER PALEOCENE
MIDDLE PALE
NP 3
NP4A
PT13
ND
PT15?
PT 1
PT 13
8850
8792'
8770'
8772'
8737'
8711'
8650'
8652'
8633'
8600'
CHALK GP.
LST: ol. gy - lt. gy, fm - mod. hd, copl mdst, (micro xln), arg, tr. py, glc
EKOFISK FM (8772'-T.D.)
MRL: md - ol. gy., sft. - fm.
CLST gn-gy to pa.gy., sft. - mod. hd, calc. i/p
8800
8700
8600
FM
LST
LST
LST
LST
CLST (calc.)
CLST (calc.)
CLST
CLST
8875' DRILLERS T.D.
8882 LOGGERS T.D.
FR
FR
FR

Report

SHELL U.K. EXPLORATION & PRODUCTION

COMPLETION LOG

SCALE 1:500

SHELL/ESSO 21/30-16

EXPLORATION WELL

S
N
"E
)m N
)m E
36' AMSL
9' BMSL
'30' AHBDF
544' AHSS
542' TVSS

LOCATION MAP QUADRANT 21/30

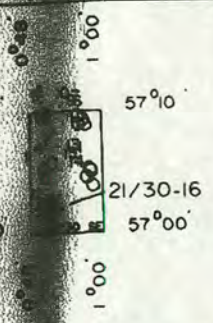

OPERATOR: SHELL UK EXPRO
DATE RIG ON LOCATION: 15.03.90
SPUDDING DATE: 18.03.90
ABANDONMENT DATE: 21.04.90
DATE RIG OFF LOCATION: 21.04.90
WELL STATUS:
PLUGGED AND ABANDONED
MUDLOGGING COMPANY:
EXLOG
LOGGING COMPANY:
SCHLUMBERGER
(+MWD LOGGING BY HALLIBURTON GEODATA)

OBJECTIVE
1. TO TEST THE HYDROCARBON POTENTIAL OF THE EOCENE ROGALAND AND TAY SANDS
2. TO TEST A SMALL STRUCTURAL CLOSURE AT TOP CHALK LEVEL

PRODUCTION LICENCE: P.013
ROUND: 1
INTERESTS:
SHELL 50%
ESSO 50%

WELL COMPLETION

TESTING PERIOD:
14.04.90-17.04.90
TESTED INTERVALS:
NB TWO STAGE PRODUCTION TEST
ZONE 1: INTERVALS PERFORATED
5995'-6005', 6021'-6026',
6035'-6049', 6067'-6078'
ZONE 2: INTERVALS PERFORATED
5925'-5951', 5974'-5986'
(SEE LOG FOR TEST RESULTS)

COMPLETION LOG PREPARED BY:
UEX/12/32/33
DATE: AUGUST 1990

DATA LOADED TO CORPORATE DATABASES BY END JULY 1990

COMPLETION LOG REVISED BY:
INTERVAL:
DATE:

SCHEMATIC

DERRICK FLOOR
MEAN SEA LEVEL
SEA BED

LOGGING (OPEN HOLE UNLESS STATED OTHERWISE)

RUN NUMBER TYPE	DATE 1990	MEASURED INTERVAL	BIT SIZE	BHT (°F)	REMARKS
[illegible]	06.04	5300'-6670'	12 1/4"	149	GR TO SEABED

MUD

TYPE	GRAD. (psi/1000')	HTHP Water loss	RESISTIVITY (Ωm/°F) Scr Surface	RESISTIVITY (Ωm/°F) Scr Bottom hole	TIME since circulated (hours)	SALINITY ppm (Cl)
KCL/POLY	.63	5.0c	.112/58	.047/149	3.5	56

FILTRATE CAKE

RESISTIVITY (Ωm/°F) Rmf	Rmc
.036/149	.117/149

[redacted]

[redacted]

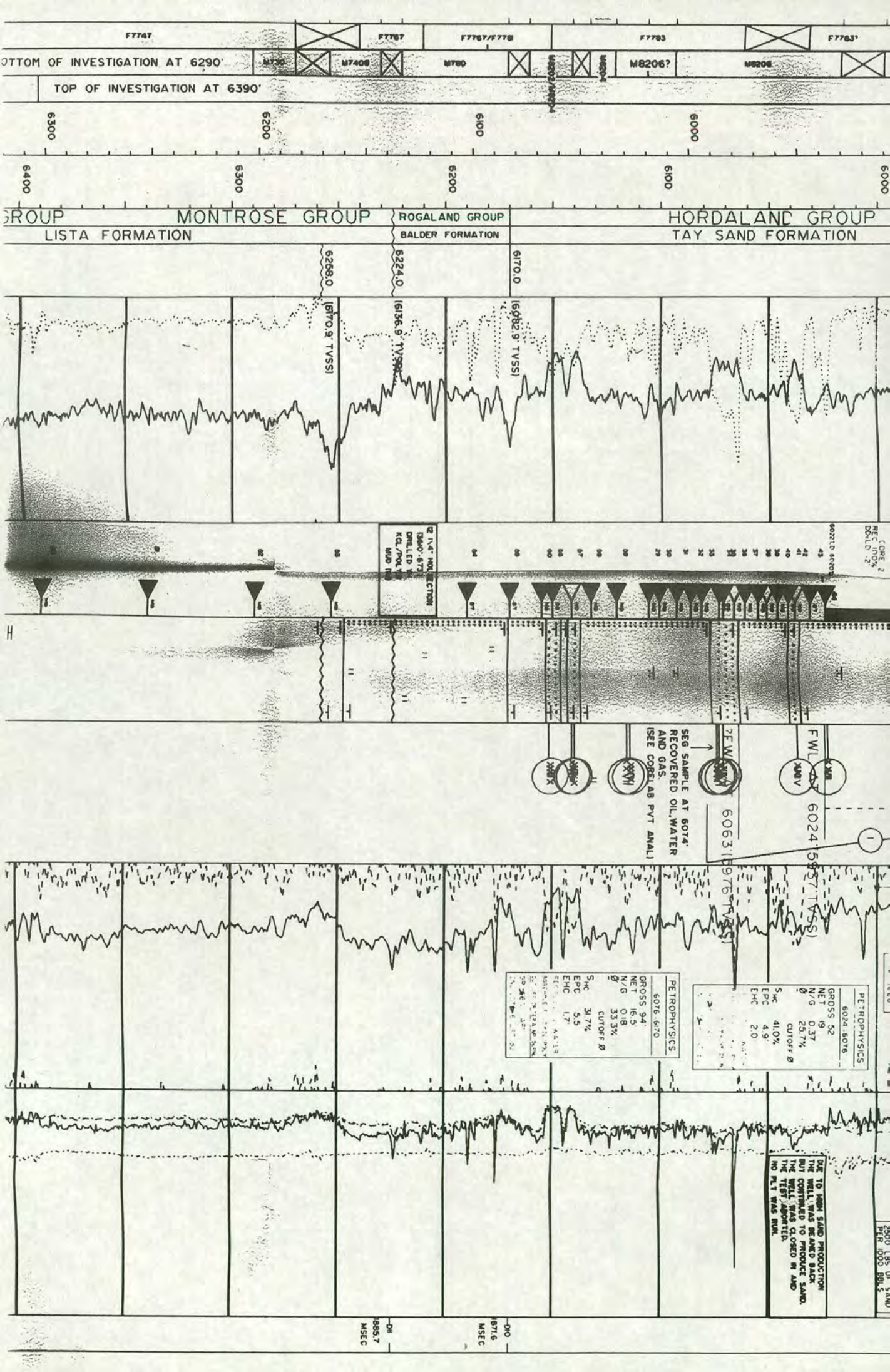
F7747
F7757
F7757/F7758
F7763
F7763'
OTTOM OF INVESTIGATION AT 6290'
M730
M7408
M780
M8206?
M8206
TOP OF INVESTIGATION AT 6390'
6300
6200
6100
6000
6400
6300
6200
6100
6000
GROUP
MONTROSE GROUP
LISTA FORMATION
ROGALAND GROUP
BALDER FORMATION
HORDALAND GROUP
TAY SAND FORMATION
6259.0
6224.0
6170.0
(6170.9' TVSS)
(6136.9' TVSS)
(6082.9' TVSS)
SEG SAMPLE AT 6074' RECOVERED OIL, WATER AND GAS. (SEE CORE LAB PVT ANAL.)
FWL
6024
6063
6076
PETROPHYSICS
6076-6070
GROSS 94'
NET 16.5
N/G 0.18
Ø 33.3%
CUTOFF Ø
Shc 31.7%
EPC 5.5
EHC 1.7
PETROPHYSICS
6024-6076
GROSS 52
NET 19
N/G 0.37
Ø 25.7%
CUTOFF Ø
Shc 41.0%
EPC 4.9
EHC 2.0
DUE TO HIGH SAND PRODUCTION THE WELL WAS BEANED BACK BUT CONTINUED TO PRODUCE SAND. THE WELL WAS CLOSED IN AND THE TEST ABORTED. NO PLT WAS RUN.
1885.7 MSEC
DH
1871.6 MSEC
DHO

MESOZOIC		CENOZOIC		CENOZOIC	
UPPER CRETACEOUS		LOWR TERTRY		LOWER TERTIARY	
U MAASTRICHTIAN		L PALEOCENE		LOWER PALEOCENE/UPPER PALEOCENE	
		PT11		PT13	PT16
F690		F730		F7743	F7746

N603 | N604 | ND

6600 | 6500 | 6400

6700 | 6600 | 6500

CHALK GROUP | MONTROSE GROUP | MONTROSE G

TOR FORMATION | EKOFISK FORMATION | MAUREEN MARL FORMATION

6730.0 | 6663.0 | 6617.0 | 6492.0

(6642.3 TVSS) | (6676.3 TVSS) | (6629.4 TVSS) | (6404. TVSS)

SONIC

GR

BCSL J 200

GAM J 330

140 40

0 150

12¼" HOLE SECTION
CEMD. 9⅝" @
DRILLED WITH
KCL/POL MUD SYSTEM

9⅝" @ AT 6643

49 | 47 | 49 | 49

6730.0 AHD (F1)
21/30-16

CNL J 330

FDC J 330

45 -15

1.95 2.95

CNL

FDT

MG .630

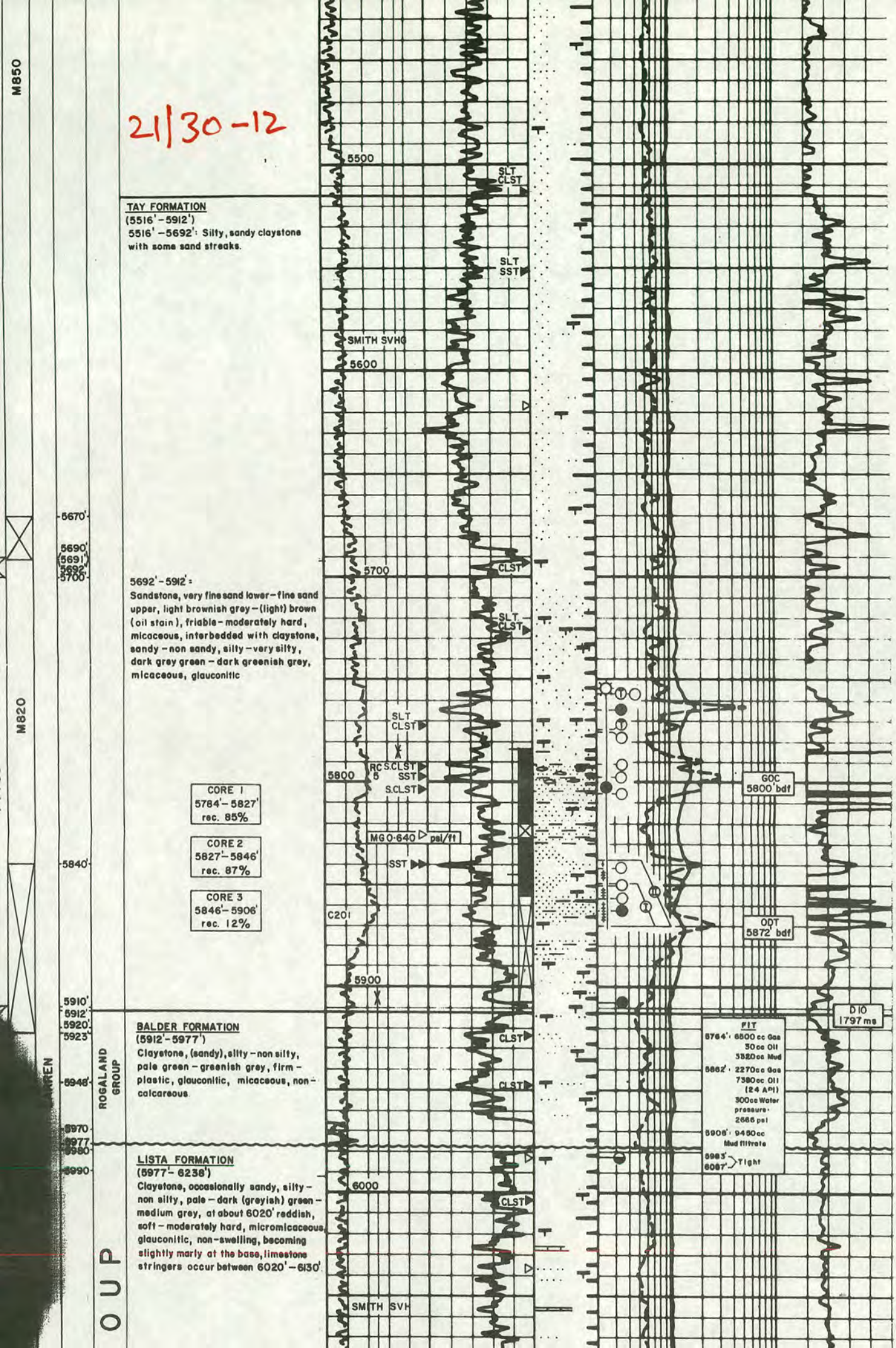
21/30-12
TAY FORMATION
(5516'-5912')
5516'-5692': Silty, sandy claystone with some sand streaks.
5692'-5912':
Sandstone, very fine sand lower-fine sand upper, light brownish grey-(light) brown (oil stain), friable-moderately hard, micaceous, interbedded with claystone, sandy-non sandy, silty-very silty, dark grey green-dark greenish grey, micaceous, glauconitic
CORE 1
5784'-5827'
rec. 85%
CORE 2
5827'-5846'
rec. 87%
CORE 3
5846'-5906'
rec. 12%
BALDER FORMATION
(5912'-5977')
Claystone, (sandy), silty-non silty, pale green-greenish grey, firm-plastic, glauconitic, micaceous, non-calcareous
LISTA FORMATION
(5977'-6238')
Claystone, occasionally sandy, silty-non silty, pale-dark (greyish) green-medium grey, at about 6020' reddish, soft-moderately hard, micromicaceous, glauconitic, non-swelling, becoming slightly marly at the base, limestone stringers occur between 6020'-6130'
ROGALAND GROUP
M850
M820
5500
5600
5700
5800
5900
6000
SMITH SVHQ
SMITH SVH
SLT CLST
SLT SST
CLST
S.CLST
SST
RC 5
MG 0-640 psi/ft
C201
GOC 5800' bdf
OOT 5872' bdf
D10 1797 ms
FIT
5764': 6500 cc Gas
30 cc Oil
3320 cc Mud
5882': 2270 cc Gas
7380 cc Oil (24 API)
300 cc Water
pressure: 2666 psi
5908': 9450 cc Mud filtrate
5983'/6087' Tight
5670'
5690'
(5691')
5692'
5700'
5840'
5910'
5912'
5920'
5923'
5948'
5970'
5977'
5980'
5990'

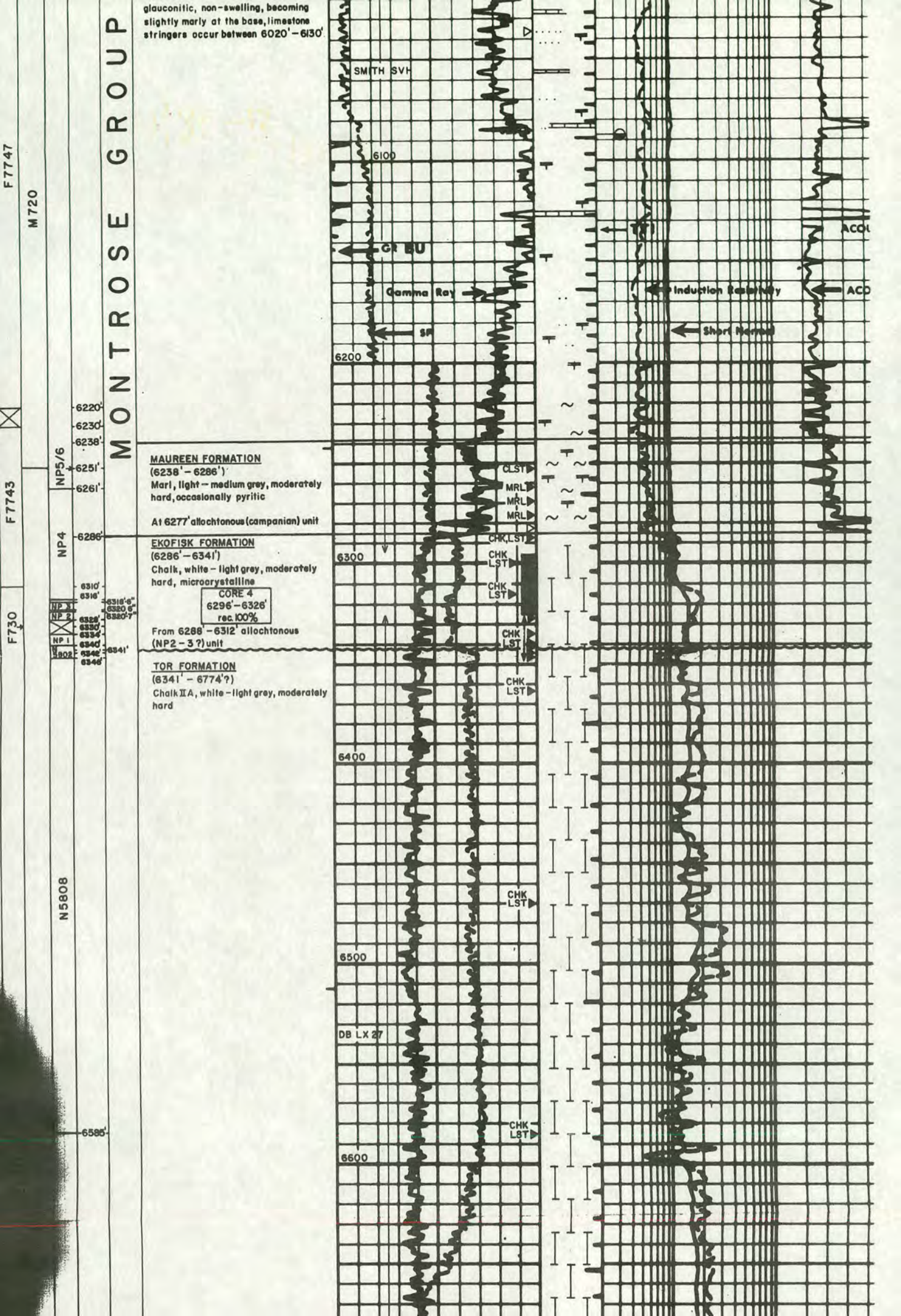
glauconitic, non-swelling, becoming slightly marly at the base, limestone stringers occur between 6020'-6130'
SMITH SVH
6100
Gamma Ray
SP
Induction Resistivity
Short Normal
6200
MONTROSE GROUP
F7747
M720
F7743
F730
N5808
NP5/6
NP4
NP 3
NP 2
NP 1
6220'
6230'
6238'
6251'
6261'
6286'
6310'
6316'
6318'6"
6320'6"
6320'7"
6328'
6330'
6334'
6340'
6344'
6346'
6341'
6585'
MAUREEN FORMATION
(6238'-6286')
Marl, light-medium grey, moderately hard, occasionally pyritic
At 6277' allochtonous (campanian) unit
EKOFISK FORMATION
(6286'-6341')
Chalk, white-light grey, moderately hard, microcrystalline
CORE 4
6296'-6326'
rec. 100%
From 6288'-6312' allochtonous (NP2-3?) unit
TOR FORMATION
(6341'-6774'?)
Chalk IIA, white-light grey, moderately hard
CLST
MRL
MRL
MRL
CHK,LST
CHK LST
CHK LST
CHK LST
CHK LST
CHK LST
CHK LST
6300
6400
6500
6600
DB LX 27

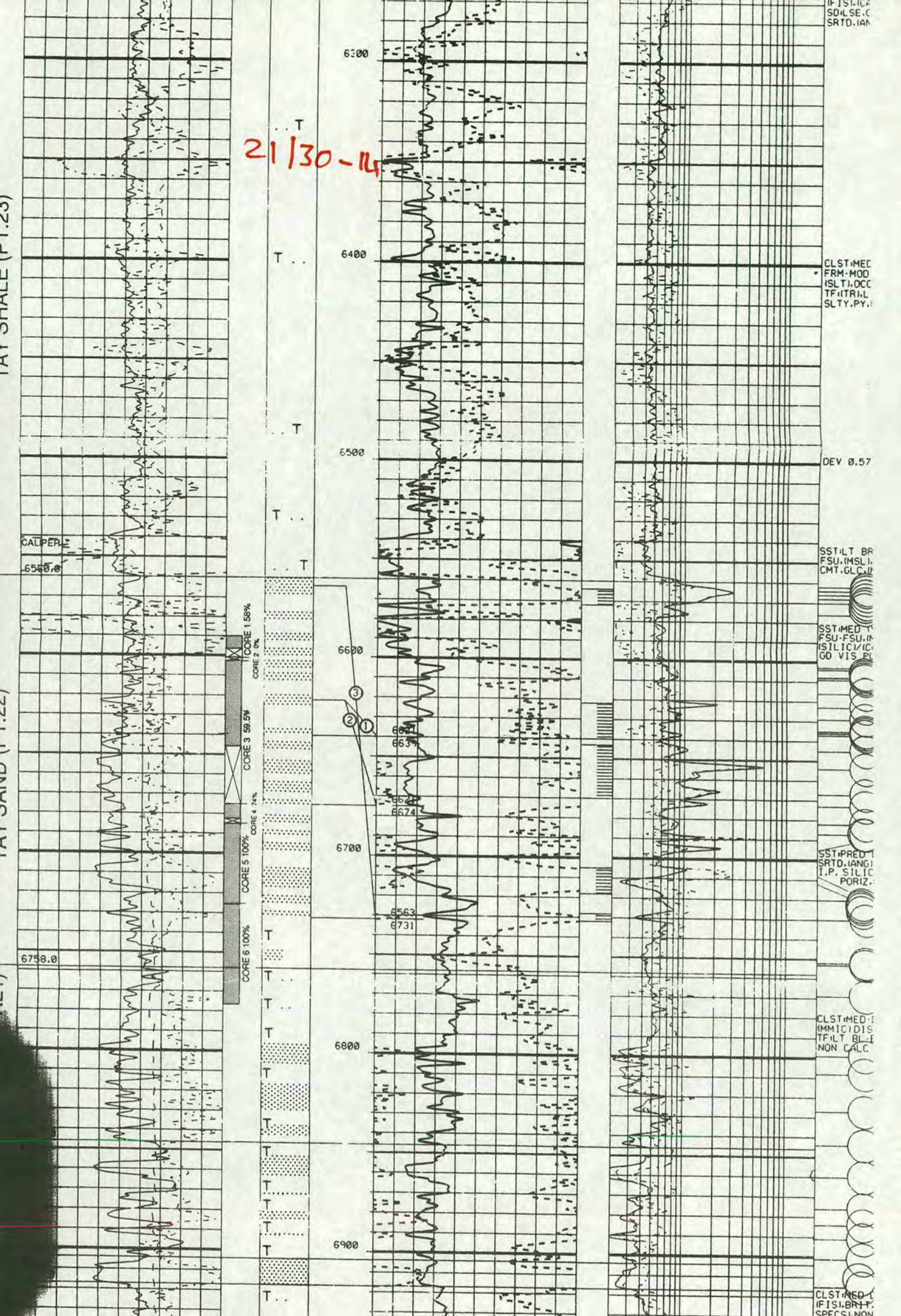
21/30-14
CALPER
6560.0
6600
6700
6758.0
6800
6900
6400
6500
CORE 1 58%
CORE 2 0%
CORE 3 59.5%
CORE 4 74%
CORE 5 100%
CORE 6 100%
6631
6634
6674
6563
6731
DEV 0.57
TAY SAND (PT.22)
TAY SHALE (PT.23)

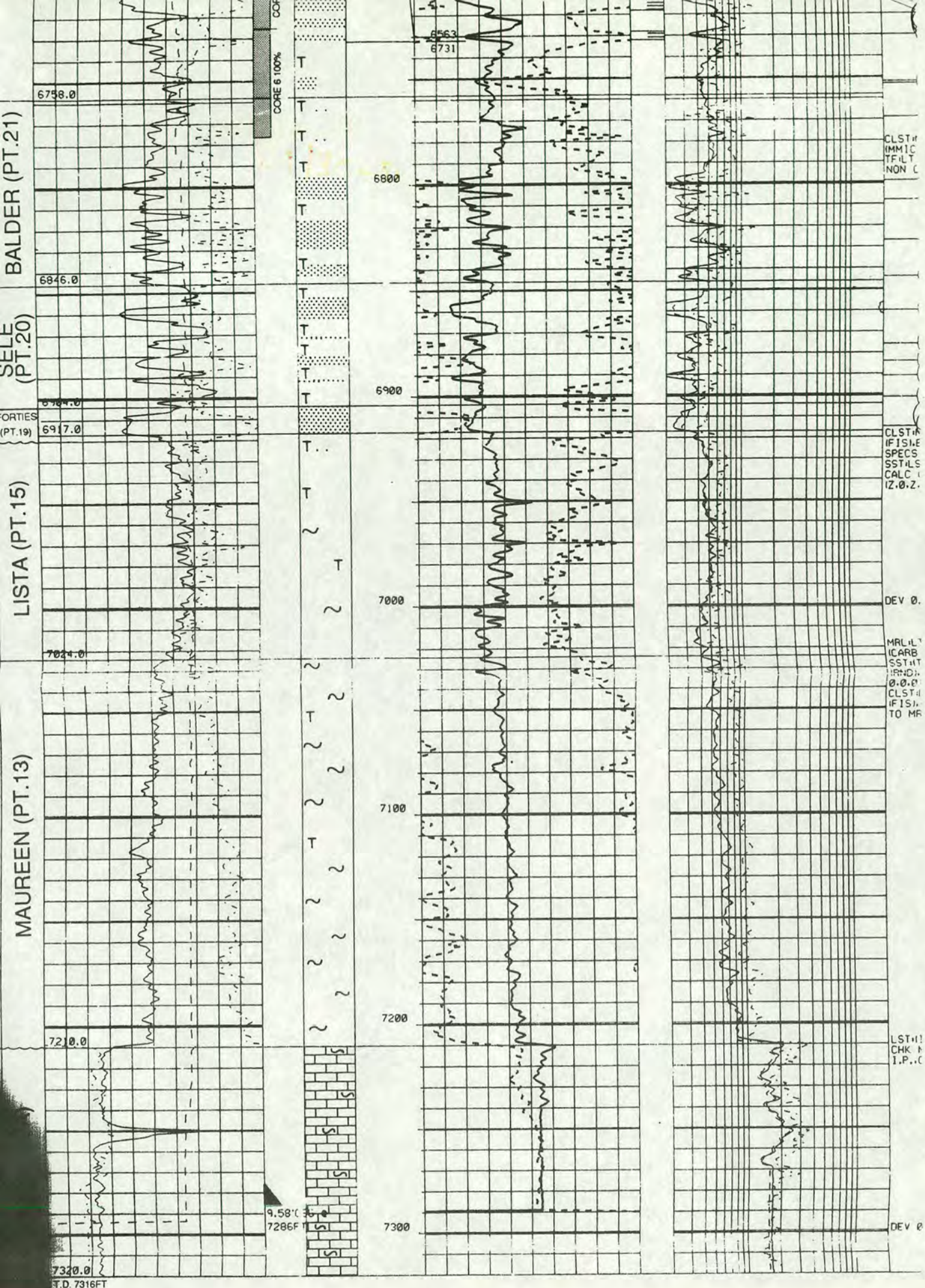
BALDER (PT.21)
SELE (PT.20)
FORTIES (PT.19)
LISTA (PT.15)
MAUREEN (PT.13)
6758.0
6846.0
6917.0
7024.0
7210.0
7320.0
T.D. 7316FT
6563
6731
6800
6900
7000
7100
7200
7300
CORE 6 100%
DEV 0.
DEV 0
BCSL R 206
200
100
GR R 330
0
150
CALF R 356
CNL R 310
45
15
FDC R 325
1.95
2.95
LL9D R 148
0.20
20
LL9S R 141
0.20
20
MILL R 151
20

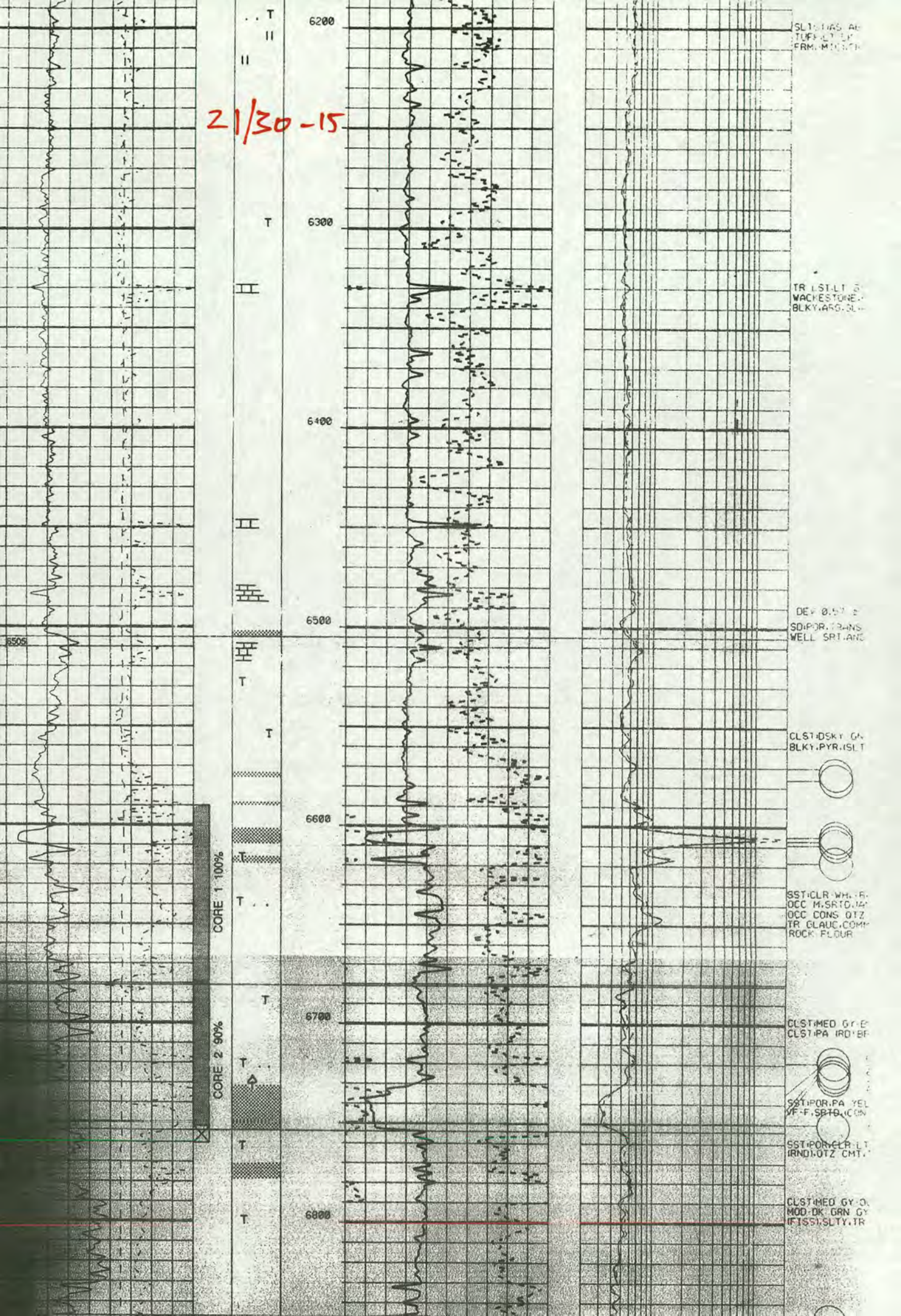
21/30-15
6200
6300
6400
6500
6505
6600
6700
6800
CORE 1 100%
CORE 2 90%
TR LST-LT
WACKESTONE
BLKY,ARG,SL
CLST-DSKY GN
BLKY,PYR,ISLT
SST-CLR WH-R
OCC M,SRTD,IA
OCC CONS QTZ
TR GLAUC,COMM
ROCK FLOUR
CLST-MED GY-BR
CLST-PA IRD-BR
SST-POR,PA YEL
VF-F,SBTD,ICON
SST-POR,CLR-LT
IRND),QTZ CMT,
CLST-MED GY-O
MOD-DK GRN GY
IFISS),SLTY,TR

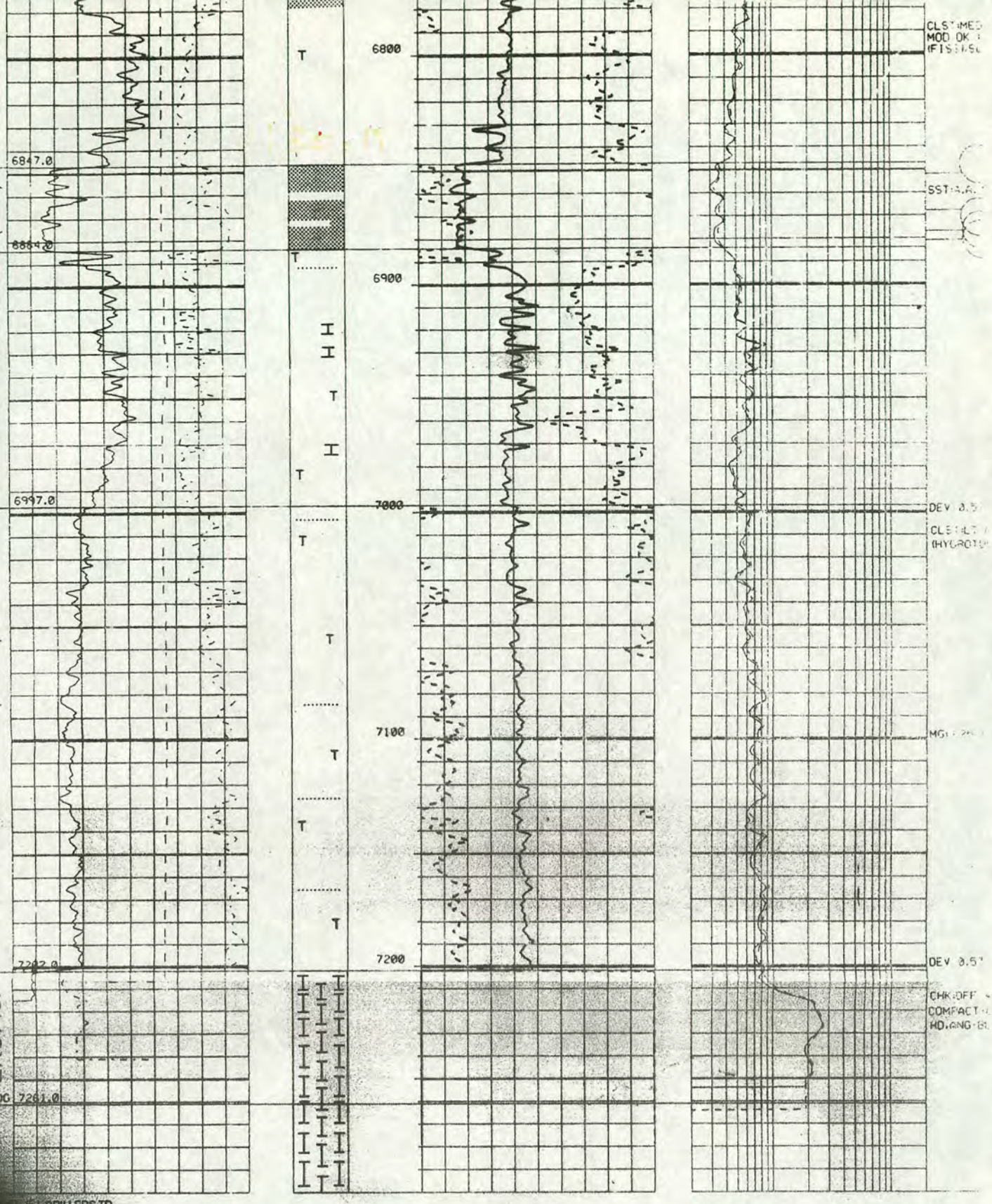
6847.0
6997.0
7202.0
7261.0
6800
6900
7000
7100
7200
DEV 8.5°
DEV 8.5°
T DRILLERS TD
BCSL R 206
100
GR R 338
150
GRIC R 337
150
CALF R 356
16
CNL R 310
45
15
FDC R 325
1.95
2.95
DILM R 115
0.20
20
DILD R 116
0.20
20

Appendix 3

Core Description Logs

Core Description

Well Name: 22/26A-1
Location:
Date: 21/2/01

Sheet: 1 of 2

Depth	Stratigraphy	Core Status	Lithology	Sedimentary Structure and Grain Size	Description and Comments	Interpretation
7529						This section represents facies association 1 which Massive sandstone. These units are deposited by medium - high density turbidity currents. It is typical of amalgamated channels - Fills or depositional lobes.
7532						
7535						
7538						
7541						
7544						
7547						
7550					- blackish grey, V.F-F, Sheet like sand, mud streaks towards top.	
7553					- Fining upward sequences, light grey to dark grey, parallel lamination f. sand to V.f & siltstone → Sheet like sand	
7556					- Light grey, consolidated, V.f-F, well sorted sand	
7559						
7562						
7565					Brownish grey, fine to medium grained, beach like unconsolidated sand.	
7568						
7571						
7574						
7577						
7580						
7583						
7586					- Brownish grey, F-M, beech like unconsolidated sand	
7589						

Coal | Clay | Silt | Very Fine | Fine | Medium | Coarse | Very Coarse | Granule | Pebble
Sandstone — Congl.

Core Description

Well Name: 22/26A-1
Location:
Date: 22/2/01

Depth	Stratigraphy	Core Status	Lithology	Sedimentary Structure and Grain Size	Description and Comments	Interpretation
7467						
7470						
7473						
7476					- greenish grey, hard, well cemented siltstone	
7479						
7482					- Brownish grey, well sorted, well cemented silty sandstone - Black, parallel laminated siltstone.	
7485						
7488						
7491						
7494						
7497					- light grey v.f massive sand. - greenish grey, parallel laminated siltstone - Light grey → dark grey intervals of VF-F, planar parallel laminated well sorted sand becoming finer & more siltier at the top with some mud clasts.	
7500		U				
7503		Q1				
7506						
7509						
7511					- Brownish grey, F-M, well sorted, non consolidated, beach-like sand.	
7514						
7517						
7520						
7523						
7526						

Coal | Clay | Silt | Very Fine | Fine | Medium | Coarse | Very Coarse | Granule | Pebble
Sandstone — Congl.

Core Description

Well 21/30-17
Sheet 1

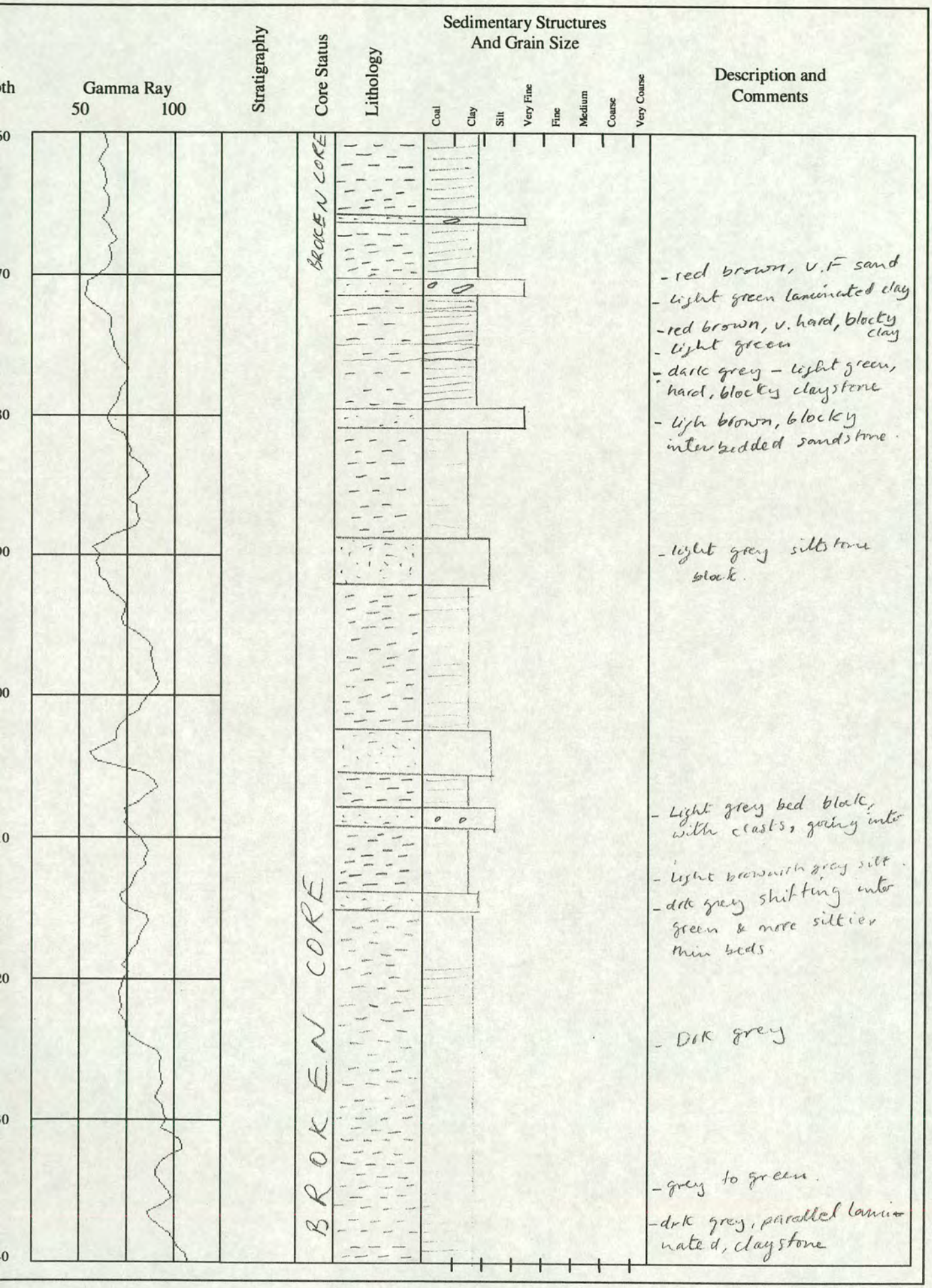

Core Description

Well 21/30-17
Sheet 2

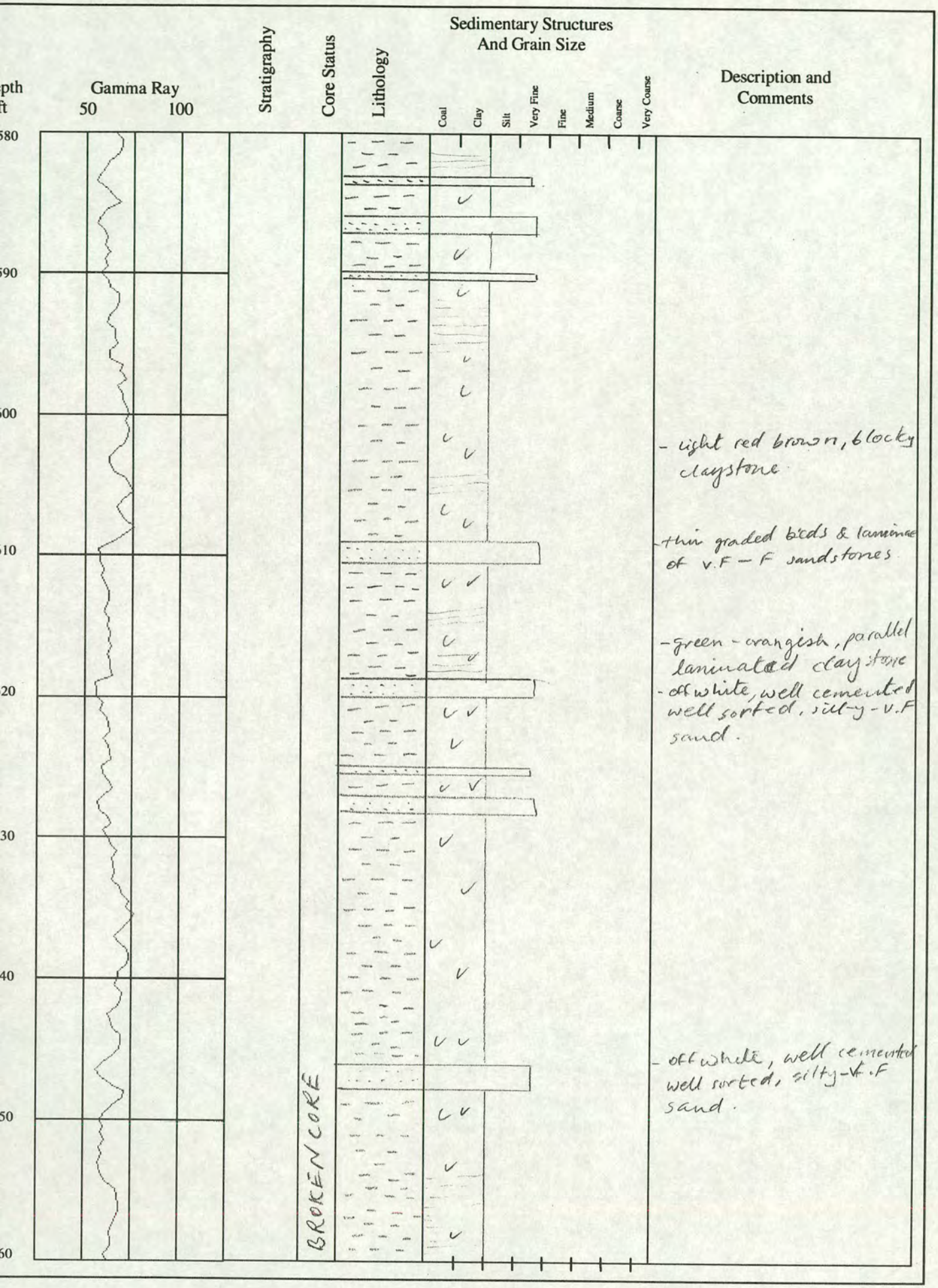

Core Description

Well 21/30-17
Sheet 3

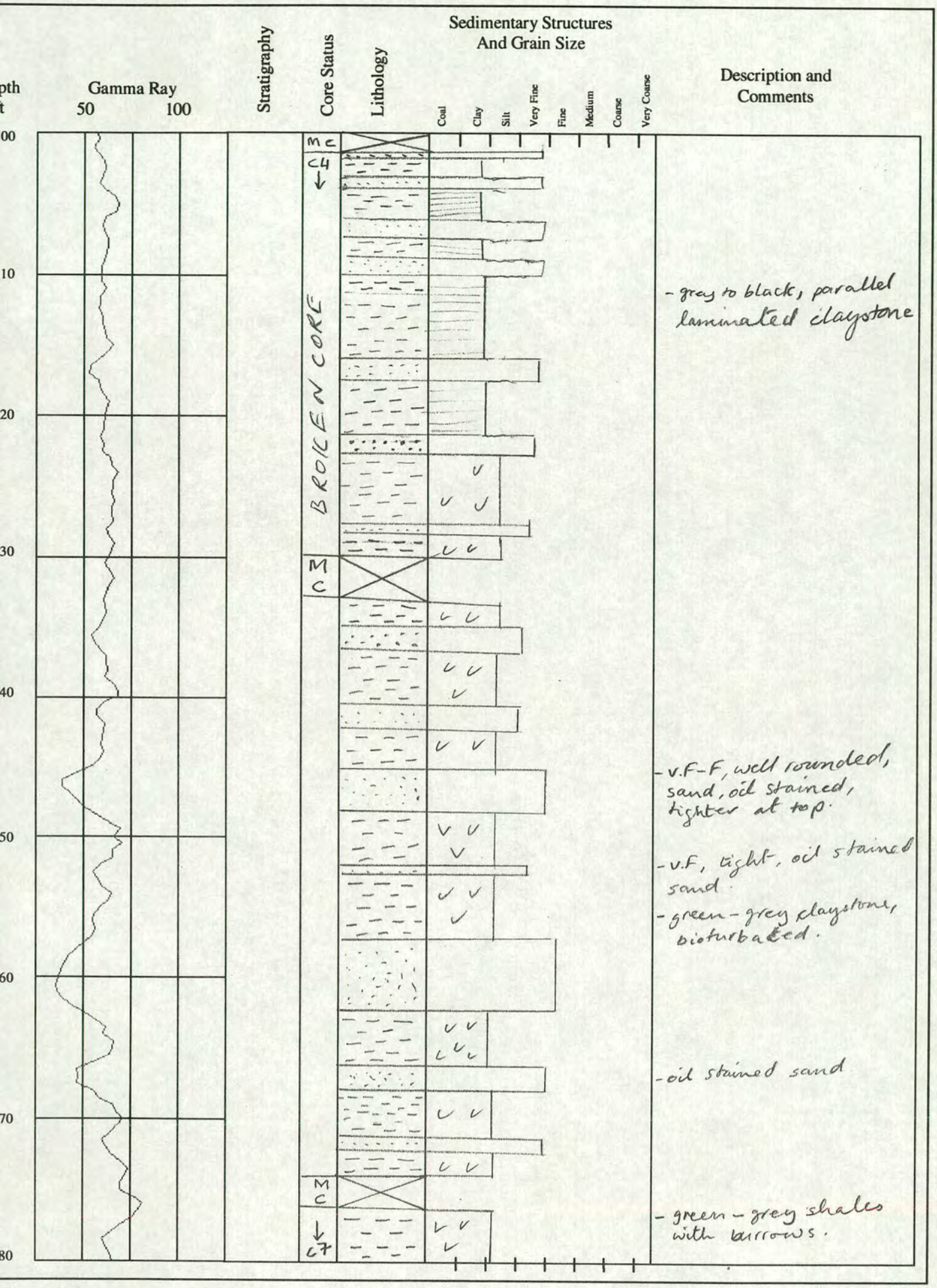

Core Description

Well 21/30-17
Sheet 4

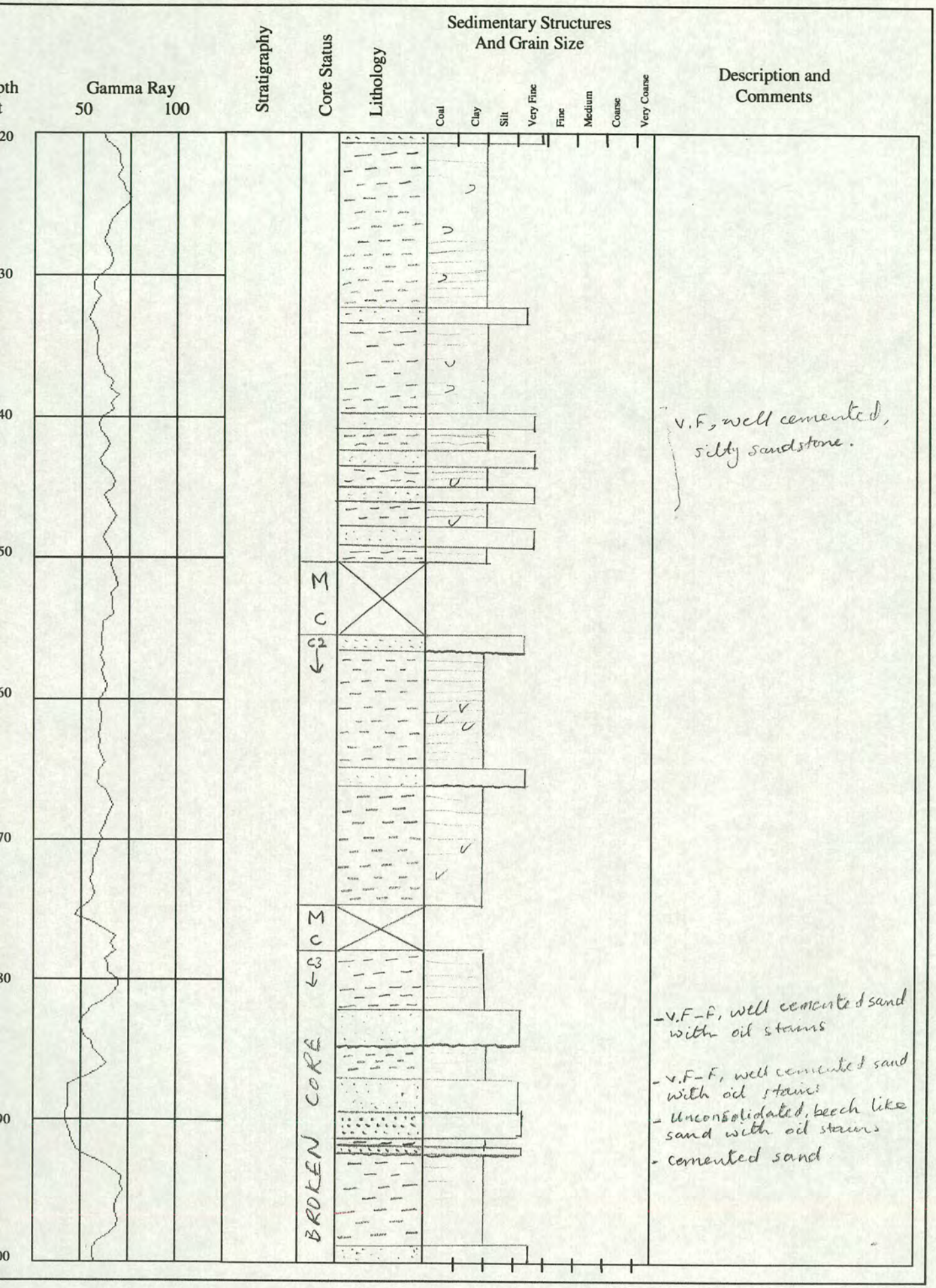

Core Description

Well 21/30-17
Sheet 5

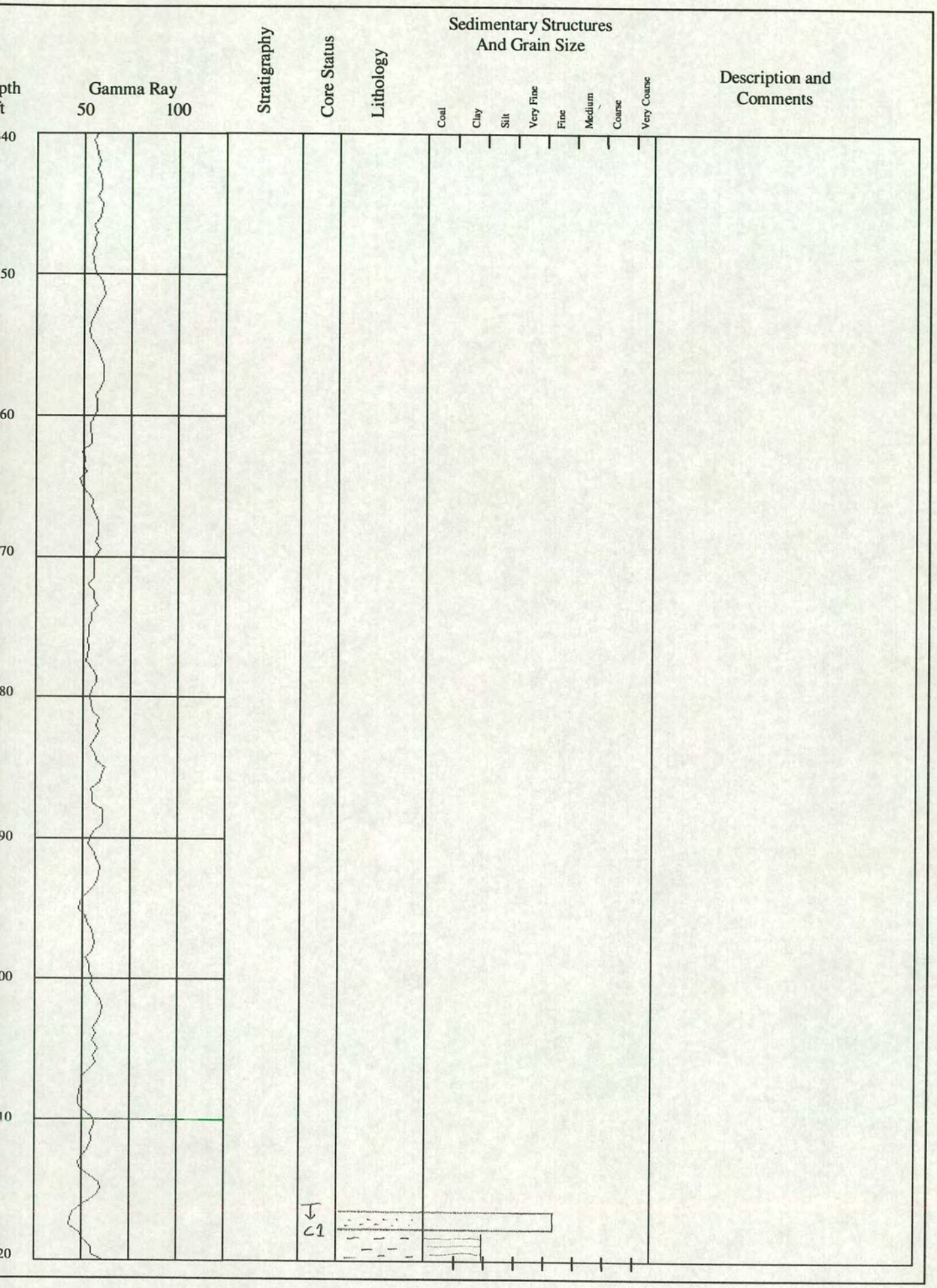

Well Name: 21/29b-9
Location:
Date: 19-2-01

Core Description
Core 5 & 6.

Sheet: 1 of 3

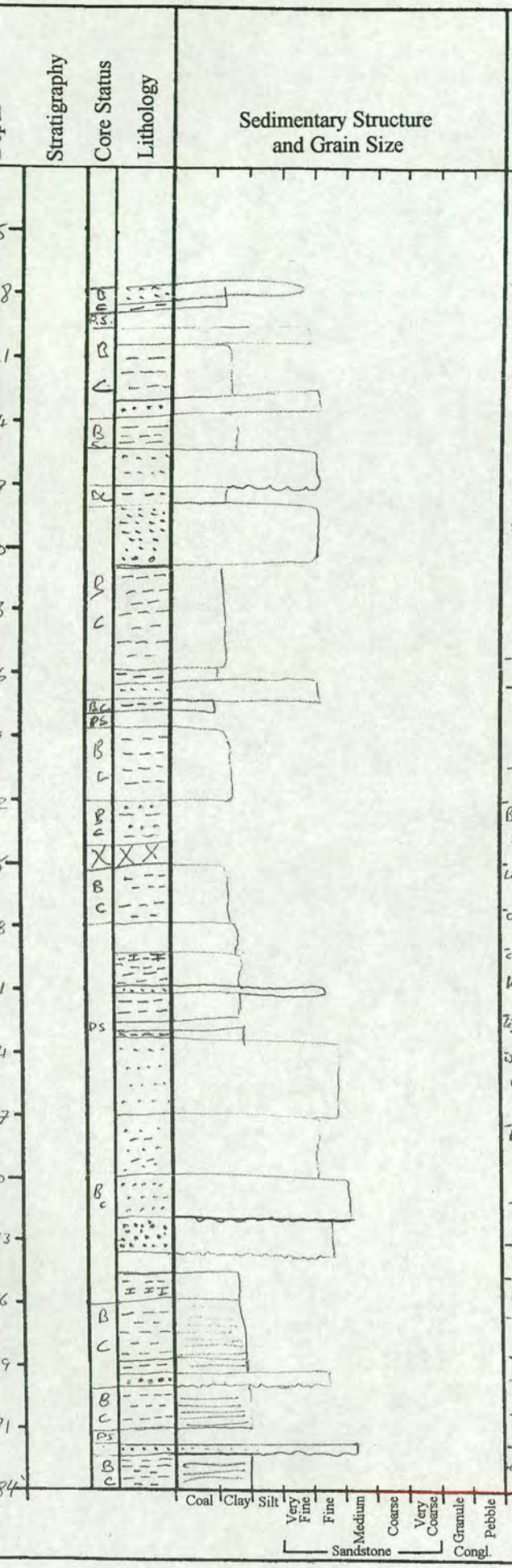

Sedimentary Structure and Grain Size	Description and Comments	Interpretation
	oil stains.	This well mostly represents interolithic facies association typical of channel-levee complexes resulting from overbank deposits &/or inter channel or basin plain environment deposition from distal turbidity currents.
	oil stains	
	sand with oil stains	
	- claystone - w/g, f/m, well cemented, sorted sand with some oil stains.	
	- claystone.	
	Broken claystone with some oil staining sandstone pieces.	
	light green, laminated claystone	
	darker claystone	
	claystone a.b. top has carbonaceous lignite high % sand, sorted with oil stains.	
	light green homogeneous claystone.	
	white/grey, fine/med, sorted sand with abrupt top going to mud.	
	highly broken core which has a mixture of sand & mud. more sand	
	- dark grey sand which coarser than below with sharp irregular base - white/grey fine/medium, well sorted, high % sand. - Green claystone with scattered red clay flakes. Carbonaceous content fizzes (HCl) - Same as below.	
	- Light green, laminated claystone - white/grey fine/medium, well sorted, high % sand. - Light green, laminated claystone.	
	- white/grey, fine/medium, well cemented, moderately sorted, high % sand light green, some grey claystone, homogeneous might be parallel laminated.	

Broken Core. ——— sharp
~~~ irregular
~~~

Well Name: 21/29b-9
Location:
Date:

Core Description
Core 3 & 4

Sheet: 2 of 3

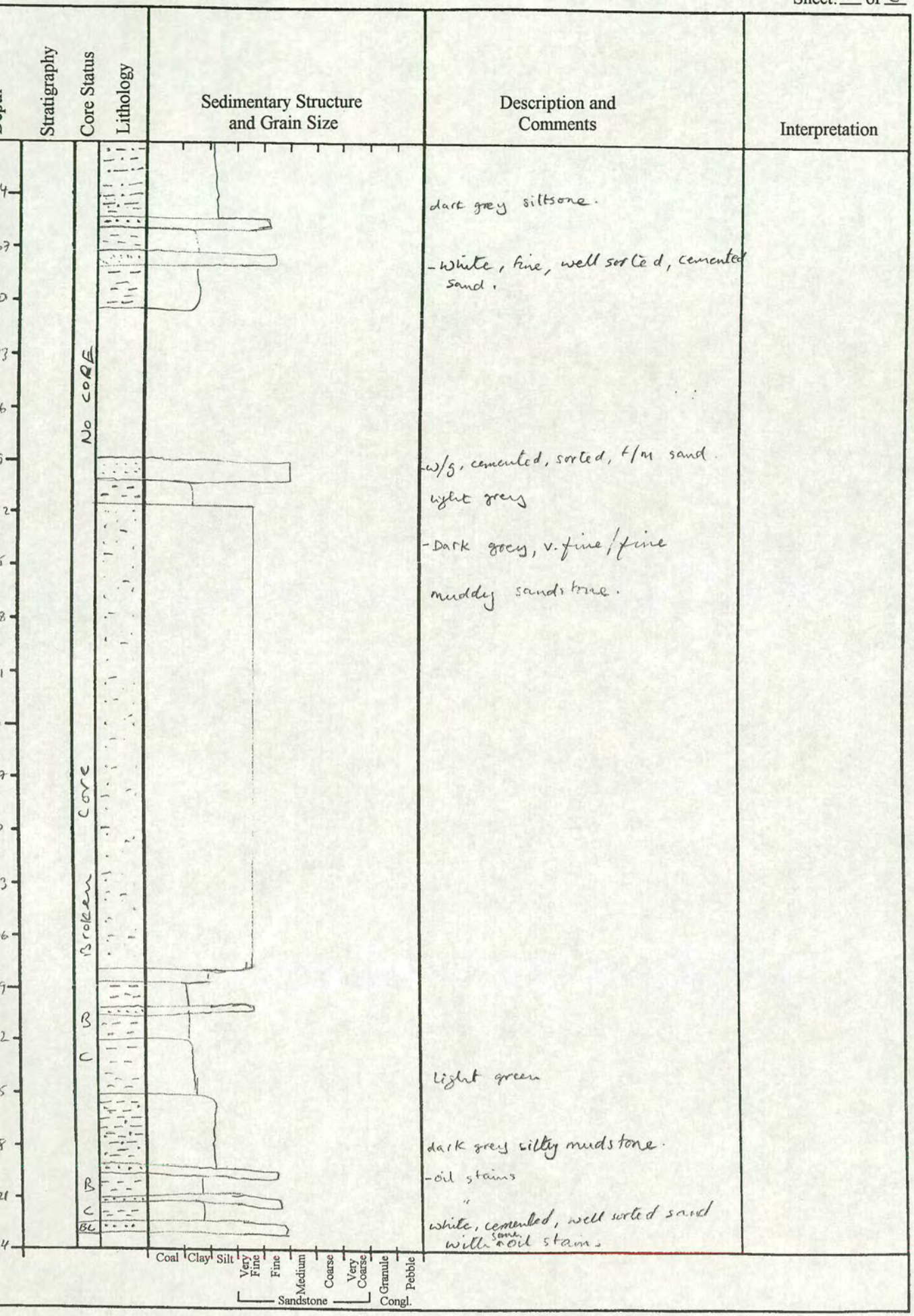

Name: 21/29b-9 Locality: _____ Grid Ref./Well Log: _____ Date: _____

Sheet: 3 of 3

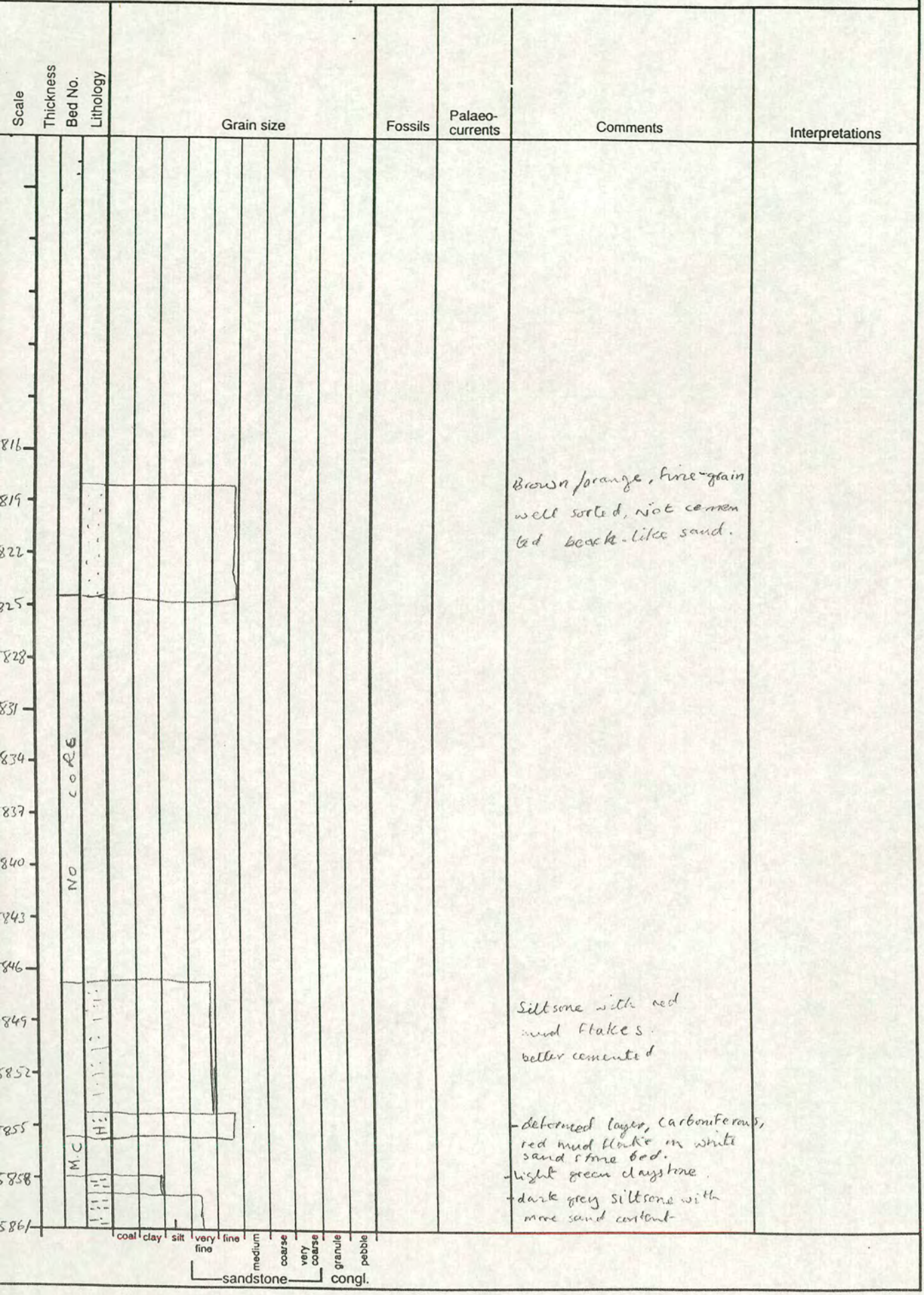

Brown/orange, fine-grain well sorted, not cemented beach-like sand.

Siltsone with red mud flakes. better cemented

- deformed layer, carboniferous, red mud flakes in white sand stone bed.
- light green claystone
- dark grey siltsone with more sand content

M.C Missing Core

Core Description

Well Name: 21/30 - 14
Location:
Date: 21/2/01

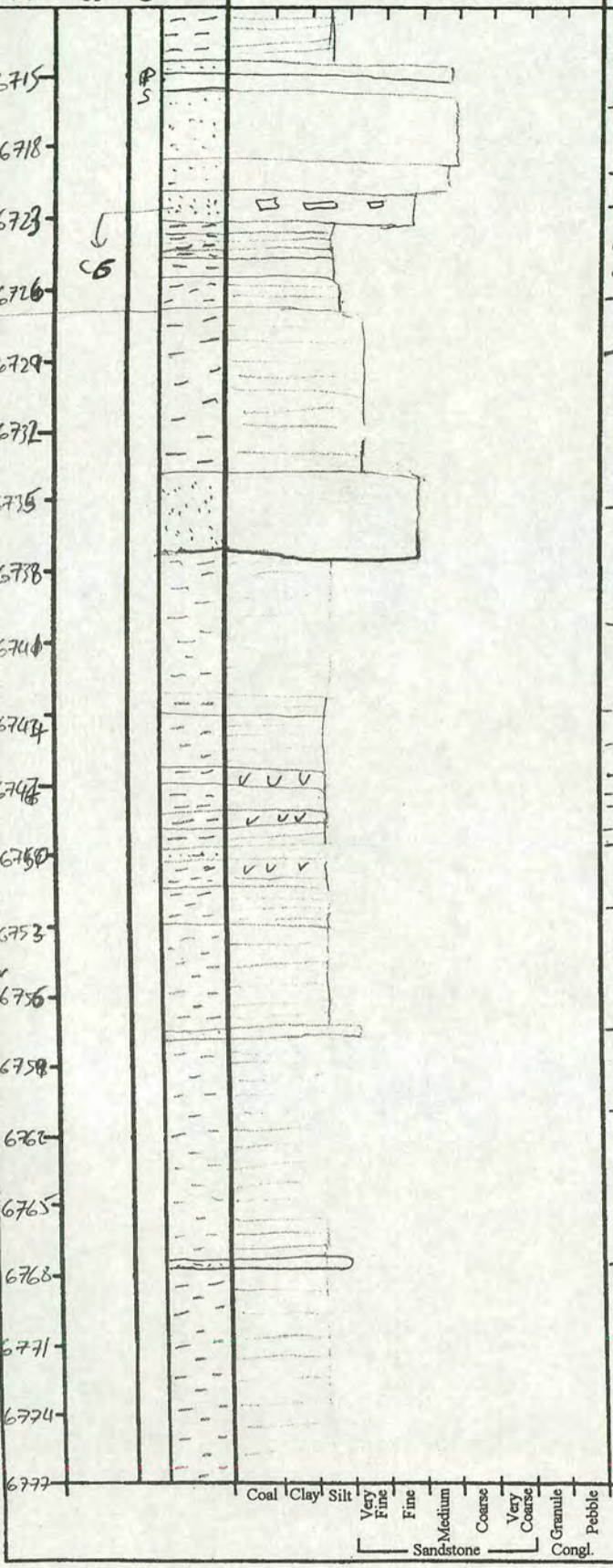

Sedimentary Structure and Grain Size

Description and Comments

- light grey going into brownish due to oil stains.
- light grey, f, well sorted, cemented
- light grey, v.f-f, well sorted, cemented with mud clasts. interbedding between drk grey & light green beds.
- light green.
- red brown, parallel laminated siltstone.
- light grey, f→m, well sorted massive sand with a sharp uprupt base.
- red brown, parrallel laminated
- green transition
- red brown
- green, massive full of burrows.
- red brown
- green full of burrows.
- red brown
- green, vf-f well cemented sand burrows.
- Colour change from grey to green then to red brown.
- light grey, v.f-f sand
- drk grey
- light grey sand, silt-v fine.
- greenish grey, parallel laminated, massive siltstone.

Interpretation

This well mostly represents heterolithic facies association typical of channel-levee complexes resulting from overbank &/or interchannel or basin plain environment deposition from distal turbidity currents.

Core Description

Well Name: 21/30-14
Location:
Date: 21/2/01

Sheet: 2 of 3

Depth	Stratigraphy	Core Status	Lithology	Sedimentary Structure and Grain Size	Description and Comments	Interpretation
6652					Missing core thought to have more sand as observed in G.R. response.	
6655						
6658		MISSING CORE				
6661						
6664						
6667						
6670						
6673						
6676		P.S.				
6679					- brownish grey, due oil, f-M, well sort well cemented, lamination towards top.	
6682					- Light grey, with parallel lamination, V.f, well sorted, well cemented sand.	
6685		M.C.				
6688					- brownish grey going into brown due to oil staining, V.f, well sorted well cemented sandstones, massive no internal structures interbedded with drk grey siltstones	
6691					- drk grey → blk siltstone	
6694						
6697					- light grey, V.F, well sorted, well cemented with mudclasts towards top	
6700		P.S.			-drk grey → blk siltone.	
6703					- Light grey going into brownish due to oil staining, V.f-f well sorted, massive sand, no structure, no grading.	
6706		P.S.				
6709					- colour changes to darker grey	
6712					- light grey, V-fine, well cemented sand interbedded with parallel laminated silt. - light green, laminated siltstone.	

Coal | Clay | Silt | Very Fine | Fine | Medium | Coarse | Very Coarse | Granule | Pebble

Sandstone — Congl.

Core Description

Well Name: 21/30-14
Location:
Date: 21-2-01

Sheet: 3 of 3

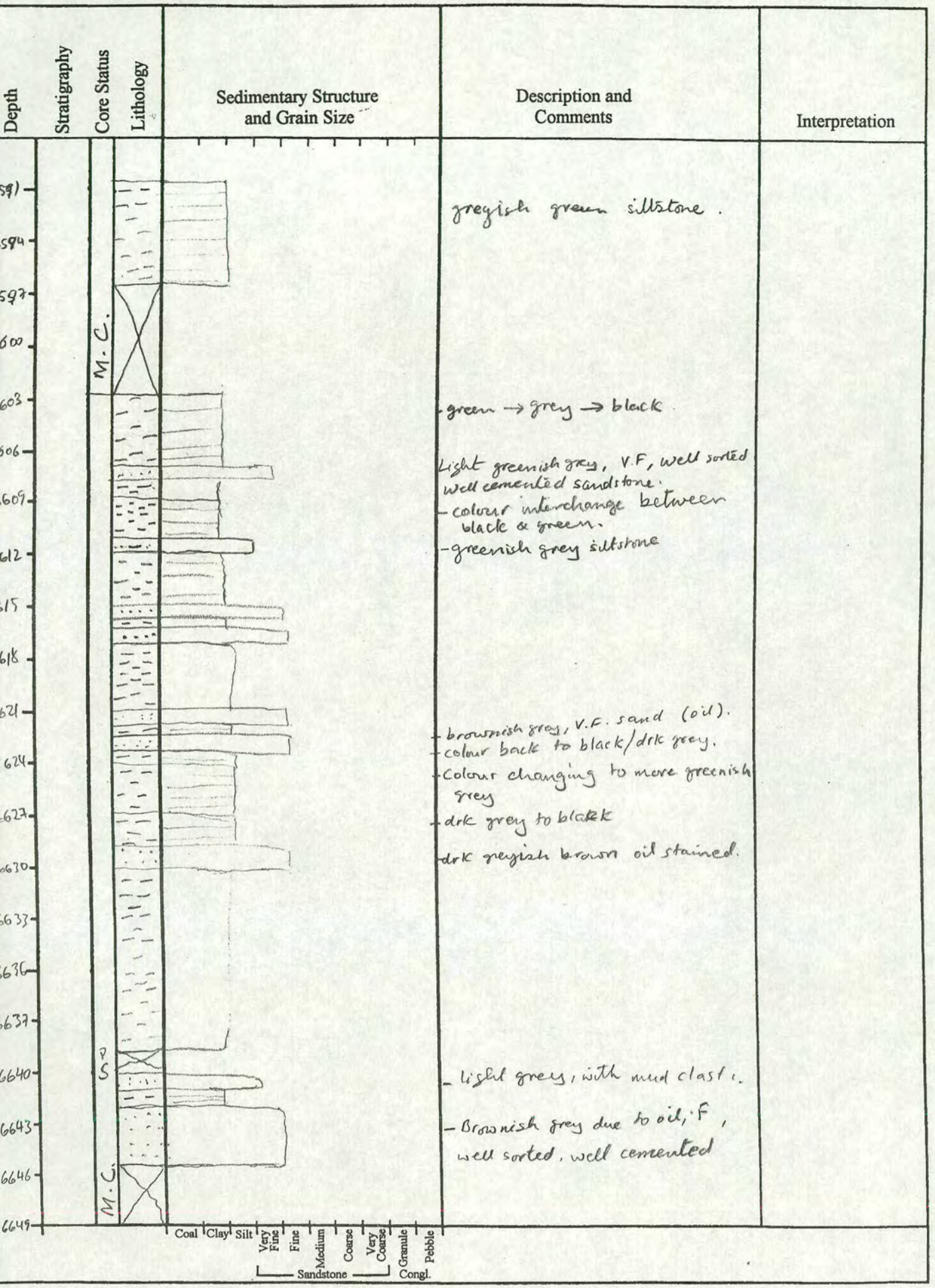

Core Description

Well Name: 21/30 - 15
Location:
Date: 21/2/01

Sheet: 1 of 3

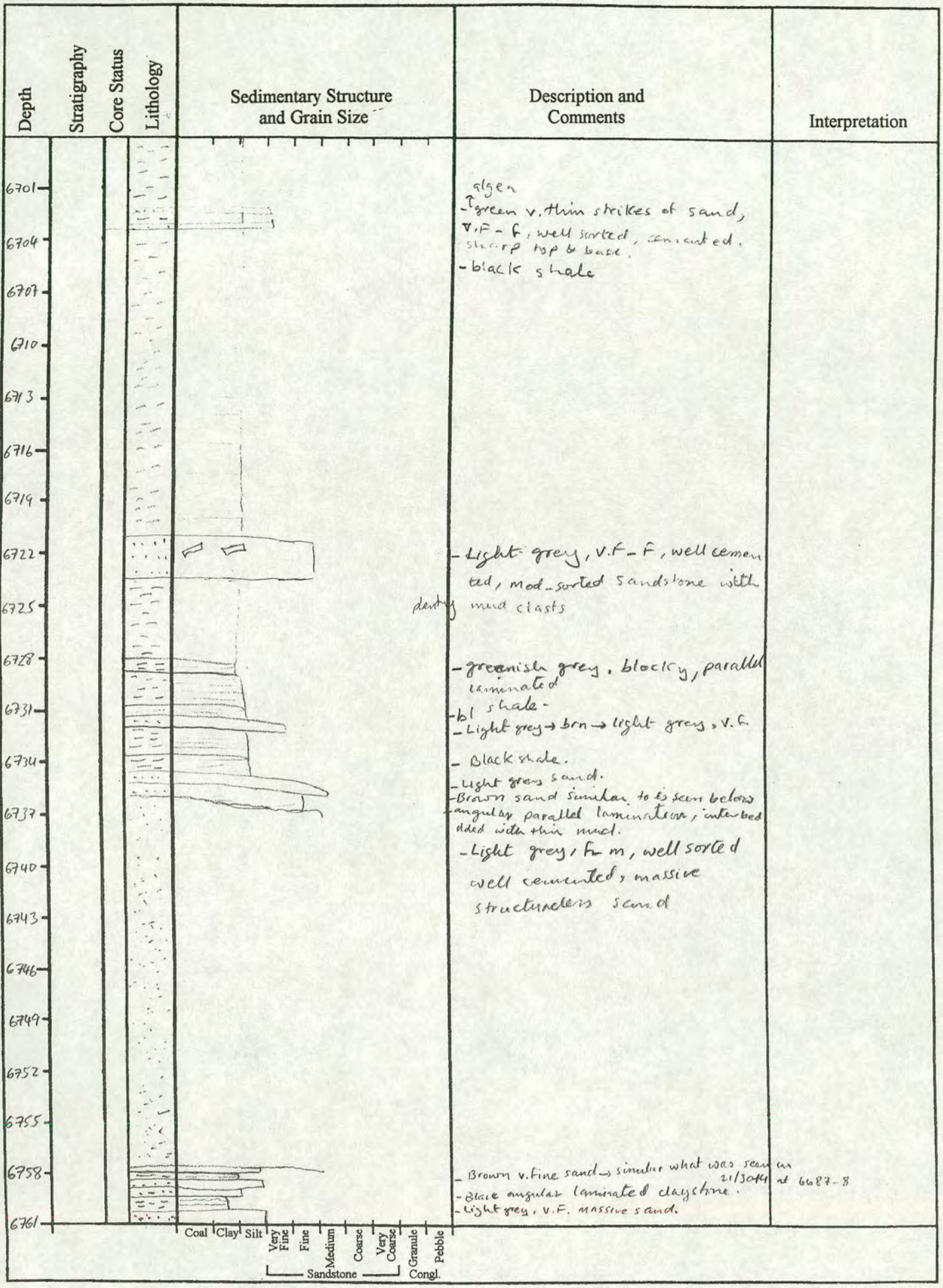

Core Description

Well Name: 21/30-15
Location:
Date: 21/2/01

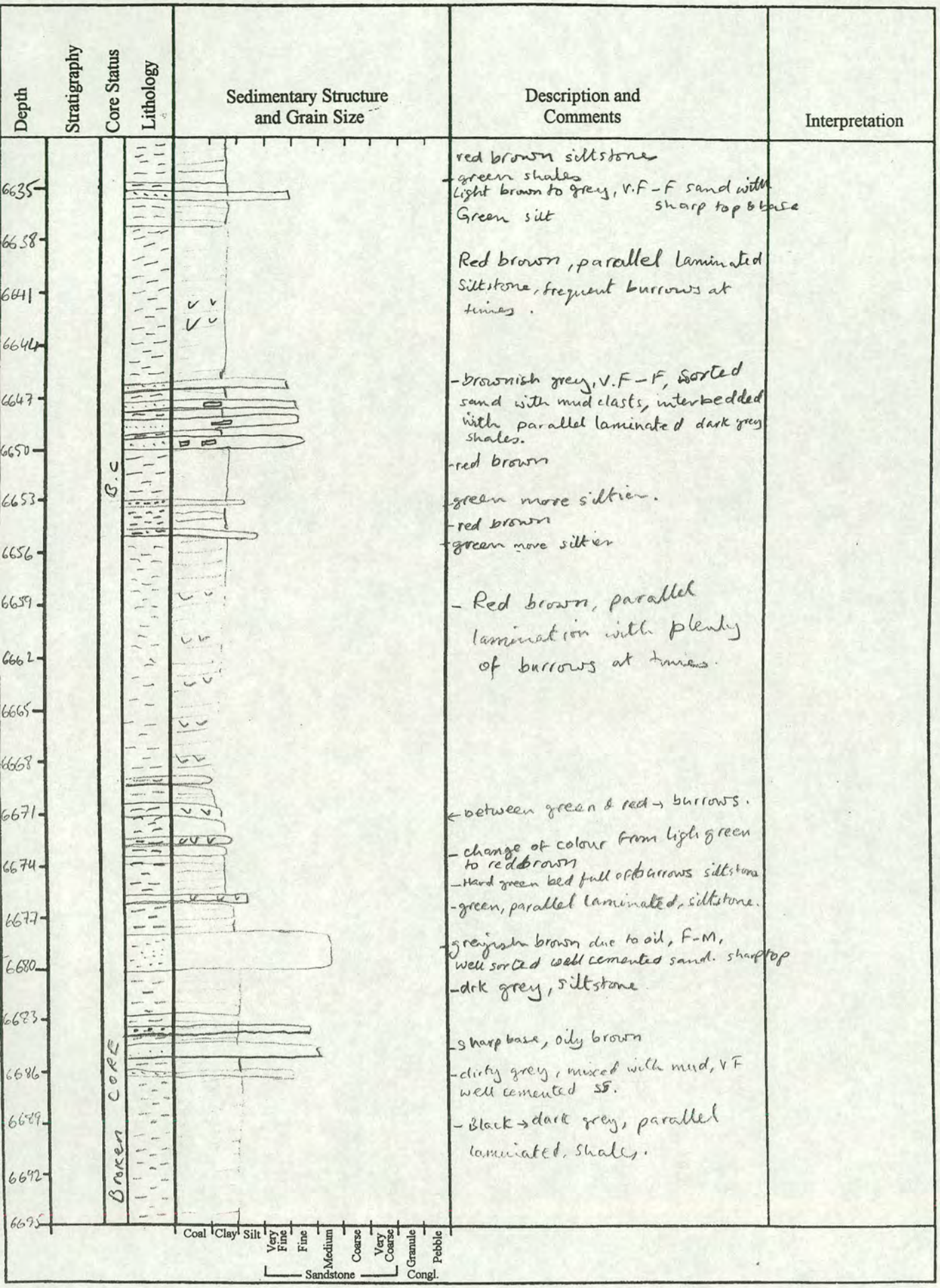

Core Description

Well Name: 21/30 - 15
Location:
Date: 21/2/01

Sheet: 3 of 3

Depth	Stratigraphy	Core Status	Lithology	Sedimentary Structure and Grain Size	Description and Comments	Interpretation
572						
575						
578						
581						
584						
587						
590					- dark grey shales.	
593					- light grey, well sorted, F, sandstone	
596					- light grey, F, well sorted SS - dark grey shales.	
599					- brownish grey, oil contained, V. F—F, well sorted consolidated sandstone	
602						
605					Burrows green	
608					- Dirty brown due to oil, non consolidated loose beech like sand.	
611						
6614					- green red brown - green - V.F.	
6617					- green shales - brownish grey, VF-F, well cemented SS. - red brown - green	
6620					- blackish brown due to oil, F-M well sorted, well cemented, SS - green shales	
6623						
6626						
6629					- full of burrows - Red brown siltstone	
6632						

Coal | Clay | Silt | Very Fine | Fine | Medium | Coarse | Very Coarse | Granule | Pebble
Sandstone — Congl.

Core Description

Well Name: 21/30-16
Location:
Date: 19/2/01

Sheet: 1 of 1

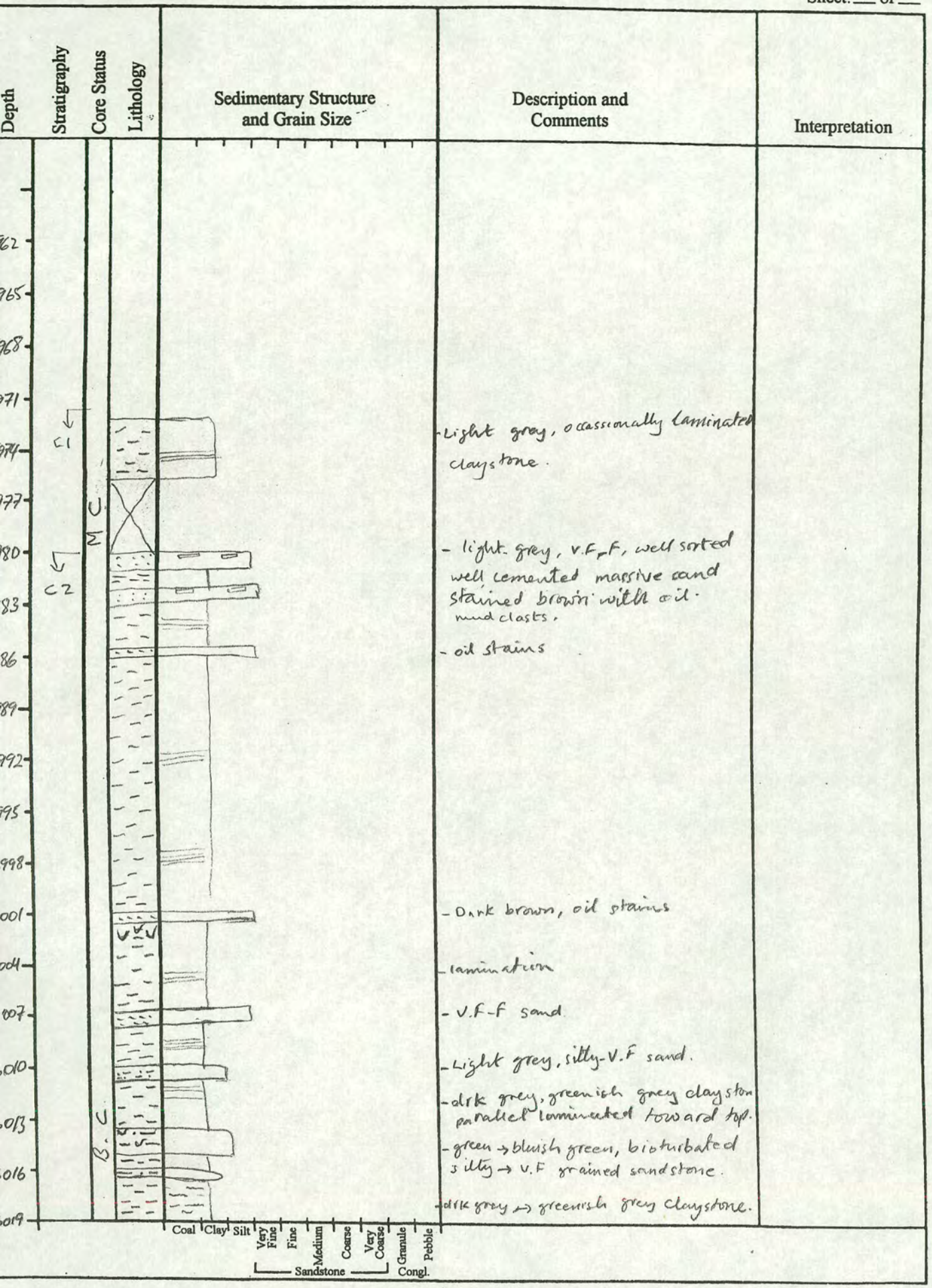

Name: 21/30-12 Locality: _____ Grid Ref./Well Log: _____ Date: _____

Sheet: 1 of 1

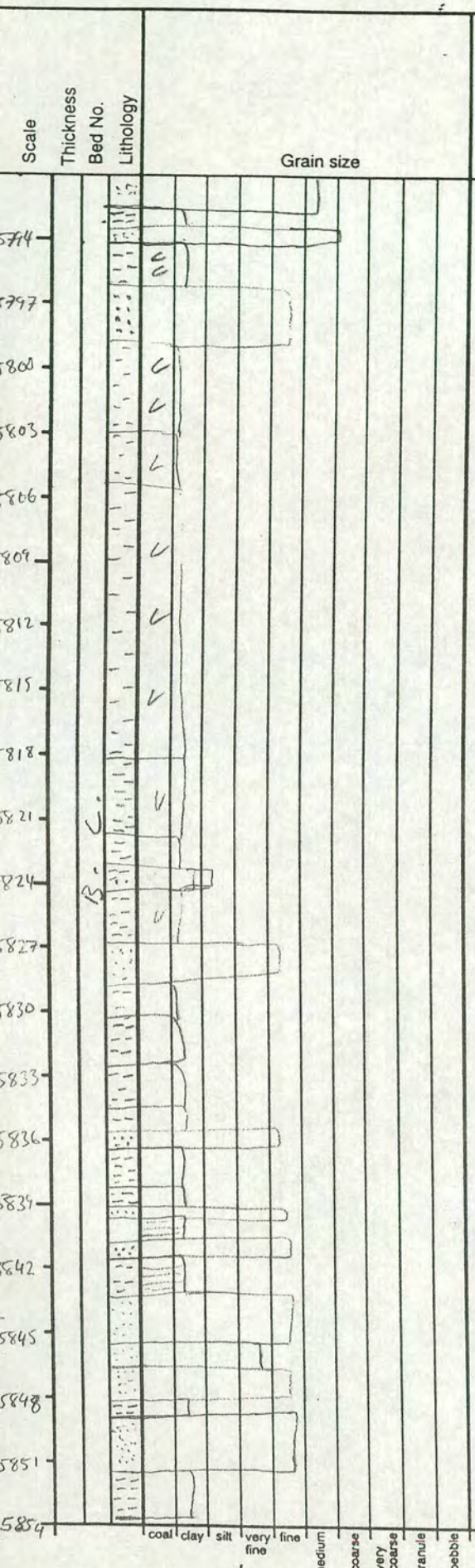

Grain size

Fossils

Palaeo-currents

Comments

- White beech-like sand.
- White/brown poorly-cemented well sorted sand
- White, V.f–f, w.sorted, poorly cemented sand. drk grey changing into light green claystone. with burrows
- drk grey claystone.
- clay flakes, drk grey
- drk grey siltstone
- cemented, poorly cemented oil stained, rangy brown sand.
- Reddish going back into drk green then light green.
- Reddish brn clay
- L.G going to darker colour than into reddish brown
- oil stained sand a/b.
- L.G. laminated mud
- drk brn oily sand a/b. grading into finer, better cemented
- * Sand same as below oil
- * L.G. clay as below
- * drk brown, fine, sorted, poorly cemented, oil stained stained
- + Light green, homogeneous clay with drk brown-black mud flakes

Interpretations

sand sharp base bright white. ↓ similar to 5973' in 296-9

Appendix 4

Horizon slices hanging of the Top Tay reflector. These slices were analysed to identify the best interval within which trace shape analysis should be performed. They were also used to establish the variation in channel sinuosity over the time.


ToyTimeslices -40
Crosslines
3000 3200 3400 3600 3800 4000 4200 4400 4600 4800 5000 5200 5400 5600
-16100
-14000
-12000
-10000
-8000
-6000
-4000
-2000
0
2000
4000
6000
8000
10000
12000
14000
16100
54 n Time= 1492 ms Data= AmplitudeSlice -40
ToyTimeslices -36
Crosslines
3000 3200 3400 3600 3800 4000 4200 4400 4600 4800 5000 5200 5400 5600
-16000
-14000
-12000
-10000
-8000
-6000
-4000
-2000
0
2000
4000
6000
8000
10000
12000
14000
16000


TayTimeslices -32
crosslines
3000
3200
3400
3600
3800
4000
4200
4400
4600
4800
5000
5200
5400
5600
TayTimeslices -28
Help
TayTimeslices -28
crosslines

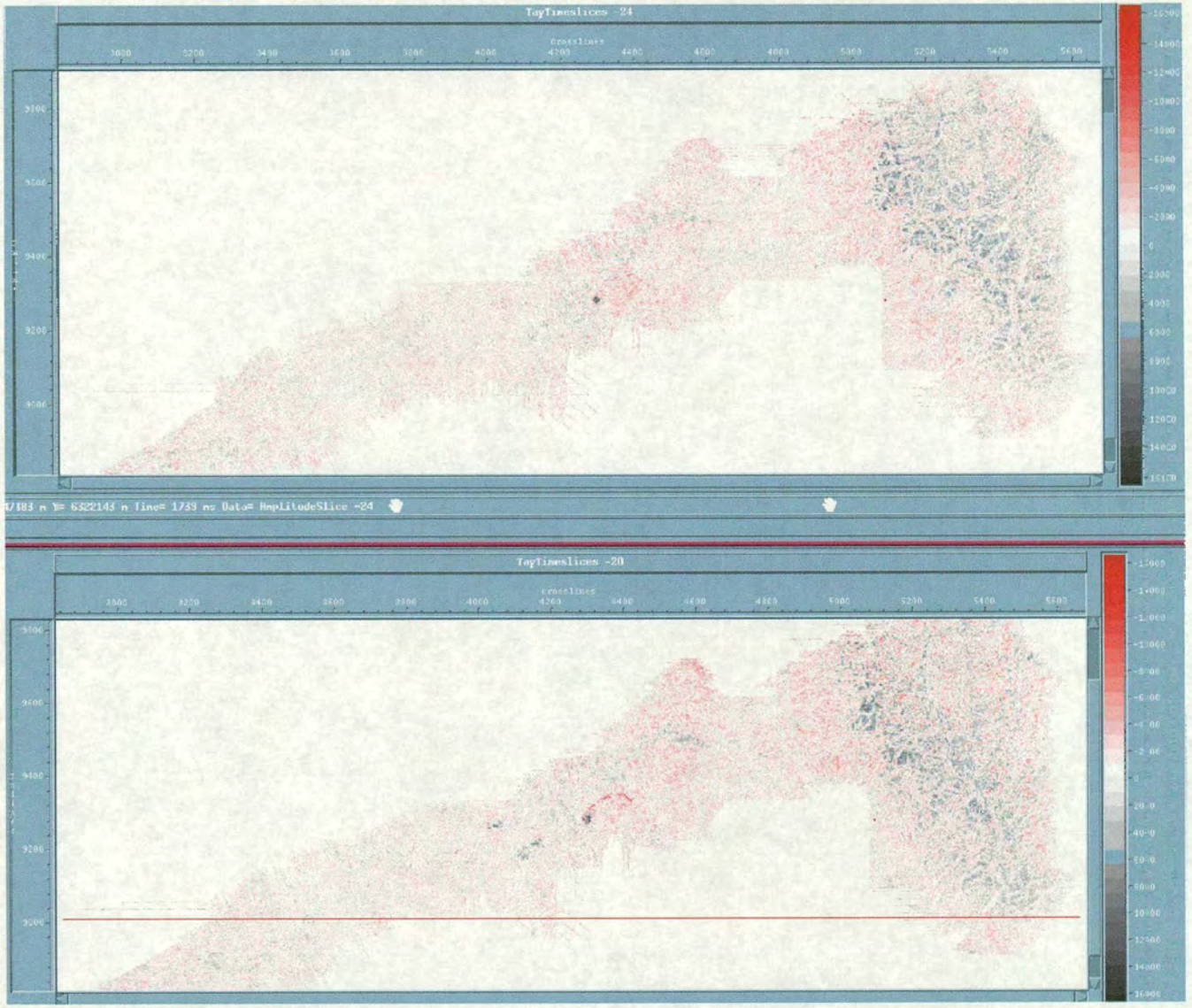
TayTimeslices -24
crosslines
3000
3200
3400
3600
3800
4000
4200
4400
4600
4800
5000
5200
5400
5600
9000
9200
9400
9600
TayTimeslices -20
crosslines
3000
3200
3400
3600
3800
4000
4200
4400
4600
4800
5000
5200
5400
5600
9000
9200
9400
9600


TayTimeslices -16
Crosslines
3000
3200
3400
3600
3800
4000
4200
4400
4600
4800
5000
5200
5400
5600
TayTimeslices -12
Help
Stop
Play
Rev
2
Increment
-12
Current slice
-12
TayTimeslices -12
Crosslines

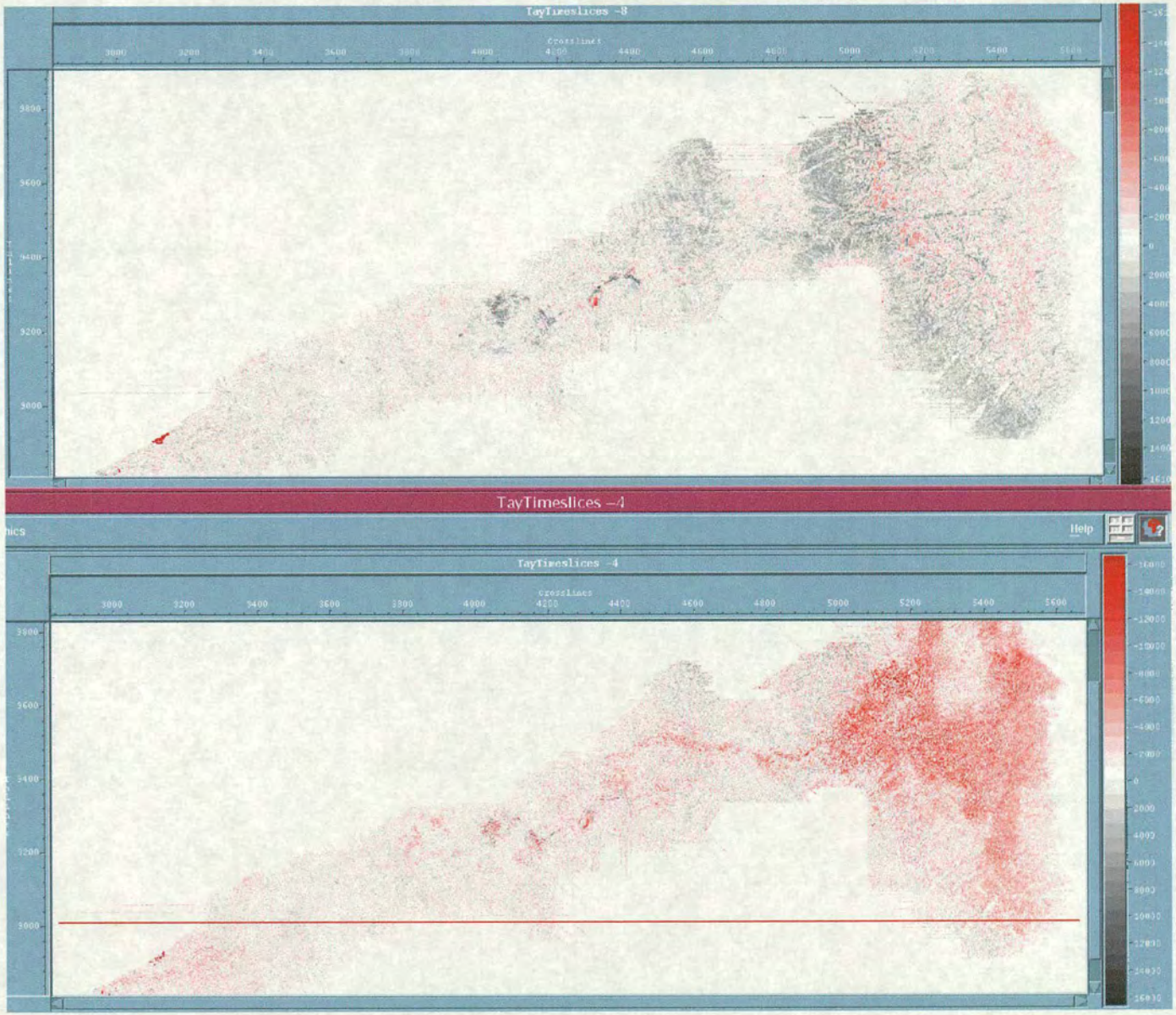
TayTimeslices -8
Crosslines
3000
3200
3400
3600
3800
4000
4200
4400
4600
4800
5000
5200
5400
5600
3800
3600
3400
3200
3000
TayTimeslices -4
Help
TayTimeslices -4
Crosslines
3000
3200
3400
3600
3800
4000
4200
4400
4600
4800
5000
5200
5400
5600
3800
3600
3400
3200
3000

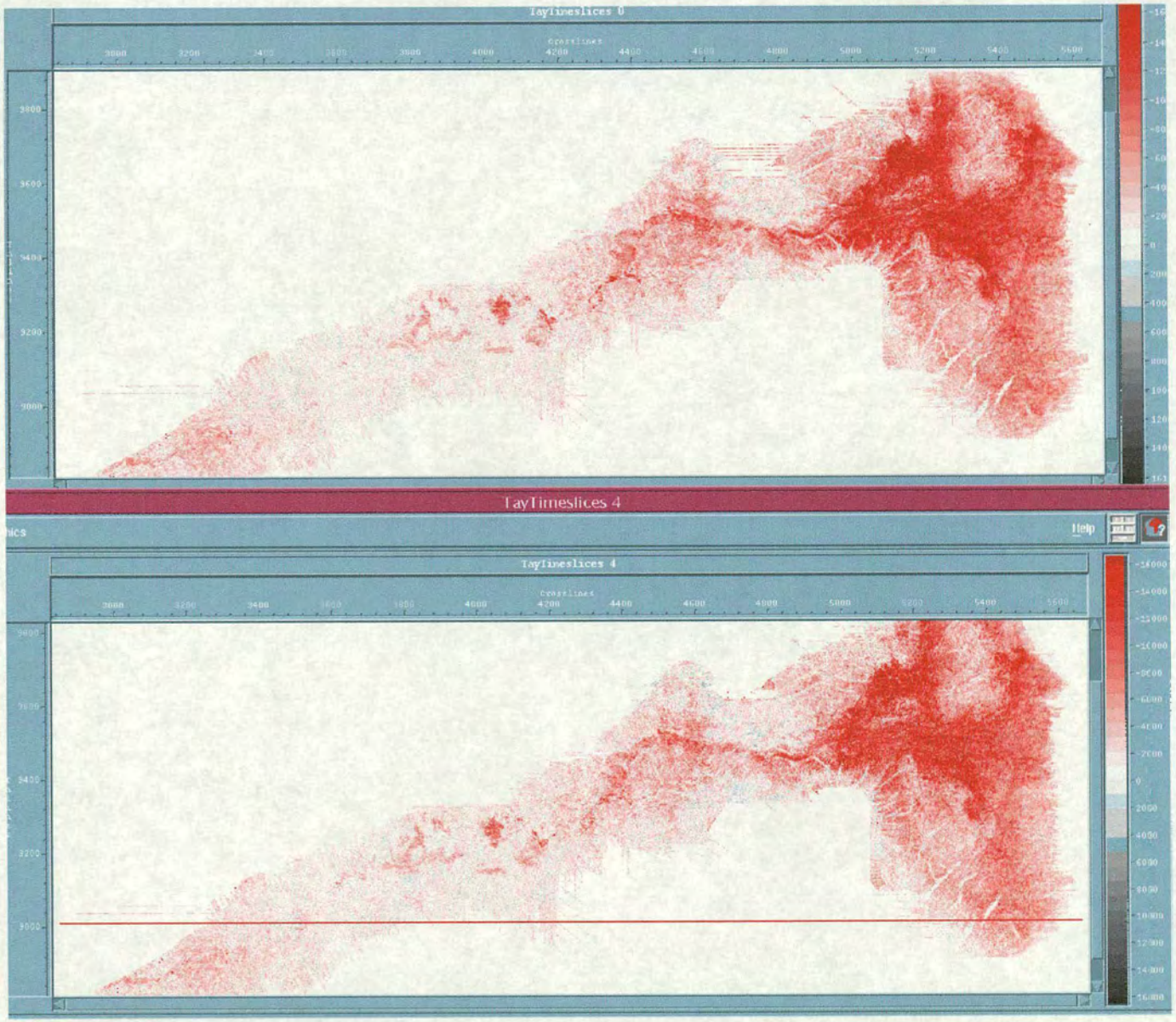
TayTimeslices 0
Crosslines
3000
3200
3400
3600
3800
4000
4200
4400
4600
4800
5000
5200
5400
5600
3800
3600
3400
3200
3000
TayTimeslices 4
Help
TayTimeslices 4
Crosslines
3000
3200
3400
3600
3800
4000
4200
4400
4600
4800
5000
5200
5400
5600
3800
3600
3400
3200
3000

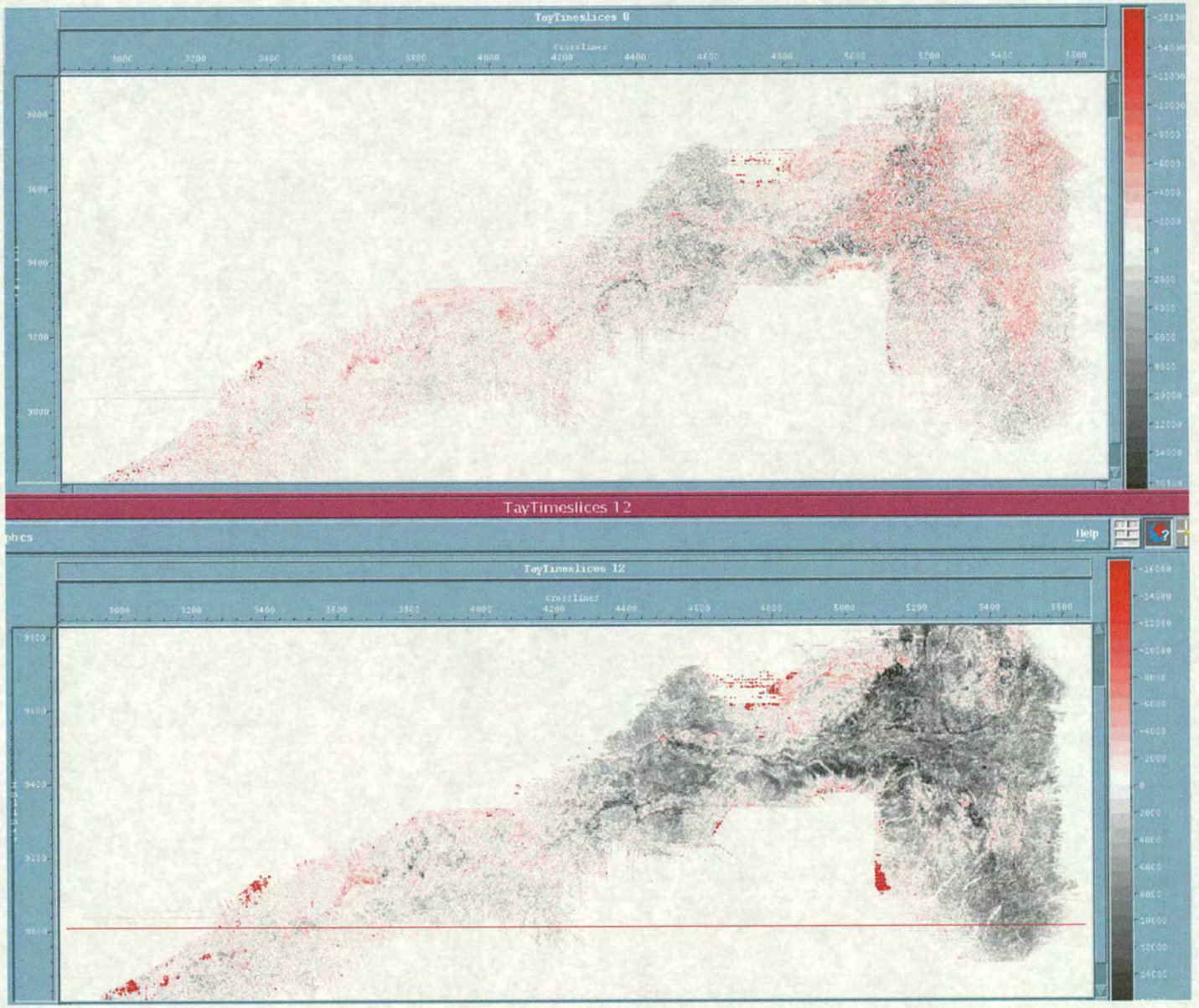
TayTimeslices 8
crosslines
TayTimeslices 12
Help
TayTimeslices 12
crosslines

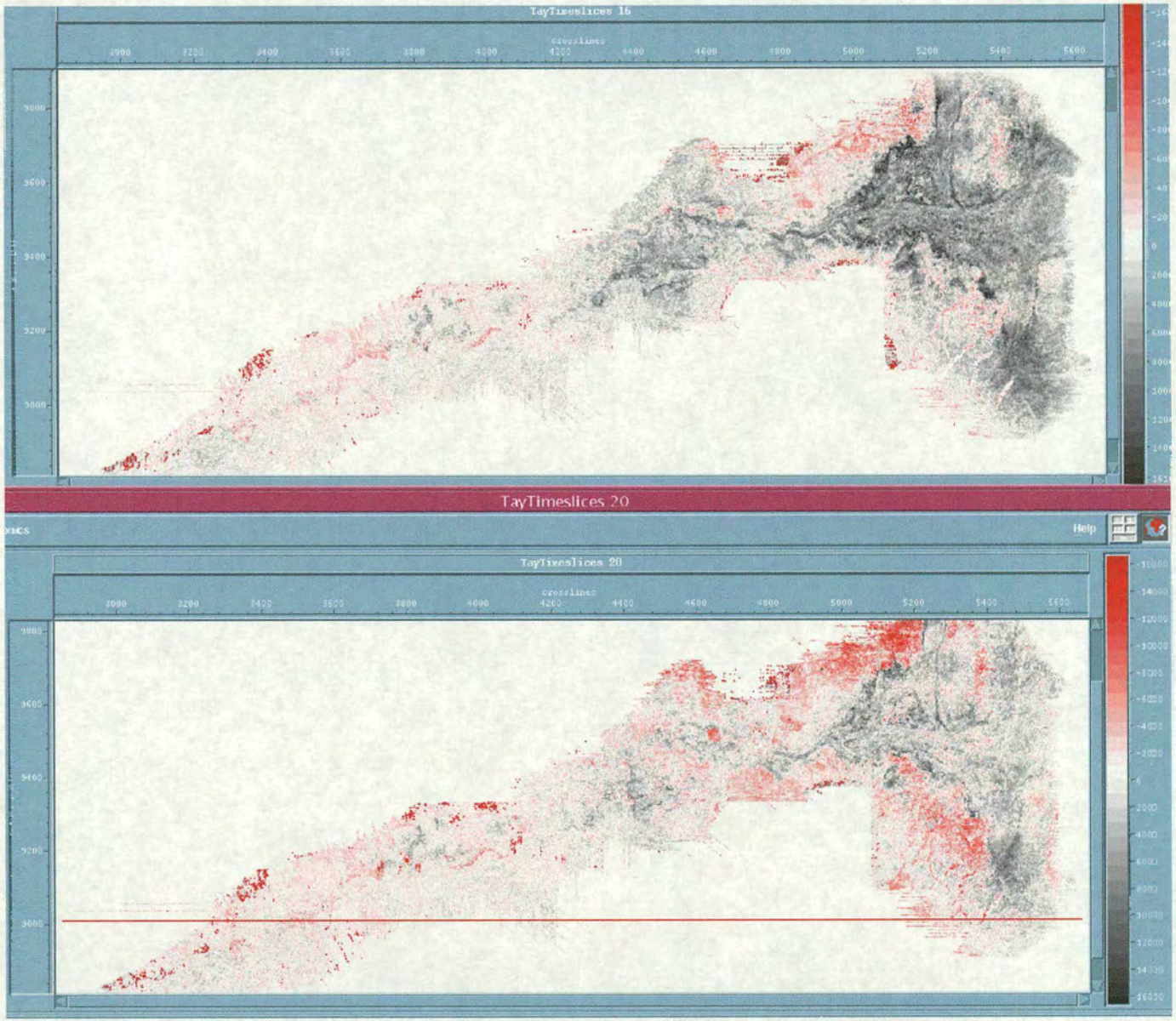
TayTimeslices 16
Crosslines
2800
3000
3200
3400
3600
3800
4000
4200
4400
4600
4800
5000
5200
5400
5600
3800
3600
3400
3200
3000
TayTimeslices 20
Help
TayTimeslices 20
Crosslines
2800
3000
3200
3400
3600
3800
4000
4200
4400
4600
4800
5000
5200
5400
5600
3800
3600
3400
3200
3000

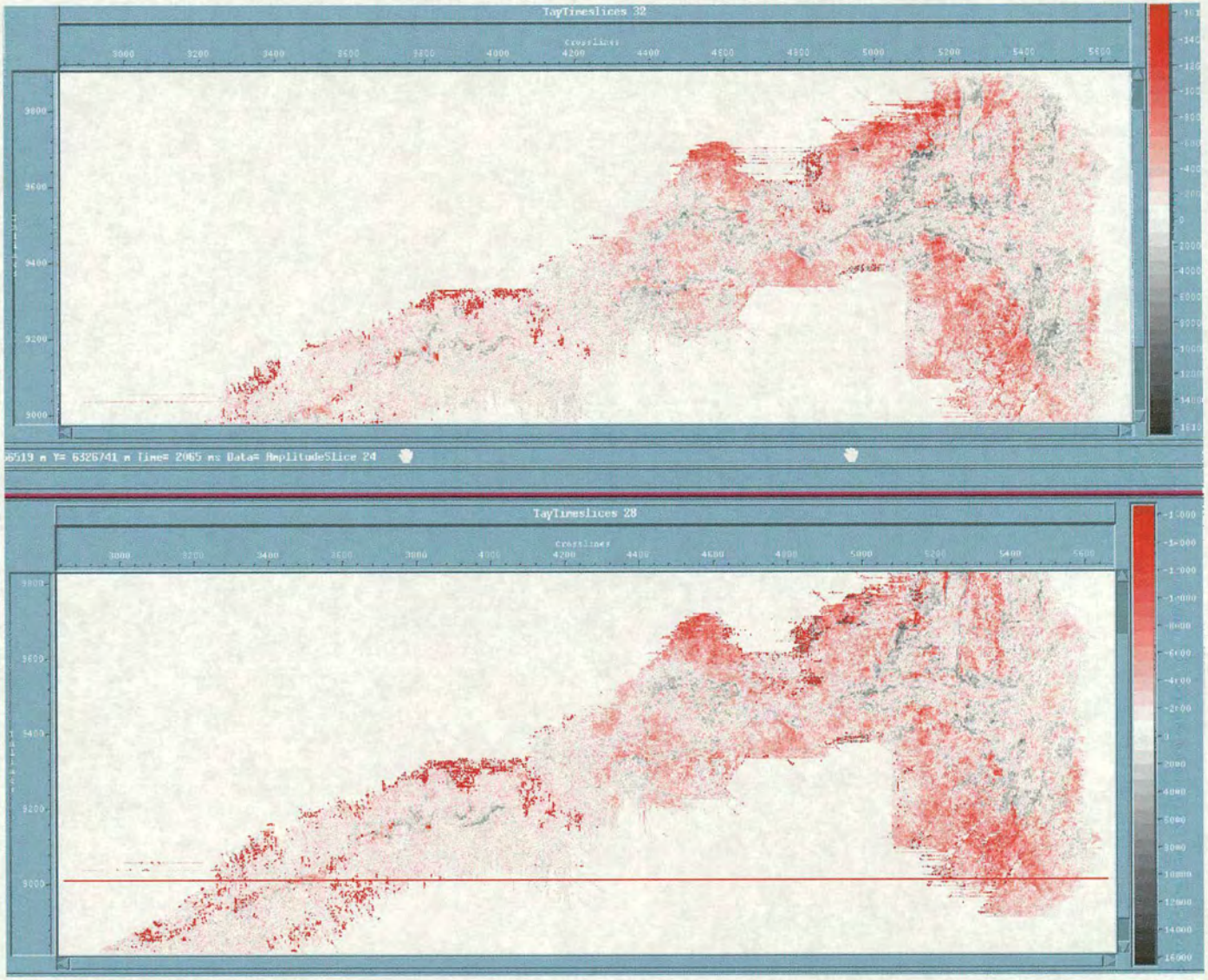
TayTimeslices 32
Crosslines
3000
3200
3400
3600
3800
4000
4200
4400
4600
4800
5000
5200
5400
5600
9800
9600
9400
9200
9000
6519 m Y= 6326741 m Time= 2065 ms Data= AmplitudeSlice 24
TayTimeslices 28
Crosslines
3000
3200
3400
3600
3800
4000
4200
4400
4600
4800
5000
5200
5400
5600
9800
9600
9400
9200
9000

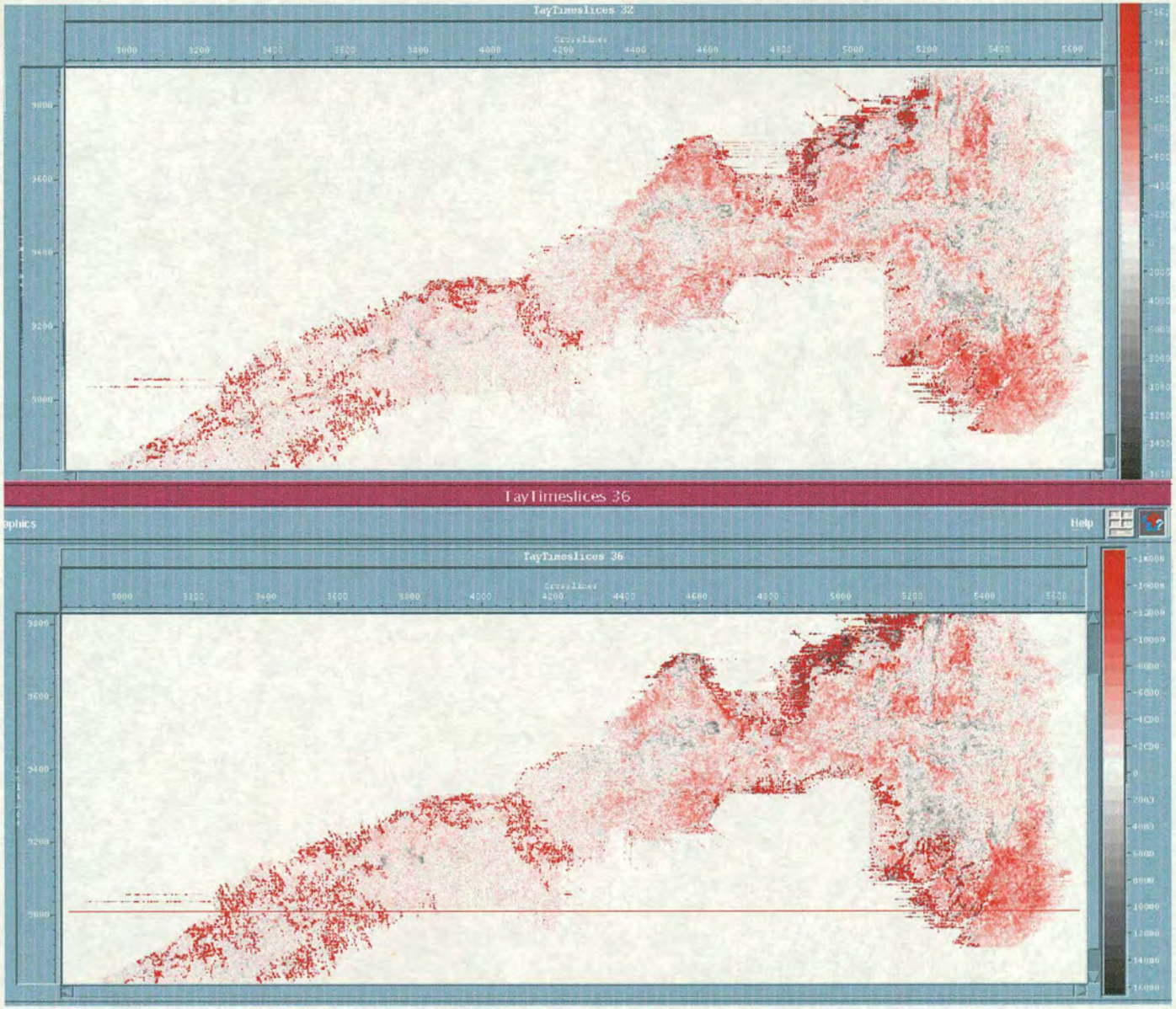
TayTimeslices 32
TayTimeslices 36
aphics
Help
TayTimeslices 36

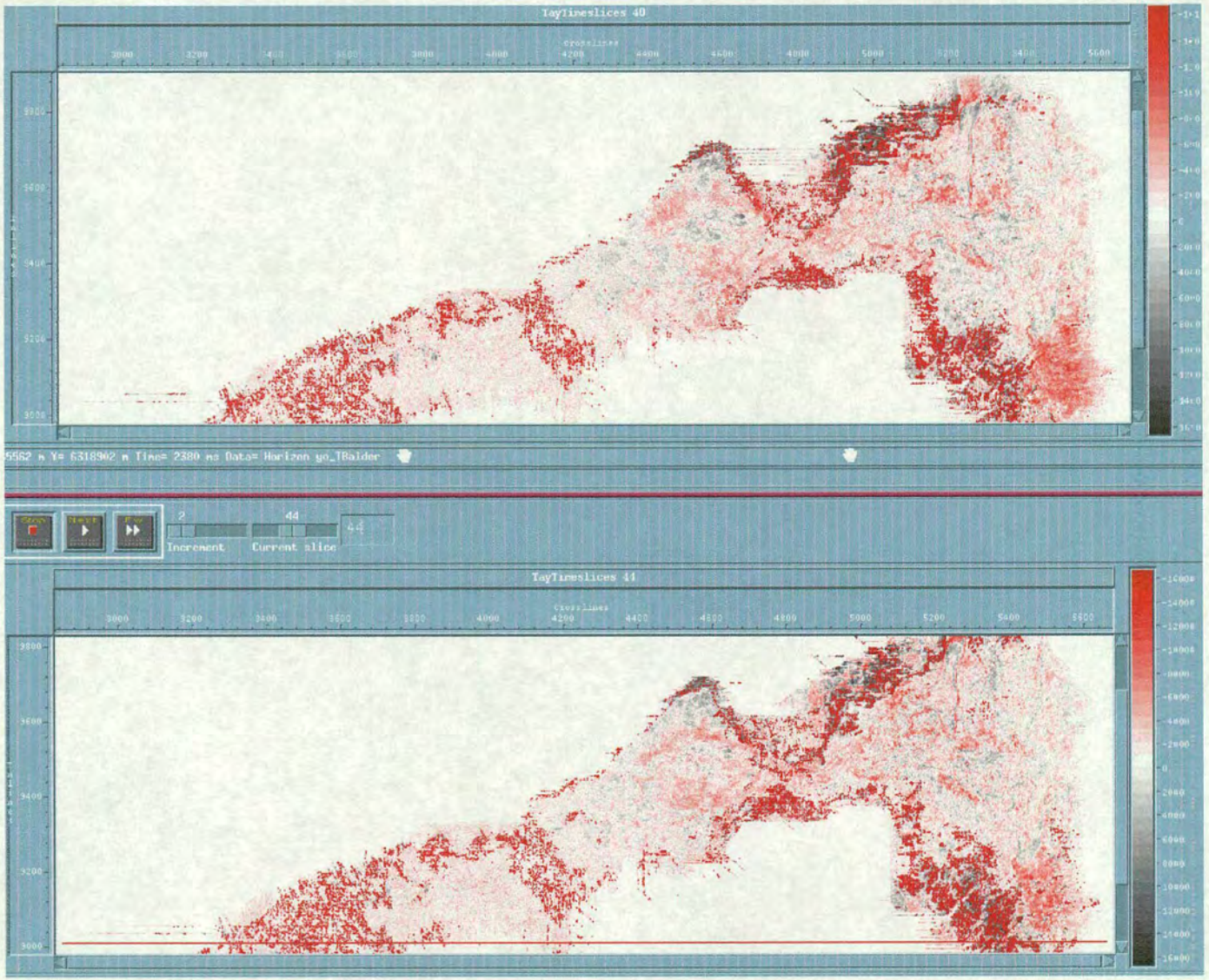
TayTimeslices 40
crosslines
TayTimeslices 44
crosslines
Increment
Current slice


ToyTimeslices 40
Crosslines
3000 3200 3400 3600 3800 4000 4200 4400 4600 4800 5000 5200 5400 5600
3300
3600
3400
3800
4000
8525 m Y= 6328408 m Time= 2501 ms Data= AmplitudeSlice 48
2
52
52
Increment
Current slice
ToyTimeslices 52
Crosslines
3000 3200 3400 3600 3800 4000 4200 4400 4600 4800 5000 5200 5400 5600
3300
3600
3400
3800
4000
-16000
-14000
-12000
-10000
-8000
-6000
-4000
-2000
0
2000
4000
6000
8000
10000
12000
14000
16000

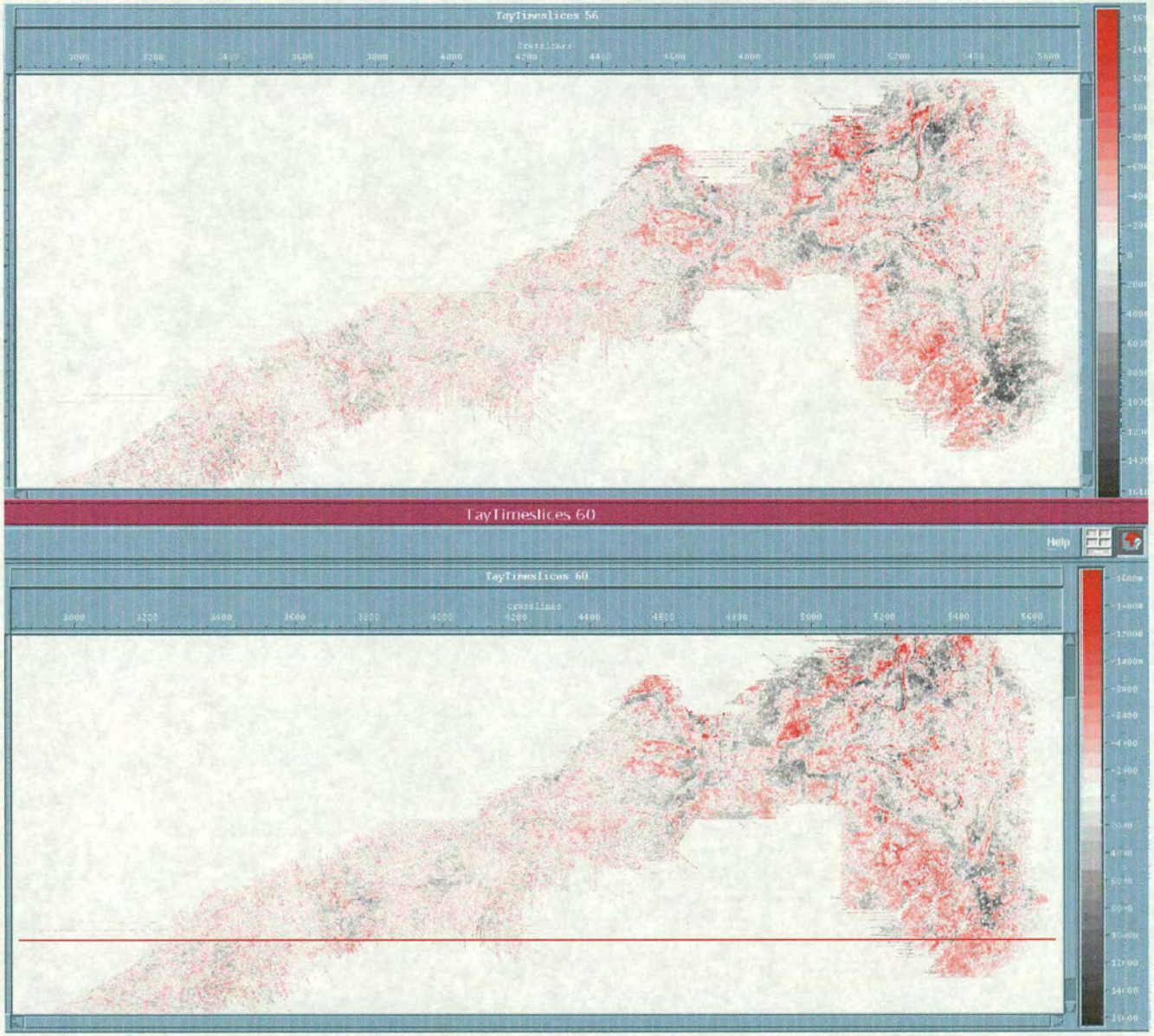
TayTimeslices 56
Crosslines:
3000
3200
3400
3600
3800
4000
4200
4400
4600
4800
5000
5200
5400
5600
TayTimeslices 60
Help
TayTimeslices 60
Crosslines:
3000
3200
3400
3600
3800
4000
4200
4400
4600
4800
5000
5200
5400
5600

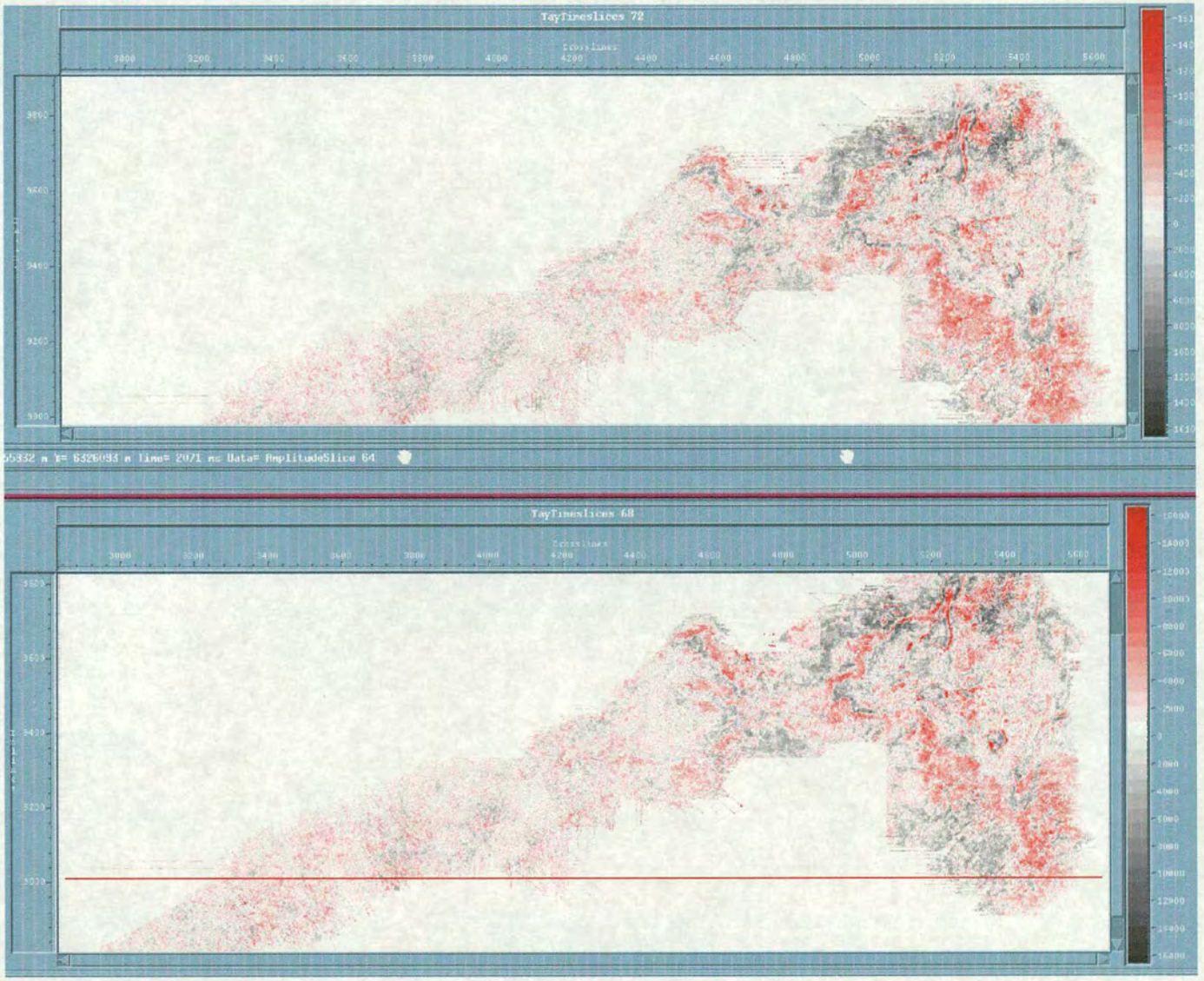
TayTimeslices 72
Crosslines
3000
3200
3400
3600
3800
4000
4200
4400
4600
4800
5000
5200
5400
5600
9800
9600
9400
9200
9000
Inlines
-140
-120
-100
-80
-60
-40
-20
0
2000
4000
6000
8000
10000
12000
14000
16000
55832 m Y= 6326093 m Time= 2071 ms Data= AmplitudeSlice 64
TayTimeslices 68
Crosslines
3000
3200
3400
3600
3800
4000
4200
4400
4600
4800
5000
5200
5400
5600
9800
9600
9400
9200
9000
Inlines
-16000
-14000
-12000
-10000
-8000
-6000
-4000
-2000
0
2000
4000
6000
8000
10000
12000
14000
16000

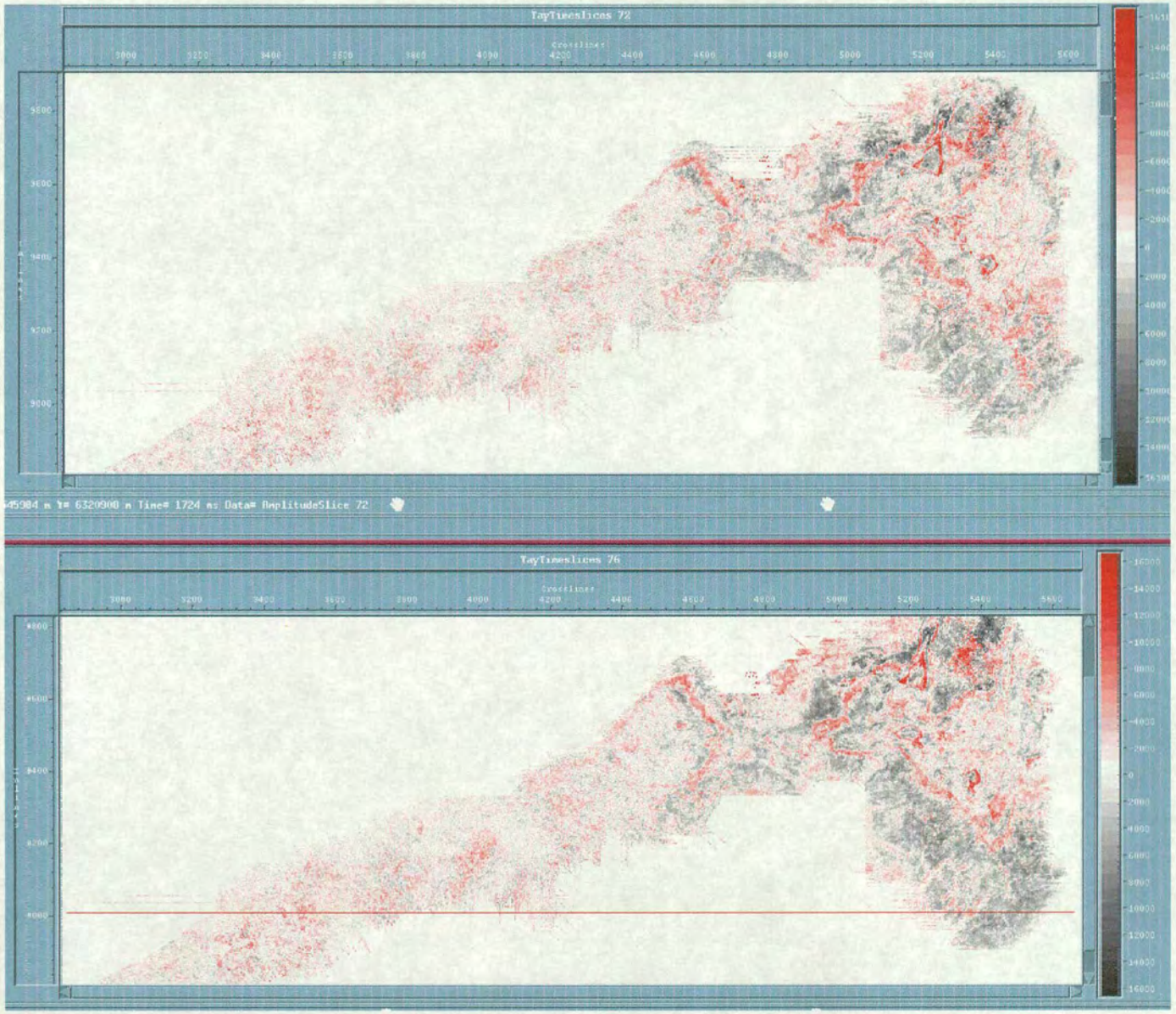
TayTimeslices 72
Crossline
3000
3200
3400
3600
3800
4000
4200
4400
4600
4800
5000
5200
5400
5600
Inline
5600
5800
6000
6200
6400
-1600
-1400
-1200
-1000
-800
-600
-400
-200
0
200
400
600
800
1000
1200
1400
1600
45984 m Y= 6320900 m Time= 1724 ms Data= AmplitudeSlice 72
TayTimeslices 76
Crossline
3000
3200
3400
3600
3800
4000
4200
4400
4600
4800
5000
5200
5400
5600
Inline
8000
8200
8400
8600
16000
14000
12000
10000
8000
6000
4000
2000
0
2000
4000
6000
8000
10000
12000
14000
16000

Appendix 5

Trace shape analysis with varying the number of model classes used with a 90 percent threshold for correlation applied. The figures also show the shape of each model trace used in the analysis.

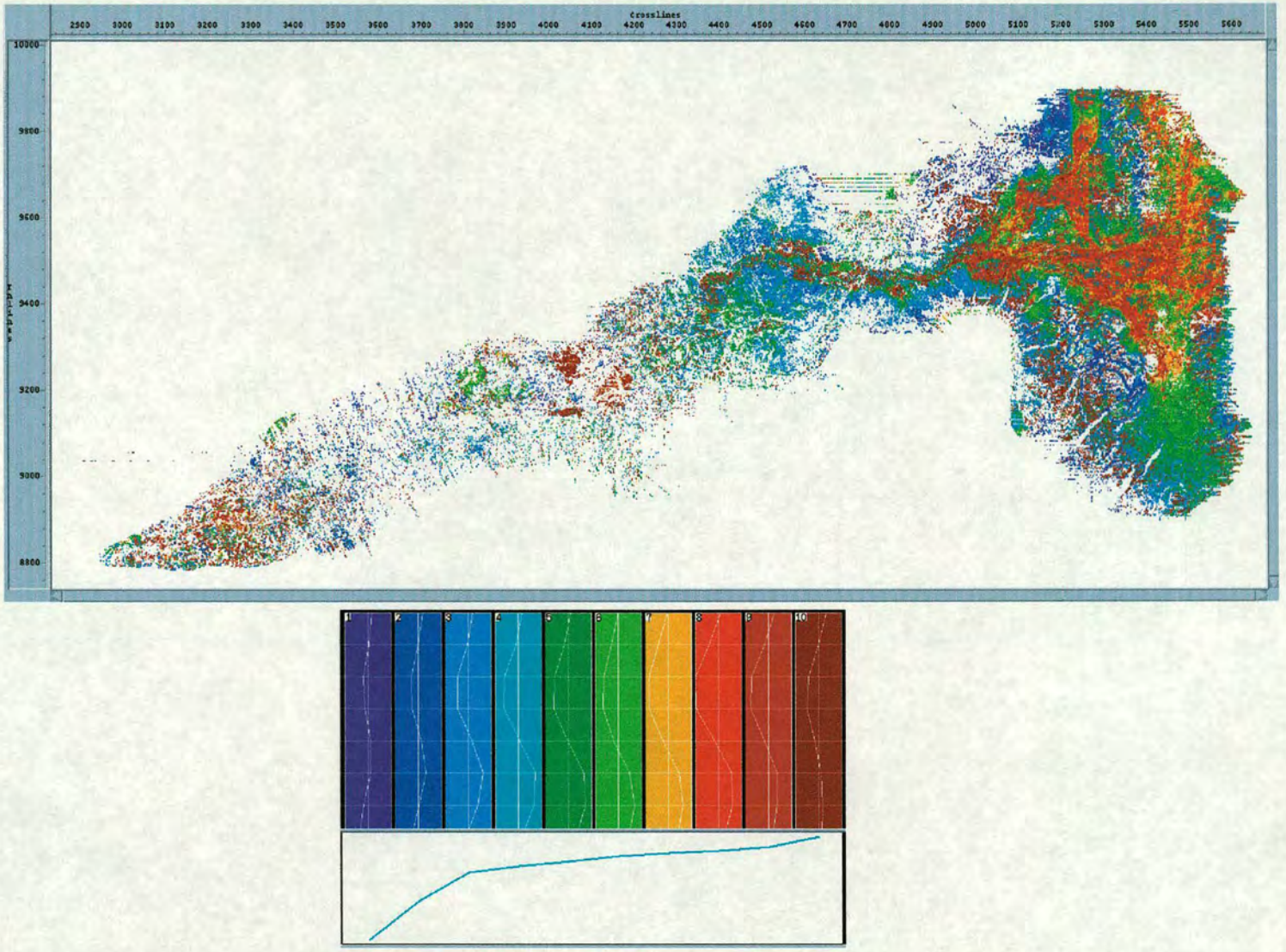

Results of unsupervised classification for the 30 ms interval hanging off the Top Tay horizon (-10 and + 20 ms) using 10 facies classes and 90% correlation threshold

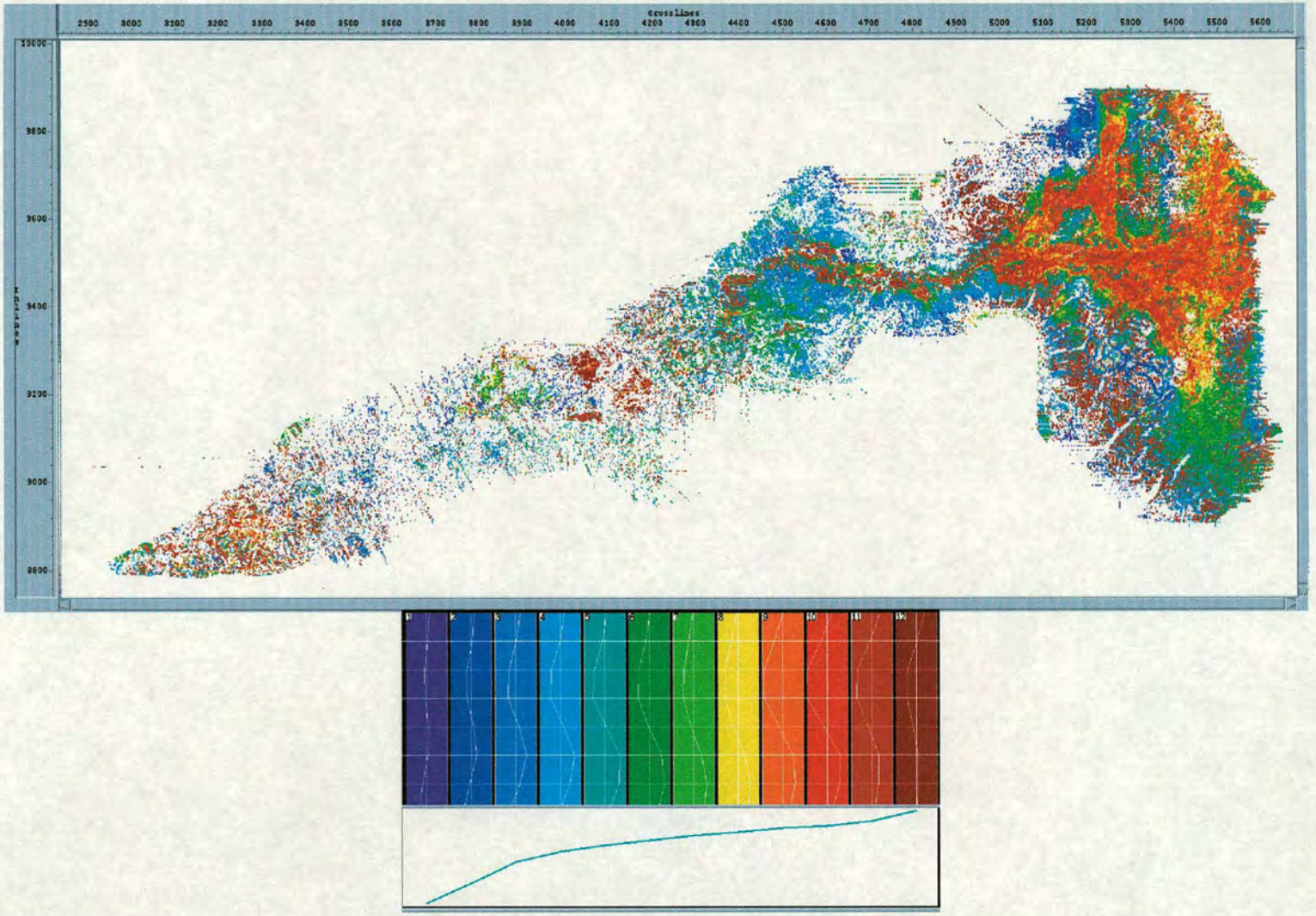

Results of unsupervised classification for the 30 ms interval hanging off the Top Tay horizon (-10 and + 20 ms) using 12 facies classes and 90% correlation threshold

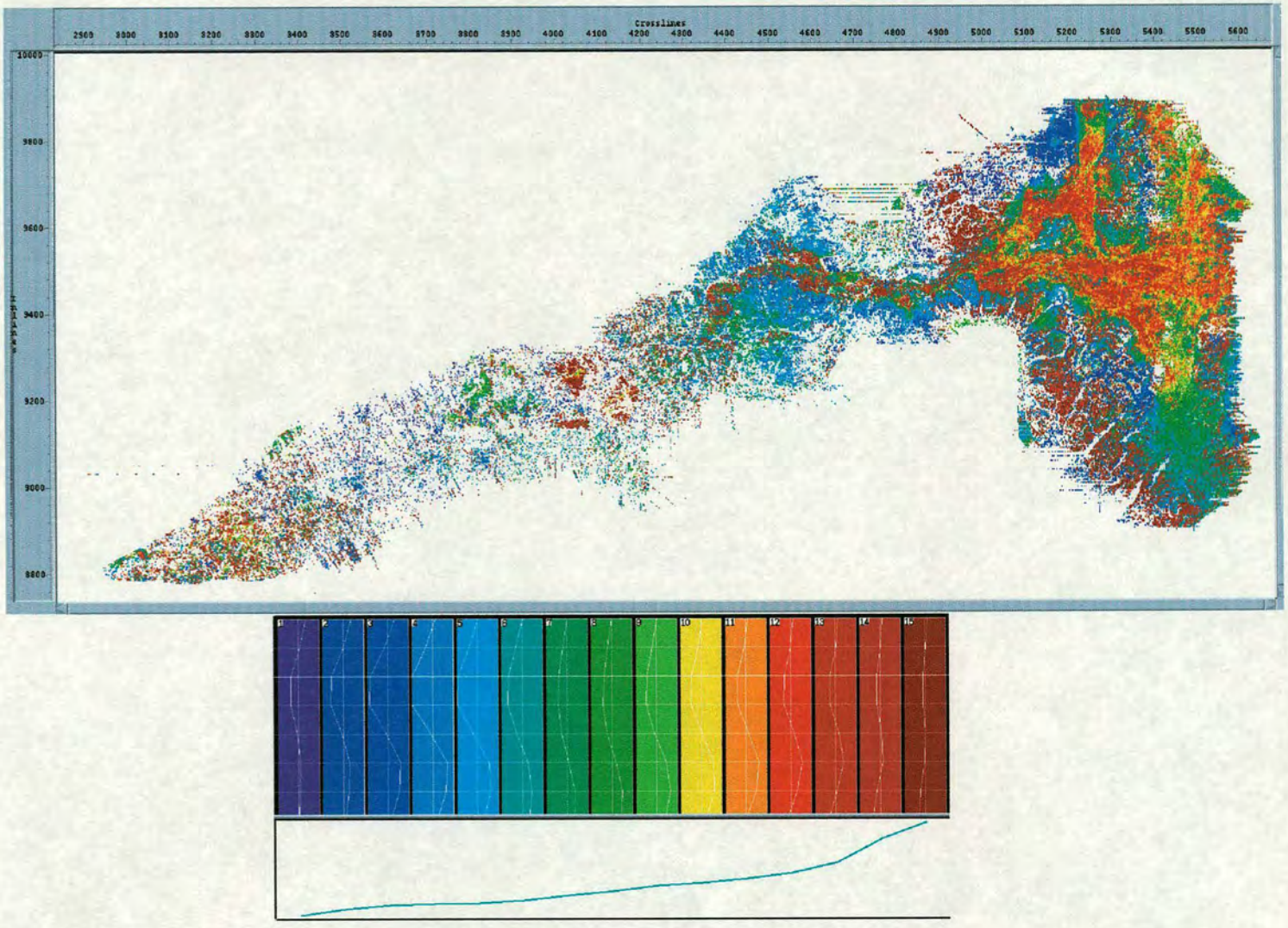

Results of unsupervised classification for the 30 ms interval hanging off the Top Tay horizon (-10 and + 20 ms) using 15 facies classes and 90% correlation threshold

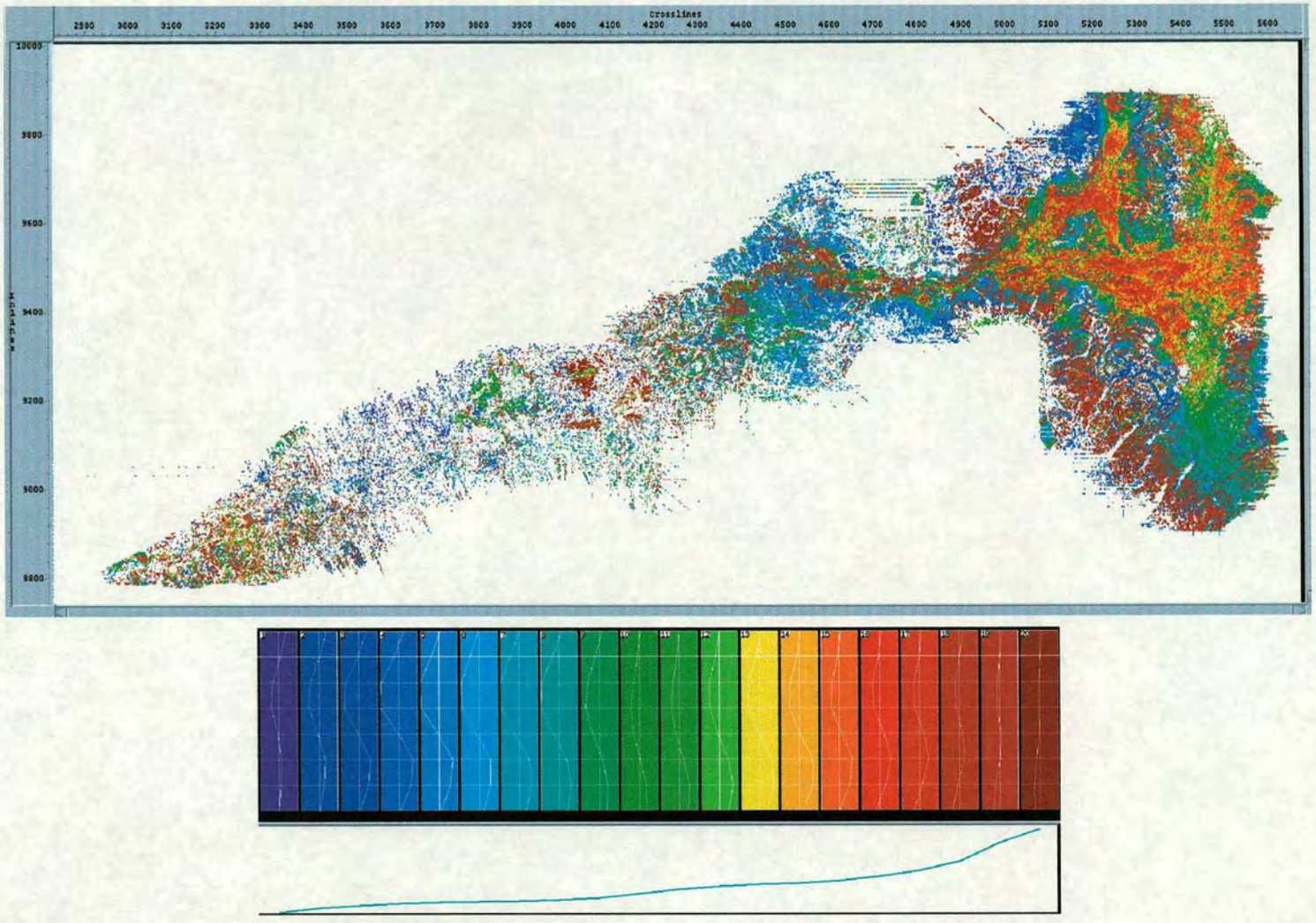

Results of unsupervised classification for the 30 ms interval hanging off the Top Tay horizon (-10 and + 20 ms) using 20 facies classes and 90% correlation threshold

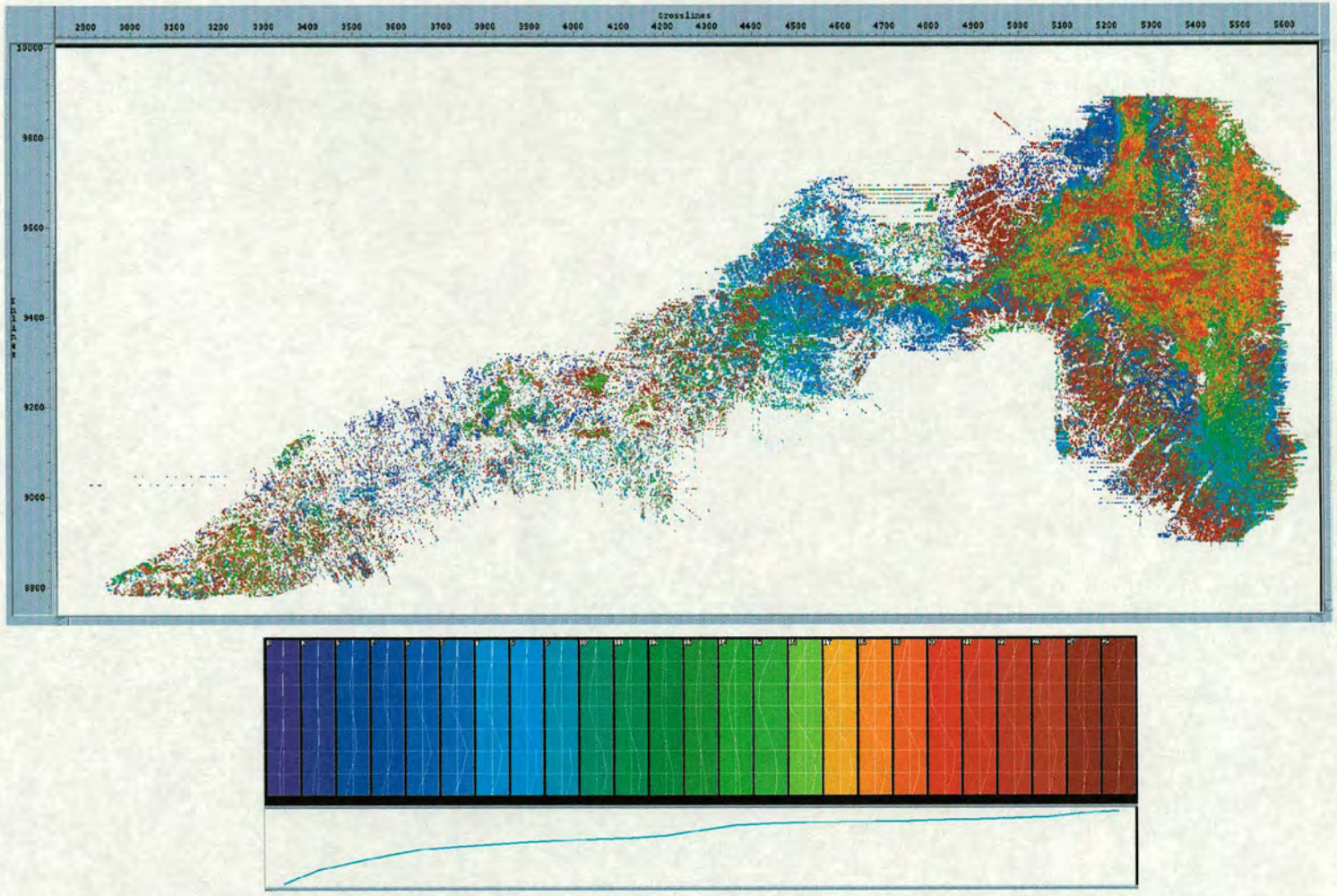

Results of unsupervised classification for the 30 ms interval hanging off the Top Tay horizon (-10 and + 20 ms) using 25 facies classes and 90% correlation threshold

Appendix 6

Results of trace shape analysis using different intervals hanging off the Top Tay Horizon. It was initially thought the these figures will reveal the temporal variation in the facies within Tay Formation. However, due to the difficulty in correlating different colours as sometimes different facies have been given the same colour, while at other times the same facies has been given different colours, making the comparison difficult.

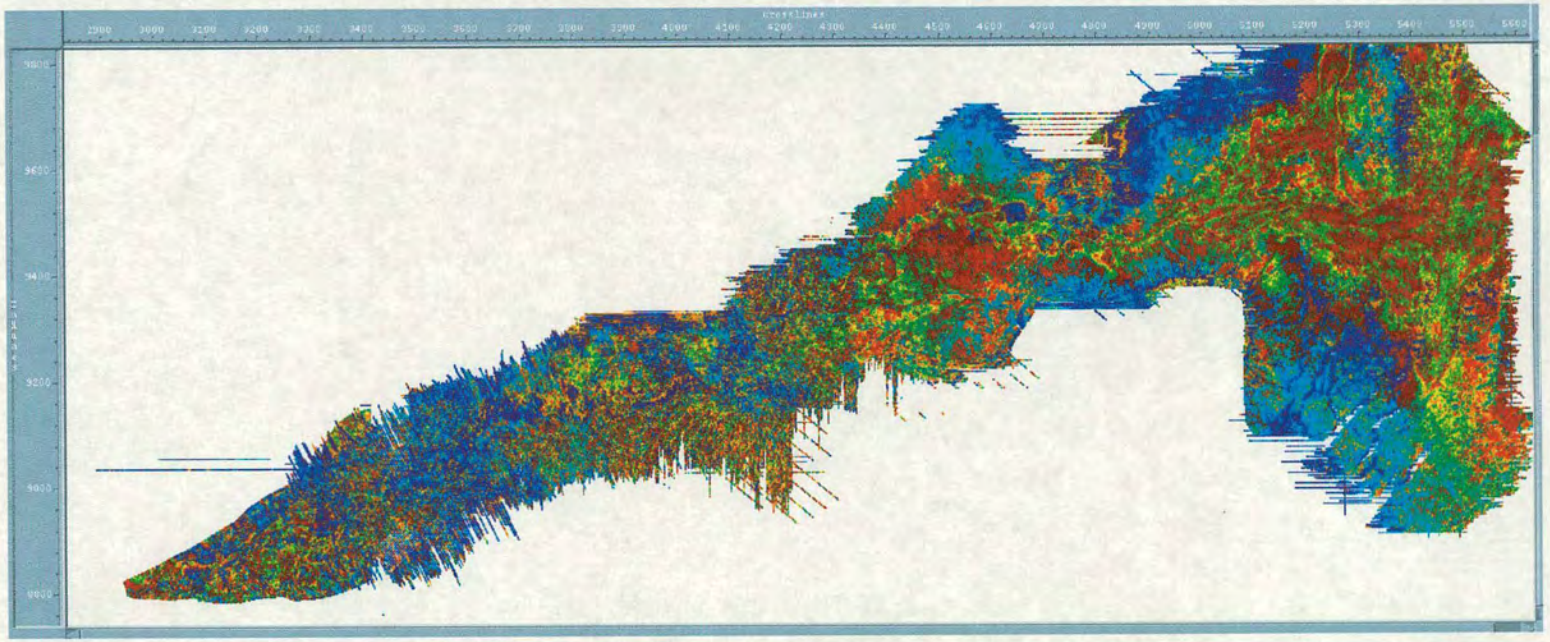

10 above and 40 below Top Tay horizon

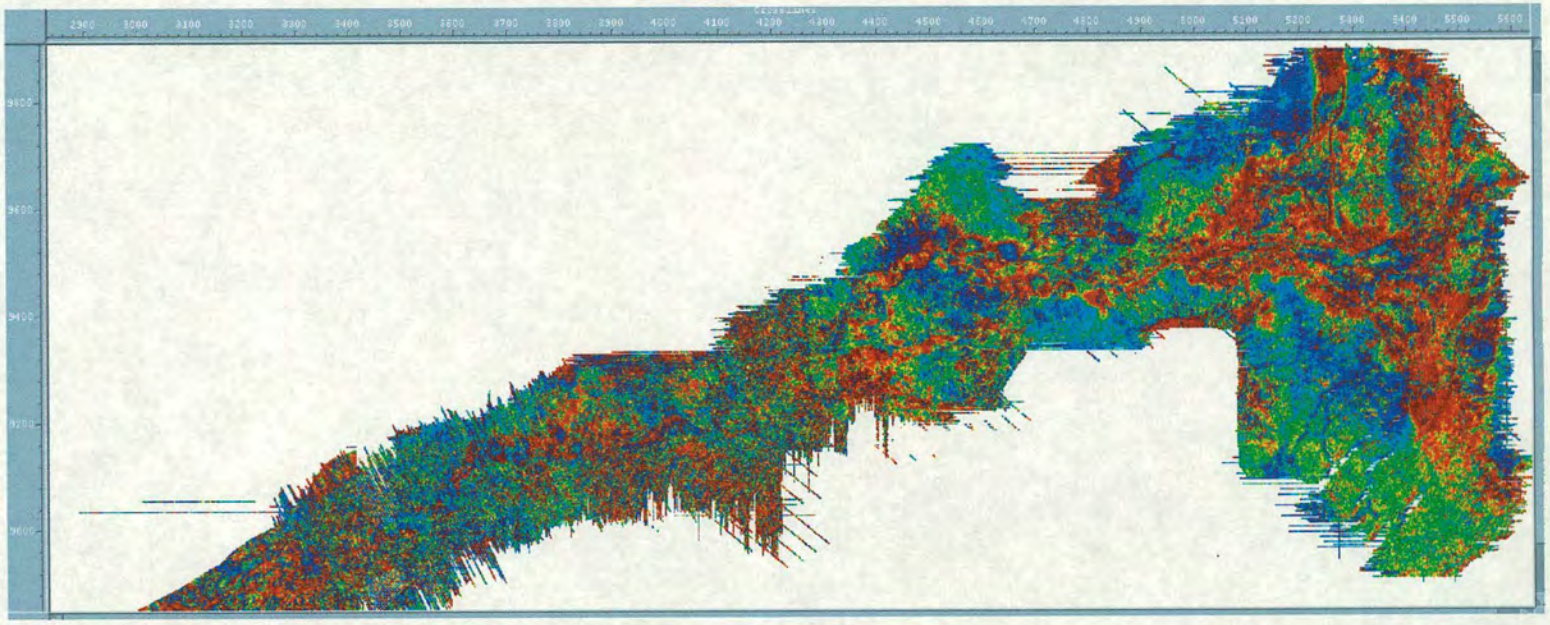

20 above and 30 below Top Tay horizon

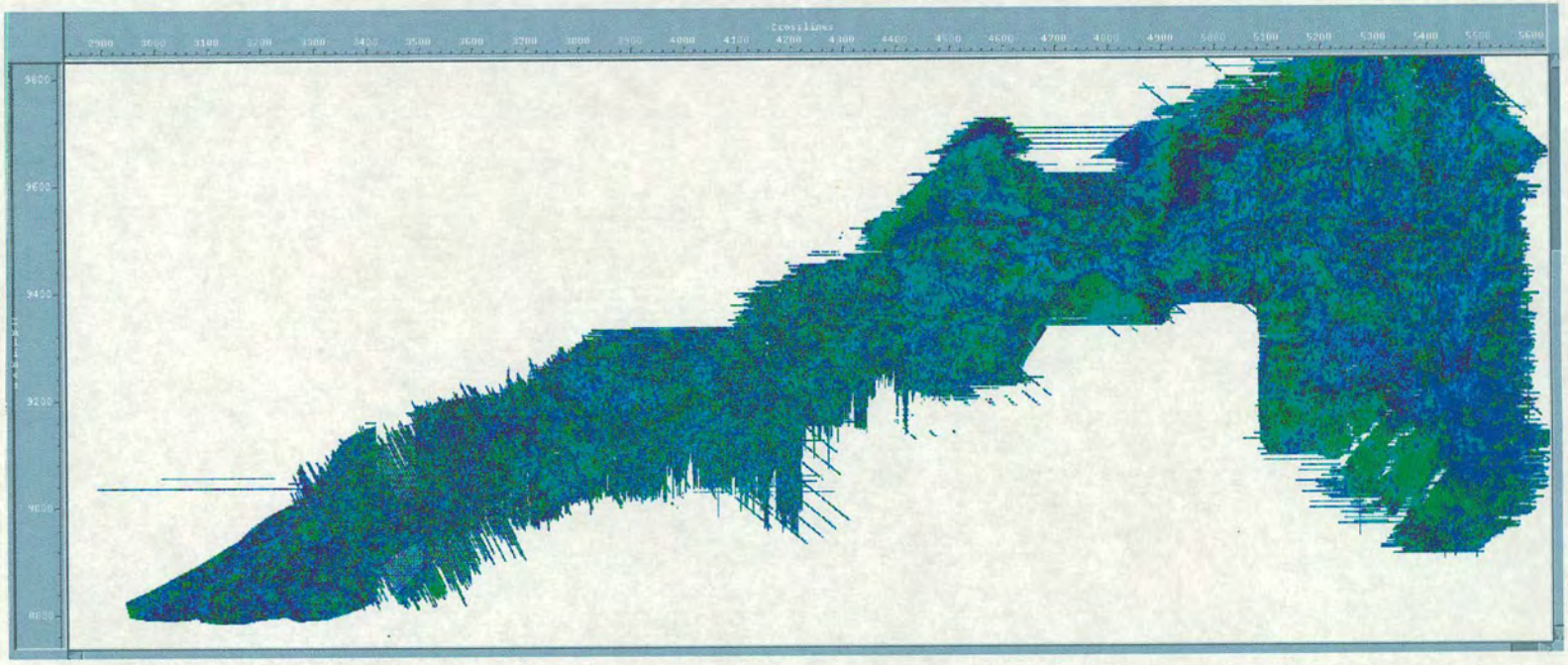

20 above and 50 below Top Tay horizon

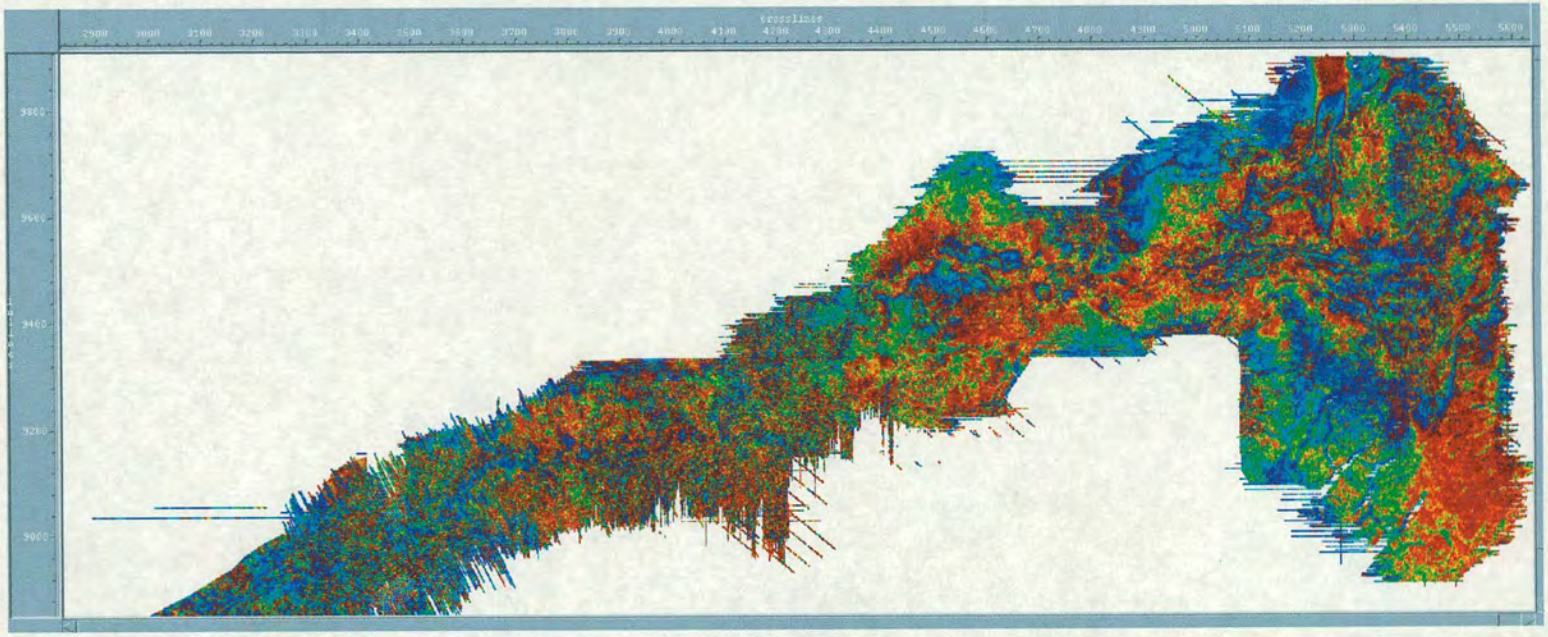

30 above and 40 below Top Tay horizon

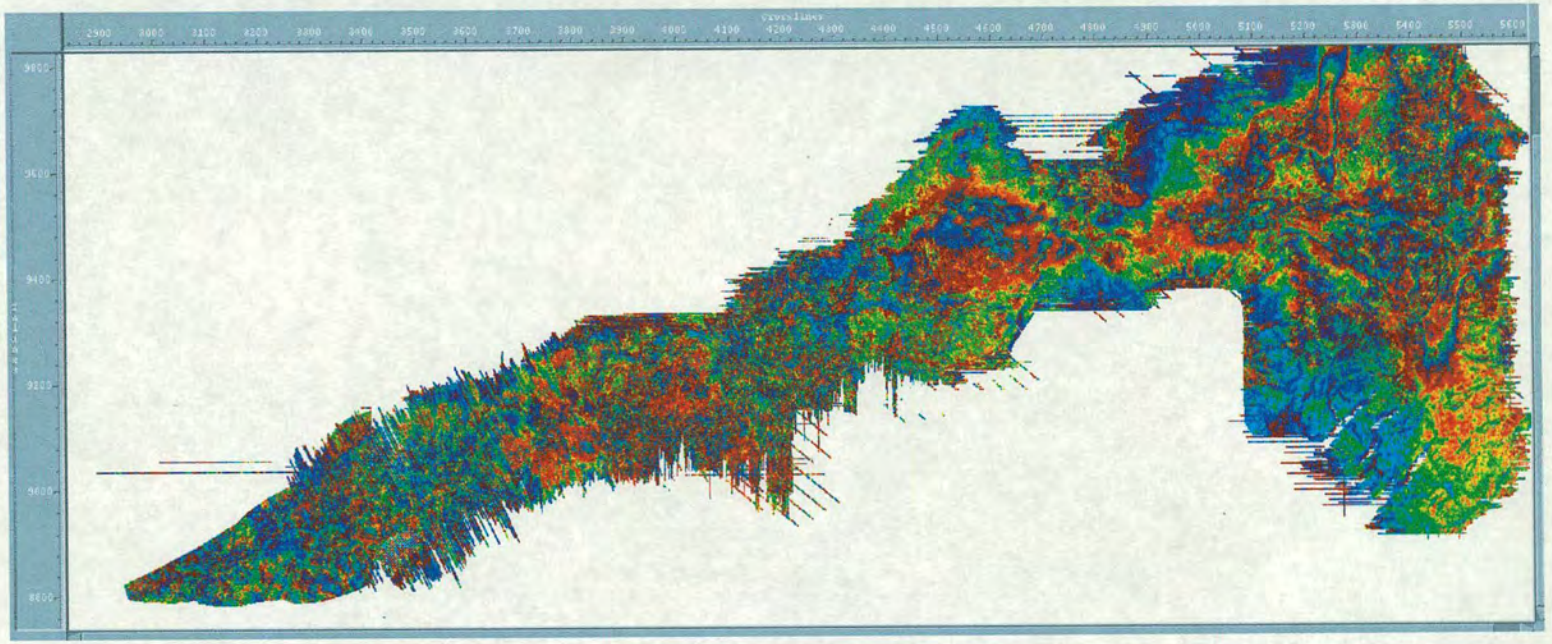

30 above and 60 below Top Tay horizon

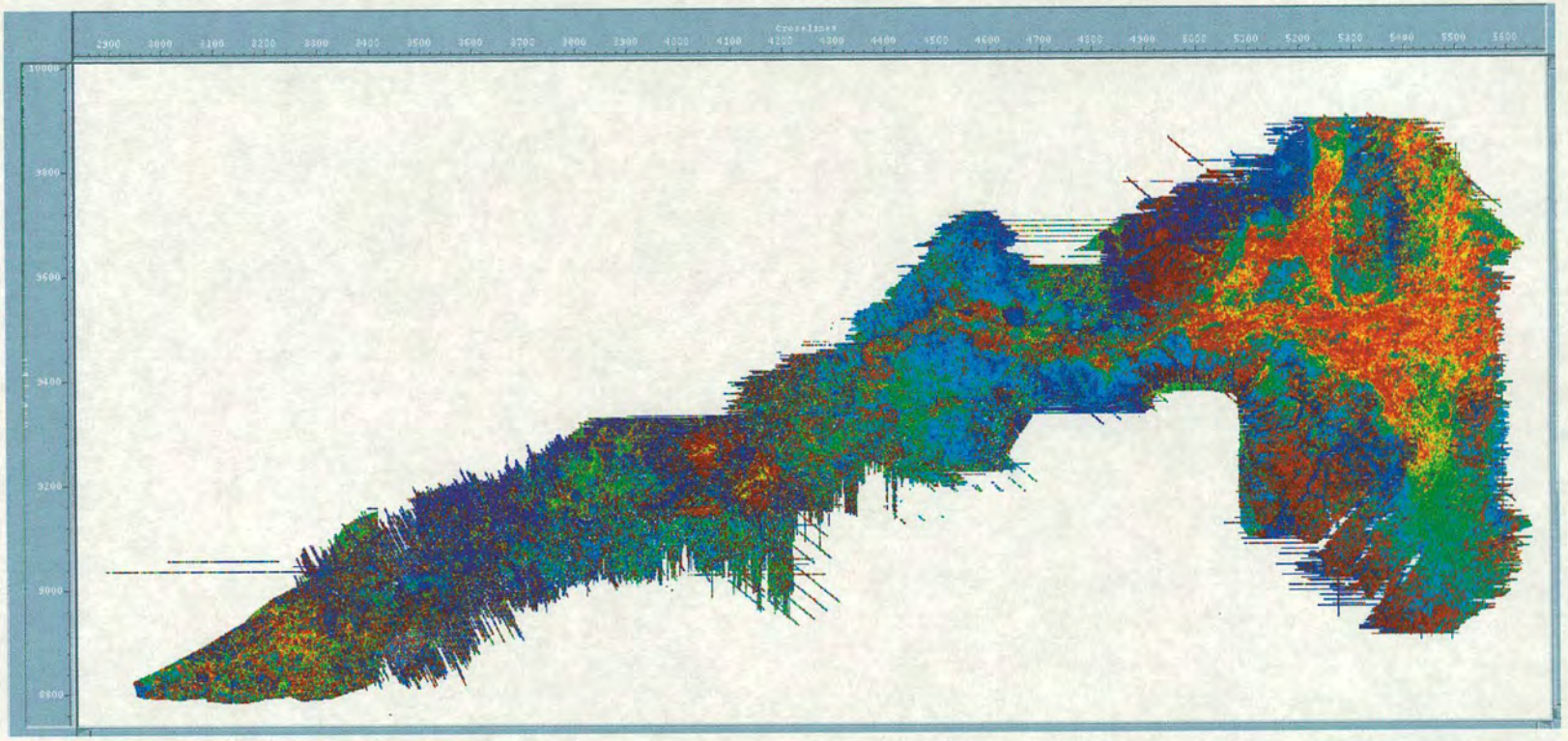

10 above and 30 below Top Tay horizon

Appendix 7

Another bird's eye view of the Tay surface, this time from the west looking towards east to salt high A. The figure shows the most recent channel flowing right through the salt high, something that cannot be possible to happen if the high was there with same relief at the time. If it was present the channel would have deflected and taken a much easier pathway. The image is not very clear on the printout but it is very convincing on the workstation.

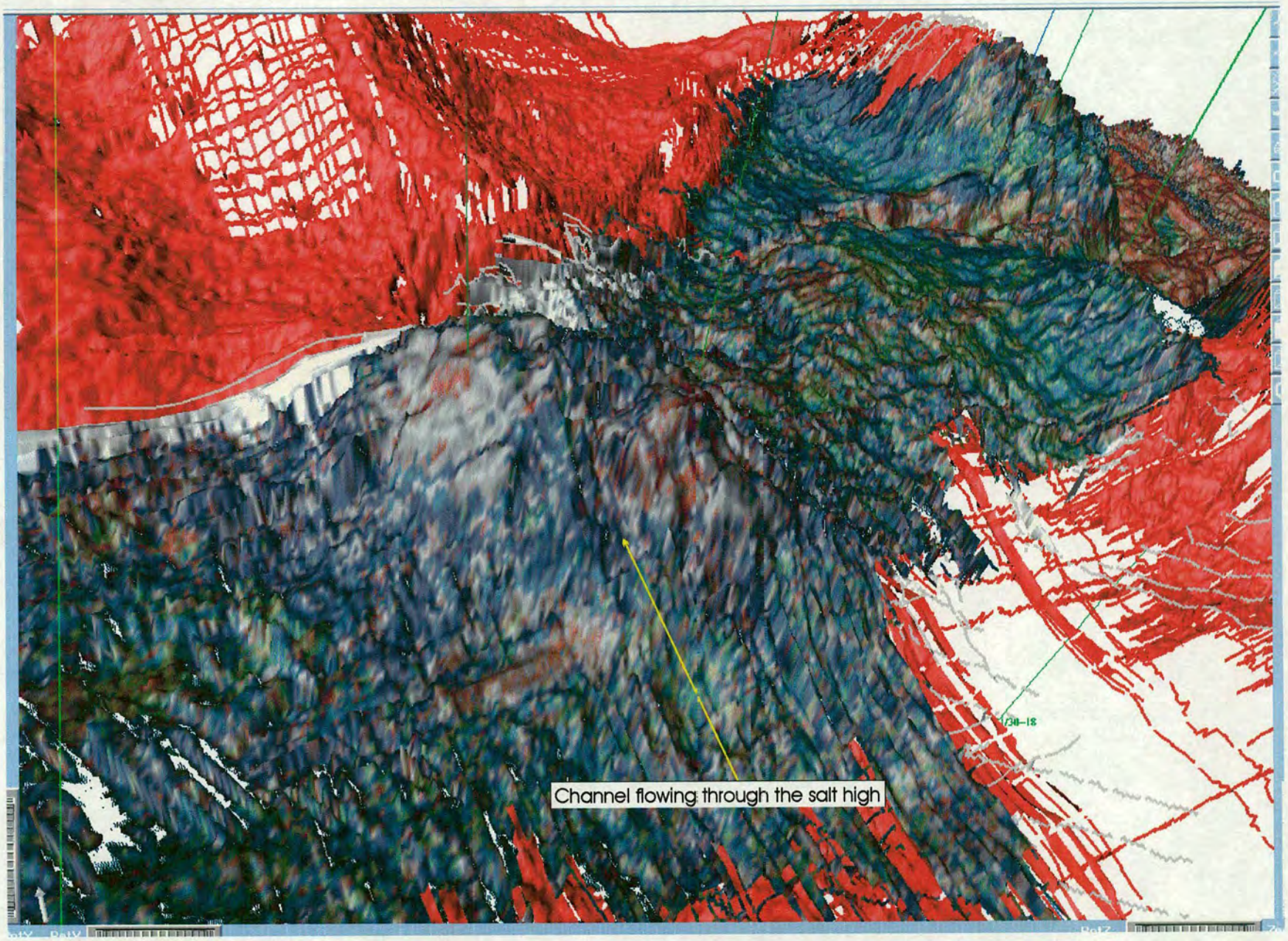
Channel flowing through the salt high

Appendix 8

Table showing the values resulted for the normalised polar representation of some simple shapes, namely; circle, square and hexagon. These values are used to plot Fig. 7.9.

Calculation of normalised polar representation of some simple shapes

ANGLE	CIRCLE	SQUARE	Hexagon
0	1	1.000000044	1.000000033
7.5	1	0.891288631	0.937379173
15	1	0.816496617	0.896575502
22.5	1	0.765366898	0.873498332
30	1	0.73205084	0.866025433
37.5	1	0.713208409	0.873498332
45	1	0.707106812	0.896575502
52.5	1	0.713208409	0.937379173
60	1	0.73205084	1.000000033
67.5	1	0.765366898	0.937379173
75	1	0.816496617	0.896575502
82.5	1	0.891288631	0.873498332
90	1	1.000000044	0.866025433
97.5	1	0.891288631	0.873498332
105	1	0.816496617	0.896575502
112.5	1	0.765366898	0.937379173
120	1	0.73205084	1.000000033
127.5	1	0.713208409	0.937379173
135	1	0.707106812	0.896575502
142.5	1	0.713208409	0.873498332
150	1	0.73205084	0.866025433
157.5	1	0.765366898	0.873498332
165	1	0.816496617	0.896575502
172.5	1	0.891288631	0.937379173
180	1	1.000000044	1.000000033
187.5	1	0.891288631	0.937379173
195	1	0.816496617	0.896575502
202.5	1	0.765366898	0.873498332
210	1	0.73205084	0.866025433
217.5	1	0.713208409	0.873498332
225	1	0.707106812	0.896575502
232.5	1	0.713208409	0.937379173
240	1	0.73205084	1.000000033
247.5	1	0.765366898	0.937379173
255	1	0.816496617	0.896575502
262.5	1	0.891288631	0.873498332
270	1	1.000000044	0.866025433
277.5	1	0.891288631	0.873498332
285	1	0.816496617	0.896575502
292.5	1	0.765366898	0.937379173
300	1	0.73205084	1.000000033
307.5	1	0.713208409	0.937379173
315	1	0.707106812	0.896575502
322.5	1	0.713208409	0.873498332
330	1	0.73205084	0.866025433
337.5	1	0.765366898	0.873498332
345	1	0.816496617	0.896575502
352.5	1	0.891288631	0.937379173
360	1	1.000000044	1.000000033